

**ANALYSIS OF STRUCTURAL TIMBER JOINTS
MADE WITH GLASS FIBRE / EPOXY**

BRUNO MASSE

**A thesis submitted in partial fulfilment
of the University's requirements
for the Degree of Doctor of Philosophy**

JUNE 2003

COVENTRY UNIVERSITY

ABSTRACT

This study investigates the potential of using glass fibre and epoxy resin to join timber members of the same thickness in the same plane. A total of 64 full-scale wood/glass/epoxy adhesive joints made with unidirectional or bidirectional glass fibres were fabricated. Joints with the load applied parallel to the grain or applied at 90°, 60° and 30° to the grain were tested in static tension. Results of strength and stiffness were compared between joint configurations.

The strength and stiffness of wood/glass/epoxy joints are mainly driven by the bond quality. The load capacity is governed by the shear strength of the timber, which appeared to be slightly affected by the grain orientation.

Finite element analysis was used to model the joints and confirmed the non-uniform load transfer that occurs on adhesive joints such as wood/glass/epoxy joints. An internal bending effect occurring at the overlap was also identified in the FE analysis. The results derived from finite element models correlate well with experimental results obtained from the sample tests.

Finally the fatigue resistance of wood/glass/epoxy joints was assessed. A total of 13 full-scale wood/glass/epoxy joints (with straight configuration) were tested in cyclic tension-tension at $R = 0.1$. The fatigue tests were carried out at a frequency of 0.33 Hz. Wood/glass/epoxy joints exhibit good fatigue resistance compared to other mechanical timber joints. The fatigue resistance was found dominated by the composite behaviour rather than the timber. Based on references, it was concluded that the joints fatigue resistance could be improved further by increasing the length of composite.

TABLE OF CONTENTS

INTRODUCTION.....	1
1.1. Introduction.....	1
1.2. Reader’s guide.....	4
LITERATURE REVIEW.....	5
2.1. Introduction.....	5
2.2. Construction environment	7
2.2.1. <i>Structural member applications.....</i>	<i>8</i>
2.2.2. <i>Structural joint applications.....</i>	<i>13</i>
2.2.3. <i>Nail plate connections</i>	<i>18</i>
2.3. Mechanical Environment	21
2.4. Review on fatigue.....	24
2.5. Summary	28
MATERIALS, PROPERTIES AND CHARACTERISTICS.....	29
3.1. Introduction.....	29
3.2. Material properties.....	30
3.2.1. <i>Timber.....</i>	<i>30</i>
3.2.1.1. <i>General.....</i>	<i>30</i>
3.2.1.2. <i>Selected timber</i>	<i>35</i>
3.2.2. <i>Glass fibres.....</i>	<i>37</i>
3.2.2.1. <i>General.....</i>	<i>37</i>
3.2.2.2. <i>Selected glass fibres.....</i>	<i>39</i>
3.2.3. <i>Epoxy resin</i>	<i>42</i>
3.2.3.1. <i>General.....</i>	<i>42</i>
3.2.3.2. <i>Selected epoxy resin</i>	<i>45</i>
3.2.4. <i>Glass fibre/epoxy composite.....</i>	<i>48</i>
3.2.4.1. <i>General.....</i>	<i>48</i>
3.2.4.2. <i>Selected glass fibre/epoxy composite.....</i>	<i>54</i>
3.3. Summary	55

EXPERIMENTAL PROGRAMME.....	56
4.1. Introduction.....	56
4.2. Testing of glass fibre/epoxy composite.....	56
4.3. Wood/glass/epoxy joints	60
4.3.1. <i>Joint geometry requirements</i>	60
4.3.2. <i>Types of test</i>	65
4.3.2.1. The choice of tests	65
4.3.2.2. Tension capacity test with load parallel to the grain.....	68
4.3.2.3. Tension capacity test with load perpendicular to the grain.....	72
4.3.2.4. Tension capacity test with load at 60° angle to the grain	74
4.3.2.5. Tension capacity test with load at 30° angle to the grain	77
4.3.3. <i>Number of samples tested</i>	81
4.3.4. <i>Testing equipment (LVDT, Translog 500, tension rig, frame).....</i>	83
4.3.5. <i>Sample fabrication process.....</i>	91
4.3.5.1. Straight configuration	93
4.3.5.2. Angle configuration	98
4.3.5.3. Samples with strain gauges.....	102
4.4. Timber properties testing.....	104
4.4.1. <i>Timber conditioning and preliminary grading</i>	105
4.4.2. <i>Determination of timber mechanical properties.....</i>	106
4.4.2.1. Determination of modulus of elasticity in bending.....	107
4.4.2.2. Determination of modulus of elasticity and strength in tension parallel to the grain	110
4.4.2.3. Determination of modulus of elasticity and strength in tension perpendicular to the grain	113
4.4.2.3.1. EN 1193: 1997 Standard test	113
4.4.2.3.2. Alternative test.....	115
4.4.2.4. Determination of shear strength parallel to the grain.....	118
4.5. Summary	119
 EXPERIMENTAL RESULTS	 120
5.1. Introduction.....	120
5.2. Preliminary tests	120
5.2.1. <i>Test of wood/glass/epoxy samples with varying lengths of composite.....</i>	120
5.2.2. <i>Test of wood/glass/epoxy samples for experimental adjustments.....</i>	123
5.3. Timber grading tests.....	127
5.4. Tension parallel to the grain tests.....	129

5.4.1.	<i>TPU00 and TPB00 Tests</i>	129
5.4.2.	<i>TPU10 and TPB30 Tests</i>	140
5.4.3.	<i>Discussion</i>	149
5.5.	Tension not parallel to the grain tests	153
5.5.1.	<i>TNU90 and TNB90 Tests</i>	153
5.5.2.	<i>TNU60 and TNB60 Tests</i>	163
5.5.3.	<i>TNU30 and TNB30 Tests</i>	172
5.5.4.	<i>Discussion</i>	182
5.6.	Samples tested with strain gauges	187
5.7.	Strength determination and timber grading	192
5.7.1.	<i>Small clear sample tests</i>	192
5.7.2.	<i>Principles and methods</i>	196
5.7.3.	<i>Small clear sample test results</i>	201
5.7.3.1.	<i>Static Bending tests</i>	201
5.7.3.2.	<i>Tension parallel to the grain tests</i>	202
5.7.3.3.	<i>Tension perpendicular to the grain tests</i>	204
5.7.3.4.	<i>Shear parallel to the grain tests</i>	206
5.7.4.	<i>Comparison and discussion</i>	207
5.8.	Conclusion	219
 THEORETICAL AND FINITE ELEMENT ANALYSES		221
6.1.	Introduction	221
6.2.	Theoretical approach to structural adhesive joints	222
6.2.1.	<i>Anisotropic and orthotropic materials</i>	223
6.2.2.	<i>Micromechanics of composite materials</i>	235
6.2.2.1.	<i>Stiffness approach to lamina with uniaxial fibres</i>	237
6.2.2.2.	<i>Stiffness approach to lamina with biaxial fibres</i>	244
6.2.3.	<i>Double lap joints</i>	246
6.2.3.1.	<i>Load transfer mechanisms in double lap joints</i>	249
6.2.3.2.	<i>Wood/glass/epoxy joints</i>	253
6.2.3.3.	<i>Existing comparable results</i>	256
6.3.	Finite element modelling	261
6.3.1.	<i>Introduction</i>	261
6.3.2.	<i>FEM procedures</i>	261
6.3.2.1.	<i>Analysis type</i>	261
6.3.2.2.	<i>Elements and mesh types</i>	265
6.3.3.	<i>Joints with load parallel to the grain</i>	268
6.3.3.1.	<i>Configuration with uniaxial fibres TPU00</i>	273

6.3.3.1.1.	2-Dimensional model.....	273
6.3.3.1.2.	3-Dimensional model.....	280
6.3.3.2.	Configuration with biaxial fibres TPB00.....	287
6.3.3.2.1.	2-Dimensional model.....	287
6.3.3.2.2.	3-Dimensional model.....	292
6.3.4.	<i>Joints with load not parallel to the grain</i>	298
6.3.4.1.	Load applied perpendicular to the grain	298
6.3.4.1.1.	Configuration with uniaxial fibres TNU90.....	298
6.3.4.1.2.	Configuration with biaxial fibres TNB90.....	304
6.3.4.2.	Load applied with an angle of 60 degrees to the grain	309
6.3.4.2.1.	Configuration with uniaxial fibres TNU60.....	309
6.3.4.2.2.	Configuration with biaxial fibres TNB60.....	315
6.3.4.3.	Load applied with an angle of 30 degrees to the grain	321
6.3.4.3.1.	Configuration with uniaxial fibres TNU30.....	321
6.3.4.3.2.	Configuration with biaxial fibres TNB30.....	327
6.4.	Internal bending effects.....	334
6.5.	Discussion and conclusion	336

FATIGUE ASSESSMENT OF WOOD/GLASS/EPOXY JOINTS.....340

7.1.	Introduction.....	340
7.2.	Fatigue test programme	341
7.2.1.	<i>Methodology</i>	341
7.2.2.	<i>Testing equipment</i>	345
7.2.3.	<i>Joint properties and configurations</i>	347
7.3.	Test results.....	351
7.3.1.	<i>Preliminary results</i>	352
7.3.2.	<i>Fatigue properties and S-N curve</i>	355
7.3.2.1.	Experimental results	355
7.3.2.2.	Fatigue properties of materials	358
7.3.2.3.	Relationship with current design codes	374
7.3.3.	<i>Other wood/glass/epoxy joints fatigue results</i>	379
7.4.	Conclusion	387

CONCLUSIONS	391
8.1. General conclusions	391
8.2. Suggestions for future work.....	393
REFERENCES	394
APPENDIX	403
A. Strains results from static tensile tests of wood/glass/epoxy joints.....	403
B. Results of small clear samples tests	406
<i>B.1. Static bending tests results.....</i>	<i>406</i>
<i>B.2. Tension parallel to the grain tests results.....</i>	<i>407</i>
<i>B.3. Tension perpendicular to the grain tests results.....</i>	<i>408</i>
<i>B.4. Shear parallel to the grain tests results</i>	<i>409</i>
C. Example of in-plane and out-of-plane bending moment calculations	410
D. Technical details for FE models.....	411
<i>D.1. Models with load parallel to the grain TPU/B00 – 2D models</i>	<i>411</i>
<i>D.2. Models with load parallel to the grain TPU/B00 – 3D models</i>	<i>413</i>
<i>D.3. Models with load perpendicular to the grain TNU/B90 – 3D models.....</i>	<i>415</i>
<i>D.4. Models with load at 60° to the grain TNU/B60 – 3D models.....</i>	<i>417</i>
<i>D.5. Models with load at 30° to the grain TNU/B30 – 3D models.....</i>	<i>420</i>

LIST OF FIGURES

1.1. <i>Typical timber truss internal joint with dowels</i>	1
1.2. <i>Typical wood/glass/epoxy sample with 60° angle configuration.....</i>	2
3.1. <i>Models of a softwood and hardwood block, showing the main planes for anisotropy</i>	31
3.2. <i>The average density at a moisture content of 15% for some common constructional timber and two woods at extremes of the density range</i>	31
3.3. <i>Lateral branches are connected to the pith of the main stem. Each successive growth ring forms continuously over the stem and branches</i>	33
3.4. <i>Tension failure of a spruce board cause by fibre inclination around a knot.....</i>	33
3.5. <i>A softwood board may show knots in clusters separated by the often clear wood of the inter-nodes.....</i>	33
3.6. <i>UT-E500 fibre layout.....</i>	40
3.7. <i>XE450 fibre layout.....</i>	41
3.8. <i>Stress/strain diagram of typical epoxy resin.....</i>	43
3.9. <i>Sketch of single fibre surrounded by the matrix</i>	50
3.10. <i>Effect of fibre orientation on the tensile strength of E-glass fibre reinforced epoxy composites</i>	53
3.11. <i>A three-dimensional weave for fibre reinforced composites.....</i>	54
4.1. <i>Dog bone sample shape.....</i>	57
4.2. <i>Moulds for dog bone samples using aluminium foil</i>	57
4.3. <i>Dog bone samples curing in moulds.....</i>	58
4.4. <i>Comparison between dog bone cross-section needed and achieved</i>	58
4.5. <i>Variable bonded length for butt end joint.....</i>	62
4.6. <i>Determination of maximum bonded length from joint geometry</i>	62
4.7. <i>Sample end with 20 mm bolt connection</i>	64
4.8. <i>Detail of sample end connection with shear-plate connectors</i>	64
4.9. <i>Sample configurations for tension test with load parallel to the grain.....</i>	68
4.10. <i>Positions of LVDTs on samples for tension test with load parallel to the grain</i>	70
4.11. <i>Strain gauge locations on samples for tension test with load parallel to the grain.....</i>	71
4.12. <i>Sample configurations for tension test with load perpendicular to the grain.....</i>	72

4.13.	<i>Positions of LVDTs on samples for tension test with load perpendicular to the grain.....</i>	73
4.14.	<i>Strain gauge locations on samples for tension test with load perpendicular to the grain.....</i>	73
4.15.	<i>Sample configurations for tension test with load at 60° angle to the grain.....</i>	74
4.16.	<i>Positions of LVDTs on samples for tension test with load at 60° angle to the grain</i>	75
4.17.	<i>Strain gauge locations on samples for tension test with load at 60° angle to the grain.....</i>	76
4.18.	<i>Sample configurations for tension test with load at 30° angle to the grain.....</i>	77
4.19.	<i>Position of LVDTs on samples for tension test with load at 30° angle to the grain.....</i>	78
4.20.	<i>Strain gauge locations on samples for tension test with load at 30° angle to the grain.....</i>	79
4.21.	<i>Rig configuration for straight pullout tests.....</i>	83
4.22.	<i>TPB00 sample ready for straight pullout test.....</i>	84
4.23.	<i>Loading arrangement for tension test with load not parallel to the grain</i>	85
4.24.	<i>Sample arrangement within the steel box.....</i>	85
4.25.	<i>Rig configuration for tension test with load not parallel to the grain</i>	87
4.26.	<i>Sample configuration when positioned within the steel box.....</i>	87
4.27.	<i>Sample configuration for tension test with load at 90° to the grain.....</i>	88
4.28.	<i>Sample configuration for tension test with load at 60° to the grain.....</i>	88
4.29.	<i>ACT1000A Spring Return LVDT Transducer configuration</i>	89
4.30.	<i>D5/300AG Spring Return LVDT Transducer configuration.....</i>	90
4.31.	<i>Drilling of each timber piece end for shear plate connector.....</i>	93
4.32.	<i>Aluminium foil positioned in the joint's gap.....</i>	94
4.33.	<i>Staples and craft tapes are placed on the sample.....</i>	95
4.34.	<i>The first layer of glass fibre is bonded on the timber</i>	96
4.35.	<i>The layer of glass fibre is bonded onto the other side</i>	96
4.36.	<i>Sample with composite excess removed.....</i>	97
4.37.	<i>Brackets are fixed onto the samples.....</i>	97
4.38.	<i>Angle sample is cut into shape.....</i>	98
4.39.	<i>Neutral axes and bolt position are drawn on the timber surfaces</i>	99
4.40.	<i>Craft tape is used to hold the sample together and to define the composite edges</i>	99
4.41.	<i>Layers of glass fibre are bonded on the sample</i>	100
4.42.	<i>A handsaw is used to remove the excess of composite.....</i>	100
4.43.	<i>Sample with final composite layout</i>	101
4.44.	<i>Brackets and timber wedges are glued on the sample sides.....</i>	101
4.45.	<i>Strain gauges are carefully positioned onto the wet composite layer</i>	102

4.46.	<i>Strain gauges and soldered to cables and isolated with craft tape</i>	103
4.47.	<i>Principles of three points bending test</i>	105
4.48.	<i>Central loading for 20 mm standard test piece</i>	107
4.49.	<i>Static bending test samples</i>	107
4.50.	<i>Contour of the loading head</i>	108
4.51.	<i>Testing frame used for the static bending test</i>	108
4.52.	<i>Test piece for tension parallel to the grain</i>	110
4.53.	<i>Some of the small clear samples for the tension test parallel to the grain</i>	111
4.54.	<i>Tension parallel to the grain test configuration</i>	112
4.55.	<i>Structural timber piece for tension test perpendicular to the grain</i>	113
4.56.	<i>Test principle with gauge length</i>	114
4.57.	<i>Structural timber test piece for alternative tension test perpendicular to the grain</i>	115
4.58.	<i>Test piece glued on Tee end steel plates</i>	115
4.59.	<i>Section through the tee end with connected bolt</i>	116
4.60.	<i>Tension perpendicular to the grain samples</i>	116
4.61.	<i>Tension perpendicular to the grain test configuration</i>	117
4.62.	<i>Test piece for the shear box test parallel to the grain</i>	118
4.63.	<i>Shear parallel to the grain test configuration</i>	118
4.64.	<i>Shear sample ready for testing</i>	119
5.1.	<i>Loading procedures in accordance with BS EN 26891</i>	124
5.2.	<i>Idealised load/displacement curve and measurements to BS EN 26891</i>	125
5.3.	<i>Load/displacement curve for sample C</i>	125
5.4.	<i>Delamination on both sides observed on the 7TPU00 - Z sample</i>	131
5.5.	<i>Delamination on both sides observed on the 8TPU00 - J sample</i>	132
5.6.	<i>Load/displacement curves for TPU00 tests</i>	133
5.7.	<i>Tension failure and delamination for the 5TPB00 - J sample</i>	136
5.8.	<i>Tension failure and delamination for the 5TPB00 - J sample</i>	136
5.9.	<i>Load/displacement curves for TPB00 tests</i>	138
5.10.	<i>Load/displacement curves for TPU10 tests</i>	143
5.11.	<i>Load/displacement curves for TPB30 tests</i>	147
5.12.	<i>Average failure loads for all load parallel to the grain tension tests</i>	149
5.13.	<i>Average stiffness for all load parallel to the grain tension tests</i>	150
5.14.	<i>Load/displacement curves for TNU90 tests</i>	156
5.15.	<i>Combined failure modes for the 1TNB90 - γ sample</i>	159
5.16.	<i>Load/displacement curves for TNB90 tests</i>	161
5.17.	<i>Load/displacement curves for TNU60 tests</i>	166
5.18.	<i>Load/displacement curves for TNB60 tests</i>	170

5.19.	<i>Top delamination on both sides at failure of sample 4TNU30 – X.....</i>	174
5.20.	<i>Top delamination on both sides at failure of sample 5TNU30 – Z.....</i>	175
5.21.	<i>Load/displacement curves for TNU30 tests.....</i>	176
5.22.	<i>Load/displacement curves for TNB30 tests.....</i>	180
5.23.	<i>Average failure loads for all tension tests with the load not parallel to the grain.....</i>	182
5.24.	<i>Average stiffness for all tension tests with the load not parallel to the grain.....</i>	184
5.25.	<i>Average elastic deformations for all tension tests with the load not parallel to the grain.....</i>	185
5.26.	<i>Strain gauge positions on a typical composite layer.</i>	188
5.27.	<i>Load/strain curves obtained for the samples with load parallel to the grain.....</i>	189
5.28.	<i>Load/strain curves obtained for the samples with load not parallel to the grain.....</i>	190
5.29.	<i>Frequency distribution of crushing strength of small clear test pieces of green hardwood keruing.....</i>	197
5.30.	<i>Central loading for 20 mm standard test piece</i>	201
5.31.	<i>Test piece for tension parallel to the grain.....</i>	203
5.32.	<i>Test piece for tension perpendicular to the grain test</i>	204
5.33.	<i>Test piece for the shear box test parallel to the grain</i>	206
6.1.	<i>Longitudinal (L), Radial (R) and Tangential (T) axes directions of timber.....</i>	224
6.2.	<i>Planes of symmetry of a unidirectionally reinforced lamina.....</i>	225
6.3.	<i>Stresses acting on a cube of material</i>	227
6.4.	<i>Double layer of glass fibres in the XE450 fabric.....</i>	233
6.5.	<i>Basic questions of micromechanics</i>	235
6.6.	<i>Composite element loaded in the X direction</i>	237
6.7.	<i>Composite element loaded in the Y direction</i>	239
6.8.	<i>Composite element with deformation loaded in the X direction.....</i>	240
6.9.	<i>Composite element loaded in shear with shear deformation.....</i>	242
6.10.	<i>Stitched fabric lamina for micromechanics analysis</i>	245
6.11.	<i>Typical double lap joint loaded in tension.....</i>	246
6.12.	<i>Typical double strap joint loaded in tension.....</i>	246
6.13.	<i>Bending moments induced in the outer adherends of a double lap joint.....</i>	248
6.14.	<i>Adhesive shear stress-strain curves and models.....</i>	249
6.15.	<i>Models of equal shear strain energy of the adhesive.....</i>	250
6.16.	<i>Development of shear stress and strain distribution in double lap joint with increasing loading</i>	250
6.17.	<i>Influence of lap length on adhesive shear stress distribution.....</i>	251

6.18. <i>Ideal models of thickness distribution of glass fibre and epoxy resin.....</i>	254
6.19. <i>Adhesive shear stress distributions in aluminium-aluminium joints.....</i>	256
6.20. <i>Adhesive shear stress distributions in CFRP-CFRP joints.....</i>	256
6.21. <i>Adherend tensile stress distributions in CFRP-CFRP double lap joints</i>	257
6.22. <i>Adhesive shear stress distributions in cross-ply CFRP-CFRP and unidirectional CFRP-CFRP double lap joints.....</i>	258
6.23. <i>Adhesive shear stress distributions in aluminium-CFRP double lap joints.....</i>	258
6.24. <i>Adhesive shear stress distributions in aluminium-CFRP double lap joints with equal and matched adherends</i>	259
6.25. <i>Example of 2D configuration for straight joint</i>	263
6.26. <i>Example of 2D configuration and symmetry for straight joint</i>	264
6.27. <i>Example of 3D configuration and symmetry for straight joint</i>	264
6.28. <i>Example of 2D straight joint model with rectangular mesh</i>	268
6.29. <i>Another example of 2D straight joint model with rectangular mesh.....</i>	268
6.30. <i>Example of 2D straight joint model with a coarse-to-fine mesh.....</i>	269
6.31. <i>Another example of 2D straight joint model with a coarse-to-fine mesh</i>	269
6.32. <i>Example of 2D straight joint model with free quadrilateral mesh generated using SmartMeshing</i>	270
6.33. <i>Convergence graph of longitudinal strain recorded on node A</i>	271
6.34. <i>Convergence graph of longitudinal strain recorded on node B</i>	271
6.35. <i>Refined of 2D straight joint model with free quadrilateral mesh (18499 elements).....</i>	272
6.36. <i>Zooms of the 2D straight joint model (18499 elements) showing locations of nodes A and B.....</i>	272
6.37. <i>Zooms of the 2D straight joint model (18499 elements) showing locations of nodes A and B.....</i>	272
6.38. <i>Graphical results of the 2D model type TPU00.....</i>	274
6.39. <i>Deformed shape at composite left end of the 2D model type TPU00</i>	275
6.40. <i>Tensile stress distributions at the interface between the composite and the timber.....</i>	276
6.41. <i>Shear stress distributions at the interface between the composite and the timber.....</i>	278
6.42. <i>Longitudinal tensile strain distribution on glass fibre/epoxy surface.....</i>	279
6.43. <i>Graphical results of the 3D model type TPU00.....</i>	281
6.44. <i>Tensile stress distributions at the interface between the composite and the timber.....</i>	282
6.45. <i>Shear stress distributions at the interface between the composite and the timber.....</i>	284
6.46. <i>Longitudinal tensile strain distribution on glass fibre/epoxy surface.....</i>	285
6.47. <i>Graphical results of the 2D model type TPB00.....</i>	288

6.48. Tensile stress distributions at the interface between the composite and the timber.....	289
6.49. Shear stress distributions at the interface between the composite and the timber.....	290
6.50. Longitudinal tensile strain distribution on glass fibre/epoxy surface.....	291
6.51. Graphical results of the 3D model type TPB00.....	293
6.52. Tensile stress distributions at the interface between the composite and the timber.....	294
6.53. Shear stress distributions at the interface between the composite and the timber.....	295
6.54. Longitudinal tensile strain distribution on glass fibre/epoxy surface.....	296
6.55. Graphical results of the 3D model type TNU90.....	299
6.56. Tensile stress distributions at the interface between the composite and the timber.....	300
6.57. Shear stress distributions at the interface between the composite and the timber.....	302
6.58. Tensile strain distribution on glass fibre/epoxy surface.....	303
6.59. Graphical results of the 3D model type TNB90.....	305
6.60. Tensile stress distributions at the interface between the composite and the timber.....	306
6.61. Shear stress distributions at the interface between the composite and the timber.....	307
6.62. Longitudinal tensile strain distribution on glass fibre/epoxy surface.....	308
6.63. Graphical results of the 3D model type TNU60.....	310
6.64. Tensile stress distributions at the interface between the composite and the timber.....	311
6.65. Shear stress distributions at the interface between the composite and the timber.....	313
6.66. Longitudinal tensile strain distribution on glass fibre/epoxy surface.....	314
6.67. Graphical results of the 3D model type TNB60.....	316
6.68. Tensile stress distributions at the interface between the composite and the timber.....	317
6.69. Shear stress distributions at the interface between the composite and the timber.....	318
6.70. Longitudinal tensile strain distribution on glass fibre/epoxy surface.....	319
6.71. Graphical results of the 3D model type TNU30.....	322
6.72. Tensile stress distributions at the interface between the composite and the timber.....	323
6.73. Shear stress distributions at the interface between the composite and the timber.....	325

6.74.	<i>Longitudinal tensile strain distribution on glass fibre/epoxy surface.....</i>	326
6.75.	<i>Graphical results of the 3D model type TNB30.....</i>	328
6.76.	<i>Tensile stress distributions at the interface between the composite and the timber.....</i>	329
6.77.	<i>Shear stress distributions at the interface between the composite and the timber.....</i>	331
6.78.	<i>Longitudinal tensile strain distribution on glass fibre/epoxy surface.....</i>	332
6.79.	<i>Deformed shape with lateral deformation $\Delta\omega$ of the 2D FE model type TPU00.....</i>	334
7.1.	<i>Typical saw tooth stress versus time waveform</i>	343
7.2.	<i>Set of σ-log N curves for tension-tension ($R = 0.1, 0.3$ and 0.5) and tension-compression ($R = -0.5$ and -1) cyclic stress configurations</i>	344
7.3.	<i>The J.J. Lloyds machine during the fatigue test of one of the sample</i>	346
7.4.	<i>Sample configuration type TPU00 for fatigue test</i>	348
7.5.	<i>LVDTs and strain gauges positions on fatigue test samples.....</i>	349
7.6.	<i>Strain gauges positions on fatigue test samples</i>	349
7.7.	<i>Sample in position ready for the fatigue test</i>	350
7.8.	<i>Three points bending test of one timber plank before joint fabrication.....</i>	352
7.9.	<i>S-N logarithmic curves for wood/glass/epoxy joints tested in tension-tension at $R = 0.1$.....</i>	356
7.10.	<i>Typical S-N curves for 1045 Steel and 2014-T6 Aluminium alloy.....</i>	359
7.11.	<i>S-N curves of reversed axial stresses for mild steel (\bullet) and 24S-T3 aluminium alloy (\times).....</i>	359
7.12.	<i>S-N curves for various construction materials at $R = 0.1$</i>	360
7.13.	<i>S-N curves for sliced Khaya laminates tested in bending at $R = 0$.....</i>	361
7.14.	<i>S-N curves for Khaya axially loaded at $R = -1, -2, -10$ and 10.....</i>	362
7.15.	<i>S-N curves for Khaya and Douglas fir tested in tension-compression at $R = -1$.....</i>	362
7.16.	<i>S-N curves for Khaya tested in shear at $R = 0.1$</i>	363
7.17.	<i>S-N curves for laminated Khaya tested in tension-tension at $R = 0.1$</i>	364
7.18.	<i>Maximum and minimum strain plotted versus log cycles for three Khaya samples tested in tension-tension fatigue at $R = 0.1$ and peak stress of 55 MPa</i>	365
7.19.	<i>S-N curves for laminated Douglas fir tested at $R = 0.1$.....</i>	365
7.20.	<i>S-N curves for timber at various frequencies</i>	366
7.21.	<i>Fatigue failure mechanisms in composites.....</i>	367
7.22.	<i>Fatigue life diagram with damage mechanisms for a unidirectional composite subjected to tension-tension stresses</i>	368

7.23.	<i>Normalised S-N curves for three unidirectional composite materials.....</i>	<i>369</i>
7.24.	<i>Extremes of normalised S-N tensile fatigue data from glass fibre laminate at R = 0.1</i>	<i>371</i>
7.25.	<i>The fatigue sensitivity coefficient for unidirectional glass fibre laminates as a function of fibre content at R = 0.1.....</i>	<i>372</i>
7.26.	<i>Effect of matrix material on tensile fatigue in glass fibre laminates with 0° and ±45° plies at R = 0.1</i>	<i>373</i>
7.27.	<i>k_{fat}-log N relationship from EC5: Pt 2 combined with bonded-in rod connections test results.....</i>	<i>375</i>
7.28.	<i>k_{fat}-log N relationship from EC5: Pt 2 combined with bonded-in rod connection test results by failure modes.....</i>	<i>376</i>
7.29.	<i>k_{fat}-log N relationship from EC5: Pt 2 and combined with the tension fatigue test results of wood/glass/epoxy joints at R = 0.1.....</i>	<i>377</i>
7.30.	<i>Maximum gap strain recorded for maximum cyclic loads for several wood/glass/epoxy joints tested in tension-tension at R = 0.1</i>	<i>379</i>
7.31.	<i>Maximum and minimum gap displacements recorded at maximum and minimum cyclic loads of 17.5 kN and 1.5 kN for two wood/glass/epoxy joints tested in tension-tension at R = 0.1</i>	<i>380</i>
7.32.	<i>Maximum and minimum gap displacements recorded at maximum and minimum cyclic loads of 16 kN and 1.4 kN for three wood/glass/epoxy joints tested in tension-tension at R = 0.1</i>	<i>381</i>
7.33.	<i>Maximum and minimum middle and end strains recorded at maximum and minimum cyclic loads of 18.5 kN and 1.6 kN for sample 4B tested in tension-tension at R = 0.1.....</i>	<i>382</i>
7.34.	<i>Maximum and minimum middle and end strains recorded at maximum and minimum cyclic loads of 16 kN and 1.4 kN for sample 11A tested in tension-tension at R = 0.1.....</i>	<i>383</i>
7.35.	<i>Visible damage in the gap zone of the composite layer after the fatigue test.....</i>	<i>384</i>
7.36.	<i>Matrix/fibre debonding details at the interface with the timber (underside of the composite layer) in the gap zone.....</i>	<i>385</i>
7.37.	<i>Matrix/fibre debonding details at the interface with the timber (underside of the composite layer) in the gap zone.....</i>	<i>385</i>
7.38.	<i>Other matrix/fibre debonding details at the interface with the timber (underside of the composite layer) in the gap zone</i>	<i>385</i>
7.39.	<i>Other matrix/fibre debonding details at the interface with the timber (underside of the composite layer) in the gap zone</i>	<i>385</i>
7.40.	<i>Fibre breaking and local debonding details at the interface with the timber in the gap zone</i>	<i>386</i>
7.41.	<i>Fibre breaking and local debonding details at the interface with the timber in the gap zone</i>	<i>386</i>

7.42.	<i>S-N normalised curves for wood/glass/epoxy joints tested in tension-tension at R = 0.1</i>	387
A.1.	<i>Strain gauges positions on a typical composite layer</i>	403
D.1.	<i>Forces, restraints and symmetries for TPU/B00 – 2D models</i>	411
D.2.	<i>Node locations for TPU/B00 – 2D models</i>	412
D.3.	<i>Forces, restraints and symmetries for TPU/B00 – 3D models</i>	413
D.4.	<i>Node locations for TPU/B00 – 3D models</i>	414
D.5.	<i>Forces, restraints and symmetries for TNU/B90 – 3D models</i>	415
D.6.	<i>Node locations for TNU/B90 – 3D models</i>	416
D.7.	<i>Forces, restraints and symmetries for TNU/B60 – 3D models</i>	417
D.8.	<i>Node locations for TNU/B60 – 3D models</i>	418
D.9.	<i>Forces, restraints and symmetries for TNU/B30 – 3D models</i>	420
D.10.	<i>Node locations for TNU/B30 – 3D models</i>	421

LIST OF TABLES

3.1.	<i>Grade stresses and moduli of elasticity for strength classes: for dry exposure condition.</i>	36
3.2.	<i>Strength classes and characteristic values for coniferous species</i>	36
3.3.	<i>Mechanical properties of typical E-glass and S-glass fibres.</i>	38
3.4.	<i>UT-E500 mechanical properties.</i>	40
3.5.	<i>Component properties for Spabond 120 resin.</i>	46
3.6.	<i>Working properties vs. temperature for Spabond 120 resin.</i>	46
3.7.	<i>Cured system properties for Spabond 120 resin.</i>	47
3.8.	<i>Typical mechanical properties for unidirectional glass fibre reinforced epoxy composite</i>	49
3.9.	<i>Mechanical properties for UT-E500 and XE-450 with Ampreg 20 resin composites.</i>	55
4.1.	<i>Summary table of wood/glass/epoxy joints test programme</i>	82
4.2.	<i>Summary of small clear timber sample tests.</i>	106
5.1.	<i>Test results of wood/glass/epoxy samples with varying lengths of composite</i>	121
5.2.	<i>Test results of wood/glass/epoxy samples for loading procedure adjustments.</i>	123
5.3.	<i>Bending moduli for TPU00 and TPB00 samples.</i>	127
5.4.	<i>Bending moduli for TPU10 and TPB30 samples.</i>	127
5.5.	<i>Bending moduli for TNU30 and TNB30 samples</i>	128
5.6.	<i>Bending moduli for TNU60 and TNB60 samples</i>	128
5.7.	<i>Bending moduli for TNU90 and TNB90 samples</i>	128
5.8.	<i>Results from TPU00 tests.</i>	130
5.9.	<i>Failure modes from TPU00 tests</i>	131
5.10.	<i>Results from TPB00 tests</i>	135
5.11.	<i>Failure modes from TPB00 tests</i>	136
5.12.	<i>Results from TPU10 tests.</i>	141
5.13.	<i>Failure modes from TPU10 tests</i>	142
5.14.	<i>Results from TPB30 tests</i>	145
5.15.	<i>Failure modes from TPB30 tests</i>	146
5.16.	<i>Results from TNU90 tests</i>	154
5.17.	<i>Failure modes from TNU90 tests.</i>	155
5.18.	<i>Results from TNB90 tests.</i>	158

5.19.	<i>Failure modes from TNB90 tests</i>	159
5.20.	<i>Results from TNU60 tests</i>	164
5.21.	<i>Failure modes from TNU60 tests</i>	165
5.22.	<i>Results from TNB60 tests</i>	168
5.23.	<i>Failure modes from TNB60 tests</i>	169
5.24.	<i>Results from TNU30 tests</i>	173
5.25.	<i>Failure modes from TNU30 tests</i>	174
5.26.	<i>Results from TNB30 tests</i>	178
5.27.	<i>Failure modes from TNB30 tests</i>	179
5.28.	<i>Table of the strain gauges positions for each tested sample</i>	187
5.29.	<i>Summary of small clear timber sample tests</i>	192
5.30.	<i>Changes in derivation of design stresses over the period before 1973 to 2005</i>	194
5.31.	<i>Summary table for grading requirements</i>	199
5.32.	<i>Summary results of the static bending tests</i>	202
5.33.	<i>Summary results of the tension parallel to the grain tests</i>	203
5.34.	<i>Summary results of the tension perpendicular to the grain tests</i>	205
5.35.	<i>Summary results of the shear parallel to the grain tests</i>	206
5.36.	<i>Summary table of mean values and standard deviations for the timber properties obtained from the small clear sample tests</i>	207
5.37.	<i>Average values (upper) and standard deviation (lower) of various mechanical properties for selected timbers at 12% moisture content from small clear test pieces</i>	208
5.38.	<i>Tensile strength parallel to the grain of certain timbers using small clear test pieces</i>	208
5.39.	<i>Approximate change (%) of clear wood properties for a one percent change of moisture content. Basis is properties at 12%</i>	210
5.40.	<i>Basic and graded values of small clear timber sample properties at 10.2% and 18% moisture content</i>	211
5.41.	<i>Dry basic and grade 65 stresses and moduli of elasticity for various species of softwoods having a moisture content not exceeding 18%</i>	211
5.42.	<i>Summary results of the full-size bending tests</i>	212
5.43.	<i>Bending MOE and density of the full-size bending tests at 11.44% and 12% moisture content</i>	214
5.44.	<i>Basic values of bending MOR and MOE from small clear samples based on the lower 5-percentile at 10.2% and 12% moisture content</i>	214
5.45.	<i>Characteristic values obtained from results compared with characteristic values given for some strength classes of poplar and conifer species</i>	216
5.46.	<i>Orthotropic properties determined for various species</i>	219
5.47.	<i>Timber orthotropic properties used for the FEA</i>	220

6.1.	<i>Contracted notation for stresses and strains</i>	228
6.2.	<i>Thickness measurement of glass fibres and composites used in wood/glass/epoxy joints</i>	253
6.3.	<i>Comparison of strains results obtained from experiments and from the FE model</i>	280
6.4.	<i>Comparison of strains results obtained from experiments and from the FE model</i>	286
6.5.	<i>Comparison of strains results obtained from experiments and from the FE model</i>	292
6.6.	<i>Comparison of strains results obtained from experiments and from the FE model</i>	297
6.7.	<i>Comparison of strains results obtained from experiments and from the FE model</i>	304
6.8.	<i>Comparison of strains results obtained from experiments and from the FE model</i>	308
6.9.	<i>Comparison of strains results obtained from experiments and from the FE model</i>	315
6.10.	<i>Comparison of strains results obtained from experiments and from the FE model</i>	320
6.11.	<i>Comparison of strains results obtained from experiments and from the FE model</i>	327
6.12.	<i>Comparison of strains results obtained from experiments and from the FE model</i>	333
6.13.	<i>Comparison of lateral deformation $\Delta\omega$ obtained from experiments and from 2D FE model type TPU00</i>	335
7.1.	<i>Summary table of cycle-profiles used for the fatigue tests</i>	345
7.2.	<i>Cyclic loading ranges for the fatigue tests</i>	351
7.3.	<i>Preliminary results from fatigue tests</i>	353
7.4.	<i>Tests results of loading ranges and cycles to failure</i>	355
7.5.	<i>Results of the static tension test for sample 12 and 13</i>	357
7.6.	<i>Relationship between k_{fat} and the number of cycles N and the corresponding values of $k_{fat,\infty}$ as presented in EC5: Part 2: 1997</i>	374

A.1.	Strain results obtained from samples made with uniaxial glass fibre	404
A.2.	Strain results obtained from samples made with biaxial glass fibre	405
B.1.	Results obtained from the static bending tests.....	406
B.2.	Results obtained from the tension parallel to the grain tests.....	407
B.3.	Results obtained from the tension perpendicular to the grain tests.....	408
B.4.	Results obtained from the shear parallel to the grain tests	409
D.1.	Materials properties for TPU00 – 2D models	412
D.2.	Materials properties for TPB00 – 2D models.....	412
D.3.	Nodes coordinates for TPU/B00 – 2D models.....	412
D.4.	Materials properties for TPU00 – 3D models	414
D.5.	Materials properties for TPB00 – 3D models.....	414
D.6.	Nodes coordinates for TPU/B00 – 3D models.....	414
D.7.	Materials properties for TNU90 – 3D models.....	416
D.8.	Materials properties for TNB90 – 3D models	416
D.9.	Nodes coordinates for TNU/B90 – 3D models	416
D.10.	Materials properties for TNU60 – 3D models.....	418
D.11.	Materials properties for TNB60 – 3D models	418
D.12.	Nodes coordinates for TNU/B60 – 3D models	419
D.13.	Materials properties for TNU30 – 3D models.....	421
D.14.	Materials properties for TNB30 – 3D models	421
D.15.	Nodes coordinates for TNU/B30 – 3D models	422

CHAPTER 1

INTRODUCTION

1.1. Introduction

Timber is a material widely used in the construction industry. Because of the very low energy required to produce timber and its fully renewable capacity, the use of this naturally grown material is likely to become more and more significant, particularly with today's environmental issues.

In structural timber engineering, connections are often the weakest part of the structure, mainly because of the wood anisotropy and its non-linear mechanical behaviour. There are many different types of joint in timber structures and most of them are mechanically fastened. The use of plates, dowels (as shown in figure 1.1) or bolts normally induces a reduction of the member's cross-section in the jointed area. Therefore larger timber sections are necessary to satisfy the member as well as the joint designs. In other words, the strength capacity of the timber is not fully exploited with mechanically fastened joints.

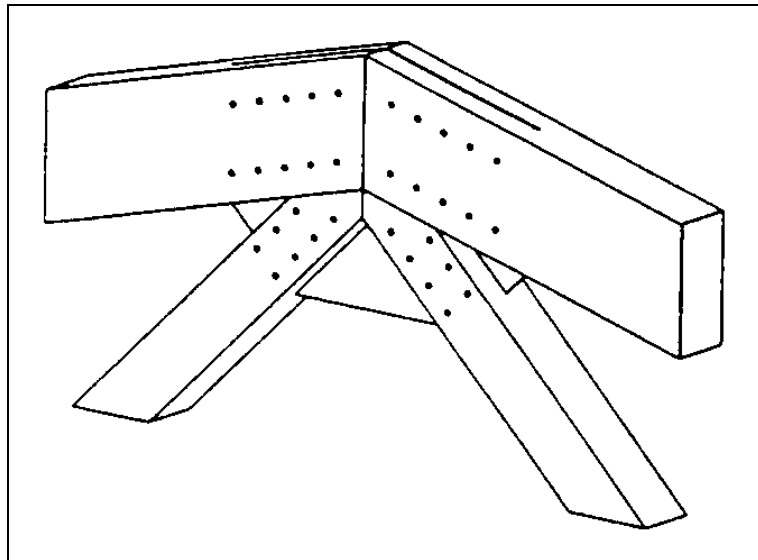


Figure 1.1 Typical timber truss internal joint with dowels (Dayer, 1994).

Many different alternatives have been proposed to reinforce the timber in the jointed area, for example by timber densification (with hardwood) or reinforcement with external steel plates, which are not particularly aesthetic.

The objectives of this research project are the development of a new kind of adhesive joint made of glass fibre strips bonded with epoxy resin on the timber as shown on figure 1.2, the analysis and understanding of its mechanical behaviour in axial tension. This joint uses a gap-filling adhesive, which means the resin does not require high pressure to acquire its full efficiency.

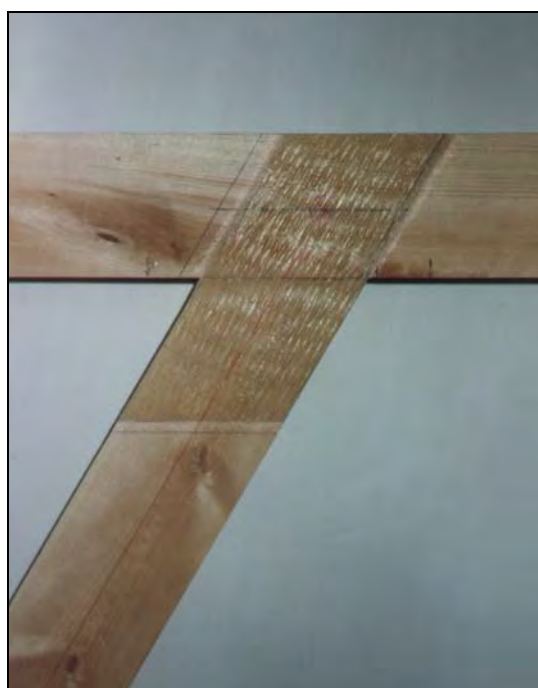


Figure 1.2 Typical wood/glass/epoxy sample with 60° angle configuration.

One of the most common mechanical fasteners for timber structures is the punched metal plate or nail plate, which is used to connect two or more pieces of timber of the same thickness in the same plane. Punched metal plate fasteners are widely used in timber trussed rafters. In this research, the wood/glass/epoxy joint is continuously referred to the punched metal plate fastener because they both show similar configurations:

- Member cross-sections are not reduced in the jointing area of both systems.
- They both display symmetrical arrangement of glass/epoxy bonding or nail plate punching on two opposite sides of timber members.

The comparison of wood/glass/epoxy joint with punched metal plate fasteners was initially planned and then abandoned because of the many different parameters that affect the strength of punched metal plate fasteners: Steel grade, gauge thickness, geometry, tooth shape and length, teeth distribution across the plate, etc.

The research on wood/glass/epoxy adhesive joints for construction applications is relatively new as there are very few references available on this topic. However these composite materials have been used for many years in the boat building industry with success to build entire yachts or structural elements (hull, deck, mast...). The outstanding mechanical properties of wood/glass/epoxy composites for a relatively low cost have developed the use of these composites.

A test programme for wood/glass/epoxy joints was then developed, based on standard tests for punched metal plate fasteners. The analysis of wood/glass/epoxy connections was only conducted on isolated joints.

Initially, tension tests of joints having the load parallel to the wood grain direction (i.e. straight configuration) were carried out. It appeared that there were many parameters that could affect the strength and stiffness of those joints. Restrictions were made on joint sizes and the materials used. Tension tests of joints having different load to grain direction (i.e. angle configurations) were carried out. Joints with the load applied at 90°, 60° and 30° to the grain were then tested in tension.

Finite Element techniques were used to model the joints in order to understand the theoretical behaviour of those joints, to be able to predict their strengths and stiffness. Results derived from finite element models and experimental sample tests were then compared.

Finally the fatigue resistance of wood/glass/epoxy joints with straight configuration was assessed in tension cyclic loading. The fatigue tests were carried out at a frequency corresponding to the action of the wind uplift on a typical roof structure.

A summary of the thesis is given in the next section to help the reader.

1.2. Reader's guide

- The review of all literature used for the development of this research is presented in chapter 2. References on the materials, on the theoretical approach of composite joints and on the fatigue resistance of materials are described.
- The characteristics and properties of the materials that compose the wood/glass/epoxy joints are presented in chapter 3. Wood, glass fibre and epoxy resin are described as materials in general terms as well as the specific products that were used in this research.
- The complete experimental programme is presented in chapter 4. From the development to the joint fabrication, all wood/glass/epoxy joint configurations that were tested in static tension are described.
- The results obtained from the experimental programme are presented and analysed in chapter 5.
- The theoretical and finite element analyses are presented in chapter 6. A theoretical approach to structural mechanics of the wood/glass/epoxy joints is given. Then the development and the results of finite element models are described and analysed, for each joint configuration that was previously tested.
- A preliminary investigation of the fatigue resistance of wood/glass/epoxy joints is presented in chapter 7.
- The conclusion and recommendations for future work are presented in chapter 8.
- Finally the references are listed, the results of strain gauges obtained experimentally are given in appendix A and the full results of small clear sample tests are given in appendix B.

Note: All the research work contained in this PhD thesis was carried out between November 1997 and December 2001 and refers to codes of practice that were current standards at the time. Nowadays some of them may be superseded, such as the BS 5268: Pt2: 1996, which is now replaced by the BS 5268: Pt2: 2002.

CHAPTER 2

LITERATURE REVIEW

2.1. Introduction

Research in composite materials has been developed for many years in a wide range of engineering fields. It started in the late 1930s, Dorman (1969) cites Dr. Pierre Castan who first synthesised epoxy resins in 1936. According to Adams et al. (1997), the first design theory of composite adhesive joint appeared with the Volkersen's analysis in 1938 of single lap joint. At this time, words like adherends and structural adhesive were first used. Then development of adhesive defined as a polymeric material was on its way:

“In 1938, an American company called Owens-Corning Fiberglas Corporation first produced and sold glass fibre and glass fibre products” (Mettes, 1969).

“In 1948, the first commercial epoxy resins became available in United States” (Dorman, 1969).

“Composites materials such as glass fibre and epoxy resins have many attractive properties such as high mechanical properties, light weight, good thermal properties, moisture, corrosion and chemical resistance. Glass fibres have relatively low cost, excellent electrical characteristics and behave perfectly elastically” (Mettes, 1969).

“Epoxy resins exhibit outstanding characteristics compared to other resins: They have a wide range of forms (resins, hardeners and modifiers), curing conditions (rapidly or slowly at almost any temperature between 5 and 180°C), low shrinkage, good toughness and strong adhesive bond” (Dorman, 1969).

Consequently these advantages of using composites, especially glass/resin combination, have developed their applications in military, transportation, construction, aircraft, aerospace, marine, electrical and goods industries.

“Research has been undertaken to develop other composite materials such as carbon fibre, graphite, boron, Aramid (Kevlar), titanium...and other adhesives like polyurethane, phenolic, polyamide or polycarbonate adhesive” (Mallick, 1997).

During the last 40 years, glass fibre/epoxy has been widely used in ship and boat building, mainly for hulls and masts. Bonding glass fibre/epoxy on a wood hull makes the structure much stronger, protects the wood from salt corrosion and water penetration and consequently reduces the maintenance of the boat.

Structural wood/glass/epoxy joints have been used on boats but no records of design methods or research exist in this field. In other words, there is no background research on structural wood/glass/epoxy joints except from Claisse and Davis (1998), who have seen in this adhesive joint a potential for use in the construction industry. They tested different configurations but irregular results were recorded. They found that wood/glass/epoxy joints are highly rigid and have good mechanical characteristics.

It was essential to review all research in which the three materials wood glass fibre and epoxy have been involved, even if it did not concern directly this particular jointing system. Such review lead to a better understanding of those materials and their properties and helped to establish a reliable research process. Further review was required about other comparable jointing system for timber structures, such as punched metal plate fasteners in order to draw an acceptable performance comparison.

Because of the lack of background for this research, the review of papers was concentrated in different engineering fields:

- The construction environment, about the structural use of wood, glass fibre and epoxy resin materials, the punched metal plate fasteners in timber trusses and other related subjects.
- The mechanical environment (aircraft, aerospace...) for the use of structural adhesive composite joints.

Finally, the review of papers and literature dealing with the fatigue of timber structures and adhesive joints is presented at the end of this chapter, as the fatigue resistance of wood/glass/epoxy joints was also assessed in this research project.

2.2. Construction environment

The use of epoxy resins in the construction industry has been mainly limited to structural applications (load bearing supports for bridge structures, repair and resurfacing of highways, roads and timber structures...) and decorative and efficient structures (epoxy floors, epoxy-aggregate walls...). On the other hand, glass fibre and GRP (Glass Reinforced Plastic) have been used in thermal applications (glass wool, insulation components...) and construction elements (panels, roofing, structural shapes, concrete pouring forms...).

Nowadays, the cost of epoxy is relatively low compared to 30 years ago because of its universal use. For the last ten years, glass-epoxy has been used more and more in other applications such as coating concrete structures in order to protect the concrete surface and to increase its strength and durability.

The use of composite materials to reinforce structural wood members is reviewed in the following section. This review is concentrated on the use of glass fibre and epoxy resin.

2.2.1. Structural member applications

Using glass fibre to reinforce wood materials began in the early 1960s with Wangaard (1964) and Biblis (1965). They analysed wood-glass fibre composite beams in elastic deflection but also in the plastic region for Biblis (1965). Both reinforced various species of wood by applying unidirectional glass fibre strands impregnated with epoxy resin to the top and bottom surface. Their studies were examining analysis techniques when core specific gravity varied from 0.08 to 1.14, using different assumptions such as neglecting or taking into consideration the shear strain, which acts in the core and contributes to the deflection. The analysis techniques gave reasonably accurate results.

Theakston (1965) first examined reinforcing laminated timber beams with glass fibre. He considered both a water base adhesive and an epoxy resin. The water base adhesive was rejected because of poor performance. He used different types of glass fibre such as roving mats, woven roving mats, cloth mats, and chopped strand mats. Unidirectional non-woven roving mats were found the most suitable. Strength and stiffness improvements were reported when the member was wrapped in the glass fibre/epoxy composite or when the composite was placed between horizontal laminations.

Further studies were developed for laminated timber using different kind of adhesive (polyester, vinyl-ester, phenol-resorcinol resins...) as described in the excellent review from Bulleit (1984). He also mentioned research for wood/glass fibre composites in other applications:

- Glass Fibre Reinforced Plastics (GFRP) were used to reinforce wood transmission poles in the early 1970s. Plywood was overlaid with glass fibre (in-depth series of tests performed by the American Plywood Association in 1972 and 1973). This reinforced board was used in the transportation industry and was extensively used in cargo shipping containers, railroad cars and vans.
- An extensive study was performed in Germany using solid wood, plywood and particleboard in 1974-1976. GFRP incorporating a polyester resin was bonded to the surfaces of the core material in a wet process. A considerable improvement in

the strength and the stiffness properties was obtained and a significant reduction in creep was reported.

A method and a prototype machine were developed by Saucier and Holman (1975) to produce structural members such as 2 by 4 inch beams made from wood particles on a continuous-belt press with special provision for incorporating continuous glass strands of high tensile strength into the structure, parallel to its length. The strands were prestressed and coated with resin. It produced poor boards when urea-melamine resin was used and slightly higher quality boards when a phenolic resin was used. No further works have followed this attempt.

Spaun (1981) undertook a study using glass fibre with phenol-resorcinol formaldehyde resin to increase the tension and bending strength of impression finger joints. Composite members were made of a core wood material (finger joint) with veneers on each side and glass fibre layers sandwiched between veneer and core. The strengths were increased from 10 to 40% over unreinforced joints, using only a glass fibre reinforcement level of 3.5% and 7% by volume. Spaun noticed that a maximum of 80% of the glass fibre strength capacity was effective in these tests.

The use of fibre reinforcement for laminated veneer lumber was evaluated by Laufenberg et al. (1984). They assessed the economic feasibility of that kind of products with different type of fibres (E-glass, S-glass, carbon and graphite). Axial, bending and concentrated stress tests were undertaken. The study revealed that the cost of E-glass reinforcement with phenol-formaldehyde resin was the cheapest for the range of strength properties obtained.

The technical feasibility of producing internally reinforced laminated beams was evaluated experimentally in a large programme performed by Rowlands et al. (1986). Ten adhesives (three epoxy resins, two resorcinol formaldehydes, two phenol resorcinol formaldehydes, two isocyanates and one phenol formaldehyde) and numerous types of fibre reinforcements (unidirectional and cross-woven glass, graphite and Kevlar) were evaluated. Reinforced laminates were tested in tension and three-point bending, with and without finger joints. They concluded that fibre reinforcements could be very advantageous in regions of stress concentration (bolted

joints, etc). Glass reinforcement was technically and economically superior for wood structures. Under normal dry conditions, epoxies exhibited superb performance with all fibre materials tested. Glass fibre reinforced Douglas fir (18% of glass by volume using epoxies) produced a 40% stiffness enhancement and doubled the strength over similar unreinforced wood.

Van de Kuilen (1991) developed a theory to predict the ultimate bending strength of laminated timber beams reinforced with glass fibre/polyester resin on the bottom face and both top and bottom faces. An experimental research program was undertaken by the TNO (Timber Research Institute - Holland) on glass fibre reinforced laminated beams. The research demonstrated that laying glass fibres in the glue lines has little effect on the stiffness of the beam. Bonding glass fibre with polyester resin on the top and bottom faces of the beam increased the stiffness by 17% having 4% of the initial height reinforced and by 55% having 16% of the initial height reinforced.

The bonding properties of the reinforcement are critical parameters in laminated timber beams. Gustafsson and Enquist (1993) produced a report, which assessed the adherence of reinforcement to wood in this matter. The experiments were concentrated on shear (tension) test with reinforcement bonded to the wood, perpendicular to the grain. They were using glass fibre/polyester and different softwood species. The failure always developed along the bond surface, and they concluded the bond strength was governed by the shear properties of the wood. The study is supported with a substantial theoretical shear analysis.

Another way of strengthening laminated timber was performed by Sonti and GangaRao (1995) with the use of composite wraps. Two materials were used: glass and carbon fibre. The composites were wrapped all around the laminated beams with an epoxy-based resin, and tested in bending to failure. Low increments in stiffness and high increments in strength were reported. Experimentally, the use of carbon fibre did not show a very large improvement of mechanical properties compare to the glass fibre (5% in stiffness and 15% in strength).

Alternatively Dorey and Cheng (1996) examined the potential for glass fibre reinforcement for laminated timber beams using the same adhesive phenolic resorcinol formaldehyde. The laminated beam was tested in four-point bending with the glass fibre bonded on its bottom side. They showed that the fibre fraction plays a major role in the mechanical capacity of the reinforced member. A range of fibre fractions was studied to determine the optimum percentage. The maximum strength and stiffness improvements of 127% and 104% respectively, were achieved by using a fibre fraction of 8.23%.

The use of composite fabrics to reinforce wood crossties was developed by GangaRao et al. (1996). They investigated the feasibility of hand wrapping for GFRC (Glass Fibre Reinforced Composites)/wood crosstie and experimentally evaluated their mechanical behaviour. Northern red oak wood and unidirectional E-glass/epoxy reinforcement were used. Results of the experimental tests indicated that only one layer of reinforcement provided noticeable enhancement to both strength and stiffness. Average increase in stiffness of 15 to 41% and strength of 14 to 31% were achieved.

The same year, the same team Sonti et al. (1996) produced a paper about accelerated ageing of wood-composites members. Using red oak wood as a core and two types of composite fabrics (glass and carbon) as external reinforcements, they undertook series of shear strength tests. Several adhesives for bonding were used. The results showed that phenolic-based resins had higher retention of shear strength after being subjected to ageing conditions. The ageing process was composed of six cycles of swelling and shrinkage effects. The best combinations were wood/glass/epoxy and wood/carbon/epoxy, which retained nearly 50% of their shear strength capacity after the ageing process.

The performance of fibre reinforced polymer composites used with wood was reviewed by Hota and GangaRao (1997). Strength, stiffness and accelerated ageing response of sawn and laminated wood beams wrapped with glass composites and bonded in place with polymeric resins were reported. They concluded that hybrid wood components exhibit increases in strength and stiffness of up to 40 and 70% respectively, over non-wrapped wood beams for a constant volume percent of fabric.

These mechanical properties could be increased further with the addition of more layers of fabric.

Finally these papers are reviewing different applications for reinforcing wood members, considering diverse material characteristics such as strength, stiffness, ageing (long term durability) and creep...

A preference appears frequently in these papers for E-glass fibre rather than carbon fibre or any other fibrous materials, because of a fairly cheap cost related to the strength properties obtained. Similarly the epoxy resin is often used with fibrous materials because of its high strength properties, chemical and water resistance, and high bonding interaction, either through the composite matrix or with wood (and wood-based) materials. Using epoxy resin is preferred when the bond strength is a major criterion. On the other hand, its use is limited by a relatively high cost, compared with other common wood adhesives, such as the phenol resorcinol formaldehyde resin.

Composite materials were also used in different ways to fabricate or reinforce structural joints in wood structures. The papers about this research area are reviewed in the following section.

2.2.2. Structural joint applications

Because of its outstanding properties and particularly its high bonding strength with wood, epoxy resin has been considered for the repair of timber structures. Avent et al. (1978, 1984, 1985 and 1986) undertook a large research programme on epoxy-repaired timber structures. The five following papers are some of the most relevant of this programme and raise different aspects of epoxy repair capabilities.

Using pressure injected epoxy to restore deteriorated timber structures, Avent et al. (1978) analysed the behaviour of epoxy-repaired full-scale timber trusses. They conducted an experimental study to determine the effectiveness of this repair method. They tested two types of trusses: Fink trusses (triangular truss with inclined internal members) and Pratt trusses (rectangular truss with inclined internal members). Some of them were made with new timber, and the epoxy repair method was applied to bolted and damaged joints. The method restored strength to a level approximately equal to the original. The results showed that the epoxy repair method was very effective: Not a single repaired joint failed during the load tests. Other tests were carried out on 30 years old timber trusses. To increase the wood deterioration, these trusses were stored outside and exposed to weather for a two years period. Bolted and split ring connections were badly rotted and damaged. The epoxy repair method was less successful and marginal at best. They acknowledged the difficulty to assess joint damage, identified the poor bonding of epoxy on highly rotted material and concluded of the high effectiveness of the epoxy repair process.

Six years later, Avent et al. (1984) investigated the fire resistance of epoxy-repaired timber. The structural efficiency and economical consideration have brought the epoxy repair for timber structure as a reliable technique of restoration. In this investigation, they conducted an experimental and theoretical programme. They determined the wood/epoxy bond strength on small shear block specimens over a wide range of temperatures, and the time required for full sized epoxy-repaired joints to fail when subjected to a sudden elevated temperature. They developed a mathematical model, which predicts with approximate accuracy the strength and duration of load for joints exposed to a sudden high heat condition. By comparison with the experiments, a 30 minutes fire rating was obtained for the glue line at

3 in. (76mm) from the heated surface and 60 minutes rating was obtained with a glue line at 4 in. (102mm) from the surface. Further investigations were required because this was one of the first studies on fire resistance for epoxy repair timber. They concluded that members with interior glue lines will not fail immediately and higher fire ratings could be predicted.

Avent (1985) conducted an experimental investigation to evaluate the effects of weathering and decay on the epoxy repair of timber. Unprotected epoxy repaired joints were exposed to natural weathering in the southern United States. Joints were periodically loaded over a 4½ years period and correlated to accelerated weathering tests on small epoxy bonded shear block samples. The strength of the repaired joints compared well with that of undamaged material. However the author concluded with the three following recommendations:

- The dry condition design shear strength of epoxy-repaired Southern pine should be reduced by 33% when the repaired member is exposed to natural weathering typical of the southern U.S.
- Preservative treatments that prevent wood decay are required on exposed timber if the expected repair life is longer than just a few years.
- Normal precautions for protecting wood will serve well in protecting epoxy-repaired timber.

One year later, Avent (1986) published a paper about an investigation into the factors affecting the strength of epoxy-repaired timber structures. He evaluated two aspects: The repair methodology and the effects of member configuration. The methodology consisted of four steps: special member preparation, joint sealing, epoxy injection and finishing. Each of these steps is described in detail with recommended procedures. To evaluate the various joint configuration parameters affecting the behaviour of epoxy-repaired timber, 200 full sized repaired members and 100 shear blocks of Southern pine were tested. The effects of mechanical connectors, length of overlap, member thickness, grain orientation, timber age and glue line thickness were considered. The author concluded that the shear bond strength was of the order of the shear strength of the wood, and the primary factors affecting strength were the ratio of lap length to member thickness and grain orientation.

Finally Avent (1986) presented a study into the design criteria for epoxy repair of timber structures. Based on theoretical and experimental studies (cited in the report), the author exposed a methodology for computing both actual and allowable glue line shear stresses. He assumed the actual glue line as an average shear stress. He established some formulae to work out the allowable shear stress. These formulae are functions of the wood species, grain orientation, allowable wood shear stress and lap length to member thickness ratio. Several epoxy formulations were considered and method for evaluating other epoxies is presented. The predicted values obtained through those formulae matched approximately the experimental results.

In this large research programme sponsored by the United States Air Force Directorate of Civil Engineering, Avent et al. brought forward a new era of jointing structures. At this stage, they thought of using bonded joints for timber repair and investigated most of the parameters, which rule the design of that kind of joint.

Using glued joints in timber structures requires a substantial analysis involving many parameters to ensure the reliability of the connection. For example, design rules for steel joints are not applicable because of different materials characteristics and a fairly complex stress combination in glued timber joints. Glos and Horstmann (1991) assessed the requirements for the design of glued joints in timber structures. In order to produce a design proposal for glued joints in timber trusses, they tested over 500 full size samples and analysed the stress distribution using the finite element modelling. They assessed the effects of joint geometry, glued area geometry and grain orientation. Their design proposal presented is very similar to the one from Avent (1986), using a wide range of safety factors.

Alternatively in the following sections, the authors thought of using composites and not as adhesive joints but as mechanically fastened joints for timber structures.

Dmitriev et al. (1991) investigated the potential of non-metallic fastening units made of high strength plastics and GFRP. The authors presented experimental research on full-size trusses under short-term and long-term loading. The fastening pieces as well as bolts, pegs, nails or straps were made in glass fibre, produced with a hot moulding process. They tested different truss configurations, detailing each jointing system.

Entirely made without metal, the connections had similar configurations to the usual ones in metal, but bolts were replaced by GFRP dowels or pegs glued in the wood. The results were satisfactory, but the cost of the final trusses was relatively high. The authors suggested this jointing system as an alternative method of producing wood trusses if corrosion resistance, non-magnetism and radio interference are key criteria for the structure.

Composite materials can also be used as a wood reinforcement for mechanically fastened joints. Haller et al. (1996) developed joints for timber truss structures. They presented a study on glass fibre reinforced and densified timber joints. In other words, connections were reinforced either by bonding glass fibre fabrics with epoxy resin on the wood members, or by removing layers of wood in the timber section on both opposite bearing sides, then bonding glass fibre fabrics in between. The densification was achieved by thermo-mechanical compression of the wood (160°C and 10 MPa of pressure). The two alternatives showed remarkable enhancement in load bearing capacity and deformation. Ultimate strength and deformation capacity were doubled. These results were obtained from tests on bottom chord joint having two bracing members. The mechanical joints were made of steel plates and dowels.

Beyond the high strength capacity obtained with glass fibre reinforcement, the embedded strength was also improved. This is an important parameter when steel fasteners are used for the connection especially when the loading acts perpendicular to the grain. Chen (1996) proposed to reinforce laterally assembled timber elements with glass fibre fabrics and epoxy resin. The premature failure was therefore avoided due to the lateral reinforcement: The member strength and stiffness was enhanced, and it prevented the splitting of timber: For example, a bolted joint tested in tension or compression parallel to the grain showed a significant ductility when the wood was reinforced with glass fibres.

Finally Claisse and Davis (1998) performed a comparison of high performance jointing systems for timber. Four different jointing systems were tested and one of them was made of uniaxial glass fibre and epoxy. Tests in tension for butt and scarf joints with varying bonded length were undertaken. The results showed that

wood/glass/epoxy joints offered some of the best performance: High stiffness and strength. However very small joint slips were recorded at failure (< 1.5 mm), which seemed to reflect a brittle failure mechanism. Therefore the authors concluded that wood/glass/epoxy joints have great potential that could be limited to some applications.

The purpose of this research in wood/glass/epoxy joints is in the continuity of Claisse and Davis's work.

Some of the research achieved on nail plate connectors, which are probably the most comparable timber jointing system with wood/glass/epoxy joints, are reviewed in the following section.

2.2.3. Nail plate connections

Nail plates have been investigated for the last 50 years in Europe as well as North America. Intensive research has been carried out in this area for several reasons: The use of nail plates is probably the cheapest way to connect timber pieces. It is relatively easy to manufacture with just one material involved and one component, the steel plate.

The first nail plates were made of a steel plate perforated with a grillage of holes. Nails were used to connect the plate to the timber. Nowadays the nails are part of the steel plate: the plate is cut in order to give the shape of the nails, which are bent afterwards to become the teeth. The manufacturing process remains simple, but the truss fabrication is made easier and quicker. The nail plate is punched into the timber pieces using a hydraulic press. That is why the nail plate is also called the punched metal plate. However the plate dimensions, the properties of the steel used, the number, the spacing, the dimensions and the shape of the teeth are some of many parameters which affect the strength of this connection system. Such variations justify the research achieved around the nail plate, particularly to produce reliable and general design methods.

Nowadays punched metal plate fasteners are widely used and mainly for timber trussed rafters. Most timber truss manufacturers use their own design procedures and products, and the design methods given by the codes are used as guidance rather than standard design procedures.

The following papers are representative of this research and contribute to the comparison with wood/glass/epoxy joint, which will be carried out further on in this thesis.

Destructive testing of punched metal plate connectors in wood truss joints were undertaken by Gupta and Gebremedhin (1990) to demonstrate the partially rigid behaviour of this joint type. Tension splice joints, heel joints and web at bottom chord joints were tested (50 samples per joint configuration). Joints were fabricated from the same softwood (Southern Pine) in 2 by 4 inch using the same metal plate characteristics but different sizes. Joints were tested in a steel frame designed to apply in-plane loads in order to simulate the loads carried by truss members. Average

strengths (and stiffnesses) under axial force for tension splice, heel and web at bottom chord joints were recorded as 27.0 kN (and 52.8 kN/mm), 22.7 kN (and 41.2 kN/mm) and 16.7 kN (and 3.8 kN/mm), respectively. Ductile failure for heel joints and brittle failure for tension splice and web at bottom chord joints were recorded as well as the fact that joint failure was mainly due to a combination of wood and teeth failure. However such uniform failure behaviour was achieved because all joints tested had a configuration used in the design of an 8.5 m span Fink truss with 5/12 roof slope. Note that all the joints were fabricated by commercial truss manufacturers.

The same year, Cramer et al. (1990) published a paper about theoretical consideration of metal-plate connected wood-splice joints in tensile and bending analysis. A typical splice joint connected with metal-plate fasteners was presented as a finite element model. A non-linear plane stress finite element formulation was used for this model to allow computation of internal deformations, stress conditions and ultimate strength. Different stiffnesses for the wood in the contact area, the steel plate and the tooth-wood interface were considered in the analysis. The model showed a strong plate-size effect in the lateral load resistance (based on strength per tooth). This research showed that current design assumptions represent realistic approximations of behaviour for small plate connections, but unrealistic ones for connectors with larger plates. Therefore this research confirmed that refinement was required in the design procedure of long span trusses containing large metal-plate connectors. Unfortunately the research only included a comparison with experimental results from references.

Gebremedhin and Crovella (1991) investigated the load distribution in metal-plate connectors of tension joints in wood trusses. By testing tension splice joints they showed the non-uniformity of load distribution along the plate member, using different plate type. The samples were made with 4 different plate types on 2 by 4 inch Southern Yellow Pine wood. The row of teeth next to the centreline was found to transfer the highest load (or to be the most highly stressed). One plate type, which had uniform tooth layout, was modified to achieve better stress distribution, by reducing gradually the number of teeth from the end to the plate centreline. The same plate type was also studied to examine the effect of tooth damage on load

redistribution. By removing 3 teeth in one row, and varying the row at each test, no substantial load redistribution was observed. Tension joints stiffnesses varying from 70.2 kN/mm to 93.5 kN/mm for a failure load from 20.7 kN to 31.7 kN were recorded for each joint configuration.

Groom and Polensek (1992) developed a theoretical model for predicting mechanisms of load transfer between a wood member and a metal-punched truss plate. The model treated a plate tooth as a beam on an inelastic foundation of wood, which predicted the load-displacement trace and the ultimate load of joints. It took into account the inelastic behaviour of the tooth due to the wood embedment (variation of bearing pressure along the tooth length) and the changing moment of inertia along the tooth length. The model was verified with the testing of 8 truss-plate joint types, 3 with variable number of teeth and 5 with different plates and wood grain angles. Theoretical and experimental load/displacement graphs showed good agreement. The theoretical model accurately predicted the ultimate load and failure modes of joints (tooth withdrawal or plate tensile failure for straight pullout joints, side grain failure perpendicular to the grain for square pullout joints).

These papers show some of the research on metal-plate connectors and also the new approach of metal plate design, which seems to be needed by the truss manufacturing industry. The non-uniformity of load transfer in the metal plate, the partially-rigid behaviour as well as the fact that tension test is the most relevant test to establish the joint strength and stiffness, are important criteria which are taken into account in this research about wood/glass/epoxy joints. Also the experimental programme was inspired by some of the procedures presented here.

The research in mechanical engineering on composite jointing is also a fundamental reference for the research in wood/glass/epoxy joints. Some of the most relevant papers are presented in the following section.

2.3. Mechanical Environment

The use of glass fibre and epoxy resin has been highly developed in engineering for 40 years in so many different applications that it would be irrelevant to summarise them here. In the automotive, boats, aircraft, aerospace and others industries, glass fibre and epoxy resin have been used as materials for a wide range of parts and components because of outstanding properties (as listed before). However, these composite materials have been used for jointing elements of different materials, with capacity to transfer significant loads and stresses. The review is therefore concentrated on this particular field of mechanical engineering, which deals with structural adhesive joints, because of the similarities with the present research.

The five following papers show a part of the research in composite joints achieved in the past 10-20 years. Since the late 1970s with the development of computer, the use of finite element methods have solved many theoretical problems too complex to be dealt with classical analysis, such as anisotropic and non-linear behaviour of composite.

In the early 1980s, Matthews et al. (1982) published an excellent review of the strength of joints in fibre-reinforced plastics. Most of the published work, mainly theoretical and relating to all aspects of adhesively bonded joints in composite material is presented. Classical analytical and finite element methods applied to metals and composites, adhesive properties and joint design procedures are reviewed considering both linear and non-linear analyses. This paper also refers to books, which are the foundation of the theoretical principles raised in this report. Most of the papers listed in this review are linked to the research in the aeronautic industry.

The same year, Marloff (1982) published a paper about finite element analysis of biaxial stress test specimen for graphite/epoxy and glass fabric/epoxy composite. A diametrically loaded circular specimen was proposed to test composite materials under biaxial stress. Using finite element analysis, a model of the specimen was developed with isoparametric mesh, refined step by step in the highly stressed areas to obtain an optimum shape for the specimen. Using elastic behaviour only, linear analysis but considering the material orthotropy, the model gave accurate results

compared to the experimental results obtained from strain gauges fixed on the test specimen. But the finite element procedure developed in this research is the most relevant point, with its meshing assumptions, choice of element and theoretical background. Nevertheless the failure mode could not be accurately predicted because non-linear behaviour of the composite was ignored.

Failure prediction of composite was overcome two years later by Harris and Adams (1984) who published a paper about strength prediction of bonded single lap joints by non-linear finite element methods. Single lap joints made of four aluminium alloys and four epoxy adhesives were tested and the results obtained compared with finite element models. The program used for the finite element analysis was able to take into account the large displacement rotations that occurred in single lap joint and allowed the effects of elasto-plasticity in both the adhesive and the adherends to be modelled. Therefore a realistic stress-strain curve of composite was obtained. A failure criterion based on the uniaxial tensile properties of the adhesive was used (modified Von Mises failure criterion) to achieve accurate failure prediction.

The two following papers were published by the same Authors, Gilibert et al. (1988) and are related to the mechanical behaviour assessment of the double lap joint using epoxy adhesive on steel or aluminium adherends. Taking into account the non-linear behaviour of the bond (i.e. non-uniform load transfer distribution), specimens were tested in axial tension while strain gauges positioned at different locations on the outer face of adherends recorded the strain distribution. Finite element method was not used in these papers but classical analytic method. According to the authors, the non-linear behaviour maybe due to the opening of micro-cracks at overlap ends.

In the second paper, different joint configuration (thinner joint) was tested. Also a different method of analysis was used. Reasonable accuracy was obtained between experiment and theory in both papers. However the theoretical analysis was developed using assumptions on parameters such as the strain distribution through the thickness of the adhesive, which could not be evaluated.

These papers are some examples of the wide research developed in the last 50 years on composite adhesive joints in different fields of engineering. Most methods developed were based on principles of mechanics of materials as shown in those papers.

References to several books of mechanics of composite were also made for the theoretical analyses that are presented throughout this thesis to describe the mechanical behaviour of wood/glass/epoxy joints.

The research papers and literature dealing specifically with the fatigue of timber structure and composite joints is presented in the following section.

2.4. Review on fatigue

The behaviour of the wood/glass/epoxy joint under fatigue was carried out as part of this project and is presented in Chapter 7. The performance of the joints was assessed in cyclic loading to establish their fatigue resistance.

The papers reviewed in this section were used to identify and understand the fatigue behaviour of the timber material and composites materials. Furthermore books were selected because of their excellent review of the research carried out on fatigue. These books and papers are used as references in the literature review presented in chapter 7. Some of the books are presented below.

In his assessment of timber's nature and behaviour, Dinwoodie (2000) defines fatigue and the theory around it, which is used to evaluate the timber's fatigue resistance. The author refers to several papers of recent work carried out to assess the fatigue life of timber materials. The conclusions from these investigations can be summarised as follow:

- Fatigue resistance is dependent on the timber species, but reduces with increasing moisture content.
- Fatigue resistance is considerably higher for axially loaded timber in tension than in compression.

The author investigates the modelling and failure criteria in fatigue, referring to other work carried out to evaluate fatigue: The use of alternative S-N curves, models based on elastic and visco-elastic work, etc are presented.

Ansell (in Timber Engineering STEP1, 1995) assesses the fatigue design for timber and wood based material and describes the life prediction techniques. The author relates the fatigue to the crack propagation (fracture mechanics) first and then introduced the S-N curves and R ratios. He refers to some of his substantial research work, and explains the constant life-lines and life prediction techniques in details.

In a book dealing with composite materials, Chawla (1998) investigates how fatigue affects composite materials. The author introduces the S-N curves, the fatigue crack propagation. He describes the fatigue behaviour of various composite materials, such

as ceramic matrix composites, particles composites and hybrids. He exposes theories of damage mechanics of fatigue, fatigue due to thermal effects and creep.

Other books are referred to in chapter 7. They are not presented in this review because of the minor references made to them.

In addition to those books, research papers were used as part of this project to understand the experimental procedures of fatigue tests. These papers are dealing with fatigue of timber, glass fibre and epoxy, as single materials or composites, as well as with fatigue of bonded-in rods in timber connections and punched metal plate fasteners. They are reviewed as follow:

By testing different species of timber (Sitka spruce, laminated Khaya and beech) under load control in four-point bending and at five different R ratios and three different moisture contents, Tsai and Ansell (1990) found that fatigue lives were independent from the species and were reducing with increasing moisture content. They have showed that the most severe mode of cyclic loading for wood material is the fully reverse loading ($R = -1$). As for the mechanical properties, the moisture content seems to be an outstanding parameter that affects the fatigue life of wood. They also found that the fatigue damage accumulation at cellular level was associated with the formation of kinks in the cell walls, compression creases and cracks in the wood.

As part of a research program for the needs of the wind turbine blade industry in the UK, Bonfield and Ansell (1991) explored the fatigue in constant amplitude tests in axial tension, compression and shear for both Douglas fir and Khaya using various R ratios. They found and confirmed that fatigue lives measured in all-tension loading are significantly longer than those in all-compression tests. The fatigue resistance of Khaya appeared to be significantly higher in all compression than in reverse modes. Finally the laminated Khaya was tested in shear in all-tension tests ($R = 0.1$). The fatigue resistance in shear was measured along two shear plane orientations: The shear fatigue resistance of Khaya was found to be significantly higher along the Tangential/Longitudinal plane than the Radial/Longitudinal plane.

Hacker and Ansell (2001) have investigated property changes and fatigue damage accumulation of wood-epoxy laminates under constant amplitude fatigue tests in tension-tension ($R = 0.1$), compression-compression ($R = 10$) and reverse loading ($R = -1$). They also found that the reverse loading is the most severe mode of cyclic loading. The wood appeared to be more tolerant in compression-compression than in tension-tension. Maximum and minimum fatigue strains were monitored during the fatigue tests. In tension-tension ($R = 0.1$), the strains remained constant through the test, but they increase significantly close to failure. The sudden increases of strains were found to correspond to the initiation and growth of fatigue cracks along the wood grain, as each crack initiation causes a small step in strain.

Spera et al. (1990) investigated the laminated Douglas fir/epoxy as materials of choice for wind turbine blades. They characterised the fatigue properties of Douglas fir/epoxy joints. They tested scarf and butt joints in tension-tension at $R = 0.1$ with respect of grades and joint sizes. It appeared that the veneer grades do not govern the joint fatigue resistance: For the butt joints, the grade A veneer outperformed the grade A+ veneer, which is a higher quality grade. A further effect that the increased surface area of the scarf joints did not translate into an increase in strength and fatigue resistance. This could be due the fact that larger bonded areas contain more voids and therefore the bond was significantly degraded.

Sutherland (1999) presented in his report a large research program about the applications of glass fibres to built wind turbine blades that was undertaken in the early 1990s in United States. This program aimed at the development of a glass fibre composite database for wind turbine applications. The DOE/MSU database for E-glass composites contains over 4500 data points for 130 material systems tested. A high frequency database provides a significant data set for unidirectional composites to 10^8 cycles. The database explores material parameters such as reinforcement fabric architecture, fibre content, matrix materials and loading parameters (R values). The results derived from this database are widely presented in chapter 7.

Fatigue tests were carried out by Bainbridge et al. (2000) on bonded-in rods in glued laminated timber, using three different types of adhesives: Epoxy, polyurethane and phenol resorcinol formaldehyde. Mild and high strength steel threaded rods were axially loaded in tension parallel to the grain of the timber at a frequency of 1Hz. S-N curves are presented for an R ratio of 0.1. The authors investigate the relationship between experimental results and the design code basis, trying to establish fatigue coefficients by comparison of the results with existing data. Fatigue coefficients were not evaluated because of lack of high number of load cycles.

The punched metal plate fasteners were tested in fatigue loading by Karadelis and Brown (2000), on two types of fasteners (two different steel grades). The joints were tested in tension from 0.78 to 7.75 kN at a frequency of 1 to 2 Hz, corresponding to one-fifth of the failure tension load. The joints were tested up to 10^5 cycles and strains in the fasteners were recorded. Larger strains occurring in the centre of the fastener than at the edges were observed and joint slips reach a peak at 60000 cycles and then reduce.

The experimental data from those papers were used as comparison with the results obtained from the wood/glass/epoxy fatigue tests that are presented in chapter 7.

2.5. Summary

The research in wood/glass/epoxy joint seems to be a relatively new idea particularly in timber engineering. In the construction environment, glass fibre and epoxy are increasingly used in various applications. This recent development is probably due to a reduction in cost of those materials compared to 10-15 years ago. Nevertheless jointing timber with glass fibre and epoxy has been a common jointing system in the boat industry for many years. Nowadays, boats are entirely made with composite materials and timber is not used anymore to form the frame skeleton. Nevertheless the properties of those materials are well known and they have been used in other engineering fields. Using glass fibre and epoxy to reinforce timber members have been studied for a long time without being developed up to a design procedure. Again this is due to a high cost compared to the performance enhancement. However using glass fibre/epoxy as an alternative to nail plates is a way to optimise the strength and the quantity of timber used, while maintaining the cost relatively low. There are also further applications in which this research could be used, particularly in the repair of damaged timber structures, reinforcement of existing structures or reinforcement of mechanically fastening joints.

CHAPTER 3

MATERIALS, PROPERTIES AND CHARACTERISTICS

3.1. Introduction

The joint performance is dependent of the materials and their properties. These joints are fabricated with three different materials: timber, epoxy resin and glass fibre. The timber is the material to be connected therefore it is an adherend. The glass fibre is also an adherend and connects the timber pieces together in order to transfer the stresses from one piece to the other. The glass fibre can be called the connecting material. The epoxy resin is the adhesive, which ensures the “link” between the timber and the glass fibre. But the epoxy is much more than a simple adhesive. In fact the glass fibre and the epoxy can be seen as only one component: the glass fibre/epoxy composite. While the glass fibre is embedded in the resin, the properties of both materials combine together to create the composite, with the fibres being the principal load-carrying component. The matrix properties are enhanced in comparison to the properties of either material. In fact, the joint could be seen as composed of two materials: the timber and the glass fibre/epoxy composite, the epoxy having a double function as an adhesive between the timber and the composite and as part of the composite itself. It is therefore relevant to summarise the characteristic and properties for each of these materials and also for the glass fibre/epoxy composite.

3.2. Material properties

3.2.1. Timber

3.2.1.1. General

“Wood is a natural, organic cellular solid. It is a composite made out of a chemical complex of cellulose, hemicellulose, lignin and extractives. Wood is highly anisotropic due mainly to the elongated shapes of wood cells and oriented structure of the cell walls. In addition, anisotropy results from the differentiation of cell sizes throughout a growth season and in part from a preferred direction of certain cell types” (Hoffmeyer, in Timber Engineering STEP 1, 1995).

Without getting too deeply into the microstructure of wood material, it is important to identify the parameters that affect the properties of the wood.

Water is always present in wood and has a profound effect on almost all its properties. It changes the mass and volume of wood, which are linked to its strength and stiffness and therefore shrinkage and durability. The moisture content (based on oven dry weight of wood) varies considerably between species, and can vary from 30% to 200% in green wood. The density appears as the best single indicator of the properties of the wood: It is determined principally by two factors: the amount of wood substance present and the moisture content.

Shrinkage and swelling of wood is normally 10 to 20 times larger in the transverse direction than in the longitudinal direction because of the longitudinal shape of the cell structure. It also explains why the wood is much stiffer in the longitudinal direction (along the grain) than in the transverse direction (perpendicular to the grain). But differences are not only in direction but also in wood species.

Wood is classified in two main categories of plants: Softwoods (gymnosperms, conifers) and hardwoods (angiosperms, deciduous), which correspond roughly to a different cell type, as shown in figure 3.1.

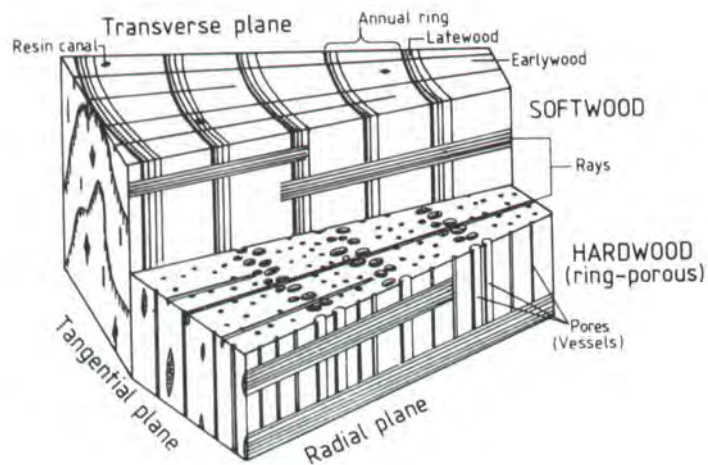


Figure 3.1 Models of a softwood and hardwood block, showing the main planes for anisotropy (adapted from Fengel and Wegener, 1984).

The timber used in this research is a softwood, which is the most common type of wood used in construction nowadays. Low cost, wider availability and a fast growing process are some of the reasons. But softwoods usually have lower densities, as shown in figure 3.2. Therefore, lower mechanical properties than hardwoods are expected and most of them are more sensitive to moisture variation and defects.

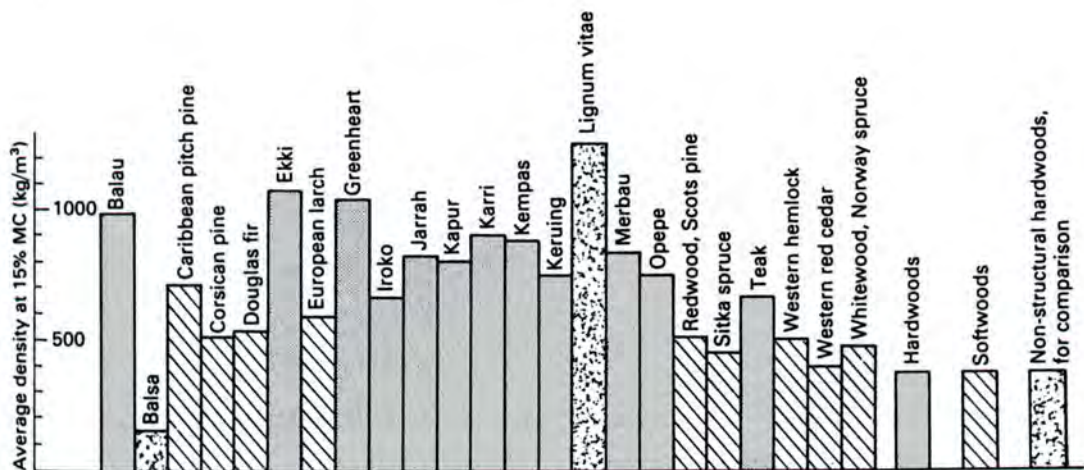


Figure 3.2 The average density at a moisture content of 15% for some common constructional timber and two woods at extremes of the density range (Mettem, 1986).

Within the softwood category, there are still large variations in properties from one species to another, and even in selected species, within a specific tree: From sapwood to heartwood, where the sensitivity to moisture decreases and from earlywood to latewood, which corresponds to the growth throughout the season. When the tree grows quickly, the density remains low (during spring and summer) and as the growing process slows down (late summer and autumn) the density increases. The latewood appears in the growth rings (darker material), also called annual rings. The characteristics of the rings also reflect the wood density: Thick rings show a fast growing process in the latewood, therefore the average density of the tree is likely to be relatively low. The number of rings reflects the age of the tree but rings spacing also show whether the wood has a high density or not. Large spacing corresponds to a fast growing process and low density on average.

The durability of timber can be threatened by certain organisms. Some species of destructive fungi damage the wood. These organisms develop in specific moisture content, temperature and air conditions. To control the moisture content (below 20%) is a way to prevent the decay of the wood.

Wood-boring insects also affect the durability of timber, by reducing the cross-sectional area of the timber, thus its strength. To prevent infestation of timber, preservatives are used either to cure damage wood or as a preventive measure (preservative impregnation) which are usually adequate unless infestation is severe.

Wood is a grown material and therefore natural defects occur such as knots. A knot is the part of the branch continuity within the main trunk as shown on the figure 3.3. “Knots are, by far, the single most important defect affecting mechanical properties of timber” (Hoffmeyer, in Timber Engineering STEP 1, 1995).

“There are many descriptions of types of knots, however generally fall into two categories. A “live” knot has complete continuity between the fibres of the branch and the tree. A “dead” knot occurs where a dead stub of a branch has been overgrown. This has no connections with the new wood formed annually, and consequently can become loose and fall out” (Reece, 1949).

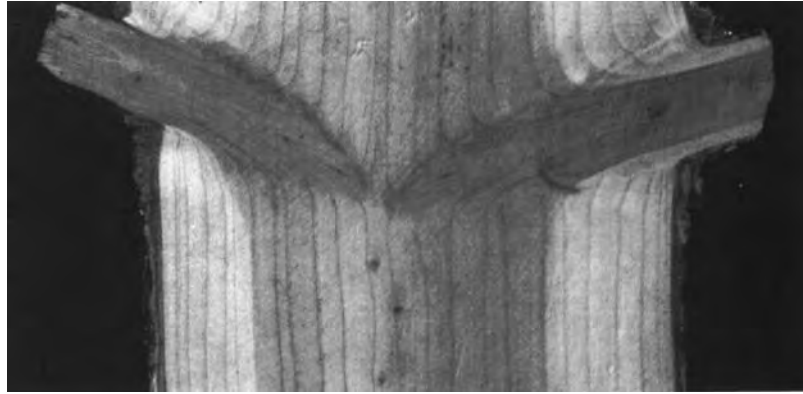


Figure 3.3 Lateral branches are connected to the pith of the main stem. Each successive growth ring forms continuously over the stem and branches (Hoffmeyer, in Timber Eng. STEP1, 1995).

A knot causes distortions in the grain that passes around it, resulting in concentration of stresses, which reduce the strength of the timber to a greater extent in tension than compression, as shown in figure 3.4. Most softwoods are characterised by having a dominant stem from which whorls of lateral branches occur at regular intervals or nodes. Softwood boards therefore show knots in clusters separated by the clear wood of the inter-nodes, as shown in figure 3.5.



Figure 3.4 Tension failure of a spruce board cause by fibre inclination around a knot (Hoffmeyer, in Timber Eng. STEP1, 1995).



Figure 3.5 A softwood board may show knots in clusters separated by the often clear wood of the inter-nodes (Hoffmeyer, in Timber Eng. STEP1, 1995).

The standards, which deal with grading of timber, contain restrictions on the proportion of knots permitted in a cross-sectional area of timber, as described further on.

Other natural defects of timber are cracks and fissures. They can occur in various part of the tree, usually along the wood fibres and have specific names: checks, shakes and splits reduce the timber resistance in shear, due to the reduction of cross-section in the radial or tangential direction. “Heart” shakes occur in the centre of the trunk, and can indicate the presence or beginnings of decay. Resin pockets are fissures containing resin, a defect that can results in strength reduction of timber depending of the number and sizes of pockets.

However restrictions on the proportion of cracks and fissures permitted in a cross-sectional area of timber are given in the standards for timber grading.

3.2.1.2. Selected timber

The timber used in this project has been bought from a local merchant who is the regular supplier for the university. The timber was delivered by the merchant who certified that all planks were from the same batch. All planks are in softwood from the same specie classified as **European Spruce**. The cross-section of these timber planks was 2 by 4 inch as specified (100 × 50 mm gross cross-section) and have been planed (94 × 44 mm net cross-section). 200 metres of timber were delivered and the planks were between 3 and 5 m long. A fair amount of distortion (twist and bow) was reported and a preliminary visual selection of the timber planks was achieved before being stored: Planks that were damaged (particularly on edges), full of knots or too twisted were taken out of the selection. According to the merchant, the timber was seasoned and left in a storage area protected from the weather for more than a year. However from the twist distortion reported on some planks, the timber was not protected from temperature and moisture variation during seasoning. The timber has also been graded and certified to be grade SC3 to SC4 by the merchant. Nevertheless, to confirm this information and to establish more accurate figures, the timber would be graded after adequate conditioning and fully tested, as developed further on in the thesis.

Strength classes for structural timber have been updated to European standards. The Strength classes (SC) noted in BS5268: Pt 2: 1996 have been changed to strength classes C for conifers (softwood) and D for deciduous (hardwood) as specified in BS EN 338: 1995 “ Structural timber - Strength classes ” and other recent standards. The two following tables show the strength characteristics from the previous classification (table 3.1) and the characteristics values from the current code (table 3.2). The grey shading shows that timber softwood previously classified SC3/SC4 would be now C16/C24. However the values are not comparable between the two tables: Grade stresses and moduli of elasticity from table 3.1 are much higher than the characteristic values from table 3.2, characteristic strength values being based on the lower 5-percentile of the timber population.

Strength class	Bending	Tension	Compression	Compression		Shear	Modulus of elasticity	
	parallel to the grain	parallel to the grain	parallel to the grain	perpendicular to the grain		parallel to the grain	Mean	Min.
	MPa	MPa	MPa	MPa	MPa	MPa	MPa	MPa
SC1	2.8	2.2	3.5	2.1	1.2	0.46	6800	4500
SC2	4.1	2.5	5.3	2.1	1.6	0.66	8000	5000
SC3	5.3	3.2	6.8	2.2	1.7	0.67	8800	5800
SC4	7.5	4.5	7.9	2.4	1.9	0.71	9900	6600
SC5	10.0	6.0	8.7	2.8	2.4	1.00	10700	7100
SC6	12.5	7.5	12.5	3.8	2.8	1.50	14100	1180
SC7	15.0	9.0	14.5	4.4	3.3	1.75	16200	1360
SC8	17.5	10.5	16.5	5.2	3.9	2.00	18700	1560
SC9	20.5	12.3	19.5	6.1	4.6	2.25	21600	1800

Table 3.1 Grade stresses and moduli of elasticity for strength classes: for dry exposure condition (from BS 5268: Pt 2: 1996).

		C14	C16	C18	C22	C24	C27	C30	C35	C40
Strength properties (in N/mm ²)										
Bending	$f_{m,k}$	14	116	18	22	24	27	30	35	40
Tension //	$f_{t,0,k}$	8	10	11	13	14	16	18	21	24
Tension \perp	$f_{t,90,k}$	0.3	0.3	0.3	0.3	0.4	0.4	0.4	0.4	0.4
Compression //	$f_{c,0,k}$	16	17	18	20	21	22	23	25	26
Compression \perp	$f_{c,90,k}$	4.3	4.6	4.8	5.1	5.3	5.6	5.7	6.0	6.3
Shear	$f_{v,k}$	1.7	1.8	2.0	2.4	2.5	2.8	3.0	3.4	3.8
Stiffness properties (in kN/mm ²)										
Mean MOE //	$E_{0,mean}$	7	8	9	10	11	12	12	13	14
5% MOE //	$E_{0,05}$	4.7	5.4	6.0	6.7	7.4	8.0	8.0	8.7	9.4
Mean MOE \perp	$E_{90,mean}$	0.23	0.27	0.30	0.33	0.37	0.40	0.40	0.43	0.47
Mean SM	G_{mean}	0.44	0.50	0.56	0.63	0.69	0.75	0.75	0.81	0.88
In kg/m ³										
Density	ρ_k	290	310	320	340	350	370	380	400	420

NOTE: // = Parallel to the grain, \perp = Perpendicular to the grain, MOE = Modulus Of Elasticity and SM = Shear Modulus.

Table 3.2 Strength classes and characteristic values for coniferous species (from BS EN 338: 1995).

3.2.2. Glass fibres

3.2.2.1. General

Glass fibres are filaments or fibres of glass.

“The commonly accepted definition of glass is an inorganic product of fusion which, when cooled, becomes rigid without crystallising (its atoms never arrange themselves into an orderly crystalline pattern)” (Dorman, 1969).

“Glass composition: The major constituent of most inorganic glasses is silica. The silicon dioxide molecule has a tetrahedral configuration consisting of a central silicon ion surrounded by four oxygen ions. The three-dimensional network of silica tetrahedra is the basis of the various and unusual properties of glass. By addition of modifying ingredients such as metallic oxides, which may become part of the silica network or disrupt it, the properties of the amorphous glass can be varied and adjusted to various levels of performance” (Dorman, 1969).

In other words, specific chemical and physical properties of glass fibres are controlled and altered through the process by which the fibres are drawn, but several properties remain characteristic of all types of glass fibres:

- High tensile strength to weight ratios.
- Perfect elasticity: Hooke’s law applies to glass fibres, without even developing plasticity or partial plasticity near failure. Typical glass fibres have a maximum elongation of 5% at break, they do not shrink or stretch.
- Moisture resistance: Glass fibres do not absorb moisture. In contact with moisture, fibres chemical composition remains identical. This is one of the main characteristics, which justifies the wide use of glass fibres in the boat industry.
- Thermal properties: Glass fibres are incombustible, with a low coefficient of thermal expansion and a high thermal conductivity. Typical fibres retain 50% of their strength at 350°C and up to 25% at 550°C.
- Corrosion resistance: Glass fibres do not rot or deteriorate and resist all organic solvents and most acids and alkalis.
- Electrical properties: Glass fibres have high dielectric strengths and low dielectric constants.

- Low cost: Particularly if compared with other high performance fibrous reinforcements such as carbon fibres.

Glass fibres in general terms have been used for many years in very wide range of applications as developed in the previous chapter. Regarding glass fibre production, the fibres are available in many different forms, such as continuous or chopped strands, mats, fabrics and woven strands. Mats are defined as a sheet made of chopped or continuous strands laid in a random pattern and held together with adhesive or with a needling process. Woven strands usually show a multidirectional pattern, but the most common is the bidirectional pattern with 90° angle.

The glass itself as inorganic glass has been produced in different forms: Mainly made of silica, by adding chemical elements in various proportions to modify the silica chemical structure, then the glass properties. Therefore, glass fibres can have various levels of performance and are classified in different categories. However only fibres made of E-glass and S-glass are summarised in this report, as they are the most common reinforced glass fibres used in mechanical applications.

The first glass developed specifically for production of continuous fibres was a lime-alumina-borosilicate glass. It was originally designed for electrical applications. This glass, which is called E-glass, was found adaptable and highly effective from decorative to structural applications and has become the standard textile glass. Most of the glass fibres produced nowadays are E-glass.

S-glass is a high strength tensile glass. Its tensile strength can be up to 33% greater and its modulus of elasticity up to 20% greater than typical E-glass. It was used for aerospace applications in the 1960s for its high strength-to-weight ratio, its superior strength retention at elevated temperatures and its high capacity to fatigue loading. It has found applications in rocket engine cases, aircraft parts, etc.

Typical properties for both types of glass fibres are summarised in the table 3.3.

Fibre	Density (g/cm ³)	Tensile strength (MPa)	Tensile modulus (GPa)	Strain to failure (%)	Coef. of thermal expansion (10 ⁻⁶ /°C)
E-glass	2.54	3450	72.4	4.8	5
S-glass	2.49	4300	86.9	5.0	2.9

Table 3.3 Mechanical properties of typical E-glass and S-glass fibres (from Mallick, 1997).

3.2.2.2. Selected glass fibres

The types of glass fibres used in these experiments have been selected according to the following criteria:

- The glass fibre has to be a relatively standard product, in other words a product already available in its existing form, which is used for other applications.
- The fibres must be continuous, as well as having the same dimensions and properties. The uniformity of the reinforcement is essential for a better understanding of the composite. Chopped strands and random arrangement of fibres cannot be considered here because the fibre orientation is a key parameter in the joint configuration as explained further on.
- The practicality of handling the material is also significant. The feasibility and simplicity of fabrication are considered. Therefore, the glass fibre as a roller of continuous strand cannot be considered, it has to come as a fabric or sheet of woven or “needled” strands. In that case, just cutting the sheet to the appropriate dimensions can ensure the uniformity of the material over the whole joint.

The glass fibres used have been supplied by SP Systems, Composite Engineering Materials, which is a large company of composite materials manufacturing. Their activities are mainly mechanical engineering in boat industry and in high performance applications such high-tech boats and cars for racing, wind power station (propellers and masts design), etc. They produce a wide range of composite materials, S-glass, E-glass, carbon, aramid fibres in various forms and sizes, as well as pre-impregnated fibres. Also they blend the adhesives required to bond the reinforcement from polyesters to epoxies.

Reinforcements made of E-glass were considered, for cost purposes and also to test a standard type of composite widely available nowadays. Two different types of fibre orientations were selected, unidirectional and bidirectional fabrics. This choice was based on the following assumptions:

- The fibre orientations may have a significant effect in the load transfer through the joint.

- The use of a multidirectional composite may produce a higher strength joint due to its “multi-isotropic” properties and therefore enhance its capacity to respond to transverse and eccentric (i.e. bending) stresses.

Unidirectional fabric type UT-E500 and Double bias fabric type XE450 were the glass fibres used in the experiment (referred to SP Systems product information guide).

Unidirectional fabric type UT-E500:

UT-E500 is a Woven fabric called “plain weave” by the manufacturer because the strand of primary fibres (which are orientated in one direction) are held in place by finer and lighter fibres through an interlacing process, as shown in figure 3.6. To avoid excessive distortion of the fabric when handling, the weft interlaces are lightly fixed into position to give more stability. With this process, the fabric can be cut into strips and shapes without falling apart.

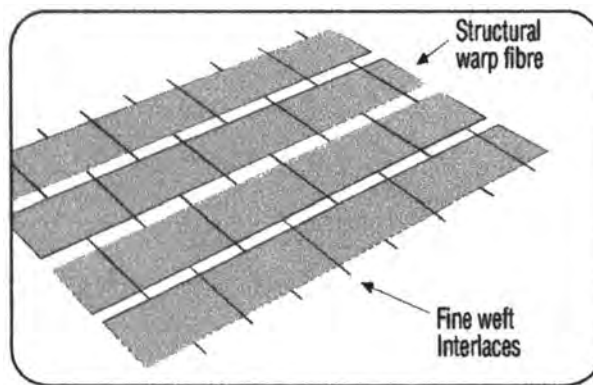


Figure 3.6 UT-E500 fibre layout (from SP Systems product information guide).

The UT-E500 fabric is available in rolls of 500 mm width. Its weight per unit area is 500 g/m² and each strand has 1200 fibres that are all continuous. The mechanical properties of the UT-E500 are summarised in table 3.4.

Fibre	Density (g/cm ³)	Tensile strength (MPa)	Tensile modulus (GPa)	Strain to failure (%)	Coef. of thermal expansion (10 ⁻⁶ /°C)
UT-E500	2.5	2400	69	3.5	7

Table 3.4 UT-E500 mechanical properties (from SP Systems product information guide).

Both UT-E500 and XE450 fabric types are made with E-Glass fibres having different diameters that range between 13 and 24 μm .

Double bias fabric type XE450:

XE450 is a multi-axial fabric. It is made of several strand layers having different fibre orientations. Layers are stitched together with polyester threads to form the fabric. The threads stop the fabric distorting, but also allow all the fibres of a given layer to be straight in the same plane continuously, without having to cross up and down alternatively transverse fibres as for woven fabrics. This is one of the main advantages of stitched fabrics over woven fabrics because it improves the mechanical properties of the composite matrix. The XE450 is fabricated with a “weave and stitch” method, as shown in figure 3.7.

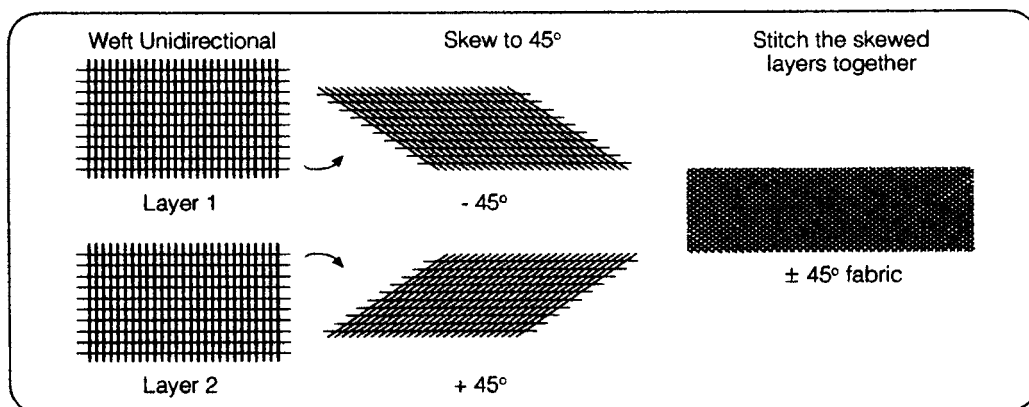


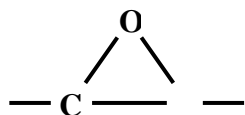
Figure 3.7 XE450 fibre layout (from SP Systems product information guide).

The method consists in weaving some unidirectional strands and skewing the fabric at $+45^\circ$ and another one at -45° , then stitching them together to form a tri-axial fabric: 0° , $+45^\circ$ and -45° . The fibres in the 0° direction (34 per strand) are much fewer than the fibres in the $+45^\circ$ and -45° directions (600 per strand). But careful considerations must be taken with multi-layer fabric to ensure an appropriate resin impregnation. The XE450 fabric is available in rolls of 1200 mm width. Its weight per unit area is precisely 467 g/m^2 . The fabric's architecture of the XE450 is made of two layers of unidirectional strands stitched together at $+45^\circ/-45^\circ$ and a negligible layer at 0° . Finally some fibres are used for the stitching the fabric.

3.2.3. Epoxy resin

3.2.3.1. General

“An *epoxy resin* is a polymer containing two or more epoxy groups:



Such groups are also referred to as *epoxide*, *ethylene Oxide*, or *oxirane* and may be by terminal, internal, or cyclic structures. *Epoxy resin* is used to designate both the uncured or thermoplastic polymer as well as the cured (hardened) or thermosetting material” (Dorman, 1969).

Epoxies are some of the most efficient resin types currently available in terms of mechanical properties and resistance to environment degradation. They are mainly classified as thermosetting material, which means once the resin and the hardener are mixed, a non-reversible chemical reaction occurs. The non-reversible reaction is the main difference between thermosetting and thermoplastic material. As thermosetting material, once the system has cured, it will not become liquid again if heated, the process of crossing the melting point can not be repeated again (and this without modifying the material properties) as it would be for a thermoplastic material. However above a specific temperature the mechanical properties of an epoxy system will change significantly (strength and stiffness). This temperature is known as the Glass Transition Temperature (T_g) and the change in mechanical properties is reversible once the temperature is below T_g .

The properties and characteristics of epoxy resins are as described in the following section:

- Versatility is probably the most outstanding characteristic of epoxy resins. They can have a wide variety of forms as far as the resin type is concerned but also their hardeners and modifiers allow them to be used in various applications, from very low viscosity to high-melting point solid.
- Curing range: Dependent upon the selection of hardener, systems can cure rapidly (or slowly) at almost any temperature from 5 to 180°C.

- Low shrinkage: Epoxy resins react with their hardeners by direct addition, without the evolution of water or volatile by-products (a “condensation” reaction) and with very little chemical rearrangement. Unlike polyester resin behaviour, the epoxies exhibit very low shrinkage during cure (less than 2%).
- Mechanical properties: Epoxy resin systems exhibit high mechanical properties due, in part, to their low shrinkage and relatively unstressed structure. These properties are usually higher than most of other resin types. Unlike the glass fibre, epoxy resin does not reveal perfectly elastic behaviour. Typical stress-strain diagram of epoxy resin is shown in figure 3.8.

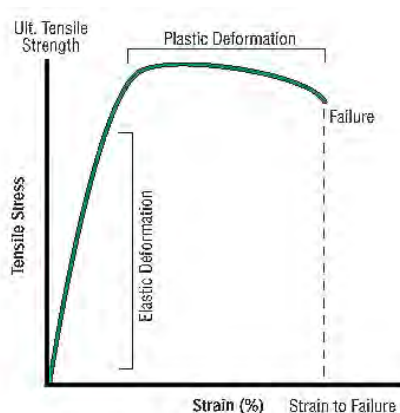


*Figure 3.8 Stress/strain diagram of typical epoxy resin
(from SP Systems product information guide).*

- Chemical resistance: Generally, epoxy resin systems exhibit extremely high resistance to alkali, good-to-excellent acid and solvent resistance. Again the epoxy system’s performance is dependent upon the choice of resin and hardener. Specific chemical resistance can be achieved with an appropriate selection of curing agent and epoxy resin.
- Durability: Combination of many of the above properties contributes to the outstanding dimensional stability and permanence of epoxy resin systems. They “age” very well, even under dynamic stressing.
- Thermal stability: The cured epoxy resin system generally exhibits good thermal stability. Systems can be selected for the desired stability and some exhibit stability at temperatures over 250°C.
- Water resistance: “Epoxy resins serve as excellent moisture barriers, exhibiting low water absorption and moisture vapour transmission, mainly due to the

absence of ester groups in the reaction (in comparison with polyester resin)” (Dorman, 1969).

Epoxies are cured by a hardener, which is often an amine, and by chemical reaction, both materials combined together. The chemistry of this reaction shows that there are usually two epoxy groups binding to each amine group. Each amine group co-reacts with epoxy groups in a fixed ratio, therefore, to ensure that complete reaction occurs, it is essential to use the correct mix ratio. If not, unreacted resin or hardener will remain in the matrix and this will affect the properties of the cured system.

Epoxies are used on a wide variety of substrates including metals, glass, wood, concrete and masonry. In any engineered fields (aircraft, aerospace, automotive, etc) where epoxy properties are relevant (such as high strength to weight ratios) and in composite structures, epoxy resins are used efficiently with strong reinforcements such as carbon, boron or glass fibres. They have applications in many industries for a multitude of bonding operations.

The outstanding adhesive strengths are due primarily to the thorough wetting, polarity and low shrinkage during cure. The good wetting assures that the adhesive will closely contact the adherends so that the strong adhesive forces may become active. This close contact is maintained after cure, and stresses, which may tend to disrupt the adhesive forces are minimised by the low shrinkage of the epoxy system. Epoxies are especially useful for the bonding of dissimilar materials, such as honeycomb structures, and where high-strength joints are required.

3.2.3.2. Selected epoxy resin

The epoxy resin used is called Spabond 120 and was supplied by SP Systems. Spabond 120 is recommended by the manufacturer as a perfect adhesive to bond a wide range of high strength materials, particularly GRP (Glass Reinforced Plastic), concrete, wood and composite components. Having been used in the boat industry for many years, Spabond 120 is ideal for all wood bonding operation, including hardwood such as teak, iroko, oak, etc. To ensure the best workability and performance of the resin, the following recommendations must be followed:

- Use the product at temperature between 15 and 25°C. Below this range, the resin will thicken and workability will become difficult (mixing procedure).
- Use the appropriate mix ratio between resin and hardener:
Resin/Hardener ratio: 2/1 by volume or 100/44 by weight.
- The choice of hardener depends whether the system needs to be cured rapidly. In the purpose of this research, slow hardener was used because the curing time was not essential, but also because a resin system cured with a slow hardener exhibits better mechanical properties and durability.
- The surface to be bonded should be prepared: For timber, it is recommended to sand the surface across the grain, to degrease and clean with water any oily and resinous timber surface.

Spabond 120 can be used for gluing, fillet bonding and fibre reinforcement. Spabond 120 has a high shear strength and toughness, which makes it suitable for bonding both high strength materials and dissimilar materials. However to optimise the resin consistency, a range of filler powders is available and will make the mix thicker. To enhance the strength of the resin, micro-fibres can be added to the mix. Acting as filler, the micro-fibres will thicken the mix but also will reinforce the adhesive against micro-cracks propagation. With its relatively low viscosity, Spabond 120 can be used with fibre reinforcement.

The following tables 3.5, 3.6 and 3.7 summarise respectively the main component properties, working properties and cured system properties of the Spabond 120 epoxy, as given by the manufacturer.

Properties	Resin	Slow hardener
Viscosity @ 15°C (cps)	5110	1200
Viscosity @ 20°C (cps)	2970	814
Viscosity @ 25°C (cps)	1730	554
Viscosity @ 30°C (cps)	997	375
Component density (g/cm ³)	1.174	0.973
Mixed density (g/cm ³)	-	1.113

Table 3.5 Component properties for Spabond 120 resin (from SP Systems product information guide).

The viscosity of the resin and the hardener are highly affected by the temperature. For a better workability, the viscosity must be kept as low as possible (more liquid). Furthermore, the low viscosity permits a better embedding and impregnation of the fibre reinforcements. Most of the experiments have been carried out in laboratory where a temperature between 20 and 25°C was maintained.

Resin/Slow hardener	15°C	20°C	25°C	30°C
Initial mixed viscosity (cps)	2780	1820	1170	792
Gel time - 150g mix in water (hrs:mins)	-	1:04	0:33	0:21
Pot life - 500g mix in air (hrs:mins)	-	0:35	-	0:18
Clamp time (hrs:mins)	13:30	8:00	4:50	3:00
Sag resistance (mm)	0.28	0.20	0.14	0.10

Table 3.6 Working properties vs. temperature for Spabond 120 resin (from SP Systems product information guide).

The gel time and pot life are standard tests, which quantify how fast the resin mix hardened.

The clamp time is the time required to obtain a degree of cure where the bonded components cannot easily be removed without damaging the adhesive layer.

Finally the sag resistance is the maximum thickness of adhesive, which can be applied to a vertical surface without slumping.

Properties	Room Temperature Cure (28 days @ 21°C)	Cured (24 hrs @ 21°C + 16 hrs @ 21°C)
Tg DMTA (Peak Tan δ)(°C)	68.2	78.1
Tg Ult - DMTA (°C)	81.3	81.3
ΔH - DSC (J/g)	13	0
Tg1 - DMTA (°C)	57.8	67.0
Cured Density (g/cm ³)	1.154	1.152
Linear shrinkage (%)	1.6	1.6
Cleavage Strength (kN)	6.37	5.83
Shear strength on steel (MPa)	19.0	17.4
Shear strength wet retention (%)	95	-

*Table 3.7 Cured system properties for Spabond 120 resin
(from SP Systems product information guide).*

Tg DMTA (Peak Tan δ), Tg Ult - DMTA and Tg1 - DMTA are sophisticated tests to measure the Glass Transition Temperature Tg, the temperature where the chemical composition of the polymer material such as the cured epoxy, will change from rigidly linked molecules to flexible molecules. The chemical structure remains intact but the cross-links are no longer effective (i.e. mechanical properties reduced).

The ΔH - DSC test is an alternative to quantify Tg by measuring the amount of energy absorbed by the polymer's chemical structure when it reaches Tg because of its molecular rearrangement.

The linear shrinkage is an indication of the amount shrinkage the epoxy develops when transitioning from liquid state to fully cured state.

Cleavage strength is a standard test in which two steel blocks are bonded together with the adhesive and pulled apart in order to cause cleavage of the adhesive. The load is given for a bond area of 25 mm \times 25 mm.

Shear strength on steel is a standard test in which two thick steel plates are bonded together with the adhesive and pulled apart. The plates are almost in pure tension due to their thickness, which stop them to bend.

Finally the lap shear strength wet retention is the same test as the previous one but the sample has been initially immersed in distilled water at 35°C for 28 days. The retention (given in percentage of pre-soak value) is an indication to the degradation of the adhesive in wet conditions.

3.2.4. Glass fibre/epoxy composite

3.2.4.1. General

The mechanical properties of the glass fibre/epoxy matrix or lamina are much higher than the mechanical properties of the epoxy resin itself. Therefore the fibres have a predominant role in the composite behaviour. In fact, with the lamina in tension, the fibres carry most of the load as the resin only hold the fibres together. On the other hand, with the lamina in compression (or in bending), the fibres behave like axially loaded columns and then the resin must resist the fibres buckling. Therefore the fibre/resin adhesion becomes an important parameter. However, different behaviours apply to the resin and fibres for adhesive joints bonded with composite, and this will be covered in the theoretical analysis of wood/glass/epoxy joints, later in this thesis.

The mechanical properties of a lamina are governed by some of the following factors:

- Mechanical properties of the fibre and the resin.
- The amount of fibre in the matrix, evaluated as the Fibre Volume Fraction (FVF).
- The fibre/matrix interaction such as bond strength.
- The fibre orientation within the lamina.
- The fibre layout (woven, needled, fabric, etc) within the matrix.

The mechanical properties of fibre and resin are usually given by manufacturers and are based on experimental testing rather than theoretical estimations. Properties are always based on a specific fibre volume fraction, as the ratio of fibre in the composite does reflect on the mechanical properties. Mechanical properties of composites can be separated in two categories: basic or static properties (elastic modulus and strength) and advanced or dynamic properties (fatigue, impact, creep and vibration behaviours). Fatigue properties were investigated in this research further to the static tests of wood/glass/epoxy joints (see chapter 7). Typical static mechanical properties of unidirectional fibre reinforced composites are density, fibre volume fraction, longitudinal/transverse tension/compression strengths, in-plane/interlaminar shear strengths, longitudinal/transverse/shear moduli, and

major/minor Poisson's ratios. All these properties are in-plane properties (in the plane containing the fibres). Properties through the thickness of the lamina (out-of-plane) are sometime required but are not easily available, because their measurement is a difficult process. However, there are some ways to estimate those out-of-plane properties based on in-plane properties (for unidirectional composite). But referring to the wood/glass/epoxy joint, only very thin composite layers were used and tangential or out-of-plane properties were assumed to be equal to transversal properties for a unidirectional layer. These assumptions will be explained and detailed later in this thesis. Typical mechanical properties are shown in table 3.8:

Property	E-glass/epoxy
Density (kg/m ³)	2100
Longitudinal tension strength (MPa)	1020
Longitudinal compression strength (MPa)	620
Transverse tension strength (MPa)	40
Transverse compression strength (MPa)	140
In-plane shear strength (MPa)	70
Interlaminar shear strength (MPa)	70
Longitudinal elastic modulus (GPa)	45
Transverse elastic modulus (GPa)	12
Shear elastic modulus (GPa)	5.5
Major Poisson's ratio	0.28

Table 3.8 Typical mechanical properties for unidirectional glass fibre reinforced epoxy composite (Mall, 1997).

Another main factor to control the composite mechanical properties is the fibre volume fraction.

“In general, the higher the fibre volume fraction, the higher the modulus, strength, and many other properties of the composite” (Mall, 1997).

However, around 60-70% of fibre volume fraction, the composite strength will reach a limit and will decrease for higher fibre volume ratio because the amount of resin will not be sufficient to hold and bond the fibres.

In theory, the fibre arrangement within the matrix is regular, and the fibre volume fraction could be calculated by dividing the fibre volume to the composite volume. This is the basic assumption of the macromechanics of composite where the material

is assumed homogeneous and its properties are based on the average properties of the constituent. In equation (3.1), the fibre volume fraction V_f is defined as:

$$V_f = \frac{\text{Volume of fibres}}{\text{Total volume of composite material}} \quad (3.1)$$

In practice, the fibres are not regularly distributed, and then theoretical fibre volume fraction is not representative and is inaccurate. The study of composite behaviour assuming the composite to be heterogeneous and where the interaction between constituents is examined in detail is called micromechanics. In equation (3.2), the actual fibre volume fraction V_f is derived from the fibre weight fraction ω_f (that is determined experimentally):

$$V_f = \frac{\omega_f / \rho_f}{\omega_f / \rho_f + \omega_m / \rho_m} \quad (3.2)$$

Where V_f = Fibre volume fraction, ω_f = Fibre weight fraction, ω_m = Matrix weight fraction, ρ_f = Fibre density and ρ_m = Matrix density.

The adhesion between the resin and the fibres is also a critical parameter in the composite performance. The strength of the composite is increased if there is a strong interfacial bond between the fibres and the matrix. The interface bond strength influences the fracture toughness of the composite. The sketch shown in figure 3.9 shows the contact area between the resin and fibre or fibre/matrix interface.

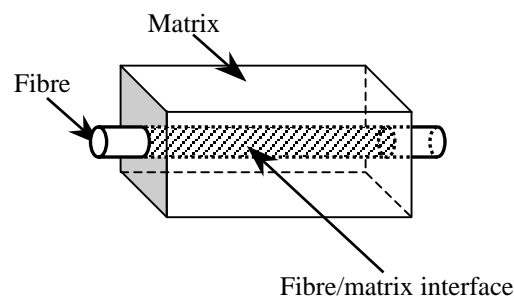


Figure 3.9 Sketch of single fibre surrounded by the matrix

The interface properties affect the crack propagation in the composite. For example, in unidirectional composite loaded in tension, the cracks occur in the transverse direction.

“If the interface debonds relatively easily, the crack propagation is interrupted by the debonding process and instead of moving through the fibre, the crack moves along the fibre surface, allowing the fibre to carry higher loads” (Mallick, 1997).

Then the fibre pullout and break occur, leading to a wider crack and finally a premature failure.

“If the pullout occurs against high frictional forces or shear stresses at the interface, there may be a significant increase in fracture toughness of the composite” (Mallick, 1997).

In normal conditions, the interface bond strength is mechanically achieved during the curing process. This bond is formed by the differential shrinkage of the matrix, which has a higher coefficient of thermal expansion than the fibres. Therefore the matrix shrinks more than the fibres during the temperature cooling down and this creates some residual stresses within the composite, which take part of the interface bond strength.

“In many polymeric matrix composites, increased interfacial bond strength is achieved by fibre surface treatment, which helps in forming a chemical linkage between the fibres and the matrix across the interface” (Mallick, 1997).

There are several methods to evaluate the fibre/matrix bond strength through series of tests, which attempt to measure interfacial shear strength (IFSS) or to measure interface-sensitive properties and microscopic inspection of failure surfaces. Eventually highly sophisticated equipment is required to carry out those tests therefore the fibre/matrix bond strength will not be assessed in the purpose of this research. However, one of the most commonly used tests is the fragmentation test:

“A single filament is embedded in the resin, which is moulded into a tensile dogbone. The coupon is pulled in tension until the filament fractures numerous times, causing the fibre to break into shorter and shorter lengths. Eventually a length is attained, called the critical length (l_c), which is too short to develop enough tensile stress for failure. This tensile stress is generated by shear loads at the fibre/matrix interface, so higher values of IFSS will produce shorter critical length” (Mallick, 1997).

The equation (3.3) relates the IFSS to the critical length l_c is:

$$IFSS = \left(\frac{\sigma_f}{2} \right) \times \left(\frac{d}{l_c} \right) \quad (3.3)$$

Where l_c is the critical length, d is the fibre diameter and σ_f is the fibre strength.

The fibre length and diameter have also an implication in the composite strength. Fibres can be short, long or even discontinuous. Their dimensions are often characterised by the aspect ratio l/d , where l is the fibre length and d is the diameter. Typical fibres have diameters from 10 microns (10E-3 mm) to 150 microns (150E-3 mm). If the fibre length l is smaller than l_c , little reinforcement effect is observed; if l is greater than $15 \times l_c$, the fibre behaves almost as if it were continuous. The strength of the composite σ_c can be estimated from equation (3.4):

$$\sigma_c = f_f \sigma_f \left(1 - \frac{l_c}{2l} \right) + f_m \sigma_m \quad (3.4)$$

Where σ_m is the stress in the matrix when the fibres break,

f_f is the force carried by the fibres, f_m is the force carried by the matrix.

Note that the total force acting on the composite $f_{composite} = f_f + f_m$ (from Askeland, 1996).

The fibre orientation within the lamina is also a critical parameter in the strength properties of the composite. Short or randomly orientated fibres can be introduced easily into the matrix and give relatively isotropic (in-plane properties) behaviour in the composite. With long or continuous fibres, arranged regularly in the same direction, the composite shows anisotropic behaviour but with particularly good strength and stiffness properties if the load is applied in the fibre direction. On the other hand, poor properties are observed with the load applied in the perpendicular direction of the fibres. The figure 3.10 shows the effect of fibre orientation on unidirectional composites.

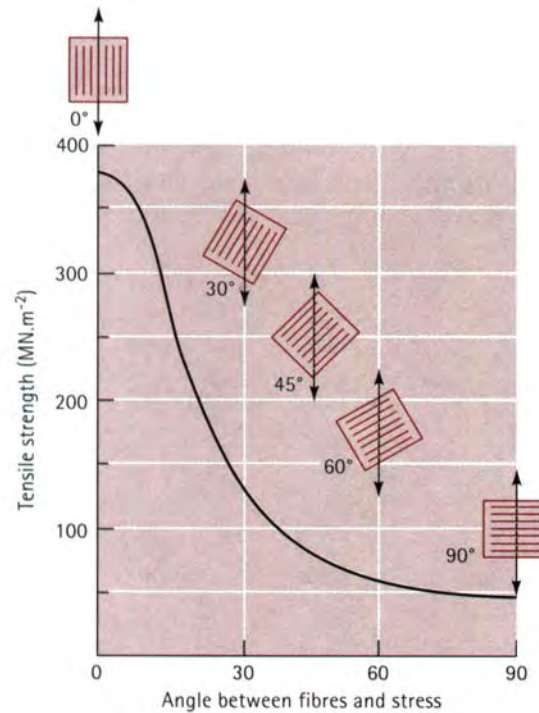


Figure 3.10 Effect of fibre orientation on the tensile strength of E-glass fibre reinforced epoxy composites (Askeland, 1996).

The angle between the fibre direction and the load direction is called the fibre orientation angle θ . As θ varies from 0° to 90° , the strength properties of the unidirectional composite decrease dramatically. To overcome this weakness, multidirectional arrangement of fibres can be used, as discussed in the section about glass fibre. Better performances are obtained for composite laminate plate by overlaying several plies of fibres having different orientation in the matrix. Orthogonal arrangements ($0^\circ/90^\circ$ plies) show good properties in the perpendicular directions considered. Multi-orientated arrangements (such as $0^\circ/+45^\circ/-45^\circ/90^\circ$ plies) provide almost isotropic properties (in-plane). More complicated three-dimensional arrangements can also be used for laminated composites, as shown in figure 3.11.

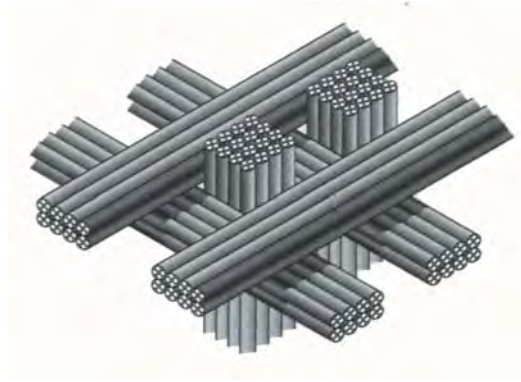


Figure 3.11 A three-dimensional weave for fibre reinforced composites (Askeland, 1996).

Finally, the mechanics of composite is relatively complex due to the anisotropic behaviour of the materials. Stiffness matrix and stress-strain transformations need to be looked at carefully to design or predict the composite strength. Also mechanics of adhesive joints with laminated materials is even more complex by adding out-of-plane parameters. The basic principles of macromechanics and micromechanics of composites materials, as well as adhesive joint theory will be treated in chapter 6 about theoretical analysis of wood/glass/epoxy joints.

3.2.4.2. Selected glass fibre/epoxy composite

As specified before, the composites used in the experiments are:

- E-Glass fibre UT-E500 (unidirectional)/Spabond 120 epoxy resin.
- E-Glass fibre XE-450 (bidirectional)/Spabond 120 epoxy resin.

The mechanical properties of these composites have been given by the manufacturer and are based on Ampreg 20 epoxy laminated system, which is an epoxy resin having similar chemical structure and properties than Spabond 120 except its viscosity which is lower and therefore more appropriate for laminated composites. According to the manufacturer, these properties are the same if Spabond 120 is used: Two sets of properties are shown in table 3.9 for the UT-E500/Ampreg 20 and one for the XE450/Ampreg 20.

Property	UT-E500 / Ampreg 20	UT-E500 / Ampreg 20	XE450 / Ampreg 20
Fibre volume fraction	0.44	0.35	0.44
Density (kg/m ³)	1764	1640	1729
Longitudinal tension strength (MPa)	597	500	279
Longitudinal compression strength (MPa)	398	300	214
Transverse tension strength (MPa)	26	20	279
Transverse compression strength (MPa)	80	70	214
Longitudinal elastic modulus (GPa)	33.18	28	18.6
Transverse elastic modulus (GPa)	5.69	5	18.6
Interlaminar shear modulus (GPa)	2.91	2.5	2.79
In-plane shear modulus (GPa)	2.91	2.5	2.79
Longitudinal Poisson's ratio	0.297	0.27	0.091
Transverse Poisson's ratio	0.045	0.05	0.091
Thickness per ply (mm)	0.44	0.5	0.54

Table 3.9 Mechanical properties for UT-E500 and XE-450 with Ampreg 20 resin composites (from SP Systems product information guide).

Each set of UT-E500/Ampreg 20 is for a specific fibre volume fraction. Note that the properties are lower with low fibre volume fraction.

3.3. Summary

In this chapter, all the materials characteristics and properties involved in this research have been described. Particular attention was given to the glass fibre and the epoxy resin, particularly to their properties because there are difficult to assess by experimentation without sophisticated equipment, as developed in the next chapter.

CHAPTER 4

EXPERIMENTAL PROGRAMME

4.1. Introduction

From the concept of testing wood/glass/epoxy joints to the actual experimental programme, many parameters have been considered and modified all along the research. The types of test, the sizes and number of samples tested and the equipment facilities are part of those parameters, which have been investigated through the research process. These assumptions and considerations will be developed through this chapter.

Beyond the experimental programme in which the joint's mechanical properties are evaluated, additional experiments must be carried out to determine, if possible, the mechanical properties of each material on its own. These parameters are essential to understand the composite behaviour of the joint, to correlate the theoretical estimation to the experimental results. Moreover, materials properties measured in the experiments will be key input data for finite element models. The difficulties in carrying out these measurements, as well as the description and number of tests undertaken are also presented in this chapter.

4.2. Testing of glass fibre/epoxy composite

To evaluate the mechanical properties of the glass fibre/epoxy systems was a task initially planned in the research programme, but was not considered anymore after unsuccessful testing and sample fabrication.

The idea was to fabricate samples having the shape of a dog bone made of glass fibres and epoxy resin, as shown in figure 4.1. Each end of the sample was drilled to accommodate a bolt to hold the sample in tension. Each sample would have different amount of fibres embedded in the resin in order to establish tension strength to fibre content relationship. Prior to this research, Kirby (1998) already did a final year project on this subject therefore all the equipment used was available. Nevertheless

his experiments did not show any valid results and did not confirm any relationships. However an attempt to carry out the same test was made.

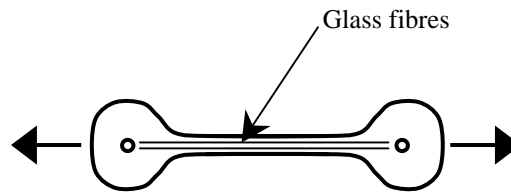


Figure 4.1 Dog bone sample shape.

Using the same moulds, samples were fabricated with slight modifications from Kirby's method:

- Aluminium foil was used instead of cling film as mould cover. This allowed the sample to be removed easily from its mould and not have the cling film remaining within the sample, as shown in figure 4.2.

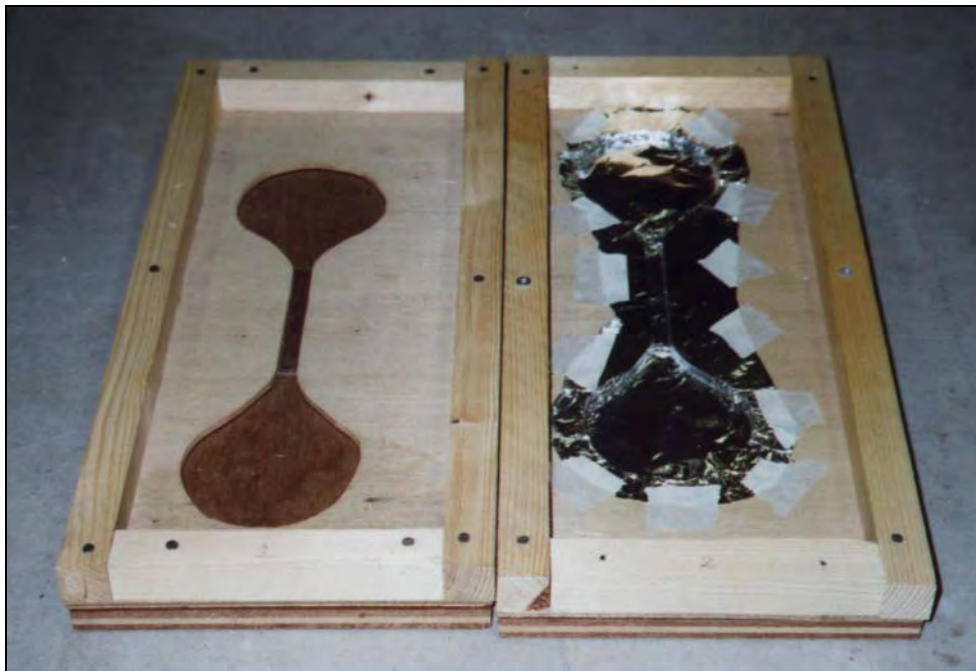


Figure 4.2 Moulds for dog bone samples using aluminium foil.

- Reinforcement of the bone ends with bidirectional glass fibre layers to avoid premature failure transverse to the holes, as shown in figure 4.3.



Figure 4.3 Dog bone samples curing in moulds.

Nevertheless, one of the samples broke while extracting it from the mould. For the other one, the edges were not properly defined after the removal of the aluminium foil. Air bubbles were trapped inside the resin matrix, and then the cross-section of the thin inner part of the dog bone was far from being rectangular, as shown in figure 4.4.

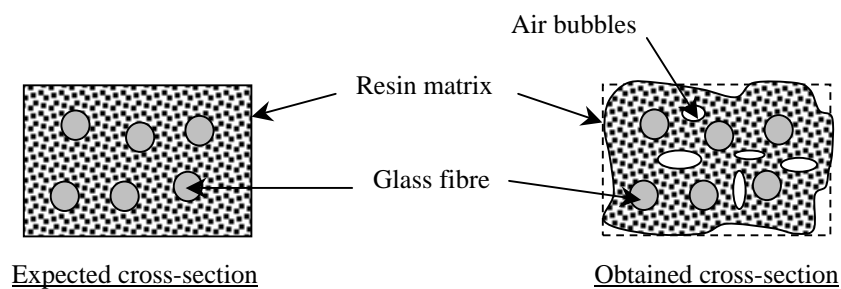


Figure 4.4 Comparison between dog bone cross-section needed and achieved.

As a result, the testing of the glass fibre/epoxy sample was abandoned and the following reasons explain this decision:

- Impracticality of sample fabrication: The difficulties to turn the sample out from its mould with a high risk of damaging or breaking the sample.

- The wooden moulds were inadequate to create the samples shape required. It was not truly symmetrical therefore bones heads did not have the same shape. Aluminium or stainless steel mould fabricated with precise dimensioning to 0.1 mm or less tolerance would have been ideal.
- With imprecise dimensions, it was difficult to measure the cross-sectional area.
- There was no system to ensure a good fibre impregnation (such as using a roller or a vibrating system) and remove the air trapped within the resin matrix.
- Maintaining the fibres in position near the cross-section neutral axis, parallel to the sample was almost impossible to achieve.
- Some extra fibres were placed in the sample bones ends to avoid tension failure around the bolt connection, therefore the amount of resin was difficult to measure, especially the exact amount, which would lead to the sample failure in the thinner part of the dog bone.

Under those considerations, the most reliable way to find out about the glass fibre/epoxy properties was to use the properties given by the manufacturer. Usually properties from manufacturers are slightly over estimated (for commercial purposes) and do not always reflect realistic conditions. However SP Systems is a large company based in the Isle of Wight, which fabricates its own products but also runs a design office. All their materials are tested and properties established experimentally with appropriate methods and equipment in order to be used for design purposes. The properties given by SP Systems are not the ones commonly given for commercial use and are therefore accurate and representative of experimental conditions. They have been recommended by SP design office for use in this research.

At this stage of the research process, it was decided to use those properties instead of measuring them for the theoretical analysis and finite element modelling.

4.3. Wood/glass/epoxy joints

The testing of wood/glass/epoxy joints was elaborated according to various parameters such as types of test, joint geometry, number of samples per type of test, standard testing method of mechanically fastened timber joints, standard testing method of adhesive joints, etc.

The programme was initially based on Claisse and Davis (1998) who looked at butt or scarf ends timber members, fully or partially connected with glass fibre/epoxy layers of various length, tested in static tension. Most of the information obtained through this research has been taken into account to develop this experimental programme, as explained in the following sections.

4.3.1. Joint geometry requirements

The initial application of wood/glass/epoxy was thought to be an alternative to mechanical fastened timber joints, particularly for timber frame such as trussed rafters. The most common jointing system used for timber truss connection is the punched metal plate. It can only be used if the members connected have the same thickness, which is normally the case for trussed rafters. The plates are 'punched' or nailed on two opposite faces of the timber members and the member cross-sections are not reduced, as it would be if bolts or dowels were used. For these reasons, the punched metal plate is probably the most comparable jointing system with wood/glass/epoxy joints in terms of geometrical configuration.

In timber frames such as trusses, connected members have different orientations, therefore glass fibre/epoxy layers can only be bonded on the two opposite sides of each members, which are in the same plane. In order to obtain an efficient bond between the composite layer and the timber, the connected members must have the same thickness.

The strength of punched metal plate timber joints varies with the member orientation. This is reflected through the anisotropic timber properties, which are a function of its grain orientation. Therefore, punched metal plate timber joints are generally tested for different grain orientation.

The same variations are likely to appear with the wood/glass/epoxy joints. The bonding area may remain the same while member orientation varies but the timber in contact with the epoxy will have the specific mechanical properties given for its grain orientation. It was therefore relevant to carry out tests where the connected timber members of the wood/glass/epoxy joints have different grain orientations.

The selected timber gross cross-section dimensions are 100×50 mm. These dimensions were set as a standard size for all samples and tests carried out. The dimensions of the glass fibre/epoxy layer could vary as required but for the purpose of this research, these dimensions had to remain constant within each type of test, in order to compare results obtained from each sample. The glass fibre/epoxy layer dimensions should be the same on each side of the sample (to have uniform stiffness through the joint cross-section). Additionally the bonded area should be equal on each connected timber member. The full width of the timber member was bonded to maximise the composite efficiency and performance of the joint. The critical remaining parameter was therefore the length of composite to be bonded. It could be selected under two criteria:

- The wood/glass/epoxy joint has to be a balanced or '**economically designed**' joint. This means that the joint has the critical bonded length of composite, which makes it fail under load in multiple failure modes. The adhesive joint tested in tension is likely to have two modes of failure: breaking of the composite in tension and failure by delamination of the composite from the bonded timber surface. In the case of a balanced joint, the failure occurs by delamination combined with tension rupture of the composite. However the determination of critical length is an iterative process, which can be laborious especially if it involves wood material with its anisotropy and varying mechanical properties. Also the critical length can be changed as well as the amount of glass fibres, which makes the balancing process even more complicated.

The joint can be balanced if the timber members are connected by a butt end joint, as shown in figure 4.5. If not, the bonded length is limited by the geometry of the joint.

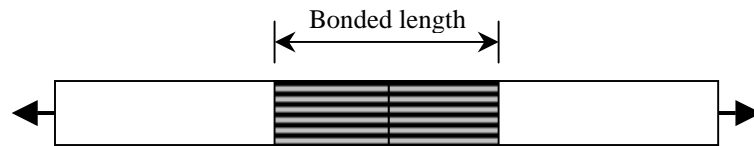


Figure 4.5 Variable bonded length for butt end joint.

- The other criterion is to look at the **joint geometry**, particularly when timber members have different orientations. In that case, the bonded length is limited to the maximum bonding area available. The minimum bonding area is available when the connected members are perpendicular to each other, as shown on figure 4.6.

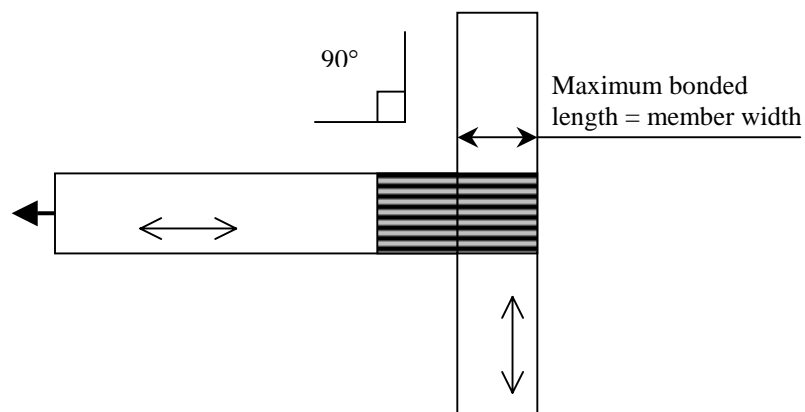


Figure 4.6 Determination of maximum bonded length from joint geometry.

The testing of balanced joint seemed to be inappropriate at this stage of the research as it might need a full experimental programme to optimise it. Moreover the natural wood property variations would complicate this task. But the wood/glass/epoxy joints expectation was a stiff and efficient joint system from the combination of these three materials (wood, glass fibre and epoxy resin). Out of those, the weakest material is the timber therefore its properties are likely to limit the joint's strength. It would be more appropriate to take this assumption into account and make sure the glass fibre/epoxy is strong enough to not fail by rupture prematurely. With sufficient length and weight of glass fibre bonded, the tension failure should occur at the bond interface, by delamination of the composite. In that case, the timber or the resin fails in shear.

Three preliminary tests were carried out for the connected members with the same orientation (i.e. straight butt ends joint) using different lengths of glass fibre bond. Samples were fabricated with 200 mm, 250 mm and 300 mm long layers of uniaxial glass fibre UT-E500 and tested in straight pull out tension. From these preliminary tests results (presented in the chapter 5) it came out that a 200 mm layer was of sufficient length to obtain the sample's failure by delamination.

It was decided to use 200 mm long layers for uniaxial and biaxial glass fibre for samples with members orientated in the same direction. For sample with different member orientation, the maximum length available from the joint geometry determined the length of glass fibre.

With the length of glass fibre determined, the geometry of the whole sample could be defined. Depending on the type of test, samples needed to be fixed to a testing rig with a fastening system, which must to be stronger than the joint tested. In the preliminary tests two 17 mm thick steel side plates connected to the rig were positioned on two opposite sides of the sample end, with a 20 mm diameter bolt connected through, as shown in figure 4.7.

The bolt was located with sufficient edge distances to avoid premature failure by wood splitting, but while testing the sample in tension, too much displacement was recorded at the bolt position and bearing failure of the timber occurred around the bolt. An alternative fastening system was then required. Several bolts were used instead of one, but there was still a fair amount of displacement. The solution came from Claisse and Davis (1998), where experiments on joints made with shear-plate connectors were carried out. These joints were formed using 67 mm diameter pressed steel shear-plate connectors with 20 mm grade 8.8 bolt, as shown in figure 4.8. These joints appeared to be extremely stiff, allowing for a more uniform distribution of stress through the timber members.

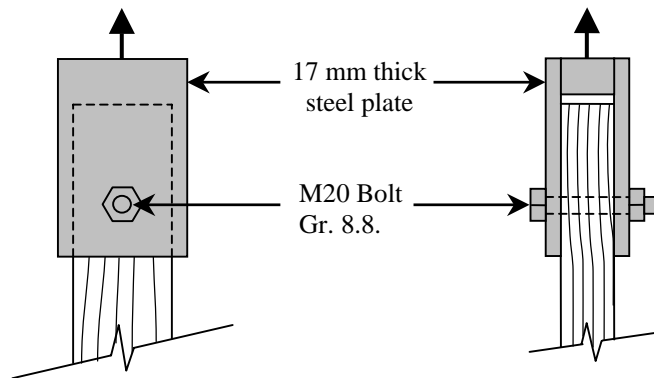


Figure 4.7 Sample end with 20 mm bolt connection.

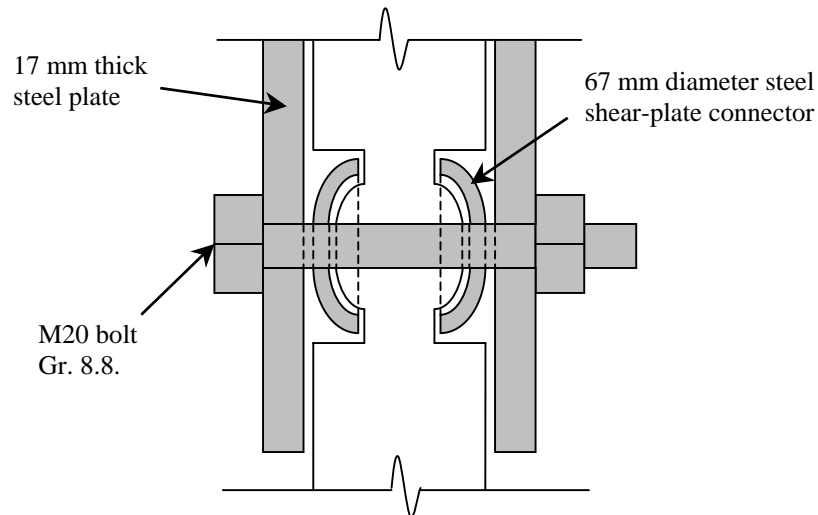


Figure 4.8 Detail of sample end connection with shear-plate connectors.

Shear-plate connectors were used to connect samples to the testing rig. A minimum distance from the connectors to the tested joint (i.e. glass fibre/epoxy layers) of 300 mm was recommended. Sufficient clearance was required to allow the stress from the shear-plates to be distributed progressively towards a uniform distribution over the whole cross-section as it reached the glass fibre layers.

The minimum geometry requirements of samples were developed through this section. The overall dimensions of the samples depend on the type of test and are defined further on in this chapter, for each particular test.

4.3.2. Types of test

4.3.2.1. The choice of tests

Wood/glass/epoxy joint strength properties depend on the materials jointed:

- Timber species, density, moisture content, mechanical properties, aspects and defects,
- Types of glass fibre, density and mechanical properties,
- Type of epoxy resin, the amount used in the joint, its density and mechanical properties.

The strength properties of wood/glass/epoxy joints also depend on the overall size, thickness, width and configuration of the joint and also on loading direction and exposure conditions to which the joint is subject in service.

There are so many factors, which can affect the strength of wood/glass/epoxy joints that restrictions such as the type and size of the glass fibre, the size of the samples and the number of specimens tested were taken in order to set up a feasible testing programme. Dimension requirements were developed in the previous section and the number of samples tested is discussed later.

To define the types of test to carry out in this programme, it was essential to recall the aim of this research, which was to develop tests to determine strength properties, capacity and stiffness of joints made of glass fibre bonded with epoxy resin for applications in load bearing timber structures.

Testing samples is an alternative way to recreate a joint within a timber structure without having to test the whole structure. Testing joints is more practical and it reduces secondary effects or problems which tend to occur in the testing of large frames, such as lateral stability, support conditions, member buckling etc. In full frame tests, the joints do not always behave as they would if they were 'isolated' from the frame. In fact it is difficult to recreate a true in-situ conditions for a full structure, such as providing a timber truss with adequate lateral restraints of the rafters (normally due to the purlins) without altering the loading conditions.

Wood/glass/epoxy joints in a frame would act in a way similar to mechanically fastened joints. They would be subject to axial forces, shear forces and bending moments. In trussed frames, joints are usually assumed as pinned joints. In fact, the frame is usually designed as a pinned frame and bending moments are only taken into account in the member design. The joints are assumed to be free to rotate, but in reality they can only rotate to a nominal degree, which depends on the type of connection, the number of fasteners, etc. However a very small amount of rotation would release partially a joint from any bending moment. This explains why it is so difficult to design a fully rigid joint, which will always have some degree of rotation and then will never attract the full bending moment it has been designed for.

When 'isolated' joints are tested, bending moments can be developed from eccentric axial force (i.e. axial force not distributed uniformly through the member cross-section), but such bending would remain small in comparison to the axial force if appropriate attention is taken to minimise that effect.

In that instance, wood/glass/epoxy joints needed to be tested under axial loading. Tests in flexion would be unrepresentative of their actual behaviour within a frame. Considerations were taken to minimise any bending moment effects due to axial force eccentricity. Axial loading meant the joints could be tested in tension as well as in compression.

The tension test means to pull one of the connected members from the other, in which the composite bond will resist, stretch under load until it reaches some plasticity and then fail.

In compression tests, one of the connected members must be 'pushed' against the other, in which the composite will have no immediate effect. The compressive stress will be transferred directly by the bearing of the timber members end to the other, which means that the compression capacity will be limited to the compression resistance of the timber. The composite will act in flexion by resisting the buckling of the joint, with in-plane shear stresses if the connected members have different orientations.

The structural role of the composite is more complex in a joint tested in compression because the composite will be subject to stresses resulting from a combination of compression, shear and possibly bending.

As part of the preliminary tests, one sample made with a straight configuration (i.e. connected members with same orientation) was tested in compression. The

sample failed after the timber started splitting in the joint area. As the sample was buckling, one of the composite layers partially broke in tension. The test was stopped at this stage before the complete failure occurred. However no measurements such as the failure load were recorded because this test was carried out at an early stage of the research, simply to observe and understand the joint behaviour.

The compression test was then excluded from the testing programme because of the complexity of the joint behaviour and for the reasons previously described.

As a result, the testing programme was then concentrated on tension tests exclusively. The main objective was to analyse the effect of glass fibre orientation with the wood grain orientation on timber samples tested in tension.

The measurements to be carried out were:

- The load-slip capacity and maximum load resulting from tension test at various angles between the direction of the applied force and glass fibre orientation (α) and the direction of the applied force and the grain of the timber (β),
- Strain values throughout the composite layers at specific locations to identify how the stresses are distributed within the composite.

The types of tests were selected among a large number of test options to reduce the experiments to a feasible programme. Each test had samples made with uniaxial and biaxial glass fibre. They are presented and developed in the following sections.

4.3.2.2. Tension capacity test with load parallel to the grain

This test was carried out with samples loaded in the timber grain direction, which means the samples were made of two pieces of timber connected with butt ends. This test is also called straight pullout test due to the straight configuration of the specimen as shown in figure 4.9.

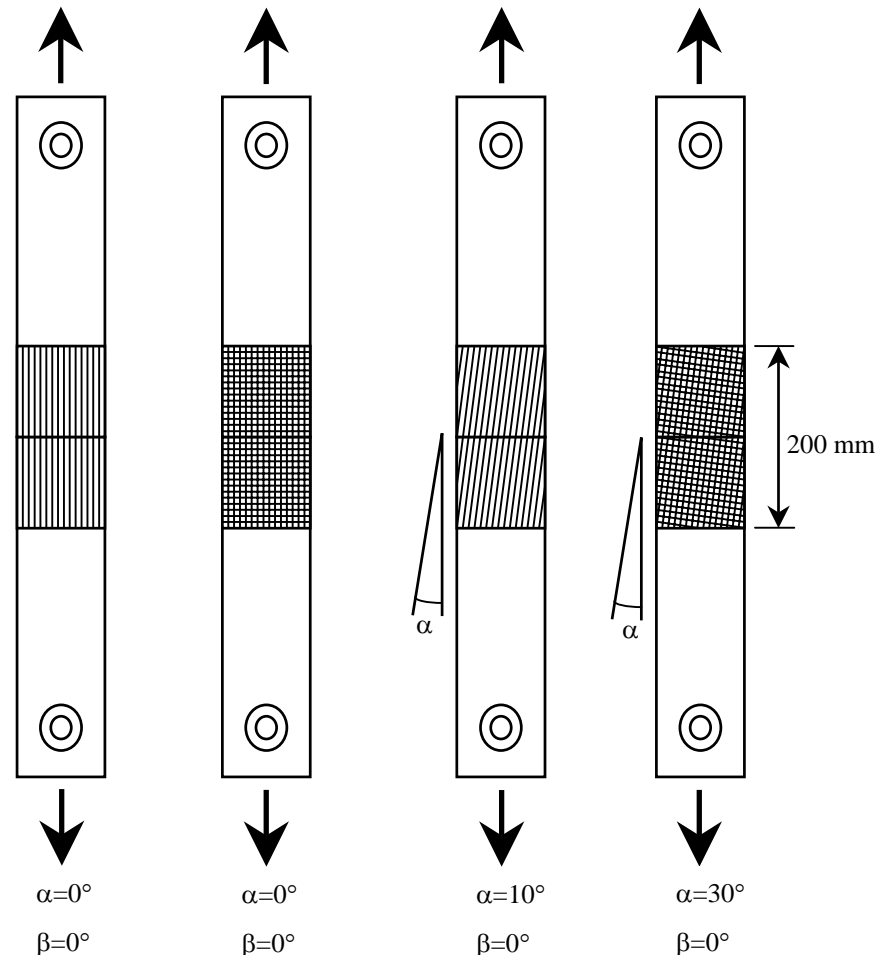


Figure 4.9 Sample configurations for tension test with load parallel to the grain.

Four different types of samples were tested in the tension with load parallel to the grain:

- **Tension Parallel with Uniaxial glass fibre UT-E500**, where the load was applied in the glass fibre direction ($\alpha = 0^\circ$) and in the same direction than the timber grain ($\beta = 0^\circ$). The sample type was classified as **TPU00**.

- **Tension Parallel with Biaxial** glass fibre XE450, where the load was applied in the glass fibre direction ($\alpha = 0^\circ$) and in the same direction than the timber grain ($\beta = 0^\circ$). The sample type was classified as **TPB00**.
- **Tension Parallel with Uniaxial** glass fibre UT-E500, where the glass fibres were orientated 10° from the load direction ($\alpha = 10^\circ$), but the load was parallel to the timber grain ($\beta = 0^\circ$). This 10° angle represented a possible misalignment of the fibres with the timber grain and the load direction. The aim of this test was to assess the implication of fibre misalignment for the joint strength. The sample type was classified as **TPU10**.
- **Tension Parallel with Biaxial** glass fibre XE450, where the glass fibres were orientated 30° from the load direction ($\alpha = 30^\circ$), but the load was parallel to the timber grain ($\beta = 0^\circ$). With the biaxial glass fibre, the properties were the same in orthogonal directions, therefore $\alpha = 0^\circ$ and $\alpha = 90^\circ$ show exactly the same configuration. For $0^\circ < \alpha < 45^\circ$, the sample had different properties but for $\alpha > 45^\circ$, the same properties applied by orthogonal symmetry. For example, with the selected angle of $\alpha = 30^\circ$, it was the same configuration for $\alpha = 60^\circ$. Combined with the test where $\alpha = 0^\circ$, this value of 30° allowed the assessment of four different configurations, $\alpha = 0, 30, 60$ and 90° with only two different sample tested. The sample type was classified as **TPB30**.

Measurements were carried out on these samples during test. The testing rig and the equipment used is explained and developed in detail further on in this chapter, but it is relevant in this section to identify which type of measurements were carried out during those tests.

As the load applied to the sample was recorded, displacements or strains at specific locations on the joint were measured. Two different types of devices were used to carry out those measurements:

- Linear Voltage Displacement Transducers or LVDTs were glued (with quick setting epoxy resin) onto the timber at various locations, using PVC and steel brackets fabricated for this purpose. These transducers measured displacements between the brackets located on either piece of timber. They measured the displacement around the gap position (small side LVDTs) and were fixed in a symmetrical arrangement to check any misalignment of the sample. For the

tension test with load parallel to the grain, the LVDTs were located as shown in figure 4.10.

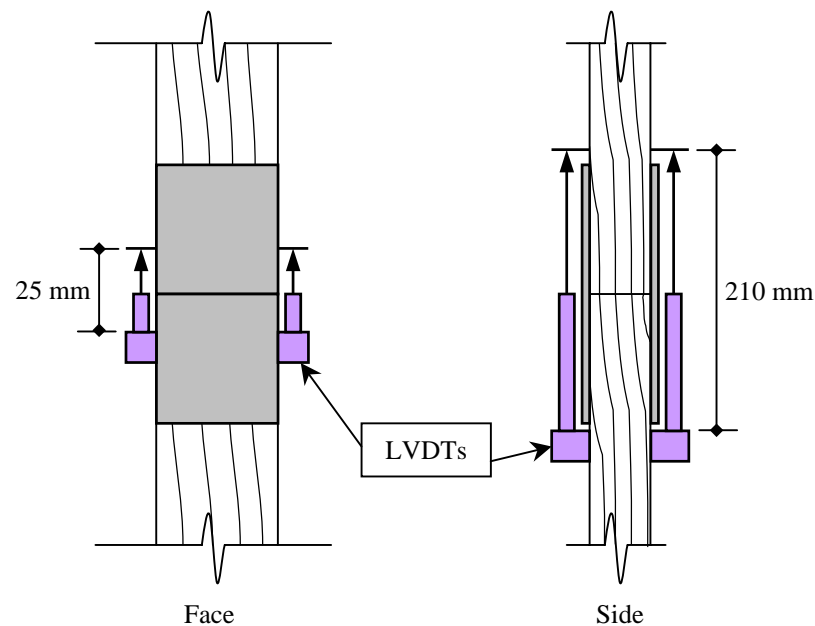


Figure 4.10 Positions of LVDTs on samples for tension test with load parallel to the grain.

Two different types of LVDTs were used, one type having a small configuration with short travelling distance (used on the sides) and another type only used to check samples misalignment having a long shape with longer travelling distance (used on the faces). The full technical information about these LVDTs is given in the section about experimental equipment.

- The other type of device used to measure displacement was the electrical resistance strain gauge. The strain gauge is a small and thin resistance made of thin wires, which measures strain directly when cemented to the specimen. Strain gauges were used only to measure strains in the glass fibre/epoxy layer. They were embedded directly at the surface of the composite matrix in the epoxy, with a thin coat added on top of it, while the samples were fabricated. Therefore the gauges were part of the composite as their cement was the matrix's epoxy. The gauges were positioned in a similar arrangement on each side of the sample. Gauge locations on samples for tension test with load parallel to the grain are as shown in figure 4.11.

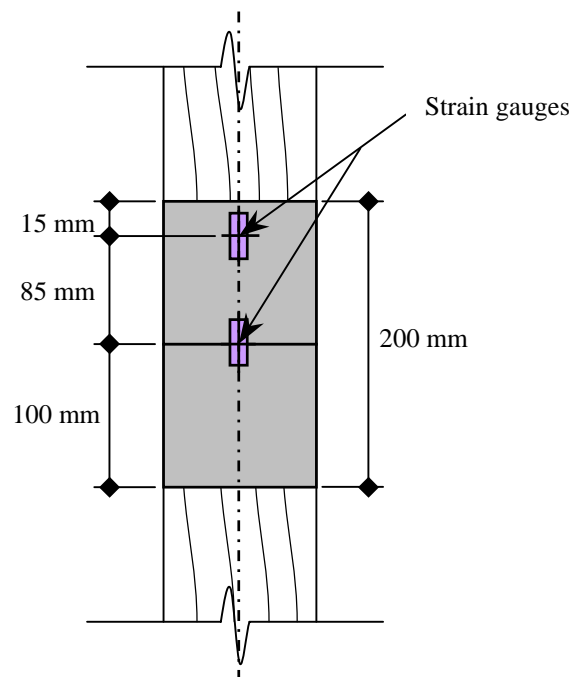


Figure 4.11 Strain gauge locations on samples for tension test with load parallel to the grain.

Strain gauges were not utilised on all samples nor all types of test but only some of them, as the LVDTs were used on all of them with the configuration presented previously. The number of samples tested with strain gauges is described in the table 4.1 further on in this chapter.

4.3.2.3. Tension capacity test with load perpendicular to the grain

This test was carried out with samples made of two timber pieces connected perpendicularly, which means one piece had the load applied perpendicular to its grain direction. The sample configurations are shown in figure 4.12.

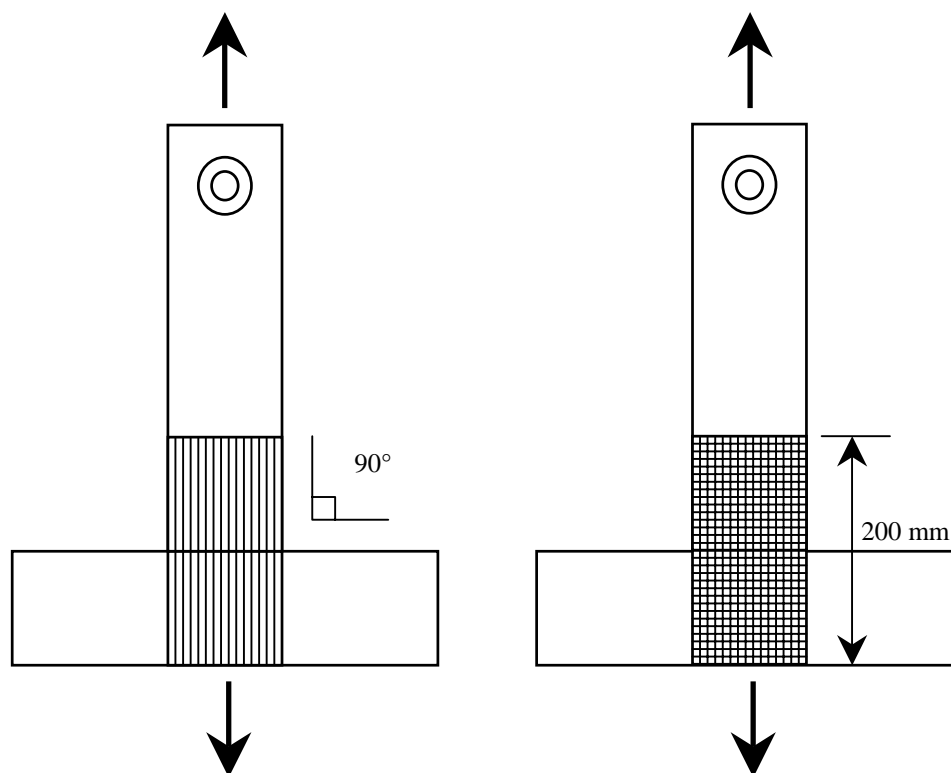


Figure 4.12 Sample configurations for tension test with load perpendicular to the grain.

Two different types of samples were tested in the tension test with load perpendicular to the grain:

- Tension Not parallel with Uniaxial glass fibre UT-E500, where the load was applied in the glass fibre direction ($\alpha = 0^\circ$) but perpendicular to the grain ($\beta = 90^\circ$) of the timber piece considered (Bottom piece in figure 4.12). The sample type was classified as **TNU90**.
- Tension Not parallel with Biaxial glass fibre XE450, where the load was applied in the glass fibre direction ($\alpha = 0^\circ$) but perpendicular to the grain ($\beta = 90^\circ$). The sample type was classified as **TNB90**.

Measurements were carried out on these samples during tests using LVDTs and strain gauges. The LVDTs were used to measure the displacement around the gap

between the two timber pieces and were located according to the sample configuration shown in figure 4.13.

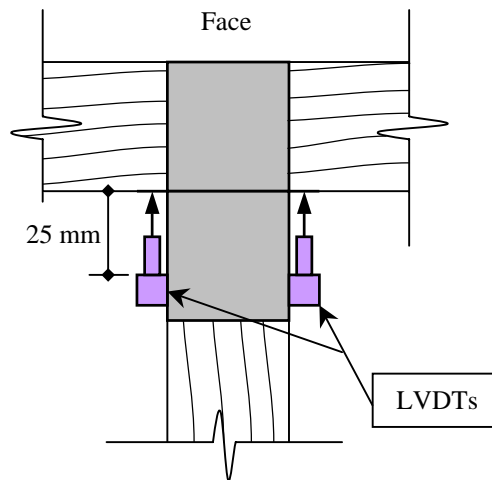


Figure 4.13 Positions of LVDTs on samples for tension test with load perpendicular to the grain.

Only two small LVDTs could be used for this test on the sample sides because the loading rig in which the sample was held did not have sufficient clearance space to accommodate any LVDTs on the faces.

Strain gauges were used on both faces of the sample and embedded in the composite layer as explained previously. Two strain gauges were placed on each face to measure the strain of the composite layer in the zone bonded perpendicular to the grain. They were positioned as shown in figure 4.14.

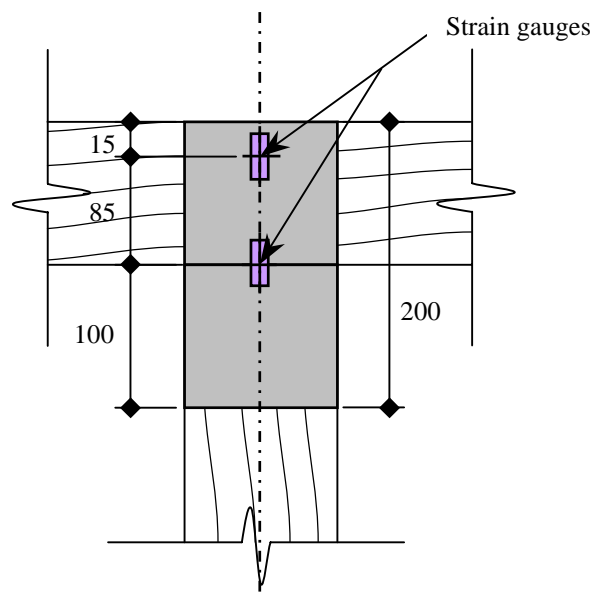


Figure 4.14 Strain gauge locations on samples for tension test with load perpendicular to the grain.

4.3.2.4. Tension capacity test with load at 60° angle to the grain

This test was carried out with samples made of two timber pieces connected together with an angle of 60°. This means one of the timber pieces had the load applied in its grain direction and transferred the load through the joint to the other piece with an angle of 60°. The sample configurations are shown in figure 4.15.

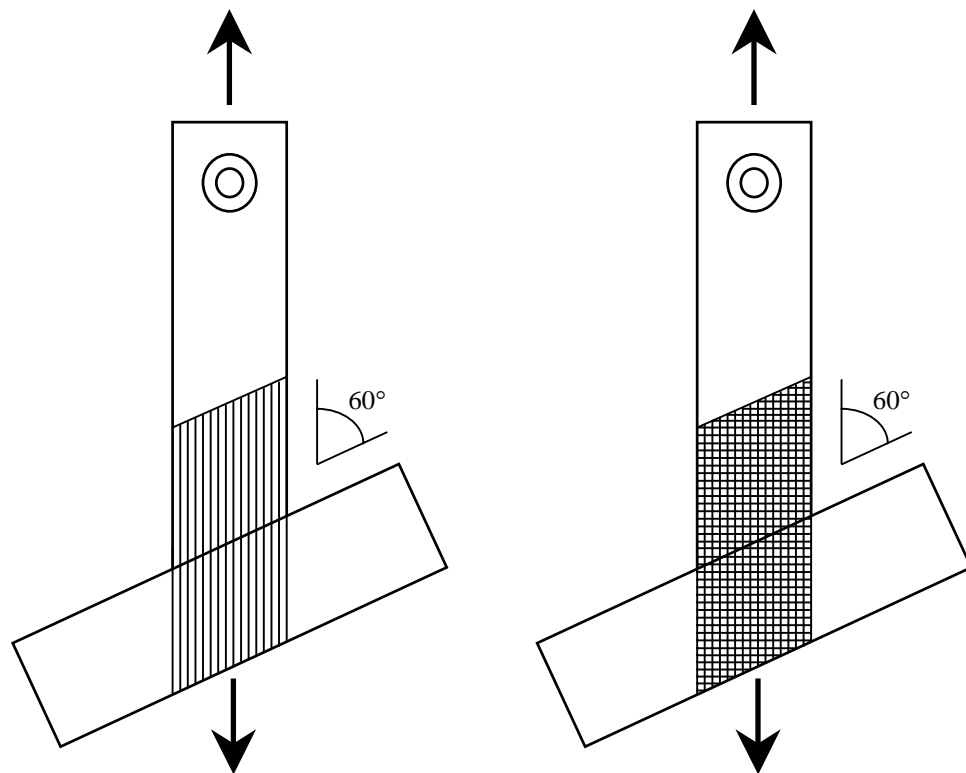


Figure 4.15 Sample configurations for tension test with load at 60° angle to the grain.

Two different types of samples were tested in tension with the load applied at an angle of 60° to the grain:

- **Tension Not parallel with Uniaxial glass fibre UT-E500**, where the load was applied in the glass fibre direction ($\alpha = 0^\circ$) but with an angle of 60° to the grain ($\beta = 60^\circ$) of the timber piece considered (Bottom piece in figure 4.15). The sample type was classified as **TNU60**.
- **Tension Not parallel with Biaxial glass fibre XE450**, where the load was applied in the glass fibre direction ($\alpha = 0^\circ$) but with an angle of 60° to the grain ($\beta = 60^\circ$). The sample type was classified as **TNB60**.

Measurements were carried out on these samples during test using LVDTs and strain gauges. The LVDTs were used to measure the displacement at the gap between the two timber pieces and were located according to the sample configuration shown in figure 4.16.

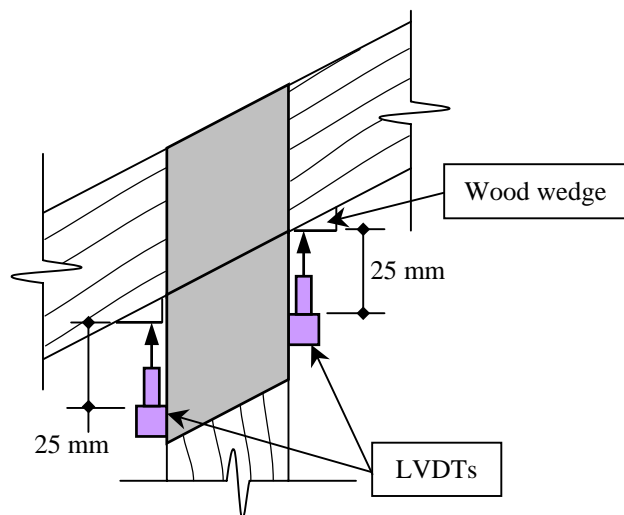


Figure 4.16 Positions of LVDTs on samples for tension test with load at 60° angle to the grain.

Only two small LVDTs were used for this test on the sample sides because the loading rig in which the sample was held did not have sufficient clearance space to accommodate any LVDTs on the faces. Timber wedges were fabricated to provide the flat contact surface perpendicular to the LVDT's end, and allow a more accurate reading of displacement. Those wedges were also bonded on the timber with quick setting epoxy resin.

Strain gauges were used on both faces of the sample and embedded in the composite layer as explained previously. Two strain gauges and one strain rosette were placed on each face to measure the strain of the composite layer in the zone bonded at an angle of 60° to the grain. They were located as shown in figure 4.17.

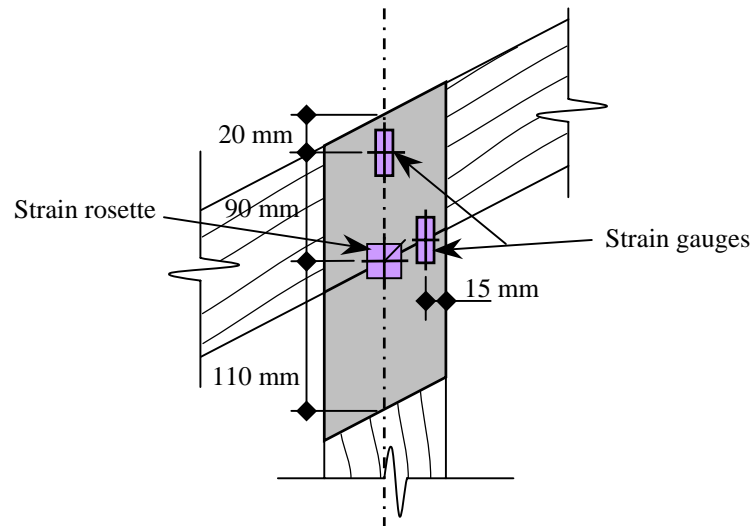


Figure 4.17 Strain gauge locations on samples for tension test with load at 60° angle to the grain.

The strain rosette is a group of three strain gauges arranged in a specified pattern. For this type of strain rosette, the axes of three strain gauges are arranged at an angle of 45°.

They were used on these samples to measure the transversal strain and to identify the state of strain at this location, in the plane of composite surface.

4.3.2.5. Tension capacity test with load at 30° angle to the grain

This test was carried out with samples made of two timber pieces connected together with an angle of 30°. This means one of the timber pieces had the load applied in its grain direction and transferred the load through the joint to the other piece with an angle of 30°. The sample configurations are shown in figure 4.18.

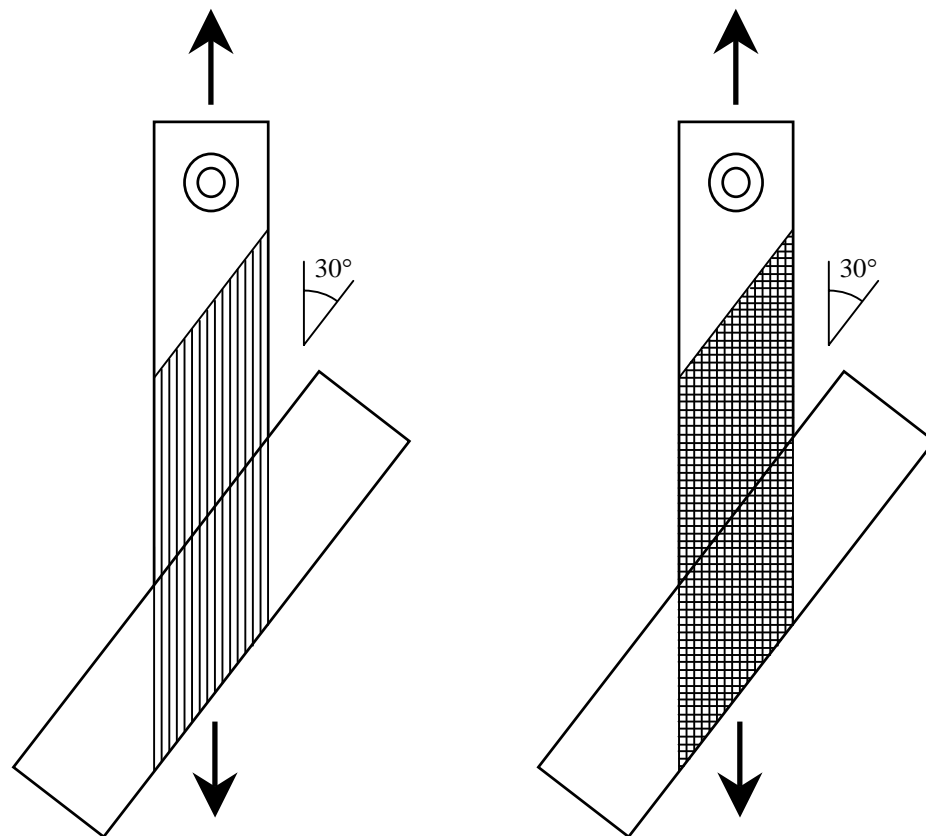


Figure 4.18 Sample configurations for tension test with load at 30° angle to the grain.

Two different types of samples were tested in tension with the load applied at an angle of 30° to the grain:

- Tension Not parallel with Uniaxial glass fibre UT-E500, where the load was applied in the glass fibre direction ($\alpha = 0^\circ$) but with an angle of 30° to the grain ($\beta = 30^\circ$) of the timber piece considered (Bottom piece in figure 4.18). The sample type was classified as **TNU30**.

- **Tension Not parallel with Biaxial glass fibre XE450**, where the load was applied in the glass fibre direction ($\alpha = 0^\circ$) but with an angle of 30° to the grain ($\beta = 30^\circ$). The sample type was classified as **TNB30**.

Measurements were carried out on these samples during test using LVDTs and strain gauges. The LVDTs were used to measure the displacement at the gap between the two timber pieces and were located according to the sample configuration shown in figure 4.19.

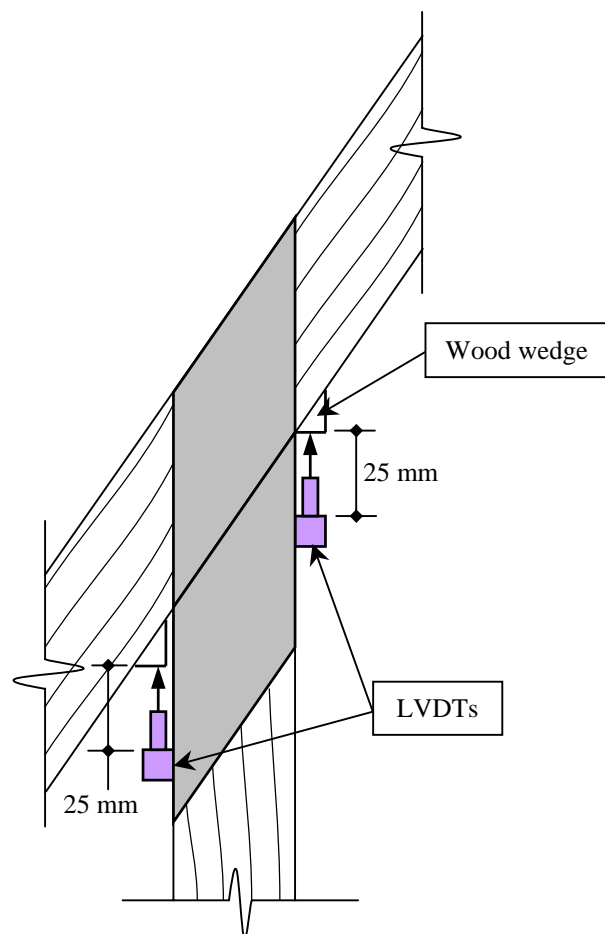


Figure 4.19 Position of LVDTs on samples for tension test with load at 30° angle to the grain.

Also for this test, only two small LVDTs were used on the sample sides. Timber wedges were fabricated to provide the flat contact surface perpendicular to the LVDT's end as explained previously. Those wedges were also bonded onto the timber with quick setting epoxy resin.

Strain gauges were used on both faces of the sample and embedded in the composite layer as explained previously. Two strain gauges and one strain rosette were placed on each face to measure the strain of the composite layer in the zone bonded at an angle of 30° to the grain. They were located as shown in figure 4.20.

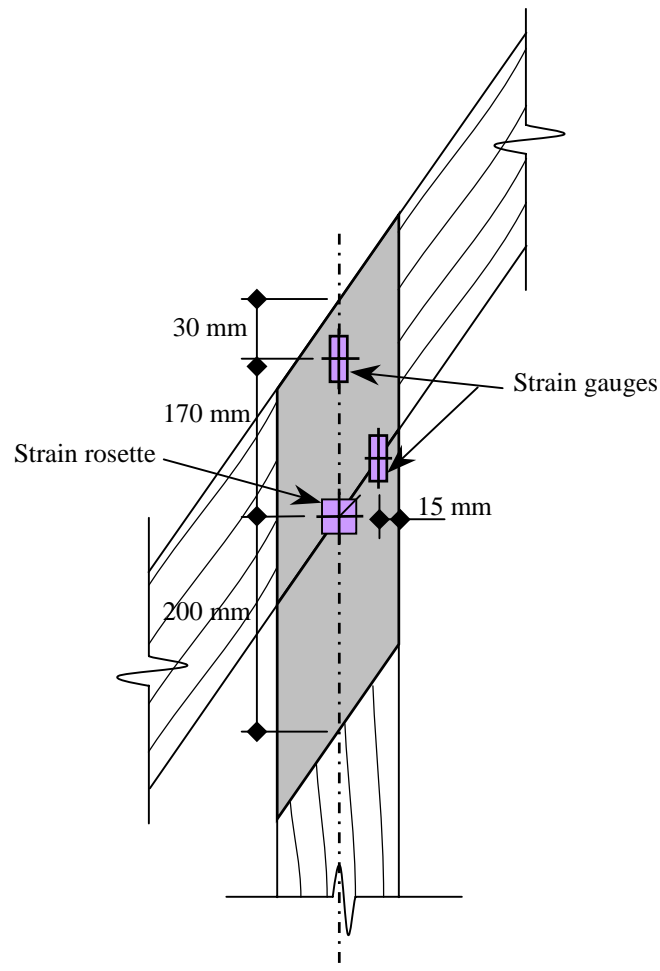


Figure 4.20 Strain gauge locations on samples for tension test with load at 30° angle to the grain.

As previous tests, the strain rosettes were used on these samples to measure the transversal strain and to identify the state of strain at this location, in the plane of composite surface.

Finally there were four different types of test, which were carried out on wood/glass/epoxy joints. All the samples tested were made of two timber pieces connected together. Therefore only two-member joints were considered in this experimental programme. Joints made of three or more members are more complicated to test because sophisticated loading rig is required to ensure that:

- The sample is tested with realistic loading conditions.
- The loads are applied axially to each member.

But in theory a multi-member joint is a combination of several two-member joints. It could be modelled as a superposition of two-member joints. But this would be regardless of the fact that the same composite layer connects all the members together. The single layer of composite would be subject to a large number of stresses, which would complicate significantly the joint behaviour and analysis.

Multi-member joints made of wood/glass/epoxy are beyond the scope of this research and could be part of further research on this topic.

Several parameters still needed to be considered for the tests carried out, such as the number of samples tested for each series of test.

4.3.3. Number of samples tested

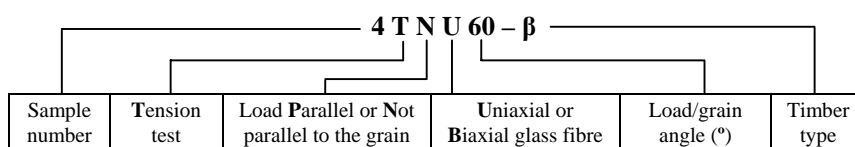
Codes of practice BS 6948: 1989 “Methods of test for mechanically fastened joints in timber and wood-based materials” gives minimum number of samples to be tested to obtain basic strength data of a particular fastener and they are:

- Not less than 15 specimens of a particular type to be tested for lateral strength.
- Not less than 20 specimens of a particular type for withdrawal and pull-through strength.

The large number of specimens required by the code is evidence of the wide variations observed with timber materials. But it is assumed through the standard, that the results obtained from those tests will be used for design purposes. It seemed difficult to carry out such series of testing for each type of tests. It was impractical in terms of costs, materials required, experimental time span, etc. Further more, the aim of this research was not orientated to design at this stage, but only to understand the structural behaviour of wood/glass/epoxy joint.

In this experimental programme, minimums of six specimens were tested in each series. It was insufficient to draw statistics out of the results, but according to the wide range of varying parameters and the limited knowledge of wood/glass/epoxy joints, it provided adequate information for a preliminary analysis. Then with minimums of six specimens per type of test, all samples were tested using Linear Voltage Differential Transducers (LVDTs) to record displacements.

Strain gauges were only provided on some of them in addition to the LVDTs because of their costs and the fact that strain gauges are not reusable. The numbers of specimens tested in respect of the type of test and measurement devices are summarised in the table 4.1. The sample symbol definition is given as follow:



Sample symbol definition.

Type of test	Number of samples with LVDTs	Number of samples with LVDTs + Strain Gauges	Total number of samples
TPU00	6	2	8
TPB00	6	2	8
TPU10	6	0	6
TPB30	6	0	6
TPU90	5	1	6
TPB90	5	1	6
TPU60	5	1	6
TPB60	5	1	6
TPU30	5	1	6
TPB30	5	1	6
Total	54	10	64

Table 4.1 Summary table of wood/glass/epoxy joints test programme.

A total of 64 wood/glass/epoxy joints samples were tested. Strain gauges were not used on test TNU10 and TNB30 because the fibres were not orientated in both load and timber grain directions. Therefore the strain recorded by the gauges would have been a combination of longitudinal, transversal and in-plane shear strains, which could not be dissociated.

At least one sample was tested with strain gauges for all other types of test. On TPU00 and TPB00 tests, two samples were tested with strain gauges for the following reasons:

- The accuracy of the measurements could be compared with two samples having the same configuration.
- TPU00 and TPB00 were the most reliable test types to carry out in terms of accessibility of samples. Misalignment could be checked in both axes (four LVDTs were fixed on the sample) therefore secondary effects were minimised.

All these tests were carried out using laboratory equipment, which is described in the following section.

4.3.4. Testing equipment (LVDT, Translog 500, tension rig, frame)

The tests of wood/glass/epoxy joints were performed on a purpose-built loading rig. This rig was made of a substantial steel frame positioned on the strong floor area of the Structures Laboratory. The load was applied with a hydraulic jack located on top of the steel frame. The sample was connected between a pair of 17 mm thick steel side plates at top and bottom of the rig, with 20 mm diameter bolts and shear plate connectors as explained previously in this chapter. The bottom plates were connected with a partially pinned system to a baseplate bolted to the strong floor. The top plates were connected with a fully pinned system bolted to the threaded end of a 24 mm diameter tie rod. The other end of the tie was connected to the jack at the top of the rig. The jack needed to be loaded manually to apply the load with accuracy. The jack used has a capacity of 300 kN in tension, which was more than required for the testing of wood/glass/epoxy joints. Readings of the load were given in tenth of a kilo Newton (0.1 kN). Figure 4.21 shows the rig configuration for straight pullout tests.

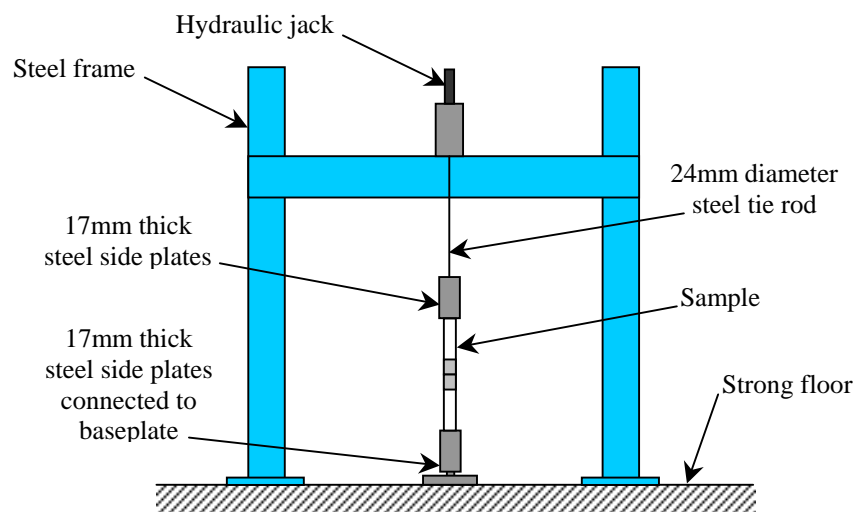


Figure 4.21 Rig configuration for straight pullout tests.

Figure 4.22 shows one of the TPB00 samples positioned in the rig with the LVDTs and brackets fixed around the joint's gap. This sample was ready to be tested.



Figure 4.22 TPB00 sample ready for straight pullout test.

A different rig configuration was used for the series of tests with load not parallel to the grain. An additional steel frame was required to hold the inclined timber piece. This frame had to be free to rotate in respect of the load direction, to allow axial loading of the sample. As explained before, the testing of wood/glass/epoxy joints was based on similarities with punched metal plate joints. There were no codes of practice specifying the testing methods of punched metal plate fasteners at the time, but only a draft standard available for public comments. This draft named prEN 1075: 1997 “Timber structures - Test methods - Joints made of punched metal plate fasteners” proposed a loading arrangement for the testing of punched metal plates with load not parallel to the grain. The steel frame used for the testing of wood/glass/epoxy joints with load not parallel to the grain was based on the one suggested in prEN 1075 as shown in figure 4.23.

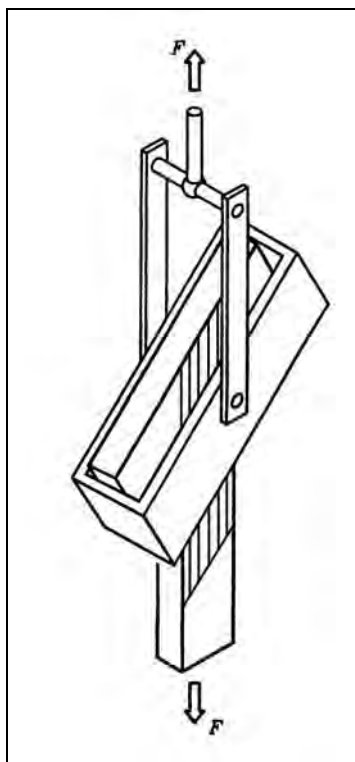


Figure 4.23 Loading arrangement for tension test with load not parallel to the grain.

The frame was made of a steel box, hanging from two steel arms connected to either side of the box with one bolt. Figure 4.24 shows sections and elevations of the frame.

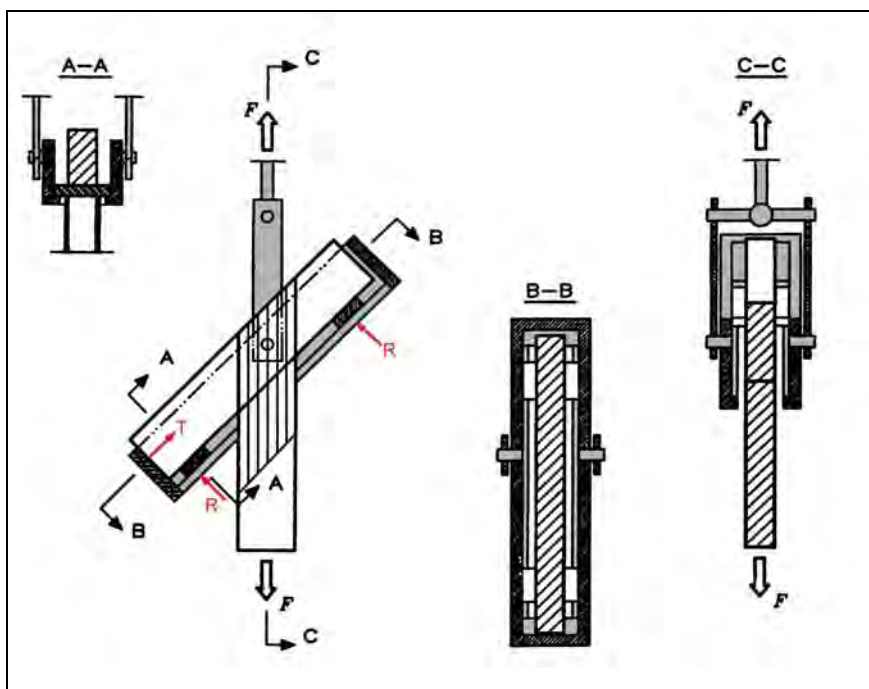


Figure 4.24 Sample arrangement within the steel box.

The bolts were not tightened and were located on the same axes to allow the box to rotate. M20 grade 8.8 bolts were used at top and bottom of the arms. The frame was designed to resist a tension force of 100 kN.

The sample was placed inside the steel box, and the inclined timber piece was supported at equal distance to the bolt centreline with hardwood plates. The internal forces in the box are the two reactions from the hardwood supports (shown as R in figure 4.24) and the reaction from the steel box side (shown as T in figure 4.24). With F as the applied tension force, the equilibrium of the forces gives for the reactions:

$$R = \frac{F \sin \beta}{2} \quad \text{and} \quad T = F \cos \beta \quad (4.1)$$

Where β is the angle between the load direction and the timber grain.

There was a continuous edge around the bottom of the steel box to support the hardwood plates (see section A-A in figure 4.24). The supports were made of hardwood and not steel to minimise the local deformation in the inclined timber piece. To ensure that the hardwood supports remained at their initial location during the test, they were drilled at their centre. A nail fixed to the underside of the inclined timber piece was positioned into that hole to keep the sample in the centreline of the steel box and also to hold the support in position during the test. While the tension was applied to the sample, the inclined timber piece deflected. To reduce this sagging effect, which creates some eccentricity in the load direction, the hardwood supports were positioned on each side of the joint, as closely as possible. If any eccentricity of load was developed in the joint, it produced bending moments. In that case, the joint was not tested in strictly pure tension. Some small bending moments were measured on the samples, due to minor eccentricities. These bending moments were so small compared to the tension force applied to the sample that they were considered as negligible.

An example of in-plane and out-of-plane bending moment calculations using LVDTs readings is presented in Appendix C.

The figure 4.25 shows the rig configuration for tension test with load not parallel to the grain.

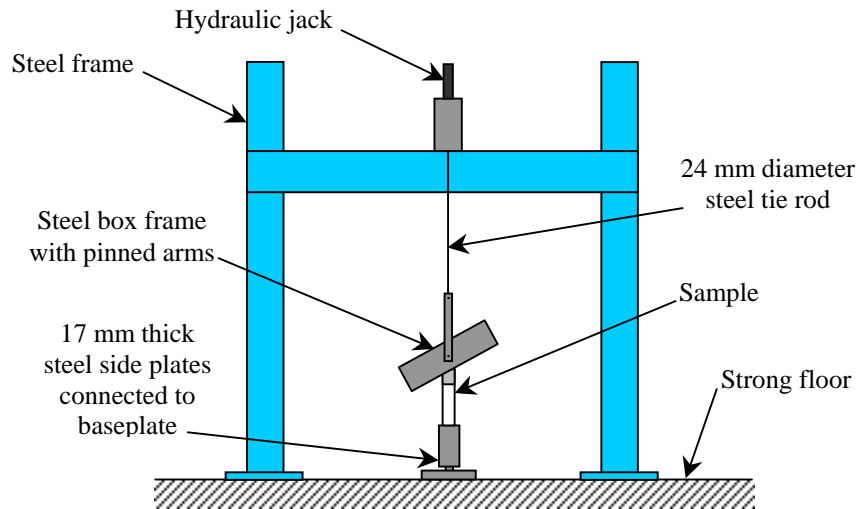


Figure 4.25 Rig configuration for tension test with load not parallel to the grain.

The figure 4.26 shows a sample ready to be placed within the steel box. In this picture, some steel plates were used on top of the hardwood supports to adjust the height of the sample inside the box. They were placed the wrong way around and should have been located underneath the hardwood plate.



Figure 4.26 Sample configuration when positioned within the steel box.

Figure 4.26 also shows the set of brackets used to hold the LVDTs in position to measure displacements. A red circle is also visible on the glass fibre, almost in the middle of the timber piece. This circle was drawn onto the timber before the sample

fabrication. It was part of the adjustments carried out prior to the tests to make sure the sample is on the centreline of the steel box. These adjustments are developed in the following section.

The following pictures in figure 4.27 and 4.28 show the configuration for a tension test with load not parallel to the grain at 90° and 60° angles.



Figure 4.27 Sample configuration for tension test with load at 90° to the grain.



Figure 4.28 Sample configuration for tension test with load at 60° to the grain.

It is clearly visible that only two LVDTs were used on those tests and they were placed on the sides of the timber piece. LVDTs as well as strain gauges were connected to a High Capacity Data Acquisition system. This system named E500 Translog Base System 1 that includes conditioning module housing units and controller/interface module, was used with a software compatible PC. The modules connected to the LVDTs or strain gauges, which were different, had 8 channels capacity. The E500 Translog Base System 1 translates the electric signals of both the LVDTs and strain gauges in displacement and micro strains respectively. The software used converts and displays those values in spreadsheets format. However the system did not record readings at regular intervals of load increments, because

the loading equipment was not linked to this data acquisition system. This procedure was done manually to obtain the displacements and strains for the appropriate load.

There were two different types of LVDTs used for the test. Both LVDTs were in fact spring return armature transducers. They had a guided armature, which was spring loaded. The spring pushed the armature to its outer end stop. The end of the armature was fitted with a ball-ended probe. This type of armature configuration only required fixing at one end. That is why the LVDTs were fixed with a bracket system to be held on the sample and at the armature end, an angle bracket was glued on the sample to stop it.

The first type of LVDTs was an ACT1000A manufactured by RDP-Electronics, which is a large international company manufacturing a wide range of measuring equipment. The ACT1000A was a long LVDT, which was used on both faces of the sample, measuring the displacement between either ends of the composite strip. The ACT1000A had a travelling capacity of ± 25 mm from the electrical zero position, which meant a full travelling length of 50 mm. The percentage of error of full scale was around 0.5%, which corresponds to 0.125 mm over 25 mm travelling. The dimensions of the ACT1000A are as shown in figure 4.29, with $L = 161$ mm, $D1 = 20.6$ mm and $X = 63$ mm.

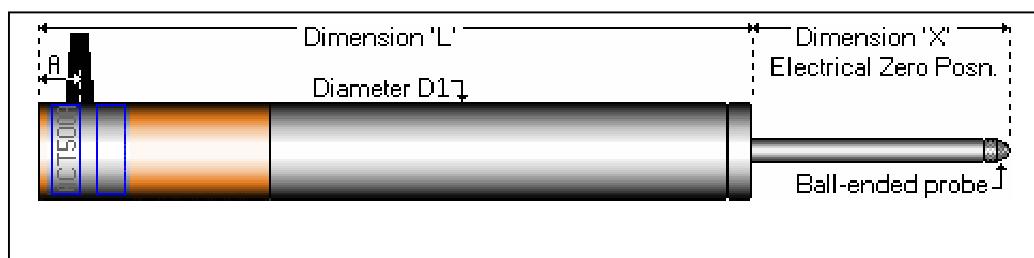


Figure 4.29 ACT1000A Spring Return LVDT Transducer configuration (picture from RDP Electronics web site).

The other type of LVDTs was a D5/300AG also manufactured by RDP-Electronics. The D5/300AG was a smaller LVDT, which was used on both sides of the sample, measuring the displacement at the gap between the timber pieces. The D5/300AG had a travelling capacity of ± 7.5 mm from the electrical zero position, which meant a full travelling length of 15 mm. The percentage of error of full scale was also around 0.5%, which corresponds to 0.0375 mm over 7.5 mm travelling. The dimensions of the D5/300AG are as shown in figure 4.30, with $L = 85$ mm, $D = 9.5$ mm and $X = 15.3$ mm.

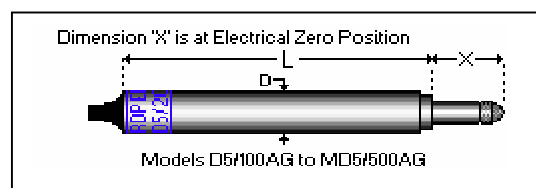


Figure 4.30 D5/300AG Spring Return LVDT Transducer configuration (picture from RDP Electronics web site).

Those two types of LVDTs were the only types used for the research. All of them were calibrated and checked before the beginning of the experiments.

Also an extended armature was fabricated to lengthen the D5/300AG LVDT, adding 40 mm to the X dimension. This extension was fixed to the threaded ends between the end of the armature and the ball-ended probe. It was used only for the TNU30 and TNB30 tests, to allow the LVDT fixed in the acute angle to reach in length the wood wedge bracket, without being in contact with the steel box frame.

Further testing equipment were used to determine the timber properties on small samples. This equipment is described in the section dealing with the timber properties testing.

4.3.5. Sample fabrication process

The fabrication of the samples was a long and carefully elaborated process, in which a large amount of time was spent. The fabrication was a repetitive procedure because it has to be done for each sample. Therefore the samples were fabricated in series corresponding to the type of test, which means for each type of test all the samples were fabricated at the same time. There were some advantages to fabricate the samples in this manner:

- It saved on the amount of resin, as it is difficult to estimate the quantity of resin required for a particular number of samples. There was always some resin left over, which could not be kept for further fabrication because it cured.
- It minimised the variation of moisture content in the glass fibre, which was cut from a large roll and for all the samples before the gluing process. Each strip of glass fibre was in the same conditions of temperature and humidity. However, these parameters did not have any significant effect on the composite strength.
- It minimised the variation in timber moisture content from one sample to another, for the particular type of test. The wood was preliminary conditioned before the sample fabrication, which took place in the wood workshop of the structures laboratory. There was not enough space available in the control temperature room to carry out the gluing process on the samples. The gluing was done in the labs, which meant the samples were not any longer in a controlled environment and this during the 48 hours required for complete drying of the resin. However the same temperature was maintained in the labs, but the relative humidity was not controlled. By fabricating all the samples of a particular type of test at the same time meant they were all in the same conditions of temperature and humidity.

Regarding the humidity in the laboratory, this had a minor effect on the samples compared to the heat produced by the thermosetting of the epoxy resin. Because it was not possible to re-condition the samples after fabrication, it was decided to measure the moisture content of the samples as soon as they were tested. On each tested sample, a small piece of wood was sawn very close to the jointing area. Its dimensions, wet weight and dry weight were recorded. The dry weight was measured after few days in the oven at a temperature of $103 \pm 2^{\circ}\text{C}$, in accordance with the relevant timber code of practice.

Prior to the sample fabrication, the selection of timber planks was carried out. This procedure is developed in the section about timber conditioning and grading. Timber planks were selected from the batch by visual inspection. The selected planks were conditioned for several weeks, then cut into smaller length corresponding to the full size of one sample and tested in three points bending for grading. Each plank was numbered to identify from which timber piece the plank came. At this stage the sample fabrication began.

The fabrication process was relatively similar for each type of test with some variations between straight and angle sample configuration. The procedure is developed for both configurations in the following sections.

4.3.5.1. Straight configuration

The straight configuration corresponded to the series of tests TPU00, TPB00, TPU10 and TPB30, where the samples were made of two pieces of timber connected with butt ends by the glass fibre/epoxy joint. The fabrication was a step-by-step procedure, which is described with pictures as follows:

- The numbered plank was sawn in two equal halves to have the two timber pieces, which will be jointed together to form the sample. The plank was cut in order to exclude any knot, wane or fissure in the jointing area. The bond needed to be free from defects of the wood, to ensure an optimum strength of the joint and to avoid any premature failure due to localised weakness of the wood.
- Using a template to ensure the timber piece fitted within the dimensions of the rig's steel plates, the positions of the connected bolt and shear connector were located on each timber piece. Widths of members were measured to ensure that the bolt was centred with the neutral axis drawn on the sample. The pieces were then drilled to accommodate the 20 mm diameter bolt. A particular drill was used for the circular ring into the timber surface, centred on the bolt's hole to accommodate the shear plate connectors, as shown in figure 4.31. The details of the shear connector have been previously developed in the section about joint geometry requirements (see figure 4.7 and 4.8).



Figure 4.31 Drilling of each timber piece end for shear plate connector.

- On the other butt end of the timber pieces, in the jointing area, a sheet of aluminium foil was positioned as shown in figure 4.32.

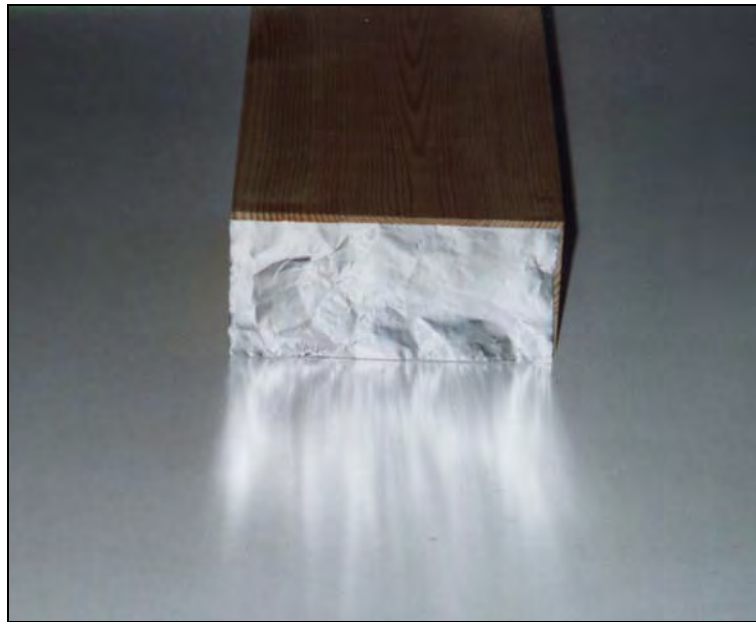


Figure 4.32 Aluminium foil positioned in the joint's gap.

The foil was clamped between the butt ends of the timber pieces to stop the epoxy resin bonding the butt ends together. During the bonding process, some epoxy resin could seep into the gap in an unknown proportion and this would strengthen the joint. Because the cross-sectional area of bonding in the gap could not be evaluated, this was a varying parameter of joint strength from one sample to another. Therefore the foil was placed to prevent butt ends bonding. If any resin seeped into the gap, it could bond the timber butts ends but with the aluminium foil in between and the resin did not bond to the aluminium foil.

- The two timber pieces were placed on a flat surface to optimise straightness of the sample. The timber pieces were jointed together by stapling their sides using paper staples, with the aluminium foil still positioned in the gap, as shown in figure 4.33. The staples were small and did not connect the timber pieces with strength, but they were sufficiently strong to hold the sample during the fabrication. The staples were removed afterwards. Then the dimensions of the bond were measured and drawn onto the timber surface to locate the exact position of the composite. If the fibre orientation was not parallel to the grain (i.e. TNU10 and TNB30 tests), lines were drawn showing the orientation in which the

fibres needed to be positioned. Because it was almost impossible to cut the glass fibres to the exact dimensions of the joint, strips of adhesive craft tape were wrapped along the end lines of the composite overlap. Because the craft tape had a sufficient bond capacity to stop the resin seeping underneath, the layer of glass fibre could be cut oversized and bonded onto the timber surface.

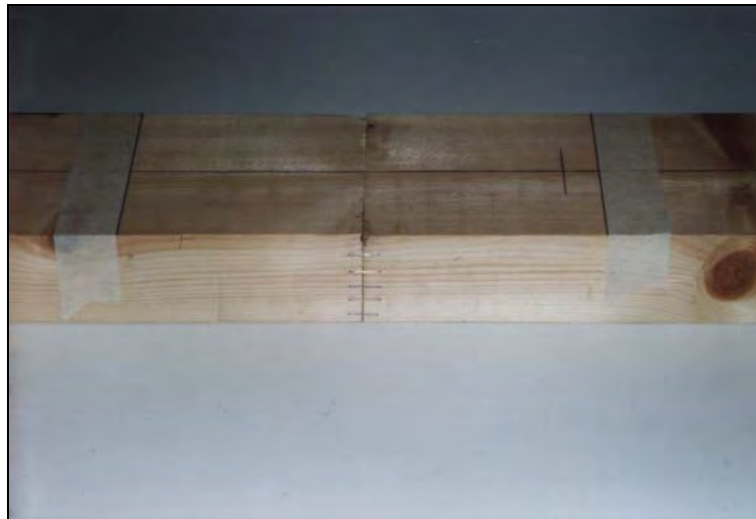


Figure 4.33 Staples and craft tapes are placed on the sample.

The excess of composite was bonded onto the craft tape and could be removed later on. The joint overlap was the same on each side of the sample, with a uniform length across the width of the member. At this stage, the whole sample weight was recorded before the gluing process.

- Once stapling, wrapping craft tape and dimensioning were done for both sides of the sample, the first layer of glass fibre was bonded onto the timber surface, as shown in figure 4.34. The layer was slightly oversized as explained before, and the lines drawn to indicate the glass fibre orientation were still visible (in figure 4.34, the lines are orientated at 30° from the grain). A roller with longitudinal grooves was used to spread the epoxy through the fabric, to obtain a good impregnation of the composite by removing the air trapped between the fibres and the excess of epoxy applied.



Figure 4.34 The first layer of glass fibre is bonded on the timber.

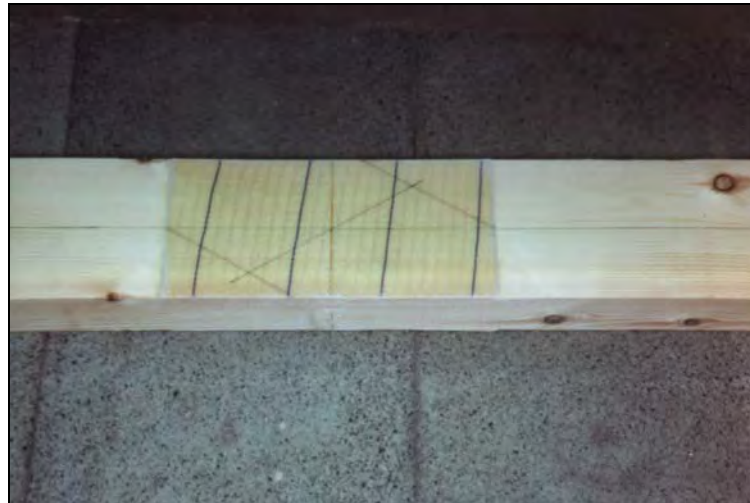
- After 12 hours, the first layer of composite was almost cured. The sample was then turned over and the other layer of glass fibre was bonded onto the timber surface, as shown in figure 4.35. The same procedure was used for the bonding.



Figure4.35 The layer of glass fibre is bonded onto the other side.

- The next day, after at least 24 hours, the composite was fully cured on both faces. The excess of composite around the joint could be removed. Using a handsaw with small teeth, the excess of composite was cut on the sides and along the end lines on the faces. The craft tapes were then removed, with the composite bonded on it. A clean uniform composite lap was obtained, as shown in figure 4.36. The side staples were also removed. A smooth file was carefully used to adjust the composite layer over the side edges, without damaging the composite. Then the

weight of the sample was recorded. As the weights of glass fibre, staples and craft tape were known, the difference of weights was the weight of resin used in the joint. The ratio of glass fibre to resin weights corresponds to the resin content of the joint. It was not the resin content of the composite because some of the resin may have been absorbed into the wood surface and may have seeped into the gap. Therefore the FVF of the composite was determined but with slight inaccuracy.



4.36 Sample with composite excess removed.

- The last step of the fabrication was the gluing and positioning of the brackets required on the four sides of the joint to hold the LVDTs and steel angles. A quick set epoxy resin was used for that purpose. The next set of brackets, on the next side of the sample could then be glued, as shown in figure 4.37.



Figure 4.37 Brackets are fixed onto the samples.

4.3.5.2. Angle configuration

The angle configuration corresponded to the series of tests TNU30, TNU60, TNU90, TNB30, TNB60 and TNB90, where the samples were made of two pieces of timber connected at an angle. The fabrication was a step-by-step procedure, which was very similar to the fabrication of straight configuration samples, as follows:

- The plank was sawn in two halves to have the two timber pieces, which were jointed together to form the sample. The plank was cut in order to exclude any defects in the jointing area. One of the timber pieces was cut at one end to form the required angle (lower member). The other piece was cut in length to fit within the steel box frame (upper member), as shown in figure 4.38.

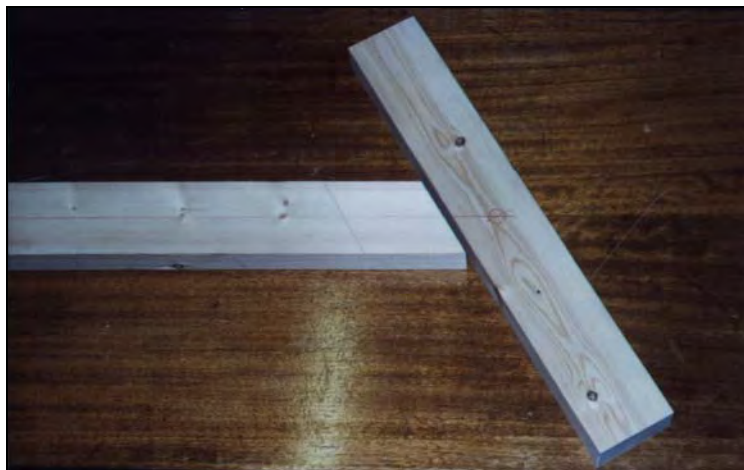


Figure 4.38 Angle sample is cut into shape.

- Using a template to ensure the lower timber piece will fit within the dimensions of the rig's steel plates, the positions of the connected bolt and shear connector were located. Widths of the members were measured to ensure that the bolt was centred with the neutral axis drawn on the sample. The upper timber piece was then placed into the steel box frame with the wood supports. The position of the steel box bolt was drawn on both faces of the timber member, to locate the neutral axis of loading. The lower piece could then be adjusted to have its neutral axis centred with the load, as shown in figure 4.39. A sheet of aluminium foil was also positioned between the timber pieces as explained before. To maintain the timber pieces along the same axis, nail staples were used to hold the timber pieces together, but only on the side forming an obtuse angle, as shown in figure 4.39.

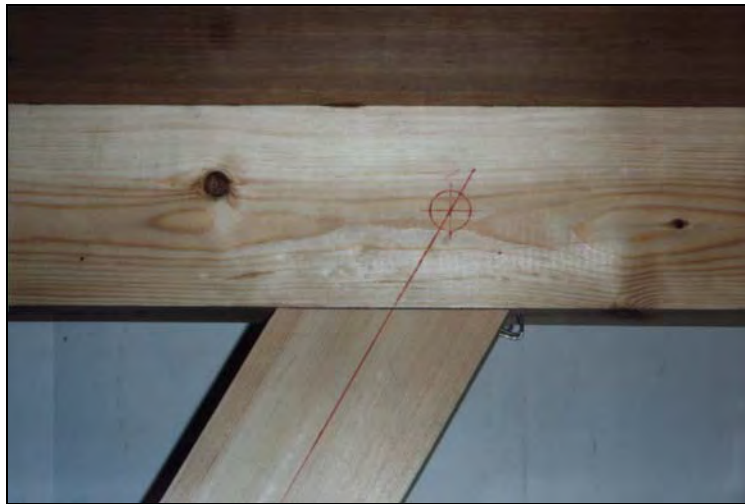


Figure 4.39 Neutral axes and bolt position are drawn on the timber surfaces.

- With nail staples only connected on one side, the members were not sufficiently restrained. Therefore, long strips of craft tape were wrapped on both faces of the samples, far enough from the jointing area, to hold the member together on the side of the acute angle, as shown in figure 4.40. For samples having a perpendicular configuration, nail staples were used on both sides. Then the dimensions of the bond were measured and drawn onto the timber surface to locate the exact position of the composite. Positions of strain gauges were also drawn on the timber of appropriate samples. Again strips of adhesive craft tape were wrapped along the end lines of the composite overlap for the same reasons explained previously. At this stage, the whole sample weight was recorded before the gluing process.



Figure 4.40 Craft tape is used to hold the sample together and to define the composite edges.

- The first layer of glass fibre was bonded onto the timber surface, as shown in figure 4.41. The layer was slightly oversized as explained before. After 12 hours when the first layer was almost cured, the second layer of glass fibre was bonded on the other face, with the same procedure.

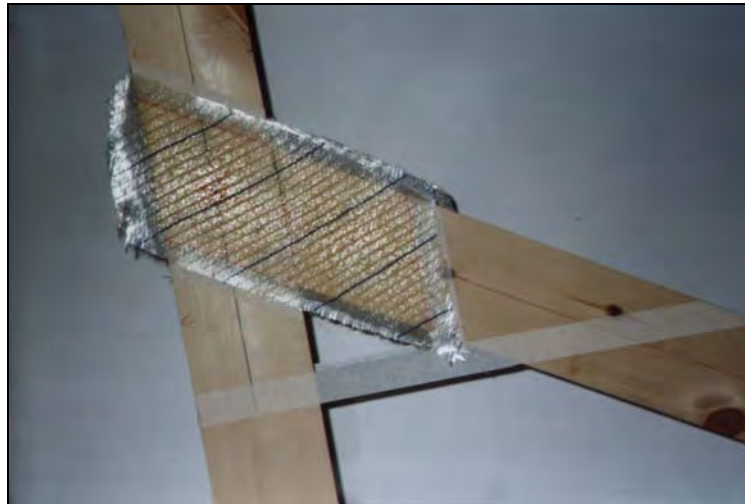


Figure 4.41 Layers of glass fibre are bonded on the sample.

- The next day, after at least 24 hours, the composite was fully cured on both faces. The excess of composite around the joint could be removed. Using a handsaw with small teeth, the excess of composite was cut on the sides and along the end lines on the faces, as shown in figure 4.42.

•



Figure 4.42 A handsaw is used to remove the excess of composite.

The craft tapes were then removed, with the composite bonded on it. A clean uniform composite lap was obtained, as shown in figure 4.43. Nail staples were also removed. A smooth file was carefully used to adjust the composite layer over the side edges, without damaging the composite. Then the weight of the sample was recorded. The resin content of the joint could be determined.

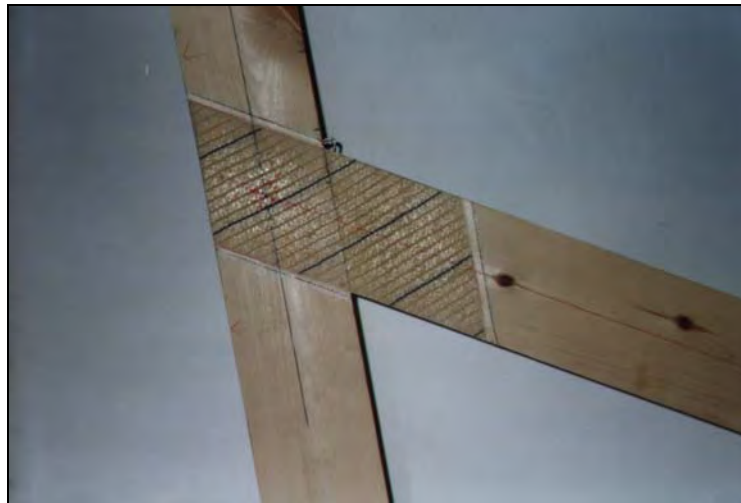


Figure 4.43 Sample with final composite layout.

- The last step of the fabrication was the gluing (with a quick set epoxy resin) and positioning of the brackets required on the two opposite short sides of the joint to hold the LVDTs and timber wedges as shown in figure 4.44.

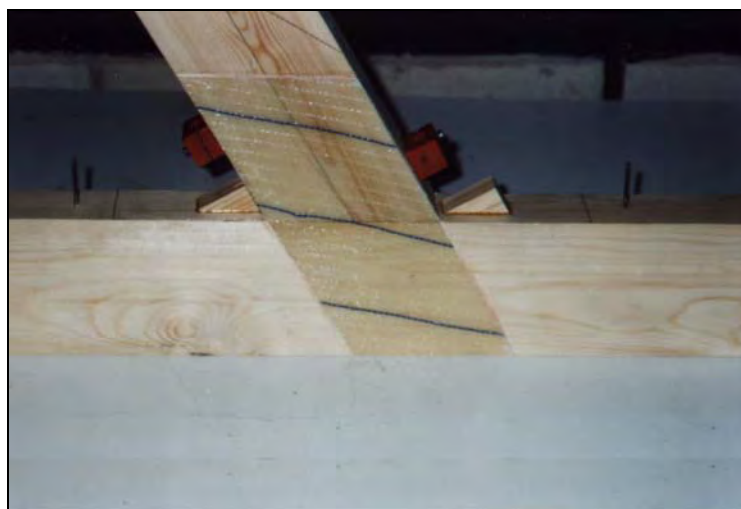


Figure 4.44 Brackets and timber wedges are glued on the sample sides.

4.3.5.3. Samples with strain gauges

It is necessary to identify the samples with strain gauges because their fabrication was slightly different. Initially, strain gauges were glued on the composite with a quick set epoxy. But the strain gauges needed to be fully embedded in the resin to work efficiently, therefore the layer of quick set epoxy had to be fairly thick, thickness relatively significant compared to the composite thickness. This extra amount of epoxy could affect the strength of the joint. For this reason, it was decided to embed to strain gauges directly in the composite during the gluing process.

The weight of the strain gauges is so small that it was ignored. However there were several advantages to place the gauges within the composite:

- The gauges were embedded in the same resin therefore the strain in the gauge was exactly the same than the strain in the composite at this particular location.
- The gauge was positioned onto the fibres and not on the surface of the composite therefore it could be assumed that the strain recorded by the gauge was the strain occurring within the composite, half way through its thickness.

Before the gluing process, the position of the strain gauges were measured and drawn on the sample. Once the first layer of glass fibre was bonded on the timber, the strain gauges were positioned on the wet resin, as shown in figure 4.45.

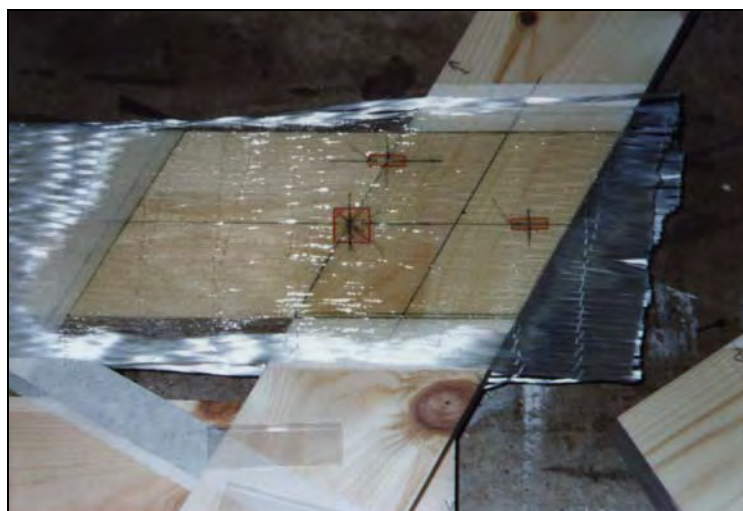


Figure 4.45 Strain gauges are carefully positioned onto the wet composite layer.

Using a small paintbrush, a thin layer of resin was laid onto the gauge surface. The two wires attached to the gauge were bent upwards to ensure they did not remain within the resin and did not touch each other. The same procedure was also used on other side. Once the composite was fully cured, care was taken to ensure the strain gauges wires were not damaged during the following steps of fabrication, particularly during the removal of composite excess. After the bracket fixing step, the sample was ready to be tested. But before, the strain gauges needed to be connected to the acquisition data system for strain recording. Some electric wires were then soldered to the gauges. To avoid any short circuit occurring in the gauge, the wires were soldered and isolated from each other using craft tape, as shown in figure 4.46. The cables were numbered to identify each strain gauge.



Figure 4.46 Strain gauges and soldered to cables and isolated with craft tape.

Finally the fabrication of wood/glass/epoxy joints was completed and the testing could be undertaken. The tests were carried out in series corresponding to the type of test. The samples were fabricated first and after a minimum of three days, they were tested.

The experiments were run in three parts. Part one was the straight pullout tests series, part two was the angle tests series because the rig needed a modified configuration using the steel box frame, as explained earlier on. The third part was the testing of all the samples having strain gauges because of the different data acquisition system requirements. The checks and preparations needed to set-up the samples only allowed one test to be carried out per day.

4.4. Timber properties testing

The properties of the timber are key parameters in the strength capacity of the joint. Also the timber is a natural grown material and its characteristics and properties vary greatly. It was therefore essential to establish clearly what were the mechanical properties of the timber used in the tested samples. Because of those variations, the determination of timber mechanical properties was required for each sample. However it seemed unrealistic to work out those properties for each of them, because of the large number of tests intended in the experimental programme. Also it is important to recall that this was not a design attempt of wood/glass/epoxy joints but only a research into their mechanical properties. Therefore an alternative method was developed to assess the required mechanical properties of each piece of timber without having to carry out all the tests on all of them. This method is summarised as follow:

- All the pieces of timber selected for the sample fabrication were conditioned as specified in the relevant codes of practice.
- All of them were preliminarily graded as explained further on, to obtain one of the timber mechanical properties: The bending modulus of elasticity.
- Out of the 40 different timber planks from which all the timber pieces were sawn, 10 of them were selected. Small clear specimens were taken from those 10 planks to determine the full range of mechanical properties required, including the bending modulus of elasticity.
- From those small clear specimen tests, timber mechanical properties profiles were established. With the bending modulus of elasticity found from the preliminary grading test, the full mechanical properties of each timber piece were assessed by correlation with the timber properties profiles obtained from the small clear specimen tests.

The method of timber properties determination is developed through the next two sections with description of the tests carried out and their validity in accordance with the codes of practice.

4.4.1. Timber conditioning and preliminary grading

The timber conditioning was based on the standards requirements for timber testing BS EN 1193: 1997, which specifies that the test pieces shall be conditioned for at least one week before the test at $(20 \pm 2)^\circ\text{C}$ temperature and $(65 \pm 5)\%$ relative humidity. The timber material was conditioned until it attained constant mass.

The timber was stored in the temperature controlled room two weeks before the experiments started. Unfortunately, this room did not have the facility to regulate the humidity. Therefore measurements of the relative humidity were carried out every weekday during the months of experiments. The measurements showed a fairly constant relative humidity, as the room was located well within the building and the summer during which the experiments were carried out was relatively cool.

It can be said that the timber was conditioned at a constant temperature of $20 \pm 2^\circ\text{C}$ and a relative humidity of $60 \pm 10\%$.

After being conditioned, each sample was graded precisely. Before being sawn to the appropriate shape and over one metre in length, each piece of timber was tested in three points bending under low loading (to 3 kN) in order to maintain the timber in the elastic range and not affect its strength properties. With mid-span deflection recorded, the bending modulus of elasticity (parallel to the grain) was established. A sketch of the test is shown in figure 4.47.

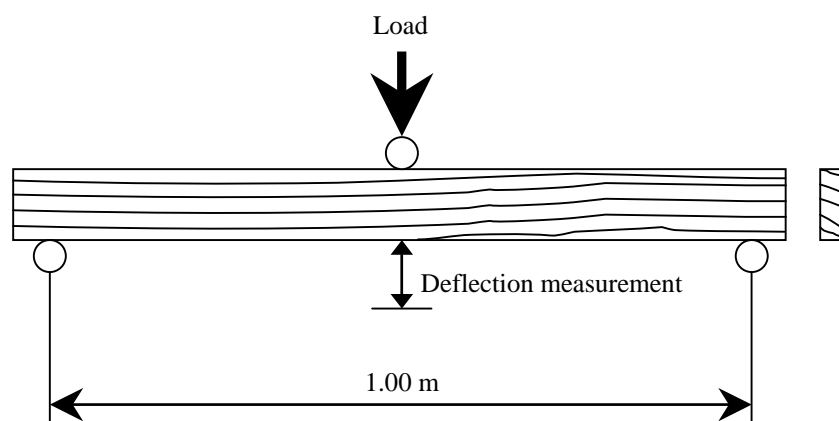


Figure 4.47 Principles of three points bending test.

This test was carried out on all timber pieces to be used for the sample fabrication and the results of that test are presented in the next chapter.

4.4.2. Determination of timber mechanical properties

Because of the need to establish the mechanical properties of the timber required for the research, tests were carried out on small clear timber samples. As explained before, the determination of the mechanical properties was carried out on a random selection of 10 different timber planks. From each plank, small clear samples were cut for different tests. Four type of test were carried out to establish the following properties: Bending MOE (Modulus Of Elasticity), tension strength and tension MOE parallel to the grain, tension strength and tension MOE perpendicular to the grain, and finally shear strength parallel to the grain. The number of samples tested per test is summarised in table 4.2. All the tests were based on standard tests, thus they refer to requirements given by the relevant code of practice.

Test number	Properties measured	Standard test from	Samples per plank	Total samples tested
1	Bending modulus of elasticity	BS373: 1986	2	20
2	Tension strength and tension MOE parallel to the grain	EN408: 1995/ BS373: 1986	2	20
3	Tension strength and tension MOE perpendicular to the grain	EN1193: 1997/ Alternative	2	20
4	Shear strength parallel to the grain	BS373: 1986	4	40

Table 4.2 Summary of small clear timber sample tests.

Alternative standard tests meant that modifications of the standard test were needed to suit the size of the sample, as explained later. But it is essential to highlight that the moisture content and specific gravity are two fundamental parameters to assess the properties of the timber and are relatively easy to measure. Consequently for all the samples tested, a piece of wood was cut from the sample immediately after each test to measure the moisture content and the specific gravity. The specific gravity was established on the same piece of wood, as its dimensions were previously measured. The specific gravity is the ratio of the dry weight over the bulk volume. The following sections describe the details of the small clear sample tests carried out as specified in table 4.2.

4.4.2.1. Determination of modulus of elasticity in bending

The static bending test was carried out using the central loading method specified in BS373: 1986 “Methods of testing small clear specimens of timber”. The test piece was a beam of dimensions 20 mm × 20 mm × 300 mm. In the central loading method the distance between the points of support of the test piece was 280 mm and the load was applied as shown in figure 4.48.

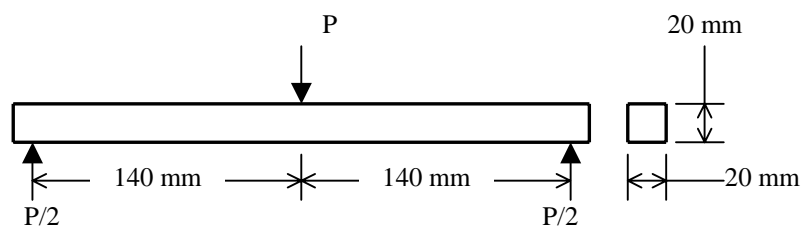


Figure 4.48 Central loading for 20 mm standard test piece.

The orientation of the annual rings in the test piece was parallel to the direction of loading as the sample was cut along the grain direction.

Using a planer, the sample dimensions were adjusted to less than 1 mm of tolerance. The cross-sectional dimensions were measured at mid-length and recorded for each sample. These values were used to calculate the bending modulus of elasticity. Samples ready to be tested are shown in figure 4.49.



Figure 4.49 Static bending test samples.

The loading rate or load head movement was at a constant speed of 2.54 mm/min (based on 0.1 in/min).

The contour of the loading head, which was in contact with the beam, had a half-circular form with a radius of 30 mm as the one shown in figure 4.50.

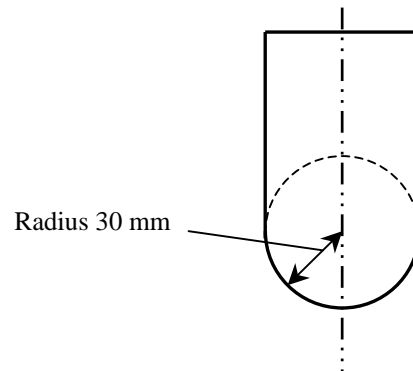


Figure 4.50 Contour of the loading head.

The frame used for this test was initially designed to fit on the J.J. Lloyds testing machine. This machine could only test samples accurately in tension. Therefore the test was carried out upside down using that particular frame, as shown in figure 4.51.

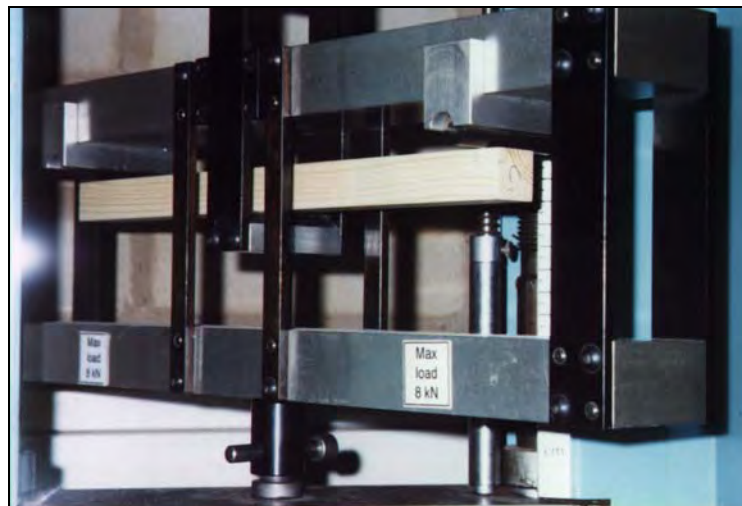


Figure 4.51 Testing frame used for the static bending test.

The load was applied upward and the end supports were orientated downwards but the principles were the same: The beam was in three points loading. The frame still complied with the standard, which specifies that the test pieces shall be supported at the ends in such a way, that they will be free to rotate and follow the bending action.

It shall not be restrained by friction otherwise it would resist the bending and tend to introduce longitudinal stresses.

The deflection of the beam at mid-span shall be measured with reference to the outer points of loading by recording the load head movement. The bending modulus of elasticity is given by equation (4.2):

$$E = \frac{FL^3}{4\delta bh^3} \quad (4.2)$$

With E = Bending modulus of elasticity (N/mm²),

F = Load (N),

L = Length of the member (mm),

δ = Deflection at mid-span (mm),

b and h = Breadth and height of the beam cross-section (mm).

4.4.2.2. Determination of modulus of elasticity and strength in tension parallel to the grain

There are currently two standard tests to establish the modulus of elasticity in tension parallel to the grain. The latest one is given in EN 408: 1995 “Timber structures - Structural timber and glued laminated timber - Determination of some physical and mechanical properties”. The standard test in EN 408: 1995 specifies that tension test parallel to the grain shall be achieved with test pieces of full structural cross-section. These test pieces must have sufficient length to provide a clear space between the testing machine grips of at least 9 times the larger cross-sectional dimension. For the timber cross-section of 96×44 mm used in this research, it means that the sample should be at least 900 mm long. Such sample could not be tested with the equipment available in the university laboratory unless using the same testing rig as for the wood/glass/epoxy joints. Furthermore the code specifies the use of gripping devices to hold the sample, which were not available at the university for such a member size. For those practical reasons, it was decided to use the standard test for small clear samples given by BS 373: 1986.

BS 373: 1986 standard test specifies that tension test parallel to the grain shall be achieved with test piece having form and dimensions as illustrated in figure 4.52.

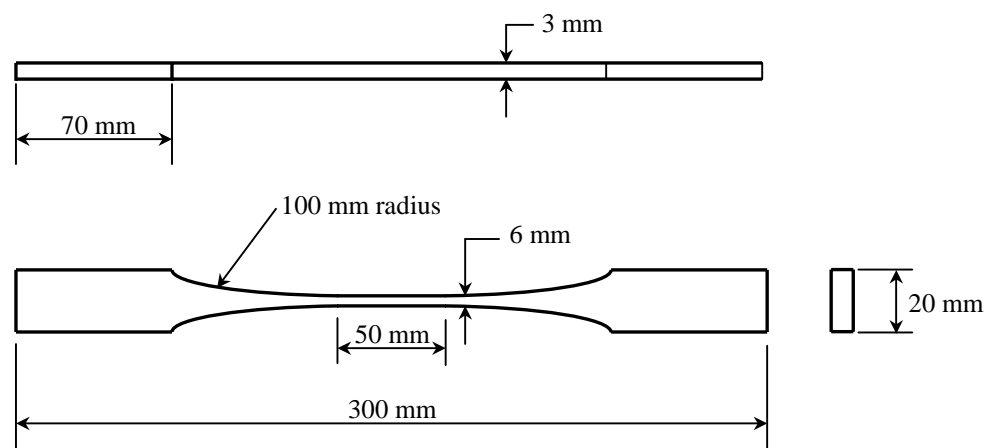


Figure 4.52 Test piece for tension parallel to the grain.

The fabrication of those samples required great care and attention. The samples were fabricated at the School of Art and Design at Coventry University. This school has a wood workshop equipped with a rotor planer machine. This machine allows accurate cutting of the wood in curved and circular shape. As far as the fabrication is

concerned, the sample was first reduced in thickness to 3 mm using a planer machine. Then the rotor was used to taper the sample towards the mid-length. Some samples ready to be tested are shown in figure 4.53.

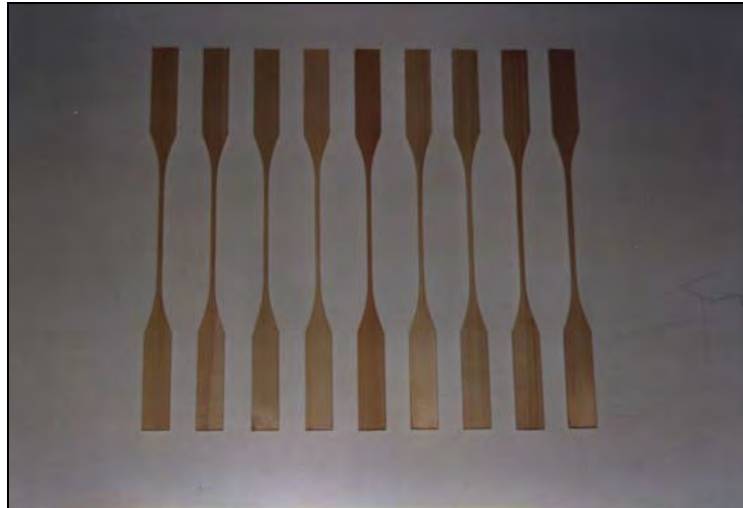


Figure 4.53 Some of the small clear samples for the tension test parallel to the grain.

The BS 373: 1986 requirements for the tensile test for tension parallel to the grain are as follow:

- The test piece shall be so orientated that the direction of the annual rings at the smaller cross-section is perpendicular to the greater cross-sectional dimensions.
- The actual dimensions at the minimum cross-section shall be measured.
- The load shall be applied to the 20 mm face of the ends of the test piece by toothed plate grips, which are forced into the wood before the test is commenced.
- Load extension curves when required shall be taken for a 50 mm central gauge length.
- The load shall be applied to the test piece at a constant head speed of 1.3 mm/min (= 0.05 in/min).

These requirements were followed for the test. The grip jaws were fixed at the top and bottom of the J.J. Lloyds machine. The 50 mm long gauge was replaced by one LVDT fixed into a cylindrical frame, which was clipped to the mid-length of the sample 50 mm apart, as shown in figure 4.54. The elongation was effectively recorded between those points therefore this system complied with the standard requirements.



Figure 4.54 Tension parallel to the grain test configuration.

The stress/strain or load/displacement diagram was obtained from this test. The tension modulus of elasticity was calculated using the diagram and applying Hooke's law or law of elasticity. After the first tension crack was heard, the LVDT was removed to run the test until the sample failed. The tension strength was recorded as the ultimate stress in the thinner cross-section at failure.

4.4.2.3. Determination of modulus of elasticity and strength in tension perpendicular to the grain

4.4.2.3.1. EN 1193: 1997 Standard test

This standard test described in EN 1193: 1997 “Timber structures - Structural timber and glued laminated timber - Determination of shear strength and mechanical properties perpendicular to the grain” specifies the following requirements:

- The test piece used shall be glued between two steel plates at both ends.
- Some specific dimensions for the test piece are given in the standard (in table 1 of EN 1193: 1997) and are shown in figure 4.55.

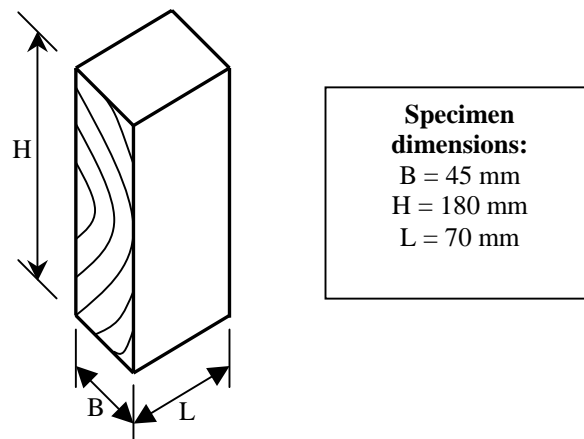


Figure 4.55 Structural timber piece for tension test perpendicular to the grain.

- The gluing process shall be capable of ensuring the specified position of the test piece during testing.
- A suitable adhesive for fixing the steel plates to the timber piece is a two-part epoxy resin.
- Immediately prior to gluing, the surfaces to be jointed should be prepared by planing the timber test piece surfaces and sandblasting the steel plates.
- The test piece shall be loaded concentrically. The longitudinal axis of the test piece shall be aligned with the axis of the machine and fixed in such a way that no initial stresses in the test piece are introduced, except those due to the weight of the test piece and the equipment.

- The test piece shall have pinned end connections to the testing machine, with the axis of the pin parallel to the grain direction.
- The load shall be applied at an adjusted constant rate of cross head movement throughout the test so that the maximum load is reached within 300 ± 120 s.
- The test piece shall be mounted vertically between the test machine platens and the appropriate tension load applied. The gauge length H_0 (approximately $0.6H$) shall be located centrally in the test piece height and not closer than $b/3$ to the loaded ends of the test piece, as shown in figure 4.56.

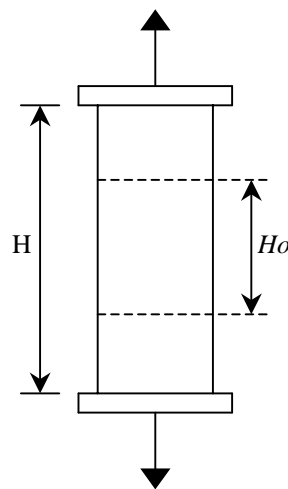


Figure 4.56 Test principle with gauge length.

However the dimensions required for the test piece were not suitable in the project because of the timber size used in the experiment was 96×44 mm. The maximum length of timber perpendicular to the grain could only be 96 mm. Furthermore it seemed to be difficult to achieve fully pinned ends connections to the test machine. Consequently another way of doing this test was investigated and an alternative test was proposed.

4.4.2.3.2. Alternative test

The first difficulty was the test piece dimensions. There were not many alternatives as the sizes were limited by a maximum height of 96 mm available. It was then decided to keep the ratios between the width, the height and the length of the test piece, but the dimensions were reduced to 50%, as shown in figure 4.57. In fact the same sample proportions were maintained but at a different scale.

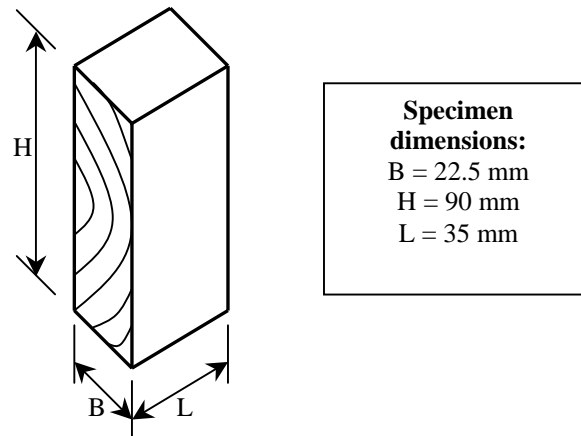


Figure 4.57 Structural timber test piece for alternative tension test perpendicular to the grain.

Both ends of the test piece shall be glued on steel plates. It was decided that these plates would have a tee shape with a hole drilled into the tee stem for bolt connection to the machine top and bottom fork ends. This is illustrated in figure 4.58.

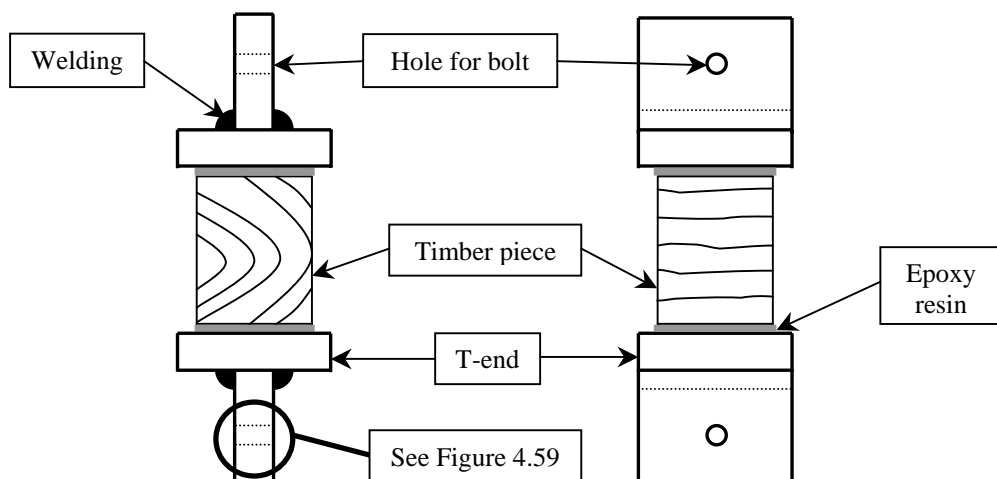


Figure 4.58 Test piece glued on Tee end steel plates.

The second difficulty was to achieve a kind of pinned connection to the testing machine. A fully pinned system would be too complex to fabricate therefore a simple alternative was developed to increase the connection capacity to rotate and obtain a partially pinned system.

The bolt used to connect the T-end to the testing machine was 10 mm diameter and the T-end had to allow lateral displacement along the bolt in order to reduce initial stresses. An arrangement is given in figure 4.59.

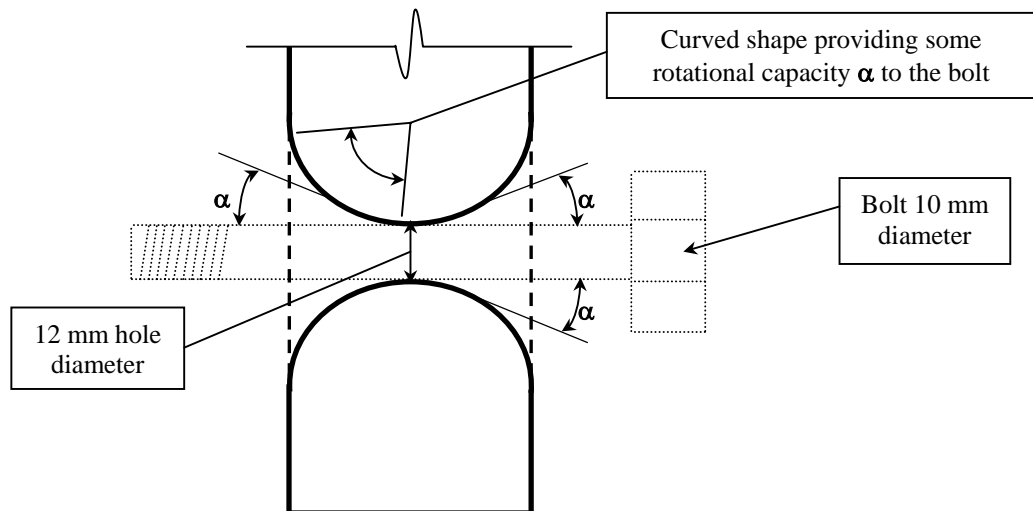


Figure 4.59 Section through the tee end with connected bolt.

The hole was tapered rather than curved and was achieved using different size of drills. The figure 4.60 shows samples ready to be tested.

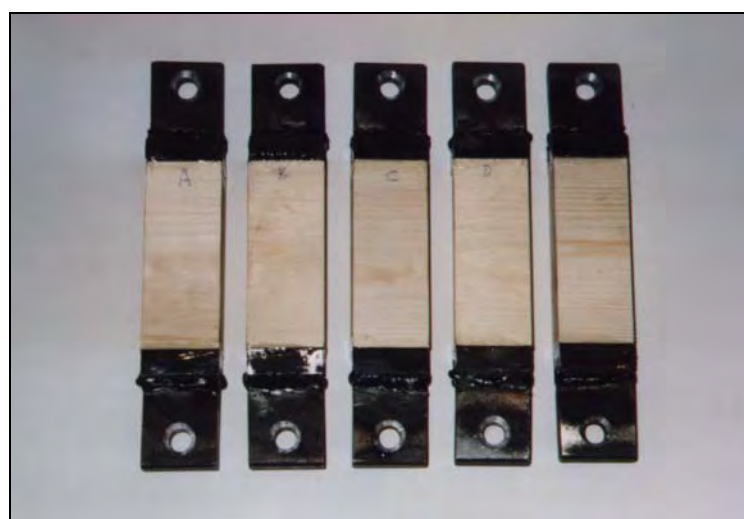


Figure 4.60 Tension perpendicular to the grain samples.

The samples were then positioned in the J.J. Lloyds machine as shown in figure 4.61.

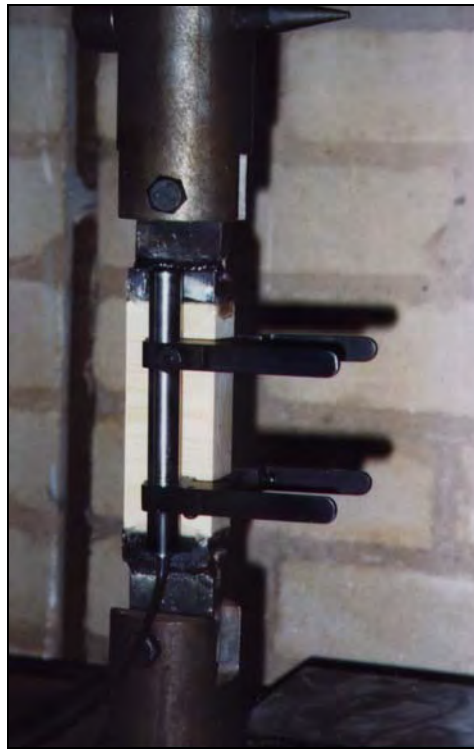


Figure 4.61 Tension perpendicular to the grain test configuration.

One LVDT was used and positioned in a way to minimise the effects of distortion. The LVDT measured the deformation in the load direction, which was referred to the centre of the loaded section and was calculated on the basis of measurements on two opposite sides of the test piece.

The load was applied at a constant rate of cross head movement throughout the test. The rate of loading was adjusted so that the maximum load was reached within 300 ± 120 s (identical to standard requirements).

The increment of load between 10% and 40% of the failure load was measured (and also the deformation corresponding to this increment) to calculate the modulus of elasticity in tension perpendicular to the grain. The LVDT was then removed and the sample tested to failure. The tension perpendicular to the grain strength was obtained from the ratio of failure load to sample cross-section (previously measured).

4.4.2.4. Determination of shear strength parallel to the grain

This standard test was taken from BS 373: 1986. The test piece for this test was a timber cube of 20 mm sides, as shown in figure 4.62.

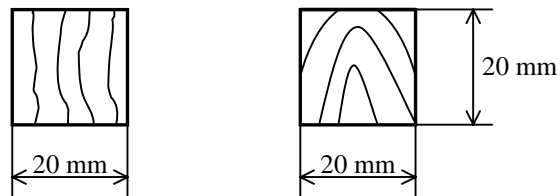


Figure 4.62 Test piece for the shear box test parallel to the grain.

The direction of shearing was parallel to the longitudinal direction of the grain. The cubes were cut from the wood plank free from any defect, where the grain direction was uniform and well defined. The shear box rig used for the test was set-up on the J.J. Lloyds machine and was applying shear to the sample in compression. The rig was effectively loaded in tension, but the inverted frame was applying the load in compression, as shown in figure 4.63.



Figure 4.63 Shear parallel to the grain test configuration.

The load was applied at constant rate of cross head movement of 0.025 in/min (or 0.635 mm/min). Figure 4.64 shows shear samples ready for testing.

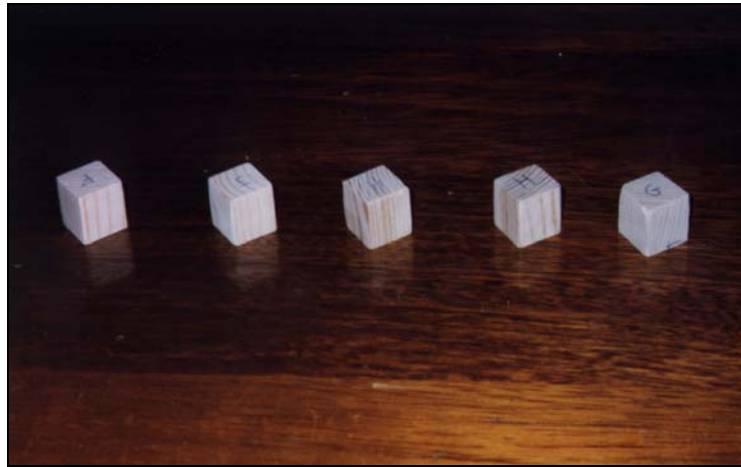


Figure 4.64 Shear sample ready for testing.

The samples were tested with the plane of shear failure parallel to the tangential direction of the grain and also with the plane of shear failure parallel to the radial direction. However it was difficult to assess the radial and tangential direction on some samples, because of uncertainty of those grain directions in the timber plank. The test was carried out to failure. The shear strength was calculated as the ratio of the failure load to the area of shear of the sample (previously measured).

4.5. Summary

This chapter covers more than the experimental programme. It includes a description of the research process, which has brought this programme forward. It describes some of the preliminary tests and should be used as a reference for the following chapter, which covers the experimental results.

CHAPTER 5

EXPERIMENTAL RESULTS

5.1. Introduction

The experiments were carried out in several parts, which correspond to the progression of the research. The preliminary tests were developed and undertaken to clarify and define the main series of tests. Those series, which are described in the previous chapter, were developed to enable the determination of the load-slip and tension capacity of the wood/glass/epoxy joints, with various load to timber grain orientations. The results obtained from these tests are presented and discussed in this chapter.

5.2. Preliminary tests

There were two series of preliminary tests. Both series were carried out to optimise the testing procedure and configuration of the straight pull out samples tested in tension. The first series was undertaken to determine the bonded length of glass fibre to be used for further tests. The second one was carried out to establish the loading procedure. The preliminary tests are described in the following sections.

5.2.1. Test of wood/glass/epoxy samples with varying lengths of composite

The length of composite to be bonded to form the joint was one of the parameters to define at this stage of the research. As explained in the previous chapter, there were two alternatives, which were to design an economical joint (i.e. balanced joint) or to restrict the joint configuration to its geometry.

Samples were fabricated using some timber softwood available in the laboratory. This timber was not conditioned and its mechanical properties were not measured. The samples were cut to size to fit in the J.J. Lloyds testing machine.

The first sample was then fabricated and connected to the testing machine using one centred 20 mm diameter bolt and two 12 mm diameter bolts slotted through the pair of steel side plates at both ends. The loading rate selected was 5 mm/min. The sample failed at a load of 32.6 kN but with an overall displacement of 39 mm (the J.J. Lloyds machine records the displacement between the top and bottom heads). In fact the failure of the sample was due to the bolts bearing onto the wood at top and bottom end connections.

It was found to be necessary to use the shear plate connectors to connect the samples to the testing machine to avoid end connection failures. As there would still be some displacement through those end connections, as the load was applied to the sample, the displacement recorded between sample ends was an overall displacement which was not representative of the actual displacement within the glass fibre/epoxy joint. It was then decided that the displacement would have to be recorded at the gap between the two timber pieces.

Three additional samples were fabricated with three different lengths of bonded composite: 200 mm, 250 mm and 300 mm. They were tested in tension at the same loading rate of 5 mm/min. The results are presented in table 5.1.

Sample	Fibre length (mm)	Failure load (kN)	Max. displ. (mm)	Comments
1	200	33.7	4.5	Delamination both sides
2	250	32.6	5.5	Delamination both sides + partial shear in wood
3	300	39.6	8	Delamination both sides

Table 5.1 Test results of wood/glass/epoxy samples with varying lengths of composite.

The modes of failures were very similar for the three tests: The glass fibre/epoxy composite was delaminated from the wood surface on both sides of the sample, remaining unbroken. However the bonded area was presenting a rough surface on the wood samples because some wood fibres had failed and remained bonded to the composite matrix contact face. On sample number two, the same mode of failure by delamination was observed. Again some bits of wood fibres (up to 3 mm thick) were still bonded to the composite surface, close to the gap area. The displacement values shown in table 5.1 are overall displacements and are not representative of the actual joint slip therefore the joint stiffness could not be evaluated. Nevertheless the results

show that the overall sample displacement increased with the composite length. In fact the contact area was larger therefore the load, which was transferred from one timber piece to the other, was distributed over a larger area, thus reducing the shear stresses. With a larger bond, the shear stress occurring at the interface is normally reduced for a given load. Higher failure load was obtained with 300 mm composite length, but smaller load with 250 mm length compared to 200 mm. This was probably due to the wood properties of the sample number two which were certainly lower than the ones for sample number one and number three.

Resulting from those tests, it was decided to use 200 mm of composite length, mainly for geometrical reasons (as explained in the previous chapter) but also it appeared that increasing the length of composite did not strengthen the joint sufficiently for the extra amount of material added to it. All three joints failed by delamination with no rupture in the composite. In other words the joints were unbalanced for the three bond lengths proposed, as the composite was much stronger than the interface bond with the wood. For the design of a balanced joint, it would have been necessary to either reduce the composite cross-section (i.e. reduce glass fibre density) or increase the bond length of composite further than 300 mm. As the glass fibre used was a commercial product, reducing and adjusting its density was not a practical option. Increasing the length of the composite was therefore the only alternative, but there would have been no possible comparison between different tests. The choice of using 200 mm bonded length was discussed and finally justified with the two following reasons:

- The samples had the same area of glass fibre bonded for two test configurations, with the load parallel to the grain and with the load perpendicular to the grain.
- For all the samples, both connected timber pieces had an equal bonded area of composite.

5.2.2. Test of wood/glass/epoxy samples for experimental adjustments

The second preliminary test was carried out at a time when the experimental programme was already defined. It was decided to test the samples in the loading rig set up in the strong floor area of the laboratory rather than the J.J. Lloyds machine. This rig configuration is described in the previous chapter. The samples were fabricated with longer timber pieces to fit in the loading rig. The aims of this experiment were mainly:

- To check whether the proposed fixings for the displacement transducers were adequate.
- To identify whether the loading procedure specified in BS EN 26891: 1991 would have to be considered for that type of composite joint.
- To establish the optimum rate of loading.

PVC and steel brackets were fabricated to fix the Linear Voltage Differential Transducers (LVDTs) in position. With brackets on both timber pieces, the LVDTs measured the displacement around the gap. The same configuration of LVDTs was used on two opposite faces of the sample in order to check any misalignment of the timber members.

For these specific preliminary tests, three samples were fabricated using uniaxial glass fibre UT-E250 in 200 mm long strips. The UT-E250 has a density of 250 g/m², which is half the density of the UT-E500. A much lighter glass fibre was selected for those tests because we wanted to know whether it was still possible to develop a balanced joint.

The results and graphs of these tests are presented in table 5.2.

Sample type	Failure load (kN)	Max. displ. at gap before failure	Comments
A	29.7	0.9 mm at 27 kN	Fibre failure both sides + partial delam. one side
B	24.9	0.65 mm at 24 kN	Fibre failure + partial delam. both sides
C	25.5	0.44 mm at 25.2 kN	Fibre failure both sides

Table 5.2 Test results of wood/glass/epoxy samples for loading procedure adjustments.

- The first sample A was tested with an estimated failure load of 40 kN. BS EN 26891 recommends a total testing time of about 10 to 15 min. With a testing time based on 10 min. the loading rate was 4 kN/min or 1 kN every 15 seconds. The failure load was smaller than estimated therefore the test was carried out in seven minutes. The sample failed by the entire rupture of the composite on both faces in the gap area. Partial delamination was also observed on one side.
- For the sample B the estimated load was adjusted to 30 kN. The loading rate was then reduced to 3 kN/min. The test was completed in less than ten minutes because once again the failure load was smaller than estimated. The sample failed by the entire rupture of the composite on both faces in the gap area. Partial delamination was also observed on both faces.
- For sample C, the loading procedure specified in BS EN 26891 was used. This standard described how to apply the load for mechanically fastened timber samples. With the estimated failure load F_{est} established, the sample must be loaded to 40% of F_{est} in 2 min. The load is maintained during 30 seconds and then reduced to 10% of F_{est} in 1 min 30 sec. The load is then maintained at 10% of F_{est} during 30 sec and the sample is loaded to failure at a rate of 20% of F_{est} per min. This loading procedure is represented on the graph in figure 5.1.

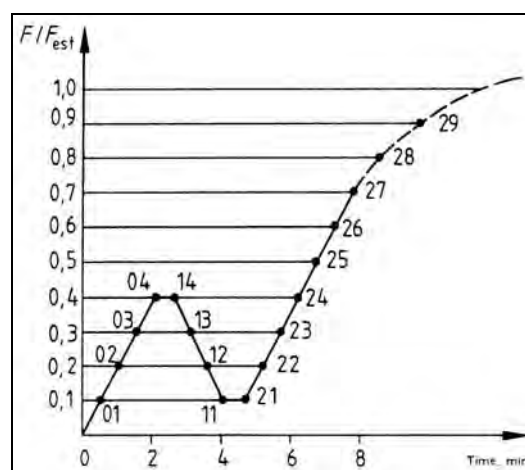


Figure 5.1 Loading procedures in accordance with BS EN 26891.

If this loading procedure is followed, the load/displacement curve should be as shown in figure 5.2. This procedure allows any fastening system to bed into the timber while pre-loaded and then the loading of the sample can be carried out.

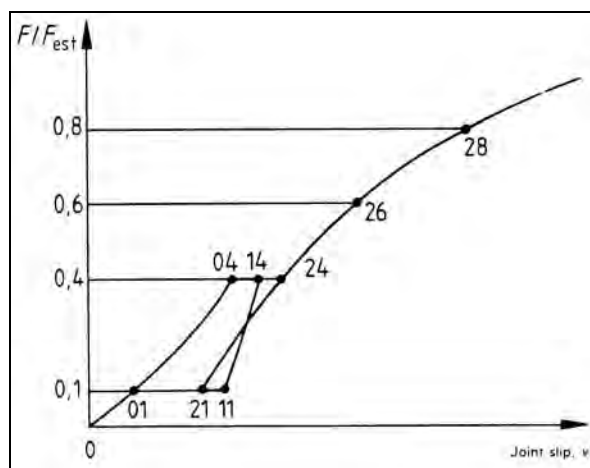


Figure 5.2 Idealised load/displacement curve and measurements to BS EN 26891.

The sample C was tested in accordance with the BS EN 26891 requirements. The wood/glass/epoxy joints were not mechanically fastened joints, but both ends of the samples are connected to the loading rig with shear plate connectors. These should not affect the joint itself, as the deformation was recorded only in the joint area. However any initial strain or slip in the joint could falsify the results. This loading procedure was applied in order to identify whether such phenomenon would occur and could have any implications on the results. The average load/displacement curve recorded through the four transducers is shown in figure 5.3.

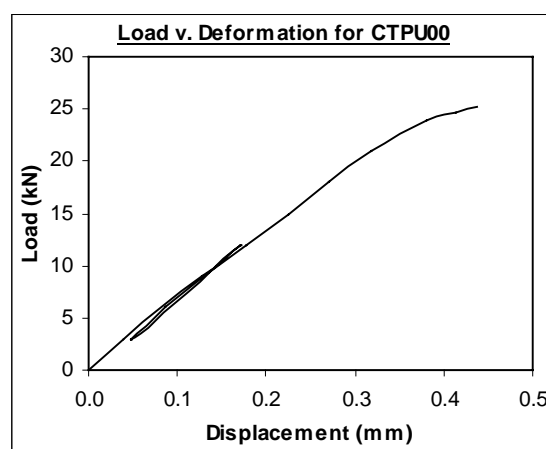


Figure 5.3 Load/displacement curve for sample C.

The sample was loaded up to 12 kN (40% of 30 kN estimated failure load), unloaded down to 3 kN and then loaded to failure. As shown in figure 5.3, the pre-loading curve is perfectly aligned with the final loading curve, with the same gradient and crossing at the same point. It means that there was no initial strain or slip occurring in the joint during the pre-loading process resulting in no loss of stiffness. This curve also shows that the requirements for mechanically fastened joints do not apply for adhesive joints. This procedure was then declared inadequate for the wood/glass/epoxy joints and it was decided not to use it for the tests.

Other properties were measured on those samples such as moisture content, wood density and resin content. These values were not considered relevant because these samples had different configuration (i.e. lighter glass fibre) than the samples from the main tests.

The modes of failure for all three samples observed were tensile rupture of the composite, combined with local delamination in some cases. Having used glass fibre of low density (UT-E250) for these samples, it showed that the joints were still unbalanced. The UT-E250 contains half the number of fibres of the UT-E500. The fibres from both fabrics have exactly the same length and characteristics. In other words, a balanced joint could be obtained by two means:

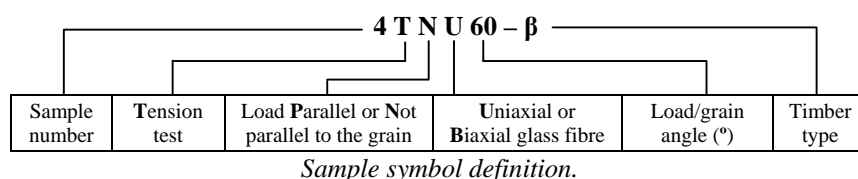
- Increasing the number of glass fibres, therefore increasing the fabric density between 250 and 500 g/m² for a given bonded length of 200 mm, which would have been impractical to achieve with accuracy.
- Keeping the same number of fibres, but increasing the bonded length to more than 200 mm, which could have been done but the balanced joint was no longer considered for the reasons explained previously.

5.3. Timber grading tests

As explained in the previous chapter, each timber sample was graded precisely after their temperature and humidity conditioning. Before being sawn to the appropriate shape and over one metre in length, each piece of timber was tested in three points bending with records of mid-span deflection under load. The load and mid-span deflection would allow the calculation of the bending modulus of elasticity (parallel to the grain) for each sample.

The tests were carried out at very low loading (up to 3 kN maximum). For each 1 kN of load applied, the mid-span deflection was recorded. At the end of the test the residual deflection was also measured.

This test was carried out on all timber pieces to be used for the sample fabrication. The results of that test are presented in tables 5.3, 5.4, 5.5, 5.6 and 5.7.



Sample	Wood	MOE (kN/mm ²)	Sample	Wood	MOE (kN/mm ²)
1TPU00	O	8.63	1TPB00	E	10.62
2TPU00	I	8.42	2TPB00	M	7.06
3TPU00	H	8.52	3TPB00	L	7.66
4TPU00	N	7.04	4TPB00	C	8.97
5TPU00	A	8.46	5TPB00	J	7.40
6TPU00	P	7.21	6TPB00	G	8.88
7TPU00	Z	6.44	7TPB00	α	7.03
8TPU00	J	7.88	8TPB00	\$	6.71

Table 5.3 Bending moduli for TPU00 and TPB00 samples.

Sample	Wood	MOE (kN/mm ²)	Sample	Wood	MOE (kN/mm ²)
1TPU10	I	9.38	1TPB30	L	6.70
2TPU10	O	6.27	2TPB30	K	8.52
3TPU10	E	8.71	3TPB30	E	9.66
4TPU10	D	7.85	4TPB30	C	8.08
5TPU10	N	8.12	5TPB30	M	7.04
6TPU10	F	6.35	6TPB30	G	10.94

Table 5.4 Bending moduli for TPU10 and TPB30 samples.

Sample	Wood	MOE (kN/mm ²)	Sample	Wood	MOE (kN/mm ²)
1TNU30	V	6.46	1TNB30	α	6.89
2TNU30	W	8.89	2TNB30	V	6.79
3TNU30	β	5.63	3TNB30	R	6.78
4TNU30	X	8.89	4TNB30	Δ	7.09
5TNU30	Z	6.36	5TNB30	Y	6.08
6TNU30	T	6.79	6TNB30	U	6.44

Table 5.5 Bending moduli for TNU30 and TNB30 samples.

Sample	Wood	MOE (kN/mm ²)	Sample	Wood	MOE (kN/mm ²)
1TNU60	Π	7.80	1TNB60	Π	8.66
2TNU60	F	7.47	2TNB60	S	6.51
3TNU60	D	8.95	3TNB60	Ω	8.02
4TNU60	γ	6.81	4TNB60	Q	6.02
5TNU60	η	6.16	5TNB60	W	6.87
6TNU60	ε	7.01	6TNB60	P	7.20

Table 5.6 Bending moduli for TNU60 and TNB60 samples.

Sample	Wood	MOE (kN/mm ²)	Sample	Wood	MOE (kN/mm ²)
1TNU90	μ	7.30	1TNB90	γ	6.04
2TNU90	Σ	9.89	2TNB90	U	6.01
3TNU90	φ	6.27	3TNB90	To	6.09
4TNU90	T	8.57	4TNB90	Σ	9.40
5TNU90	Ω	8.00	5TNB90	Y	6.61
6TNU90	R	6.97	6TNB90	φ	6.10

Table 5.7 Bending moduli for TNU90 and TNB90 samples.

The bending moduli were calculated using the cross-section dimensions of each sample. But they should be related to the wood type (A, B, C, etc.) rather than the sample number. The roman or Greek alphabet characters identified the plank from which the samples were sawn. Therefore there should be some similarities between bending moduli from the same plank. The tables show that bending moduli vary significantly even within the same wood plank. Those variations are usually expected with timber material. Those results are used further on in this chapter with the small clear sample tests to assign a profile of timber properties for wood/glass/epoxy joints.

5.4. Tension parallel to the grain tests

As developed in the previous chapter, the first experimental tests were carried out on samples having straight configuration: Tension load applied parallel to the timber grain. All the samples were made of two pieces of timber connected with butt ends and were tested using the same rig configuration, loading rate and equipment. There were four different series of tests, which consisted of samples made with uniaxial or biaxial glass fibres positioned with various orientations to the load and timber grain direction. The results of these tests are presented in the following sections.

5.4.1. TPU00 and TPB00 Tests

TPU00 and TPB00 were load-slip and tension capacity tests with load parallel to the grain:

- TPU00 means **T**ension **P**arallel with **U**niaxial glass fibre UT-E500, where the load was applied in the glass fibre direction ($\alpha = 0^\circ$) and in the same direction as the timber grain ($\beta = 0^\circ$).
- TPB00 means **T**ension **P**arallel with **B**iaxial glass fibre XE450, where the load was applied in the glass fibre direction ($\alpha = 0^\circ$) and in the same direction as the timber grain ($\beta = 0^\circ$).

Various measurements were carried out on these samples during test. The testing rig and the equipment used are presented in the previous chapter.

The samples were positioned between the pair of steel plates at the top and bottom connection and bolted through the shear plate connectors. LVDTs were fixed between brackets and adjusted to have sufficient travelling distance. The rig was loaded until the sample was effectively held (i.e. a small load was applied to the sample). At this stage, the LVDTs were initialised through the data acquisition system as zero position. Using a loading rate of 6 kN/min, the load was constantly applied to the sample. The load and displacements were recorded at every 1.5 kN increment (every 15 sec.) and as the load came closer to the estimated failure load,

they were recorded at every 0.6 kN increment (every 6 sec.). Adequate precautions were taken to prevent the LVDTs from falling and being damaged near sample failure.

After the test, a sample of wood was sawn from one of the timber pieces. The sample dimensions were recorded as well as the wet weight. After at least one week in the oven, the dry weight was recorded. From those data, the specific gravity (i.e. bulk density), the nominal specific gravity (i.e. dry density) and the moisture content of the timber were calculated.

Also the sample weights were recorded at different stages of the fabrication process to enable the evaluation of the amount of resin contained in the sample, therefore the Fibre Volume Fraction of the composite could be calculated.

The table 5.8 summarises all the results obtained for TPU00 tests.

Sample	1TPU00 - O	2TPU00 - I	3TPU00 - H	4TPU00 - N	5TPU00 - A	6TPU00 - P	7TPU00 - Z	8TPU00 - J	Average Values	Standard Deviation
Failure Load (kN)	32.4	36	34.8	35.7	36.6	36.6	34.2	33	34.9	1.6
Elastic Zone (%)	76	77	86	91	89	72	96	80	83.4	8.4
Plastic Zone (%)	24	23	14	9	11	28	4	20	16.6	8.4
Stiffness (kN/mm)	83	103	84	84	82	78	61	66	80.1	12.7
Elastic Deformation (mm)	0.29	0.27	0.36	0.39	0.44	0.34	0.54	0.40	0.38	0.09
Bending MOE (kN/mm ²)	8.63	8.42	8.52	7.04	8.46	7.21	6.44	7.88	7.83	0.83
Moisture Content (%)	13.7	11.4	10	10.9	12.9	12.2	11.1	10.7	11.6	1.2
Fibre Volume Fraction	0.31	0.25	0.27	0.26	0.27	0.25	0.27	0.28	0.27	0.02
Specific Gravity (kg/m ³)	478	516	496	517	464	495	413	454	479	35
Nominal S.G. (kg/m ³)	430	463	451	467	411	442	372	410	431	32

Table 5.8 Results from TPU00 tests.

The failure load corresponds to the last load and displacement measurements recorded before the sample's failure. Typical load/displacement curves as shown in figure 5.6 clearly indicate the range of elastic and plastic behaviour of the sample, which is expressed in percent of failure load in table 5.8.

Some curves show a change in slope (or stiffness) in the elastic range with a sudden increment of displacement (shows as a step in the curve). This is due to the failure in

tension of some epoxy resin infiltrated accidentally between the timber piece butt ends (in the gap).

The joint stiffness was calculated over the elastic range of the sample.

The modes of failure of each sample were also recorded during the tests and are summarised in table 5.9.

Samples	Failure Load (kN)	Modes of failure
1TPU00 - O	32.4	Delamination both sides
2TPU00 - I	36	Delamination both sides
3TPU00 - H	34.8	Delamination both sides
4TPU00 - N	35.7	Top shear plate connector failure
5TPU00 - A	36.6	Delamination both sides
6TPU00 - P	36.6	Delamination both sides
7TPU00 - Z	34.2	Delamination both sides
8TPU00 - J	33	Delamination both sides

Table 5.9 Failure modes from TPU00 tests.

The modes of failure observed through the tests were very consistent and of the same nature for most of the samples. The samples failed by delamination of the composite layers from the timber surface on both sides. Figures 5.4 and 5.5 show some of the TPU00 samples after failure.

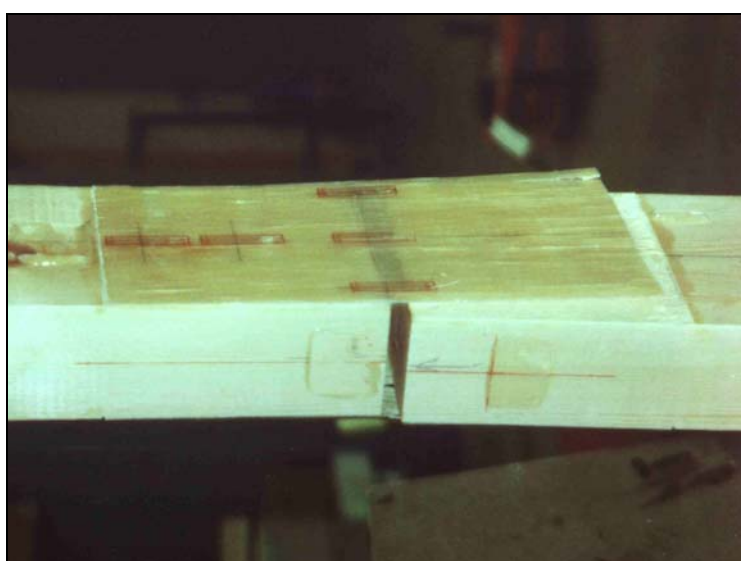


Figure 5.4 Delamination on both sides observed on the 7TPU00 - Z sample.

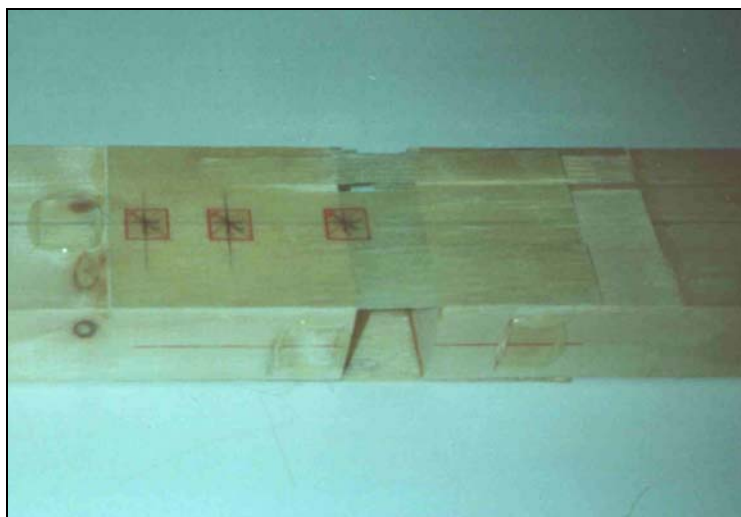


Figure 5.5 Delamination on both sides observed on the 8TPU00 - J sample.

Except on the sample shown in figure 5.5, there was no longitudinal shear failure detected in the composite layer. This means the tension stresses at failure in the composite were fairly uniformly distributed on each face and across the width. There might be two reasons for that:

- The samples tested were in fact axially loaded or “tension only”, with a negligible eccentricity if there was any.
- There was effectively an eccentricity of the load, but the longitudinal shear resistance of the composite layer was high enough to re-distribute the stresses across the whole width and enable the composite layer to delaminate entirely at failure.

Figure 5.6 summarises the load/displacement curves obtained for the samples from the TPU00 tests.

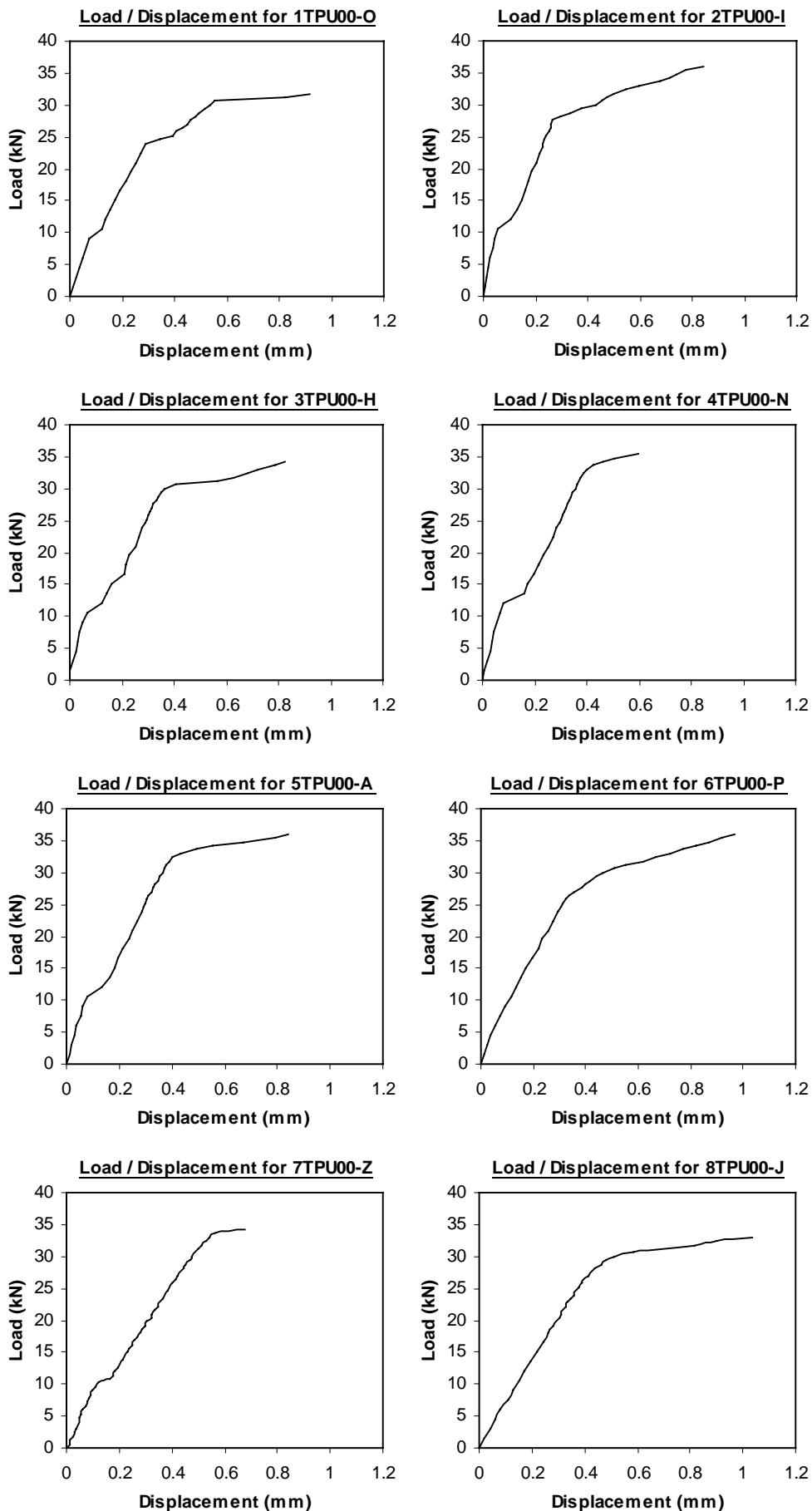


Figure 5.6 Load/displacement curves for TPU00 tests.

The displacements were measured using the average readings from the small LVDTs positioned on the samples sides. However strain gauges were also used on some of the tested samples, such as samples 7TPU00 - Z and 8TPU00 - J of the TPU00 Test. Measurements of strains were carried out at precise locations on the surface of the glass fibre/epoxy composite layers. Strain gauges were used on the sample shown in figures 5.4 and 5.5.

These results are presented later in this chapter, in § 5.6.

The load/displacement curves for the TPU00 tests show that the displacements recorded around the gap between the connected members never exceed 1.1 mm, which is a very small value of slip at failure in comparison with mechanically fastened timber joints such as bolted connection.

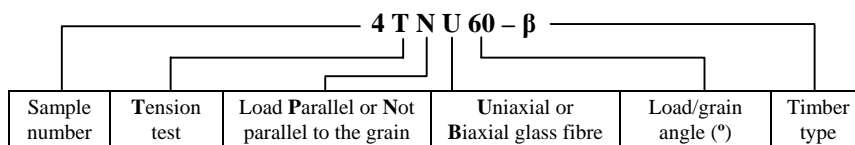
The failure loads recorded for the eight samples are relatively uniform, ranging between 32.4 and 36.6 kN.

The elastic behaviour of the samples exceeds 72% of the overall recorded joint slip for a maximum elastic displacement of 0.54 mm.

The samples develop a plastic behaviour generally, except on samples No 4 and No 7 where the curves stop suddenly as they start to show some plasticity. In fact the curves do not reflect the full behaviour, especially as the load reached its maximum. The equipment did record the load at 1.5 kN increment and at 0.6 kN increment as the sample came up to the failure load. Therefore the position where the curve stopped corresponds to the last load/displacement record before the failure. Most of the time, the exact failure load was higher than this value but not high enough to reach the next 0.6 kN increment. As a consequence, the exact displacement at failure could not be measured and therefore could be much larger than the recorded value, especially as the sample developed plasticity.

The comparison of various parameters obtained from these tests is presented in the discussion section, in § 5.4.3.

The same tests were carried out on the TPB00 samples. The table 5.10 summarises all the results obtained for the TPB00 tests.



Sample symbol definition.

Sample	1TPB00 - E	2TPB00 - M	3TPB00 - L	4TPB00 - C	5TPB00 - J	6TPB00 - G	7TPB00 - α	8TPB00 - β	Average Values	Standard Deviation
Failure Load (kN)	26.4	28.2	26.1	28.5	28.2	26.4	24.6	28.8	27.2	1.5
Elastic Zone (%)	84	87	87	78	83	86	85	87	84.6	3.1
Plastic Zone (%)	16	13	13	22	17	14	15	13	15.4	3.1
Stiffness (kN/mm)	60	50	54	58	55	64	60	56	57.1	4.3
Elastic Deformation (mm)	0.35	0.49	0.42	0.38	0.43	0.36	0.35	0.45	0.40	0.05
Bending MOE (kN/mm ²)	10.62	7.06	7.66	8.97	7.4	8.88	7.03	6.71	8.04	1.34
Moisture Content (%)	13.9	13.1	12.7	12.3	12.8	13.8	10.3	10.7	12.5	1.3
Fibre Volume Fraction	0.29	0.28	0.27	0.27	0.27	0.3	0.27	0.29	0.28	0.01
Specific Gravity (kg/m ³)	505	499	503	447	445	494	468	485	481	24
Nominal S.G. (kg/m ³)	443	442	446	398	394	434	425	439	428	21

Table 5.10 Results from TPB00 tests.

The failure load corresponds to the last load and displacement measurements recorded before the sample’s failure. Typical load/displacement curves as shown in figure 5.9 clearly indicate the range of elastic and plastic behaviour of the sample, which is expressed in percent of failure load in table 5.10.

As explained before, some curves show a change in slope (or stiffness) in the elastic range with a sudden increment of displacement that is due to the failure in tensile failure of some epoxy resin infiltrated between the timber piece butt ends.

The joint stiffness was calculated over the elastic range of the sample.

The modes of failure of each sample were also recorded during the tests and are summarised in table 5.11.

Samples	Failure Load (kN)	Modes of failure
1TPB00 - E	26.4	Tension one side/Delamination other side
2TPB00 - M	28.2	Tension one side/Delamination + tension other side
3TPB00 - L	26.1	Tension one side/Delamination + tension other side
4TPB00 - C	28.5	Tension one side/Partial delamination other side
5TPB00 - J	28.2	Tension one side/Delamination other side
6TPB00 - G	26.4	Delamination + partial tension both sides
7TPB00 - α	24.6	Tension one side/Delamination other side
8TPB00 - $\$$	28.8	Tension both sides

Table 5.11 Failure modes from TPB00 tests.

The modes of failure observed through the tests were not of the same nature except that the tension failure of the composite seemed to happen most of the time. In fact the samples failed initially by tension failure of one of the composite layers in the gap area. The figures 5.7 and 5.8 show some of the TPB00 samples after failure.

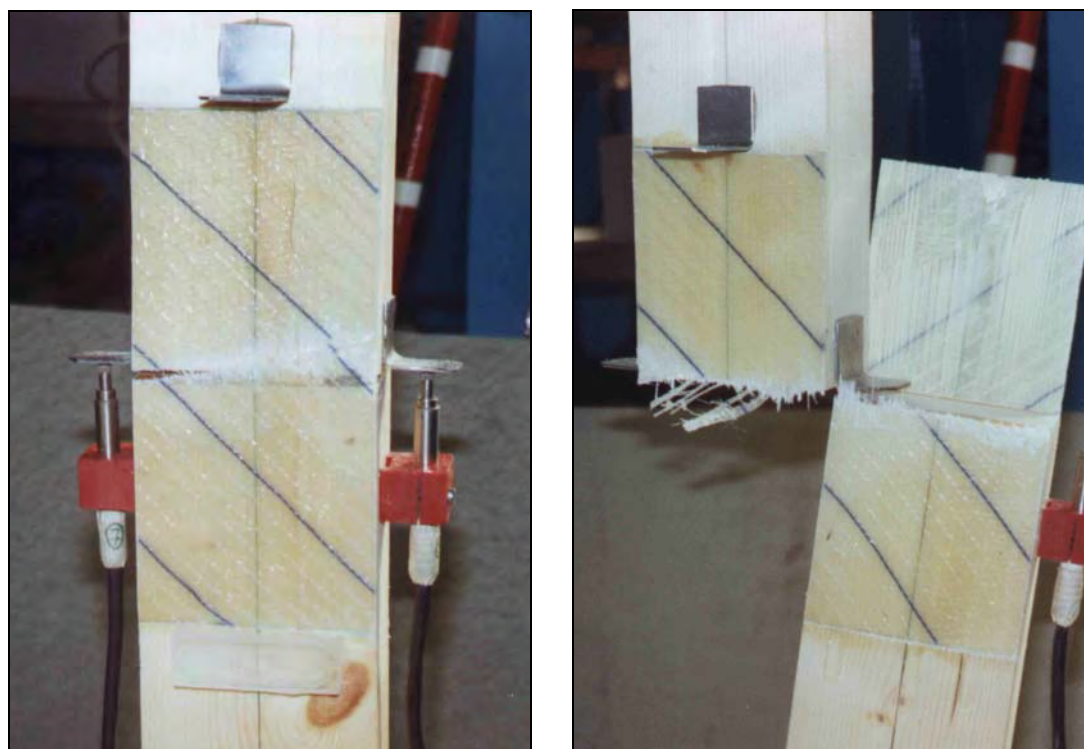


Figure 5.7 and 5.8 Tension failure and delamination for the 5TPB00 - J sample.

Only half of the fibres were orientated in the load direction with the biaxial glass fibre fabric. The other half was orientated perpendicular to the grain and was providing strength only to transversal effects or stresses, which are minimal in a tension only test of that configuration. It shows that this type of joint was still unbalanced, with insufficient amount of fibres provided in the loading direction.

When the composite layer of one side of the joint failed in tension as shown in figure 5.7, all tension stresses were then transferred to the other layer, which failed soon after in multiple modes of failure. This was probably due to the suddenness of this high stress transfer from one face to the other. In figure 5.8, the other layer failed by Delamination.

There was generally no longitudinal shear failure detected in the composite layer.

Figure 5.9 summarises the load/displacement curves obtained for the samples from the TPB00 tests.

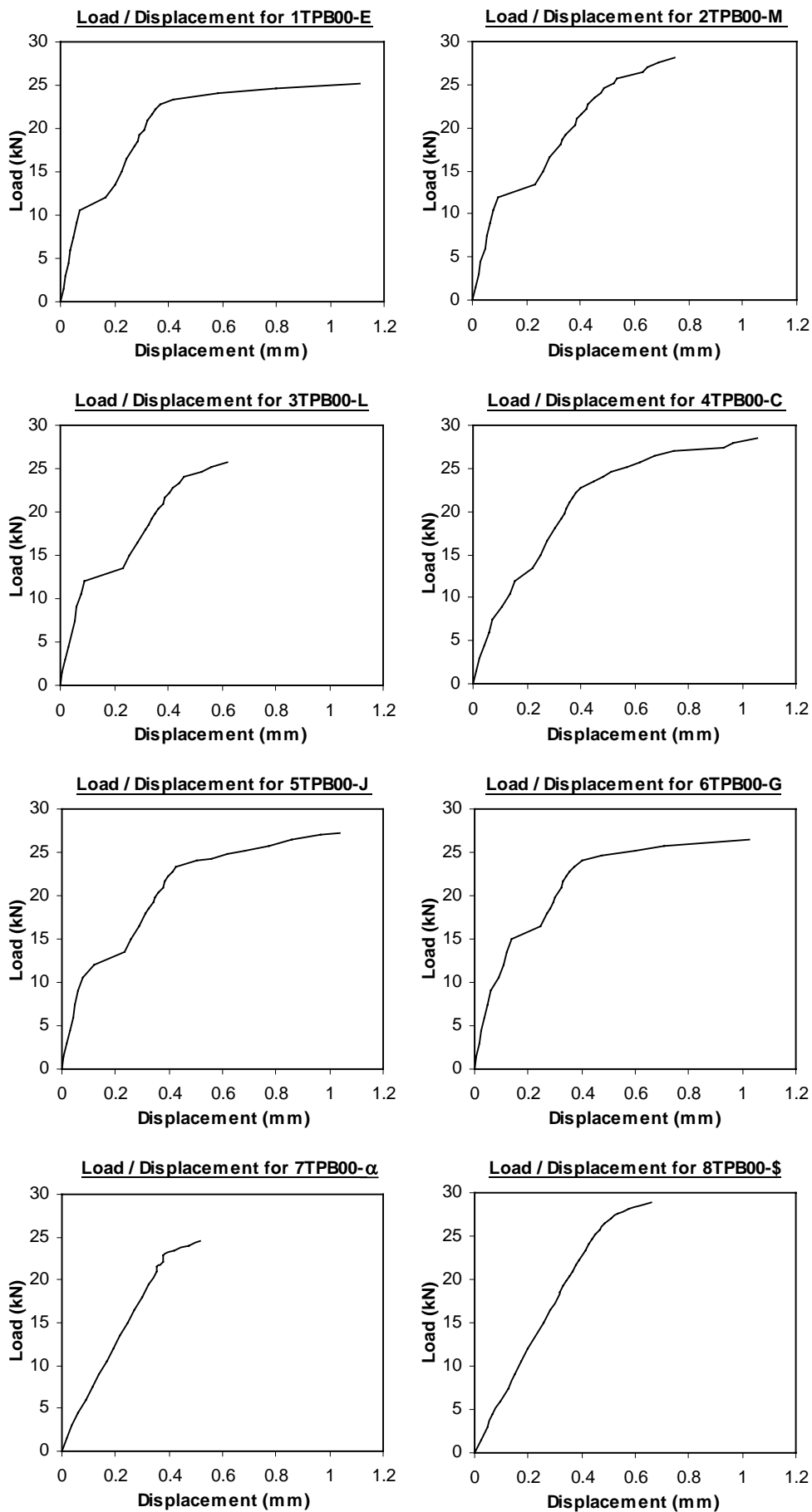


Figure 5.9 Load/displacement curves for TPB00 tests.

The displacements were measured using the average readings from the small LVDTs positioned on the samples sides. However strain gauges were also used on some of the tested samples, such as on samples 7TPB00 - α and 8TPB00 - β . Measurements of strains at precise locations on the surface of the glass fibre/epoxy composite layers were carried out. These results are presented in § 5.6.

The load/displacement curves for the TPB00 tests show that the displacements recorded around the gap between the connected members are relatively small, because they never exceed 1.2 mm at failure.

The failure loads recorded for the eight samples are relatively uniform, ranging between 24.6 and 28.8 kN.

The elastic behaviour of the samples exceeds 78% of the overall recorded joint slip for a maximum elastic displacement of 0.49 mm.

The samples develop a plastic behaviour generally, except on samples No 2, No 3, No 4 and No 7 where the curves stop suddenly as they start to show some plasticity. In fact the curves do not reflect the full behaviour, as explained previously.

The comparison of various parameters obtained from these tests is presented in the discussion section, in § 5.4.3.

5.4.2. TPU10 and TPB30 Tests

As explained previously, TPU10 and TPB30 tests were load-slip and tension capacity tests with load parallel to the grain but the glass fibre direction was orientated with an angle to the load:

- **Tension Parallel with Uniaxial** glass fibre UT-E500, where the glass fibres were orientated 10° from the load direction ($\alpha = 10^\circ$), but the load was parallel to the timber grain ($\beta = 0^\circ$). This 10° angle represented a possible misalignment of the fibres with the timber grain and the load direction. The aim of this test was to assess the implication of fibre misalignment for the joint strength. The sample type was classified as **TPU10**.
- **Tension Parallel with Biaxial** glass fibre XE450, where the glass fibres were orientated 30° from the load direction ($\alpha = 30^\circ$), but the load was parallel to the timber grain ($\beta = 0^\circ$). With the biaxial glass fibre, the properties were the same in orthogonal directions, therefore $\alpha = 0^\circ$ and $\alpha = 90^\circ$ showed exactly the same configuration. For $0^\circ < \alpha < 45^\circ$, the sample had different properties but for $\alpha > 45^\circ$, the same properties applied by orthogonal symmetry. For example, with the selected angle of $\alpha = 30^\circ$, it was the same configuration for $\alpha = 60^\circ$. Combined with the test where $\alpha = 0^\circ$, this value of 30° allowed the assessment of four different configurations, $\alpha = 0, 30, 60$ and 90° with only two different sample tested. The sample type was classified as **TPB30**.

Various measurements were carried out on these samples during test. The testing rig and the equipment used are presented in the previous chapter.

The samples positioning, displacement measurements using LVDTs through the data acquisition system, loading rates, the moisture content, density and FVF measurements were all carried out as for TPU00 and TPB00 tests.

The table 5.12 summarises all the results obtained for TPU10 tests.

Sample	1TPU10 - I	2TPU10 - O	3TPU10 - E	4TPU10 - D	5TPU10 - N	6TPU10 - F	Average Values	Standard Deviation
Failure Load (kN)	30	30	30.9	27.6	25.8	31.8	29.4	2.2
Elastic Zone (%)	82	80	82	89	81	79	82.2	3.5
Plastic Zone (%)	18	20	18	11	19	21	17.8	3.5
Stiffness (kN/mm)	67	53	63	59	59	60	60.2	4.7
Elastic Deformation (mm)	0.38	0.5	0.4	0.42	0.36	0.43	0.42	0.05
Bending MOE (kN/mm ²)	9.38	6.27	8.71	7.85	8.12	6.35	7.78	1.25
Moisture Content (%)	12.65	13.35	13.2	11.85	11.65	13	12.6	0.7
Fibre Volume Fraction	0.32	0.29	0.27	0.26	0.27	0.25	0.28	0.03
Specific Gravity (kg/m ³)	545	455	473	445	442	485	474	38
Nominal S.G. (kg/m ³)	484	402	418	398	396	430	421	33

Table 5.12 Results from TPU10 tests.

The failure load corresponds to the last load and displacement measurements recorded before the sample's failure. Typical load/displacement curves as shown in figure 5.10 clearly indicate the range of elastic and plastic behaviour of the sample, which is expressed in percent of failure load in table 5.12.

It is also relevant to identify that only six samples of that type were tested. In fact for the TPU10 tests, no samples were tested with the use of strain gauges.

As for TPU00 and TPB00 tests, the change in slope for some curves, in the elastic range with a sudden increment of displacement is due to the failure in tension of some epoxy resin infiltrated accidentally between the timber pieces.

The joint stiffness was also calculated over the elastic range of the sample.

The modes of failure of each sample were also recorded during the tests and are summarised in table 5.13.

Samples	Failure Load (kN)	Modes of failure
1TPU10 - I	30	Delamination both sides
2TPU10 - O	30	Delamination both sides
3TPU10 - E	30.9	Delamination both sides
4TPU10 - D	27.6	Delamination both sides
5TPU10 - N	25.8	Delamination both sides
6TPU10 - F	31.8	Delamination both sides

Table 5.13 Failure modes from TPU10 tests.

Only one mode of failure was observed through the tests of these samples. In fact all the samples failed by delamination of both composite layers. The orientation of the fibres (i.e. 10 degrees to the loading and grain direction) seemed to have no effect on the mode of failure. The same failure pattern was observed here as for the TPU00 tests.

Although there was no longitudinal shear failure detected in the composite layers.

It appeared that this type of joint was still unbalanced and the 10 degrees orientation of fibres did not directly affect the tension strength of the composite. However the samples failed at a much lower load than for the TPU00 tests, therefore it appeared that the strength of the bond at the interface between the composite matrix and the timber was affected by the glass fibre orientation.

Figure 5.10 summarises the load/displacement curves obtained for the samples from the TPU10 tests.

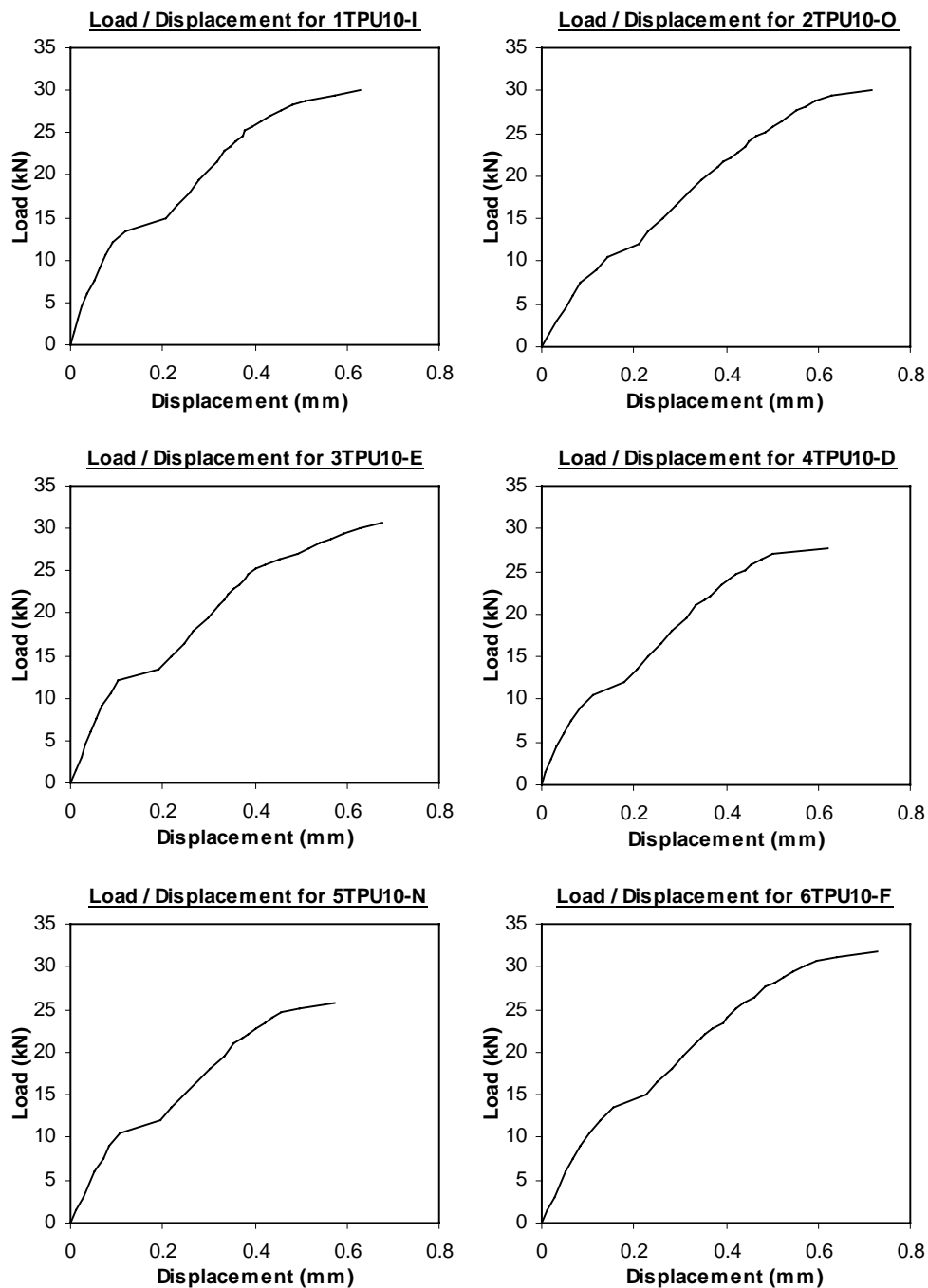


Figure 5.10 Load/displacement curves for TPU10 tests.

The displacements were measured using the average readings from the small LVDTs positioned on the samples sides. However strain gauges were not used on the tested samples of the TPU10 tests, mainly because the glass fibres were not orientated in the same direction than the load. Standard strain gauges are measuring strain in their longitudinal direction. With a strain gauge orientated 10 degrees to the load direction, there is no direct relation between the tension load and the strain recorded by the gauge. The use of strain rosette, which is a strain gauge reading strains from three directions and giving the state of strain at a point, would have been more appropriate. However strain rosettes tend to work efficiently on homogeneous and isotropic materials, but not for composite or anisotropic materials. This was the main reason for not using strain gauges on the TPU10 tests.

The load/displacement curves for the TPU10 tests show that the displacements recorded around the gap between the connected members are even smaller than for TPU00 tests, because they never exceed 0.75 mm at failure.

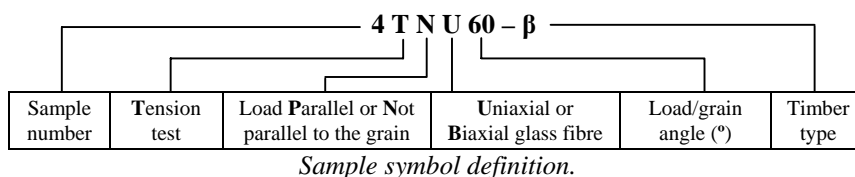
The failure loads recorded for the six samples are relatively uniform and are also lower than for TPU00 tests, ranging between 25.8 and 31.8 kN.

The elastic behaviour of the samples exceeds 79% of the overall recorded joint slip for a maximum elastic displacement of 0.50 mm.

All the samples develop a plastic behaviour generally in a fairly similar pattern. Although the curves are reflecting a more elastic-plastic behaviour than for the TPU00 and TPB00 tests, because of the absence of point of flexure between the linear elastic and the plastic parts of the curve. In fact the transition appears to be progressive and therefore not leading to full plasticity.

The comparison of various parameters obtained from these tests is presented in the discussion section, in § 5.4.3.

The table 5.14 summarises all the results obtained for TPB30 tests.



Sample	1TPB30 - L	2TPB30 - K	3TPB30 - E	4TPB30 - C	5TPB30 - M	6TPB30 - G	Average Values	Standard Deviation
Failure Load (kN)	22.8	20.4	19.8	22.8	21.6	20.4	21.3	1.3
Elastic Zone (%)	84	82	94	87	83	88	86.3	4.4
Plastic Zone (%)	16	18	6	13	17	12	13.7	4.4
Stiffness (kN/mm)	50	55	53	51	47	57	52.2	3.6
Elastic Deformation (mm)	0.39	0.31	0.35	0.39	0.39	0.32	0.36	0.04
Bending MOE (kN/mm ²)	6.7	8.52	9.66	8.08	7.04	10.94	8.49	1.60
Moisture Content (%)	12.55	13.15	13.25	11.45	12.85	13.05	12.7	0.7
Fibre Volume Fraction	0.23	0.24	0.27	0.24	0.26	0.26	0.25	0.02
Specific Gravity (kg/m ³)	477	483	486	549	482	556	506	37
Nominal S.G. (kg/m ³)	424	427	429	488	427	492	448	33

Table 5.14 Results from TPB30 tests.

The failure load corresponds to the last load and displacement measurements recorded before the sample’s failure. Typical load/displacement curves as shown in figure 5.11 clearly indicate the range of elastic and plastic behaviour of the sample, which is expressed in percent of failure load in table 5.14.

Once again, only six samples of that type were tested. In fact, no samples were tested with the use of strain gauges.

The joint stiffness was calculated over the elastic range of the sample.

As for all previous test series, the change in slope for some curves, in the elastic range with a sudden increment of displacement was due to the tensile failure of some epoxy resin infiltrated accidentally between the timber pieces.

For the TPB30 tests, the increment of displacement and the change in stiffness were relatively pronounced, revealing how much the epoxy’s infiltration in the gap zone was strengthening the samples.

The modes of failure of each sample were also recorded during the tests and are summarised in table 5.15.

Samples	Failure Load (kN)	Modes of failure
1TPB30 - L	22.8	Tension one side/Delamination other side
2TPB30 - K	20.4	Tension one side/Delamination other side
3TPB30 - E	19.8	Tension both sides
4TPB30 - C	22.8	Tension both sides
5TPB30 - M	21.6	Tension one side/Delamination other side
6TPB30 - G	20.4	Tension both sides

Table 5.15 Failure modes from TPB30 tests.

The modes of failure observed through the tests were generally of the same nature, with the initial tension failure of one of the composite layers in the gap area. In some case the samples failed in tension failure of both composite layers. However the orientation of the fibres (i.e. 30 and 60 degrees to the loading and grain direction) seemed to have some influence on the mode of failure unlike for the TPB00 tests. Transversal failure of the composite was observed on some of the samples, probably because of the fibres not being orientated in the loading direction. With the tension applied to the samples, the fibres would try to move into longitudinal position and this fact would induce bending stresses to the composite plate and other twisting effects.

It appeared that this type of joint was still unbalanced, and the fibres orientation seemed to affect the tension strength of the composite. In fact the samples failed at a lower load than for the TPB00 tests.

Figure 5.11 summarises the load/displacement curves obtained for the samples from the TPB30 tests.

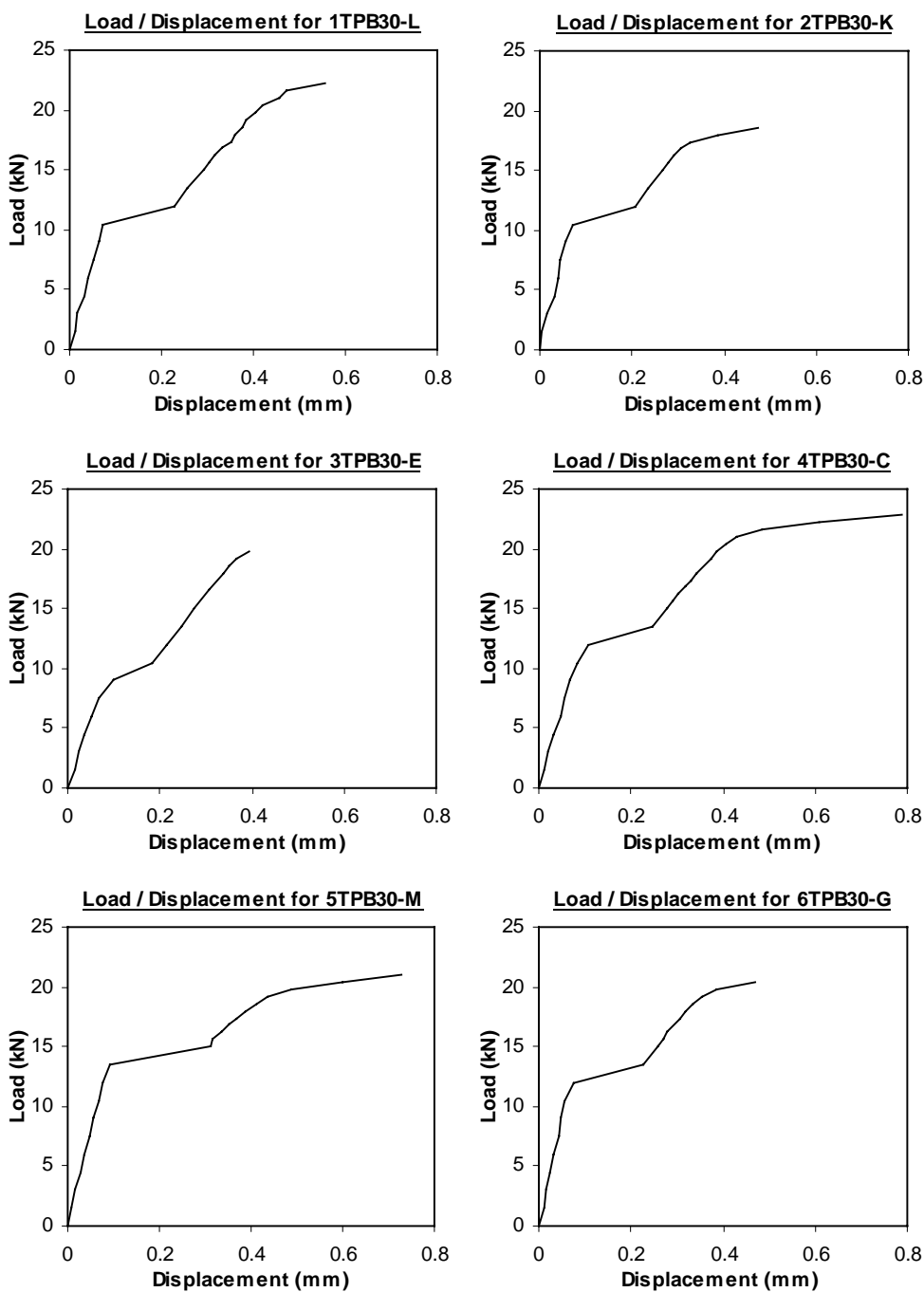


Figure 5.11 Load/displacement curves for TPB30 tests.

The displacements were measured using the average readings from the small LVDTs positioned on the samples sides. However strain gauges were not used on the tested samples of the TPU10 tests for the same reasons explained before. Because both perpendicular strands glass fibres strands of the biaxial fabric were not orientated in the loading direction, significant bending and twisting effects have occurred during the test within the composite layers. This would have made the use of strain gauges even more ineffective.

The load/displacement curves for the TPB30 tests show that the displacements recorded around the gap between the connected members are even smaller than for TPB00 tests, because they never exceed 0.8 mm at failure.

The failure loads recorded for the six samples are relatively uniform and are also lower than for TPB00 tests, ranging between 19.8 and 22.8 kN.

The elastic behaviour of the samples exceeds 82% of the overall recorded joint slip for a maximum elastic displacement of 0.39 mm.

All the samples develop a plastic behaviour. As mentioned before, the sudden increment of displacement due to the tension failure of the epoxy resin infiltrated in the gap area is dramatically affecting the stiffness of the samples. This change of slope (and stiffness) is bringing the curve towards the horizontal, which may be assumed as an elastic-plastic behaviour. In fact the sample is still behaving elastically and unlike for the TPU10 tests, the curves generally show a point of flexure between the linear elastic and the plastic parts of the curve.

The comparison of various parameters obtained from these tests are presented and discussed in the following section.

5.4.3. Discussion

There were four different configurations of samples considered for the load parallel to the timber grain tension tests. Those configurations depended of the type of glass fibre used, whether it was uniaxial or biaxial strands, but also of the glass fibre's orientation in relation to the timber grain and load direction.

The primary assessment can be drawn from the comparison of failure loads for each configuration. For each type of test considered, the failure loads appeared to be relatively uniform. Therefore it was found acceptable to use average values as a realistic representation of the whole test series.

The figure 5.12 shows a graph of the average failure loads for all the load parallel to the grain tension tests including standard deviations.

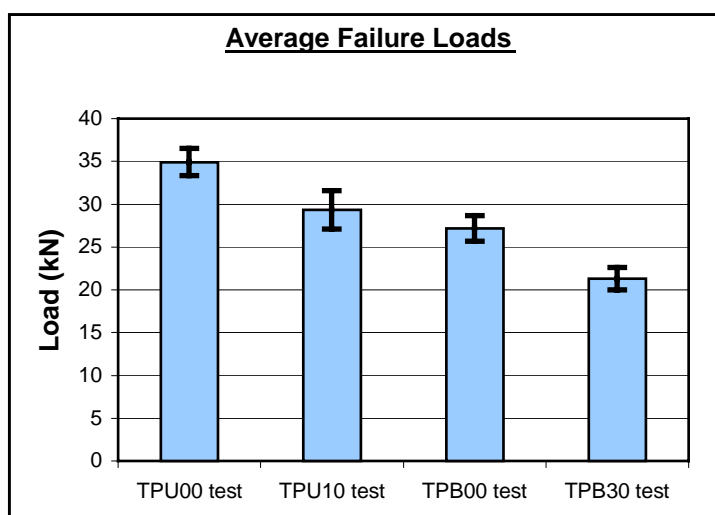


Figure 5.12 Average failure loads for all load parallel to the grain tension tests.

Considering the tests with uniaxial glass fibres materials, when all the fibres are orientated in the load direction such as the TPU00 test, it is clear that this system is the strongest in terms of failure loads and stiffness, as shown in figure 5.12 and 5.13. All the fibres are working efficiently in tension. Consequently the tension strength of the composite is significant. Because of the large amount of fibres, each fibre is carrying less load. Working at a lower stress, the elongation of each fibre is reduced, resulting in a higher stiffness for the whole system.

The figure 5.13 shows a graph of the average stiffness for all the load parallel to the grain tension tests including standard deviations.

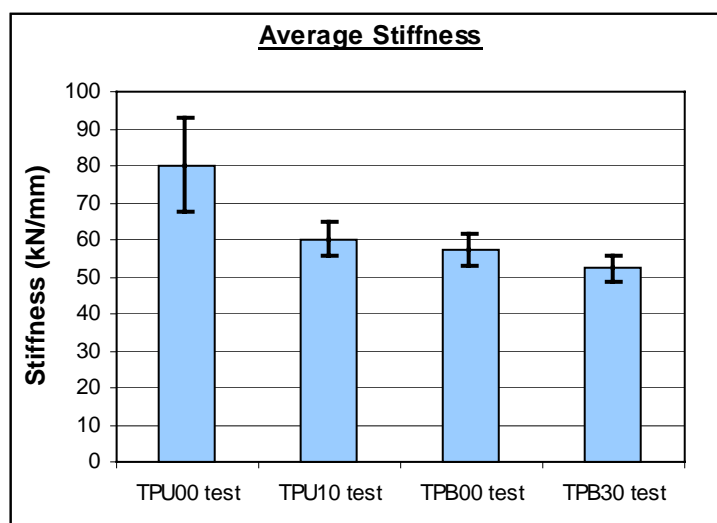


Figure 5.13 Average stiffness for all load parallel to the grain tension tests.

Looking at the TPU10 test, the only difference from the previous test is that the fibres were bonded to the timber with an inclination of 10 degrees to the grain and load direction. It results in failure loads more than 15% lower and in stiffness more than 25% lower than for the TPU00 test. The slight orientation of fibres is weakening the system significantly. The same mode of failure by delamination occurred for TPU00 and TPU10 Tests, revealing that the tension strength of the composite matrix is still higher than the bond strength.

As explained before, premature delamination is observed on the TPU10 test because the system is not tension only any longer. With the load applied, the composite layer appeared to be “pulled” in the longitudinal direction. In fact, with tension applied longitudinally, the anisotropy of the composite does not allow it to resist the tension directly. Only the fibres are able to carry a substantial amount of tension in the composite layer, but because of their orientation, only a reduced area of the composite is effective. The “reduced” composite plate is subject to a combination of tension and bending stresses. This combined system is leading to the premature failure by delamination at the interface between the composite and the wood.

The maximum slip in the gap at failure did not exceed 0.75 mm for the TPU10 test, which is to be compared with the maximum slip of 1.1 mm for TPU00 test. However the maximum elastic displacement calculated from the curves, did not exceed

0.5 mm for the TPU10 test, which is to be compared with the maximum 0.54 mm for TPU00 test. The fact that the TPU10 test had a limited slip at failure compared to the TPU00 test, and that the elastic slip for TPU10 and TPU00 tests were of the same magnitude, confirmed the premature failure of the TPU10 tests in relation to its strength. Moreover the curves of TPU10 test showed that the samples did not reach a plastic behaviour and only remained in an elastic/plastic stage before failure, as explained previously.

Considering now the tests with biaxial glass fibres materials, when half the fibres are orientated in one direction and the other half in the perpendicular direction. For the TPB00 test, half of the fibres were orientated in the load direction, the other half were perpendicular to it. Because of the configuration, which was a tension only test, the fibres in the load direction were effectively carrying all the loads. With a smaller amount of fibres working than for the TPU00 test, the fibres were exposed to higher stresses and thus the tension capacity of the composite was reduced. On the other hand, the bonding area remained the same and if the fibres of the TPB00 test could carry the load, the same range of failure load than TPU00 test could be expected. The mode of failure observed for TPB00 test was however tension rupture of the fibres and delamination. These reasons explained why the failure loads obtained from the TPB00 test were lower than for TPU00 test.

Working at high stresses, the elongation of each fibre in the load direction was significant, resulting in a high slip in the gap area, with a maximum of 1.2 mm, similar value to TPU00 test. High slip but lower failure load would give the TPB00 test a lower stiffness than the TPU00 test, as shown in figure 5.13.

Finally, the TPB30 test was a variation where one half of the fibres was orientated 30 degrees from the grain and load direction and because they were perpendicular, the other half of the fibres was orientated 60 degrees from the grain and load direction. The modes of failure observed here were similar to the TPB00 test because of the tension failure of the fibres and partial Delamination. As a result, transversal rupture of the fibres was observed (due to the combined failure modes), following the orientation to the load direction (30 degrees).

The failure load was generally 20% lower than for the TPB00 test. Once again, it seemed that premature failure was due to the fibre orientation, which weakened the

joint significantly. The slip-load curves showed an elastic and plastic behaviour before failure. The maximum displacement did not exceed 0.8 mm, a much smaller value than for the TPB00 test. The stiffness based on elastic behaviour was only 10% less than for the TPB00 test. The fact that both strands of fibres were bonded to the timber with an angular orientation to the load (unlike TPB00 configuration where only one strand is in fact loaded) improved the stiffness of the system.

Probably the combination of stresses was less significant at the interface between the composite and the wood, as it was for the TPU10 test. Because of the two strands, the combined stresses partially cancelled each other in a way, but the fibres were still trying to reach a longitudinal position, within the composite. This explained the tension rupture and the partial Delamination, which occurred at failure.

Those four series of tests were only considering the tension load applied in the timber grain direction. The series of tests presented in the next section were carried out to assess the effects on joints where the tension load was applied with an angle to the timber grain direction.

5.5. Tension not parallel to the grain tests

The second experimental tests with load not parallel to the grain were carried out on samples made of two timber pieces connected together with a defined angle. In fact, one of the timber pieces had the load applied in its grain direction and transferred the load through the joint to the other piece with that defined angle. A different rig configuration was used for this series of tests. An additional steel frame including a steel box was required to hold the inclined timber piece. This frame had to be free to rotate in respect of the load direction, to allow axial loading of the sample, as explained in details in chapter 4. There were six different series of tests, which consisted of samples made with uniaxial and biaxial glass fibres positioned with various orientations to the timber grain direction. The results of these tests are presented in the following sections.

5.5.1. TNU90 and TNB90 Tests

These tests were carried out with samples made of two timber pieces connected perpendicularly, which means that one piece had the load applied perpendicular to its grain direction. Two different types of samples were tested in tension with the load applied perpendicular to the grain:

- **Tension Not parallel with Uniaxial** glass fibre UT-E500, where the load was applied in the glass fibre direction ($\alpha = 0^\circ$) but perpendicular to the grain ($\beta = 90^\circ$) of the timber piece considered. The sample type was classified as **TNU90**.
- **Tension Not parallel with Biaxial** glass fibre XE450, where the load was applied in the glass fibre direction ($\alpha = 0^\circ$) but perpendicular to the grain ($\beta = 90^\circ$). The sample type was classified as **TNB90**.

Various measurements were carried out on these samples during test. The testing rig and the equipment used were presented in the previous chapter.

The bottom piece of the sample was positioned between the pair of steel plates and bolted through the shear plate connectors. The top piece was fitted within the steel

box and supported on both sides. Only two LVDTs were fixed from the lower brackets and adjusted to have sufficient travelling distance to the upper timber piece. The same procedure was used for these tests as before:

The rig was loaded until the sample was effectively held. At this stage, the LVDTs were initialised through the data acquisition system as zero position. Using a loading rate of 6 kN/min, the load was constantly applied to the sample. The load and displacements were recorded at every 1.5 kN increment (every 15 sec) and as the load came closer to the estimated failure load, they were recorded at every 0.6 kN increment (every 6 sec). Adequate precautions were taken to prevent the LVDTs from falling and being damaged as the sample failed.

Specific gravity and moisture content were measured and calculated in the same way as for the tension parallel to the grain tests.

The sample weights were recorded at different stages of the fabrication process to enable the evaluation of the amount of resin contained in the sample. Therefore the Fibre Volume Fraction of the composite could be calculated.

The table 5.16 summarises all the results obtained for TNU90 tests.

Sample	1TNU90 - μ	2TNU90 - Σ	3TNU90 - ϕ	4TNU90 - T	5TNU90 - Ω	6TNU90 - R	Average Values	Standard Deviation
Failure Load (kN)	34.2	38.4	37.8	30	39	37.8	36.2	3.5
Elastic Zone (%)	72	72	84	84	83	80	79.2	5.7
Plastic Zone (%)	28	28	16	16	17	20	20.8	5.7
Stiffness (kN/mm)	35	40	33	36	32	34	35.0	2.8
Elastic Deformation (mm)	0.71	0.70	0.98	0.70	1.03	0.92	0.84	0.15
Bending MOE (kN/mm ²)	7.30	9.89	6.27	8.57	8.00	6.97	7.83	1.29
Moisture Content (%)	10.92	10.46	11.53	11.20	9.95	11.22	10.9	0.6
Fibre Volume Fraction	0.25	0.25	0.25	0.26	0.27	0.23	0.25	0.01
Specific Gravity (kg/m ³)	455	554	462	494	445	435	474	44
Nominal S.G. (kg/m ³)	411	501	414	444	404	392	428	40

Table 5.16 Results from TNU90 tests.

The failure load corresponds to the last load and displacement measurements recorded before the sample's failure. Typical load/displacement curves as shown in figure 5.14 clearly indicate the range of elastic and plastic behaviour of the sample, which is expressed in percent of failure load in table 5.16.

There were six samples of that type that were tested. In fact, there was only one sample tested with strain gauges.

As shown in figure 5.14, the load/displacement curves do not display the usual change in slope (or stiffness), which is due to the failure in tension of some epoxy resin infiltrated between the timber pieces. This is down to a more sophisticated and careful fabrication process.

The joint stiffness was calculated over the elastic range of the sample.

The modes of failure of each sample were also recorded during the tests and are summarised in table 5.17.

Samples	Failure Load (kN)	Modes of failure
1TNU90 - μ	34.2	Top delamination both sides
2TNU90 - Σ	38.4	Top delamination one side/Bottom delamination other side
3TNU90 - φ	37.8	Top delamination both sides
4TNU90 - T	30	Top delamination both sides
5TNU90 - Ω	39	Bottom delamination both sides
6TNU90 - R	37.8	Top delamination both sides

Table 5.17 Failure modes from TNU90 tests.

Only one mode of failure was observed through the tests of these samples. In fact all the samples failed by delamination of both composite layers. Delamination of the top lap of the composite layers occurred for all samples except sample 5TNU90 - Ω . This seemed to indicate that the grain direction affects the bond strength of the joint. There was no longitudinal shear failure detected in the composite layers. This mode of failure also confirmed that this type of joint was still unbalanced.

Figure 5.14 summarises the load/displacement curves obtained for the samples from the TNU90 tests.

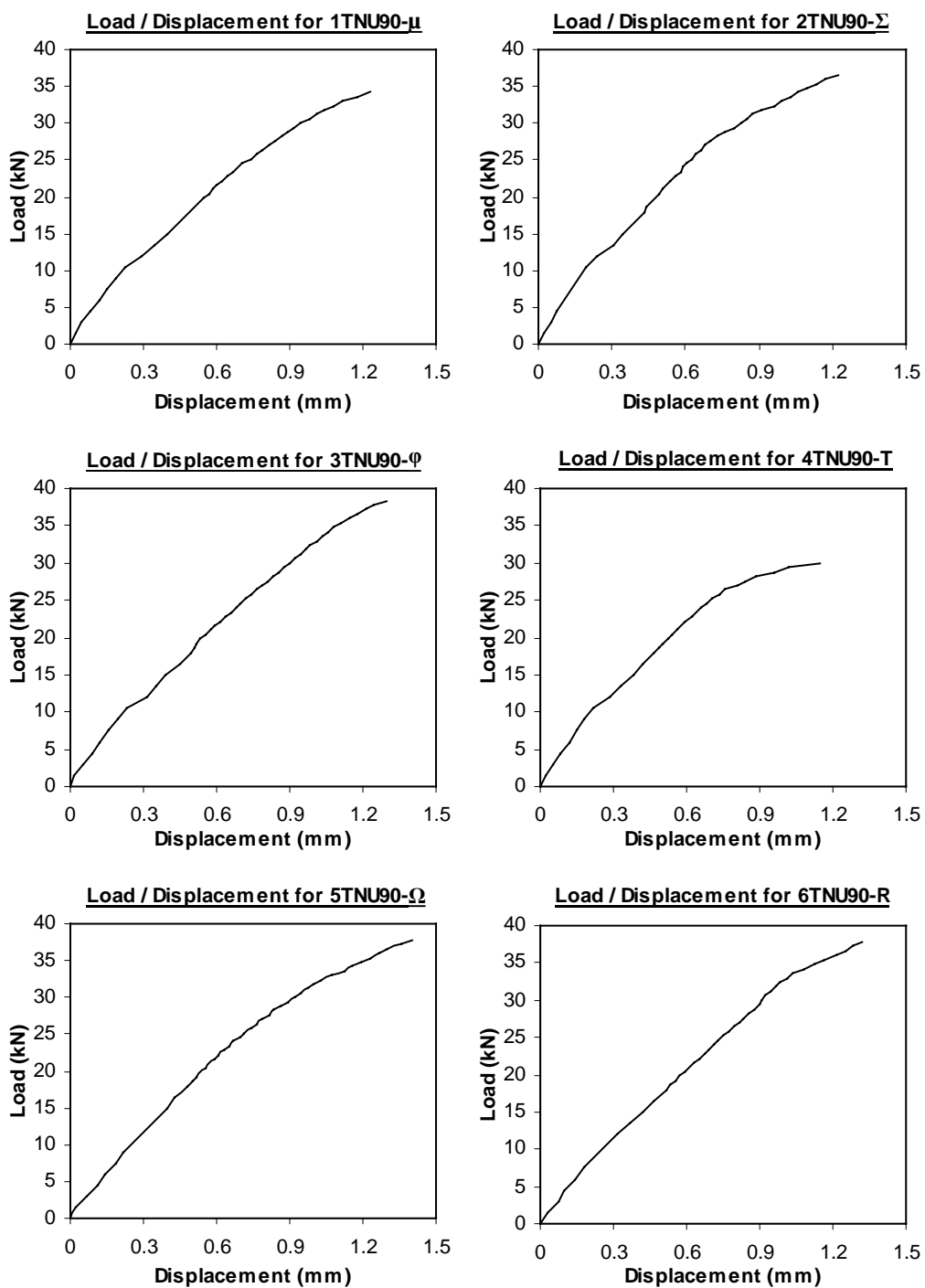


Figure 5.14 Load/displacement curves for TNU90 tests.

The displacements were measured using the average readings from the small LVDTs positioned on the samples sides. However strain gauges were also used on of the tested samples, the sample 5TNU90 - Ω . Measurements of strains at precise locations on the surface of the glass fibre/epoxy composite layers were carried out. These results are presented later in this chapter, in § 5.6.

The load/displacement curves for the TNU90 tests show that the displacements recorded around the gap between the connected members never exceed 1.4 mm at failure.

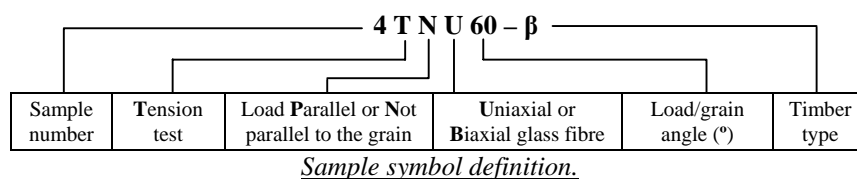
The failure loads recorded for the six samples are relatively uniform, ranging between 30 and 39 kN.

The elastic behaviour of the samples exceeds 72% of the overall recorded joint slip for a maximum elastic displacement of 1.03 mm.

Not all the samples seemed to reach a plastic behaviour at failure. The curves are reflecting an elastic-plastic behaviour, in a similar manner than the TPU10 tests. Even the curve from the sample 3TNU90 - ϕ is not showing any sign of plasticity. The absence of point of flexure shows that the transition is progressive and does not highlight the plastic region.

The comparison of various parameters obtained from these tests is presented in the discussion section, in § 5.5.4.

The same tests were carried out on the TNB90 samples. The table 5.18 summarises all the results obtained for TNB90 tests.



Sample	1TNB90 - γ	2TNB90 - U	3TNB90 - τ	4TNB90 - Σ	5TNB90 - Y	6TNB90 - ϕ	Average Values	Standard Deviation
Failure Load (kN)	25.8	28.2	27	27.6	29.4	25.8	27.3	1.4
Elastic Zone (%)	84	98	80	87	78	86	85.5	7.0
Plastic Zone (%)	16	2	20	13	22	14	14.5	7.0
Stiffness (kN/mm)	26	27	30	32	26	28	28.2	2.4
Elastic Deformation (mm)	0.83	1.03	0.73	0.75	0.89	0.81	0.84	0.11
Bending MOE (kN/mm ²)	6.04	6.01	6.09	9.4	6.61	6.1	6.71	1.34
Moisture Content (%)	10.87	10.95	10.06	10.49	10.49	9.89	10.5	0.4
Fibre Volume Fraction	0.29	0.27	0.24	0.27	0.27	0.23	0.26	0.02
Specific Gravity (kg/m ³)	493	429	438	534	464	455	469	39
Nominal S.G. (kg/m ³)	445	386	398	484	420	414	424	35

Table 5.18 Results from TNB90 tests.

The failure load corresponds to the last load and displacement measurements recorded before the sample's failure. Typical load/displacement curves as shown in figure 5.16 clearly indicate the range of elastic and plastic behaviour of the sample, which is expressed in percent of failure load in table 5.18.

There were six samples of that type, which were tested. In fact, there was only one sample tested with strain gauges.

The joint stiffness was calculated over the elastic range of the sample.

Because of a more careful fabrication process, the load/displacement curves shown in figure 5.16 do not display the usual change in slope that results from tensile failure of some epoxy resin infiltrated between the timber pieces.

The modes of failure of each sample were also recorded during the tests and are summarised in table 5.19.

Samples	Failure Load (kN)	Modes of failure
1TNB90 - γ	25.8	Top delamination one side/Bottom delamination ($\frac{1}{2}$ width) + Tension ($\frac{1}{2}$ width) other side
2TNB90 - U	28.2	Top delamination one side/Bottom delamination ($\frac{1}{2}$ width) + Tension ($\frac{1}{2}$ width) other side
3TNB90 - τ	27	Top delamination both sides
4TNB90 - Σ	27.6	Top delamination one side/Bottom delamination ($\frac{1}{2}$ width) + Tension ($\frac{1}{2}$ width) other side
5TNB90 - Y	29.4	Top delamination one side/Bottom delamination ($\frac{1}{2}$ width) + Tension ($\frac{1}{2}$ width) other side
6TNB90 - ϕ	25.8	Top delamination both sides

Table 5.19 Failure modes from TNB90 tests.

The modes of failure observed through the tests of these samples were not of the same nature, but the delamination of the top lap of the composite layers occurred for all samples. The figure 5.15 shows the combined modes of failure of one of the TNB90 samples after failure.

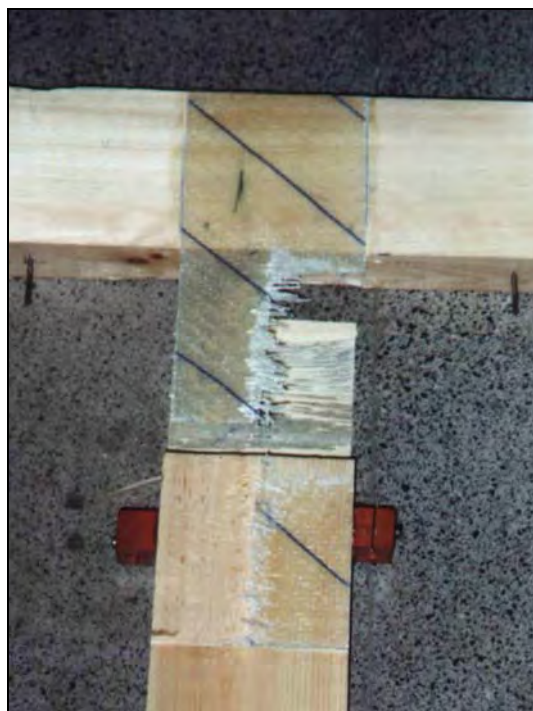


Figure 5.15 Combined failure modes for the 1TNB90 - γ sample.

It was difficult to identify which part of the composite failed first because the joint was hidden by the steel box. However it is likely that the delamination at the top of one side occurred first, all the loads were then transferred to the other layer, which failed soon after in multiple modes of failure. With such high loads applied to only one layer, rupture of the fibres would have started and followed by the delamination. Because only half the width failed by fibre rupture, longitudinal shear failure occurred as a result of the delamination of the other half width. In figure 5.15, the broken fibres along the middle of the bottom lap of the composite are confirming these comments.

Because the joint failed in delamination and tension modes, with the composite failing in the top and bottom zones, this type of joint could be considered as balanced.

Figure 5.16 summarises the load/displacement curves obtained for the samples from the TNB90 tests.

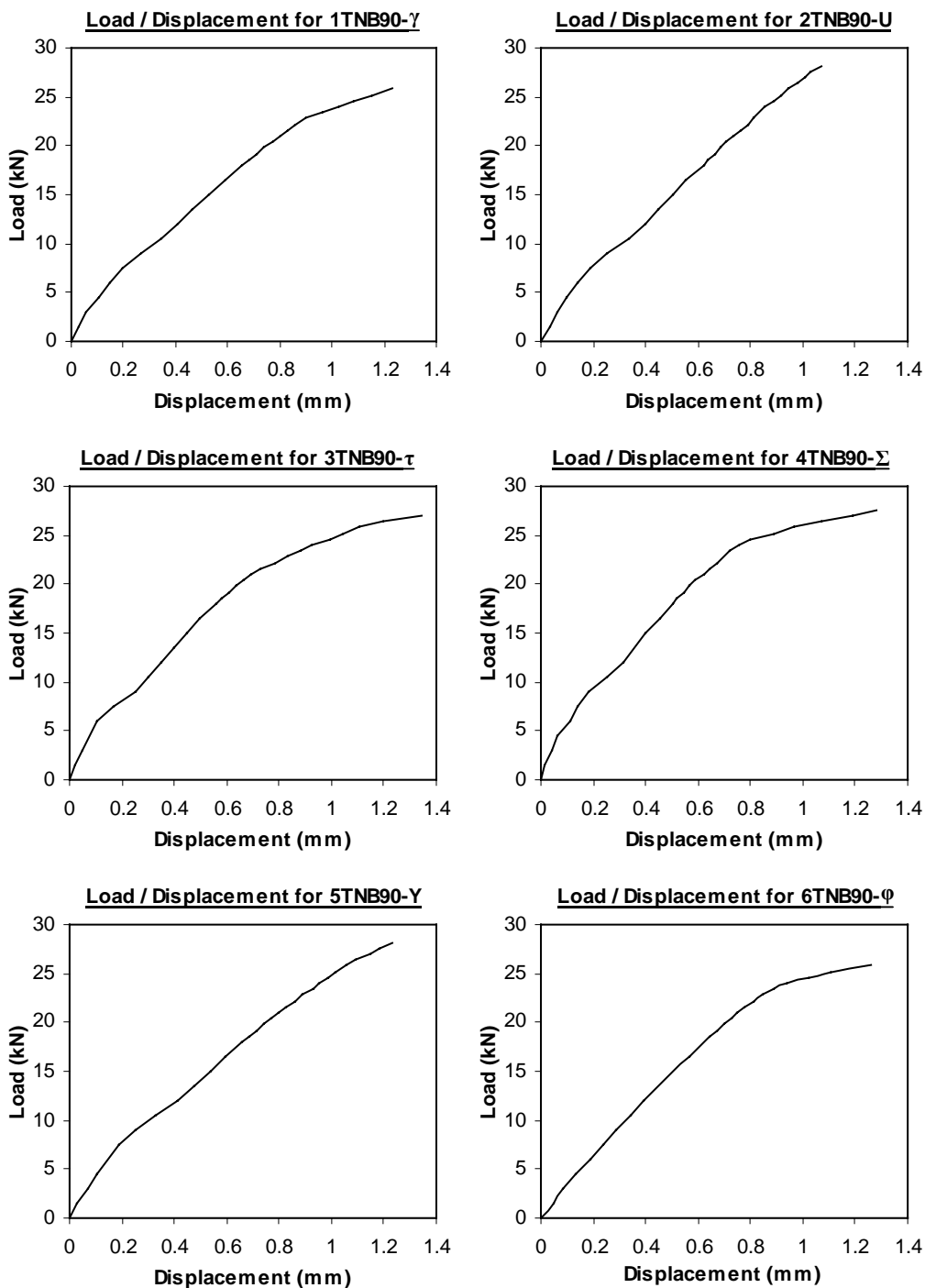


Figure 5.16 Load/displacement curves for TNB90 tests.

The displacements were measured using the average readings from the small LVDTs positioned on the samples sides. However strain gauges were also used on of the tested samples, the sample 6TNB90 - ϕ . Measurements of strains at precise locations on the surface of the glass fibre/epoxy composite layers were carried out. These results are presented in § 5.6.

The load/displacement curves for the TNB90 tests show that the displacements recorded around the gap between the connected members never exceed 1.4 mm at failure.

The failure loads recorded for the six samples are relatively uniform, ranging between 25.8 and 29.4 kN.

The elastic behaviour of the samples exceeds 78% of the overall recorded joint slip for a maximum elastic displacement of 1.03 mm.

Here again, not all the samples seemed to reach a plastic behaviour at failure. The curves are reflecting an elastic-plastic behaviour, in a similar manner than the TNU90 tests. However four samples out of the six showed significant signs of plasticity at failure. Even two of them displayed a point of flexure, confirming that some plastic behaviour was occurring at failure and that the transition is less progressive than for the TNU90 tests.

The comparison of various parameters obtained from these tests is presented in the discussion section, in § 5.5.4.

5.5.2. TNU60 and TNB60 Tests

As explained previously, TNU60 and TNB60 tests were carried out with samples made of two timber pieces connected together with an angle of 60 degrees. This means one of the timber pieces had the load applied in its grain direction and transferred the load through the joint to the other piece with an angle of 60 degrees.

Two different types of samples were tested in tension with the load applied at an angle of 60 degrees to the grain:

- **Tension Not parallel with Uniaxial** glass fibre UT-E500, where the load was applied in the glass fibre direction ($\alpha = 0^\circ$) but with an angle of 60° to the grain ($\beta = 60^\circ$) of the timber piece considered. The sample type was classified as **TNU60**.
- **Tension Not parallel with Biaxial** glass fibre XE450, where the load was applied in the glass fibre direction ($\alpha = 0^\circ$) but with an angle of 60° to the grain ($\beta = 60^\circ$). The sample type was classified as **TNB60**.

Various measurements were carried out on these samples during test. The testing rig and the equipment used were presented in the previous chapter.

The samples positioning, displacement measurements using LVDTs through the data acquisition system, loading rates, the moisture content, density and FVF measurements were all carried out as for TNU90 and TNB90 tests.

The table 5.20 summarises all the results obtained for TNU60 tests.

Sample	1TNU60 - II	2TNU60 - F	3TNU60 - D	4TNU60 - γ	5TNU60 - η	6TNU60 - ϵ	Average Values	Standard Deviation
Failure Load (kN)	29.4	36	31.2	29.4	35.4	35.4	32.8	3.1
Elastic Zone (%)	100	72	79	76	88	90	84.2	10.4
Plastic Zone (%)	0	28	21	24	22	10	17.5	10.5
Stiffness (kN/mm)	32	41	44	36	35	39	37.8	4.4
Elastic Deformation (mm)	0.9	0.63	0.56	0.63	0.91	0.83	0.74	0.15
Bending MOE (kN/mm ²)	7.8	7.47	8.95	6.81	6.16	7.01	7.37	0.96
Moisture Content (%)	11.40	11.01	9.74	11.16	10.01	10.19	10.6	0.7
Fibre Volume Fraction	0.4	0.32	0.26	0.33	0.25	0.36	0.32	0.06
Specific Gravity (kg/m ³)	466	480	517	462	425	461	468	30
Nominal S.G. (kg/m ³)	418	432	471	416	386	418	424	28
Exact Angle (Degrees)	62	62	62	62	61	62	N/A	N/A

Table 5.20 Results from TNU60 tests.

The failure load corresponds to the last load and displacement measurements recorded before the sample's failure. Typical load/displacement curves as shown in figure 5.17 clearly indicate the range of elastic and plastic behaviour of the sample, which is expressed in percent of failure load in table 5.20.

There were six samples of that type that were tested. In fact only one sample was tested with strain gauges.

Again with a more careful fabrication process, the load/displacement curves shown in figure 5.17 do not display the usual change in slope that results from tensile failure of some epoxy resin infiltrated between the timber pieces.

The joint stiffness was calculated over the elastic range of the sample.

An additional parameter was added to the table 5.20: The angles of the joint were measured during the test of each sample to identify the precise load to timber grain orientation.

The modes of failure of each sample were also recorded during the tests and are summarised in table 5.21.

Samples	Failure Load (kN)	Modes of failure
1TNU60 - Π	29.4	Top delamination both sides
2TNU60 - F	36	Top delamination both sides
3TNU60 - D	31.2	Top delamination both sides
4TNU60 - γ	29.4	Top delamination both sides
5TNU60 - η	35.4	Top delamination both sides
6TNU60 - ε	35.4	Top delamination both sides

Table 5.21 Failure modes from TNU60 tests.

Only one mode of failure was observed through the tests of these samples. In fact all the samples failed by delamination of the top lap of both composite layers. Once again, this seemed to indicate that the grain direction affects the bond strength of the joint. The same failure pattern was observed here than for the TNU90 tests.

There was no longitudinal shear failure detected in the composite layers.

This mode of failure also confirmed that this type of joint was still unbalanced.

Figure 5.17 summarises the load/displacement curves obtained for the samples from the TNU60 tests.

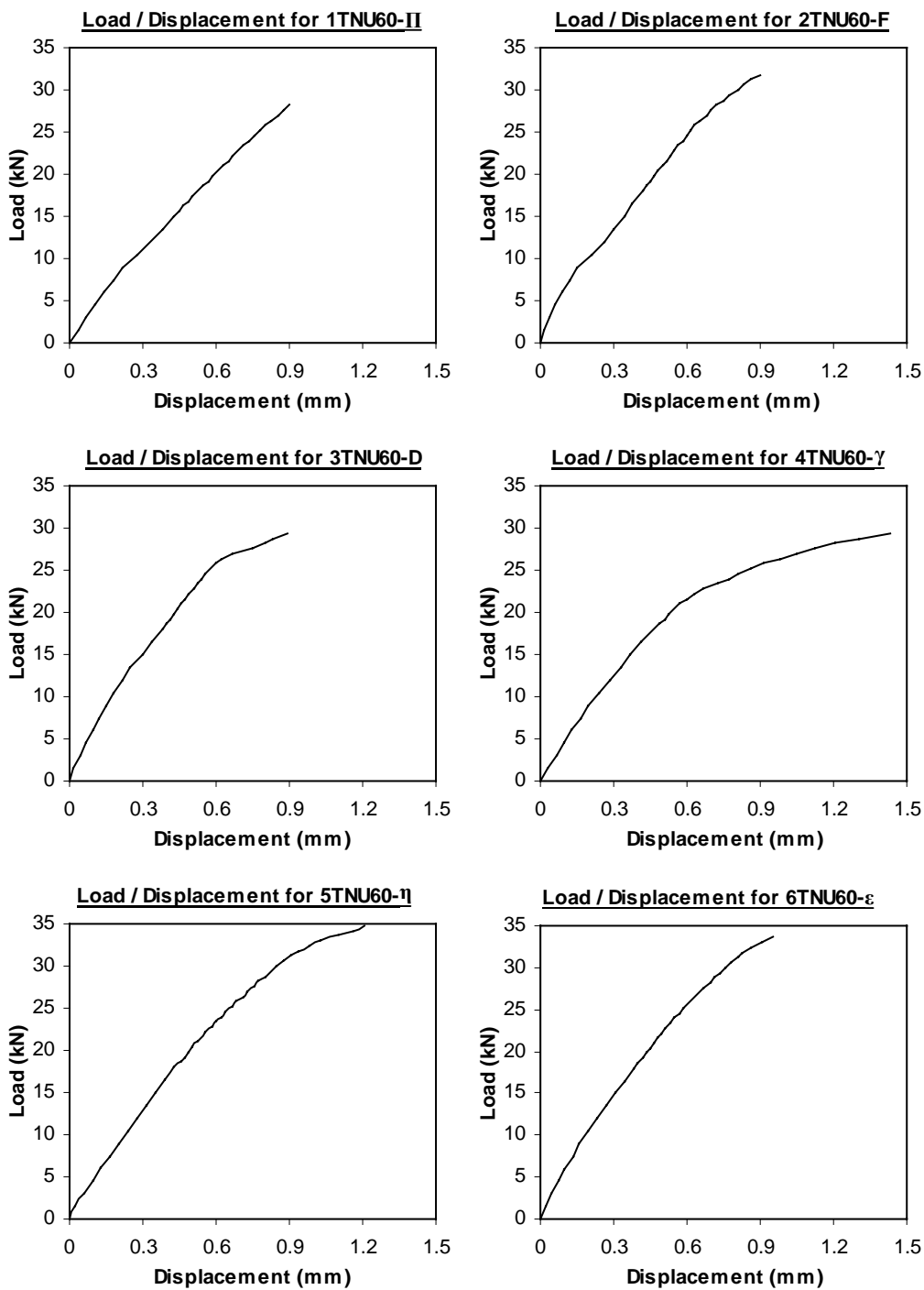


Figure 5.17 Load/displacement curves for TNU60 tests.

The displacements were measured using the average readings from the small LVDTs positioned on the samples sides. However strain gauges were also used on of the tested samples, the sample 5TNU60 - η . Measurements of strains at precise locations on the surface of the glass fibre/epoxy composite layers were carried out. These results are presented in § 5.6.

The load/displacement curves for the TNU60 tests show that the displacements recorded around the gap between the connected members never exceed 1.5 mm at failure.

The failure loads recorded for the six samples are relatively uniform, ranging between 29.4 and 35.4 kN.

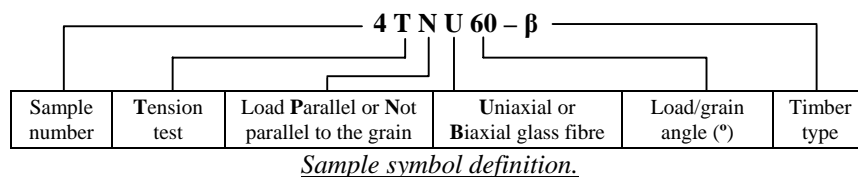
The elastic behaviour of the samples exceeds 72% of the overall recorded joint slip for a maximum elastic displacement of 0.91 mm.

Here again, not all the samples seemed to reach a plastic behaviour at failure. The curves are reflecting an elastic-plastic behaviour, in a similar manner than the TNU90 tests. However the last two samples failed at a higher load than the curves end indicated on the graph, because of large deformation occurring before failure.

Points of flexure are visible, particularly on sample No 3, 4 and 5. This confirms that some plastic behaviour developed at failure, and the transition was less progressive than for the TNU90 tests.

The comparison of various parameters obtained from these tests is presented in the discussion section, in § 5.5.4.

The same tests were carried out on the TNB60 samples. The table 5.22 summarises all the results obtained for TNB60 tests.



Sample	1TNB60 - H	2TNB60 - S	3TNB60 - Ω	4TNB60 - Q	5TNB60 - W	6TNB60 - P	Average Values	Standard Deviation
Failure Load (kN)	28.8	27	28.2	26.4	24	25.8	26.7	1.7
Elastic Zone (%)	90	76	79	91	83	79	83.0	6.2
Plastic Zone (%)	10	24	21	9	17	21	17.0	6.2
Stiffness (kN/mm)	34	33	34	31	33	35	33.3	1.4
Elastic Deformation (mm)	0.78	0.63	0.67	0.79	0.61	0.59	0.68	0.09
Bending MOE (kN/mm ²)	8.66	6.51	8.02	6.02	6.87	7.2	7.21	0.98
Moisture Content (%)	11.84	11.87	11.26	10.58	10.20	10.72	11.1	0.7
Fibre Volume Fraction	0.41	0.27	0.37	0.25	0.2	0.35	0.31	0.08
Specific Gravity (kg/m ³)	523	487	445	397	458	466	463	42
Nominal S.G. (kg/m ³)	468	436	400	359	416	421	417	36
Exact Angle (Degrees)	62	62	62	62	61	60	N/A	N/A

Table 5.22 Results from TNB60 tests.

The failure load corresponds to the last load and displacement measurements recorded before the sample's failure. Typical load/displacement curves as shown in figure 5.18 clearly indicate the range of elastic and plastic behaviour of the sample, which is expressed in percent of failure load in table 5.22.

There were six samples of that type that were tested, with one having strain gauges. With a more careful fabrication process, the load/displacement curves shown in figure 5.18 do not display the usual change in slope due to the tensile failure of some epoxy resin infiltrated between the timber pieces, except for sample No 6.

The joint stiffness was calculated over the elastic range of the sample.

The modes of failure of each sample were also recorded during the tests and are summarised in table 5.23.

Samples	Failure Load (kN)	Modes of failure
1TNB60 - II	28.8	Top delamination one side/Bottom delamination other side
2TNB60 - S	27	Top delamination one side/Bottom delamination other side
3TNB60 - Ω	28.2	Top delamination both sides
4TNB60 - Q	26.4	Top delamination both sides
5TNB60 - W	24 (*)	Top delamination both sides
6TNB60 - P	25.8	Top delamination one side/Tension other side

Table 5.23 Failure modes from TNB60 tests.

The sign (*) Indicates that this sample failed prematurely because of poor fabrication process: The resin used on one of the composite layers started hardening before being laid properly with the roller, resulting in a poor quality bond.

The modes of failure observed through the tests were not of the same nature except that the delamination of the top lap of one of the composite layer seemed to occur every time. Once again it was difficult to identify which part of the composite failed first because the joint was hidden by the steel box. However it is likely that the delamination at the top (or bottom) of one side occurred first, all the loads were then transferred to the other layer, which failed soon after in a multiple modes of failure. Tension failure was not a common mode of failure for the TNB60 tests. The failure loads were in the same range than the TNB90 tests, delamination of the top lap occurred well before the fibres could have broken. It seemed that the bond strength was affected by the grain orientation of the timber sample.

The lap length of the composite for the TNU/TNB60 tests was longer (232 mm) than for the TNU/TNB90 tests (200 mm). This should normally improve the bond strength of the composite, but the bond failure occurred at nearly the same range of loads. It confirmed that the timber grain has a strong impact on the bonding strength. There was no longitudinal shear failure detected in the composite layers.

Figure 5.18 summarises the load/displacement curves obtained for the samples from the TNB60 tests.

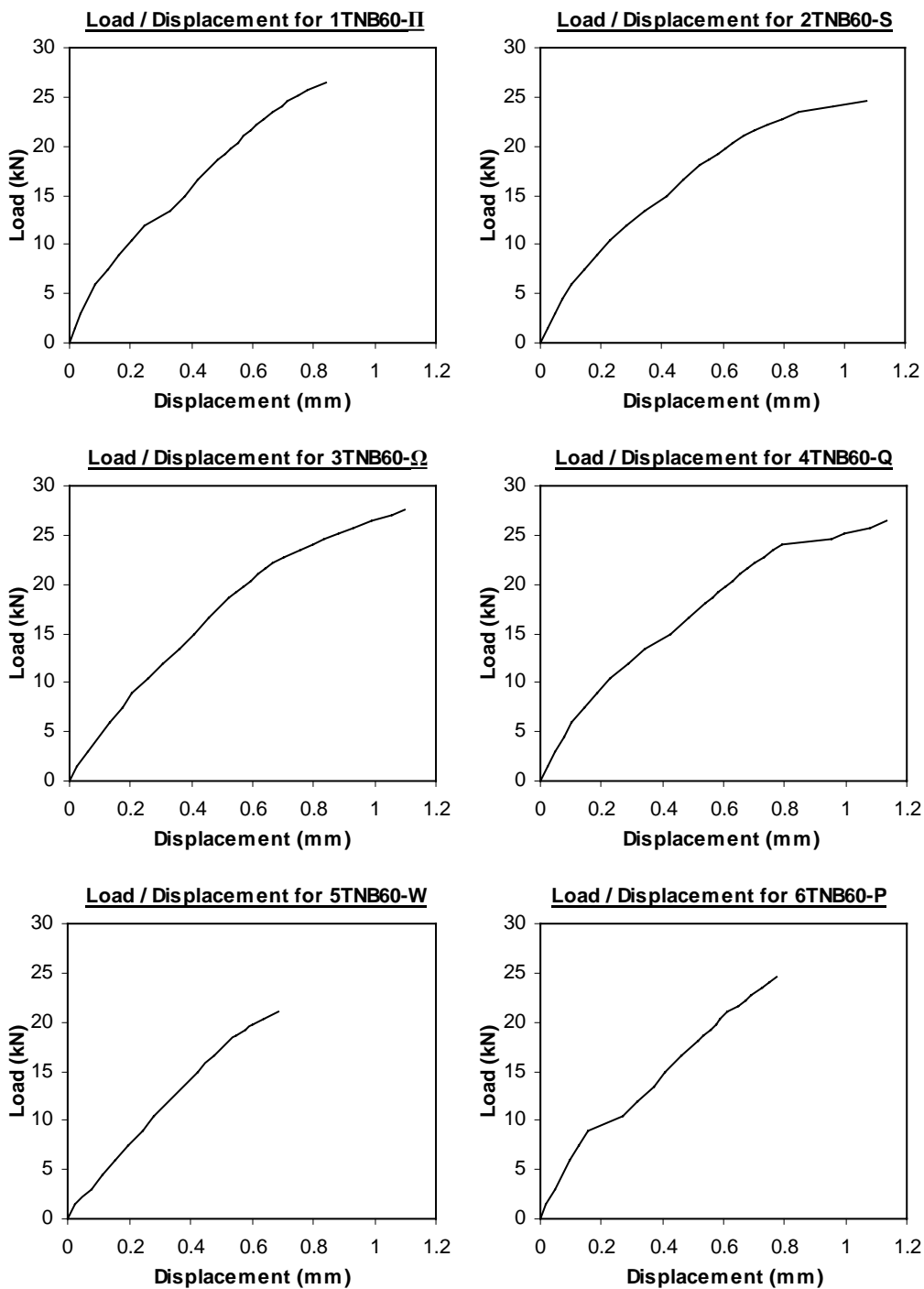


Figure 5.18 Load/displacement curves for TNB60 tests.

The displacements were measured using the average readings from the small LVDTs positioned on the samples sides. However strain gauges were also used on of the tested samples, the sample 5TNB60 - W. Measurements of strains at precise locations on the surface of the glass fibre/epoxy composite layers were carried out. These results are presented in § 5.6.

The load/displacement curves for the TNB60 tests show that the displacements recorded around the gap between the connected members never exceed 1.2 mm at failure.

The failure loads recorded for the six samples are relatively uniform, ranging between 24 and 28.8 kN.

The elastic behaviour of the samples exceeds 76% of the overall recorded joint slip for a maximum elastic displacement of 0.79 mm.

Here again, not all the samples seemed to reach a plastic behaviour at failure. The curves are still reflecting an elastic-plastic behaviour, in a similar manner than the TNU90 tests. However the first and last two samples failed at a higher load than the curves end indicated on the graph, because of large deformation occurring before failure. Only sample No 4 displayed a point of flexure, confirming that some plastic behaviour was occurring at failure. The curves show that the transition between elastic and plastic is progressive and does lead to some plasticity at failure.

The comparison of various parameters obtained from these tests is presented in the discussion section, in § 5.5.4.

5.5.3. TNU30 and TNB30 Tests

As explained previously, TNU30 and TNB30 tests were carried out with samples made of two timber pieces connected together with an angle of 30 degrees. This means one of the timber pieces had the load applied in its grain direction and transferred the load through the joint to the other piece with an angle of 30 degrees.

Two different types of samples were tested in tension with the load applied at an angle of 30 degrees to the grain:

- **Tension Not parallel with Uniaxial** glass fibre UT-E500, where the load was applied in the glass fibre direction ($\alpha = 0^\circ$) but with an angle of 30° to the grain ($\beta = 30^\circ$) of the timber piece considered. The sample type was classified as **TNU30**.
- **Tension Not parallel with Biaxial** glass fibre XE450, where the load was applied in the glass fibre direction ($\alpha = 0^\circ$) but with an angle of 30° to the grain ($\beta = 30^\circ$). The sample type was classified as **TNB30**.

Various measurements were carried out on these samples during test. The testing rig and the equipment used are presented in the previous chapter.

The samples positioning, displacement measurements using LVDTs through the data acquisition system, loading rates, the moisture content, density and FVF measurements were all carried out as for TNU90 and TNB90 tests.

The table 5.24 summarises all the results obtained for TNU30 tests.

Sample	1TNU30 - V	2TNU30 - W	3TNU30 - β	4TNU30 - X	5TNU30 - Z	6TNU30 - T	Average Values	Standard Deviation
Failure Load (kN)	37.8	31.8	37.2	31.8	31.2	28.8	32.2	3.1
Elastic Zone (%)	87	85	71	80	71	83	78	6.6
Plastic Zone (%)	13	15	29	20	29	17	22	6.6
Stiffness (kN/mm)	42	54	44	55	41	52	49.2	6.3
Elastic Deformation (mm)	0.8	0.5	0.6	0.48	0.55	0.47	0.52	0.05
Bending MOE (kN/mm ²)	6.46	8.89	5.63	8.89	6.36	6.79	7.31	1.50
Moisture Content (%)	10.15	11.25	11.06	10.16	10.78	11.35	10.92	0.48
Fibre Volume Fraction	0.24	0.22	0.23	0.23	0.23	0.25	0.23	0.01
Specific Gravity (kg/m ³)	401	504	493	460	400	478	467	41
Nominal S.G. (kg/m ³)	364	453	444	418	361	429	411	40
Exact Angle (Degrees)	32	32	32	33	32.5	32	N/A	N/A

Table 5.24 Results from TNU30 tests.

The failure load corresponds to the last load and displacement measurements recorded before the sample's failure. Typical load/displacement curves as shown in figure 5.21 clearly indicate the range of elastic and plastic behaviour of the sample, which is expressed in percent of failure load in table 5.24.

There were six samples of that type that were tested. In fact, there was only one sample tested with strain gauges.

The joint stiffness was calculated over the elastic range of the sample.

The modes of failure of each sample were also recorded during the tests and are summarised in table 5.25.

Samples	Failure Load (kN)	Modes of failure
1TNU30 - V	37.8	Top delamination both sides
2TNU30 - W	31.8	Top delamination both sides
3TNU30 - β	37.2	Top delamination one side/Bottom delamination other side
4TNU30 - X	31.8	Top delamination both sides
5TNU30 - Z	31.2	Top delamination both sides
6TNU30 - T	28.8	Top delamination one side/Partial tension other side

Table 5.25 Failure modes from TNU30 tests.

One mode of failure was predominant through the tests of these samples. In fact all the samples failed by delamination of at least one of the top lap of the composite layers. Once again, this seemed to indicate that the grain direction affects the bond strength of the joint. The figure 5.19 and 5.20 show two of the TNU30 samples after failure.



Figure 5.19 Top delamination on both sides at failure of sample 4TNU30 - X.

The figure 5.19 clearly shows that the sample failed by delamination of both top laps of the composite layers. The wood at the edge of the top member failed in tension along its annual rings and remained bonded to the composite. This phenomenon occurred in many of the sample tested throughout all the experiments. It was observed on most of the TNU30 samples tests, as also shown in figure 5.20.



Figure 5.20 Top delamination on both sides at failure of sample 5TNU30 - Z.

Once again it is likely that the delamination at the top (or bottom) of one side occurred first, all the loads were then transferred to the other layer, which failed soon after in a multiple modes of failure.

This mode of failure also confirmed that this type of joint was still unbalanced.

The lap length of the composite for the TNU/B30 tests was even longer (400 mm) than for the TNU/B60 tests (232 mm) or the TNU/B90 tests (200 mm).

This increased lap length improved the bond strength of the composite, as the failure occurred at higher loads. It still confirmed that the timber grain has a strong impact on the bonding strength.

There was no longitudinal shear failure detected in the composite layers.

Figure 5.21 summarises the load/displacement curves obtained for the samples from the TNU30 tests.

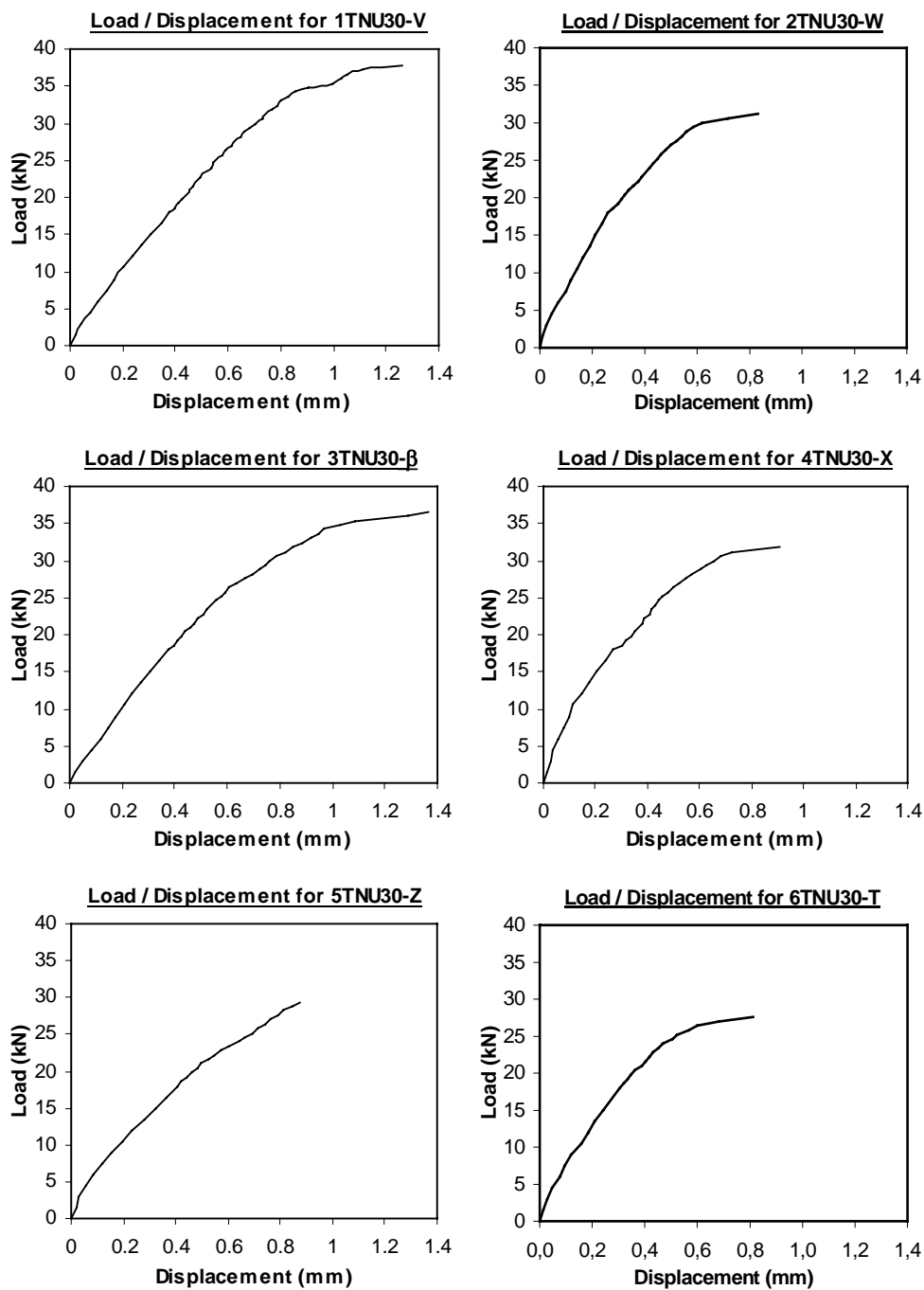


Figure 5.21 Load/displacement curves for TNU30 tests.

The displacements were measured using the average readings from the small LVDTs positioned on the samples sides. However strain gauges were also used on of the tested samples, the sample 1TNU30 - V. Measurements of strains at precise locations on the surface of the glass fibre/epoxy composite layers were carried out. These results are presented in § 5.6.

The load/displacement curves for the TNU30 tests show that the displacements recorded around the gap between the connected members never exceed 1.4 mm at failure.

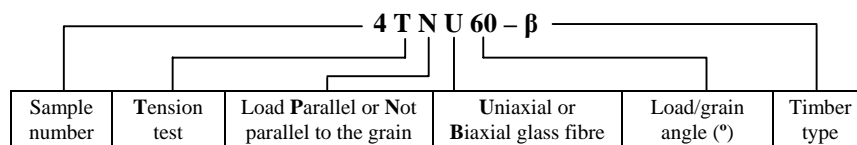
The failure loads recorded for the six samples are relatively uniform, ranging between 28.8 and 37.8 kN.

The elastic behaviour of the samples exceeds 71% of the overall recorded joint slip for a maximum elastic displacement of 0.8 mm.

The samples developed a plastic behaviour generally. The curves are still reflecting an elastic-plastic behaviour. However samples No 2, 4, 5 and 6 failed at a higher load than the curves end indicated on the graph, because of large deformation occurring before failure. The absence of point of flexure shows that the transition between elastic and plastic is progressive and do lead to some plasticity at the failure.

The comparison of various parameters obtained from these tests is presented in the discussion section, in § 5.5.4.

The same tests were carried out on the TNB30 samples. The table 5.26 summarises all the results obtained for TNB30 tests.



Sample symbol definition.

Sample	1TNB30 - α	2TNB30 - V	3TNB30 - R	4TNB30 - Δ	5TNB30 - Y	6TNB30 - U	Average Values	Standard Deviation
Failure Load (kN)	27	32.4	31.8	27	29.4	30	29.6	2.3
Elastic Zone (%)	91	83	74	76	78	78	80	6.2
Plastic Zone (%)	9	17	26	24	22	22	20	6.2
Stiffness (kN/mm)	48	69	54	65	63	44	57.2	10.0
Elastic Deformation (mm)	0.52	0.39	0.44	0.32	0.36	0.53	0.43	0.09
Bending MOE (kN/mm ²)	6.89	6.79	6.78	7.09	6.08	6.44	6.68	0.36
Moisture Content (%)	11.21	10.97	11.20	11.11	10.24	10.29	10.8	0.5
Fibre Volume Fraction	0.25	0.24	0.24	0.25	0.29	0.22	0.25	0.02
Specific Gravity (kg/m ³)	525	409	467	517	429	422	462	50
Nominal S.G. (kg/m ³)	473	369	420	465	389	383	416	44
Exact Angle (Degrees)	33	33.5	33	32.5	28	32	N/A	N/A

Table 5.26 Results from TNB30 tests.

The failure load corresponds to the last load and displacement measurements recorded before the sample's failure. Typical load/displacement curves as shown in figure 5.22 clearly indicate the range of elastic and plastic behaviour of the sample, which is expressed in percent of failure load in table 5.26.

There were six samples that were tested, with one having strain gauges.

The joint stiffness was also calculated over the elastic range of the sample.

The modes of failure of each sample were also recorded during the tests and are summarised in table 5.27.

Samples	Failure Load (kN)	Modes of failure
1TNB30 - α	27	Top delamination one side/Tension other side
2TNB30 - V	32.4	Top delamination one side/Tension other side
3TNB30 - R	31.8	Top delamination one side/Tension other side
4TNB30 - Δ	27	Top delamination both sides
5TNB30 - Y	29.4	Top delamination one side/Tension other side
6TNB30 - U	30	Top delamination one side/Tension other side

Table 5.27 Failure modes from TNB30 tests.

The modes of failure observed through the tests were not of the same nature except that the delamination of the top lap of one of the composite layer seemed to occur every time. Once again it was difficult to identify which part of the composite failed first because the joint was hidden by the steel box. However it is likely that the delamination at the top of one side occurred first, all the loads were then transferred to the other layer, which failed soon after in a multiple modes of failure. Tension failure was a common mode of failure for the TNB30 tests. Again the bond strength seemed to be affected by the grain orientation of the timber sample.

Because the joint failed in delamination and tension modes, with the composite failing in the top and bottom zones, this type of joint could be considered as balanced.

There was no longitudinal shear failure detected in the composite layers.

Figure 5.22 summarises the load/displacement curves obtained for the samples from the TNB30 tests.

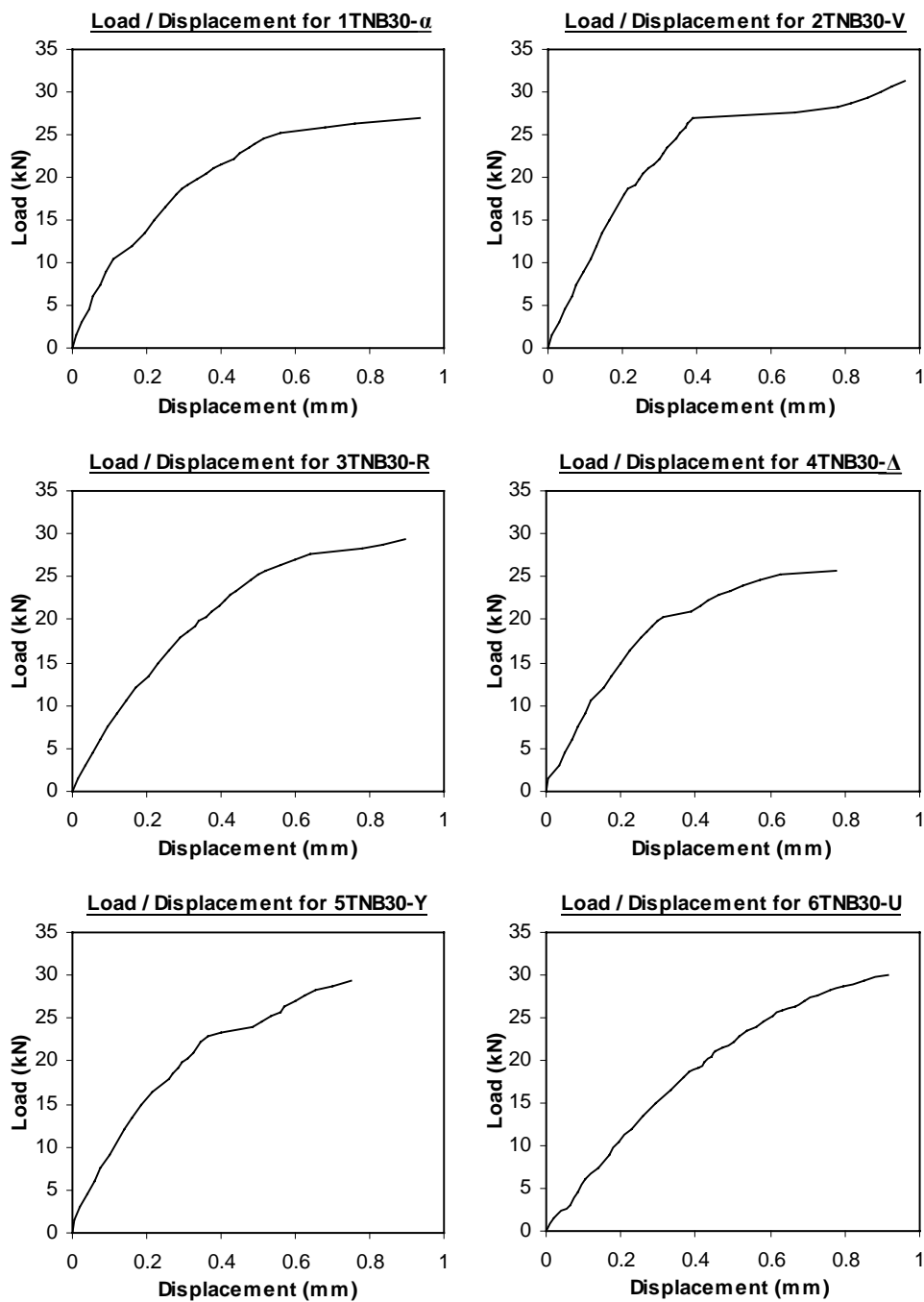


Figure 5.22 Load/displacement curves for TNB30 tests.

The displacements were measured using the average readings from the small LVDTs positioned on the samples sides. However strain gauges were also used on of the tested samples, the sample 6TNB30 - U. Measurements of strains at precise locations on the surface of the glass fibre/epoxy composite layers were carried out. These results are presented in § 5.6.

The load/displacement curves for the TNB30 tests show that the displacements recorded around the gap between the connected members never exceed 1 mm at failure.

The failure loads recorded for the six samples are relatively uniform, ranging between 27 and 32.4 kN.

The elastic behaviour of the samples exceeds 74% of the overall recorded joint slip for a maximum elastic displacement of 0.53 mm.

The samples develop a plastic behaviour generally. The curves are still reflecting an elastic-plastic behaviour. Three samples displayed a point of flexure, confirming that some plastic behaviour was occurring at failure. The other curves shows that the transition between elastic and plastic is progressive and do lead to some plasticity at the failure.

The comparison of various parameters obtained from these tests are presented and discussed in the following section.

5.5.4. Discussion

There were six different configurations of samples considered for the tension tests with load not parallel to the timber grain. Those configurations depended of the type of glass fibre used, whether it was uniaxial or biaxial strands, but also of the angle between the timber members in relation to the glass fibre and load direction.

The primary assessment can be drawn from the comparison of failure loads for each configuration. For each type of test considered, the failure loads appeared to be relatively uniform. Therefore it was found acceptable to use average values as an approximate representation of the whole test series.

The figure 5.23 shows a graph of the average failure loads for all the tension tests with load not parallel to the grain including standard deviations.

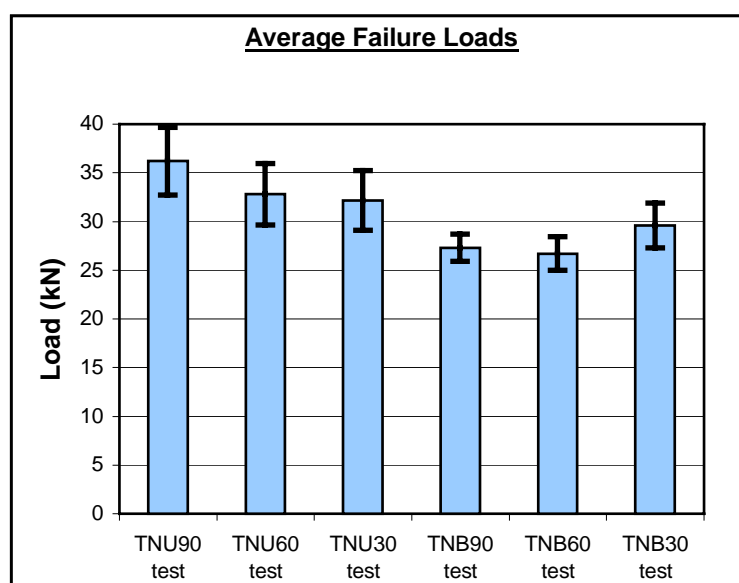


Figure 5.23 Average failure loads for all tension tests with the load not parallel to the grain.

There are major differences between the TNU (uniaxial glass fibres) and the TNB (biaxial glass fibres) systems, which need to be identified to enable the explanation of these results: The modes of failure observed for both systems were clearly different. The TNU tests always failed by delamination of the composite, whereas the TNB tests failed by combination of delamination and tension rupture of the composite. This observation was confirmed by the fact that failure loads for the

TNB tests were lower than failure loads for the TNU tests, whatever angle configuration was considered. In fact for the TNU tests, all the fibres of the uniaxial glass are orientated in the load direction: They are working to lower stresses than the fibres in the TNB tests where the biaxial glass allow only 50% of the fibres to work directly in tension. With fewer fibres available to transfer the loads, the TNB tests failed at lower loads, whether it was delamination failure or fibre rupture.

Considering all joint configurations, the length of the composite layer was defined by the geometry of the joints. For the 90 degrees grain/load angle, the length of composite was of 200 mm, the same length than for the load parallel to the grain tension tests. But for other grain/load angles, different lengths of composite were used: 232 mm long for the 60 degrees and 400 mm long for the 30 degrees. Consequently the bonding length and area were increased for those types of tests, resulting in a potentially higher bond strength capacity. For example, in a system where the joint is unbalanced so that it always fails by delamination (i.e. bond stress failure), by increasing the length of composite, the joint would develop higher bond capacity. With higher bond capacity and sufficient fibre strength, the joint should have failed at higher loads. But this was not the case for the TNU and TNB tests.

For the TNU tests, where the joints were clearly unbalanced (the joints always failed by Delamination), the failure loads seemed to decrease as the grain/load angle reduced from 90 to 30 degrees. In this situation, the longer the composite layers, the lower the failure loads. In fact the grain orientation was an important parameter to take into account: Failure by delamination always occurred on the timber members, where the composite was orientated with an angle to the grain. This indicated that the bond strength of the composite was reduced when the timber grain was not orientated in the same direction than the composite fibres and the loading. When the fibres are orientated perpendicular to the timber grain direction such as the TNU90 test, it is clear that this system is the strongest in terms of failure loads, as shown in figure 5.23. The average failure loads decrease as the angle to the grain reduces. But this reduction is not as significant as it could be, if the length of composite were equal for all the TNU tests.

The situation was rather different for the TNB tests. The modes of failure were less consistent and were generally combinations of various modes, such as fibre tension rupture, delamination and longitudinal shear failures. As a result, the failure loads did not decrease as the grain/load angle reduced from 90 to 30 degrees. The failure loads

appeared to be fairly uniform for the TNB90 and TNB60 tests, and slightly higher for TNB30. This inconsistency was probably due to the fact that only one half of the fibres were directly stressed in tension, then the tension capacity of the composite was lower than for the TNU tests. Furthermore, the biaxial fabric XE450 used for the TNB tests had two layers of fibres, skewed and stitched together, one on top of the other, as explained in chapter 3. Because the fibres were not woven, the bond between the composite and the timber only affected the layer of fibres in direct contact with the interface. This was certainly a reducing factor of the composite bond strength for the TNB tests. With lower bond and tension strengths, the length of composite became a major factor in the strength of the joint. Longer strands of fibres improved the bond strength significantly, but the grain orientation was still having a reducing effect on it.

The figure 5.24 shows a graph of the average stiffness for all the tension tests with load not parallel to the grain including standard deviations.

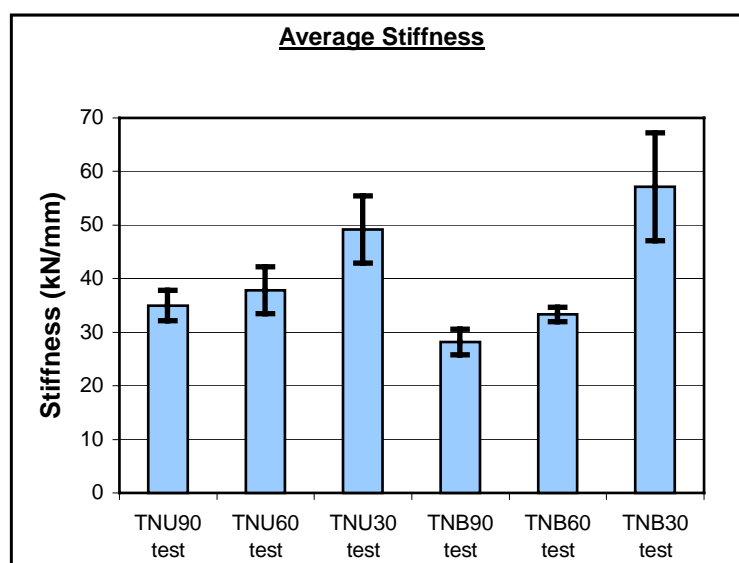


Figure 5.24 Average stiffness for all tension tests with the load not parallel to the grain.

The average stiffness for each type of test was derived from values across the elastic region of the load/displacement curves. The epoxy resin infiltration in the gap area of some joints increased the initial stiffness significantly. Ultimately the epoxy in the gap failed in tension, resulting in a large displacement on the load/displacement curves. The stiffness was in fact calculated over the portion of the elastic region of

the curve, which follows this large displacement, in order to disregard this local and unwanted stiffening effect of the joints.

It is also important to relate the stiffness to the elastic deformation, which is the overall elastic joint slip (or displacement). The figure 5.25 shows a graph of the average elastic deformation for all the tension tests with load not parallel to the grain including standard deviations.

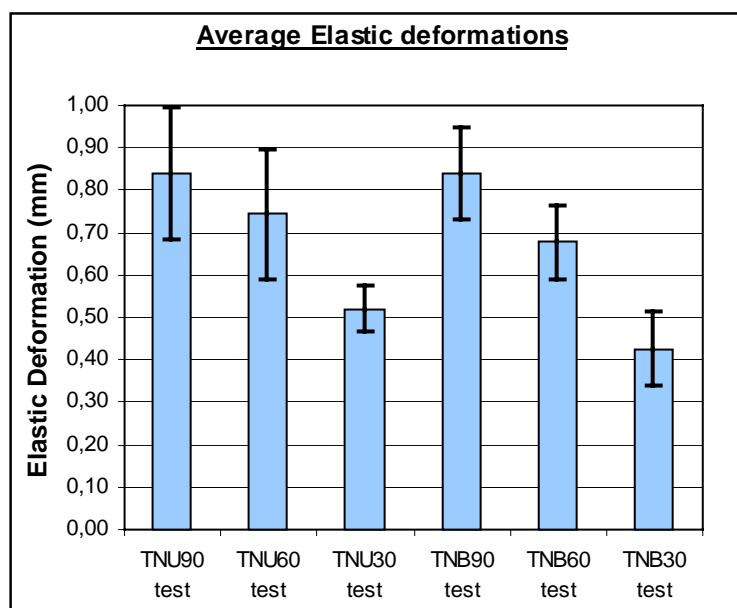


Figure 5.25 Average elastic deformations for all tension tests with the load not parallel to the grain.

The figure 5.24 clearly shows that for both TNU tests and TNB tests, the joint stiffness increased as the angle between the timber grain and the load direction decreased from 90 to 30 degrees. There are two major factors, which explain those results:

- The length of composite increased while the angle decreased from 90 to 30 degrees, therefore the elastic deformation decreased (less gap displacement), as shown in figure 5.25, and the joint stiffness increased. But for the TNB tests with longer strands of composites, there was no guarantee that the stiffness would increase because the fibres could fail in tension rupture. However for the TNB tests, the elastic deformation also decreased with the angle, as shown in figure 5.25, and the joint stiffness increased. With a longer layer of composite, there is less elastic deformation of the joint.

- The timber grain orientation has a direct effect on the joint stiffness. For the TNU90 and TNB90 tests, when the load was applied perpendicular to the grain, the elastic deformations were the largest, as shown in figure 5.25. The timber properties are generally much lower in the radial or tangential directions than in the longitudinal direction of the grain.

“Approximate values of the moduli of elasticity may be found by taking E_L (longitudinal modulus of elasticity) equal to 1.1 times the bending modulus, E_T (tangential modulus of elasticity) equal to $0.05 \times E_L$ and E_R (radial modulus of elasticity) equal to $0.10 \times E_L$.” (Booth et al., 1967).

As for the moduli of elasticity, tension strength of the timber in the tangential or radial direction is significantly lower than in the longitudinal direction. Based on the Hooke’s Law of elasticity ($\sigma = \mathbf{E} \times \epsilon$), if the modulus of elasticity \mathbf{E} is reduced, the strain ϵ must increase to achieve the same stress σ . The larger elastic deformations observed on the tension tests with load perpendicular to the grain TNU90 and TNB90 indicate that larger strains occur in the timber materials. As the load/grain angle reduce from 90 to 30 degrees, the timber properties would improve, as they are optimum in the grain direction. With higher tension strength, then higher modulus of elasticity, the strain would be reduced to achieve an equivalent stress. Consequently the elastic deformation reduces with the load/grain angle.

The length of the composite layer and the timber grain orientation are the parameters, which affect the failure loads, the stiffness and elastic deformations of the joints tested in tension with load not parallel to the grain.

The results of the tension tests with load parallel and with load not parallel to the grain are summarised in the conclusion of this thesis.

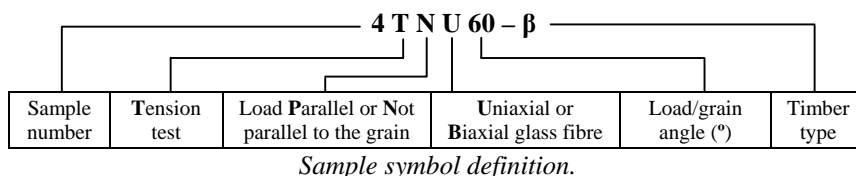
The results of all the samples tested with the use of strain gauges are presented and discussed in the following section.

5.6. Samples tested with strain gauges

Through all the samples that were tested in tension with load parallel and load not parallel to the grain, strain gauges were used on 10 samples. Those gauges were of two different types and were glued on top of the glass fibre/epoxy composite layers, at precise locations. The technical information about the gauges and their positions on each type of samples was described in the previous chapter.

The strain gauges were used to record the level of strain within the composite layers at precise locations for specific loads. These results would help to understand how the stresses are distributed through the composite and how the load is transferred from one piece of timber to the other.

The table 5.28 summarises the strain gauge positions on the composite layers for each type of sample.



Sample	Position on composite	End	Middle	Gap		Side
	Type of gauge	Straight gauge	Straight gauge	Straight gauge	Rosette gauge	Straight gauge
7TPU00 - Z		✓	✓	✓	✗	✗
8TPU00 - J		✓	✗	✓	✗	✗
1TNU30 - V		✓	✗	✗	✓	✓
5TNU60 - η		✓	✗	✗	✓	✓
5TNU90 - Ω		✓	✗	✓	✗	✗
7TNB00 - α		✓	✗	✓	✗	✗
8TNB00 - \$		✓	✗	✓	✗	✗
6TNB30 - U		✓	✗	✗	✓	✓
5TNB60 - W		✓	✗	✗	✓	✓
6TNB90 - φ		✓	✗	✓	✗	✗

Table 5.28 Table of the strain gauges positions for each tested sample.

The strain gauge positions were specific of the type of test considered. All the samples had strain gauges positioned in the gap location because it is an area where

the strain in the composite is likely to be the highest when any tension is applied to the sample. The choice of straight gauge or Rosette gauge was based on the geometry of the sample: All the samples tested in straight or perpendicular configuration were equipped with straight gauges in the gap area. These samples were loaded in tension and most of the strain occurring in the gap area was due to the tension forces acting in the longitudinal direction and the lateral contraction resulting from this tension (Poisson's ratio).

For the samples tested in configuration with load not parallel nor perpendicular to the grain, the state of strain in the gap area was also due to the tension forces acting in the longitudinal direction as well as the lateral contraction resulting from this tension (Poisson's ratio), but the inclination of the upper timber piece induced additional transversal strains along the inclination as the loads pulled the timber pieces apart. These samples were equipped with strain Rosette gauges to enable the measurement of this transversal strain. Additional straight gauges were provided on one side of the composite, still in the gap area, to check whether this transversal shear effect would induce lateral bending of the lower timber piece.

The figure 5.26 shows all the gauges locations on a typical composite layer.

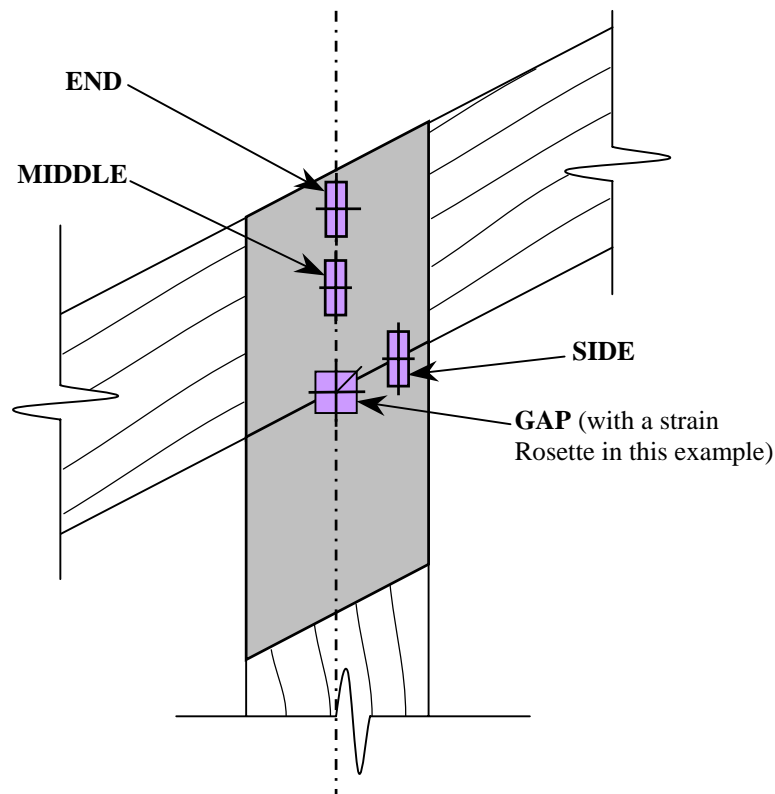


Figure 5.26 Strain gauge positions on a typical composite layer.

The strains measured by the gauges were plotted against the load for each sample. Figure 5.27 summarises the load/strain curves obtained for the samples with load parallel to the grain, tested with strain gauges.

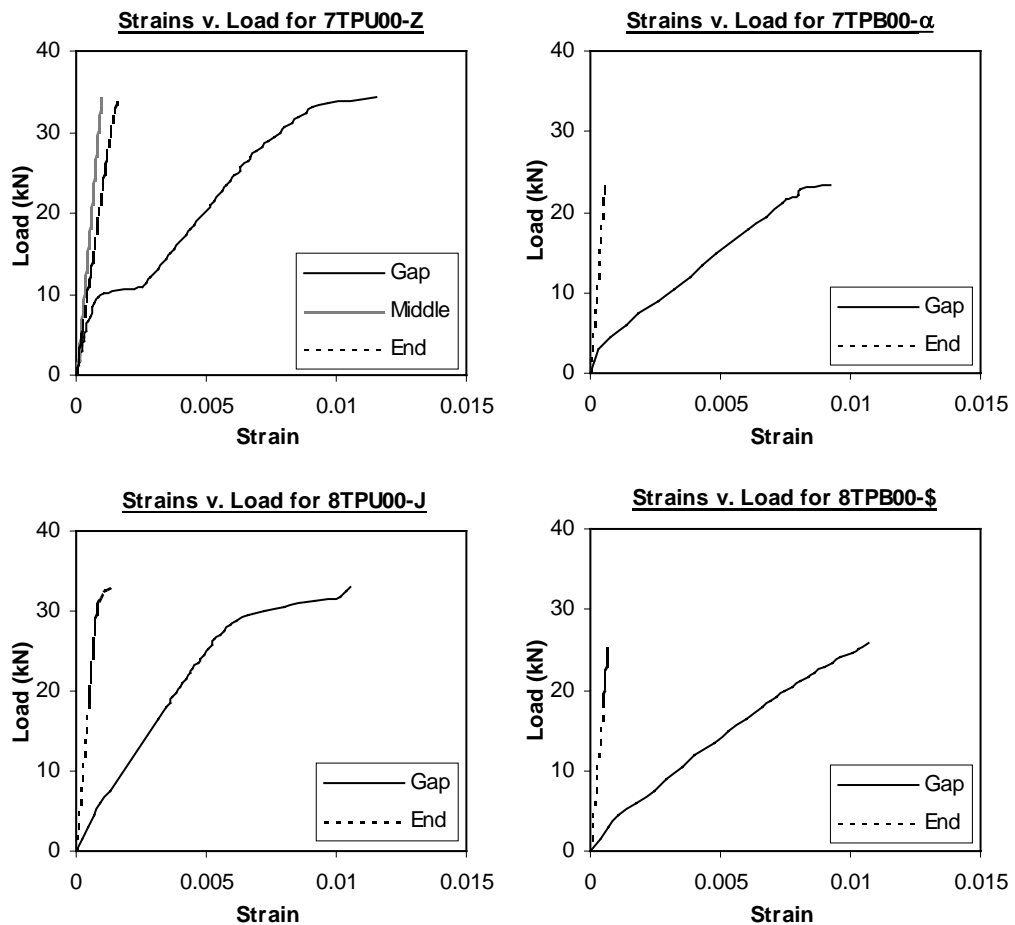


Figure 5.27 Load/strain curves obtained for the samples with load parallel to the grain.

The shape of the curves shown in figures 5.27 and 5.28 are similar to the load/displacement curves of the same sample configurations shown on previous figures. For example, the load/strain curve of sample 7TPU00 - Z shows the same step in the elastic range than the load/displacement curve of the same sample. As previously explained, this step is caused by the tensile failure of the epoxy resin infiltrated in the gap between the timber pieces.

Figure 5.28 summarises the load/strain curves obtained for the samples with load not parallel to the grain, tested with strain gauges.

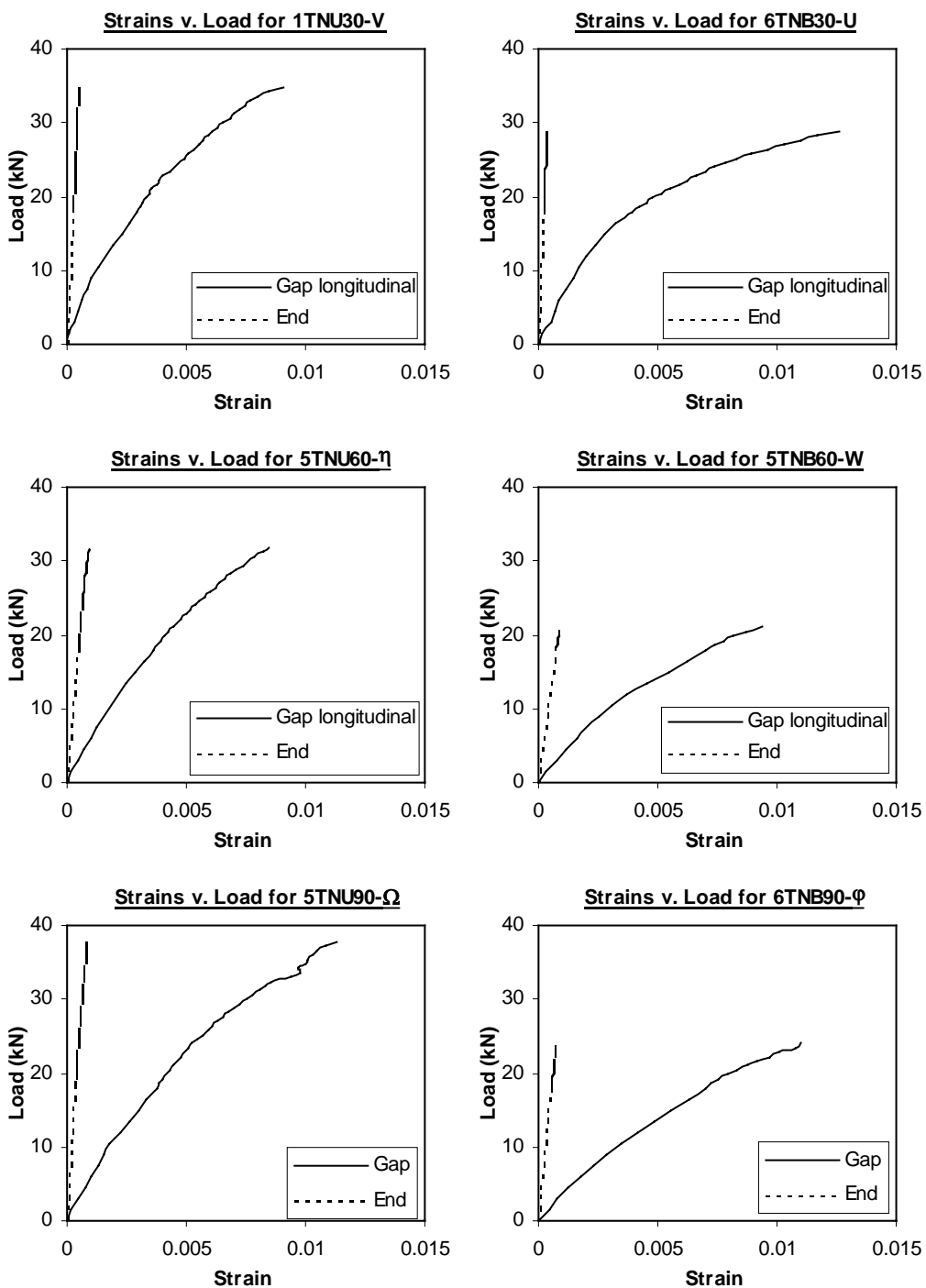


Figure 5.28 Load/strain curves obtained for the samples with load not parallel to the grain.

The strain gauges were used on some of the samples in order to identify how the stresses are distributed through the composite. The strain gauges were positioned on top of the composite layer. It would have been interesting to place some strain gauges as well at the interface between the timber and the composite to evaluate whether the strain was varying through the thickness of the composite. However it was impractical to do so, because of the gauge wires to be connected to the data acquisition system. The wires could not be driven through the composite without affecting the quality of the bond. Furthermore strain gauges do not behave properly on timber, as the glue used for the bond is always of much higher stiffness than the wood itself. Nevertheless the composite was a very thin layer of material (less than 1 mm) and it is reasonable to assume that the strain would only vary by a slight amount across the thickness.

The load transfer through double lap bonded joints such as the wood/glass/epoxy joints is generally non linear. The shear stress observed at the interface when the joint was loaded in tension varied along the length of the lap: It was high in the gap area and then decreased towards the middle of the lap length and increased as it reached the end of the lap. This distribution depended on the lap length and also of the loading applied.

The strains recorded from two oppositely positioned strain gauges on the composite layers of a sample were of similar magnitude for a given load, except at high loads when the sample reached failure. It showed that the tension applied through the samples was equally distributed between both layers.

The results of the strain values obtained through those tests are summarised in a table presented in Appendix A. Only the values recorded for loads of 6, 12, 18, 24 and 30 kN are reported. This data will be used as a comparison for the results obtained from the finite element modelling of the samples. The theoretical approach and the FE modelling process are described in the chapter 6.

The properties of timber were derived mainly from small clear sample tests. The results are presented and discussed in the following section, which deals with timber grading.

5.7. Strength determination and timber grading

5.7.1. Small clear sample tests

Small clear timber sample tests were carried out in order to calculate the mechanical properties of timber, which were required as input parameters for the finite element modelling of the wood/glass/epoxy joints. Furthermore, the small clear timber sample tests were necessary to grade the timber in order to check the information provided by the timber supplier.

As explained in the previous chapter, the determination of the mechanical properties was carried out on a random selection of 10 different timber planks. From each plank, small clear samples were cut for different tests.

Four different types of test were carried out to establish the following properties:

- Modulus of Elasticity (MOE) in bending and bending strength, which is also called Modulus of Rupture (MOR)
- Tension strength and tension MOE parallel to the grain
- Tension strength and tension MOE perpendicular to the grain
- Shear strength parallel to the grain.

The numbers of sample tested per test are summarised in table 5.29.

Test number	Properties measured	Number of sample tested
1	Bending MOE and MOR	20
2	Tension strength and tension MOE parallel to the grain	20
3	Tension strength and tension MOE perpendicular to the grain	20
4	Shear strength parallel to the grain	40

Table 5.29 Summary of small clear timber sample tests.

For each full-size sample tested, a piece of wood was cut from the sample immediately after the test to measure the moisture content and the specific gravity.

The determination of mechanical properties of timber and the timber grading were two different processes, which needed to be carried out.

The tests used to evaluate the timber properties were mainly undertaken on small clear timber samples, based on the existing code BS 373:1986. One test not based on this standard was the MOE and tension strength perpendicular to the grain test, which was an adapted test from the standard on structural-size timber given by the code EN 1193: 1997. The facilities to fabricate the samples required for the tension perpendicular to the grain in the code BS 373: 1986 were not available. The alternative was to use the standard test on structural-size timber given by the code EN 1193: 1997 but the sizes of timber available were too small to satisfy the standards requirements. By scaling down the sample sizes, the test could not be considered as a standard test any longer. Nevertheless the pieces of timber selected for this test were defect-free therefore this test could also be treated as a small clear sample test.

The timber properties could have been calculated from structural-size timber tests, but the equipment required for such test is relatively sophisticated and is usually available in specialised timber research laboratories.

From a design consideration, small clear sample tests have been superseded in the timber industry since the mid-1970s by the structural-size timber tests. But they remain valid for characterising timber and for academic purposes. Small clear samples are defect-free pieces carefully selected to provide the best quality of timber that can be obtained. In fact they do not reflect the quality of structural-size timber.

Before 1973, small clear sample tests were carried out to obtain the working stresses of the timber. Because the samples were not representative of structural-size timber, several reduction factors were used to take into account the defects of the wood material.

After 1973 the tests on structural-size timber were developed as a radical change of method to establish the timber working stresses occurred.

“The realisation in the 1970s that the duration of load values derived from testing of small clear test pieces were not appropriate for structural timber led to the derivation of grade stresses directly from actual structural-size timber” (Dinwoodie, 2000).

It was then necessary to develop the process of timber grading, with the visual or mechanical methods. Although before 1973, visual grading was already part of the derivation of the timber grade stresses. The small clear sample tests enabled the calculation of basic stresses, on which reduction factors based on the visual grading of the corresponding full-size timber were applied to obtain grade stresses. The

method is fully described in the excellent but superseded book “The structural use of timber” (Booth et al., 1967). This book is a commentary on the British Standard CP112: 1967, the timber code prior to the BS 5268.

A further inconvenience of the small clear sample tests was that they enabled the derivation of a complete set of grade stresses for a specific species, without relating it to any strength class. The new approach with structural-size timber tests was such that it defined the grade stresses and derived them either in form of strength classes or for the individual species.

“The advantage of the strength class system over the listing of stresses for individual species and grades is that it allows suppliers to meet a structural timber specification by supplying any combination of species and grade listed in BS 5268: Part 2: 1996 as satisfying the specified class” (Dinwoodie, 2000).

The table 5.30 summarises the changes in derivation of design stresses since 1973.

	UK			EUROPE			
→ 1973	1973–1995			1995 – about 2005			1996 →
Data from testing small clear test pieces	Structural timber			Structural timber			Structural timber
↓	↓			↓			↓
Mean value less 2.33s	Grading		Tests ^o	Grading		Tests ^o	Grading Tests ^o
↓	↓		BS 5820	↓		EN 408	↓
Divided by safety factor* to give Basic stress	Visual BS 4978 (1988) BS 5756 (1980)	Machine BS 4978 (1988)	↓	Visual BS 4978 (1996) BS 5756 (1997)	Machine EN 519	EN 384 ↓	Visual EN 518 ↓
↓	↓		↓	↓		↓	↓
Multiplied by strength ratio	Grade or Strength classes BS 4978 (1988)		↓	Strength classes and Characteristic values EN 338		↓	Strength classes and Characteristic Values EN 338, EN 1912
↓	↓		↓	↓		↓	↓
Derived Grade stresses in BS 5268 Part 2	Stresses in standard BS 5268 Pt. 2		↓	factored ↓ → Grade stresses		↓	↓
↓	↓		↓	↓		↓	↓
Design code BS 5268 Pt. 2	Design code BS 5268 Pt. 2		↓	Design code BS 5268 Pt. 2		↓	Design code ENV 1995-1-1

s = standard deviation
 * = safety factor (1.4 for compression || to the grain; 2.25 for all other modes) to cover effects of specimen size and shape, rate of loading and duration of load
^o = testing used only to derive values for inclusion in the standards

Table 5.30 Changes in derivation of design stresses over the period before 1973 to 2005 (Dinwoodie, 2000).

The current British European Standard EN 384: 1995 which deals with the determination of characteristic values of mechanical properties and density of timber, does not cover the use of small clear samples if they are used on their own. This standard clearly states: “Factors to determine characteristic values of bending strength and modulus of elasticity may be derived where both small, clear and structural size data are available for at least three other species”. In other words, the current code does not recommend the derivation of timber properties if only small clear sample tests are carried out.

The determination of the timber mechanical properties used in this research was thus based on the method from small clear sample tests given in CP112: 1967 “The Structural Use of Timber”. This method provided:

- The timber mechanical properties necessary for the finite element modelling. The properties were the mean values of the results obtained from the tests.
- The grade stresses for the timber, which were used to check the strength class given by the timber suppliers. However the grade stresses had no direct use for the research in wood/glass/epoxy joints: Grade stresses are useful as far as design is concerned, but this research did not take into account any design consideration. The investigation on wood/glass/epoxy joints was too preliminary to get into design matters.

The following section deals with the grading process used to relate results derived from small clear sample tests with current standards specifications.

5.7.2. Principles and methods

The timber Code of Practice CP112: 1967 gives the definitions of those two types of stresses:

- The basic stress in timber is the stress, which can safely be permanently sustained by timber containing no strength reducing characteristics.
- The grade stress in timber is the stress, which can safely be permanently sustained by timber of a particular grade.

The first definition clearly identifies the basic stresses as the stresses derived for the material itself. The method employed for the calculation of the basic stresses is based on the results obtained from tests on small clear samples of timber. A number of reduction factors would then be applied to these results to take into account several strength-reducing effects that timber can endure during its design life. Those factors are the moisture content, the load duration, the size and shape of the members, the variability of strength and the factor of safety.

As timber is a naturally grown material, wide variations of properties are observed within a particular species, even within the same tree. Rate of growth, age, knots and defects are some of the factors, which increase those variations. However if more and more samples of the same timber are tested, the variations will progressively show a Gaussian distribution curve on which the standard methods of statistical analysis are used. The figure 5.29 shows an example of frequency distribution of maximum crushing strength, tested from small clear samples of green tropical hardwood Keruing. It becomes clear that for any number of samples tested, there will be always one or more samples, which will not fall above an acceptable level. Using the properties of the Gaussian distribution, it is possible to calculate the failure level at which there is a specified probability of a sample failing.

The mean values and the standard deviation from the results are then calculated. The mean value m and the standard deviation s are defined as:

$$m = \frac{\sum x}{n} \quad (5.1)$$

$$\text{and } s = \sqrt{\frac{n \sum x^2 - \sum x^2}{n(n-1)}} \quad (5.2)$$

Where x stand for every value and n is the number of values.

It was decided that for most strength properties, the chance of getting a lower value than the estimated minimum one in a hundred times was acceptable. This failure level is marked on the graph shown in figure 5.29 as the theoretical value above which 99% of the test results should fall.

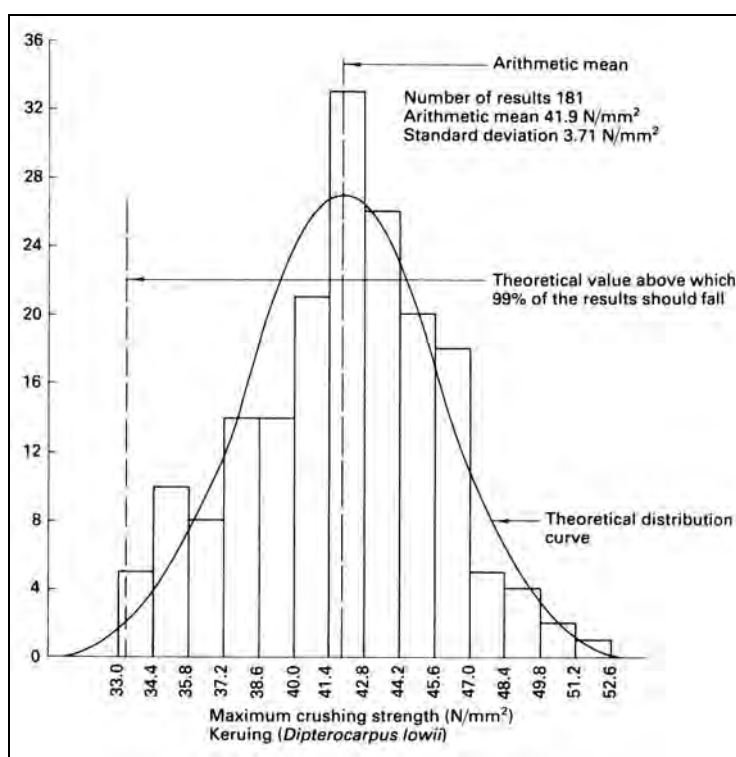


Figure 5.29 Frequency distribution of crushing strength of small clear test pieces of green hardwood keruing (Mettem, 1986).

The failure level above which 99% of the test results should fall is expressed as the mean value minus 2.33 times the standard deviation. This failure level can also be called the value of the lower 1-percentile of the population.

$$f_{01} = m - 2.33s \quad (5.3)$$

Where f_{01} is the failure level.

In the current British Standards and Eurocodes, when the test are carried out on structural-size samples, the same procedure is applied using the value of the lower 5-percentile of the population instead.

A reduction factor is then applied to the minimum value calculated with the equation (5.3) above. This factor allows for the load duration, the sample size and shape as well as a factor of safety. It is taken as 1.4 for compression strength and 2.25 for all other strengths. However this factor of safety does not apply to modulus of elasticity, which can be expressed as a mean value and a standard deviation. Depending on the requirements, it can also be expressed as a mean value and a minimum value calculated as the lower 1-percentile of the population.

The values obtained from the previous calculations are known as basic stresses. In this research, the tests were carried out on small clear samples cut from seasoned dry timber, which means the timber moisture content did not exceed 18%. Therefore the basic stresses are in fact dry basic stresses.

The next step is to grade the timber in order to derive the grade stresses.

Grade stresses in timber are related to the basic stresses of the individual species and are governed by the effect of visible gross features such as knots, sloping grain, etc.

The grade stresses are derived from the basic stresses using strength ratios. Those ratios are assigned to grade numbers: 40, 50, 65 and 75. The grading rules were given in CP112: 1967. The four grades are allocated in relation to the requirements of each timber characteristic defined as follow:

- Rate of growth. Measurement of the rate of growth is carried out at one end of a timber section, over a straight line 3 inches long (76.2 mm), normal to the growth rings and passing through the centre of the member. The table 5.31 gives minimum number of growth rings per inch to qualify for a particular grade.
- Fissures. Measurement of fissures is carried out at one end of the member, between lines enclosing the fissures. Fissures occurring on the surface should be measured to assess its depth. The table 5.31 gives maximum size of fissure expressed as a fraction of the member thickness to qualify for a particular grade.
- Slope of grain. Measurement is carried out using a grain detector. The table 5.31 gives maximum slope of grain that a member should not exceed to qualify for a particular grade.

- Wane. The amount of wane on any surface should be the sum of the wane at the two edges. The table 5.31 gives the maximum amount of wane, expressed as a fraction of the width of the surface on which it occurs to qualify for a particular grade.
- Knots. There are various types of knots, such as splay, arris, edge, margin or face knots. The measurement is carried out by careful observation of the timber planks, measuring knots sizes, numbers and positions relative to each other. The table is not presented here, but the visual observation of knots and the selection of the timber for the research would give a grade 75, maybe grade 65 for some few planks in terms of permissible knots.

Timber grade	75	65	50	40
Minimum number of growth rings per inch	8	6	4	4
Max size of fissure (fraction of the member thickness)	1/4	1/3	1/2	3/5
Maximum slope of grain	1 in 14	1 in 11	1 in 8	1 in 6
Max amount of wane (fraction of the member surfaces)	1/8	1/8	1/4	1/4

Table 5.31 Summary table for grading requirements.

The visual grading of the timber was carried out on some of the full size timber pieces. Some of the planks were rejected from the timber batch when too many knots or defects were apparent. The summary of visual grading is detailed as follow:

- Knots. As explained before, the amount of knots distributed on the timber planks was satisfactory to grade the timber as Grade 65 minimum.
- Rate of growth. The measurement were carried out on 20 pieces of timber, giving an average number well above 8 growth rings per inch therefore the timber was classified as Grade 75.
- Fissures. Very few fissures were found on those 20 timber pieces. The largest one found was about 10 mm along the thickness of the member (44 mm). The timber was then classified as Grade 75.
- Slope of grain. The grain was measured on three pieces of timber, using a swivel-handled scribe. No spiral grain was reported. The slope was measured and did not exceed 4 degrees (equivalent to a slope of 1 in 14.3). The timber was then classified as Grade 75.

- Wane. No waness were found on the selected timber planks. The timber was then classified as Grade 75.

Finally the visual grading demonstrated that the timber had a limited amount of defects, providing the pieces were selected from the whole batch. The overall timber grade is taken as **Grade 65**, mainly because of the sizes and amount of knots observed on some planks.

The basic and grade stresses calculated from the results of the small clear sample tests as well as the comparison with published data on softwoods are presented in the following section.

5.7.3. Small clear sample test results

The results of the small clear sample tests are presented for each type of test and are summarised in this section. Not all the standards tests were carried out. Tests such as compression parallel to the grain or cleavage were not undertaken because the timber properties calculated through those tests were not of any interest for the purpose of the research. The experimental procedures for each of the following tests are presented and described in the chapter 4.

5.7.3.1. Static Bending tests

The static bending test was carried out using the central loading method specified in BS 373: 1986 “Methods of testing small clear specimens of timber”. The test piece is a beam of dimensions 20 mm × 20 mm × 300 mm. The beam is loaded in three points loading as shown in figure 5.30.

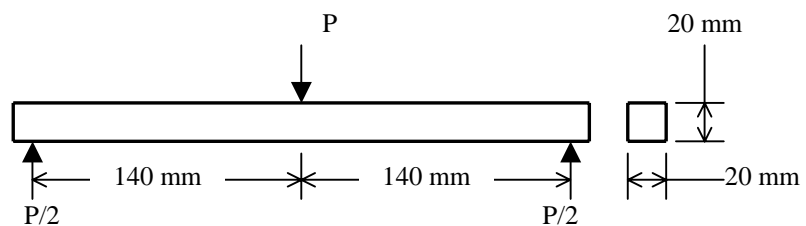


Figure 5.30 Central loading for 20 mm standard test piece.

The deflection of the beam at mid-span were measured with reference to the outer points of loading by recording the load head movement. The modulus of rupture (MOR), which is a measure of the ultimate bending strength and the bending modulus of elasticity are given as:

$$MOR = \frac{3FL}{2bh^2} \quad (5.4)$$

$$\text{and } E = \frac{PL^3}{4\delta bh^3} \quad (5.5)$$

Where MOR = Modulus of Rupture or bending strength (N/mm^2),

E = Modulus of Elasticity in bending (N/mm^2),

F = Load at failure (N),

L = Length of the member (mm),

P = Change of load in elastic range (N),

δ = Change of deflection at mid-span in elastic range (mm),

b and h = Breadth and height of the beam cross-section (mm).

A total of 20 sample beams were tested and the full results are available in Appendix B.1. The summary of the results is presented in table 5.32.

	E (N/mm^2)	MOR (N/mm^2)
Mean value	8283	81
Standard deviation	1551	8.73
Reduction factor	1	2.25
Basic value	4669	27.1
Grade 65 value	N/A	17.6

Table 5.32 Summary results of the static bending tests.

These results are discussed in the section § 5.7.4.

5.7.3.2. Tension parallel to the grain tests

This test was carried out using the tension parallel to the grain tests for small clear samples given in BS 373: 1986 “Methods of testing small clear specimens of timber”. The standard test pieces had the forms and dimensions as illustrated in figure 5.31.

The tension modulus of elasticity $E_{//}$ was calculated using the diagram of load/displacement recorded using a LVDT positioned in the 50 mm long thinner central region of the sample. The calculations of modulus of elasticity were based on elastic range values. The tension strength $\sigma_{//}$ was recorded as the ultimate stress in the thinner cross-section at failure. These two parameters are given as:

$$\sigma_{//} = \frac{F}{bh} \tag{5.6}$$

and $E_{//} = \frac{P \times 50}{\delta bh}$ (5.7)

Where $\sigma_{//}$ = Tension strength parallel to the grain (N/mm²),

$E_{//}$ = Modulus of Elasticity in tension parallel to the grain (N/mm²),

F = Load at failure (N),

P = Change of load in elastic range (N),

δ = Elongation in elastic range (mm),

b and h = Breadth and height of the thinner central region of the sample (mm).

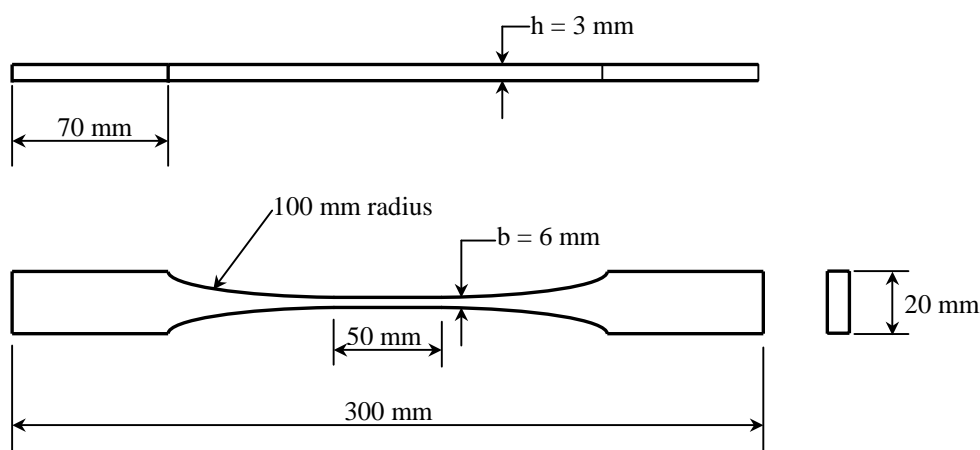


Figure 5.31 Test piece for tension parallel to the grain.

A total of 20 tension samples were tested and the full results are available in Appendix B.2. The summary of the results is presented in table 5.33.

	$E_{//}$ (N/mm ²)	$\sigma_{//}$ (N/mm ²)
Mean value	11416	82.6
Standard deviation	3034	23.07
Reduction factor	1	2.25
Basic value	4347	12.8
Grade 65 value	N/A	8.3

Table 5.33 Summary results of the tension parallel to the grain tests.

These results are discussed in the section § 5.7.4.

5.7.3.3. Tension perpendicular to the grain tests

This test was carried out using an alternative to the standard test for tension perpendicular to the grain given in EN 1193: 1997 as explained before. By scaling down the sample sizes, the samples could be fabricated. However the pieces of timber selected for this test were defect-free and therefore this test was considered as a small clear sample test. The test pieces had the forms and dimensions as illustrated in figure 5.32.

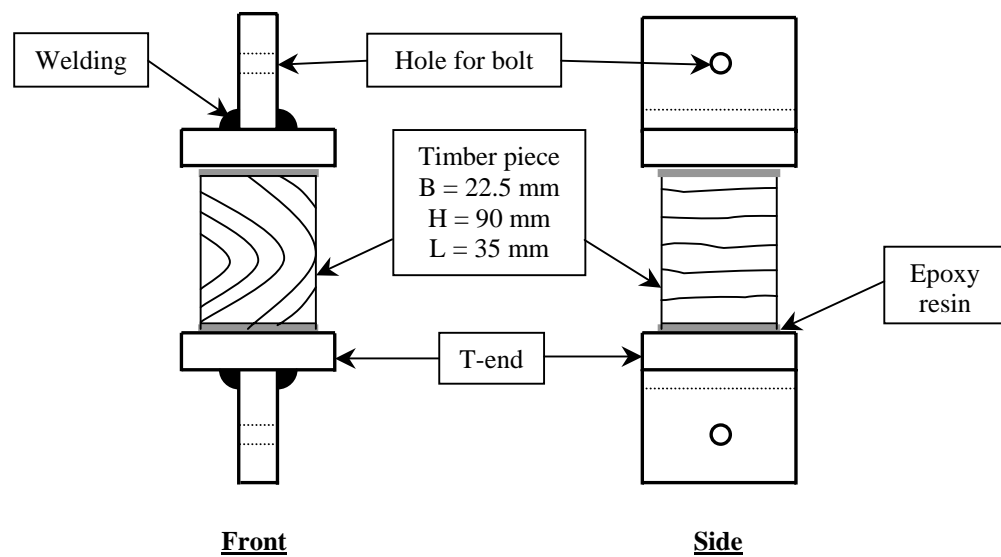


Figure 5.32 Test piece for tension perpendicular to the grain test.

The tension modulus of elasticity E_{\perp} was calculated using the diagram of load/displacement recorded using a LVDT positioned in the 54 mm long central region of the sample. The calculations of the modulus of elasticity were based on elastic range values. The tension strength σ_{\perp} was recorded as the ultimate stress at failure, but this parameter was treated with caution as the sample failure was most of the time due to resin failure between the metal T-ends and the timber sample. These two parameters are given as:

$$\sigma_{\perp} = \frac{F}{bh} \quad (5.8)$$

$$\text{and } E_{\perp} = \frac{P \times 54}{\delta bh} \quad (5.9)$$

Where σ_{\perp} = Tension strength perpendicular to the grain (N/mm²),

E_{\perp} = Modulus of Elasticity in tension perpendicular to the grain (N/mm²),

F = Load at failure (N),

P = Change of load in elastic range (N),

δ = Elongation in elastic range (mm),

b and h = Breadth and height of the thinner central region of the sample (mm).

A total of 20 tension samples were tested and the full results are available in Appendix B.3. The summary of the results is presented in table 5.34.

	E_{\perp} (N/mm ²)	σ_{\perp} (N/mm ²)
Mean value	227	1.86
Standard deviation	63	0.61
Reduction factor	1	2.25
Basic value	81	0.20
Grade 65 value	N/A	0.13

Table 5.34 Summary results of the tension perpendicular to the grain tests.

These results are discussed in the section § 5.7.4.

5.7.3.4. Shear parallel to the grain tests

This test was carried out using the shear parallel to the grain tests for small clear samples given in BS 373: 1986 “Methods of testing small clear specimens of timber”. The test piece for this test is a cube of 20 mm sides, as shown in figure 5.33.

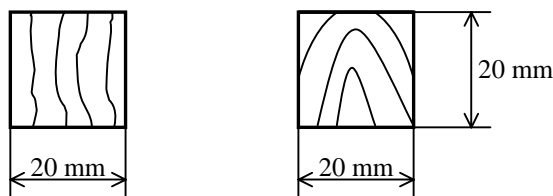


Figure 5.33 Test piece for the shear box test parallel to the grain.

The direction of shearing was parallel to the longitudinal direction of the grain. The test was carried out to failure. The shear strength τ was calculated as the ratio of the failure load to the area of shear of the sample (previously measured). This parameter is given as:

$$\tau = \frac{F}{bh} \quad (5.10)$$

Where τ = Shear strength parallel to the grain (N/mm^2), F = Load at failure (N), b and h = Breadth and height of the surface of shear of the sample (mm).

A total of 40 shear samples were tested and the full results are available in Appendix B.4. The summary of the results is presented in table 5.35.

	τ (N/mm^2)
Mean value	12.8
Standard deviation	1.63
Reduction factor	2.25
Basic value	3.98
Grade 65 value	2.59

Table 5.35 Summary results of the shear parallel to the grain tests.

These results are discussed in the following section.

5.7.4. Comparison and discussion

The results obtained through the small clear sample tests were gathered for two main reasons:

- To carry out our own timber grading in order to check the limited information provided by the supplier. This exercise would also enable one to compare the properties of this specific timber with existing information on similar species.
- To determine the timber properties necessary for the research and particularly for the finite element modelling.

The results presented in table 5.36 are mean values and standard deviations for the mechanical properties and moduli of elasticity of timber obtained from the small clear sample tests.

For dry conditions with an average moisture content = 10.24 %

	Mean value	Standard deviation
Density (kg/m ³)	465	N/A
Bending strength or MOR (N/mm ²)	81	8.73
MOE in bending (N/mm ²)	8283	1551
Tension strength parallel to the grain (N/mm ²)	82.6	23.07
MOE in tension parallel to the grain (N/mm ²)	11416	3034
Tension strength perpendicular to the grain (N/mm ²)	1.86	0.61
MOE in tension perpendicular to the grain (N/mm ²)	227	63
Shear strength parallel to the grain (N/mm ²)	12.8	1.63

Table 5.36 Summary table of mean values and standard deviations for the timber properties obtained from the small clear sample tests.

The mean values shown in this table are the values, which will be retained and used in the finite element analysis, to model some of the mechanical properties of the timber.

The values shaded in grey are the results that can be compared with existing data on small clear sample tests. The results presented in table 5.37 are compiled data presented in Bulletin 50 of the Forest Products Research Laboratory in 1969, which lists data for both the dry and green states of 200 timber species.

	Density when dry (kg/m ³)	Static bending in three-point loading				Impact: drop of hammer (m)	Compression: parallel to grain (N/mm ²)	Hardness: on side grain (N)	Shear: parallel to grain (N/mm ²)	Cleavage	
		Modulus of rupture (N/mm ²)	Modulus of elasticity (N/mm ²)	Energy to max. load (mm N/mm ²)	Energy to fracture (mm N/mm ²)					Radial plane (N/mm width)	Tangential plane (N/mm width)
Hardwoods											
Balsa	176	23 7.3	3200 1060	0.018 0.007	0.035 0.017		15.5 4.43		2.4 0.62		
Obeche	368	54 6.5	5500 620	0.058 0.010	0.095 0.015	0.48 0.072	28.2 3.00	1910 268	7.7 0.67	9.3 1.82	8.4 1.58
Mahogany (Khaya ivorensis)	497	78 15.0	9000 1520	0.070 0.026	0.128 0.044	0.58 0.149	46.4 8.45	3690 816	11.8 2.56	10.0 2.08	14.0 2.90
Sycamore	561	99 11.0	9400 1160	0.121 0.028	0.163 0.049	0.84 0.136	48.2 4.83	4850 639	17.1 2.32	16.8 2.95	27.3 3.91
Ash	689	116 16.6	11 900 2170	0.182 0.045	0.281 0.097	1.07 0.216	53.3 7.73	6140 1158	16.6 2.52		
Oak	689	97 16.8	10 100 1960	0.093 0.026	0.167 0.051	0.84 0.209	51.6 7.98	5470 911	13.7 2.38	14.5 2.86	20.1 2.08
Afzelia	817	125 26.6	13 100 1760	0.100 0.043	0.203 0.087	0.79 0.215	79.2 12.02	7870 914	16.6 2.28	10.5 2.00	13.3 2.49
Greenheart	977	181 20.9	21 000 1990	0.213 0.047	0.395 0.088	1.35 0.207	89.9 8.49	10450 1531	20.5 3.06	17.5 4.79	22.2 4.97
Softwoods											
Norway spruce (European)	417	72 10.2	10 200 2010	0.086 0.022	0.116 0.040	0.58 0.116	36.5 5.26	2140 353	9.8 1.44	8.4 1.07	9.1 1.20
Yellow pine (Canada)	433	80 10.9	8300 1440	0.089 0.015	0.097 0.019	0.56 0.100	42.1 6.14	2050 473	9.3 1.61	8.2 1.57	11.6 1.77
Douglas fir (UK)	497	91 16.9	10 500 2160	0.097 0.038	0.172 0.081	0.69 0.200	48.3 8.03	3420 865	11.6 2.29	9.5 1.90	11.4 2.17
Scots pine (UK)	513	89 16.9	10 000 2130	0.103 0.032	0.134 0.053	0.71 0.167	47.4 9.25	2980 697	12.7 2.45	10.3 1.82	13.0 2.47
Caribbean pitch pine	769	107 14.5	12 600 1800	0.126 0.042	0.253 0.060	0.91 0.196	56.1 7.76	4980 1324	14.3 2.81	12.1 1.23	13.3 1.58

Table 5.37 Average values (upper) and standard deviation (lower) of various mechanical properties for selected timbers at 12% moisture content from small clear test pieces (Dinwoodie, 2000).

The results presented in table 5.37 do not include any tension tests, mainly because of the difficulties experienced through the sample fabrication and the testing procedure. Tension tests are rarely performed and as a result, there is little tensile data available. However tensile strength parallel to the grain reported for certain timbers are listed in table 5.38.

Timber	Moisture content (%)	Tensile strength (N/mm ²)
Hardwoods		
Ash (home grown)	13	136
Beech (home grown)	13	180
Yellow poplar (imported)	15	114
Softwoods		
Scots pine (home grown)	16	92
Scots pine (imported)	15	110
Sitka spruce (imported)	15	139
Western hemlock (imported)	15	137

Table 5.38 Tensile strength parallel to the grain of certain timbers using small clear test pieces (Dinwoodie, 2000).

By comparing the mechanical properties derived from the small clear sample tests with the existing data shown in tables 5.37 and 5.38, there are some undeniable similarities. But first, it is essential to recall that the timber species selected for the research was known as **European Spruce**.

Looking at the results obtained from the static bending test, the modulus of rupture (MOR) and the modulus of Elasticity are almost identical to the values given for Yellow pine species in table 5.37. However the Norway spruce (European) is probably of the same species than the timber used for this research. The results derived from the test should be compared with those from Norway spruce. In fact the MOR value is higher and the modulus of elasticity smaller than the values given for Norway spruce. Even the density obtained is higher than Norway spruce density and is more within the range of Yellow pine density. The other parameter, which can be compared, is the shear parallel to the grain. The results are relatively high and match with shear properties of harder softwoods such as Scots pine. From the comparison of properties with existing data, it seems that this European spruce exhibits some fairly high properties for its species.

The table 5.38 shows typical tensile strength parallel to the grain for some timber species derived from small clear test pieces. The result obtained from the test is slightly lower than the tensile strength given for a home grown Scots pine. However the tensile strength standard deviation derived from the test is very high. This shows some inconsistency in the results and maybe further samples should have been necessary to establish a more representative value of tensile strength. On the other hand Scots pine species would exhibit higher strength properties than a typical European spruce therefore the tensile strength obtained from the test certainly falls within the range of its species.

It appears at this stage that the mechanical properties obtained from the small clear samples are in harmony with published figures of similar species. This confirms the validity of the tests carried out and the reliability of the properties derived from them.

The next step is to associate a grade or a grading class to the timber tested in accordance with the codes from the 1970s, from which timber grades were derived from small clear sample tests.

The grading system in all those standards are expressed for timber in dry conditions, which means for timber with moisture content of 18% or below. The timber properties obtained from the tests were derived from timber at moisture content of 10.2% therefore the first step is to adjust those values for this timber at moisture content of 18%.

“The mechanical properties of wood are dependent on moisture content. An increase in moisture produces lower strength and elasticity values. This effect is partly explained by the cell wall swelling, whereby less cell wall material per unit area is available” (Hoffmeyer, in Timber Engineering STEP1, 1995).

The values for the effect of moisture on the mechanical properties of clear wood properties are given in table 5.39. A linear relationship between moisture content and properties was assumed for moisture content between 8% and 20%.

Property	Change (%)
Compression strength parallel to the grain	5
Compression strength perpendicular to the grain	5
Bending strength parallel to the grain	4
Tension strength parallel to the grain	2,5
Tension strength perpendicular to the grain	2
Shear strength parallel to the grain	3
Impact bending strength parallel to the grain	0,5
Modulus of elasticity parallel to the grain	1,5

Table 5.39 Approximate change (%) of clear wood properties for a one percent change of moisture content. Basis is properties at 12% (Hoffmeyer, in Timber Eng. STEP1, 1995).

Using table 5.39 relationships, the mechanical properties obtained from the tests were calculated for 18% moisture content. The results are presented in table 5.40.

The timber code CP112: 1967 “The Structural Use of Timber” gives the dry graded stresses and moduli of elasticity for various species of softwoods and hardwoods. An extract from this table is presented in table 5.41 showing relevant properties to enable the comparison with the results derived in table 5.40.

		M.C. = 10.2 %		M.C. = 18 %	
		Basic	Grade 65	Basic	Grade 65
Bending strength or MOR (N/mm ²)		27.1	17.6	19.7	12.8
Tension strength parallel to the grain (N/mm ²)		12.8	8.3	10.5	6.8
Tension strength perpendicular to the grain (N/mm ²)		0.20	0.13	0.17	0.11
Shear strength parallel to the grain (N/mm ²)		3.98	2.59	3.14	2.04
Modulus of Elasticity in bending (N/mm ²)	Mean	8283		7362	
	Minimum	4669		4150	
Modulus of Elasticity in tension parallel to the grain (N/mm ²)	Mean	11416		10147	
	Minimum	4347		3864	
Modulus of Elasticity in tension perpendicular to the grain (N/mm ²)	Mean	227		202	
	Minimum	81		72	

Table 5.40 Basic and graded values of small clear timber sample properties at 10.2% and 18% moisture content.

Softwood species	Bending & tension // to grain (N/mm ²)		Shear // to grain (N/mm ²)		MOE (kN/mm ²)	
	Basic	Grade 65	Basic	Grade 65	Basic	Minimum
<i>A. Imported</i>						
Douglas fir	18.62	11.03	1.93	1.21	11723	6551
Western hemlock (unmixed)	15.86	9.31	1.66	1.07	9999	5862
Western hemlock (commercial)	14.48	8.62	1.52	0.97	9310	5517
Parana pine	14.48	8.62	1.66	1.07	8965	4827
Pitch pine	18.62	11.03	1.93	1.21	11723	6551
Redwood	14.48	8.62	1.52	0.97	8275	4482
Whitewood	14.48	8.62	1.52	0.97	8275	4482
Canadian spruce	13.79	7.93	1.52	0.97	8965	5517
Western red cedar	11.03	6.55	1.38	0.83	6896	4138
<i>B. Home-grown</i>						
Douglas fir	17.93	10.69	1.52	0.97	9999	4827
Larch	17.24	10.34	1.72	1.07	9654	4827
Scots pine	15.17	7.93	1.52	0.97	9654	5517
European spruce	11.03	5.86	1.24	0.76	6896	3793
Sitka spruce	10.34	5.52	1.24	0.76	7241	3793
Results from small clear sample tests	10.5	6.8	3.14	2.04	7362	3864

Table 5.41 Dry basic and grade 65 stresses and moduli of elasticity for various species of softwoods having a moisture content not exceeding 18% (from CP112: 1967).

The table 5.41 clearly shows that the results derived from the small clear sample tests correspond to the minimum requirements of the European spruce species, for the grade 65. The basic tension strength parallel to the grain obtained from the small

clear sample tests is the only parameter, which is slightly lower than the minimum dry basic stress given for the species. However the grade 65 value is well within the range.

Globally it confirms that the results from the tests were accurate and that the timber was correctly graded.

The next and final step in this grading process is to examine the results obtained from the full-size bending tests of the main samples that are presented at the beginning of this chapter, and compare them with the results obtained from the small clear sample tests, in order to grade the timber in accordance with the current standards. It is essential to keep in mind that this step is necessary mainly because the current codes of practice only recommend full-size tests to determine timber properties.

The timber used for the fabrication of the main samples was tested in three points bending over a span of 1 metre length. The test procedure is described in the chapter 4 and was non-destructive. The timber planks selected for the sample fabrication were cut to a size sufficiently long to obtain the two timber pieces, which formed the sample. Prior to the cutting, the planks were tested in three points bending up to a maximum point load of 3 kN with record of mid-span deflection. This procedure enabled the calculation of the modulus of elasticity in bending for each plank.

All the 64 timber planks of the main samples were tested. The summary of the results is presented in table 5.42. Minimum values are given for the lower 1-percentile and 5-percentile of the population.

	E (N/mm²)	Density (Kg/m³)	M.C. (%)
Mean value	7537	473.6	11.44
Standard deviation	1222	38.0	N/A
Reduction factor	1	1	N/A
Minimum value (1%)	4691	385.1	N/A
Minimum value (5%)	5533	411.3	N/A

Table 5.42 Summary results of the full-size bending tests.

The mean and the minimum values are the two parameters, which are computed and used for the grading process.

The bending MOE values obtained from the full-size tests are very similar to the values obtained from the static bending test of small clear samples. The mean MOE from the full-size tests is slightly lower than from the small clear tests. This reflects the fact that higher values should be expected from small clear samples because they are defect-free timber pieces. However the minimum MOE values (calculated as the lower 1-percentile of the population) are almost identical from both types of tests.

This test is the only full-size test carried out through this research. The test was non-destructive therefore the only timber property that was established is the bending MOE of each sample. EN 384: 1995 “Structural timber - Determination of characteristic values of mechanical properties and density” explains how to derive characteristic values of timber mechanical properties. This standard is based on full-size tests, but it also considers the use of small clear sample tests to determine bending strength and bending MOE: When both full-size and small clear sample tests data are available for at least three other species, the factors to determine the characteristic values can be derived from ratios of characteristic values of full-size tests data to the mean values of small clear sample tests data. These factors can then be applied to species where only small clear sample tests data exist. Characteristic values determine in this way shall be reduced by multiplying by 0.9.

In the current situation, data from both full-size and small clear sample tests are available, but only from the timber species used for the research and only for two timber properties, which are the bending MOE and the density. Therefore the use of factors between full-size and small clear sample tests is not strictly acceptable from a grading point of view, but it can give some reasonable approximations of the characteristic values.

In EN 384: 1995, characteristic values and mean values of properties shall be adjusted to the standard reference conditions, which correspond for most softwoods to moisture content of 12 %. For full-size tests, the average moisture content was 11.44% therefore a slight adjustment of the bending MOE is necessary. This

adjustment is presented in table 5.43. Note that the minimum values correspond to the lower 5-percentile values in EN 384: 1995.

		M.C. = 11.44 %	M.C. = 12 %
Modulus of Elasticity in bending (N/mm ²)	Mean	7537	7474
	Minimum	5533	5487
Specific density (kg/m ³)	Mean	474	475
	Minimum	411	412

Table 5.43 Bending MOE and density of the full-size bending tests at 11.44% and 12% moisture content.

However the same adjustment of moisture content is required for the results obtained from small clear sample tests to enable the comparison. Furthermore the results must be based on the lower 5-percentile of the population (and not 1-percentile as it was in 1970s standards). The table 5.44 shows the values adjusted to the lower 5-percentile and 12% moisture content.

		M.C. = 10.2 %	M.C. = 12 %
		Basic (5-percentile)	Basic (5-percentile)
Bending strength or MOR (N/mm ²)		29.6	27.5
Modulus of Elasticity in bending (N/mm ²)	Mean	8283	8061
	Minimum	5724	5570

Table 5.44 Basic values of bending MOR and MOE from small clear samples based on the lower 5-percentile at 10.2% and 12% moisture content.

EN 384: 1995 describes how to derive characteristic values of bending strength and MOE when both small clear and full-size samples results are available. As explained before, the ratios can be calculated as shown in the equation (5.11).

$$Ratio = \frac{\text{Characteristic value of full - size data}}{\text{Mean value of small clear data}} \times 0.9 \quad (5.11)$$

The bending MOE is the only parameter available from both full-size and small clear sample tests. The ratio is then calculated from those results. This ratio is then used to calculate the characteristic value of bending strength $f_{m,k}$ based on the result of bending strength obtained from small clear sample tests.

$$Ratio = \frac{5487}{8061} \times 0.9 = 0.613$$

Hence

$$f_{m,k} = 0.613 \times 27.5 = 16.9 \text{ N/mm}^2$$

When no full-size results are available for other timber properties, EN 384: 1995 recommends that characteristic values shall be determined from the characteristic values of bending strength $f_{m,k}$, mean modulus of elasticity $E_{0,\text{mean}}$ and density ρ_k . Note that the characteristic density ρ_k is the lower 5-percentile value of density. These characteristic values are:

$$f_{m,k} = 16.9 \text{ N/mm}^2$$

$$E_{0,\text{mean}} = 7474 \text{ N/mm}^2$$

$$\rho_k = 412 \text{ kg/m}^3$$

This method of determining the timber properties is probably more accurate than applying the ratio to the properties derived from small clear sample tests. In fact, full-size tests to determine other relevant properties, such as tension parallel or tension perpendicular to the grain strengths, etc, are entirely different from equivalent small clear sample tests used to determine the same properties.

The characteristic values of tension strength parallel to grain $f_{t,0,k}$, tension strength perpendicular to grain $f_{t,90,k}$, compression strength parallel to grain $f_{c,0,k}$, compression strength perpendicular to grain $f_{c,90,k}$, shear strength $f_{v,k}$, mean MOE perpendicular to grain $E_{90,\text{mean}}$ and shear modulus G_{mean} shall be calculated from the equations (5.12) to (5.18) respectively:

$$f_{t,0,k} = 0.6 f_{m,k} \tag{5.12}$$

$$f_{t,90,k} = 0.001 \rho_k \tag{5.13}$$

$$f_{c,0,k} = 5(f_{m,k})^{0.45} \tag{5.14}$$

$$f_{c,90,k} = 0.015 \rho_k \tag{5.15}$$

$$f_{v,k} = 0.2(f_{m,k})^{0.8} \tag{5.16}$$

$$E_{90,mean} = \frac{E_{0,mean}}{30} \tag{5.17}$$

$$G_{mean} = \frac{E_{0,mean}}{16} \tag{5.18}$$

The results are presented in table 5.45 with the characteristic values of some strength classes given in EN 338: 1995 “Structural timber - Strength classes”.

		Results	Strength classes - Characteristic values						
			C14	C16	C18	C22	C24	C27	C30
Strength properties (N/mm²)									
Bending	$f_{m,k}$	16.9	14	16	18	22	24	27	30
Tension parallel	$f_{t,0,k}$	10.1	8	10	11	13	14	16	18
Tension perpendicular	$f_{t,90,k}$	0.41	0.3	0.3	0.3	0.3	0.4	0.4	0.4
Compression parallel	$f_{c,0,k}$	17.8	16	17	18	20	21	22	23
Compression perpendicular	$f_{c,90,k}$	6.2	4.3	4.6	4.8	5.1	5.3	5.6	5.7
Shear	$f_{v,k}$	1.92	1.7	1.8	2	2.4	2.5	2.8	3
Stiffness properties (kN/mm²)									
Mean MOE parallel	$E_{0,mean}$	7.48	7	8	9	10	11	12	12
5% MOE parallel	$E_{0,05}$	5.49	4.7	5.4	6	6.7	7.4	8	8
Mean MOE perpendicular	$E_{90,mean}$	0.25	0.23	0.27	0.3	0.33	0.37	0.40	0.40
Mean shear modulus	G_{mean}	0.47	0.44	0.5	0.56	0.63	0.69	0.75	0.75
Density (kg/m³)									
Density	ρ_k	412	290	310	320	340	350	370	380
Average density	ρ_{mean}	475	350	370	380	410	420	450	460

Table 5.45 Characteristic values obtained from results compared with characteristic values given for some strength classes of poplar and conifer species (from EN 338: 1995).

In table 5.45, most of the timber properties determined with the previous method appear to fall within the range of strength class C16. However because of a low value of mean MOE parallel to grain $E_{0,mean}$, the mean MOE perpendicular to grain $E_{90,mean}$ and the shear modulus G_{mean} fall within the range of strength class C14. This can be explained by comparing the test method used in this research for the determination of $E_{0,mean}$ and the test method recommended in the current standards.

In EN 408: 1995 “Timber structures - Structural timber and glued laminated timber - Determination of some physical and mechanical properties”, the test method to determine $E_{0,\text{mean}}$ is based on a loading arrangement where the test piece is symmetrically loaded in bending at two points over the span. In other words, the timber piece is tested in four points bending to determine the MOE in bending E_m . Furthermore the standard specifies a test method to determine the shear modulus G where the test piece is loaded in three points bending. This test is used for the determination of the apparent MOE in bending $E_{m,\text{app}}$. This test method is very similar to the one used in the research. This means that the three points bending method would only determine the apparent MOE in bending, and not the proper MOE in bending. This confirmed with the equation (5.19) which enables the calculation of the shear modulus G having determined E_m and $E_{m,\text{app}}$.

$$G = \frac{k_G h^2}{l_1^2 \left[\frac{1}{E_{m,\text{app}}} - \frac{1}{E_m} \right]} \quad (5.19)$$

With $k_G = 1.2$ for rectangular or square cross-sections,

h = height of cross section,

l_1 = gauge length = $5h$

This equation shows that there is a clear discrepancy between the values of E_m and $E_{m,\text{app}}$. It also clarifies that the apparent MOE in bending $E_{m,\text{app}}$ is always lower than the MOE in bending E_m . Having said that, a relationship between E_m and $E_{m,\text{app}}$ can be derived by combination of equations (5.18) and (5.19). In fact:

$$E_m \approx 1.768 E_{m,\text{app}} \quad (5.20)$$

This equation is not strictly true (as shown with the sign \approx) because equation (5.18) applies to mean characteristic values, which gives only an approximation of the relationship between the shear modulus G and the MOE. In addition to that, this relationship does not specify whether $E_{0,\text{mean}}$ is derived from the bending MOE, tension or compression MOE parallel to grain.

All things considered, the characteristic value of MOE parallel to grain $E_{0,\text{mean}}$ is based on bending test carried out using the three points bending method. Therefore the value of $E_{0,\text{mean}}$ may reflect an apparent bending MOE, which would explain the relatively low figure shown in table 5.45.

As a result it can be confirmed that the timber used in the research corresponds to the strength class C16.

Finally the results obtained from the small clear sample tests reflect how representative they are in the grading process in accordance to the 1970s standards. When the timber properties are derived from the ratio obtained from full-size bending tests to enable the grading in accordance with current standards, the results are also relevant as they confirm the strength class C16 that corresponds to the strength class SC3 given initially by the timber supplier.

The timber properties, which are to be retained for the finite element analysis, are summarised in the conclusion.

5.8. Conclusion

Timber is not a truly elastic material as its behaviour is time dependent. The load duration has an effect on its deformation, which defines the material as viscoelastic. However timber is treated as elastic in timber design codes using safety factors to take into account the duration of load. The theory of elasticity will be used for the finite element analysis, allowing for the anisotropy of the material.

Wood is often considered as an orthotropic material, which means that the material has symmetry about three orthogonal planes. The assumption is made that the three principal elasticity directions coincide with the longitudinal, radial and tangential directions in the tree. The mechanical behaviour of wood is explained in detail in the following chapter.

Orthotropic materials are characterised by six moduli of elasticity, three in the principal directions E and three in the orthotropic planes G . The orthotropic materials are also characterised by having six Poisson's ratios. Three of them are independent because they are linked with the three moduli of elasticity E . The three others can be derived accordingly.

The table 5.46 shows orthotropic properties measured for various species.

Species	Density (kg/m ³)	Moisture content (%)	E_L	E_R	E_T	ν_{TR}	ν_{LR}	ν_{RT}	ν_{LT}	ν_{RL}	ν_{TL}	G_{LT}	G_{LR}	G_{TR}
Hardwoods														
Balsa	200	9	6 300	300	106	0.66	0.018	0.24	0.009	0.23	0.49	203	312	33
Khaya	440	11	10 200	1130	510	0.60	0.033	0.26	0.032	0.30	0.64	600	900	210
Walnut	590	11	11 200	1190	630	0.72	0.052	0.37	0.036	0.49	0.63	700	960	230
Birch	620	9	16 300	1110	620	0.78	0.034	0.38	0.018	0.49	0.43	910	1180	190
Ash	670	9	15 800	1510	800	0.71	0.051	0.36	0.030	0.46	0.51	890	1340	270
Beech	750	11	13 700	2240	1140	0.75	0.073	0.36	0.044	0.45	0.51	1060	1610	460
Softwoods														
Norway spruce	390	12	10 700	710	430	0.51	0.030	0.31	0.025	0.38	0.51	620	500	23
Sitka spruce	390	12	11 600	900	500	0.43	0.029	0.25	0.020	0.37	0.47	720	750	39
Scots pine	550	10	16 300	1100	570	0.68	0.038	0.31	0.015	0.42	0.51	680	1160	66
Douglas fir ^a	590	9	16 400	1300	900	0.63	0.028	0.40	0.024	0.43	0.37	910	1180	79

Source: Hearmon (1948), but with different notation for the Poisson's ratios.

^a Listed in the original as Oregon pine.

E is the modulus of elasticity in a direction indicated by the subscript (N/mm²).

G is the modulus of rigidity in a plane indicated by the subscript (N/mm²).

ν_{ij} is the Poisson's ratio for an extensional stress in the j direction, given by

$$\nu_{ij} = \frac{\text{compressive strain in the } i \text{ direction}}{\text{extensional strain in the } j \text{ direction}}$$

Table 5.46 Orthotropic properties determined for various species (Dinwoodie, 2000).

To define the orthotropic properties of timber, particularly for the finite element analysis, six components are strictly required. The three moduli of elasticity E and the three major Poisson's ratios. Having those, the three shear moduli G and the three minor Poisson's ratios can be deduced.

Poisson's ratios are extremely difficult to measure in wood. Using table 5.46, it was decided to use the values corresponding to the species, which is the most representative of the timber used in the research. In fact, the modulus of elasticity in the longitudinal direction E_L is the only component, which can strictly be compared as it corresponds to the modulus of elasticity in tension parallel to the grain. Other moduli of elasticity in radial and tangential directions cannot be compared because the other measured property (i.e. the modulus of elasticity in tension perpendicular to the grain) was determined without distinction of the orthotropic direction.

Sitka spruce has the most similar properties to the timber used in the research therefore the orthotropic properties presented in table 5.47 are to be used for the finite element analysis.

E_L (N/mm ²)	E_R (N/mm ²)	E_T (N/mm ²)	ν_{RL}	ν_{TR}	ν_{TL}
11600	900	500	0.37	0.43	0.47

Table 5.47 Timber orthotropic properties used for the FEA.

The orthotropy and other mechanical behaviour of timber, as well as other materials such as glass fibre and epoxy behaviour are developed in the following chapter, dealing with theoretical and finite element analysis.

CHAPTER 6

THEORETICAL AND FINITE ELEMENT ANALYSES

6.1. Introduction

The theory behind the wood/glass/epoxy joint is based on principles of structural and solid mechanics. The anisotropy of the timber and the glass fibre/epoxy composite materials makes the theoretical analysis even more complex and cannot be approached by simple calculations.

The mechanics of the wood/glass/epoxy joint will be developed in this chapter as well as the theoretical analysis, which will be carried out using finite element modelling (FEM). The computer software used for the FEM is the ANSYS package product, version 5.4.

The finite element modelling enables the theoretical analysis of the joint with the computer carrying the fastidious calculations to a degree of accuracy, which could not be reached otherwise. There are many parameters, which must be set to an appropriate level in order to obtain accurate and reliable results. These parameters are specific for each model and will be identified and developed in this chapter.

The mechanical behaviour of the joints will be studied in the elastic and plastic range, but the finite element modelling will not be considered for plasticity. This is justified by the fact that the joints did not develop plasticity to any extent, which would enable the analysis to be carried out in that range. Modelling the non-linear behaviour of the joints would have required different experimental procedures, such as using many more strain gauges to measure the state of strain throughout the joints. The objectives are the global understanding of the mechanical behaviour of the joints rather than the achievement of accurate finite element models. Other reasons to limit the FEM to the elastic range lie in the true nature of wood material, which is fairly complex, when the material develops creep and its microscopic structure start to change. These are the subjects that are developed in the following sections.

6.2. Theoretical approach to structural adhesive joints

Structural adhesive joints have been used for many years in the industry. In wood structures, it started many centuries ago with carpentry joints. At that time carpenter's glue was used, but it was only to prevent mechanical joints made for example with a tenon to become loose. Load-bearing structural adhesive joints are a recent innovation. They were initially studied for wood structures in the 1950s and were becoming essential with the development of composite materials. The wide range of applications of composite materials to high-tech industries such as aerospace and aircraft engineering have brought much research and many developments in this area. Structural adhesive joints appeared to have a great advantage over mechanically fastened joints: uniform stress transfer (i.e. no stress concentration around a fastener) resulting in greater fatigue resistance.

Today structural adhesive joints are well understood and Computer Aided Design (CAD) tools can help engineers to design very efficient adhesive joints without having to derive by hand and therefore by trial and error, the principles of mechanics, which apply to those joints. However it is necessary to understand clearly how the joints behave under load in order to use the appropriate assumptions for an accurate design.

This section will describe the theory that applies to wood/glass/epoxy joints. But first it is necessary to introduce the principles of mechanics for anisotropic materials such as wood and glass fibre/epoxy composites.

6.2.1. Anisotropic and orthotropic materials

A material, which has the same properties at any point, is known as homogeneous. And if the properties are the same in any direction, the material is isotropic. Many metals and ceramics are approximately isotropic. Amorphous materials such as glass are also isotropic. Isotropic laws of elasticity (e.g. Hooke's Law) are generally used for those materials.

The behaviour of wood and glass fibre/epoxy composites, which are the components of the wood/glass/epoxy joints, is presented in this section.

Wood is known as a highly anisotropic material because of the orientation of its wood cells, as discussed in chapter 3. Wood is a homogenous material, but the properties vary with the direction considered, therefore it is anisotropic.

The load-deformation relationship for wood is rather complex, as the material behaviour is time dependent. In fact timber does not behave in a truly elastic mode and is defined as a viscoelastic material. Timber will deform under load but if the load is maintained in time, the deformation increases but the rate of deformation decreases with time. This is the effect of creep. On removal of the load, the deformation decreases by a proportion approximately equal to the initial elastic deformation. The remaining deformation will decrease with time until no further reduction occurs. This is known as a delayed-elastic behaviour. The remaining deformation, which will not be recovered, is known as plastic or viscous deformation.

Many factors can also affect the timber response under load. These factors are part of the material properties, such as grain orientation or density. Other factors are dependent on the environment in which the wood is used: Moisture content (relative humidity) and temperature. With such complexity in its behaviour, wood is usually treated in design terms as an elastic material.

“Perhaps the greatest incentive for this viewpoint is the fact that classical elasticity theory is well established and, when applied to timber, has been shown to work very well. The question of time in any stress analysis can be accommodated by the use of safety factors in design calculations” (Dinwoodie, 2000).

The use of elastic theory for timber gives good approximation of what really happens in the material. This is why the material is treated as elastic in timber design codes using safety factors to take into account the duration of load.

The theory of elasticity will be used for the finite element analysis, allowing for the anisotropy of the material. However wood is often considered as an orthotropic material, which means that the material has symmetry about three orthogonal planes. Orthotropic properties applied to Hooke's Law of elasticity are of intermediate complexity between the isotropic and the general anisotropic cases.

“In applying the elements of orthotropic elasticity to timber, the assumption is made that the three principal elasticity directions coincide with the longitudinal, radial and tangential directions in the tree. The assumption implies that the tangential faces are straight and not curved, and that the radial faces are parallel and not diverging. However, by dealing with small pieces of timber removed at some distance from the centre of the tree, the approximation of rhombic symmetry for a system possessing circular symmetry becomes more and more acceptable” (Dinwoodie, 2000).

The three axes of longitudinal, tangential and radial directions of the tree are presented in figure 6.1.

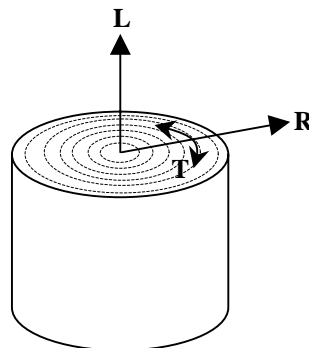


Figure 6.1 Longitudinal (L), Radial (R) and Tangential (T) axes directions of timber.

Composite materials presented in the form of a lamina are also anisotropic because of the presence of stiff fibres in particular directions. A lamina is defined as a flat (or curved as in a shell) arrangement of unidirectional or woven fibres in a supporting matrix, such as the glass fibre/epoxy laminae used for the joints. When several laminae are bonded together to form an integral structural element, it is called a laminate. Laminates usually have more complex behaviour than a single lamina because of the multiple orientations of the fibres.

However they will not be described in this thesis, as they were not used for the wood/glass/epoxy joints.

As for wood, a lamina shows material property symmetry about the three orthogonal planes. The three orthogonal planes of symmetry for a lamina are shown on figure 6.2.

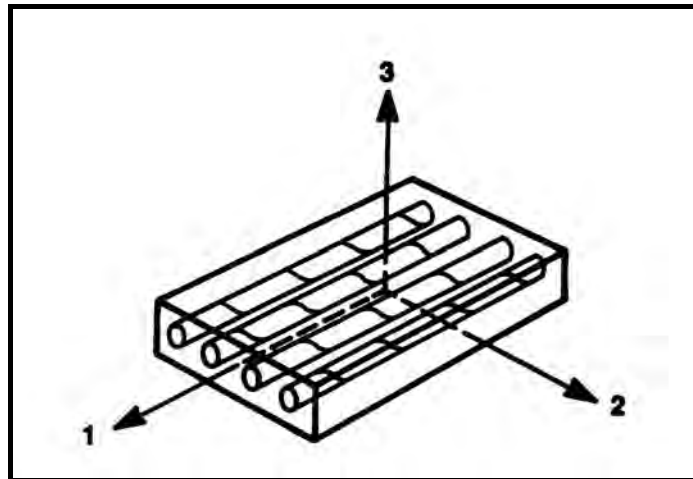


Figure 6.2 Planes of symmetry of a unidirectionally reinforced lamina (Jones, 1999).

A lamina behaves as an orthotropic material, but within each orthogonal plane, there are different properties as the lamina is made of both fibres and resin matrix.

“Because a composite is made of several materials, which interact between each other, the knowledge of mechanical behaviour of composites is defined in two parts:

- **Micromechanics:** The study of composite material behaviour wherein the interaction of the constituent materials is examined in detail as part of the definition of the behaviour of the heterogeneous composite material.
- **Macromechanics:** The study of composite material behaviour wherein the material is assumed *homogeneous* and the effects of the constituent materials are detected only as averaged apparent properties of the composite material” (Jones, 1999).

In this section, only the macromechanics of lamina is described. Macromechanics assumes the composite material as homogeneous therefore the same principles are applied for the glass fibre/epoxy lamina and for the wood, as both materials are orthotropic. The principles of micromechanics will be developed later.

The stress-strain relationship and theory of elasticity for orthotropic materials presented below apply for both the timber and the glass fibre/epoxy composite.

But first it is necessary to define the basic principles of elastic deformation.

A material subject to a stress will deform. The relationship between deformation and a low stress is linear if the material is said to be elastic. This relationship is known as Hooke's Law and is presented as:

$$E(N/mm^2) = \frac{\sigma(N/mm^2)}{\varepsilon(\text{unitless})} \quad (6.1)$$

Where E = Modulus of elasticity (constant), σ = Stress (load/cross-sectional area) and ε = strain (change in dimension/original dimension).

A second elastic constant is the shear modulus G . It is derived from the proportionality of the shearing stress and shearing strain:

$$G(N/mm^2) = \frac{\tau(N/mm^2)}{\gamma(\text{unitless})} \quad (6.2)$$

Where G = Shear modulus (constant), τ = Shearing stress and γ = Shearing strain.

A third constant is known as the Poisson's ratio and is the most physically visible of all. On a body subjected to a stress, the Poisson's ratio is the ratio of contraction or expansion strain to the applied strain.

$$\nu_{ij} = \frac{-\varepsilon_i}{\varepsilon_j} \quad (6.3)$$

Where ν = Poisson's ratio (constant), ε_i and ε_j = Strains in the i and j directions resulting from an applied stress in the i direction.

These relationships are the basis of the theory of elasticity, and are often used as such for isotropic materials.

In the three-dimensional case and for an anisotropic material, let us assume a cube of material orientated in a coordinated system (1-2-3) subjects to stresses acting on each face, as shown in figure 6.3.

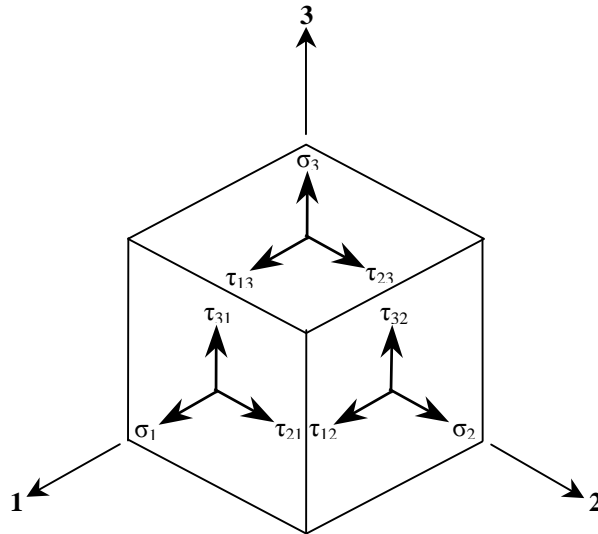


Figure 6.3 Stresses acting on a cube of material.

There is a set of three perpendicular stresses acting on each face. Stresses are labelled with the notation σ_{ij} where i is the direction of stress and j the direction perpendicular to the face on which this stress acts. With the cube prevented from rotating, the following relationship applies:

$$\sigma_{ij} = \sigma_{ji} \quad (6.4)$$

Therefore there are six components of stresses working on the cube, three normal and three shear stresses. As a result there are six corresponding strain components.

It is more convenient to use a contracted notation of those double suffixes, which are presented in the table 6.1.

Stresses		Strains	
Tensor Notation	Contracted Notation	Tensor Notation	Contracted Notation
$\sigma_{11} (\sigma_1)$	σ_1	$\varepsilon_{11} (\varepsilon_1)$	ε_1
$\sigma_{22} (\sigma_2)$	σ_2	$\varepsilon_{22} (\varepsilon_2)$	ε_2
$\sigma_{33} (\sigma_3)$	σ_3	$\varepsilon_{33} (\varepsilon_3)$	ε_3
$\tau_{23} = \sigma_{23}$	σ_4	$\gamma_{23} = 2\varepsilon_{23}$	ε_4
$\tau_{13} = \sigma_{13}$	σ_5	$\gamma_{13} = 2\varepsilon_{13}$	ε_5
$\tau_{12} = \sigma_{12}$	σ_6	$\gamma_{12} = 2\varepsilon_{12}$	ε_6

Table 6.1 Contracted notations for stresses and strains.

The generalised form of the Hooke's Law can be written as:

$$\sigma_i = C_{ij} \varepsilon_j \tag{6.5}$$

Where σ_i = stress components, C_{ij} = stiffness matrix and ε_j = strain components.

The stress is expressed in terms of strain and elastic stiffness matrix. However the strain can be expressed in terms of stress and compliance matrix, defined by the inverse of the stress-strain relationship:

$$\varepsilon_i = S_{ij} \sigma_j \tag{6.6}$$

Where ε_i = strain components, S_{ij} = compliance matrix and σ_j = stress components.

There are now six components of strain, which can be expressed in terms of six products of appropriate stresses and compliances.

$$\begin{aligned}
 \varepsilon_1 &= S_{11}\sigma_1 + S_{12}\sigma_2 + S_{13}\sigma_3 + S_{14}\sigma_4 + S_{15}\sigma_5 + S_{16}\sigma_6 \\
 \varepsilon_2 &= S_{21}\sigma_1 + S_{22}\sigma_2 + S_{23}\sigma_3 + S_{24}\sigma_4 + S_{25}\sigma_5 + S_{26}\sigma_6 \\
 \varepsilon_3 &= S_{31}\sigma_1 + S_{32}\sigma_2 + S_{33}\sigma_3 + S_{34}\sigma_4 + S_{35}\sigma_5 + S_{36}\sigma_6 \\
 \varepsilon_4 &= S_{41}\sigma_1 + S_{42}\sigma_2 + S_{43}\sigma_3 + S_{44}\sigma_4 + S_{45}\sigma_5 + S_{46}\sigma_6 \\
 \varepsilon_5 &= S_{51}\sigma_1 + S_{52}\sigma_2 + S_{53}\sigma_3 + S_{54}\sigma_4 + S_{55}\sigma_5 + S_{56}\sigma_6 \\
 \varepsilon_6 &= S_{61}\sigma_1 + S_{62}\sigma_2 + S_{63}\sigma_3 + S_{64}\sigma_4 + S_{65}\sigma_5 + S_{66}\sigma_6
 \end{aligned}
 \tag{6.7}$$

The equation (6.4) also applies to the stiffness and compliance matrix, thus reducing the number of components from 36 to 21 compliances in the above equations.

$$C_{ij} = C_{ji} \text{ and } S_{ij} = S_{ji} \tag{6.8}$$

But these apply to general anisotropic case. When orthotropic material is considered where the three perpendicular planes have symmetry, the general Hooke’s Law of elasticity becomes:

$$\begin{bmatrix} \varepsilon_1 \\ \varepsilon_2 \\ \varepsilon_3 \\ \varepsilon_4 \\ \varepsilon_5 \\ \varepsilon_6 \end{bmatrix} = \begin{bmatrix} S_{11} & S_{12} & S_{13} & 0 & 0 & 0 \\ S_{21} & S_{22} & S_{23} & 0 & 0 & 0 \\ S_{31} & S_{32} & S_{33} & 0 & 0 & 0 \\ 0 & 0 & 0 & S_{44} & 0 & 0 \\ 0 & 0 & 0 & 0 & S_{55} & 0 \\ 0 & 0 & 0 & 0 & 0 & S_{66} \end{bmatrix} \begin{bmatrix} \sigma_1 \\ \sigma_2 \\ \sigma_3 \\ \sigma_4 \\ \sigma_5 \\ \sigma_6 \end{bmatrix}
 \tag{6.9}$$

The compliance matrix is then symmetrical and has nine independent parameters.

“Now an orthotropic material is characterised by six elastic moduli, three of which are the ratios of normal stress to strain in the principal directions (E) and three are the ratio of shear stress to strain in the orthotropic planes (G)” (Dinwoodie, 2000).

The orthotropic material is also characterised by having six Poisson’s ratios. Three of them are independent because they are linked with three moduli of elasticity (E). The three others can be derived accordingly.

The equation (6.9) can be rearranged by replacing the compliances with moduli and Poisson's ratios applying the equations (6.1), (6.2), (6.3) and (6.6). The general Hooke's Law of elasticity equation for orthotropic material becomes:

$$\begin{bmatrix} \varepsilon_1 \\ \varepsilon_2 \\ \varepsilon_3 \\ \varepsilon_4 \\ \varepsilon_5 \\ \varepsilon_6 \end{bmatrix} = \begin{bmatrix} 1/E_1 & -\nu_{12}/E_2 & -\nu_{13}/E_3 & 0 & 0 & 0 \\ -\nu_{21}/E_1 & 1/E_2 & -\nu_{23}/E_3 & 0 & 0 & 0 \\ -\nu_{31}/E_1 & -\nu_{32}/E_2 & 1/E_3 & 0 & 0 & 0 \\ 0 & 0 & 0 & 1/G_{44} & 0 & 0 \\ 0 & 0 & 0 & 0 & 1/G_{55} & 0 \\ 0 & 0 & 0 & 0 & 0 & 1/G_{66} \end{bmatrix} \begin{bmatrix} \sigma_1 \\ \sigma_2 \\ \sigma_3 \\ \sigma_4 \\ \sigma_5 \\ \sigma_6 \end{bmatrix} \quad (6.10)$$

This equation applies for all materials considered in this project: Wood and glass fibre/epoxy composite. However it is preferable to adapt it for each particular case as it gives a better understanding of the specific material behaviour.

When wood material is considered, the material is truly orthotropic and the suffixes used in equation (6.10) can be replaced by the three perpendicular axes of the material such as 1 corresponds to the Longitudinal direction (L), 2 corresponds to the Tangential direction (T) and 3 corresponds to the Radial direction (R). The equation becomes:

$$\begin{bmatrix} \varepsilon_{LL} \\ \varepsilon_{TT} \\ \varepsilon_{RR} \\ 2\varepsilon_{TR} \\ 2\varepsilon_{LR} \\ 2\varepsilon_{LT} \end{bmatrix} = \begin{bmatrix} 1/E_L & -\nu_{LT}/E_T & -\nu_{LR}/E_R & 0 & 0 & 0 \\ -\nu_{TL}/E_L & 1/E_T & -\nu_{TR}/E_R & 0 & 0 & 0 \\ -\nu_{RL}/E_L & -\nu_{RT}/E_T & 1/E_R & 0 & 0 & 0 \\ 0 & 0 & 0 & 1/G_{TR} & 0 & 0 \\ 0 & 0 & 0 & 0 & 1/G_{LR} & 0 \\ 0 & 0 & 0 & 0 & 0 & 1/G_{LT} \end{bmatrix} \begin{bmatrix} \sigma_{LL} \\ \sigma_{TT} \\ \sigma_{RR} \\ \sigma_{TR} \\ \sigma_{LR} \\ \sigma_{LT} \end{bmatrix} \quad (6.11)$$

This equation refers to the nine independent constants, which are required to specify the elastic behaviour of wood:

- Three moduli of elasticity (E) in the Longitudinal, Tangential and Radial directions,
- Three moduli of rigidity (G) in the principal planes LT , LR and TR ,

- Three of the six Poisson's ratio, knowing that three can be related to three others with the relationship given in equation (6.12). The set of three Poisson's ratios ν_{RT} , ν_{LR} and ν_{TL} or ν_{TR} , ν_{RL} and ν_{LT} will have to be specified.

Due to the symmetry of the matrix presented in the equation (6.8), the relationship between dependent Poisson's ratios is:

$$\frac{\nu_{ij}}{E_i} = \frac{\nu_{ji}}{E_j} \quad (6.12)$$

The properties used to model the wood material are presented in the previous chapter. They are the input values for the finite element modelling as the analysis is applying the orthotropic theory of elasticity presented here.

When glass fibre/epoxy composite matrix is considered, there are two different cases to specify:

- Uniaxial glass fibre UT-E500/epoxy matrix,
- Biaxial glass fibre XE450/epoxy matrix.

These two types of lamina were used in this project and they have to be treated separately as they have different properties.

The UT-E500 is a unidirectional glass fibre fabric. When presented in a single layer with an epoxy resin matrix, such as used for the wood/glass/epoxy joints, it can be represented as shown in figure 6.2.

The lamina is orientated in the three perpendicular axes (1-2-3). The fibres are orientated in the 1 axis direction, but there are no fibres in the 2 and 3 axes directions. It means that similar properties are expected in the 2 and 3 directions. The material is known as transversely isotropic because the material has an axis of material symmetry (axis 1 in this particular case) in addition of the three perpendicular planes of symmetry.

Transversely isotropic material has five independent constants. In this particular case the 2-3 plane becomes an isotropic plane therefore properties in the 2 and 3 directions are equal.

By rearranging the general equation (6.9) of Hooke's Law of elasticity, the equation becomes:

$$\begin{bmatrix} \varepsilon_1 \\ \varepsilon_2 \\ \varepsilon_3 \\ \varepsilon_4 \\ \varepsilon_5 \\ \varepsilon_6 \end{bmatrix} = \begin{bmatrix} S_{11} & S_{12} & S_{12} & 0 & 0 & 0 \\ S_{21} & S_{22} & S_{23} & 0 & 0 & 0 \\ S_{21} & S_{32} & S_{22} & 0 & 0 & 0 \\ 0 & 0 & 0 & 2(S_{22} - S_{23}) & 0 & 0 \\ 0 & 0 & 0 & 0 & S_{55} & 0 \\ 0 & 0 & 0 & 0 & 0 & S_{55} \end{bmatrix} \begin{bmatrix} \sigma_1 \\ \sigma_2 \\ \sigma_3 \\ \sigma_4 \\ \sigma_5 \\ \sigma_6 \end{bmatrix} \quad (6.13)$$

By applying the following equation, which relates E , G and ν for isotropic condition, the compliance matrix S_{44} can be modified:

$$G = \frac{E}{2(1 + \nu)} \quad (6.14)$$

The derivation is carried out as shown below:

$$S_{44} = \frac{1}{G_{44}} \quad \text{and} \quad G_{44} = \frac{\sigma_4}{\varepsilon_4} = \frac{\tau_{23}}{2\varepsilon_{23}}$$

As 2 and 3 are isotropic, equation (6.14) can be introduced and rearranged as shown:

$$S_{44} = (G_{44})^{-1} = \left(\frac{E_2}{2(1 + \nu_{23})} \right)^{-1} = \frac{2(1 + \nu_{23})}{E_2} = 2 \left(\frac{1}{E_2} + \frac{\nu_{23}}{E_2} \right) = 2(S_{22} - S_{23})$$

The final equation of Hooke's Law of elasticity for the UT-E500/epoxy with the fibre orientated in the l axis direction becomes:

$$\begin{bmatrix} \varepsilon_1 \\ \varepsilon_2 \\ \varepsilon_3 \\ \varepsilon_4 \\ \varepsilon_5 \\ \varepsilon_6 \end{bmatrix} = \begin{bmatrix} 1/E_1 & -\nu_{12}/E_2 & -\nu_{12}/E_2 & 0 & 0 & 0 \\ -\nu_{21}/E_1 & 1/E_2 & -\nu_{23}/E_2 & 0 & 0 & 0 \\ -\nu_{21}/E_1 & -\nu_{32}/E_2 & 1/E_2 & 0 & 0 & 0 \\ 0 & 0 & 0 & 2 \left(\frac{1}{E_2} + \frac{\nu_{23}}{E_2} \right) & 0 & 0 \\ 0 & 0 & 0 & 0 & 1/G_{12} & 0 \\ 0 & 0 & 0 & 0 & 0 & 1/G_{12} \end{bmatrix} \begin{bmatrix} \sigma_1 \\ \sigma_2 \\ \sigma_3 \\ \sigma_4 \\ \sigma_5 \\ \sigma_6 \end{bmatrix} \quad (6.15)$$

The XE450 is bidirectional glass fibre fabric. It was used for the wood/glass/epoxy joints presented as a double layer of glass fibre strands within an epoxy resin matrix. It is important to highlight that the fibres were stitched together but the fabric was not woven. This will have some importance regarding the micromechanics of this lamina in the next section.

The fibres are laid in the epoxy matrix as shown in figure 6.4.

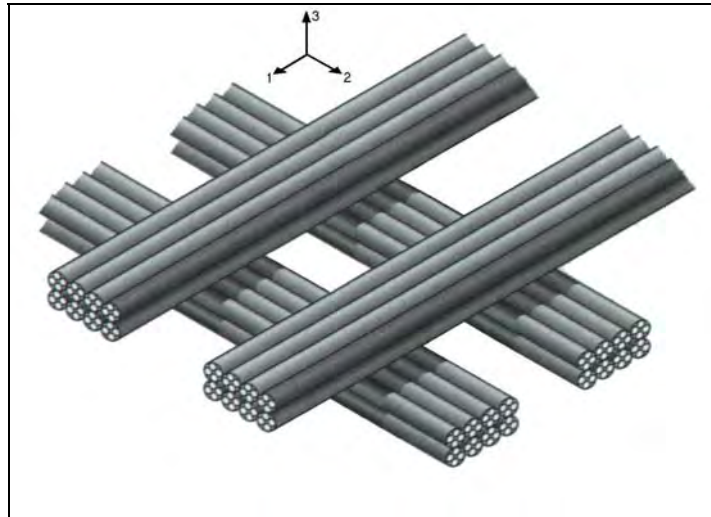


Figure 6.4 Double layer of glass fibres in the XE450 fabric.

The lamina is orientated in the three perpendicular axes ($1-2-3$). The fibres are orientated in the 1 and 2 axes directions, but there are no fibres in the 3 -axis direction. This means that similar properties are expected in the 1 and 2 directions. The material is also transversely isotropic because the material has an axis of material symmetry (axis 3 in this particular case) in addition of the three perpendicular planes of symmetry.

As mentioned before, transversely isotropic materials have five independent constants. In this particular case the $1-2$ plane becomes an isotropic plane therefore the properties in the 1 and 2 directions are identical.

By rearranging the general equation (6.9) of Hooke's Law of elasticity, the equation becomes:

$$\begin{bmatrix} \varepsilon_1 \\ \varepsilon_2 \\ \varepsilon_3 \\ \varepsilon_4 \\ \varepsilon_5 \\ \varepsilon_6 \end{bmatrix} = \begin{bmatrix} S_{11} & S_{12} & S_{13} & 0 & 0 & 0 \\ S_{21} & S_{11} & S_{13} & 0 & 0 & 0 \\ S_{31} & S_{31} & S_{33} & 0 & 0 & 0 \\ 0 & 0 & 0 & S_{44} & 0 & 0 \\ 0 & 0 & 0 & 0 & S_{44} & 0 \\ 0 & 0 & 0 & 0 & 0 & 2(S_{11} - S_{12}) \end{bmatrix} \begin{bmatrix} \sigma_1 \\ \sigma_2 \\ \sigma_3 \\ \sigma_4 \\ \sigma_5 \\ \sigma_6 \end{bmatrix} \quad (6.16)$$

Using equation (6.14), which relates E , G and ν for isotropic condition, the compliance matrix S_{66} can be modified and derived as shown below:

$$S_{66} = \frac{1}{G_{66}} \quad \text{and} \quad G_{66} = \frac{\sigma_6}{\varepsilon_6} = \frac{\tau_{12}}{2\varepsilon_{12}}$$

As 1 and 2 are isotropic, equation (6.14) can be introduced and rearranged as shown:

$$S_{66} = (G_{66})^{-1} = \left(\frac{E_1}{2(1 + \nu_{12})} \right)^{-1} = \frac{2(1 + \nu_{12})}{E_1} = 2 \left(\frac{1}{E_1} + \frac{\nu_{12}}{E_1} \right) = 2(S_{11} - S_{12})$$

The final equation of Hooke's Law of elasticity for the XE450/epoxy with the fibre orientated in the 1 and 2 axes directions becomes:

$$\begin{bmatrix} \varepsilon_1 \\ \varepsilon_2 \\ \varepsilon_3 \\ \varepsilon_4 \\ \varepsilon_5 \\ \varepsilon_6 \end{bmatrix} = \begin{bmatrix} 1/E_1 & -\nu_{12}/E_1 & -\nu_{13}/E_3 & 0 & 0 & 0 \\ -\nu_{21}/E_1 & 1/E_1 & -\nu_{13}/E_3 & 0 & 0 & 0 \\ -\nu_{31}/E_1 & -\nu_{31}/E_1 & 1/E_3 & 0 & 0 & 0 \\ 0 & 0 & 0 & 1/G_{23} & 0 & 0 \\ 0 & 0 & 0 & 0 & 1/G_{23} & 0 \\ 0 & 0 & 0 & 0 & 0 & 2 \left(\frac{1}{E_1} + \frac{\nu_{12}}{E_1} \right) \end{bmatrix} \begin{bmatrix} \sigma_1 \\ \sigma_2 \\ \sigma_3 \\ \sigma_4 \\ \sigma_5 \\ \sigma_6 \end{bmatrix} \quad (6.17)$$

These equations are the theory of elasticity for stress-strain relationship applied to each of the orthotropic materials used in the wood/glass/epoxy joints. However it is necessary to define the basis of micromechanics for composites materials, as composites are not truly homogenous, as assumed throughout this section.

6.2.2. Micromechanics of composite materials

The micromechanics of the laminae studied in this research will not be included as part of the finite element modelling because it necessitates the analysis of the laminae at a microscopic level. In fact this was not carried out in the experiments and the absence of experimental results of strains within particular locations in the glass fibre/epoxy matrix will bring some limitations to the micromechanical approach.

“For example, a perfect bond between fibres and matrix is a usual analysis restriction that might well not be satisfied by some composite materials. An imperfect bond would presumably yield a material with properties degraded from those of the micromechanical analysis. Thus, micromechanical theories must be validated by careful experimental work” (Jones, 1999).

Composite materials usually perform as homogeneous materials therefore macromechanical analysis is satisfactory. The mechanical properties of the composites used for the finite element modelling were determined from macromechanical tests. They are apparent values of the composite itself therefore they are perfectly suitable for the finite element modelling as long as the composite is modelled as a homogeneous material.

Micromechanics are required to understand how the stresses are transferred from the matrix to the fibres, or how the composite materials behave close to failure. In fact micromechanics asks the basic question of how does the fibre and the matrix interact to form the averaged properties of the composite? This basic question of micromechanics is illustrated in figure 6.5.

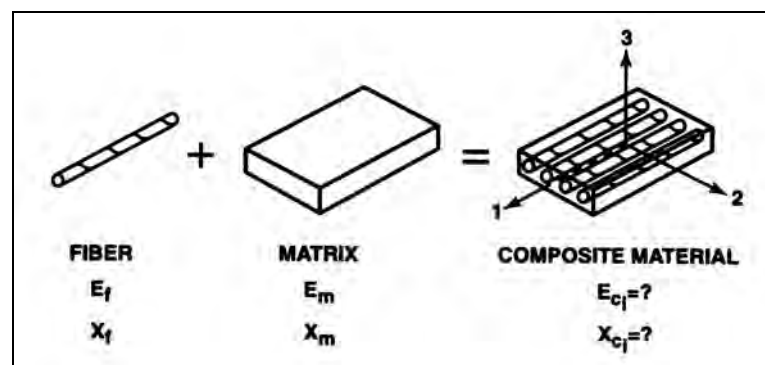


Figure 6.5 Basic questions of micromechanics (Jones, 1999).

“The objective of all micromechanics approaches is to determine the elastic moduli or stiffnesses or compliances of a composite material in terms of the elastic moduli of the constituent materials” (Jones, 1999).

The following assumptions must be considered to validate any micromechanics approaches:

- The fibres are homogeneous, linear elastic, isotropic, regularly spaced, perfectly aligned and perfectly bonded (without voids),
- The matrix is homogeneous, linear elastic, isotropic and void-free,
- The whole lamina is initially stress-free, linear elastic and macroscopically homogeneous and orthotropic.

For the purpose of this research, only in-plane tension stress of lamina with unidirectional and bidirectional fibres will be considered. Compression stress, out of plane stress, bending or buckling of the lamina will not be treated, as the glass fibre/epoxy overlaps used in the wood/glass/epoxy joints are not directly subjected to that type of loading. All additional stresses, which occur on structural adhesive joints such as the wood/glass/epoxy joints, will be presented later in this chapter.

The principles of mechanics of materials to determine the stiffness of unidirectional and bidirectional laminae are presented and discussed in the following sections. The bound solution using energy equations, approximate and exact solution approaches will not be discussed here, as these methods are largely specific to composite material design as they were derived from experimental work.

6.2.2.1. Stiffness approach to lamina with uniaxial fibres

The stiffness approach enables the calculation of the stiffness properties of the lamina, using the assumptions previously described.

Consider a unidirectionally fibre-reinforced composite material with a uniaxial stress σ_x parallel to the fibres in the X-axis direction as shown in figure 6.6.

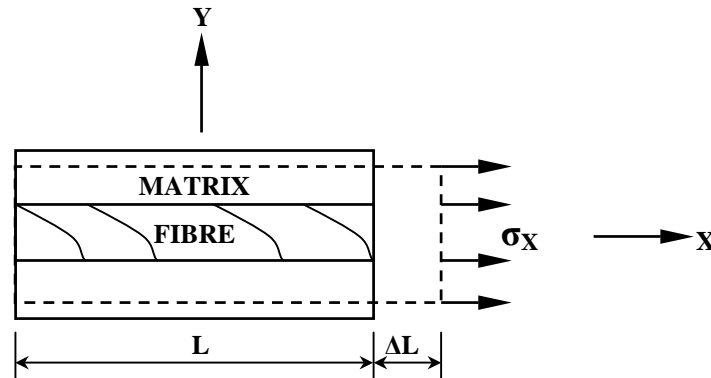


Figure 6.6 Composite element loaded in the X direction.

“The most prominent assumption is that the strains in the fibre direction of a unidirectional fibre reinforced composite material are the same in the fibres as in the matrix [...]. If the strains were not the same, then a fracture between the fibres and the matrix is implied” (Jones, 1999).

The first step is to determine the apparent modulus of elasticity of the composite in the X-axis direction E_x .

The total cross-sectional area A is equal to the area of fibres A_f and the area occupied by the matrix A_m :

$$A = A_f + A_m \quad (6.18)$$

Hooke's law of elasticity can be derived for the stress in the composite σ_X , the stress in the fibres σ_f and the stress in the matrix σ_m :

$$\sigma_X = E_X \varepsilon_X, \quad \sigma_f = E_f \varepsilon_f, \quad \sigma_m = E_m \varepsilon_m \quad (6.19)$$

In terms of strain, we also have:

$$\varepsilon_X = \frac{\Delta L}{L} \quad (6.20)$$

The applied force F is equal to the sum of the forces acting on the fibres and on the matrix:

$$F = \sigma_X A = \sigma_f A_f + \sigma_m A_m \quad (6.21)$$

By substitution of equation (6.19) into (6.21), we have:

$$E_X = E_f \frac{A_f}{A} + E_m \frac{A_m}{A} \quad (6.22)$$

The ratios A_f/A and A_m/A are also known as the *Volume Fraction* of fibres V_f and matrix V_m respectively:

$$V_f + V_m = 1 \quad V_f = \frac{A_f}{A} \quad V_m = \frac{A_m}{A} \quad (6.23)$$

Then equation 6.22 can be written as:

$$E_X = E_f V_f + E_m V_m \quad (6.24)$$

This is known as the *rule of mixtures* for the apparent modulus of elasticity of a composite material in the direction of the fibres. The modulus E_X is regarded as fibre dominated, as E_f is usually much higher than E_m .

The second step is to determine the apparent modulus of elasticity of the composite in the Y -axis direction E_Y .

Now consider the unidirectionally fibre reinforced composite material with a uniaxial stress σ_Y perpendicular to the fibres in the Y -axis direction as shown in figure 6.7.

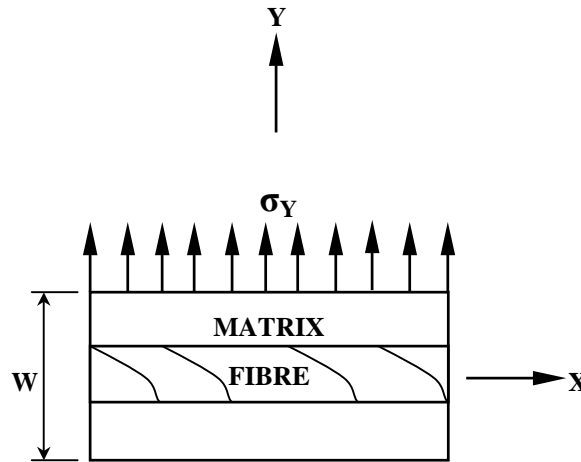


Figure 6.7 Composite element loaded in the Y direction.

The strains in the fibre ε_f and in the matrix ε_m are:

$$\varepsilon_f = \frac{\sigma_Y}{E_f} \qquad \varepsilon_m = \frac{\sigma_Y}{E_m} \qquad (6.25)$$

The transverse dimension over which ε_f acts, is approximately $V_f W$ and the transverse dimension over which ε_m acts, is over approximately $V_m W$. These values are approximate because they assume that the fibre is of square cross-section. The total transverse deformation ΔW is then:

$$\Delta W = \varepsilon_Y W = \varepsilon_f V_f W + \varepsilon_m V_m W \qquad (6.26)$$

Then

$$\varepsilon_Y = \varepsilon_f V_f + \varepsilon_m V_m \qquad (6.27)$$

Using equation (6.25), equation (6.27) becomes:

$$\varepsilon_Y = \frac{\sigma_Y}{E_f} V_f + \frac{\sigma_Y}{E_m} V_m \tag{6.28}$$

Using the total stress-strain equation, we have:

$$\sigma_Y = E_Y \varepsilon_Y = E_Y \left(\frac{\sigma_Y V_f}{E_f} + \frac{\sigma_Y V_m}{E_m} \right) \tag{6.29}$$

Removing the stress parameter σ_Y , the equation (6.29) becomes:

$$E_Y = \frac{E_f E_m}{V_f E_m + V_m E_f} \tag{6.30}$$

This is the relation for the apparent modulus of elasticity of a composite material in the transverse direction of the fibres.

The third step is to determine the major Poisson's ratio ν_{XY} . ν_{XY} is obtained using a similar approach to the one used to determine E_X .

The unidirectionally fibre-reinforced composite material with a uniaxial stress σ_X parallel to the fibres in the X-axis direction is considered including the deformations, as shown in figure 6.8.

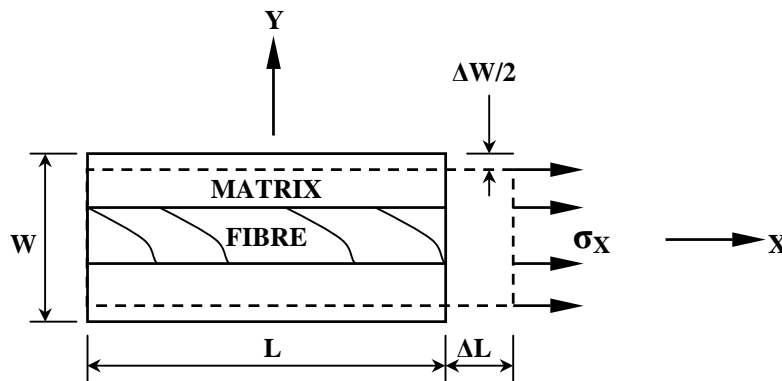


Figure 6.8 Composite element with deformation loaded in the X direction.

The major Poisson's ratio ν_{XY} is expressed as:

$$\nu_{XY} = -\frac{\varepsilon_Y}{\varepsilon_X} \quad (6.31)$$

Assuming the fibre strain is identical to the matrix strain (as assumed before), the transverse deformation ΔW can be expressed as:

$$\Delta W = -W\varepsilon_Y = W\nu_{XY}\varepsilon_X \quad (6.32)$$

But at microscopic level, the transverse deformation ΔW is also equal:

$$\Delta W = \Delta_{fW} + \Delta_{mW} \quad (6.33)$$

The transverse deformation of the fibre Δ_{fW} and the matrix Δ_{mW} can be approximately expressed as previously carried out for the determination of E_Y .

$$\Delta_{fW} = WV_f\nu_f\varepsilon_X \quad \Delta_{mW} = WV_m\nu_m\varepsilon_X \quad (6.34)$$

Combining equations (6.32), (6.33) and (6.34), it becomes:

$$W\nu_{XY}\varepsilon_X = WV_f\nu_f\varepsilon_X + WV_m\nu_m\varepsilon_X \quad (6.35)$$

Dividing equation (6.35) by $W\varepsilon_X$, the Poisson's ratio ν_{XY} can finally be expressed as:

$$\nu_{XY} = V_f\nu_f + V_m\nu_m \quad (6.36)$$

This is known as the *rule of mixtures* for the major Poisson's ratio of a composite material in the direction of the fibres. The Poisson's ratio of the fibre ν_f and the Poisson's ratio of the matrix ν_m are usually not significantly different therefore the composite material major Poisson's ratio is considered as neutral in terms of domination of one of the two constituents.

The fourth and final step is to determine the in-plane shear modulus of the lamina G_{XY} . For this analysis, the assumption is made that the shearing stresses are the same on the fibre as on the matrix, which is not the case in reality.

The shear strains for the fibre γ_f and for the matrix γ_m can be expressed as:

$$\gamma_f = \frac{\tau}{G_f} \qquad \gamma_m = \frac{\tau}{G_m} \qquad (6.37)$$

Ignoring non-linear shear stress-strain behaviour of composite material, the behaviour is considered linear, as it would be for an isotropic material.

The unidirectionally fibre-reinforced composite material with a shear stress τ with the resulting shear deformations is shown in figure 6.9.

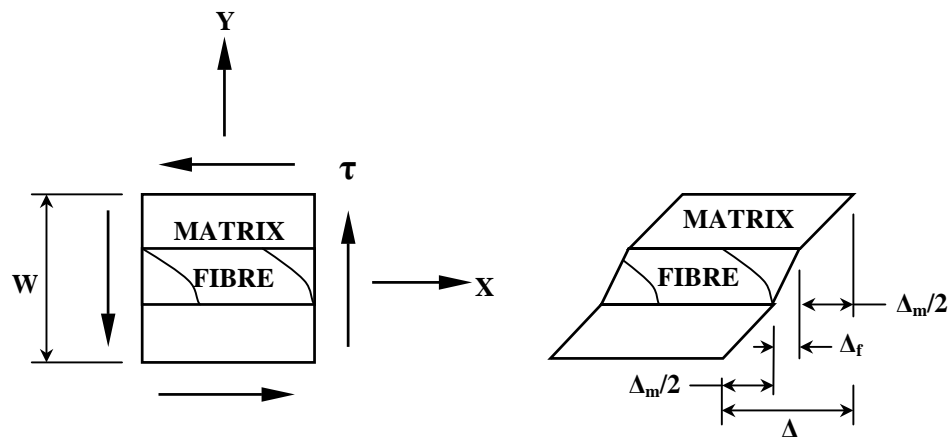


Figure 6.9 Composite element loaded in shear with shear deformation.

The total shear deformation is equal to:

$$\Delta = \gamma W \qquad (6.38)$$

The total shear deformation is made of the following approximate deformations of the fibre and the matrix:

$$\Delta = \Delta_f + \Delta_m \qquad (6.39)$$

$$\Delta_f = W V_f \gamma_f \qquad \Delta_m = W V_m \gamma_m \qquad (6.40)$$

Combining equations (6.39) and (6.40) and dividing by W , it becomes:

$$\gamma = V_f \gamma_f + V_m \gamma_m \quad (6.41)$$

Using the general equation of shear modulus:

$$\gamma = \frac{\tau}{G_{XY}} \quad (6.42)$$

Equation (6.41) can be written as:

$$\frac{\tau}{G_{XY}} = V_f \frac{\tau}{G_f} + V_m \frac{\tau}{G_m} \quad (6.43)$$

Removing the shear stress τ , the shear modulus G_{XY} becomes:

$$G_{XY} = \frac{G_f G_m}{G_f V_m + G_m V_f} \quad (6.44)$$

This equation is of the same form as the equation obtained for the transverse modulus of elasticity E_Y .

The calculation of the moduli of elasticity in two directions, the major Poisson's ratio and the shear modulus are the basic stiffness properties of a unidirectional lamina. These calculations are taking a series of assumptions into account, which are not realistic in practical terms. However these calculations are recognised as reliable and give generally accurate approximations of the exact values.

The next step is the presentation and discussion of the principles of mechanics of materials to determine the stiffness of bidirectional lamina.

6.2.2.2. Stiffness approach to lamina with biaxial fibres

Using the same assumptions as previously described, the stiffness approach, which enables the calculation of the stiffness properties of a bidirectionally reinforced lamina, is far more complex than for a unidirectionally reinforced lamina.

For a lamina where the fibres are woven in two perpendicular directions, the fibres are no longer straight and when they are in the matrix, the fibres will behave in a rather different mode than previously assumed.

The fibres in both directions are curved because of the weaving geometry. Taking this geometry into account will affect the buckling capacity of the fibres but also their efficiency to carry the loads.

For example, a curved fibre surrounded in a matrix under axial tension loading is less efficient because the straight parts of the fibre will transfer load at their full potential as the inclined parts will develop shear across its section and will carry less load. Such an approach usually necessitates the use of finite element models to represent both the curved fibres and the surrounding matrix.

The biaxial fabric used in this research is rather different because the fibres are not woven in the two perpendicular directions. As described in chapter 3, the XE450 glass fibre fabric consists of two layers of unidirectional fibres laid perpendicularly and stitched together.

This fabrication process is more complicated but provides better mechanical properties to the fabric. In fact, the fibres are no longer curved and therefore can work to their full capacity.

The great advantage of using the XE450 stitched fabric in a composite is that the lamina can be simplified in terms of micromechanics analysis. Because the fibres are not woven, the lamina can be treated as a laminate made of two laminae with the fibres orientated perpendicularly and bonded together. The thread used to stitch the two layers together is ignored, as it does not provide any capacity of strength.

The XE450/epoxy composite could be decomposed into two perpendicular layers of unidirectional glass fibre/epoxy laminae, as shown in figure 6.10.

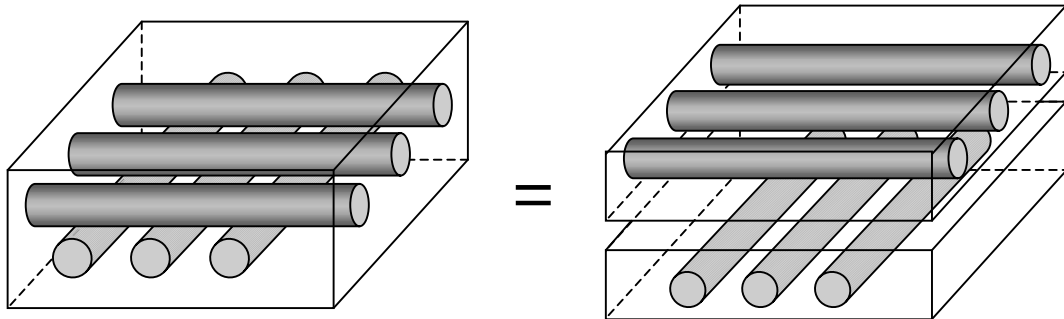


Figure 6.10 Stacked fabric lamina for micromechanics analysis.

The micromechanics of the laminate is very complex as all the assumptions used for a single lamina cannot be applied to several laminae bonded together. If so, the analysis would be unrealistic as each lamina is inter-dependent of the other. How are stresses or strains from one lamina transferred to the other? This phenomenon is highly non-linear. The tension applied to one lamina will result in compression in the other but the amount of stresses transferred necessitates the assessment of interlaminar stresses.

Laminates are usually approached in macromechanics, using apparent stiffness properties of each lamina. This approach was previously described and is particularly appropriate for the current situation where the laminate is made for two layers of fibres perpendicular to each other, such as the XE450/epoxy composite. The laminate is therefore treated as a transversely isotropic material.

The theories developed and applied to structural adhesive joints, made of composites or non-composites materials are described in the following section.

6.2.3. Double lap joints

The science of structural adhesive joints is well developed and several theories exist, depending on the joints type and geometry. In this section, double lap joints will be considered because its configuration corresponds to the wood/glass/epoxy joint.

The double lap joint is often considered as two members bonded on the opposite sides of one inner member, as shown in figure 6.11.

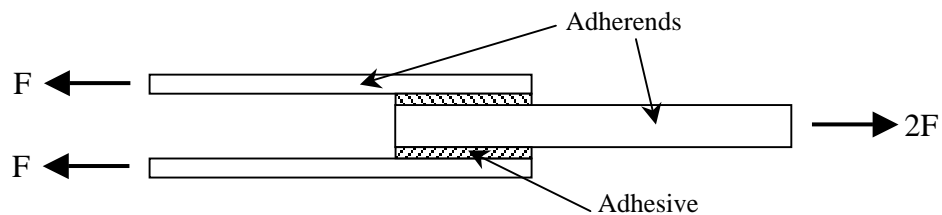


Figure 6.11 Typical double lap joint loaded in tension.

The standard configuration of the wood/glass/epoxy is in fact a double-double lap joint. It could also be called a double strap joints. Assuming there is not butt jointing between the two inner adherends, the wood/glass/epoxy joint behaves as double lap joint, with an axis of symmetry in the gap area, as shown in figure 6.12.

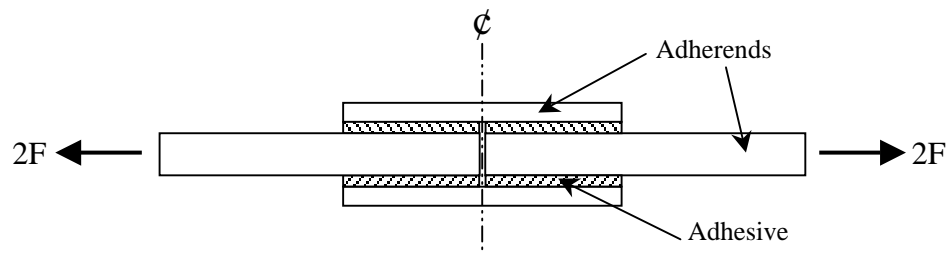


Figure 6.12 Typical double strap joint loaded in tension.

The analysis of the double lap joints is mainly based on single lap joints, which were initially developed by Volkersen back in 1938. The analysis assumed elastic deformation of the adhesive. However the approach ignored the eccentricity of the loading for that type of joint, which results in bending effect in the joints. As a result, this analysis type is only acceptable for double lap joints. The work from Goland and Reissner in 1944 introduced a bending moment factor to allow for the eccentricity of the loading in a single lap joint. Other authors have also participated in the development of theories for the analysis of structural adhesive joints, but the most

comprehensive analytical approach of adhesive joints was mainly developed by Hart-Smith in the 1970s and remains the most accessible theory nowadays. Other attempts were made to represent non-linear behaviour of the adhesive, such as shear stress/shear strain relationship, through the thickness stress distributions but these theories are too complex to be used analytically.

The Hart-Smith analysis of double lap joints is summarised in this section, with additional work and research from Baker (1997) and Adams et al. (1997).

The Hart-Smith analysis is based on the non-linear elastic/plastic behaviour of the adhesive. The theory is based on the fact that adequate joint design should be based on the adhesive strength being much higher than the adherends' strengths to avoid peel stresses failure. Therefore the adhesive failure depends on the shear strain applied to the adhesive.

“Inevitably, many of the complications in real joints are neglected or inadequately dealt with in these relatively simple studies. These include:

1. Through the thickness variation of shear stresses
2. Through the thickness stresses
3. The stress-free state at the ends of the adhesive
4. The (highly beneficial) effect of adhesive spew, excess adhesive that forms a fillet at the edge of the joint
5. True shear stress/strain behaviour, including time dependency” (Baker, 1997).

The through the thickness stress variations are ignored but these effects are significant. One example is the effect of bending in double lap joints. It was previously highlighted that double lap joints are not subject to direct loading eccentricity as for single lap joints, resulting in bending of the whole joint.

“Although there is no net bending moment on a symmetrical double lap joint, as there is with single lap joint, because the load is applied through the adhesive to the adherend plates away from their neutral axes, the double lap joint experiences internal bending [...]. In a symmetrical double lap joint, the centre adherend experiences no net bending moment, but the outer adherends bend, giving rise to tensile stresses across the adhesive layer at the end of the overlap where they are not loaded, and compressive stresses at the end where they are loaded [...]” (Adams et al., 1997).

The internal bending effect of the overlaps is illustrated in figure 6.13.

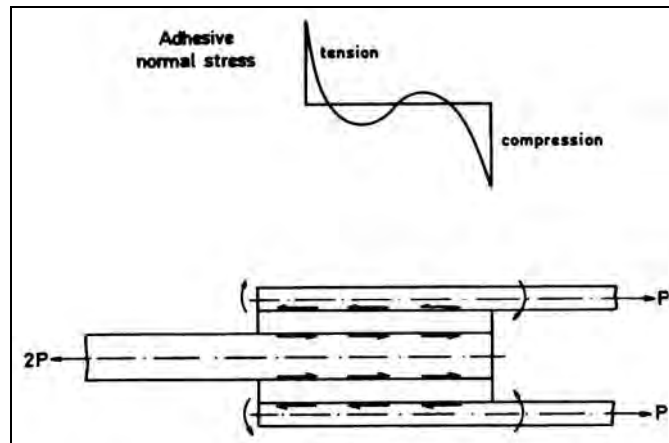


Figure 6.13 Bending moments induced in the outer adherends of a double lap joint (Adams et al., 1997).

This effect of internal bending of the outer adherends is not taken into account in the Hart-Smith analysis method. However it is suggested that finite element modelling reflects those effects happening through the thickness of the adhesive and is the best and easiest approach to the true behaviour of adhesive joints. This phenomenon will be discussed again in the section dealing with the results obtained from the FE analysis.

“Another effect that is ignored by the analysis is the stress-free state at the ends of the adhesive. The analysis predicts that the maximum shear stress occurs at the free ends of the overlap. In fact the stress in the bond line should fall to zero at the free edge, as the principles of complementary shears of the horizontal shear force cannot be balanced by the vertical shear force which is zero at the free edge. FE modelling should demonstrate that effect. However, the shear stress distribution along the bond line and the magnitude of the maximum stress predicted by the simple analytical procedures turn out to be approximately correct. Similar observations have been made concerning normal or peel stresses” (Baker, 1997).

The Load transfer mechanisms in double lap joints according to the Hart-Smith method are developed in the following section.

6.2.3.1. Load transfer mechanisms in double lap joints

The Hart-Smith approach take into account the elastic and plastic deformations of the adhesive. If the adhesive is only considered within its elastic range, the analysis is greatly simplified. However elastic analysis is only acceptable if the fatigue of the joint is critical and if plasticity is to be avoided. For static analysis of the joint strength, it is more economical to look at its elastic/plastic behaviour.

The Hart-Smith analysis considers an ideal elastic/plastic behaviour of the adhesive, where the bi-linear model is the best approximation to the real curve, as shown in figure 6.14.

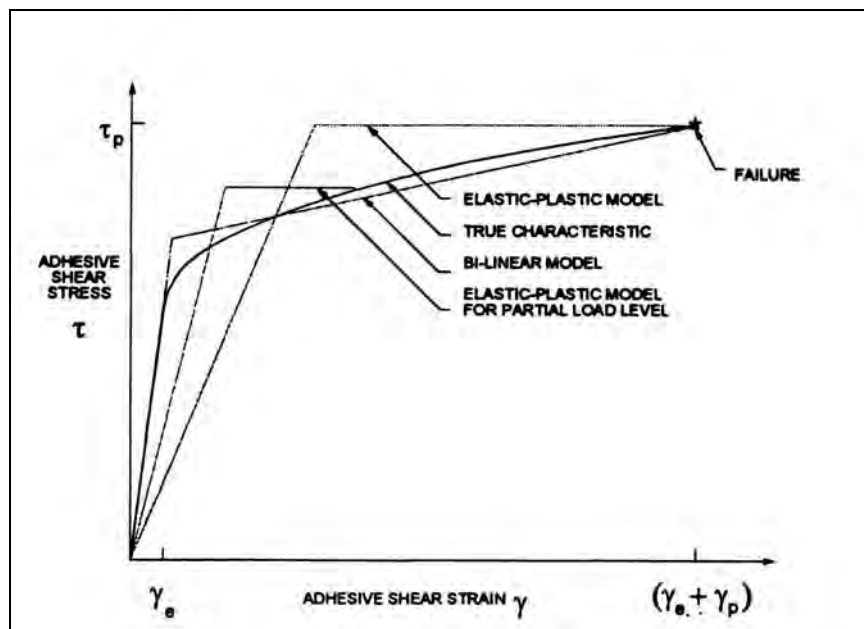


Figure 6.14 Adhesive shear stress-strain curves and models (Hart-Smith, 1981).

The ideal elastic/plastic models simplify the analysis, which still remains mathematically complex.

“Hart-Smith shows that the requirement for the elastic/ideally plastic model is that it has the same shear strain energy (area under the curve) as the actual curve and intersects it at the required level of shear stress. Thus [...] the effective shear modulus G_A and shear yield stresses used in the model vary with the strain level” (Baker, 1997).

The equal shear strain energy model is shown in figure 6.15.

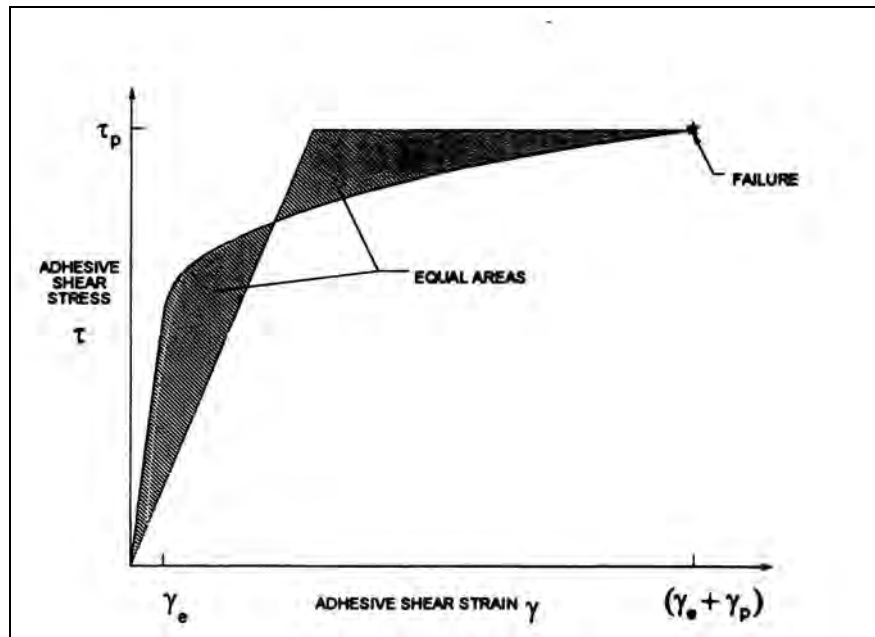


Figure 6.15 Models of equal shear strain energy of the adhesive (Hart-Smith, 1981).

The load transfer is non-uniform in double lap joints (or double strap joints) and the distribution of shear stress and shear strain of the adhesive vary along the overlap length. Furthermore the shape of the distribution curves also change as the load increases, as shown in figure 6.16.

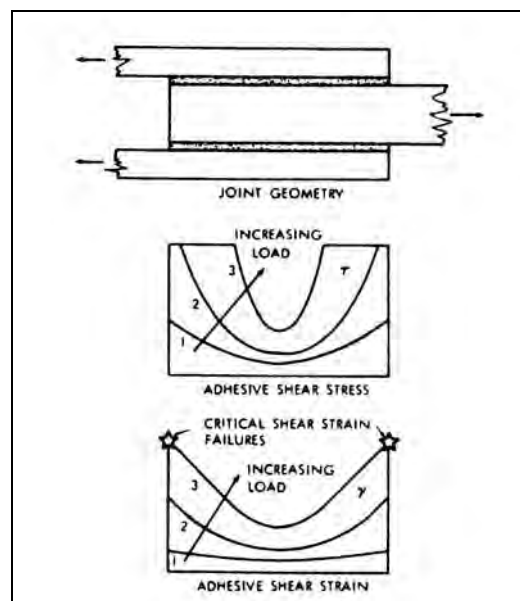


Figure 6.16 Development of shear stress and strain distribution in double lap joint with increasing loading (Hart-Smith, 1981).

Hart-Smith also demonstrated that the length of the overlap has a great significance in the shear stress distribution, particularly when the joint has reached plastic deformation of the adhesive. This is illustrated in figure 6.17.

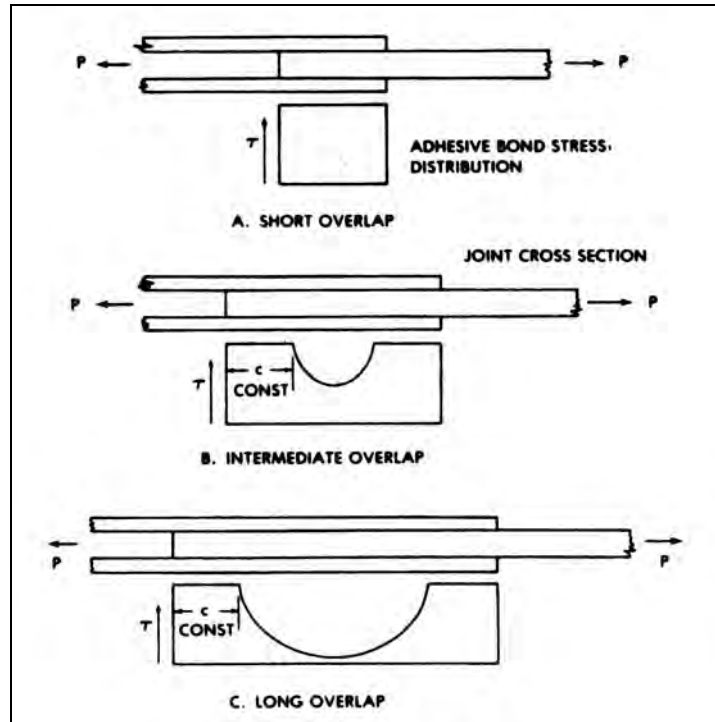


Figure 6.17 Influence of lap length on adhesive shear stress distribution (Hart-Smith, 1981).

The design approach developed by Hart-Smith look at the shear stress and strain in the adhesive. The failure of the joint occurs when the adhesive shear strain capacity is reached. The mathematical model is rather complex and considers balanced joints, which are defined in that particular case by the following equation:

$$E_1 t_1 = E_2 t_2 \quad (6.45)$$

Where: E_1 = Elastic modulus of the outer adherend,

t_1 = Thickness of the outer adherend,

E_2 = Elastic modulus of the inner adherend,

t_2 = Thickness of the inner adherend.

The model becomes even more complex when the joint is unbalanced. The equations, which enable the calculations of the joint strength, are not presented in this report because they cannot be used to establish the strength of the wood/glass/epoxy joints. These equations require the measurement of shear strain in the adhesive developed in the elastic range γ_e and in the plastic range γ_p . In fact, none of those values were recorded during the test. Values of shear strain in the bond line are highly impractical to measure because of the infinitely small thickness of the adhesive. It is obviously not possible to position a strain rosette vertically in the adhesive layer (in order to measure shear strain acting across the thickness of the adhesive), the alternative would have been to place two strain gauges on top and underneath the adhesive layer. However this was also impractical to achieve for the same reasons.

The elastic/plastic analysis developed by Hart-Smith ignores all through the thickness stresses and strain, as mentioned previously.

“[...] the basic Hart-Smith approach entails neglecting the normal or ‘peel’ stresses acting across the glue line. However, in practice these may be the main contributors to joint failure, even in double lap joints. Hart-Smith has recognised this possibility and in one of his analyses (1972) combined elastic peel stresses with plastic shear stresses” (Adams et al., 1997).

The formulation proposed is not presented in this report but reflects that the thickness of the outer adherends has an effect on the ‘peel’ stresses. In fact, the thinner the outer adherends, the less critical the ‘peeling’ stresses.

There are significant differences between the double lap joint as it is presented in this section and the wood/glass/epoxy joints. Those differences, as well as the effect they have on the joint are described in the following section.

6.2.3.2. Wood/glass/epoxy joints

The wood/glass/epoxy joint cannot be treated as a standard double lap joint, as presented before. In fact the outer adherends of the wood/glass/epoxy joint are very thin, typically 0.7 mm thick including the adhesive layer. The outer adherends are made of glass fibre/epoxy but they were laid wet, directly on the timber surface. They were not fabricated prior to the bonding process to the timber therefore it is difficult to evaluate the thickness of the adhesive layer.

The wood/glass/epoxy joint has in fact a very thin glue line, but the outer adherends are also relatively thin. Measurements of the thickness for the UT-E500/epoxy and XE450/epoxy composite layers were carried out after the sample tests. The composite layer was removed manually from the timber surface and the thickness was measured at various locations, where the composite was free from remaining timber fibres.

Using an electronic vernier, 10 thickness readings were carried out at random positions on each of the 20 layers collected for the measurement. 10 layers were made of UT-E500/epoxy composite and 10 made of XE450/epoxy composite. The thickness of the glass fibre fabrics UT-E500 and XE450 were also measured using the same electronic vernier. The results are presented in the table 6.2.

	Average thickness (mm)
UT-E500 fabric	0.4
XE450 fabric	0.4
UT-E500/epoxy layer	0.65
XE450/epoxy layer	0.65

Table 6.2 Thickness measurement of glass fibres and composites used in wood/glass/epoxy joints.

These results are consistent. The XE450 fabric contains a large amount of stitching threads, which were ignored in the thickness measurement. It is reasonable to assume that the threads represent 0.05 mm of the thickness, leaving 0.4 mm for the glass fibres. The resin thickness contained in both types of composite layer is around 0.25 mm. The question now is to identify how the resin thickness is distributed

across the overall thickness of the composite layer. It is then necessary to examine the wood/glass/epoxy joints fabrication process.

The wet epoxy resin was laid onto the timber surface using a paintbrush. That layer of resin was relatively thick in order to have a sufficient amount of resin to impregnate the glass fibre, which was laid on top of it. Using a roller, the glass fibre was pressed into the resin layer to achieve the impregnation and remove the air trapped around the fibres. Using the paintbrush, another layer of epoxy resin was laid on top. Again, the roller was used to remove the voids and the resin in excess, and complete the impregnation of the fibres.

It is reasonable to assume from the fabrication process that the thickness of resin located below the glass fibre is likely to be similar to the thickness of resin located on top. The ideal models of glass fibre fabric and resin thickness distribution for the UT-E500/epoxy and XE450/epoxy composites are presented in figure 6.18.

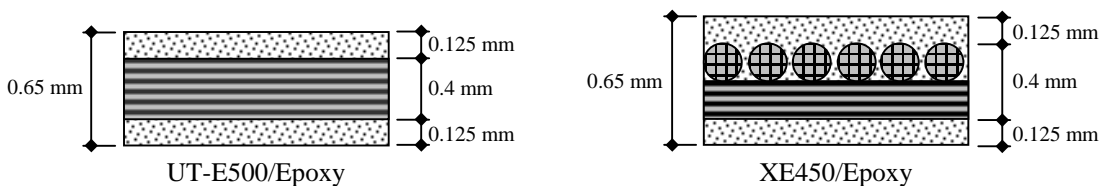


Figure 6.18 Ideal models of thickness distribution of glass fibre and epoxy resin.

Because of the uncertainty around the thickness of the bond line, the adhesive layer between the outer and inner adherends cannot be defined as a separated material from the composite layer. The wood/glass/epoxy joint will be modelled in the finite element analysis with two materials defined: The timber material and the composite material, both of them being bonded or ‘connected’ together. But this bond will not be modelled as a third material. The two materials will be directly connected or linked from their common nodes. However this will be explained in detail in the finite element procedures described later on in this chapter.

The wood/glass/epoxy joint is a joint made of materials with different stiffness properties: If a balanced joint must satisfy the equation (6.45), the wood/glass/epoxy joint is highly unbalanced. However, a balanced joint was initially defined as a joint that fails in combined modes: Delamination and tension failure of the fibres. This option represents the most economical design of a joint. Nevertheless it was decided

that tension failure of the fibres was a mode of failure to avoid, in order to limit the joint strength to the timber capacity.

The outer adherends as well as the bond line are very thin in the wood/glass/epoxy joint. The Hart-Smith theory ignores the through the thickness stresses and strains, which can be significant in terms of joint strength. However with thin bond line and outer adherends, the stress and strain variations through the thickness are limited because of the small amount of material (in thickness). As a result, the Hart-Smith analysis would probably suit better the wood/glass/epoxy joint than a typical double lap joint with thicker bond line and outer adherends.

The stresses and strains acting through the thickness of the material will be taken into account because the finite element modelling will allow for all mechanical effects occurring on the joint: The analysis will show how the stresses and strains vary through the thickness of the composite layer.

Internal bending of the outer adherends was previously defined and is a characteristic of double lap joints. For the wood/glass/epoxy joint, which has very thin outer adherends, this effect is likely to be more significant because the moment of inertia of the outer adherends is relatively small. Once again the finite element analysis will probably highlight this effect.

The finite element analysis of the wood/glass/epoxy joint will show how the joint behaves under tension load. It should provide information on stress and strain distribution over the whole joint.

As no other research work was found on that particular subject, comparison will have to be drawn, based on experimental results available for other types of double lap joints. The following section summarises the experimental results found on double lap joints, which could be relevant for the comparison with the wood/glass/epoxy joint.

6.2.3.3. Existing comparable results

There is significant research work available, which was carried out in the field of double lap joint analysis. Of course not all research work dealing with double lap joints can be referred to, but all the information gathered in this section has been taken from the excellent book “Structural adhesive joints in engineering” of Adams et al., (1997). The research team led by one of the authors carried out most of the work presented here. This extensive research work was undertaken on a variety of joint types, using different materials and different adherend thickness.

Using finite element techniques, the authors carried out analyses of various types of joint made of aluminium-aluminium and CFRP-CFRP (Carbon Fibre Reinforced Plastics). The adhesive shear stress distribution obtained for those joints are presented in figures 6.19 and 6.20.

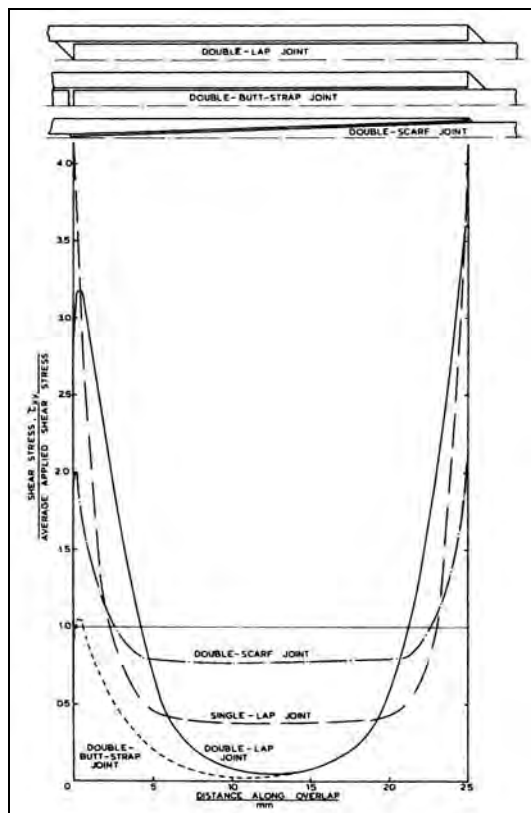


Figure 6.19 Adhesive shear stress distributions in aluminium-aluminium joints (Adams et al., 1997).

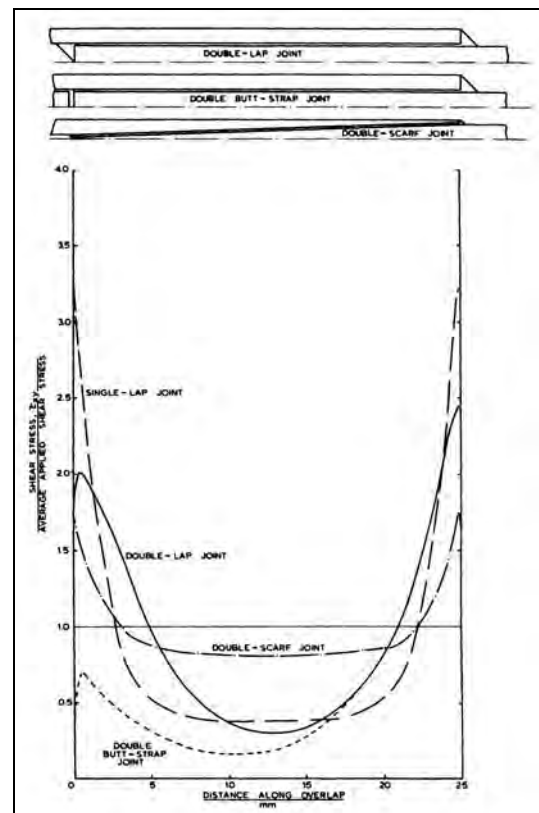


Figure 6.20 Adhesive shear stress distributions in CFRP-CFRP joints (Adams et al., 1997).

The analyses were based on the adhesive being perfectly elastic, and the adhesive properties used were typical of an epoxy. Depending on the joint configuration, there are significant differences in shear stress distribution. However, the double lap joint is the only configuration to be considered. Aluminium-aluminium and CFRP-CFRP double lap joints with the same geometry are compared. There is less shear stress concentration observed in the CFRP-CFRP joint than in the aluminium-aluminium joint, because of the greater longitudinal stiffness of the CFRP. The highest shear stress concentration occurs at the lap end of the outer adherends for both types of joint.

The applied tensile stresses at various locations of the adherends of the CFRP-CFRP double lap joint were also recorded. The adherend tensile stress distributions are shown in figure 6.21.

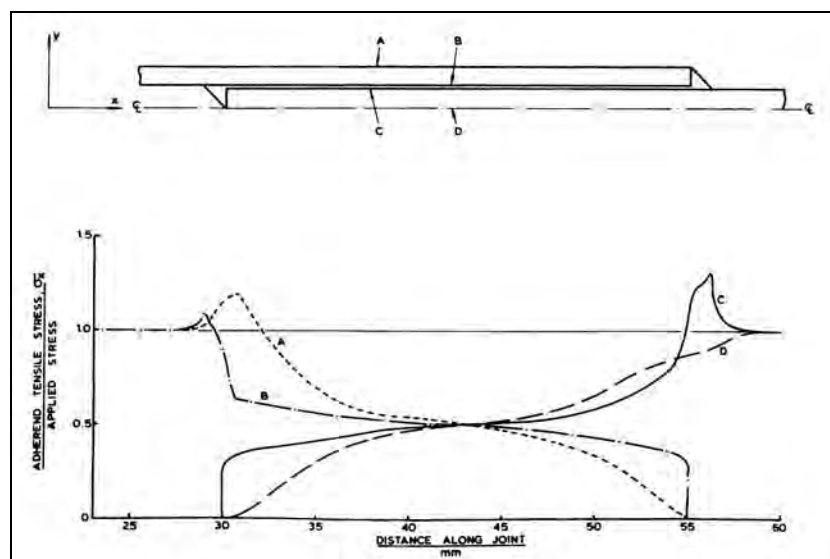


Figure 6.21 Adherend tensile stress distributions in CFRP-CFRP double lap joints (Adams et al., 1997).

These results are particularly useful as they can be linked to the experimental results obtained from the wood/glass/epoxy joint tests. Strain gauges were used to record tensile strain on the free surface of the glass fibre/epoxy composite. The stiffness properties of the glass fibre/epoxy layer are known therefore tensile strain can be converted easily to tensile stress as long as the materials behave elastically. However this conversion will be carried out through the finite element analysis, the results

obtained from the strain gauges being used as check points between the experimental and the theoretical results.

Further work was carried out by the same authors: The comparison of the elastic shear stress distribution between double lap joint made of $0^\circ/90^\circ/90^\circ/0^\circ$ CFRP cross-ply adherends and double lap joint made of unidirectional CFRP, having both the same geometry. The results are shown in figure 6.22.

Double lap joints made of metal (aluminium) and composite (unidirectional CFRP) were also analysed. The elastic shear stress distribution is compared between a double lap joint having the aluminium as outer adherends and the CFRP as inner adherend and a double lap joint having the CFRP as outer adherends and the aluminium as inner adherend. The results are shown in figure 6.23.

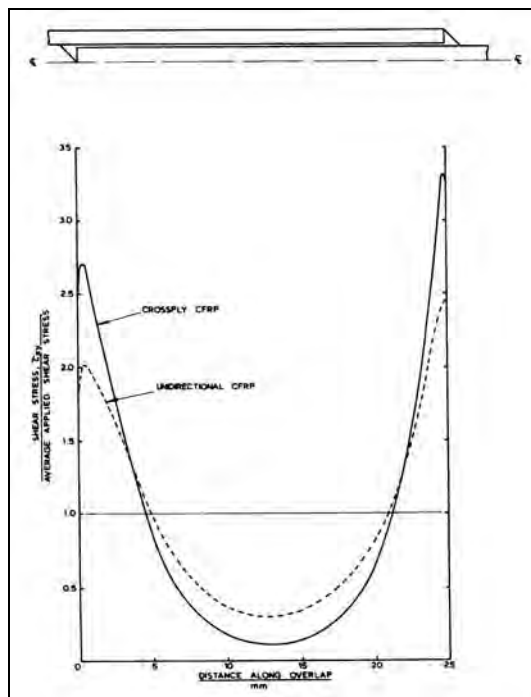


Figure 6.22 Adhesive shear stress distributions in cross-ply CFRP-CFRP and unidirectional CFRP-CFRP double lap joints (Adams et al., 1997).

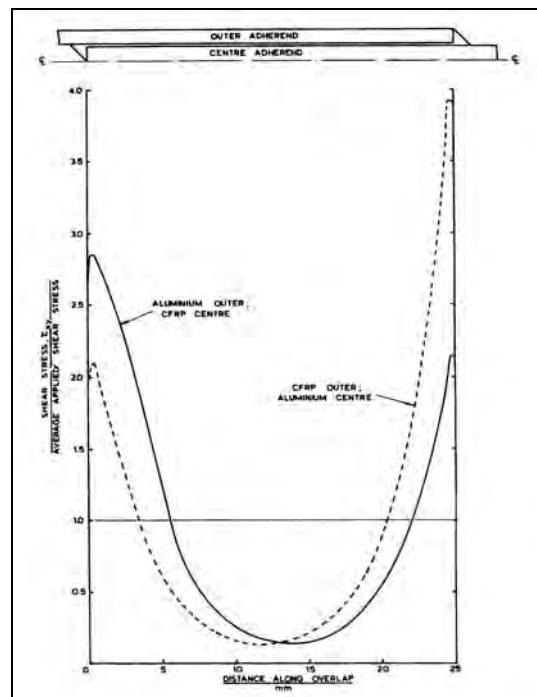


Figure 6.23 Adhesive shear stress distributions in aluminium-CFRP double lap joints (Adams et al., 1997).

In figure 6.22, higher stress concentration is observed for the cross-ply CFRP-CFRP double lap joint. This is caused by the lower tensile stiffness of the cross-ply adherends. Similar comparison will be carried out between the shear stress

distribution obtained from the wood/glass/epoxy joints models made of unidirectional fibres and bidirectional fibres.

In figure 6.23, when the aluminium is the outer adherends and the CFRP the inner adherend, the highest shear stress concentration occurs at the gap end. This is due to the lower tensile stiffness of the aluminium compared to the CFRP inner adherend. However the adhesive shear stress concentrations are in the same range at both ends of the joint. Alternatively, when the CFRP is the outer adherends and the aluminium the inner adherend, the highest shear stress concentration occurs at the lap end. The shear stress concentration at the lap end is at least two times higher than the shear stress concentration at the gap end. This phenomenon reduces significantly the joint efficiency.

The double lap joint made of equal thickness adherends, with aluminium as outer adherends and CFRP as inner adherend, was compared with the same joint made with matched adherends, as shown in figure 6.24.

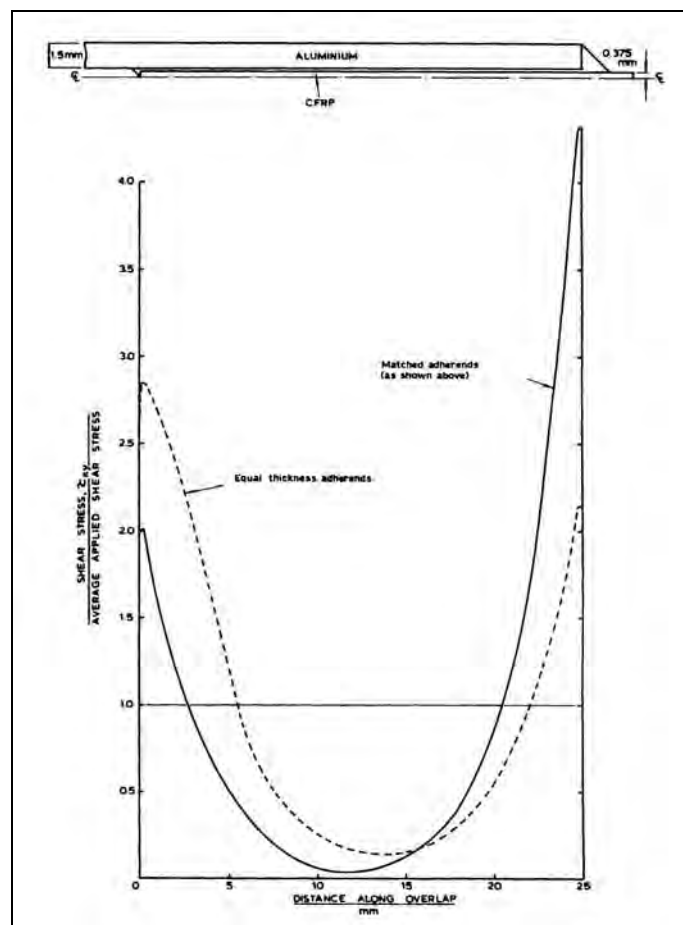


Figure 6.24 Adhesive shear stress distributions in aluminium-CFRP double lap joints with equal and matched adherends (Adams et al., 1997).

To optimise the use of high strength CFRP (typical yield strength of 1550 MPa) with aluminium (typical yield strength of 325 MPa), the thickness of the CFRP must be reduced to about one quarter of the thickness of the aluminium. This was carried out to match the adherends, as shown in figure 6.24. The aluminium outer adherends are 1.5 mm thick each, and the CFRP inner adherend is only 0.75 mm thick. As a result, the shear stress concentration of the adhesive is reduced at the gap end but significantly increased at the lap end. This shows that adherend thickness affects considerably the shear strain distribution in the adhesive.

There are many factors, which affect the double lap joint. Those factors are multiplied when the joint is made of different materials, with different thickness and if it is unbalanced. The wood/glass/epoxy joint is certainly behaving like a very unbalanced double lap joint and the finite element analysis, which is presented in the next section, will expose its mechanical behaviour under tension load.

6.3. Finite element modelling

6.3.1. Introduction

The finite element modelling was performed using the professional edition of the ANSYS software, version 5.4.

The advantages of using a well-known FEA product were the wide range of capabilities offered to the user to develop the models, to run the analysis and to make the most of the results obtained.

One finite element model was developed and analysed for each wood/glass/epoxy joint configuration that was elaborated in experiments. In other words there are eight models that were analysed. The results obtained are presented throughout this chapter and are compared thereafter with experimental results.

But firstly, many other models were built up and “tested” until the final ones were achieved. This procedure was a long exercise in model development, as various types of analysis, element types, and mesh sizes were looked at and compared. The following section summarises most procedures, which have lead to the model development.

6.3.2. FEM procedures

6.3.2.1. Analysis type

A fundamental premise of using finite element modelling is that the model is subdivided into small discrete regions known as finite elements. These elements are defined by nodes and interaction functions. Equations are written for each element and these elements are combined in a global matrix. Loads and constraints are applied and the solution is then determined.

There are various types of structural analysis available in most FE programs. For the purpose of modelling wood/glass/epoxy joint loaded in tension, a linear static analysis was performed. The static analysis can be defined as an analysis, which determines primarily displacements under static loading conditions. Other quantities,

such as strains, stresses and reaction forces are then derived from the displacements. When only linear static analysis is carried out, the stress-strain relationship and theory of elasticity are applied to the models. On the other hand, when non-linear static analysis is carried out, the non-linearities are defined as plasticity, stress stiffening, large deflection, large strain, creep, etc. A non-linear analysis consists of a set of simultaneous linear analysis, which predicts the response of the model. However a non-linear behaviour cannot be represented directly with a simple set of linear equations: Successive linear approximations with corrections are needed. Non-linear solutions can be approached using load increments, which means breaking the load into a series of load steps. For each load step, the program adjusts the stiffness matrix to reflect the non-linear behaviour and converges to a solution before proceeding to the next load increment. It means that the non-linear behaviour of the model must be predicted by the user, prior to the analysis.

The tension tests of wood/glass/epoxy joints revealed that plastic behaviour occurred at a very late stage of the test, just before the failure of the samples. The main difficulty encountered was the recording of strains and displacement in the plastic region: The equipment used was recording strains and displacements for every load increment of 1.5 kN. When plastic behaviour occurs, the strains and displacements keep increasing, as the load remains approximately identical. In fact, the equipment did not record strains and displacements while the samples were developing plastic behaviour because the load was not increasing anymore. As a result, insufficient data are available to predict the plastic response of the wood/glass/epoxy joints. The load/displacement graphs presented in chapter 5 confirm this lack of results.

The finite element analysis was then limited to a simple linear static analysis, mainly because of this inability of measuring the plastic behaviour of wood/glass/epoxy joints. Further reasons were based on the objectives of using the FEA in the first instance: FEA was a tool to be used for understanding how stresses and strains are distributed across the joints, in order to compare them with data collected from the experimental tests. The FEA was not considered as a way to design or to achieve the design of the joint. The approach is rather different: If joint design is considered, the FEA is a tool to predict its strength and behaviour, with possible improvements. In order to make the analysis reliable, the behaviour of the joint must be predicted

before the analysis is carried out and therefore must be based on theoretical or experimental data. This is even more necessary when non-linear analysis is carried out, as convergence criteria must be set by the user in order to generate the non-linear response: The analysis must converge to a predicted value, for a given load or stress, within some tolerances also set by the user.

The approach of linear static analysis was based on setting a given load (within the elastic range of the joint behaviour) and to apply it to the model, and compare the results obtained from the analysis with experimental results obtained from the tests. The load to apply to the models should range within the elastic zone of the load/displacement graphs obtained from the tests. A tension load of 18 kN seemed to correspond to the adequate value as it falls within the elastic zone of each joint tested. Consequently all the models were analysed with a tension load of 18 kN.

The finite element models could be generated as 2-Dimensional or 3-Dimensional, depending on the geometry and shape of the joint as well as the type of elements used (i.e. planar or solid elements). Joints with the load parallel to the grain (straight configuration) could be modelled in 2D or 3D. If the joint is modelled in 2D, the joint is defined in two orthogonal planes. The third orthogonal plane can be defined as a thickness, which means that the model is made of planar elements in which a thickness is given. The figure 6.25 shows an example of 2D geometry that could be used for straight configuration.

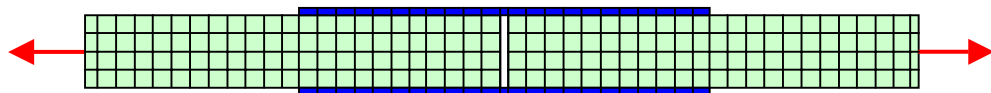


Figure 6.25 Example of 2D configuration for straight joint.

Beyond the scope of using 2D or 3D modelling, planes of symmetry can be observed on each joint configuration. The finite element modelling allows the use of symmetry to reduce the size of the model, if the symmetry is in all respects (geometry, loads, constraints and materials properties). This tool improves the efficiency of the model because on the one hand this reduces the area or volume to be modelled with elements and on the other hand, the remaining area or volume can be modelled with a finer mesh.

When a 2D configuration is used in combination with plane symmetry, the model of a straight configuration joint can be reduced as shown in figure 6.26.

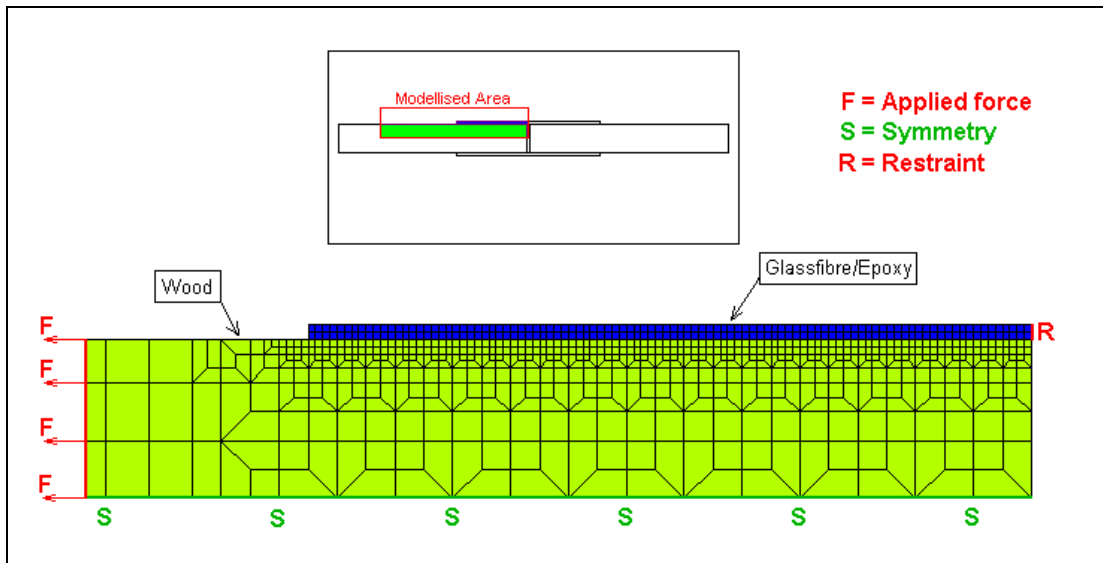


Figure 6.26 Example of 2D configuration and symmetry for straight joint.

When 3D modelling is used, the straight joint can be reduced in the same manner, using symmetries in the three orthogonal axes of the joint.

An example of 3D model for straight joint is shown in figure 6.27.

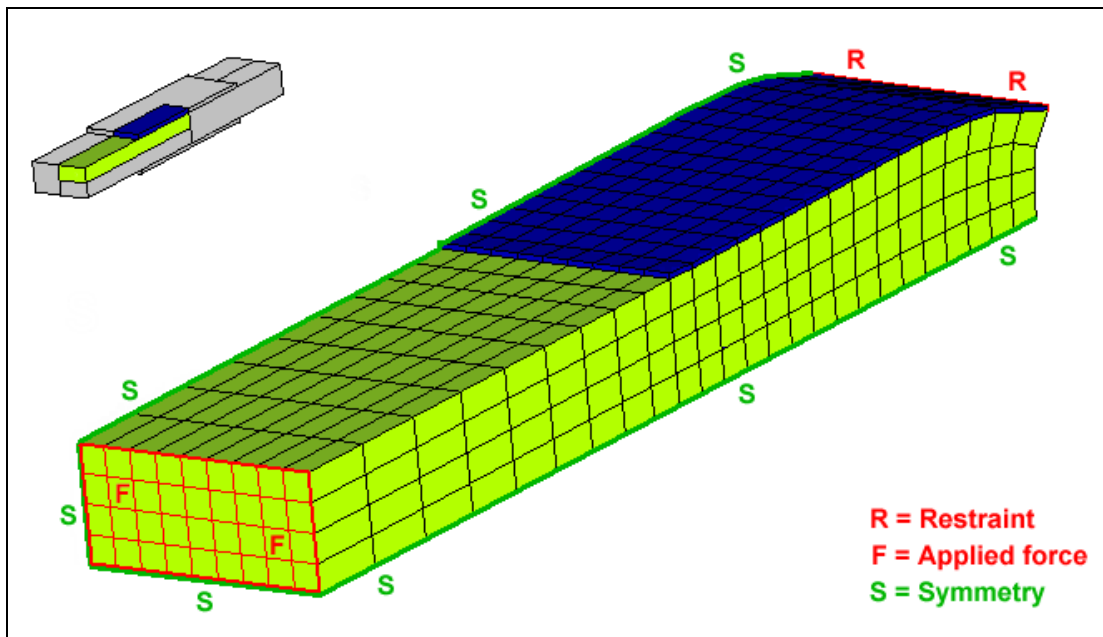


Figure 6.27 Example of 3D configuration and symmetry for straight joint.

As a result, 2D and 3D models were developed and analysed for joints with load parallel to the grain (straight configuration). However for joints with load not parallel to the grain (30°, 60° and 90° configurations), only 3D models were used, as the irregular joint geometry did not enable to have a 2D approach.

Symmetry was used on each model of all the joints:

- Three orthogonal planes of symmetry for 3D models of straight joints,
- Two orthogonal planes of symmetry for 2D models of straight joints, as well as 3D models of 90° configuration, and
- One orthogonal planes of symmetry for 3D models of 30° and 60° configurations.

The full geometrical details, boundary conditions, loading and restraints for each FE model presented in this chapter are given in Appendix D.

6.3.2.2. Elements and mesh types

There are two main types of analysis available in this FE software, which depend of the type of finite element used. These are known as h-element and p-element. The standard finite element is the h-element, as it was developed from the early years of finite element analysis. The p-element is a more recent improvement. They have both advantages and disadvantages. Using h-elements, the user must vary the meshing parameters in order to obtain the desired accuracy. With p-elements, a constant mesh only is required (usually a coarser mesh than for h-elements) to achieve a user-specified accuracy. In other words the p-element uses a variable polynomial level to obtain the results (such as displacements, stresses and strains) as specified. The p-elements seem to be user-friendly because they are easy to use, with no mesh refinement. However they require significantly greater computational resources. And this is one of the main reasons that all the models were analysed using h-elements.

A large h-element library is available to the user. As far as structural elements are concerned, many of them were used in the various preliminary models that were developed in the early days of this research. Different types of elements could be intermixed in one model as long as specific compatibility, particularly among degrees of freedom were maintained. Another choice to make was that elements could be either linear or quadratic. Linear elements have no midside nodes, only

corner nodes. For example, a linear triangular 2D element would have 3 corner nodes and the equivalent quadratic element would have 3 corner nodes and 3 midside nodes. Linear elements usually give an accurate solution in a reasonable amount of computer time, and quadratic elements give a more precise solution in a longer computer time, for a similar model. However both types have their own characteristics, which can improve or worsen the analysis depending on what is needed. Some examples of models where various element types for structural static analysis were used are presented as follow:

- Planar elements, having either a triangular or quadrilateral geometry, are used for 2D modelling. Planar elements with 4 nodes usually yield more accurate results than with 3 nodes in static analysis. Therefore they were used for all 2D models that were developed for straight configuration models.
- Solid elements, having either tetrahedral or hexahedron geometry, are used for 3D solid modelling. Solid hexahedron elements have 8 nodes if linear and 20 nodes if quadratic. Solid tetrahedral elements have 4 nodes if linear and 10 nodes if quadratic. These elements were always used to model the wood material of all 3D models. Solid elements were also used at a final stage to model the glass fibre/epoxy composite.
- Shell elements, having either a triangular or quadrilateral geometry, to be used in 2D or 3D modelling. Shell elements are defined as a plate (4 nodes if quadrilateral, etc) with a thickness. These elements were used to model the glass fibre/epoxy composite in 3D models. However there was some incompatibility at the interface with the solid elements used for the wood. This incompatibility was mainly due to a different number of degrees of freedom between the jointed elements. Another reason is that one particular solid element was used throughout the FE models as it showed the best results in a reasonable amount of computer time. This element type could not be connected to any different element type without causing erroneous results: The model had insufficient rigid body constraints. Finally, the glass fibre/epoxy composite was modelled with the same solid elements and shell elements were not used.
- Composite elements were available in the library. They are highly specialised elements called layered elements. They are specially designed to model a laminate. In other words composite elements could be used when each layer of a

laminate have different orientations, with different orthotropic properties. Because the glass fibre/epoxy composites used in this research are made of either one or two perpendicular layers of fibres, there was no need of using those elements.

All the models presented in this chapter were finally developed in 3D, with either linear or quadratic solid elements, depending on the complexity of the model, and enabling anisotropic material properties.

The mesh density is another important point to consider in order to obtain reasonably good results. This is one of the most fundamental questions that arise in finite element analysis. In theory, the finer is the mesh, the more accurate the results are. If the mesh is too coarse, the results can contain serious errors and if the mesh is too fine, it will waste computer time, and the model could be too large to run on a normal computer. As a result, the mesh density becomes a key issue during the model generation.

Various meshing techniques were used through the modelling process, mainly because the software offers different ways of mesh generation. But firstly, it is important to understand that the mesh geometry and density must always satisfy some rules in order to be acceptable as far as the analysis is concerned. Each element type has some geometric restrictions, which are known as the aspect ratio. The aspect ratio is characterised by the element shape: The height to width ratio, the angle between two adjacent ridges, etc. An element having an aspect ratio that falls outside the limits set for its type would be too distorted and therefore would produce erroneous results. For the FE models that were developed in this research, structural stress analysis was used to determine the stress (or strain) at particular locations. For that particular use of FE analysis, poorly shaped elements would generally produce more severe errors than for any other type of analysis (deflection, modal, thermal analysis, etc). In other words, special attention was given to mesh density in order to avoid element shape errors. For each model developed, they were preliminarily developed using very coarse mesh, gradually refined until the results obtained were accurate enough without showing any errors or warning in the mesh density.

The preliminary models developed for the joints with load parallel to the grain summarises the different meshing techniques used throughout the research. They are presented in the following section.

6.3.3. Joints with load parallel to the grain

The models developed for the joints with load parallel to the grain were initially developed in 2D. The three planes of symmetry of the straight configuration joints enabled 2D modelling, as shown on the figure 6.26.

The first problem encountered was the mesh density. The joint was made of the timber member, materialised as a large rectangular area (in 2D) and the glass fibre/epoxy composite layer, materialised as a very thin rectangle. The difference of the two materials thicknesses was such that the size of the elements could not be the same. The figure 6.28 shows an example of mesh with rectangular elements.

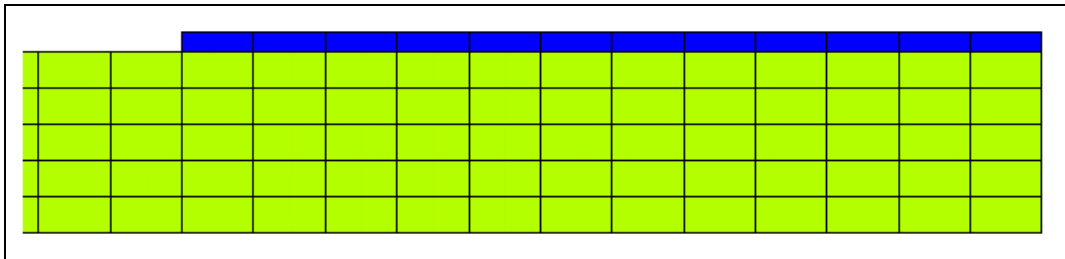


Figure 6.28 Example of 2D straight joint model with rectangular mesh.

With this model, there are just a few elements to materialise the glass fibre/epoxy composite. But the load is applied through the composite layer: It is therefore a high stress region of the model. The interface between the composite and the timber is also critical because the load is transferred from the glass fibre/epoxy to the timber. The strain gauges were only positioned on the surface of the composite. It was therefore necessary to refine the mesh in the composite and at the interface with the timber, as shown in figure 6.29.

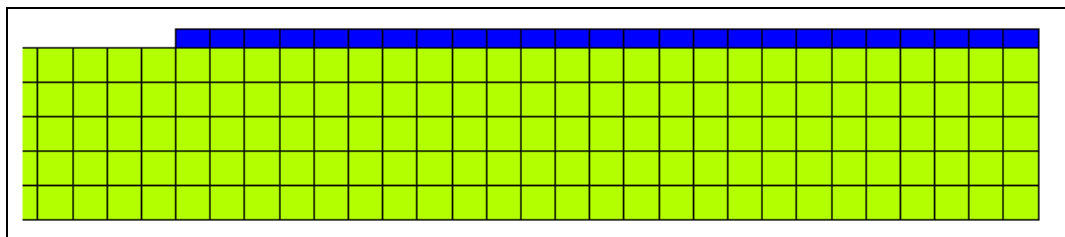


Figure 6.29 Another example of 2D straight joint model with rectangular mesh.

But this mesh refinement was not sufficient to generate acceptable results. The concept of generating a dense mesh in the composite layer and at the interface with the timber was becoming more obvious. The model could be made of a very dense square mesh and the number of elements could potentially be very large. However there was no need to generate a dense mesh beyond the composite and interface zone. It was therefore necessary to develop a mesh that could be gradually refined, from the timber member neutral axis to the composite material layer. An example of that mesh is presented in figure 6.30.

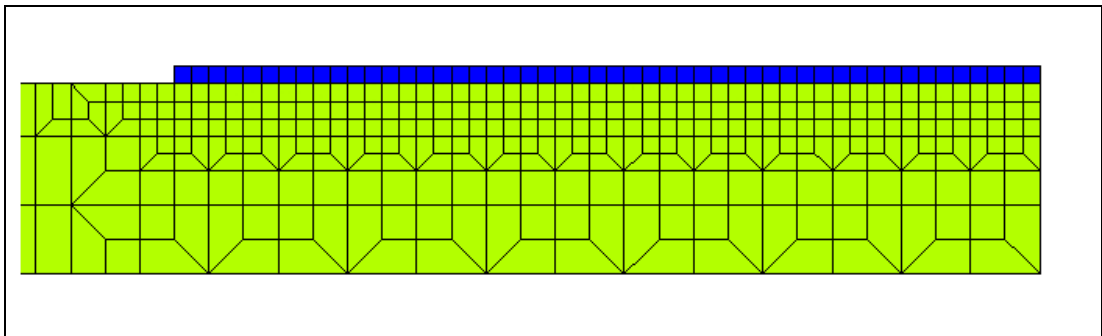


Figure 6.30 Example of 2D straight joint model with a coarse-to-fine mesh.

The mesh was even more refined by introducing two layers of elements in the composite, as shown in figure 6.31.

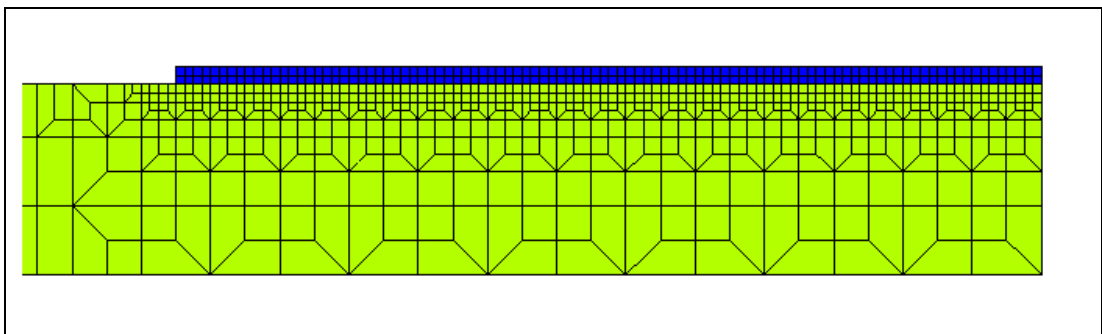


Figure 6.31 Another example of 2D straight joint model with a coarse-to-fine mesh.

But the mesh was still too coarse to produce acceptable results, even with quadratic planar elements. The composite layer was such a high stress regions that the number of elements should be radically increased. For the mesh presented in figures 6.30 and 6.31, the Cartesian coordinates of each nodes and elements was generated manually. It was then almost impossible to refine the mesh at specific locations.

SmartMeshing is another tool available in the FE software that was used as a possible alternative. This tool creates initial element sizes for free or mapped meshing operations. By specifying the mesh size level, SmartMeshing can mesh any volume or area. The advanced options enable one to refine or enlarge the mesh in a particular location. However this tool does not control the element shape and therefore requires further refinement to obtain an accurate mesh. The example presented in figure 6.32 was generated using SmartMeshing.

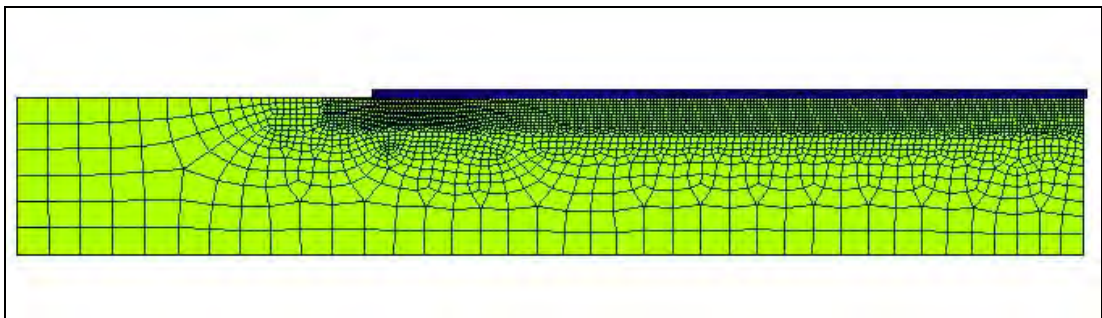


Figure 6.32 Example of 2D straight joint model with free quadrilateral mesh generated using SmartMeshing.

This model contains 3820 elements. It is a fairly large model made of linear planar quadrilateral elements. The results obtained were relatively accurate compared to those from the previous models. However, because the accuracy of the results could not be confirmed from calculated results, the adequacy of the mesh could only be confirmed by conducting a convergence tests. The convergence test consists of beginning the analysis with what seems to be an acceptable mesh, then recording the solution. Subsequently repeat the analysis with a finer mesh and compare the solution with the previous one. If the results are nearly similar, then the first mesh is probably good enough for that particular geometry, loading and constraints. If the results differ by a large amount, it is necessary to try a finer mesh. Ultimately, by repeating this operation, the results converge to the exact solution. For this exercise, the longitudinal axial strains results recorded at two nodes A and B, located in the

higher stress region of the model were used (see figure 6.37). The FE model was then refined 11 times, from 3830 to 18499 elements. For each refinement, the longitudinal strains on nodes A and B were recorded. The results are presented in two graphs shown in figures 6.33 and 6.34 for node A and node B respectively.

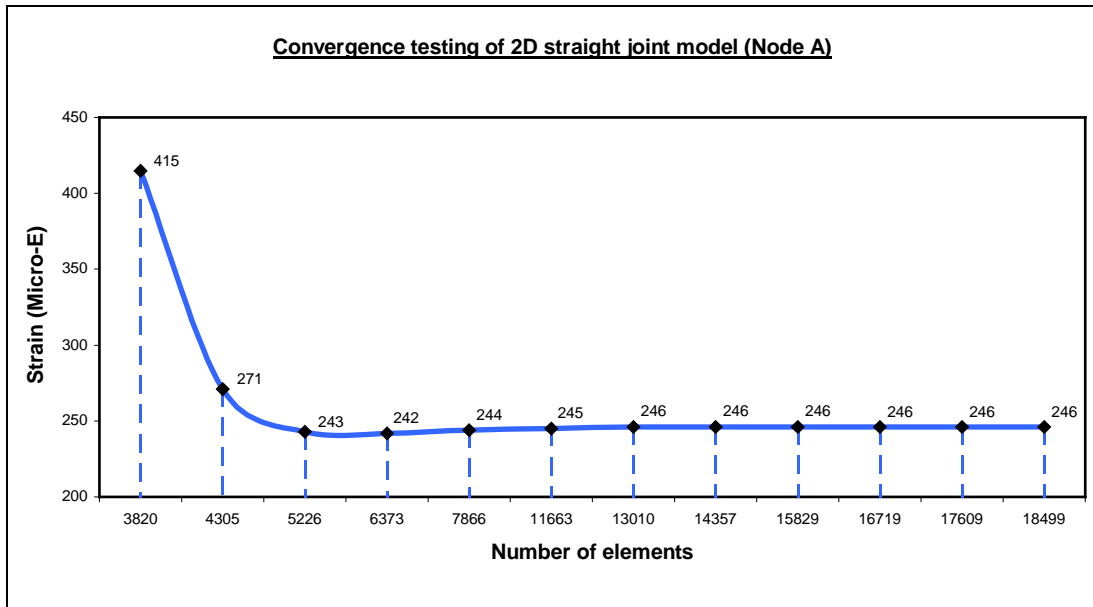


Figure 6.33 Convergence graph of longitudinal strain recorded on node A.

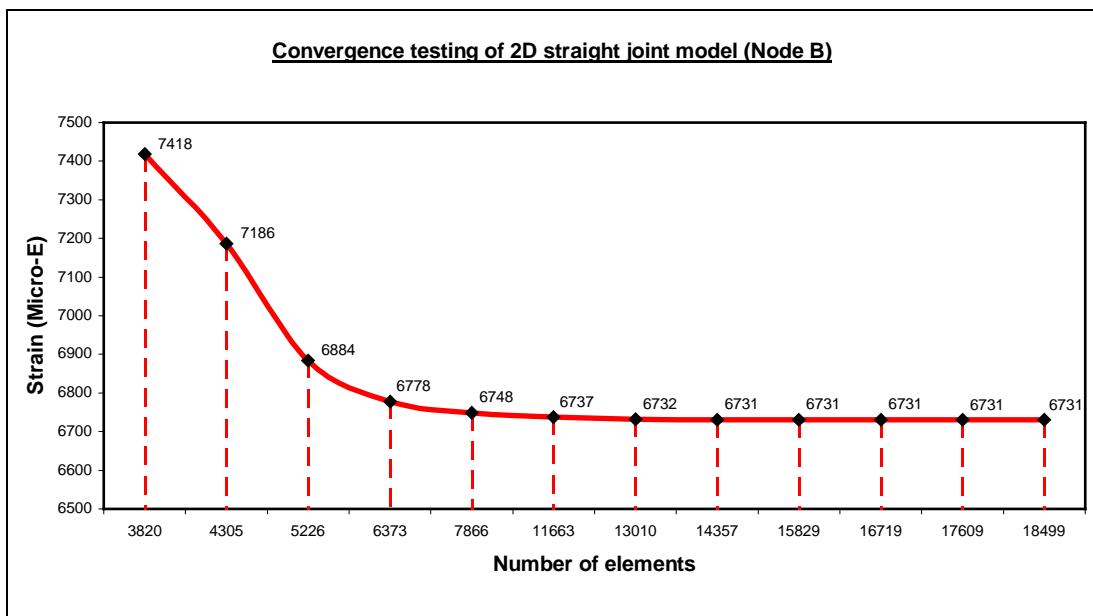


Figure 6.34 Convergence graph of longitudinal strain recorded on node B.

The two graphs show that the values of longitudinal strains on node A and B converge when the model is refined to 13010 elements. The mesh refinement exercise was extended up to an 18499 elements model in order to check whether the results have truly converged. The 18499 elements model has a very dense mesh around the nodes A and B. The geometry of the model is shown in figures 6.35, 6.36 and 6.37. The glass fibre/epoxy composite, which is of 0.65 mm thickness, is divided in 64 rows of elements at the right edge (see figure 6.37).

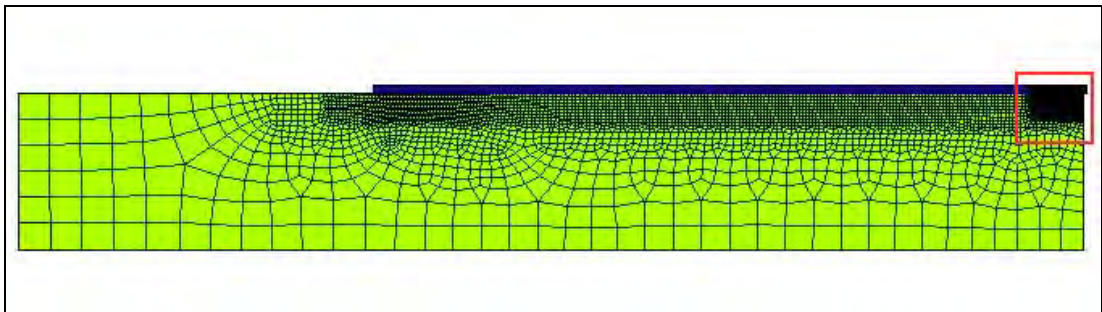
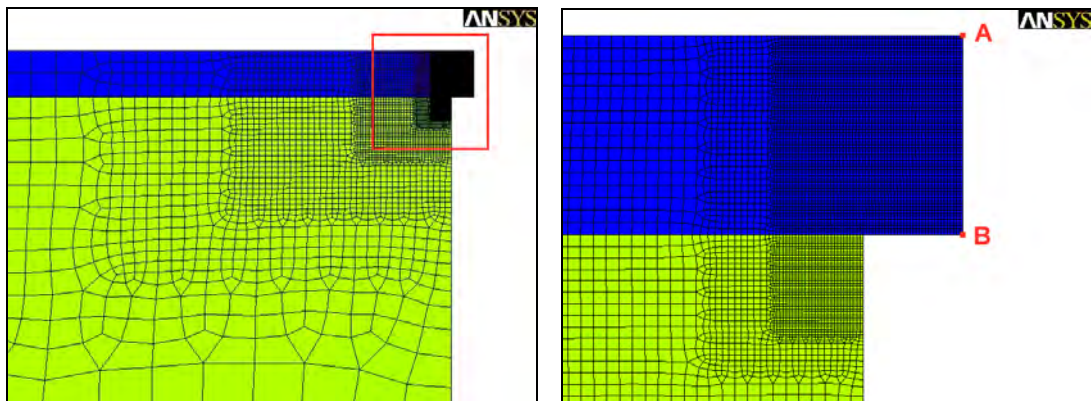


Figure 6.35 Refined of 2D straight joint model with free quadrilateral mesh (18499 elements).



Figures 6.36 and 6.37 Zooms of the 2D straight joint model (18499 elements) showing locations of nodes A and B.

But this model has large memory requirements and the calculation time is too extensive. The best option is to use a model that requires the minimum number of elements and gives a converged solution. This model converges with about 13000 elements.

As far as 2D modelling of straight joints is concerned, two models were developed with a mesh of 12393 elements. With linear planar elements, these models are presented in the following section.

3D models were also developed, in order to take into account any edge effects that cannot be detected in 2D because they occur across the joint width. However the meshing of 3D models was not developed in the same way as previously explained. The methods used are described for each FE model.

Both 2D and 3D models of joints with load parallel to the grain are presented in the following sections.

6.3.3.1. Configuration with uniaxial fibres TPU00

The two models presented in this section were generated in 2D and 3D respectively. For this configuration, glass fibres are unidirectional: The material properties of the composite reflect these characteristics. The thickness of the composite corresponds to the measured thickness of 0.65 mm.

6.3.3.1.1. 2-Dimensional model

The characteristics of the 2D model are as follow:

File name:	Am12-Plane42
Materials number:	2 - Anisotropic
Element type:	PLANE42 - 2D Structural solid
Element description:	4 nodes planar element
Analysis type:	Static - Linear
Loading:	18 kN in tension
Number of Elements:	12393
Number of Nodes:	12685

The linear element type PLANE42 is defined by a quadrilateral shape with four nodes having two degrees of freedom at each node: translations in the nodal x and y directions. The element input data includes four nodes, a thickness for the plane stress option used in this case, and orthotropic material properties.

Full details for the FE model (geometry, material properties, boundary assumptions, etc) are available in Appendix D.1.

The graphical results are presented in figure 6.38.

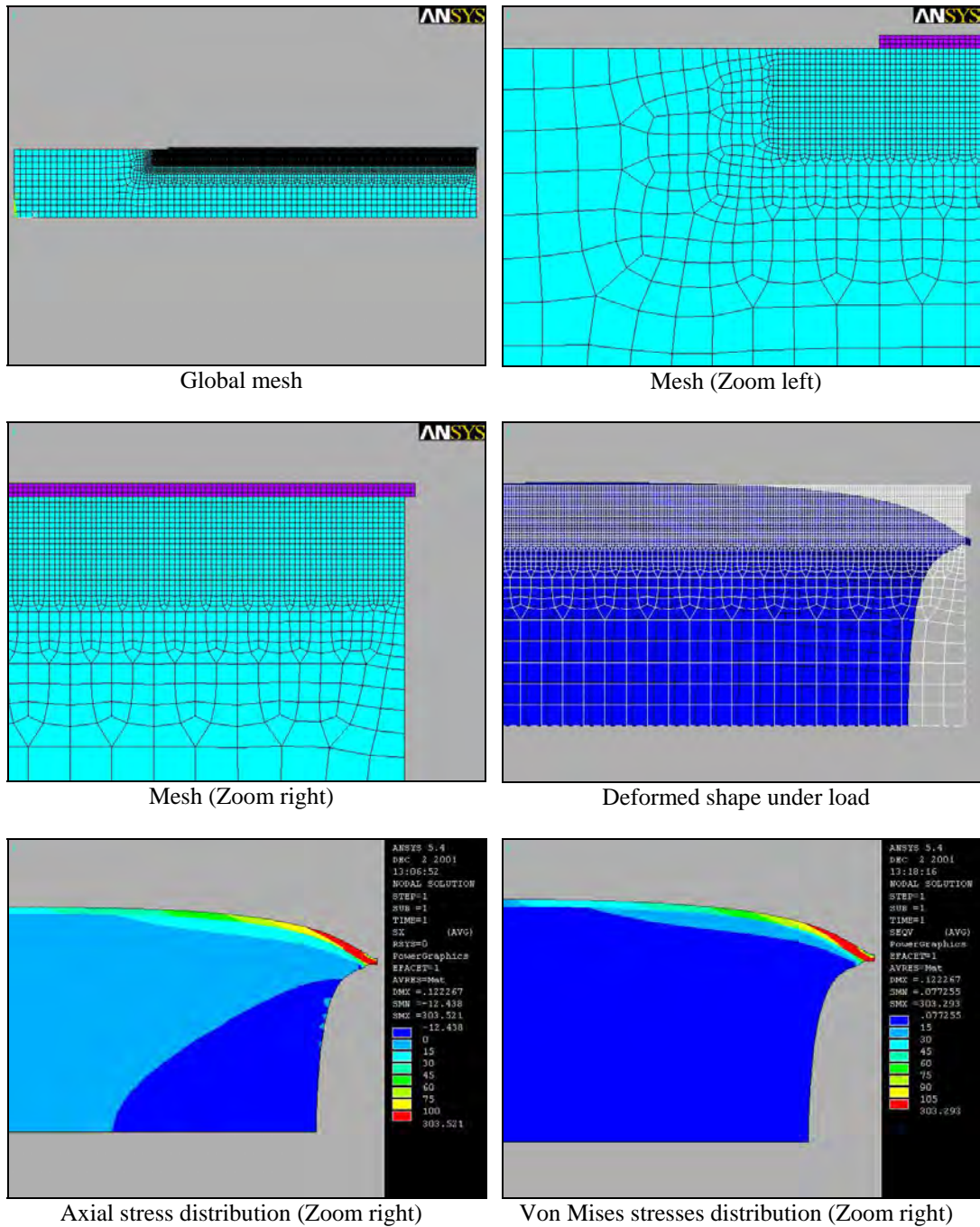


Figure 6.38 Graphical results of the 2D model type TPU00.

On the model shown in figure 6.38, the meshing of the glass fibre/epoxy composite layer is relatively dense, with three rows of elements. The mesh becomes progressively coarser as it reaches the neutral axis of the timber area.

The deformed shape indicates that the composite layer is bending downwards at the right end. This is due to the internal bending effects of the overlap, as previously

discussed in the § 6.2.3. This effect is due to the through the thickness stress variations. But the phenomenon is significantly different than the one observed on the symmetrical double lap joint shown in figure 6.13. In fact the bending effect is much more pronounced at the right end of the composite than at the left end. The deformed shape of the composite at the left end is shown in figure 6.39.

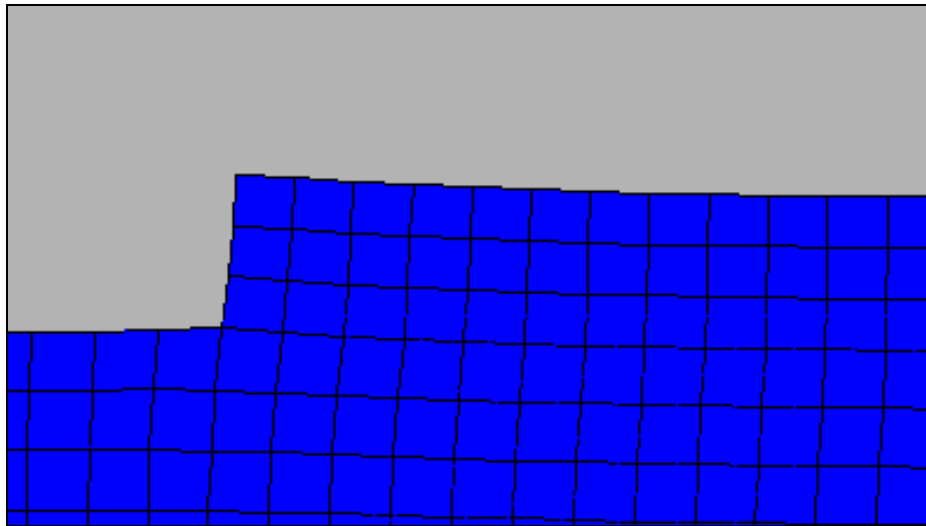


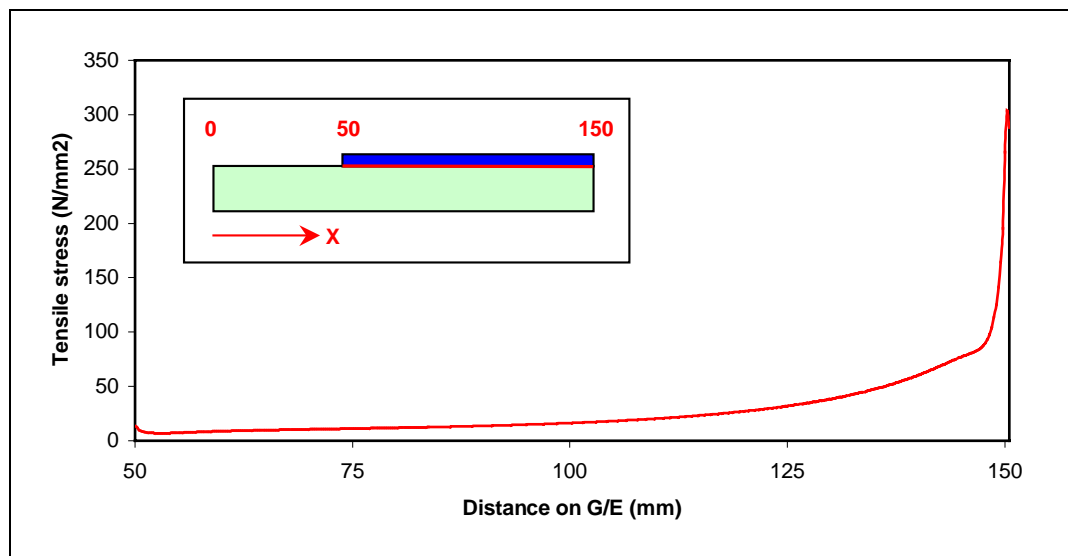
Figure 6.39 Deformed shape at composite left end of the 2D model type TPU00.

It appears clearly that the left end of the composite layer is bending upwards, but in a less significant mode than the right end. Those effects are mainly due to the tensile stresses acting across the interface of the two materials for the left end of the overlap, and to the compressive stresses for the right end of the overlap. The effect is more significant at the right end for the two following reasons:

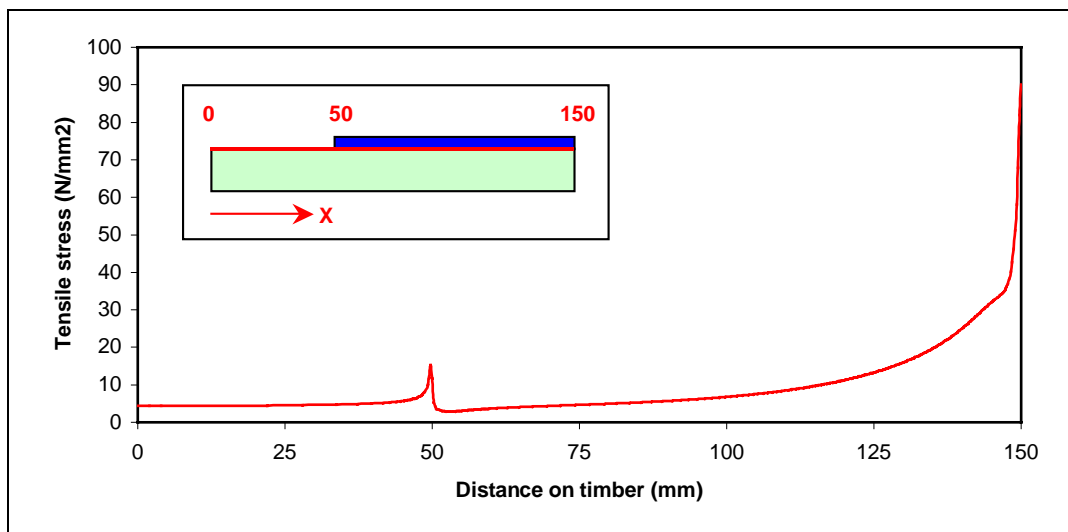
- There are much higher stresses transferred between the two materials around this particular location.
- The differences in stiffness between the timber and the glass fibre/epoxy composite are important. The timber is subject to higher deformation under stresses than the composite. Under tension load, the right edge of the timber is sagging substantially and therefore this phenomenon induces the bending of the composite layer that has higher stiffness but a very small inertia, because of its thin thickness.

Experimental measurement of the internal bending effects of the overlap was carried out on one of the sample to confirm whether the results given by the FE models were acceptable. This experiment and results are presented and discussed in § 6.4.

The axial and shear stress distributions are obviously affected by this fact. The following graphs presented in figures 6.40 and 6.41 indicate the tensile and shear stress distribution calculated by the FE model at the interface between the composite and the timber.



Tensile stress distribution on glass fibre/epoxy interface



Tensile stress distribution on timber interface

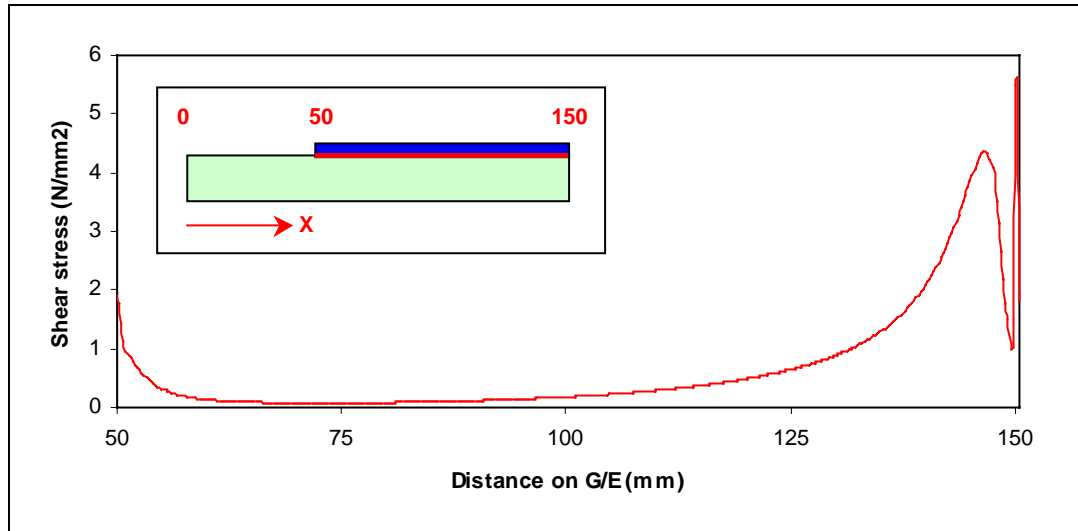
Figure 6.40 Tensile stress distributions at the interface between the composite and the timber.

These graphs show the tensile stress distribution at the interface between the two materials. The first one denotes the tensile stresses in the composite (calculated on nodes between 50 mm and 150 mm in the x direction) and the second one denotes the tensile stresses in the timber (calculated on nodes between 0 and 150 mm in the x direction). Those graphs clearly show that the distribution of tensile stress has the same shape whether it is at the timber or at the composite interface. The amplitude of tensile stress at the right end, which is expressed in ratio of tensile stress at a particular node to the average tensile stress applied to the material considered, is much higher in the timber (around 20) than in the composite (around 2). It corresponds to a local tensile stress in the composite of 305 MPa and 90 MPa for the timber. With a tensile strength of around 500 MPa for the composite, the material can sustain such a stress, but with an average tensile strength of 82.6 MPa for the timber, the stress observed has reached its limit and the timber should have failed in this zone. However, those results must be carefully considered because of two reasons:

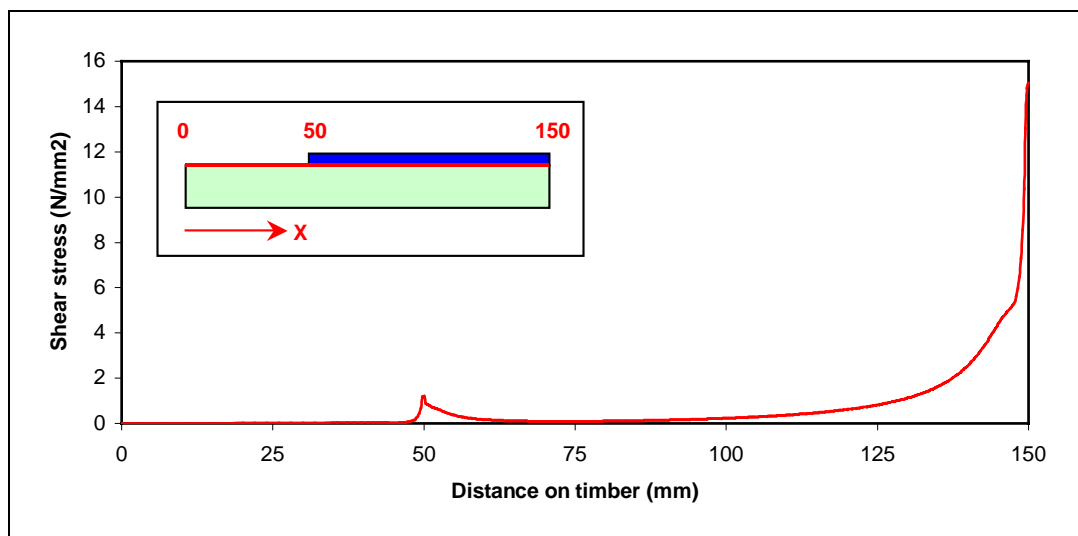
- The stresses peak in a very steep slope at the right end: The stresses may not be very accurate because the right end is a high stress region, and the finite elements may not be sufficiently refined around the right corner between the timber and the composite.
- For a tension load of 18 kN, it is unlikely that the timber would start to fail at the right corner with the composite. Nevertheless, the timber could have reached plasticity in that zone. In that case, the results could be considered as relatively accurate.

The certainty is that the timber tensile stress at the right corner of the model is very high compared to its strength, therefore any mechanism of failure (i.e. delamination of the composite) is likely to start around this location.

The shear stress distributions must also be considered. The following graphs presented in figure 6.41 show the shear stress distribution calculated by the FE model at the interface between the composite and the timber.



Shear stress distribution on glass fibre/epoxy interface



Shear stress distribution on timber interface

Figure 6.41 Shear stress distributions at the interface between the composite and the timber.

The shear stress distributions appear to have the same shape and intensity between the end of the overlap ($x = 50$ mm) up to the last 15 mm before the gap zone ($x = 135$ mm), at the interface for both the composite and the timber. Towards the gap zone, the shear stress in the composite reaches a peak at around 4 MPa, then decreases steeply to 1 MPa, and peaks again to 5.5 MPa then finally reduces to nearly 2 MPa. Those high variations of shear stresses around the right end of the

overlap are the result of the internal bending of composite in that zone. For the timber, the shear stress peaks to 15 MPa at the right end. Once again, the shear stress observed has reached the timber shear strength of approximately 13 MPa and the timber should have failed in this zone. Shear plasticity or failure could be on the verge of occurring.

The reliability of the FE model can be validated by comparing it with the samples tested in experiment. Longitudinal strains were recorded from strain gauges on the composite surface, at specific locations, as explained in chapter 4. Figure 6.42 shows a graph of longitudinal strain distribution along the composite surface, derived from the FE model.

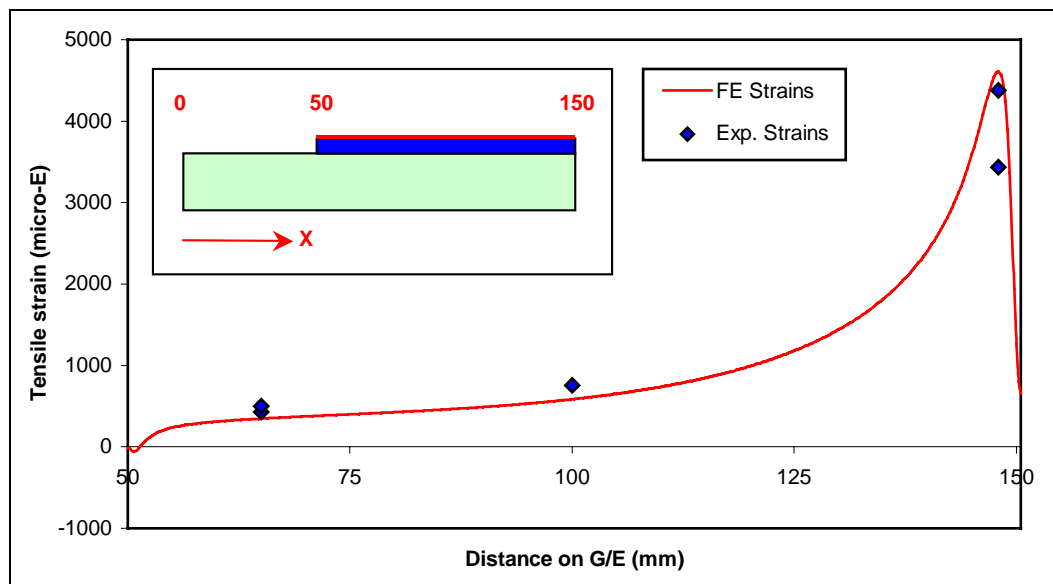


Figure 6.42 Longitudinal tensile strain distribution on glass fibre/epoxy surface.

The tensile strain distribution on the composite is progressive from the left end of the overlap to the gap area, following a parabolic shape. However the strains abruptly fall down towards the end. This is again an effect of the internal bending of the composite. Experimental strain results are also plotted in figure 6.42 and match relatively well the FE distribution.

The tensile strain results derived by the FE model and measured experimentally are also presented in table 6.3.

Sample	End strain gauge	Middle strain gauge	Gap strain gauge
	x = 65 mm	x = 100 mm	x = 150 mm
7TPU00 - Z	503	758	4376
8TPU00 - J	428	N/A	3433
Plane42 FE model	347	585	4607

Table 6.3 Comparison of strains results obtained from experiments and from the FE model.

Strain gauge positions are described in § 4.3.2.2. The results of tensile strains obtained from the FE model are relatively close to those obtained from experiments. However, the FE results tend to be lower for end and middle strains and higher for the gap strain. These results have to be compared with those obtained from the 3-dimensional FE model that is presented in the next section.

6.3.3.1.2. 3-Dimensional model

The characteristics of the 3D model are as follow:

File name:	Am01-solid72
Materials number:	2 - Anisotropic
Element type:	SOLID72 - 3D Structural solid
Element description:	4 nodes tetrahedral solid element with rotations
Analysis type:	Static - Linear
Loading:	18 kN in tension
Number of Elements:	58886
Number of Nodes:	11788

The linear element type SOLID72 is defined by a tetrahedral solid shape with four nodes having six degrees of freedom at each node: translations in the nodal x, y and z directions and rotations about the nodal x, y and z directions. The element input data includes four nodes and orthotropic material properties. The element is well suited to model irregular meshes because of its tetrahedral geometry. It can often be replaced by the SOLID92 element, which is a quadratic tetrahedral solid element, with 10 nodes. Although SOLID72 has additional degrees of freedom per node, it is not as accurate as the SOLID92 element. This model was initially developed using the SOLID92 (quadratic) element. In order to enable the analysis of the model in an acceptable computer time, the mesh was initially reduced. However the composite layer was not refined enough to give accurate results, and using mesh refinements in

that zone of the model was only generating poorly shaped elements. As a result, the linear element SOLID72 was used in order to keep a refined and correct mesh, while reducing the solution time of the model.

Full details for the FE model are available in Appendix D.2.

The graphical results are presented in figure 6.43.

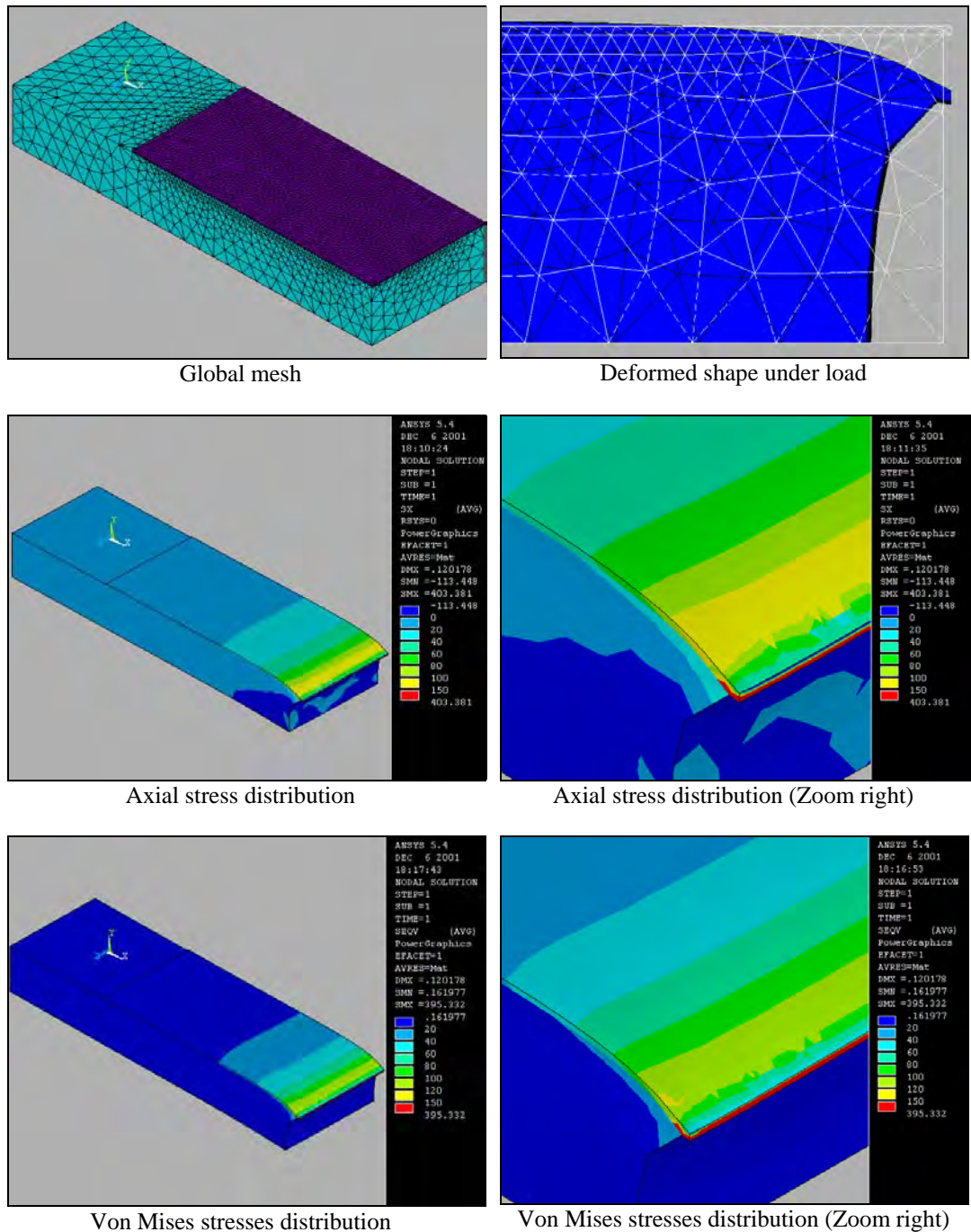
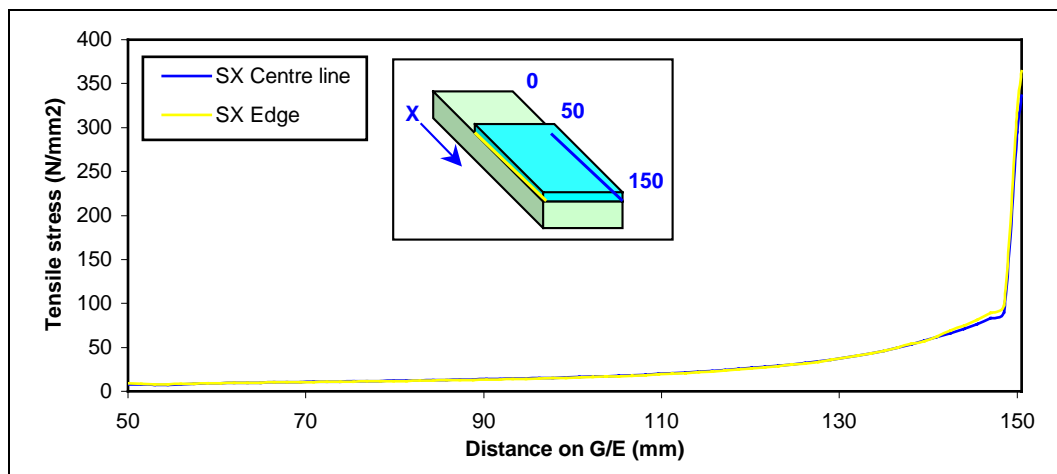


Figure 6.43 Graphical results of the 3D model type TPU00.

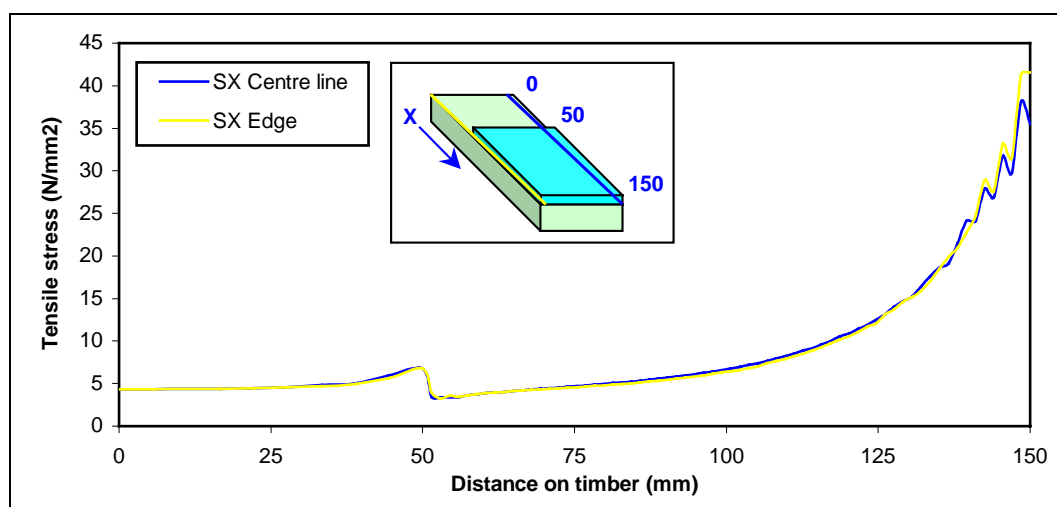
On the model shown in figure 6.43, the meshing of the glass fibre/epoxy composite layer is relatively dense, becoming progressively coarser as it reaches the neutral axis of the timber area.

On this model again, the deformed shape indicates that the composite layer is bending downwards at the right end. This reflects the internal bending effects of the overlap, as discussed before.

The graphical results of axial stress and Von Mises stress distributions do not clearly show any stress variations in the transverse direction (z direction) or any edge effects. However the FE results of axial and shear stress distributions at the interface between the composite and the timber that are presented in the following graphs (figures 6.44 and 6.45), are given along the centre line and the edge of the joint.



Tensile stress distribution on glass fibre/epoxy interface



Tensile stress distribution on timber interface

Figure 6.44 Tensile stress distributions at the interface between the composite and the timber.

These two graphs show the tensile stress distribution at the interface between the two materials, calculated from the composite and from the timber respectively.

The distribution of tensile stress has a relatively similar shape whether it is at the timber or at the composite interface. The tensile stress in the composite abruptly increases towards the right end (gap area) rising from around 100 MPa to more than 350 MPa. This increment of stress is steadier in the timber, showing a parabolic shape that rises to around 45 MPa. This value of tensile stress in the timber appears to be fairly low compared to the one of 90 MPa obtained from the 2D model. It is important here to detect which result is likely to be accurate.

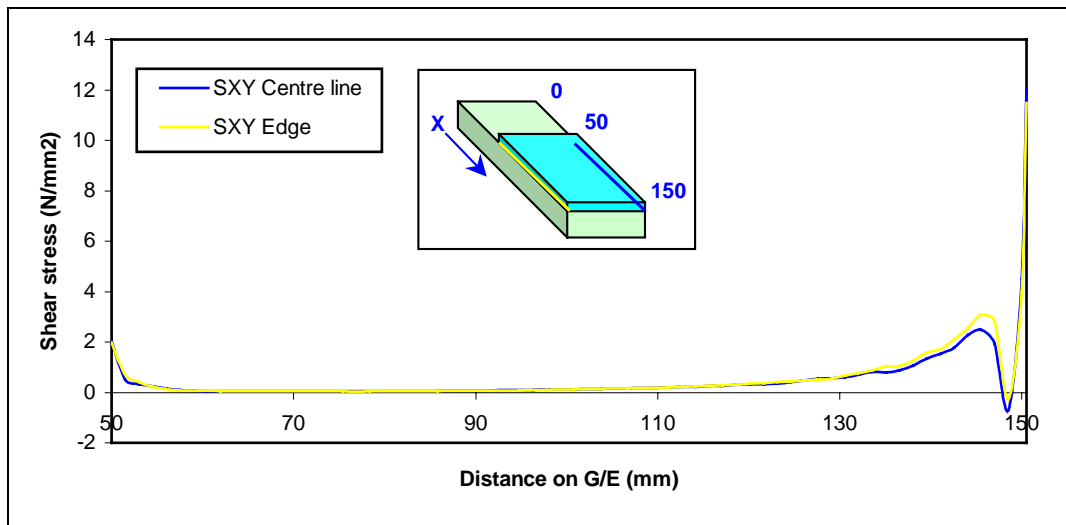
At the right end, the tensile stress in the composite is around 350 MPa, which is relatively similar to the one of 300 MPa obtained from the 2D model. Using the Hooke's Law, the longitudinal modulus of elasticity of 28 GPa for the composite and of 11.6 GPa for the timber, the tensile stresses at the same node between the two materials and for the same strain, are likely to be approximately proportional to the ratio of both moduli:

$$R = 28/11.6 \approx 2.5$$

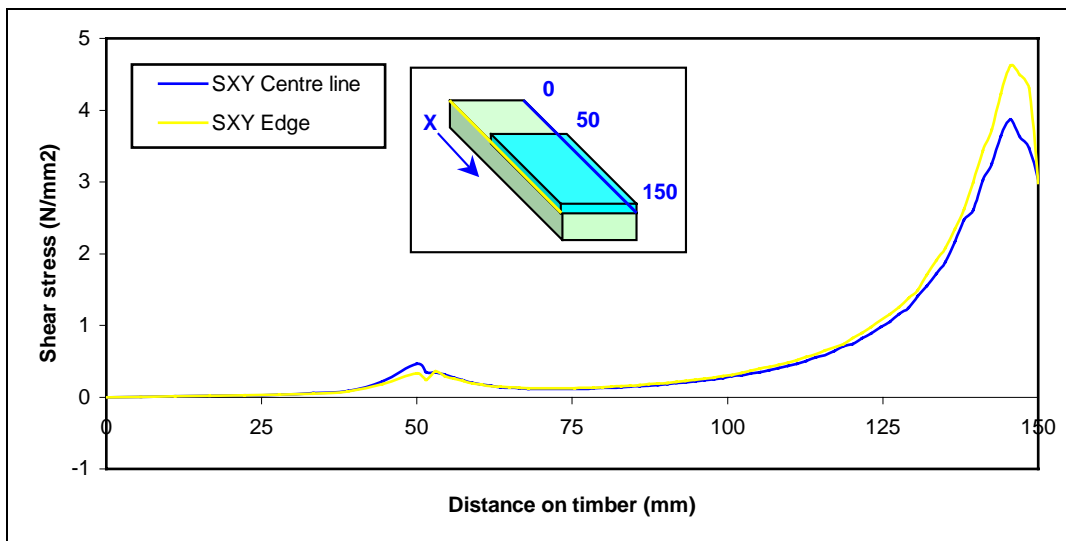
With a tensile stress in the composite of around 300 MPa, the tensile stress in the timber should range around $300 \div 2.5 = 120$ MPa. But this not strictly true as other direction stresses are ignored as well as shear stresses. The 2D model shows more accurate results because the ratio is maintained, and the mesh is much more refined than on the 3D model in that right end zone. As a result, the peak tensile stress in the timber of 45 MPa is probably inaccurate due to the coarse mesh in that region. The chaotic (wobbly) end of the curve confirms this inaccuracy. On the other hand, the denser mesh of the composite shows some relatively accurate results.

The differences between the tensile stresses recorded along the centre line and the (free) edge of the model are relatively small. However the stresses at the edge seem to be slightly higher in the high stress region (right end) than the stresses at the centre line, reflecting an insignificant edge effect.

The shear stress distributions calculated by the FE model at the interface between the composite and the timber are presented in figure 6.45.



Shear stress distribution on glass fibre/epoxy interface



Shear stress distribution on timber interface

Figure 6.45 Shear stress distributions at the interface between the composite and the timber.

The shear stress distributions appear to be similar in terms of shape and intensity except around both ends of the overlap (around $x = 50$ mm for the left end and $x = 140$ mm for the right end). Towards the right end (gap zone), the shear stress in the composite reaches a peak at around 3.5 MPa, then decreases steeply to around -0.7 MPa and peaks again to 12 MPa. Those high variations of shear stresses around the right end of the overlap are the result of the internal bending of composite in that

zone. For timber, the shear stress peaks to 4.5 MPa at the right end. There are some significant differences of shear stresses in this model with those of the 2D model:

- Much higher shear stress in the composite at the right end: 12 MPa to compare with 5.5 MPa for the 2D model,
- Much lower shear stress in the timber at the right end: 4.5 MPa to compare with 15 MPa for the 2D model.

Those differences are probably due to the coarser mesh in the timber, inducing lower deformations of the finite elements. The phenomenon produces lower values in terms of tensile and shear stresses in the timber. The load transfer between the composite and the timber is therefore affected, resulting in higher stresses in the composite in the right end.

In this situation, the shear stress observed did not reached the timber shear strength of approximately 13 MPa.

The figure 6.46 shows a graph of longitudinal strain distribution along the composite surface, derived from the FE model.

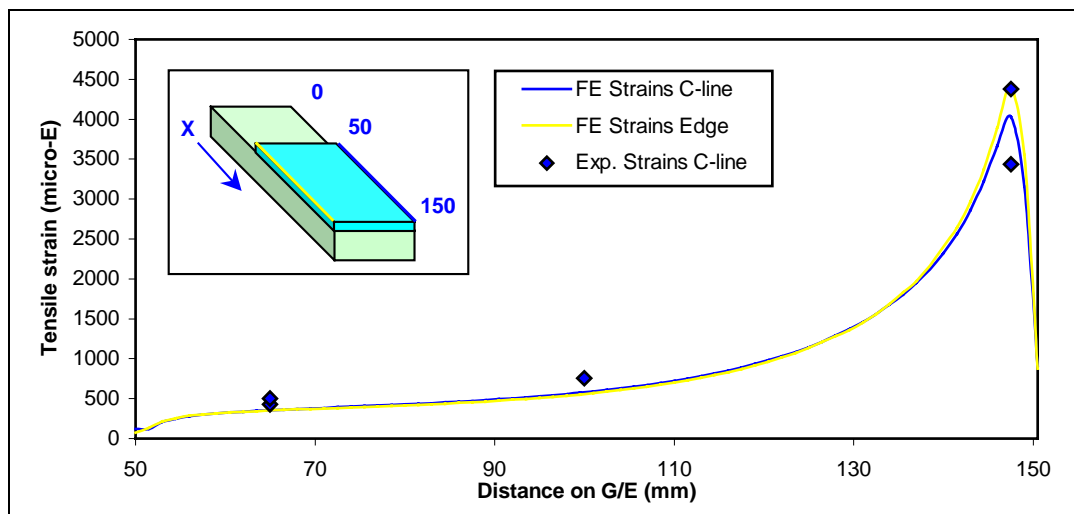


Figure 6.46 Longitudinal tensile strain distribution on glass fibre/epoxy surface.

The tensile strain distribution on the composite is progressive from the left end of the overlap to the gap area, following a parabolic shape. However the strains steeply decrease towards the right end. This is an effect of the internal bending of the composite. The FE strains at the edge seem to be slightly higher in the high stress region (right end) than the FE strains at the centre line. This difference is due to the

edge effect. Internal bending effects are discussed in greater details in § 6.4. Experimental strain results are also plotted in figure 6.46 and match relatively well the FE distribution.

The tensile strain results derived by the FE model and measured experimentally are also presented in table 6.4.

Sample	End strain gauge	Middle strain gauge	Gap strain gauge
	x = 65 mm	x = 100 mm	x = 150 mm
7TPU00 - Z	503	758	4376
8TPU00 - J	428	N/A	3433
Solid72 FE model	354	578	4031

Table 6.4 Comparison of strains results obtained from experiments and from the FE model.

Strain gauge positions are described in § 4.3.2.2. The results of tensile strains obtained from the FE model tend to be lower for end and middle strains. However, the strain result obtained for the gap is relatively close to those obtained from experiments.

Finally the comparison between the 2D and 3D models shows that the results obtained are relatively similar except in the high stress region, i.e. the gap zone. Advantages and disadvantages of both models can be considered:

- The strains and stresses are of comparable magnitude except in the high stress region where there are large differences: The 3D model shows inaccurate results due to its relatively coarse mesh, compared to those obtained with the finer mesh of the 2D model.
- The 2D model does not show whether the strain and stresses vary across the width of the joint. In fact the 3D model reveals that there is a relatively small edge effect in the high stress region, as strains and stresses are slightly higher along the edge than along the centre line of the joint.

6.3.3.2. Configuration with biaxial fibres TPB00

The two models presented in this section were generated in 2D and 3D respectively. The glass fibres are bidirectional, therefore the material properties of the composite reflect these characteristics (identical material properties in the x and z directions). The thickness of the composite corresponds to the measured thickness of 0.65 mm, which is the same than the one measured for uniaxial fibres samples TPU00.

6.3.3.2.1. 2-Dimensional model

The characteristics of the 2D model are as follow:

File name:	Am14-plane42
Materials number:	2 - Anisotropic
Element type:	PLANE42 - 2D Structural solid
Element description:	4 nodes plane element
Analysis type:	Static - Linear
Loading:	18 kN in tension
Number of Elements:	12393
Number of Nodes:	12685

The PLANE42 linear element characteristics are already defined in § 6.3.3.1.1.

Full details for the FE model (geometry, material properties, boundary assumptions, etc) are available in Appendix D.1.

The graphical results are presented in figure 6.47.

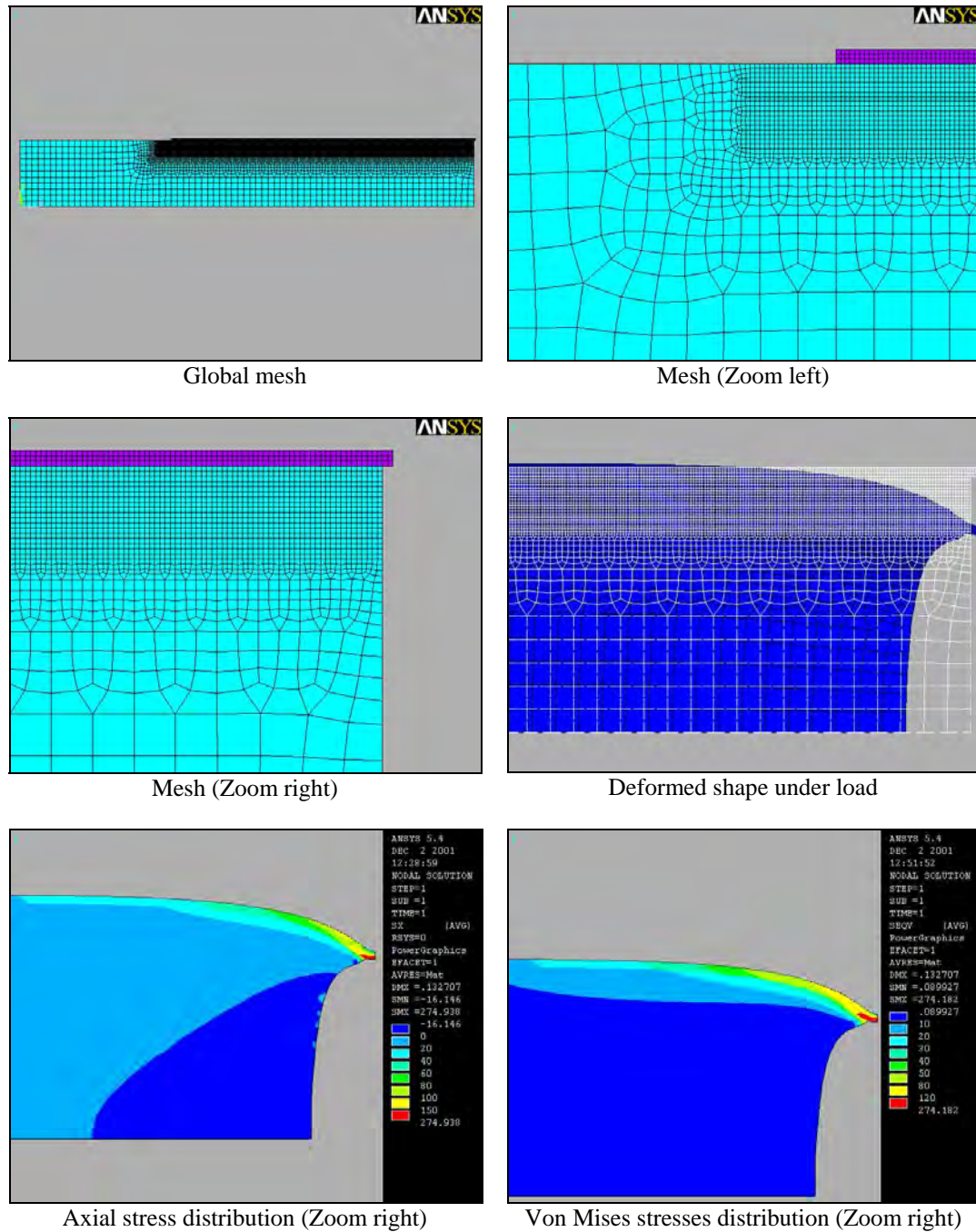
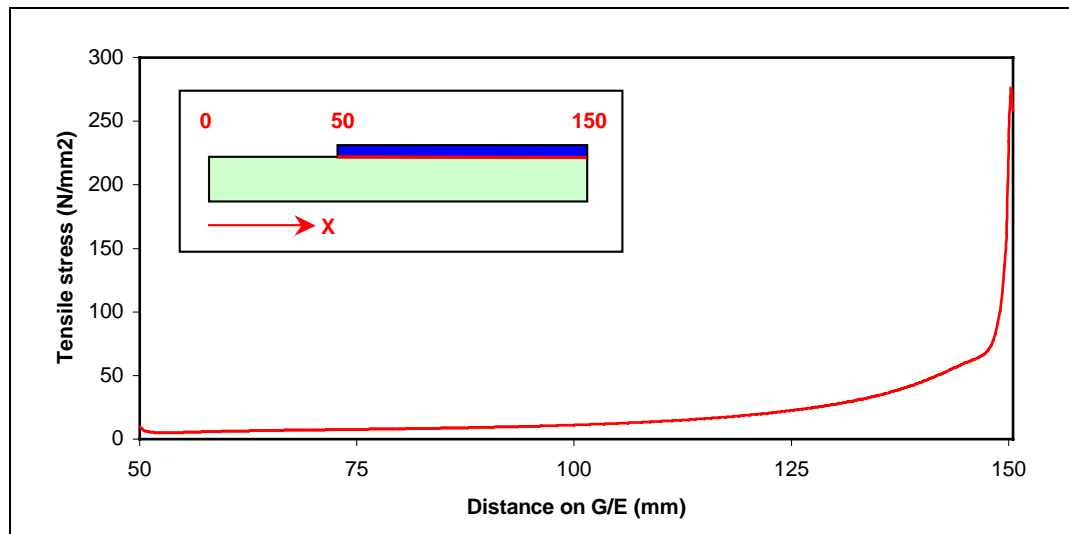


Figure 6.47 Graphical results of the 2D model type TPB00.

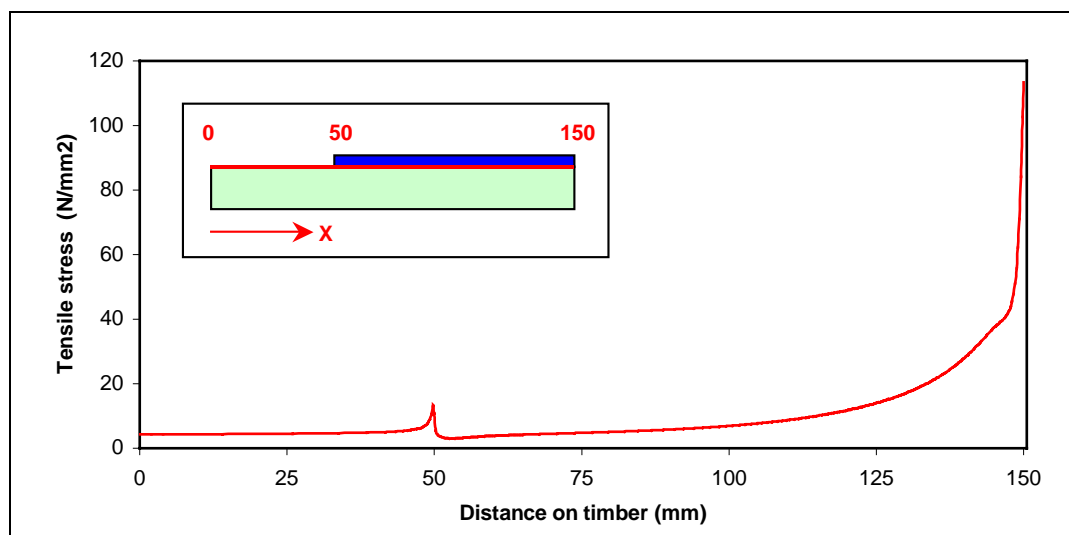
The model shown in figure 6.47 has the same number of nodes and elements, the same mesh geometry than the 2D model developed for sample TPU00.

The deformed shape also indicates that the composite layer is bending downwards at the right end, due to the internal bending effects of the overlap.

The axial and shear stress distributions at the interface between the composite and the timber are presented in the following graphs (figures 6.48 and 6.49).



Tensile stress distribution on glass fibre/epoxy interface



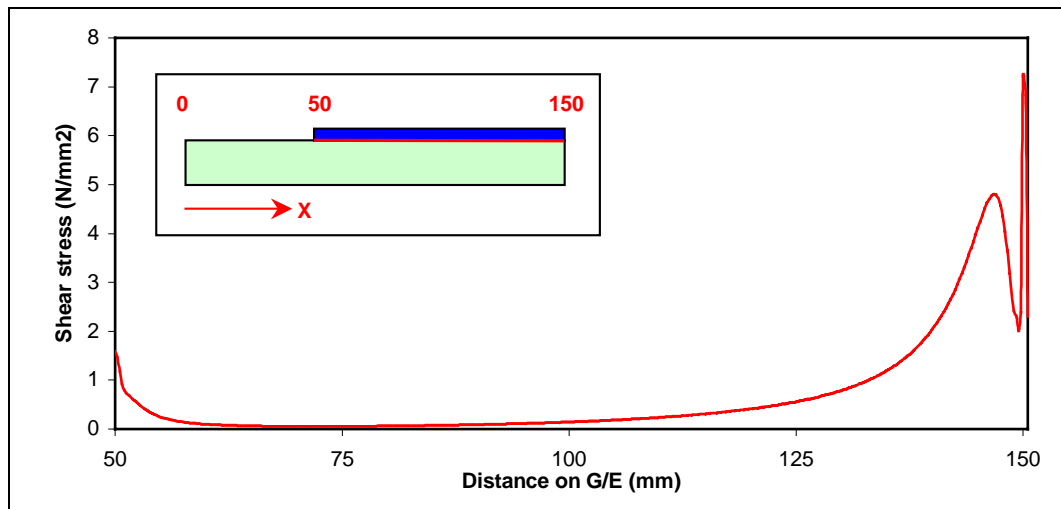
Tensile stress distribution on timber interface

Figure 6.48 Tensile stress distributions at the interface between the composite and the timber.

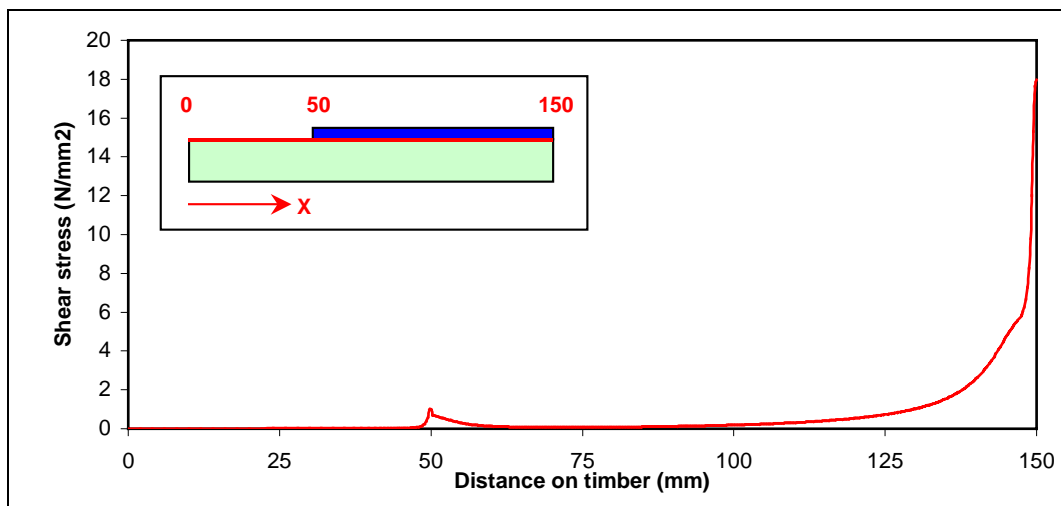
These two graphs show the tensile stress distribution at the interface between the two materials, calculated from the composite and from the timber respectively.

The distribution of tensile stress has a relatively similar shape whether it is at the timber or at the composite interface up to $x = 125$ mm. The tensile stress in the composite abruptly increases towards the right end (gap area) rising from around 60 MPa to around 275 MPa. This increment of stress is similar in the timber, rising from 40 MPa to around 110 MPa.

The shear stress distributions calculated by the FE model at the interface between the composite and the timber are presented in figure 6.49.



Shear stress distribution on glass fibre/epoxy interface



Shear stress distribution on timber interface

Figure 6.49 Shear stress distributions at the interface between the composite and the timber.

The shear stress distributions appear to be similar in terms of shape and intensity except at the right end of the overlap (after $x = 140$ mm). In that zone, the shear stress in the composite reaches a peak at around 5 MPa, then decreases steeply to 2 MPa and then peaks again to 7 MPa. Those high variations of shear stresses around the right end of the overlap are the result of the internal bending of composite in that zone. For the timber, the shear stress peaks abruptly to 18 MPa at the right end. Once again, the shear stress observed has reached the timber shear strength of

approximately 13 MPa and the timber should have failed in this zone. Shear plasticity or failure could be on the verge of occurring.

The figure 6.50 shows a graph of longitudinal strain distribution along the composite surface, derived from the FE model.

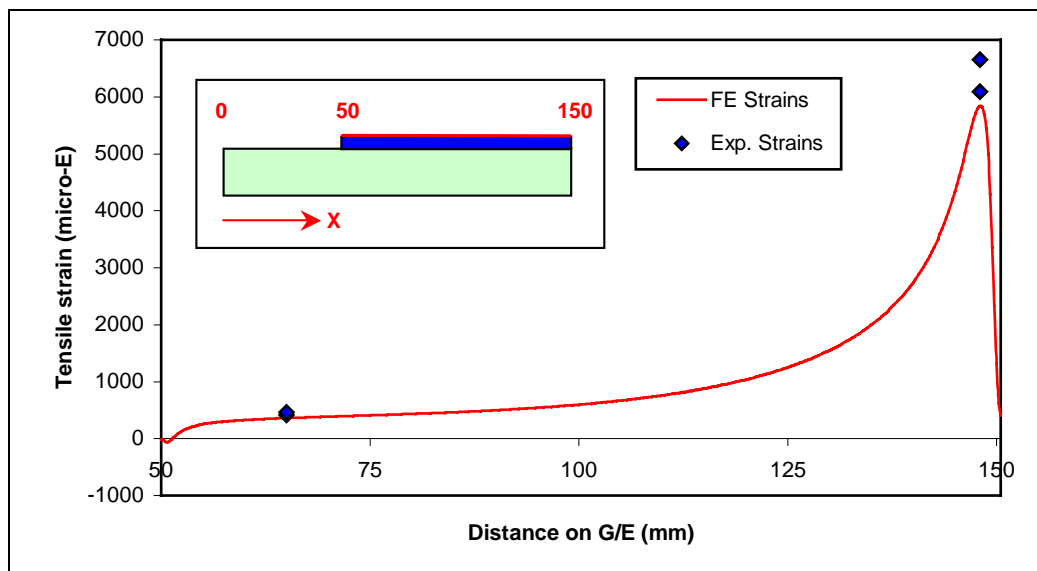


Figure 6.50 Longitudinal tensile strain distribution on glass fibre/epoxy surface.

The tensile strain distribution on the composite is progressive from the left end of the overlap to the gap area, following a parabolic shape. However the strains steeply decrease towards the right end. This is due to the internal bending of the composite. Internal bending effects are discussed in greater details in § 6.4. Experimental strain results are also plotted in figure 6.50.

The tensile strain results derived by the FE model and measured experimentally are presented in table 6.5.

Sample	End strain gauge	Gap strain gauge
	x = 65 mm	x = 150 mm
7TPB00 - α	411	6093
8TPB00 - β	463	6653
Plane42 FE model	361	5840

Table 6.5 Comparison of strains results obtained from experiments and from the FE model.

Strain gauge positions are described in § 4.3.2.2. The results of tensile strains obtained from the FE model tend to be lower than those measured in experiments but remain within the range.

These results must be compared with those obtained from the 3-dimensional FE model that is presented in the next section.

6.3.3.2.2. 3-Dimensional model

The characteristics of the 3D model are as follow:

File name:	Am02-solid72
Materials number:	2 - Anisotropic
Element type:	SOLID72 - 3D Structural solid
Element description:	4 nodes tetrahedral solid element with rotations
Analysis type:	Static - Linear
Loading:	18 kN in tension
Number of Elements:	58886
Number of Nodes:	11788

The SOLID72 linear element characteristics are already defined in § 6.3.3.1.2.

Full details for the FE model are available in Appendix D.2.

The graphical results are presented in figure 6.51.

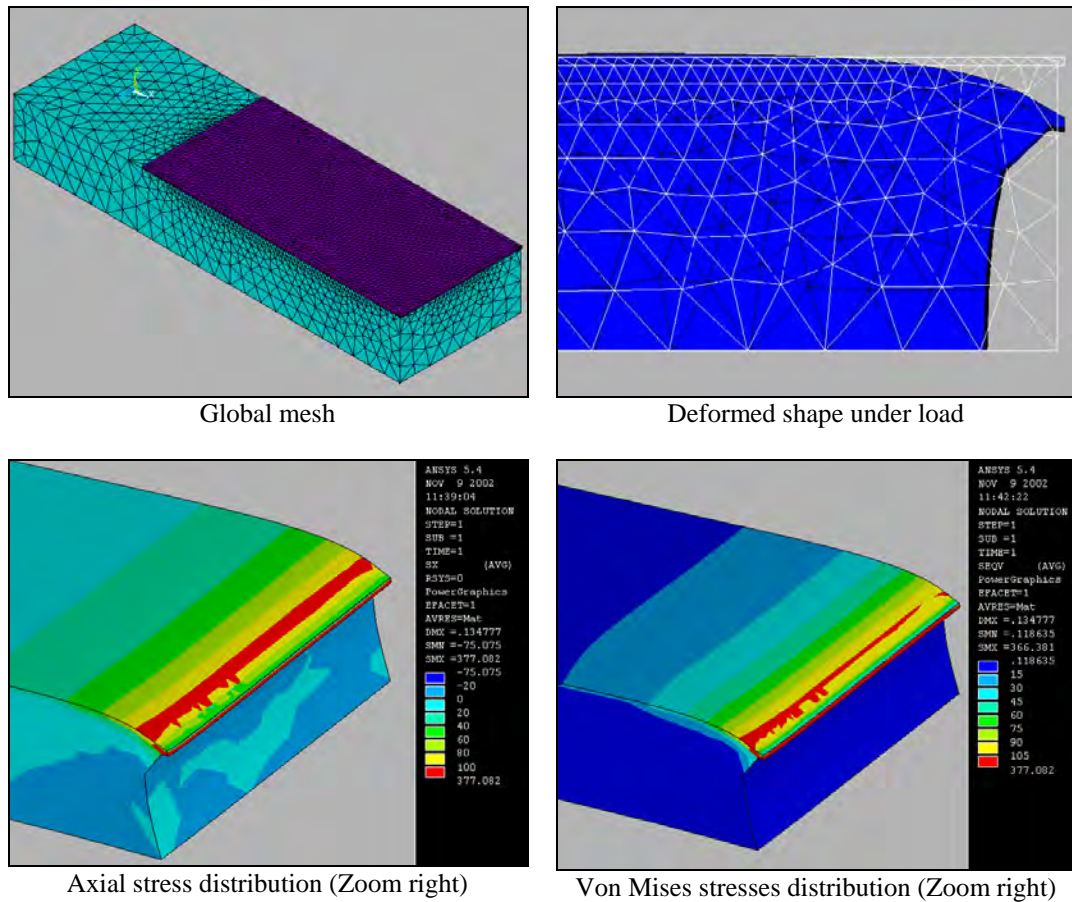
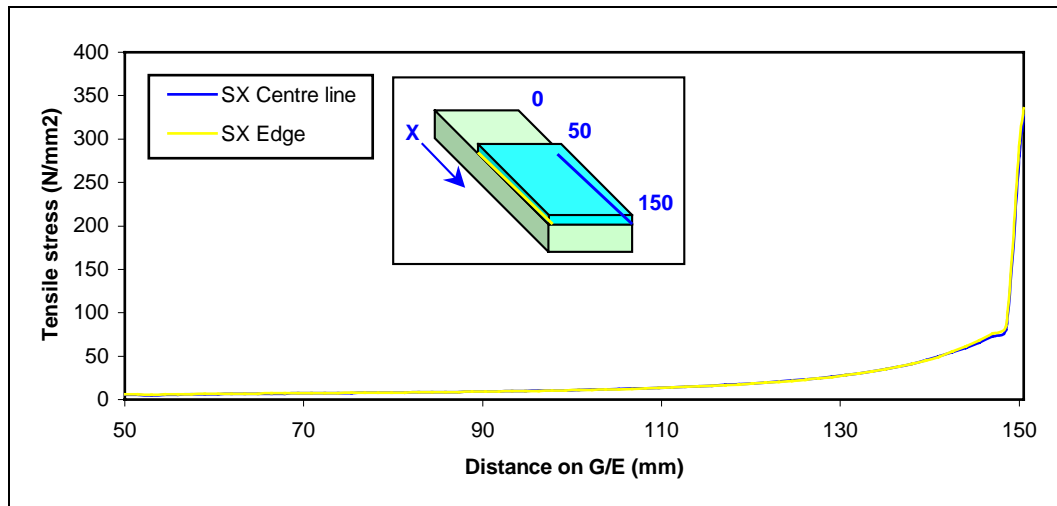


Figure 6.51 Graphical results of the 3D model type TPB00.

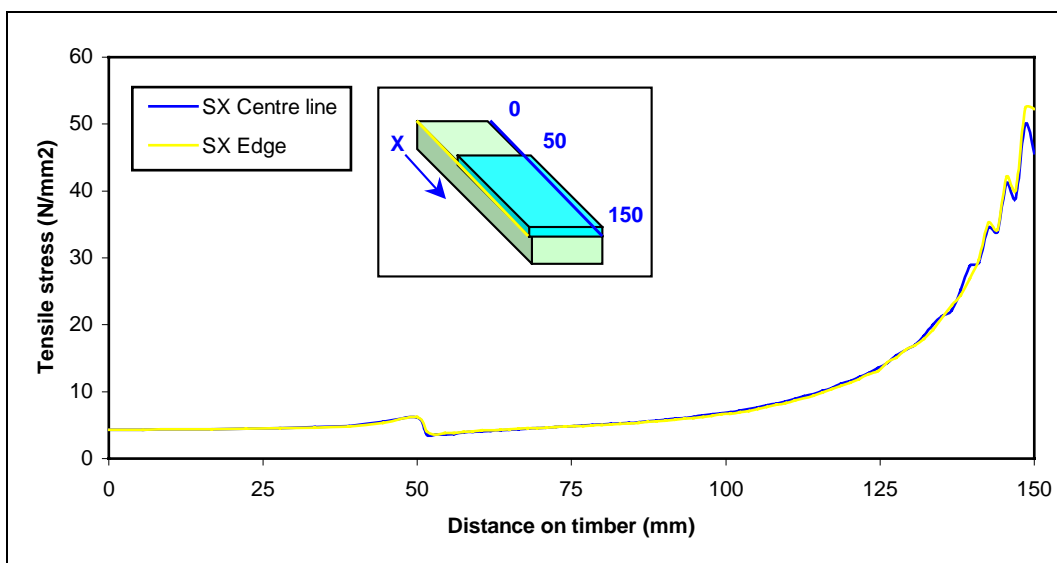
The model shown in figure 6.51 has the same number of nodes and elements, the same mesh geometry than the 3D model developed for sample TPU00.

The deformed shape also indicates that the composite layer is bending downwards at the right end, due to the internal bending effects of the overlaps, as discussed before. The graphical results of axial stress and Von Mises stress distributions clearly show some stress variations in the transverse direction (z direction) due to the edge effects.

The axial and shear stress distributions at the interface between the composite and the timber are presented in the following graphs (figures 6.52 and 6.53), with results given along the centre line and the edge of the joint.



Tensile stress distribution on glass fibre/epoxy interface



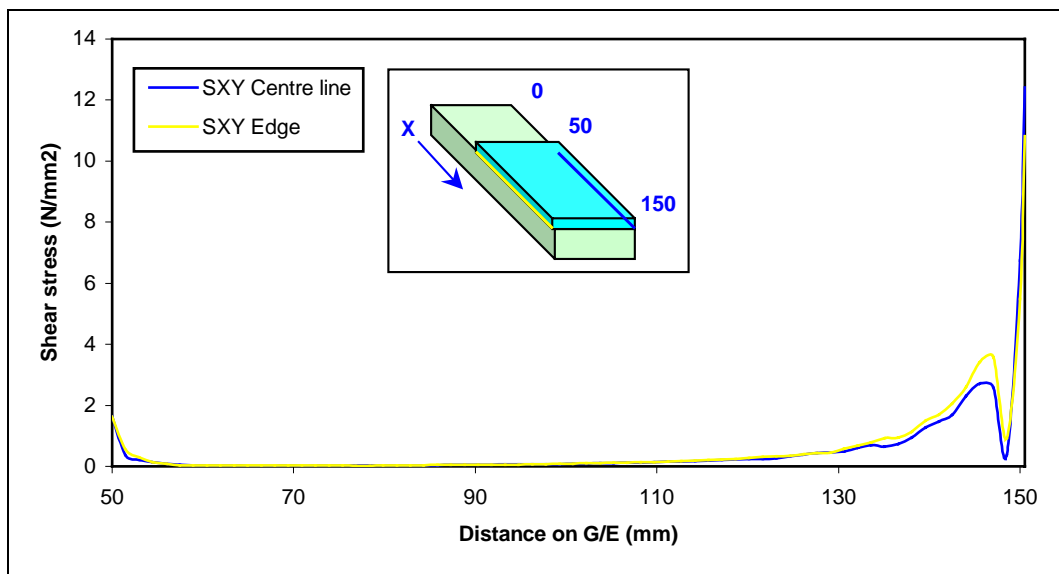
Tensile stress distribution on timber interface

Figure 6.52 Tensile stress distributions at the interface between the composite and the timber.

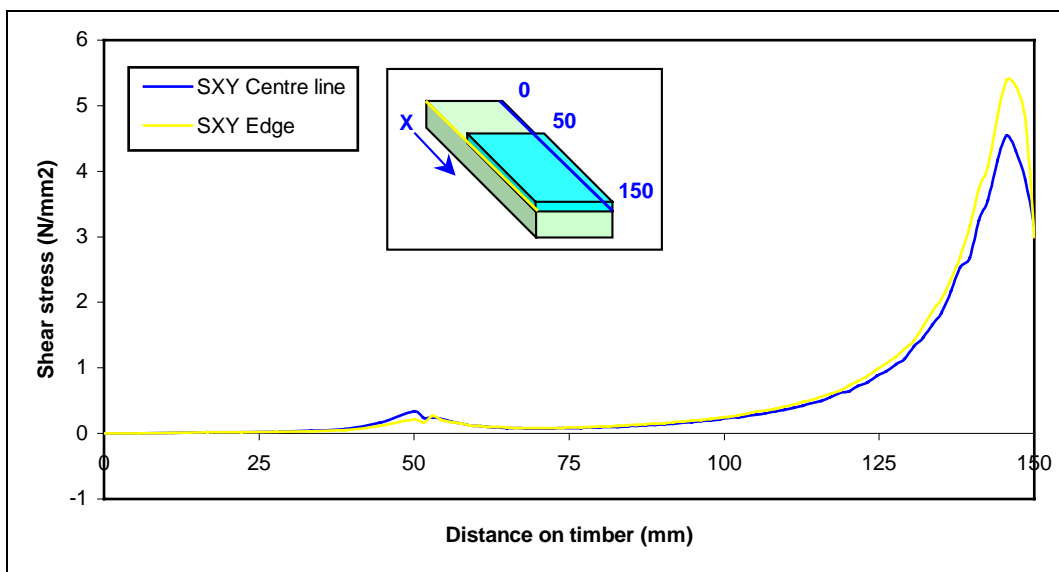
The distribution of tensile stress has a relatively similar shape whether it is at the timber or at the composite interface. The tensile stress in the composite steeply increases towards the right end ($x = 148$ mm) rising from 80 MPa to around 330 MPa. This increment of stress is steadier in the timber, showing a parabolic shape that rises to around 55 MPa. This value of tensile stress in the timber appears to be fairly low compared to the one of 110 MPa obtained from the 2D model. As for the previous 3D model, the tensile stress in the timber of 55 MPa is probably inaccurate due to the coarse mesh in that region. Again, the wobbly end of the curve confirms the inaccuracy in the finite solution.

There is no difference between the tensile stress in the composite recorded along the centre line and the (free) edge of the model. However there is a very small difference for the tensile stress in the timber, where the stress at the edge is slightly higher in the high stress region (right end) than the stresses at the centre line, showing some edge effect.

The shear stress distributions calculated by the FE model at the interface between the composite and the timber are presented in figure 6.53.



Shear stress distribution on glass fibre/epoxy interface



Shear stress distribution on timber interface

Figure 6.53 Shear stress distributions at the interface between the composite and the timber.

The shear stress distributions are similar in terms of shape and intensity except around both ends of the overlap (around $x = 50$ mm for the left end and $x = 145$ mm for the right end). At the right end, the shear stress in the composite reaches a peak at around 3 MPa, then decreases abruptly to 0.5 MPa, and peaks again to 11 MPa. The internal bending of the composite in that zone causes those variations of shear stresses around the right end of the overlap. For the timber, the shear stress distribution is steadier, following a parabolic shape, rising to 5 MPa and then reducing to 3.5 MPa at the gap end. The low shear stress observed in the timber is due to the coarse mesh of elements in that high stress zone, as previously mentioned. In accordance with these results, the shear stress did not reach the timber shear strength of approximately 13 MPa. The shear stress distribution near the right end is slightly higher along the edge than along the centre line of the joint, reflecting some edge effects.

The figure 6.54 shows a graph of longitudinal strain distribution along the composite surface, derived from the FE model.

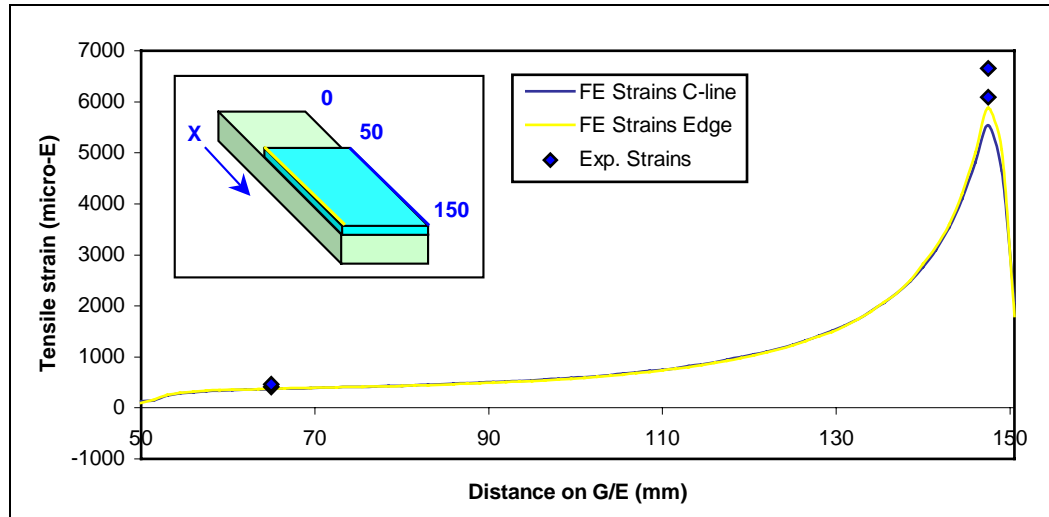


Figure 6.54 Longitudinal tensile strain distribution on glass fibre/epoxy surface.

Following a parabolic shape, the tensile strain distribution on the composite is progressive from the left end of the overlap to the gap area. However the drop in strains towards the right end is due to the internal bending of the composite. Because of a minor edge effect, the strains at the right end are slightly higher at the edge than at the centre line. Experimental strain results are also plotted in figure 6.54.

The tensile strain results derived by the FE model and measured experimentally are presented in table 6.6.

Sample	End strain gauge	Gap strain gauge
	x = 65 mm	x = 150 mm
7TPB00 - α	411	6093
8TPB00 - β	463	6653
Plane42 FE model	371	5534

Table 6.6 Comparison of strains results obtained from experiments and from the FE model.

Strain gauge positions are described in § 4.3.2.2. The results of tensile strains obtained from the FE model tend to be lower but remain relatively close to those measured in experiments.

Finally the comparison between the 2D and 3D models shows that the results obtained are relatively similar except in the high stress region, i.e. the gap zone. Advantages and disadvantages of both models are identical to those developed in § 6.3.3.1.2:

- The 3D model shows inaccurate results due to its relatively coarse mesh in the high stress region, compared to those obtained with the finer mesh of the 2D model.
- The 3D model reveals a relatively small edge effect in the high stress region, where strains and stresses are slightly higher along the edge than along the centre line of the joint. The 2D model does not show whether the strain and stresses vary across the width of the joint.

As a conclusion, the 3D model seems to be more appropriate to model the straight configuration joint as it identifies stress and strain variations across the width of the joint, but suffers a lack of accuracy, particularly regarding the stress and strain results where the meshing could not be refined sufficiently. Further refinements could not be achieved without generating poorly shaped elements, producing even more inaccurate results.

These findings will be taken into account through the modelling of joints with load not parallel to the grain, as developed in the next section.

6.3.4. Joints with load not parallel to the grain

The FE models developed for joint configurations with load not parallel to the grain are 3-dimensional models mainly because of their geometry.

The element types used in these FE models always have tetrahedral shape. Hexahedron elements could not be used to fit to the geometry, without generating errors in their aspect ratios. A mixture of hexahedron and tetrahedral elements could have been the appropriate solution, but the program user manual does not recommend the use of both types within the same model.

The mesh geometry was set in order to generate only well shaped elements. Many different mesh sizes were generated without success. For each configuration, there was only one specific mesh that fit adequately to the model.

6.3.4.1. Load applied perpendicular to the grain

The two models presented in this section were generated in 3D respectively. The glass fibres are unidirectional and bidirectional respectively, therefore the material properties of the composite reflect these characteristics. The thickness of the composite corresponds to the measured thickness of 0.65 mm.

6.3.4.1.1. Configuration with uniaxial fibres TNU90

The characteristics of the 3D model are as follow:

File name:	Am03-solid92
Materials number:	3 - Anisotropic
Element type:	Solid92 - 3D Structural solid
Element description:	10 nodes tetrahedral solid quadratic element
Analysis type:	Static - Linear
Loading:	18 kN in tension
Number of Elements:	12650
Number of Nodes:	20557

The quadratic element type SOLID92 is defined by a tetrahedral solid shape with ten nodes having three degrees of freedom at each node: translations in the nodal x, y and z directions. The element input data includes ten nodes and orthotropic material

properties. The element is well suited to model irregular meshes because of its tetrahedral geometry. It can often be replaced by the less accurate but faster in solution time SOLID72 linear element that is already presented in § 6.3.3.1.2.

With a mesh that could not be refined without generating poorly shaped elements, the choice of using quadratic element was made, in order to increase the accuracy of the solution. As a result, the quadratic element SOLID92 was used to improve the solution of the analysis while using a relatively coarse mesh.

Full details for the FE model are available in Appendix D.3.

The graphical results are presented in figure 6.55.

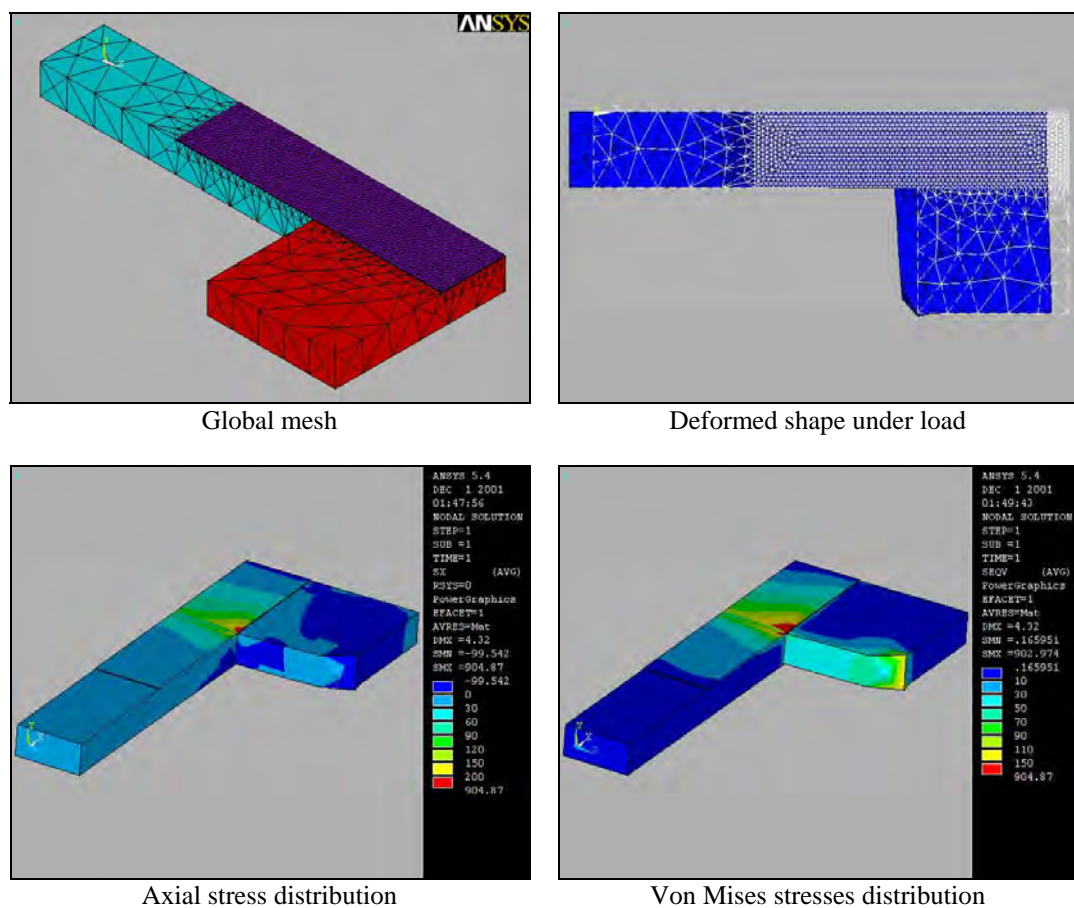


Figure 6.55 Graphical results of the 3D model type TNU90.

On the model shown in figure 6.55, the mesh of the glass fibre/epoxy composite layer is rather dense, becoming progressively coarser as it reaches the plane of symmetry of the timber members.

The deformed shape is viewed from the top. Therefore it does not show the internal bending of the composite around the gap area. On the other hand, it shows the

deflection of the perpendicularly orientated timber member. This member is simply supported at both ends (on the model, there is only one support as only half of the model was generated, using plane symmetry) and is in fact bending under the tension load applied through the glass fibre/epoxy composite layer.

The graphical results of axial stress and Von Mises stress distributions confirm the bending of the perpendicular timber member as the stresses are higher along the edge of the composite than along the centre line.

The FE results of axial and shear stress distributions at the interface between the composite and the timber that are presented in the following graphs in figures 6.56 and 6.57, and are given along the centre line and the edge of the joint.

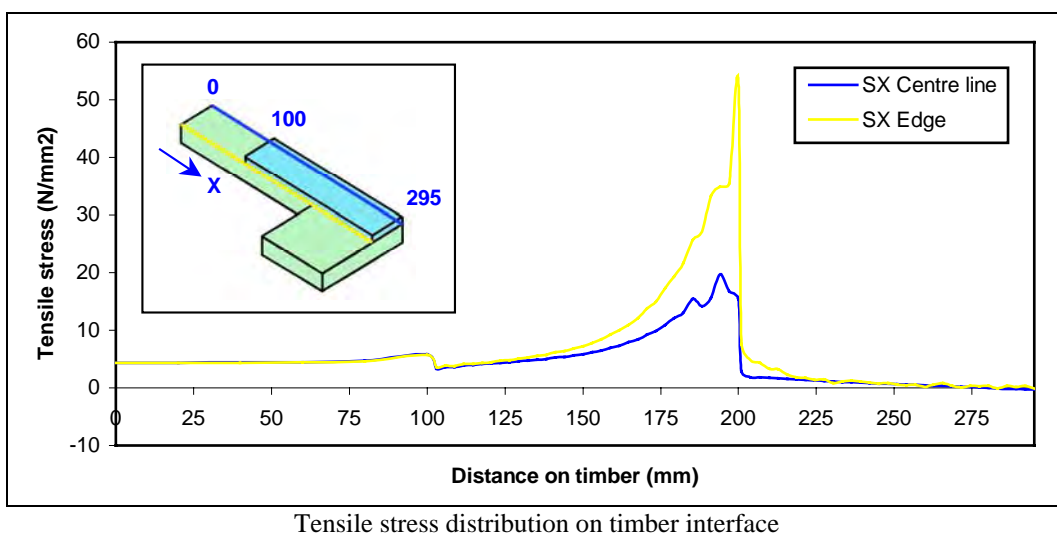
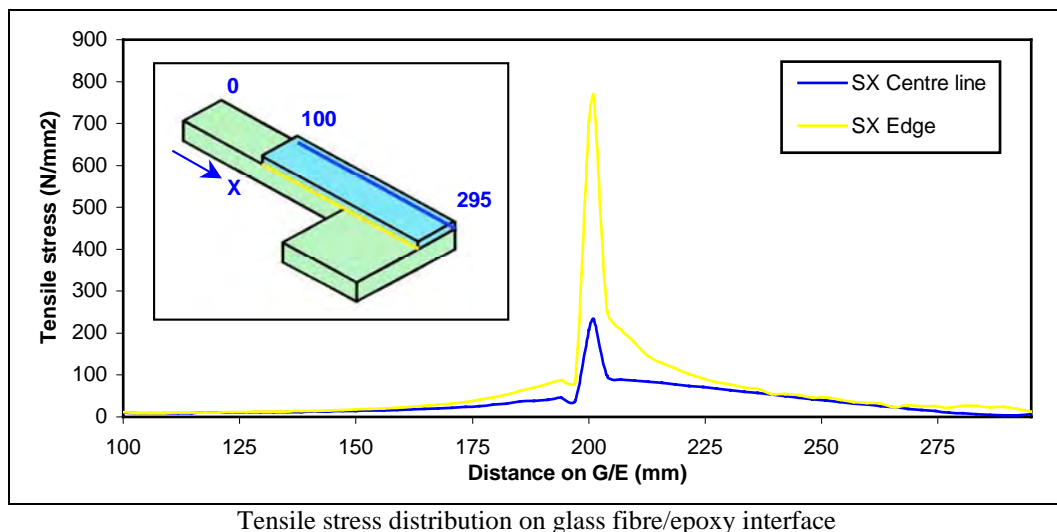


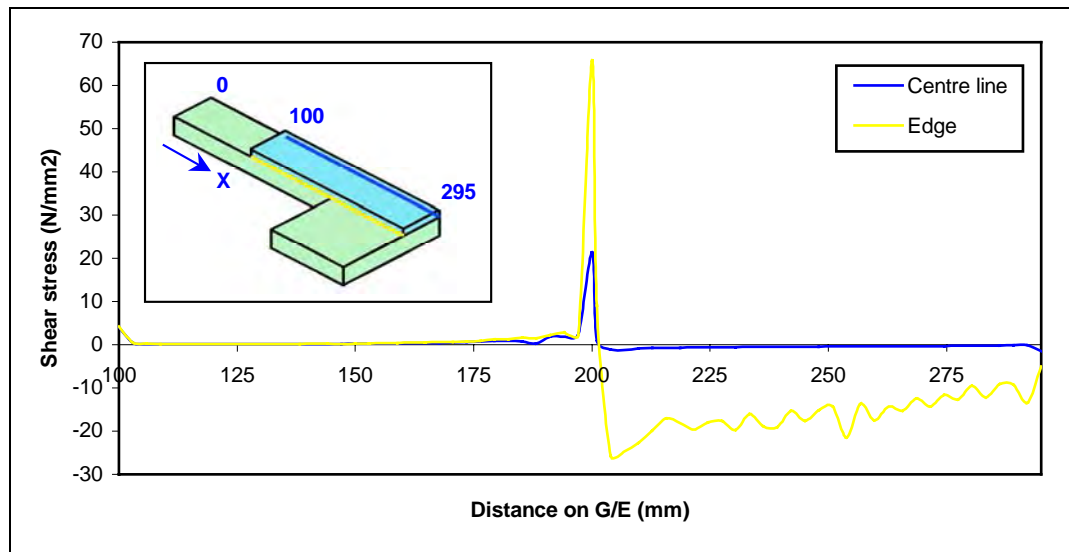
Figure 6.56 Tensile stress distributions at the interface between the composite and the timber.

The distribution of tensile stress is significantly different in shape and intensity whether it is at the timber or at the composite interface.

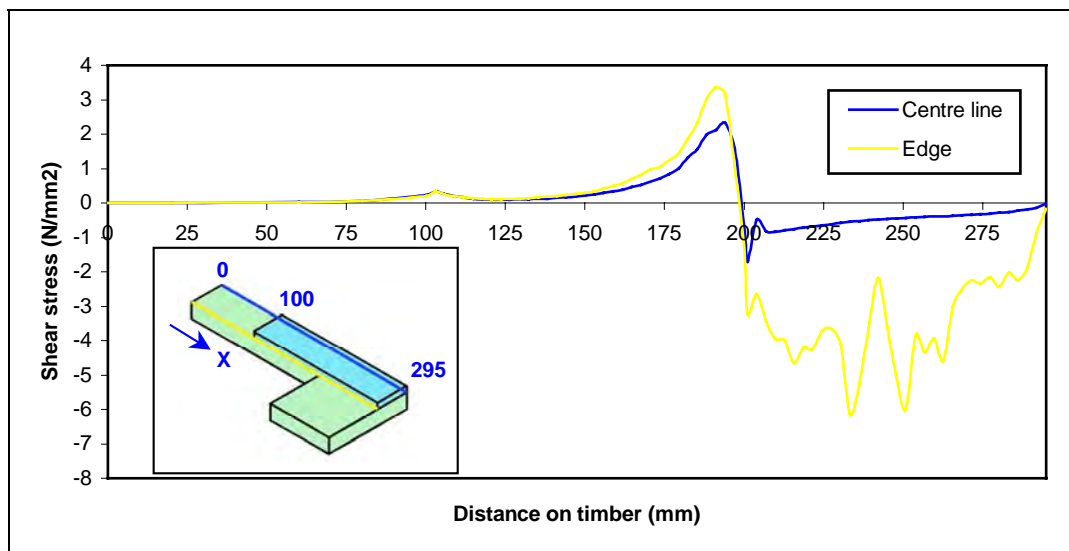
The tensile stress in the composite abruptly increases towards the gap zone ($x = 200$ mm). Along the centre line, the tensile stress rises from 50 MPa to around 240 MPa, and along the edge, it rises from 80 MPa to nearly 760 MPa.

For the tensile stress in the timber, the progression of stress is steadier and rises to 20 MPa along the centre line. Along the edge, it rises to 55 MPa. Because of a coarse mesh of elements in the timber, it was already established that the stresses are underestimated. Furthermore, the bending under load of the perpendicular timber member increases the gap in stress distribution between the edge and the centre line. In other words, the edge effect is amplified by the bending of the perpendicular timber member. The tensile stresses of the composite observed in the gap zone are very high along the edge (760 MPa) and reach the tensile strength of the composite, and this for a tension load of 18 kN. But the average failure load of the TNU90 tests is 36.2 kN and the failure mode consists of delamination of the composite. This means that for a tension load of 18 kN, the composite tension stress of 760 MPa is probably over-estimated. As a result, the mesh size is not sufficiently refined in that zone.

The shear stress distributions calculated by the FE model at the interface between the composite and the timber are presented in figure 6.57.



Shear stress distribution on glass fibre/epoxy interface



Shear stress distribution on timber interface

Figure 6.57 Shear stress distributions at the interface between the composite and the timber.

The shear stress distributions are very different in terms of shape and intensity.

For the composite, the shear stress along the centre line peaks to 20 MPa in the gap zone ($x = 200$ mm) and becomes negative (close to zero) in the perpendicularly orientated timber member (between $x = 200$ mm and $x = 294$ mm). For the timber, the shear stress along the centre line rises progressively to 3.5 MPa in the gap zone and peaks to -2 MPa then increasing progressively to zero. The negative shear stress indicates the change in direction of shear, due to the fact that the “pulling action” of

the composite on the timber is acting in the opposite direction in the perpendicularly orientated timber member.

Looking at the shear stress distributions along the edge, the results are more inconsistent. The shear stress is in fact distorted by the bending of the perpendicular timber member, and those distortions are visible on the graphs: In the composite interface, the chaotic part of the curve (right hand side) reflects insufficient mesh refinement but still give some reasonable results. In the timber interface, the curve on the right hand side is very chaotic due to a combination of complex stress variations (i.e. member bending) and insufficient mesh refinement.

The shear stress distribution along the edge is always higher than along the centre line of the joint, for the reasons explained previously.

The figure 6.58 shows a graph of longitudinal strain distribution along the composite surface, derived from the FE model.

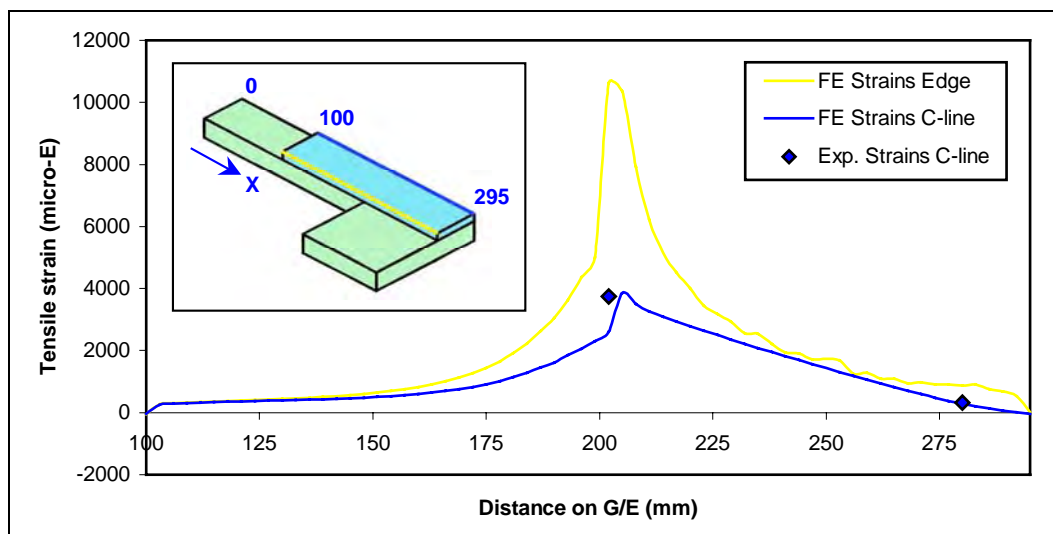


Figure 6.58 Longitudinal tensile strain distribution on glass fibre/epoxy surface.

Following a parabolic shape, the tensile strain distributions on the composite are progressive from the left end of the overlap ($x = 100$ mm) and peak in the gap zone. Then the strain reduces gradually to zero, on the right hand side of the model (to $x = 294$ mm). The internal bending of the composite in the gap zone still occurs but does not appear on the graph because the bending effect of the perpendicular timber member is prominent. As a result the FE strains along the edge are much higher in the high stress region (gap zone) than the FE strains along the centre line. The

experimental strain results are also plotted in figure 6.58 and are very close to the FE results.

The tensile strain results derived by the FE model and measured experimentally are presented in table 6.7.

Sample	Gap strain gauge	End strain gauge
	x = 200 mm	x = 280 mm
5TNU90 - Ω	3738	325
Solid92 FE model	3845	284

Table 6.7 Comparison of strains results obtained from experiments and from the FE model.

Strain gauge positions are described in § 4.3.2.3. The results of tensile strains obtained from the FE model are relatively close to those measured in experiments.

6.3.4.1.2. Configuration with biaxial fibres TNB90

The characteristics of the 3D model are as follow:

File name:	Am04-solid92
Materials number:	3 - Anisotropic
Element type:	Solid92 - 3D Structural solid
Element description:	10 nodes tetrahedral solid quadratic element
Analysis type:	Static - Linear
Loading:	18 kN in tension
Number of Elements:	12650
Number of Nodes:	20557

The quadratic element type SOLID92 was defined in the previous section.

Full details for the FE model (geometry, material properties, boundary assumptions, etc) are available in Appendix D.3.

The graphical results are presented in figure 6.59.

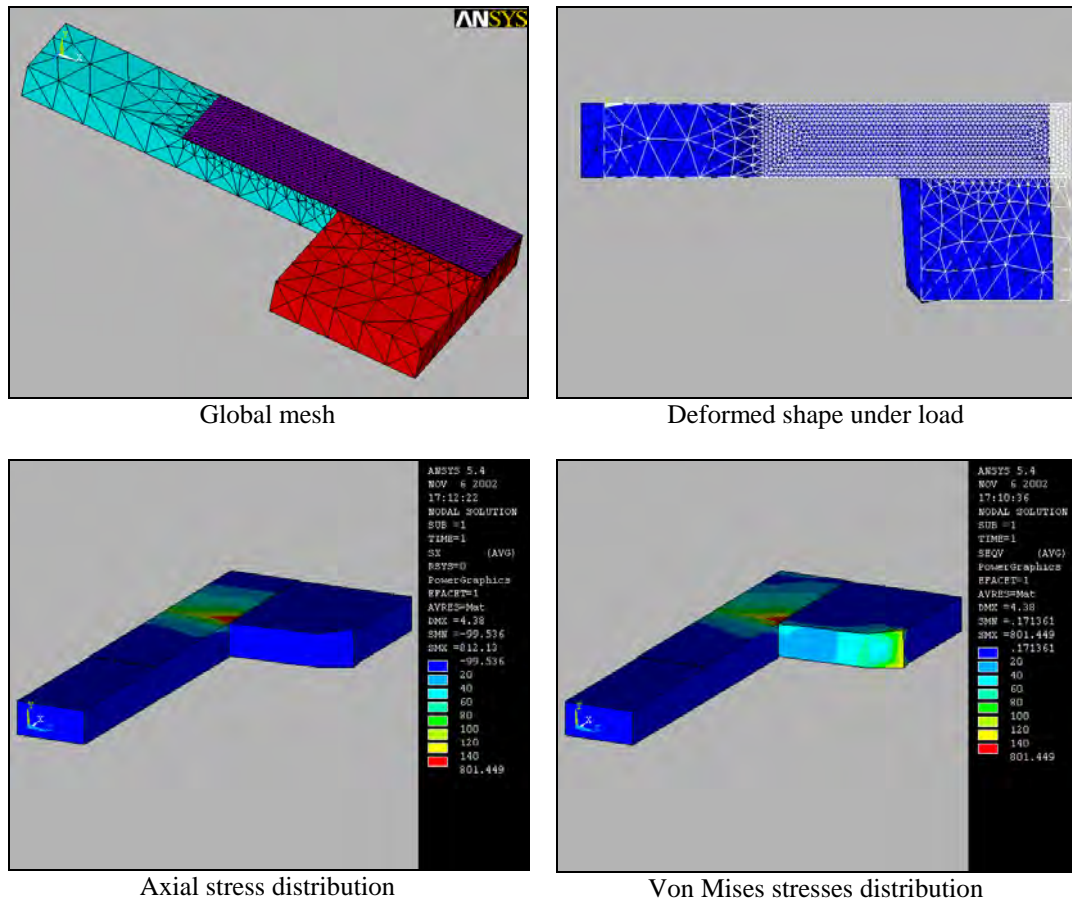
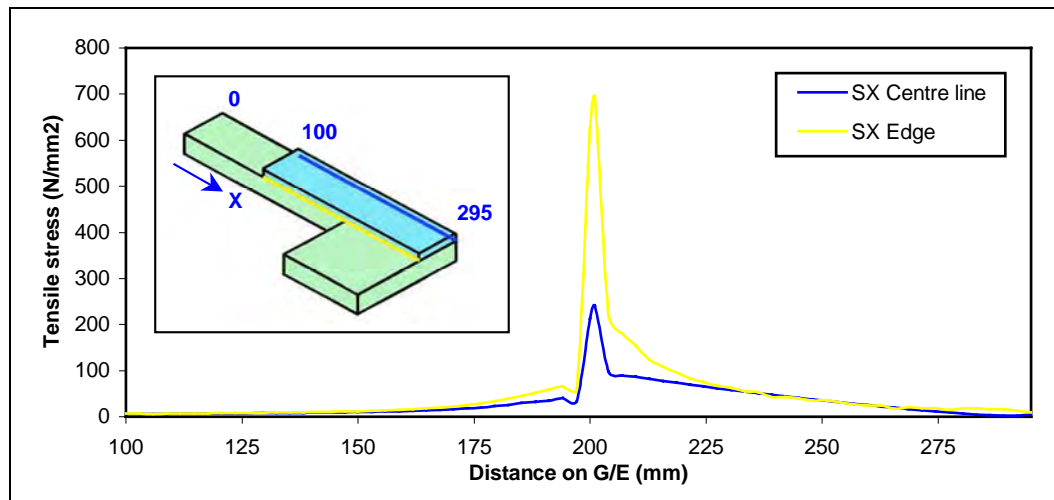


Figure 6.59 Graphical results of the 3D model type TNB90.

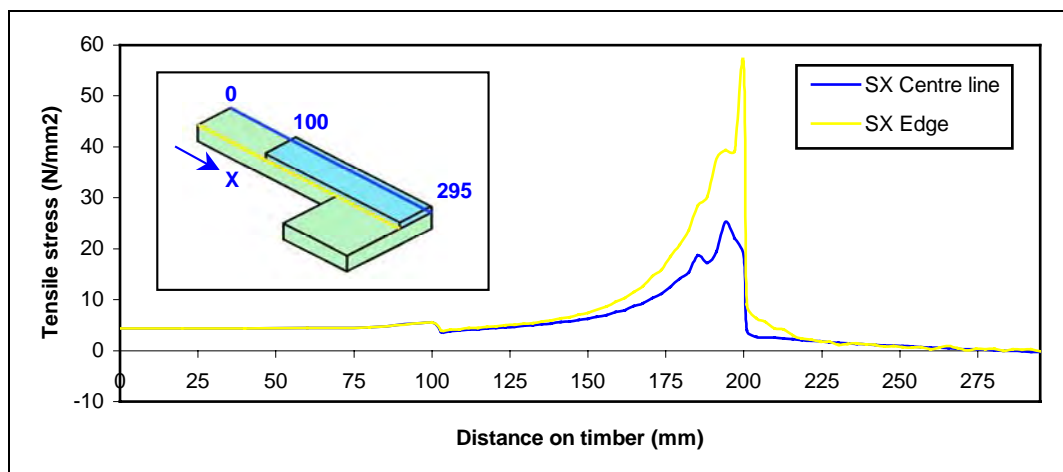
On the model shown in figure 6.59, the same mesh configuration was used than on the TNU90 model. The deformed shape shows the deflection of the perpendicularly orientated timber member that is in fact bending under the tension load applied through the composite.

The graphical results of axial stress and Von Mises stress distributions confirm the bending of the perpendicular timber member as the stresses are higher along the edge of the composite than along the centre line.

The FE results of axial and shear stress distributions at the interface between the composite and the timber are presented in figures 6.60 and 6.61.



Tensile stress distribution on glass fibre/epoxy interface



Tensile stress distribution on timber interface

Figure 6.60 Tensile stress distributions at the interface between the composite and the timber.

The distribution of tensile stress at the interface between the composite and the timber exhibits the same shape than on the TNU90 model.

Along the centre line, the tensile stress in the composite rises from 35 MPa to around 240 MPa and from 60 MPa to nearly 700 MPa along the edge. For the tensile stress in the timber, a steady progression rises to 25 MPa along the centre line and to 58 MPa along the edge.

On this model as well, the bending under load of the perpendicular timber member increases the disparity in stress distribution between the edge and the centre line.

The shear stress distributions calculated by the FE model at the interface between the composite and the timber are presented in figure 6.61.

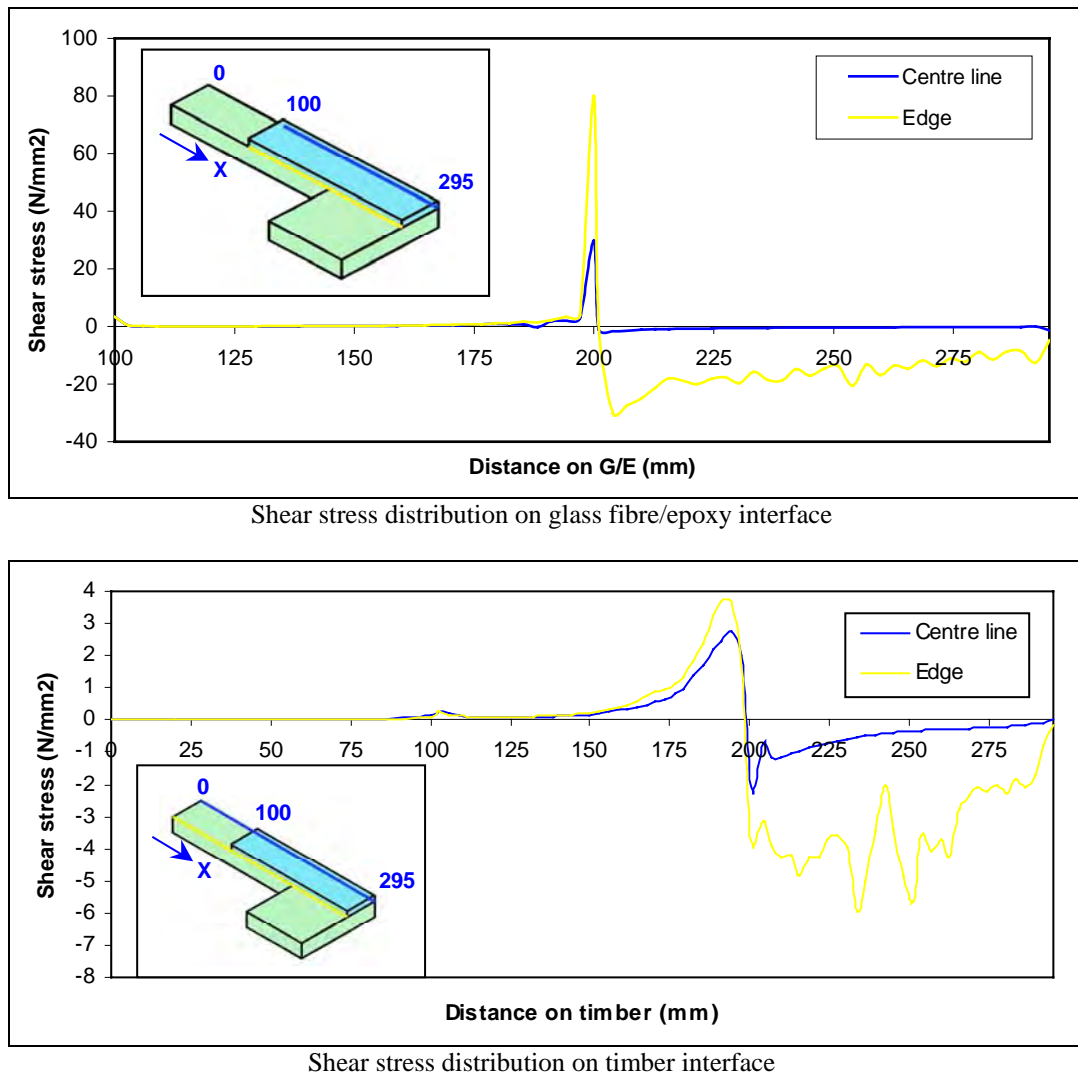


Figure 6.61 Shear stress distributions at the interface between the composite and the timber.

The shear stress distributions display the same shape than on the TNU90 model.

For the composite, the shear stress along the centre line peaks at 30 MPa in the gap zone and drops to -3 MPa in the perpendicularly orientated timber member. For the timber, the shear stress along the centre line rises progressively to 3 MPa in the gap zone and peaks to -2.5 MPa then increasing progressively to zero.

In this case again, the shear stress is distorted by the bending of the perpendicular timber member and insufficient mesh refinement. Note that the shear stress distribution along the edge is higher than along the centre line of the joint.

The figure 6.62 shows a graph of longitudinal strain distribution along the composite surface, derived from the FE model.

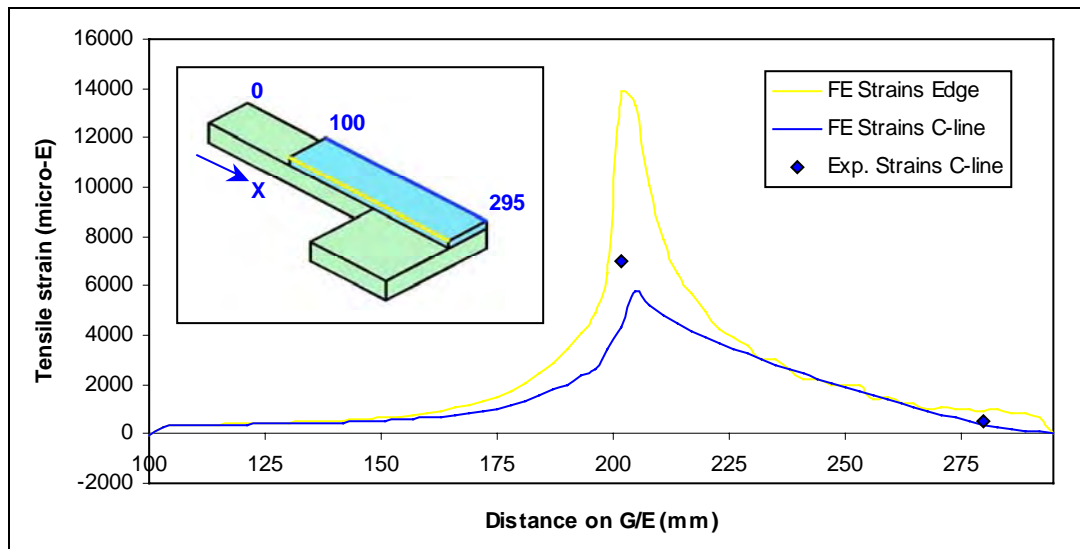


Figure 6.62 Longitudinal tensile strain distribution on glass fibre/epoxy surface.

Following a parabolic shape, the tensile strain distributions on the composite are progressive from the left end of the overlap and gradually rise in the gap zone. Then the strain reduces on the right hand side of the model gradually to zero.

As mentioned before, the FE strains along the edge are much higher in the high stress region (gap zone) than the FE strains along the centre line, resulting from the bending effect of the perpendicular timber member. The experimental strain results recorded along the centre line are also plotted in figure 6.62 and are relatively close to the FE results.

The tensile strain results derived by the FE model and measured experimentally are presented in table 6.8.

Sample	Gap strain gauge	End strain gauge
	x = 200 mm	x = 280 mm
6TNB90 - ϕ	7007	522
Solid92 FE model	5788	392

Table 6.8 Comparison of strains results obtained from experiments and from the FE model.

Strain gauge positions are described in § 4.3.2.3. The results of tensile strains of the FE model are relatively lower than those measured in experiments. This could be due to experimental errors as results from only one sample are available, or it could be the thickness of the composite layer that is slightly too high. A slight change of thickness of the composite would affect the results significantly.

6.3.4.2. Load applied with an angle of 60 degrees to the grain

The two models presented in this section were generated in 3D respectively, with the 60° configurations. The glass fibres are unidirectional and bidirectional respectively. The thickness of the composite corresponds to the measured thickness of 0.65 mm.

6.3.4.2.1. Configuration with uniaxial fibres TNU60

The characteristics of the 3D model are as follow:

File name:	Am05-solid72
Materials number:	3 - Anisotropic
Element type:	Solid72 - 3D Structural solid with rotations
Element description:	4 nodes tetrahedral solid element
Analysis type:	Static - Linear
Loading:	18 kN in tension
Number of Elements:	28932
Number of Nodes:	6753

The linear element type SOLID72 is already described in § 6.3.3.1.2. This element was used for this model because the more accurate quadratic element SOLID92 required too much computer time to reach the solution. In fact a higher number of elements than for the TNU90 and TNB90 models was needed to generate a precise mesh.

Full details for the FE model (geometry, material properties, boundary assumptions, etc) are available in Appendix D.4.

The graphical results are presented in figure 6.63.

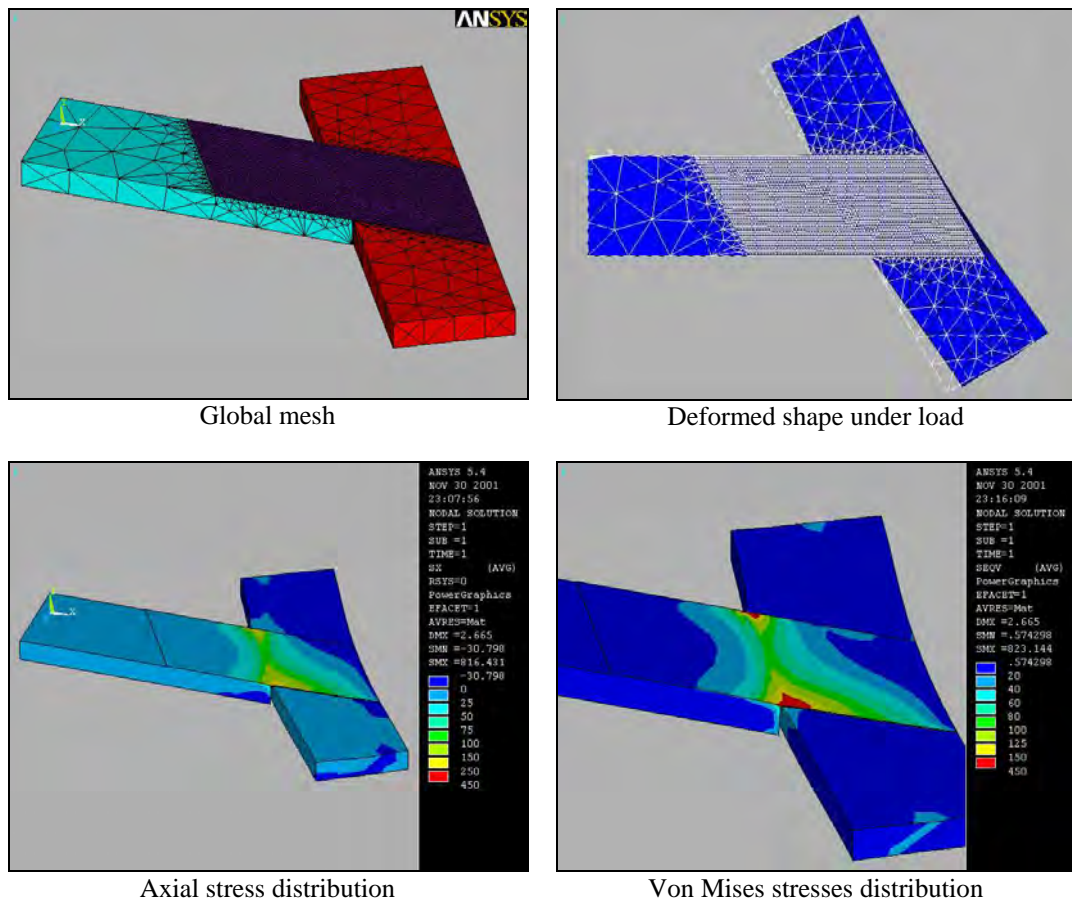


Figure 6.63 Graphical results of the 3D model type TNU60.

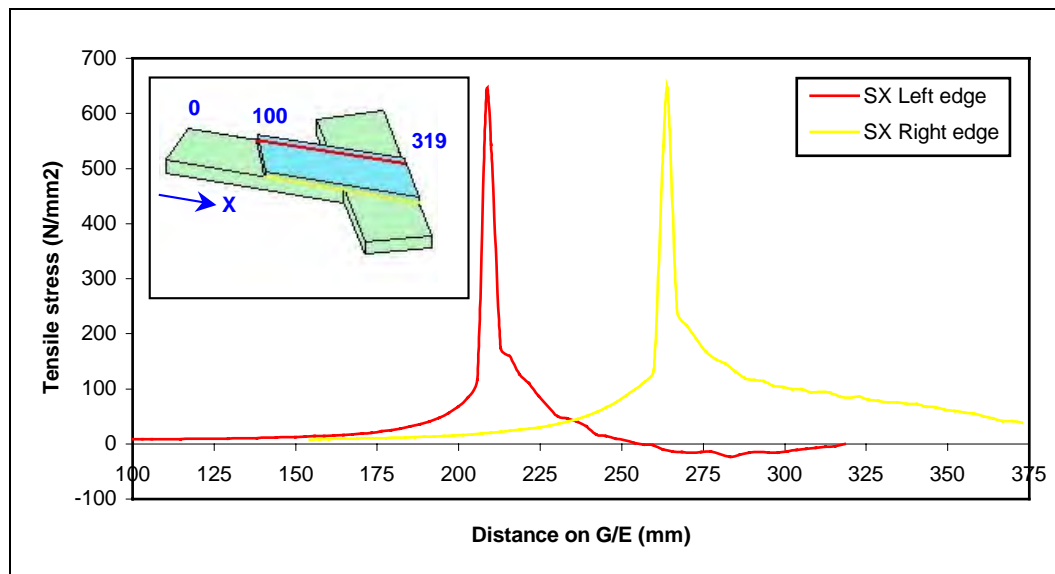
On the model shown in figure 6.63, the mesh of the glass fibre/epoxy composite layer is rather dense, becoming progressively coarser as it reaches the plane of symmetry of the timber members.

The deformed shape is viewed from the top and shows the deflection of the inclined timber member. This member is simply supported at both ends and as a result, it is bending under the tension load applied through the composite layer.

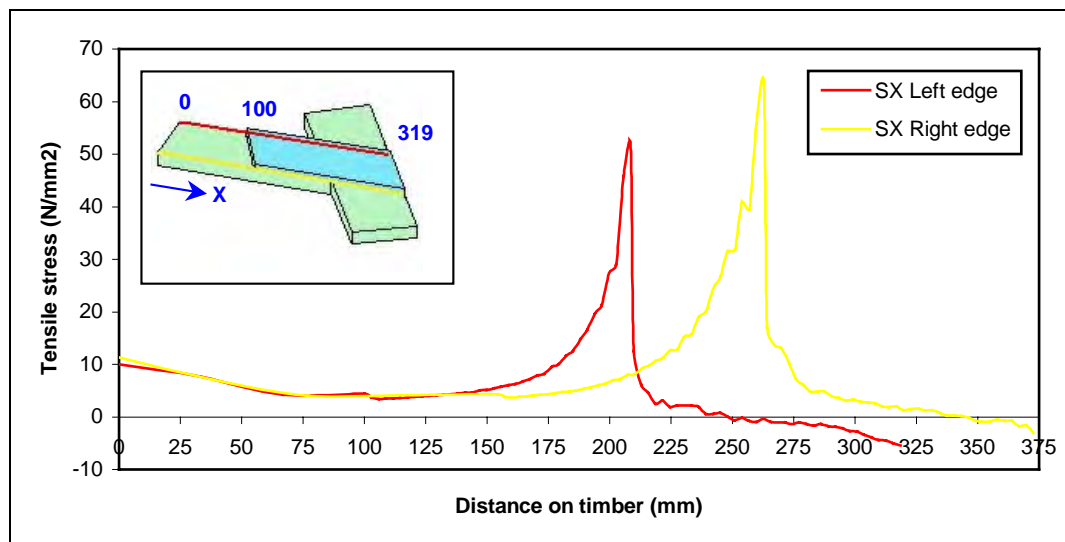
The graphical results of axial stress and Von Mises stress distributions shows that the bending of the inclined timber member induces an eccentricity of the stresses. The stresses are still higher along the edges of the composite than along the centre line. However, the left edge stresses (top edge of the composite layer in figure 6.63) are lower than the right edge stresses (bottom edge of the composite layer in figure 6.63), particularly in the gap zone. Because of the slope at which the inclined timber

member is connected, the tension load that is applied axially moves out of plane while the inclined member deflects.

The FE results of axial and shear stress distributions at the interface between the composite and the timber are presented in the following graphs in figures 6.64 and 6.65, and are given along the two edges of the joint.



Tensile stress distribution on glass fibre/epoxy interface



Tensile stress distribution on timber interface

Figure 6.64 Tensile stress distributions at the interface between the composite and the timber.

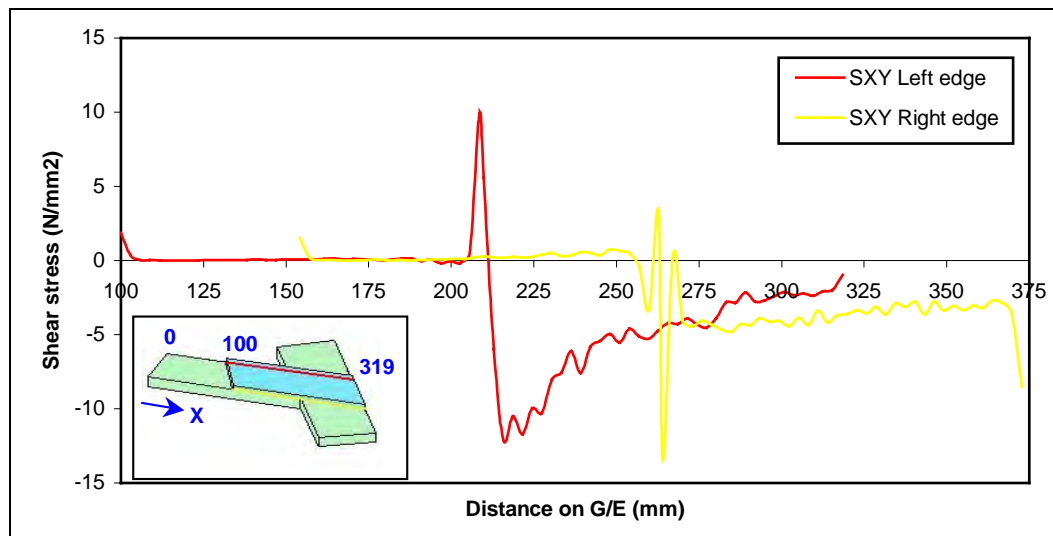
The tensile stress distribution in the composite interface has the same shape and intensity whether it is along the left or right edges. The results could not be derived along the centre line, as the element nodes are not positioned along that axis.

The tensile stresses along both edges rise progressively to approximately 100 MPa, peak to 640 MPa in the gap zone and drop to roughly 200 MPa. Then the stress reduces progressively across the inclined timber member and becomes compressive towards the end.

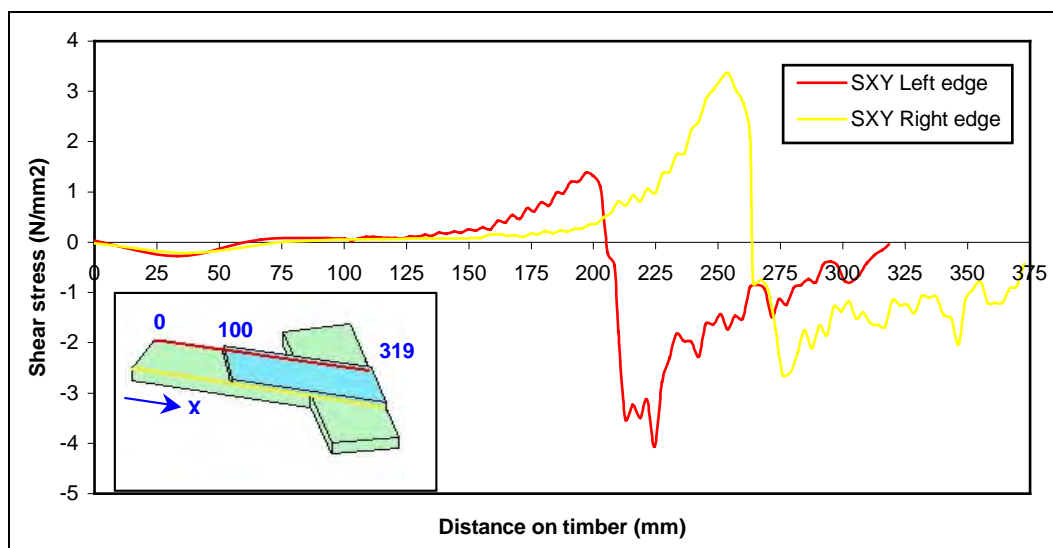
The tensile stress distribution in the timber interface has also a similar shape along the left or right edges, but reach a higher peak on the right edge than on the left edge. The tensile stresses along both edges rise progressively following a parabolic curve to approximately 60 MPa in the gap zone and drops abruptly. Then the stress reduces progressively across the inclined timber member and becomes compressive towards the end.

Tensile stress distributions appear to be accurate, except in the gap zone: Peak stress values are probably over-estimated due to the finite element coarse mesh size in that high stress region. However the inclined timber member is bending under the tension load therefore peak stresses at both ends of the gap zone are expected to be relatively high. Peak stresses along the right and left edges are certainly much higher than along the centre line.

The shear stress distributions calculated by the FE model at the interface between the composite and the timber are presented in figure 6.65.



Shear stress distribution on glass fibre/epoxy interface



Shear stress distribution on timber interface

Figure 6.65 Shear stress distributions at the interface between the composite and the timber.

The shear stress distributions are very different in terms of shape and intensity.

For the composite, the shear stress along the left edge peaks to 10 MPa in the gap zone ($x = 200$ mm) and drops to -12 MPa then progressively increases to zero. Along the right edge, the shear stress varies abruptly in the gap zone and several times between -13 MPa and 3 MPa, and then increases to zero.

For the timber, the shear stress along the left edge rises progressively to 1.4 MPa in the gap zone and peaks to -4 MPa then increasing progressively to zero. Along the

right edge, the shear stress rises progressively to 3.5 MPa in the gap zone and peaks to -2.7 MPa then increasing progressively to zero.

Looking at the shear stress distributions along the edge, the results are quite consistent. As mentioned before, the shear stress is distorted by the bending of the inclined timber member, resulting in different shape and peak values between right and left edge distributions. Those distortions are emphasized by an insufficient mesh refinement that is reflected in the wobbly shape of the curves, particularly on the inclined timber member side.

The figure 6.66 shows a graph of longitudinal strain distribution along the centre line of the composite surface, derived from the FE model.

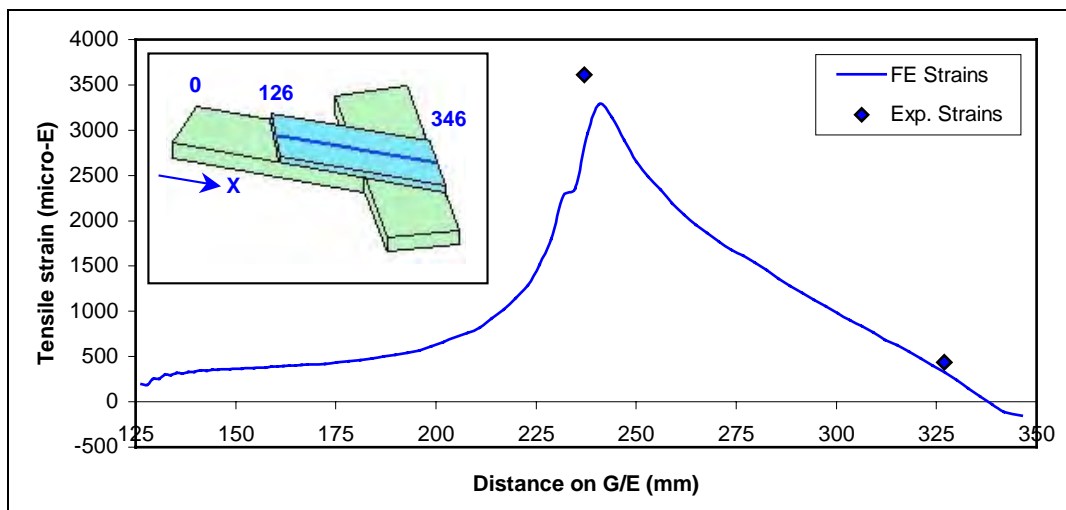


Figure 6.66 Longitudinal tensile strain distribution on glass fibre/epoxy surface.

Following a parabolic shape, the tensile strain distributions on the composite are progressive from the left end of the overlap ($x = 126$ mm) and peak in the gap zone. Then the strain reduces gradually to zero, across the inclined timber member. The experimental strain results are also plotted in figure 6.66 and are slightly higher than the FE results, mainly in the gap zone.

The tensile strain results derived by the FE model and measured experimentally are presented in table 6.9.

Sample	Longitudinal			Transverse
	End SG x = 327 mm	Gap SG x = 237 mm	Side SG x = 256 mm	Gap SG x = 237 mm
5TNU60 - η	438	3613	3767	- 820
Solid72 FE model	465	3288	4329	- 503

Table 6.9 Comparison of strains results obtained from experiments and from the FE model.

Strain gauge positions are described in § 4.3.2.4. The results of tensile strains obtained from the FE model are higher than those measured in experiments for the end and side strain gauges. For the longitudinal and transverse strain in the gap zone the FE results are lower.

6.3.4.2.2. Configuration with biaxial fibres TNB60

The characteristics of the 3D model are as follow:

File name:	Am06-solid72
Materials number:	3 - Anisotropic
Element type:	Solid72 - 3D Structural solid with rotations
Element description:	4 nodes tetrahedral solid element
Analysis type:	Static - Linear
Loading:	18 kN in tension
Number of Elements:	28932
Number of Nodes:	6753

The linear element type SOLID72 is already described in § 6.3.3.1.2. This element was used for this model for the reasons described in the previous section.

Full details for the FE model are available in Appendix D.4.

The graphical results are presented in figure 6.67.

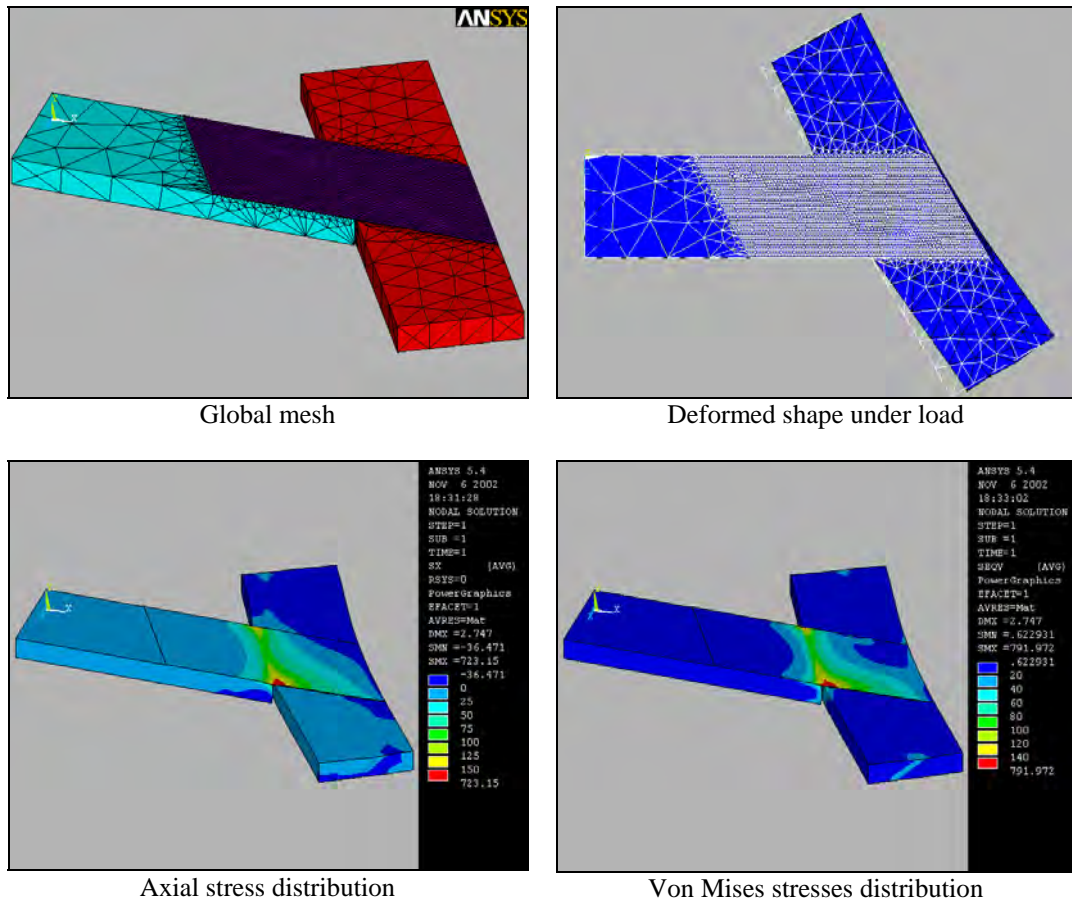
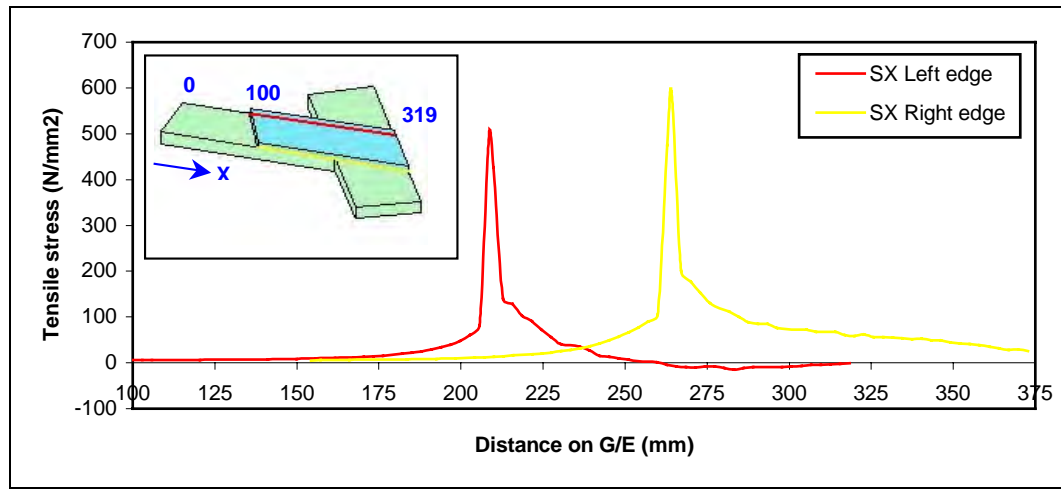


Figure 6.67 Graphical results of the 3D model type TNB60.

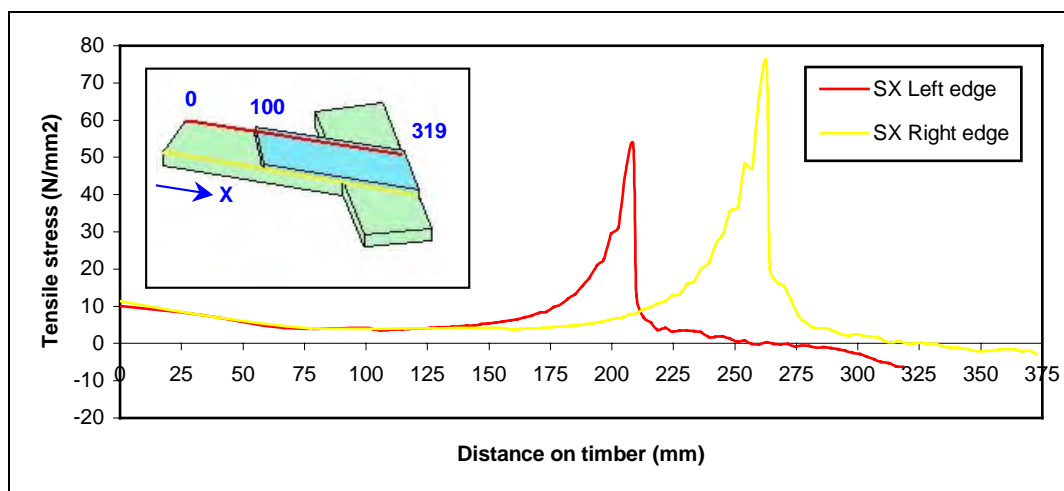
On the model shown in figure 6.67, the mesh geometry is identical to the one used for the TNU60 model. The deformed shape is viewed from the top and shows the deflection of the inclined timber member. This member is simply supported at both ends and is bending under the tension load applied through the composite layer.

On this model as well, the bending of the inclined timber member induces an eccentricity of the stresses. As a result, the tension load that is applied axially moves out of plane while the inclined member deflects.

The FE results of axial and shear stress distributions at the interface between the composite and the timber are presented in the following graphs in figures 6.68 and 6.69, and are given along the two edges of the joint.



Tensile stress distribution on glass fibre/epoxy interface



Tensile stress distribution on timber interface

Figure 6.68 Tensile stress distributions at the interface between the composite and the timber.

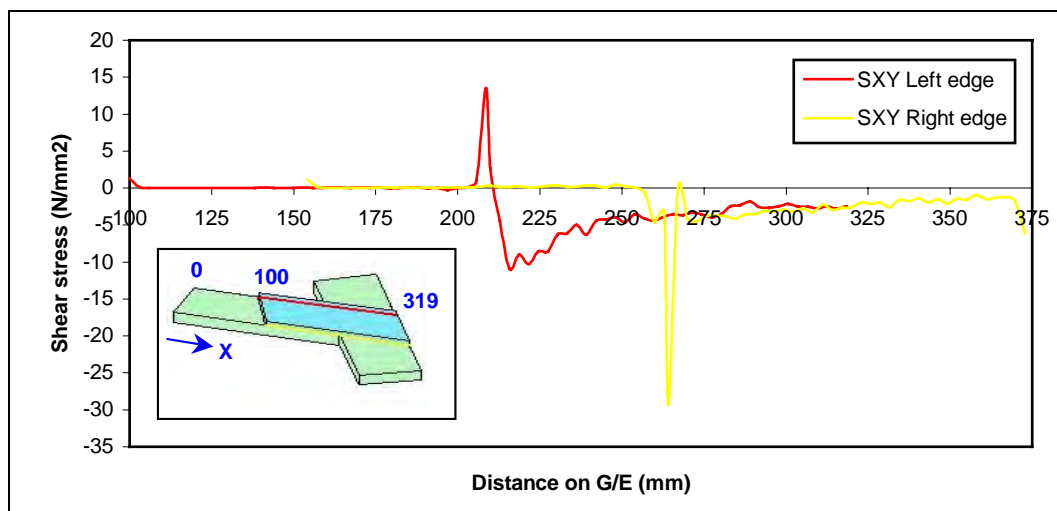
The tensile stress distribution in the composite interface has the same shape along the left and right edges, but the peak value is higher on the right than on the left edge.

The tensile stress along the left and right edges rise progressively to 80 and 105 MPa, peaks to 500 and 590 MPa in the gap zone and drops to 140 and 200 MPa respectively. Then the stress reduces progressively across the inclined timber member.

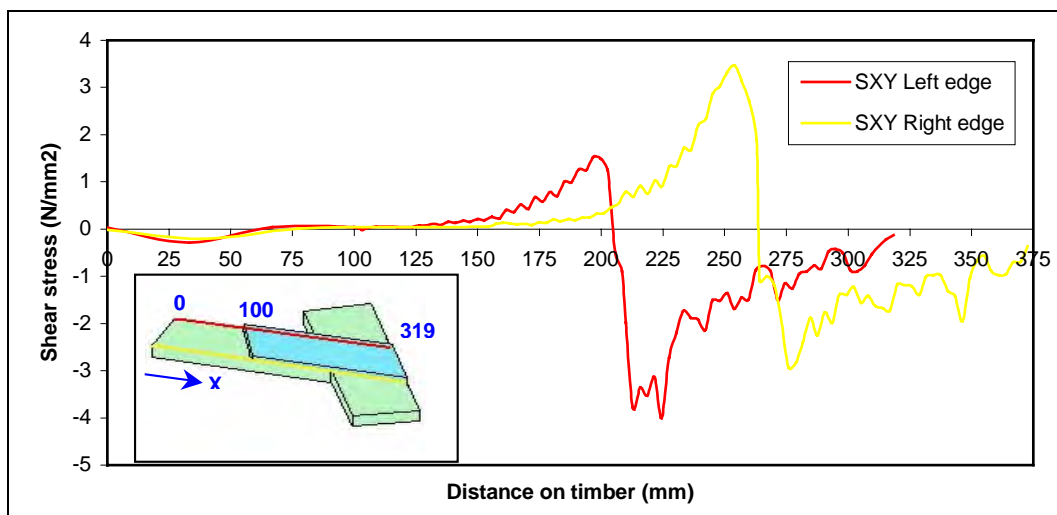
The tensile stress distribution in the timber interface has also a similar shape along the left or right edges and reaches a higher peak on the right edge than on the left edge. The tensile stress along the left and right edges rise progressively following a parabolic curve to 55 and 75 MPa in the gap zone and drops abruptly to 10 and 15 MPa respectively. Then the stress reduces progressively across the inclined timber member and becomes compressive towards the end to -6 and -3 MPa respectively.

As previously mentioned, the tensile stress distributions appear to be accurate, except in the gap zone: Peak stress values are probably over-estimated due to insufficient mesh refinement in that high stress zone. However peak stresses at both ends of the gap zone are expected to be high because of the bending effect of the inclined timber member under the tension load. Peak stresses along the right and left edges are certainly much higher than along the centre line.

The shear stress distributions calculated by the FE model at the interface between the composite and the timber are presented in figure 6.69.



Shear stress distribution on glass fibre/epoxy interface



Shear stress distribution on timber interface

Figure 6.69 Shear stress distributions at the interface between the composite and the timber.

As for the previous model, the shear stress distributions are very different in terms of shape and intensity.

For the composite, the shear stress along the left edge peaks to 13.5 MPa in the gap zone and drops to -11 MPa then progressively increases to -2.5 MPa. Along the right edge, the shear stress drops abruptly in the gap zone to -30 MPa, increases to zero and down to -4 MPa. Then the shear stress increases progressively and steeply decreases to -6 MPa at the end.

For the timber, the shear stress along the left edge rises progressively to 1.5 MPa in the gap zone and peaks to -4 MPa then increasing progressively to zero. Along the right edge, the shear stress rises progressively to 3.5 MPa in the gap zone and peaks to -3 MPa then increasing progressively to zero.

The results of shear stress distributions are fairly consistent. As mentioned before, the distortion of shear stress is induced by the bending of the inclined timber member, resulting in different right and left edge distributions in terms of shape and peak values. Those distortions are accentuated by a coarse mesh size of finite elements that is reflected in the wobbly shape of the curves, particularly on the inclined timber member side.

The figure 6.70 shows a graph of longitudinal strain distribution along the centre line of the composite surface, derived from the FE model.

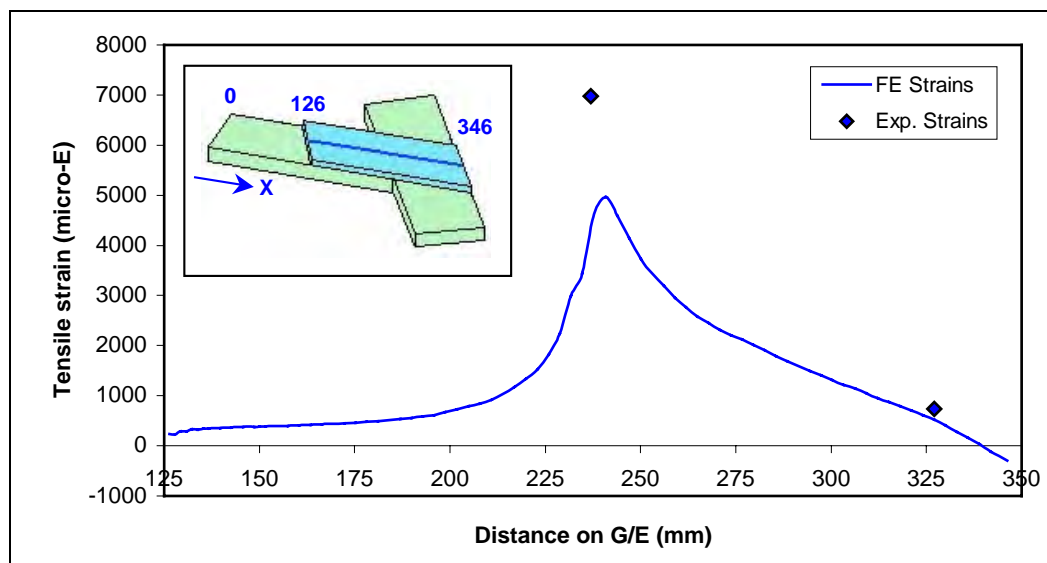


Figure 6.70 Longitudinal tensile strain distribution on glass fibre/epoxy surface.

Following a parabolic shape, the tensile strain distributions on the composite are progressive from the left end of the overlap ($x = 126$ mm) and peak in the gap zone. Then the strain reduces gradually to zero, across the inclined timber member. The experimental strain results are also plotted in figure 6.70 and are much higher than the FE results in the gap zone.

The tensile strain results derived by the FE model and measured experimentally are presented in table 6.10.

Sample	Longitudinal			Transverse
	End SG $x = 327$ mm	Gap SG $x = 237$ mm	Side SG $x = 256$ mm	Gap SG $x = 237$ mm
5TNB60 - W	731	6981	6364	- 466
Solid72 FE model	679	4966	6095	- 368

Table 6.10 Comparison of strains results obtained from experiments and from the FE model.

Strain gauge positions are described in § 4.3.2.4. The results of tensile strains obtained from the FE model are lower than those measured in experiments. This could be due to experimental errors or it could be the thickness of the composite layer that is slightly too thin. A slight change of thickness of the composite would affect the results significantly.

6.3.4.3. Load applied with an angle of 30 degrees to the grain

The two models presented in this section were generated in 3D respectively, with the 30° configurations. The glass fibres are unidirectional and bidirectional respectively. The thickness of the composite corresponds to the measured thickness of 0.65 mm.

6.3.4.3.1. Configuration with uniaxial fibres TNU30

The characteristics of the 3D model are as follow:

File name:	Am07-solid72
Materials number:	3 - Anisotropic
Element type:	Solid72 - 3D Structural solid with rotations
Element description:	4 nodes tetrahedral solid element
Analysis type:	Static - Linear
Loading:	18 kN in tension
Number of Elements:	67687
Number of Nodes:	15253

The linear element type SOLID72 is already described in § 6.3.3.1.2. This element was used for this model because of the large number of elements that was required to generate an adequate mesh. The more accurate quadratic element SOLID92 required too much computer time to reach the solution.

Full details for the FE model (geometry, material properties, boundary assumptions, etc) are available in Appendix D.5.

The graphical results are presented in figure 6.71.

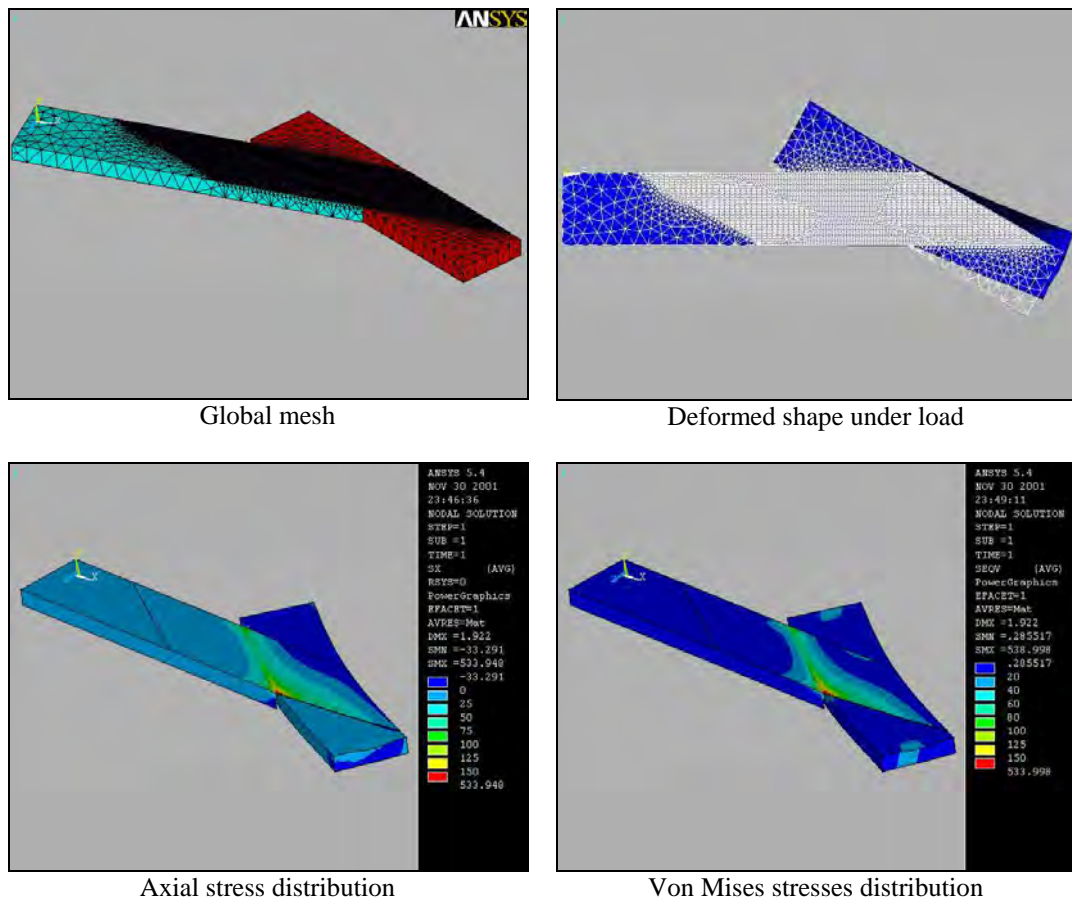


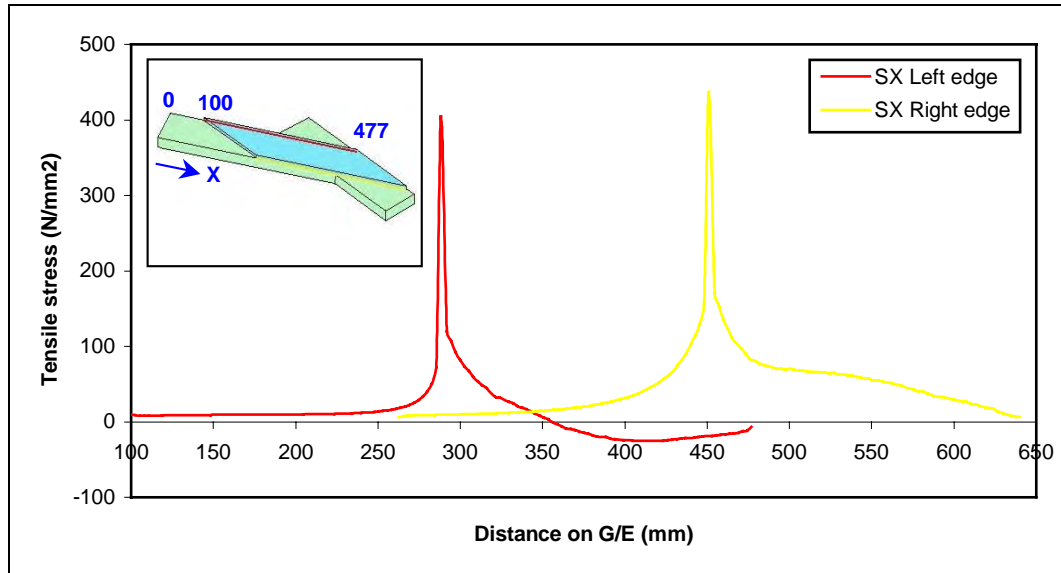
Figure 6.71 Graphical results of the 3D model type TNU30.

On the model shown in figure 6.71, the meshing follows the same geometry as used on the previous 3D models: Dense in the glass fibre/epoxy composite layer, becoming progressively coarser as it reaches the plane of symmetry of the timber members.

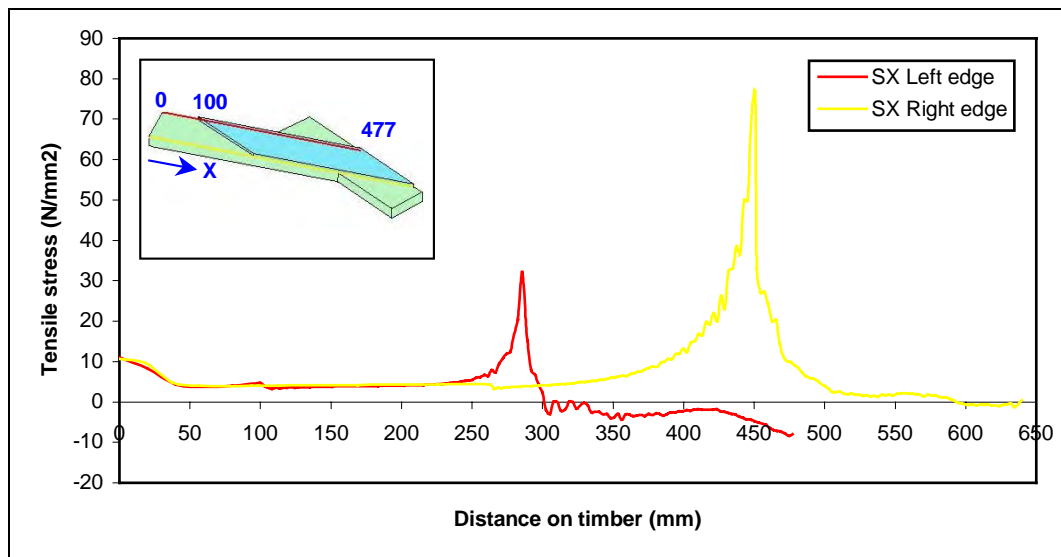
The deformed shape is viewed from the top and shows the simply supported inclined timber member deflecting under the tension load applied through the composite layer.

The graphical results of axial stress and Von Mises stress distributions show that the bending of the inclined timber member induces a significant eccentricity of the stresses. The stresses are therefore higher along the edges of the composite than along the centre line and particularly along the right edge (bottom edge of the composite layer in figure 6.71).

The FE results of axial and shear stress distributions at the interface between the composite and the timber are presented in the following graphs in figures 6.72 and 6.73, and are given along the two edges of the joint.



Tensile stress distribution on glass fibre/epoxy interface



Tensile stress distribution on timber interface

Figure 6.72 Tensile stress distributions at the interface between the composite and the timber.

The tensile stress distribution in the composite interface has the same shape but different amplitude whether it is along the left or right edges.

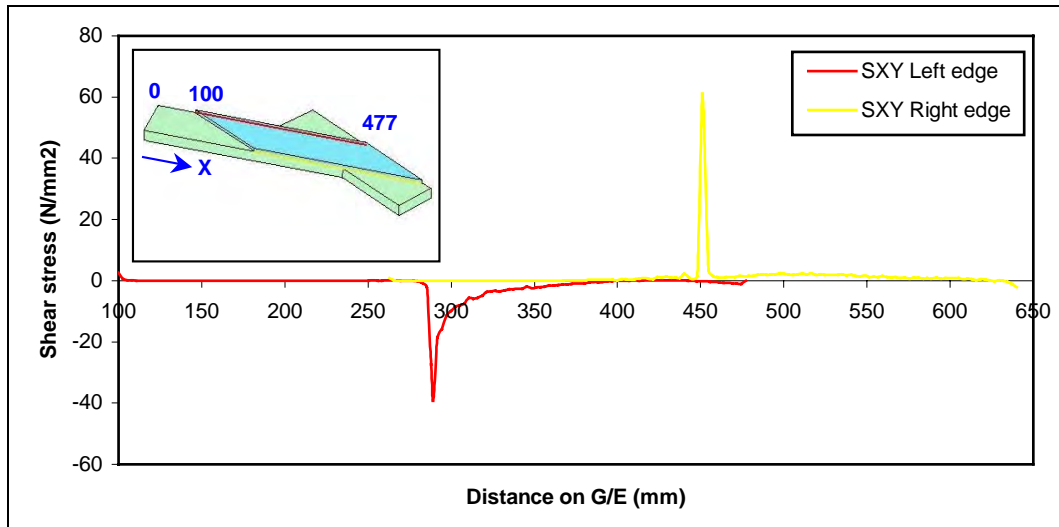
The tensile stress along the left and right edges rise following a parabolic curve to 400 and 435 MPa in the gap zone and drops to 120 and 170 MPa respectively. Then the stress reduces progressively across the inclined timber member to around 7 MPa

along the right edge, and becomes compressive to -25 MPa then reduces towards the end to -7 MPa along the left edge.

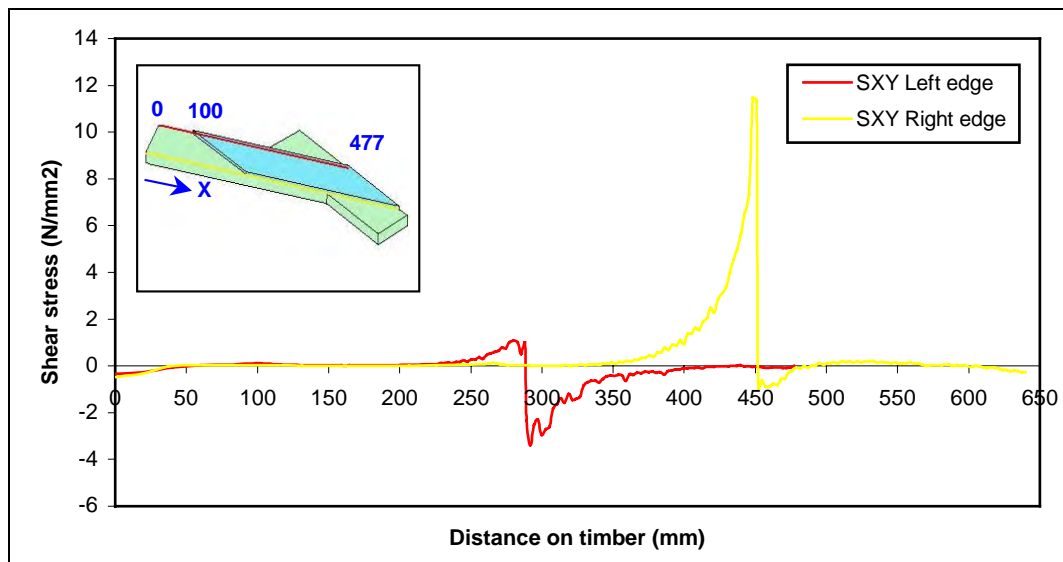
The tensile stress distribution in the timber interface has also a similar shape along the left or right edges, but reach a higher peak on the right edge than on the left edge. The tensile stress along the left edge rises progressively following a parabolic curve from 4 MPa to 32 MPa in the gap zone and drops steeply to -3 MPa. Then the stress fluctuates in compressive zone across the inclined timber member and reaches -8 MPa at the end. The tensile stress along the right edge follows the same shape, rising progressively from 4 MPa to 76 MPa in the gap zone and decreases progressively to zero.

As notified on previous models, tensile stress distributions seem to be relatively accurate in terms of shape but the peak values that occur in the gap zone are certainly over-estimated. Whether this is due to insufficient mesh refinement, peak stresses at both ends of the gap zone are expected to be much higher than along the centre line.

The shear stress distributions calculated by the FE model at the interface between the composite and the timber are presented in figure 6.73.



Shear stress distribution on glass fibre/epoxy interface



Shear stress distribution on timber interface

Figure 6.73 Shear stress distributions at the interface between the composite and the timber.

For the composite, the shear stress along the left edge peaks to -40 MPa in the gap zone and then progressively increases to zero. Along the right edge, the shear stress peaks to 60 MPa in the gap zone and then progressively reduces to zero.

For the timber, the shear stress along the left edge rises progressively from nearly zero to 1 MPa in the gap zone and peaks to -3.5 MPa then increasing progressively to zero. Along the right edge, the shear stress rises progressively from nearly zero to 11.5 MPa in the gap zone and peaks to -1 MPa then increasing progressively to zero.

For the shear stress distributions along the edge, the results are relatively consistent in terms of shape. As mentioned before, the shear stress is distorted by the bending of the inclined timber member, and those distortions are visible on the graphs: The amplitude of shear stress is higher along the right edge than along the left edge, particularly in the gap zone.

The figure 6.74 shows a graph of longitudinal strain distribution along the centre line composite surface, derived from the FE model.

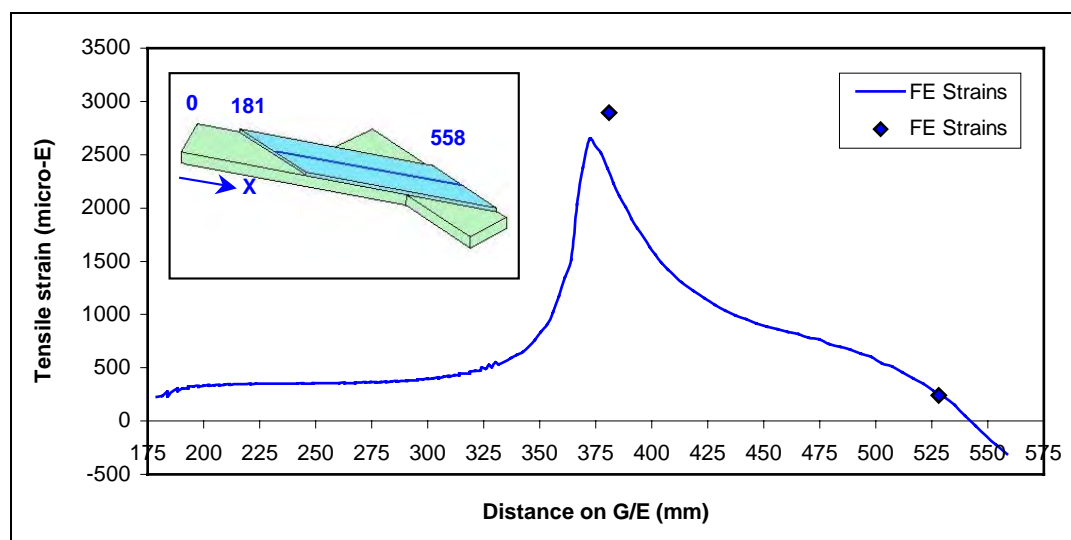


Figure 6.74 Longitudinal tensile strain distribution on glass fibre/epoxy surface.

Following a parabolic shape, the tensile strain distributions on the composite are progressive from the left end of the overlap ($x = 181$ mm) and peak in the gap zone. Then the strain reduces gradually to zero, across the inclined timber member. The experimental strain results are also plotted in figure 6.74 and are slightly higher than the FE results in the gap zone.

The tensile strain results derived by the FE model and measured experimentally are presented in table 6.11.

Sample	Longitudinal			Transverse
	End SG x = 528 mm	Gap SG x = 381 mm	Side SG x = 437 mm	Gap SG x = 381 mm
1TNU30 - V	239	2893	3274	- 1315
Solid72 FE model	227	2643	3831	- 1587

Table 6.11 Comparison of strains results obtained from experiments and from the FE model.

Strain gauge positions are described in § 4.3.2.5. The results of tensile strains obtained from the FE model are lower than those measured in experiments except for the longitudinal side strain gauge. This could be due to experimental errors or it could be the thickness of the composite layer that is slightly thinner than the one modelled.

6.3.4.3.2. Configuration with biaxial fibres TNB30

The characteristics of the 3D model are as follow:

File name:	Am08-solid72
Materials number:	3 - Anisotropic
Element type:	Solid72 - 3D Structural solid with rotations
Element description:	4 nodes tetrahedral solid element
Analysis type:	Static - Linear
Loading:	18 kN in tension
Number of Elements:	67687
Number of Nodes:	15253

The linear element type SOLID72 is already described in § 6.3.3.1.2. As for the previous model, this element was used because of the large number of elements that was required to generate an adequate mesh. The more accurate quadratic element SOLID92 required too much computer time to reach the solution.

Full details for the FE model are available in Appendix D.5.

The graphical results are presented in figure 6.75.

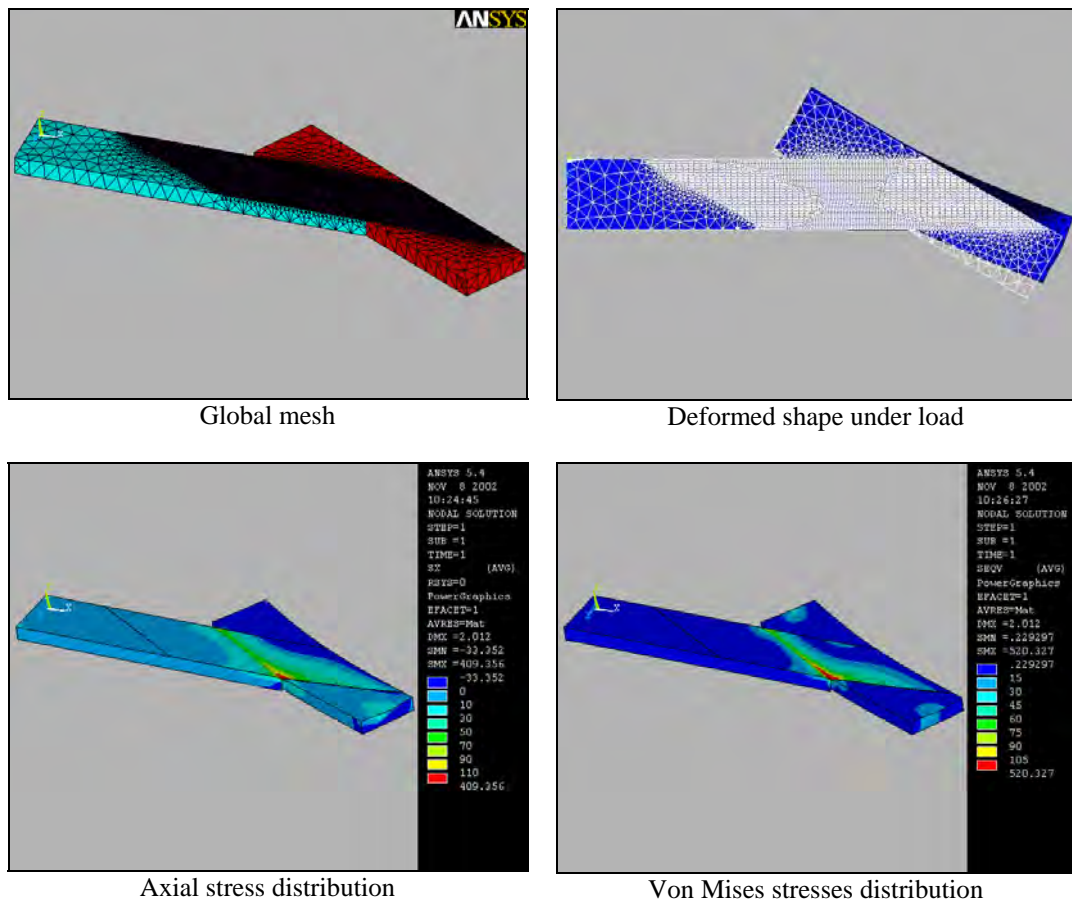


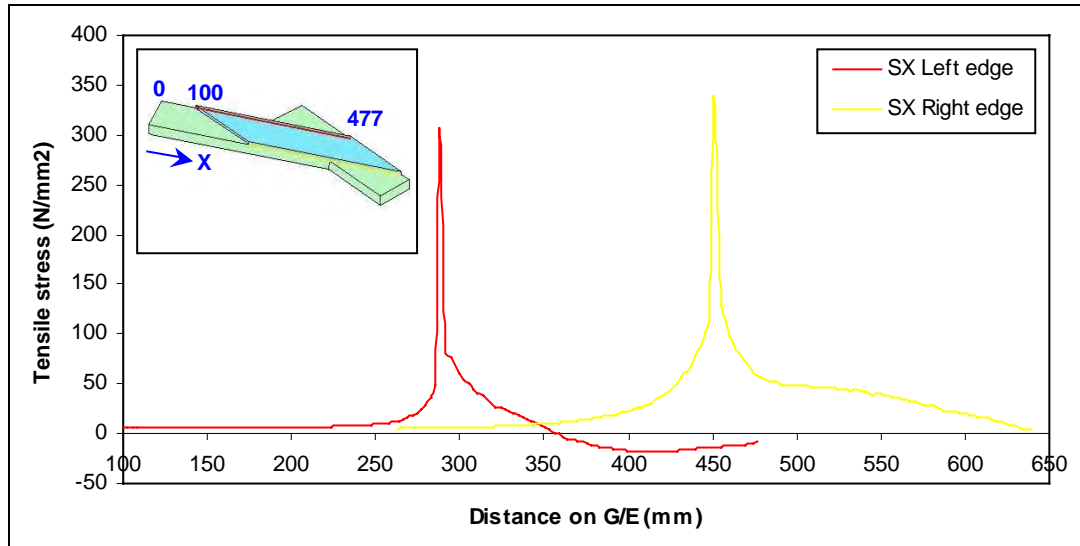
Figure 6.75 Graphical results of the 3D model type TNB30.

On the model shown in figure 6.75, the meshing follows the same geometry as used on the previous 3D models: Dense in the glass fibre/epoxy composite layer, becoming progressively coarser as it reaches the plane of symmetry of the timber members.

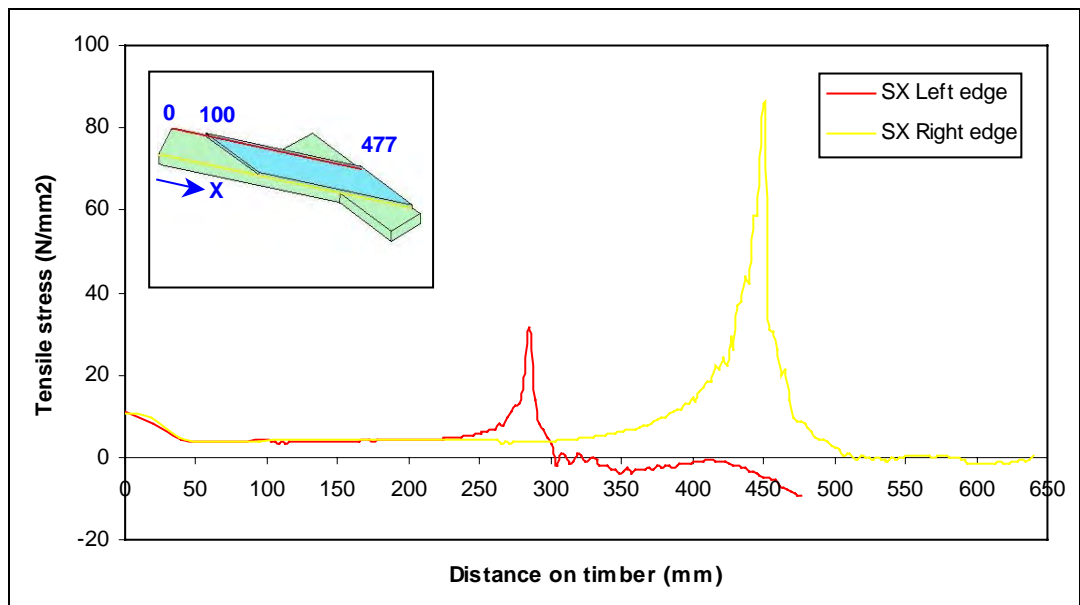
The deformed shape is viewed from the top and shows the simply supported inclined timber member deflecting under the tension load applied through the composite layer.

The axial and Von Mises stresses are higher along the edges of the composite than along the centre line and particularly along the right edge (bottom edge of the composite layer in figure 6.75). This is due to the bending of the inclined timber member that induces a significant eccentricity of the stresses.

The FE results of axial and shear stress distributions at the interface between the composite and the timber are presented in the following graphs in figures 6.76 and 6.77, and are given along the two edges of the joint.



Tensile stress distribution on glass fibre/epoxy interface



Tensile stress distribution on timber interface

Figure 6.76 Tensile stress distributions at the interface between the composite and the timber.

The tensile stress distribution in the composite interface has the same shape and intensity whether it is along the left or right edges.

The tensile stress along the left and right edges rise to 305 and 340 MPa in the gap zone and drops to 85 and 130 MPa respectively. Then the stress reduces progressively across the inclined timber member to 4 MPa for the right edge,

becomes compressive to -18 MPa then reduces towards the end to -7 MPa for the left edge.

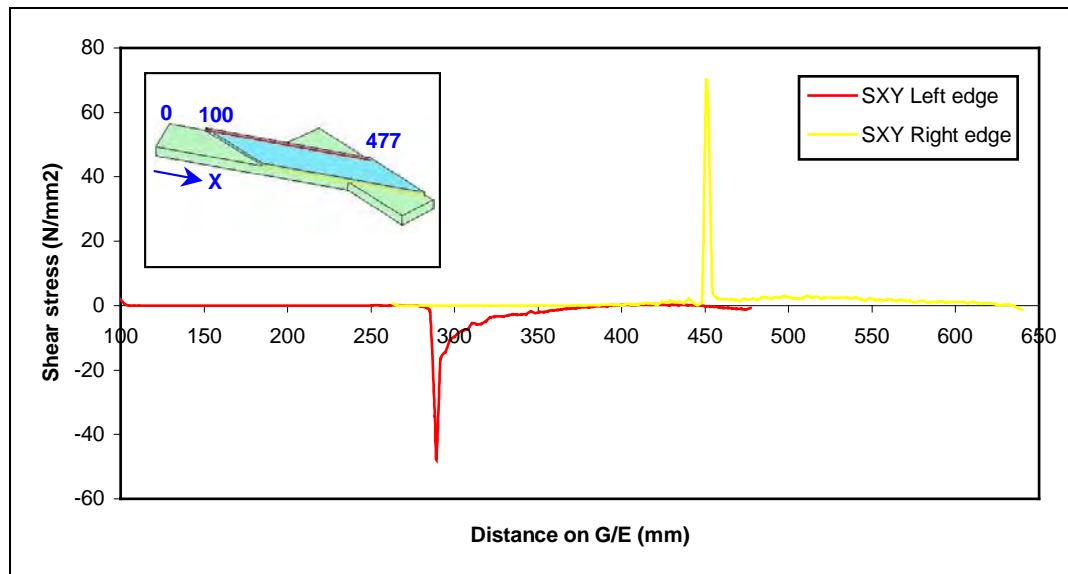
The tensile stress distribution in the timber interface has also a similar shape along the both edges, but reach a much higher peak on the right edge than on the left edge.

The tensile stress along the left edge rises progressively following a parabolic curve to 31 MPa in the gap zone and drops steeply to -2 MPa. Then the stress fluctuates in compression across the inclined timber member and reaches -9 MPa at the end.

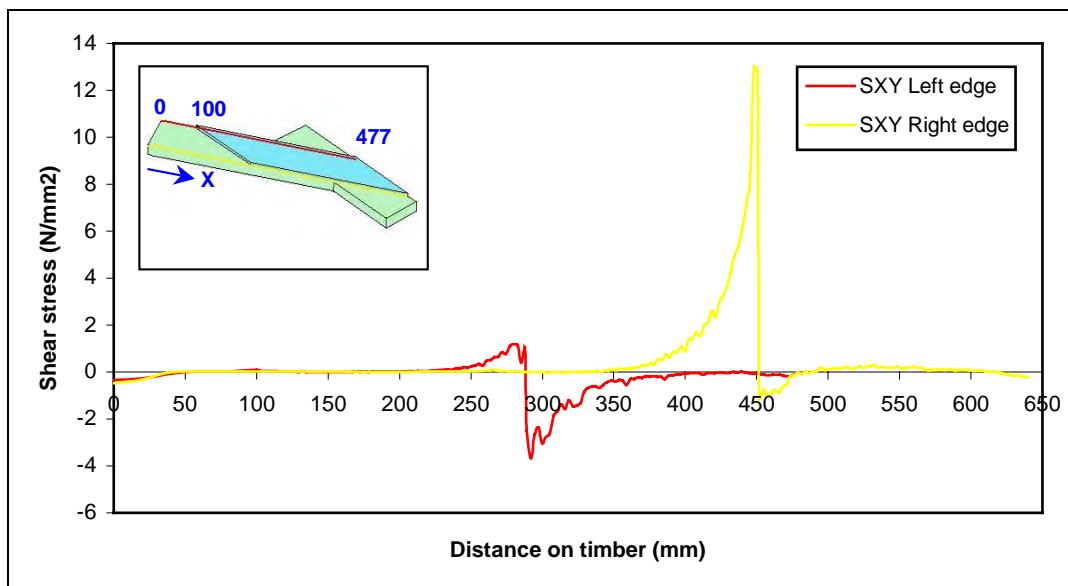
The tensile stress along the right edge follow the same shape, rising progressively to 86 MPa in the gap zone and reduces gradually to zero.

As mentioned before, tensile stress distributions seem to be relatively accurate in terms of shape but the peak values that occur in the gap zone are certainly over-estimated. This is probably due to insufficient mesh refinement. However the peak stresses at both ends of the gap zone are expected to be relatively high and certainly much higher than at the centre line. This is due to the bending effect of the inclined timber member.

The shear stress distributions calculated by the FE model at the interface between the composite and the timber are presented in figure 6.77.



Shear stress distribution on glass fibre/epoxy interface



Shear stress distribution on timber interface

Figure 6.77 Shear stress distributions at the interface between the composite and the timber.

At the composite interface, the shear stress along the left edge peaks to -47 MPa in the gap zone and then progressively increases to zero. Along the right edge, the shear stress peaks to 70 MPa in the gap zone and then progressively reduces to zero.

For the timber interface, the shear stress along the left edge rises progressively from nearly zero to 1.1 MPa in the gap zone and peaks to -3.7 MPa then increasing progressively to zero. Along the right edge, the shear stress rises progressively from

nearly zero to 13 MPa in the gap zone and peaks to -1.1 MPa then increasing progressively to zero.

For the shear stress distributions along the edge, the results are relatively consistent in terms of shape. As mentioned before, the shear stress is distorted by the bending of the inclined timber member therefore the amplitude of shear stress is higher along the right edge than along the left edge, particularly in the gap zone.

The figure 6.78 shows a graph of longitudinal strain distribution along the centre line composite surface, derived from the FE model.

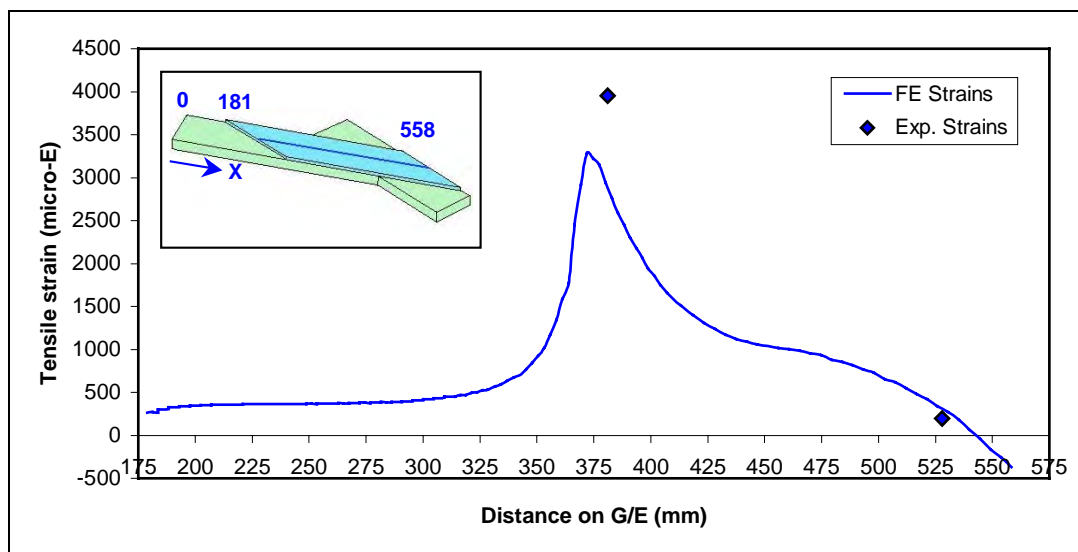


Figure 6.78 Longitudinal tensile strain distribution on glass fibre/epoxy surface.

Following a parabolic shape, the tensile strain distributions on the composite are progressive from the left end of the overlap ($x = 181$ mm) and peak in the gap zone. Then the strain reduces gradually to zero, across the inclined timber member. The experimental strain results are also plotted in figure 6.78 and are much higher than the FE results in the gap zone.

The tensile strain results derived by the FE model and measured experimentally are presented in table 6.12.

Sample	Longitudinal			Transverse
	End SG x = 528 mm	Gap SG x = 381 mm	Side SG x = 437 mm	Gap SG x = 381 mm
1TNB30 - U	197	3956	3666	- 1603
Solid72 FE model	264	3280	4496	- 1381

Table 6.12 Comparison of strains results obtained from experiments and from the FE model.

Strain gauge positions are described in § 4.3.2.5. The results of tensile strains obtained from the FE model are higher than those measured in experiments except for the longitudinal gap strain gauge. As previously mentioned, it could be due to experimental errors or with the thickness of the composite layer.

The experimental measurement of internal bending effects of the overlap carried out to confirm the results obtained from FE models are presented in § 6.4.

6.4. Internal bending effects

All the FE models presented throughout this chapter displayed to some extent internal bending of the composite overlap in the gap region. Less significant bending effects were also observed at the free ends of each composite overlap.

The stress and strain distributions in the load transfer of most FE models were so affected by the internal bending effects of the outer adherends that experimental verification was necessary. It was then decided to load one of the spare wood/glass/epoxy joints in order to measure the internal bending effects of the outer adherends in the gap zone. One sample type TPU00 was used for this experiment and was positioned in the J.J. Lloyds machine ready for the test. Using a micrometer, the thickness of the sample was measured across the joint in the gap zone at various tension loads, in order to establish the lateral deformation defined as $\Delta\omega$ on figure 6.79.

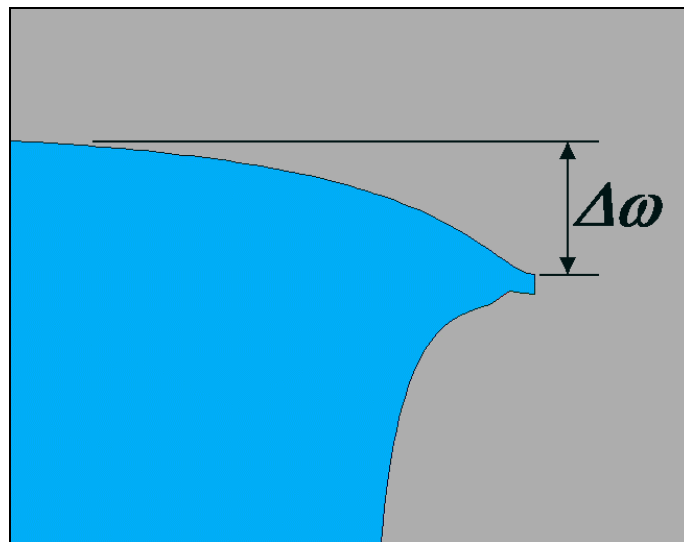


Figure 6.79 Deformed shape with lateral deformation $\Delta\omega$ of the 2D FE model type TPU00.

Figure 6.79 indicates the location of the lateral deformation $\Delta\omega$ on the deformed shape of the 2D FE model type TPU00. This FE model was presented in § 6.3.3.1.1. The lateral deformation $\Delta\omega$ was measured at four different positions along the gap zone of the joint. The values of $\Delta\omega$ presented in table 6.13 are average values from those positions for each given load.

In table 6.13, the lateral deformation $\Delta\omega$ obtained experimentally and from the 2D FE model type TPU00 are presented. These values are given for various tension loads.

Load (kN)	Average $\Delta\omega$ measured experimentally (mm)	$\Delta\omega$ calculated from 2D FE model type TPU00 (mm)
0	0	0
5	-0.02	-0.02245
10	-0.045	-0.0449
18	-0.085	-0.08

Table 6.13 Comparison of lateral deformation $\Delta\omega$ obtained from experiments and from 2D FE model type TPU00.

The lateral deformations $\Delta\omega$ measured experimentally appear to be very similar to those obtained from the FE model. This clearly indicates that the internal bending effects of the outer adherends, which are the glass fibre/epoxy composite layers, have an important role in the load transfer process. This phenomenon seems to be very well simulated by the FE models. It confirms how relevant finite element modelling was in the assessment and understanding of the structural behaviour of wood/glass/epoxy joints.

Finally the internal bending effects observed in the FE models of wood/glass/epoxy joints are the result of the lateral deformation of the inner adherend. With the outer adherend being loaded intension, the inner adherend that has much lower mechanical properties, is subject to larger thickness deformation due to significant Poisson's ratio effect. The outer adherend is therefore bending near the gap: Tensile and compressive stresses can be observed through the composite layer, alternatively at its interface with the timber and at its surface. Those effects were highlighted through most FE models.

All the results derived from the FE analysis and presented in this chapter are finally discussed in the following section.

6.5. Discussion and conclusion

Considering the straight joint configurations TPU00 and TPB00, both 2D and 3D models were developed.

The 2D models were generated based on a convergence testing that was carried out in order to establish how refined the meshing needed to be to generate an accurate solution. But with 2D models, the stress variations across the width of the joint could not be identified, therefore 3D model were necessary.

The development of 3D model was even more restrictive. With straight or angle joint configurations, the geometry only allowed tetrahedral meshing, hexahedron elements could be used but they always exceeded their aspect ratio limits. Another obstacle was that convergence testing could not be carried out: Only a few meshing configurations could be used without generating errors, and the number of elements was limited by the solution time and computer memory capacity.

Nevertheless, all the 3D models that are presented in this chapter produced some solutions without errors or warnings. The accuracy of these solutions must be examined carefully, particularly in the high stress regions where the meshes are often not sufficiently refined.

The comparison between the 2D and the 3D models developed for the TPU00 and TPB00 configurations are a good start for identifying the accuracy of the results.

Looking at the maximum tensile stresses observed at the composite interface, the results are:

- For the TPU00 configuration, the 2D model give 305 MPa and the 3D model 350 MPa,
- For the TPB00 configuration, the 2D model give 275 MPa and the 3D model 305 MPa,

The results are relatively close, with a slight over-estimation from the 3D models.

The same comparison can be made for the maximum tensile stresses observed at the timber interface:

- For the TPU00 configuration, the 2D model gives 90 MPa and the 3D model 45 MPa,
- For the TPB00 configuration, the 2D model gives 105 MPa and the 3D model 55 MPa.

In this case, the results are very different. In fact the 3D models peak results are only approximately half the 2D models results.

Similar disparities in results can be observed comparing the maximum shear results from both 2D and 3D models. In other words, the 2D models generally show higher results of maximum shear and tensile stresses in the timber, and lower results of maximum shear and tensile stresses in the composite than 3D models.

3D models would normally generate more accurate results than 2D models because they take into account edge effects and stress variations through the third dimension. But surprisingly in this FE analysis, the 2D models generate more accurate solutions (particularly in high stress regions) than 3D models mainly because convergence testing was preliminarily carried out. It is clear that the results obtained from the 3D models tend to over-estimate the stresses in the composite and under-estimate the stresses in the timber. Those considerations need to be taken into account in the analysis of the results obtained from the 3D models, particularly for the joints with load not parallel to the grain, because of the lack of convergence testing as explained before. Another argument is that displacements (i.e. strains solutions) usually converged more rapidly than stresses, in finite element analysis.

The FE results of strains are relatively consistent with those obtained from the tests. They are very close as far as the joints made of unidirectional glass fibre are concerned. However the FE results are generally lower than those measured for the joints made of bidirectional glass fibre. There might be different reasons for that:

- The thickness of the bidirectional glass fibre could well be slightly thicker than 0.65 mm. The stitching threads were ignored when the glass fabric thickness measurement was carried out. The threads have no mechanical purposes, they are just keeping the fibres in position. In other words, they thickened the composite locally up to 0.75 mm. Therefore the average composite thickness could well be around 0.7 mm.

- The material properties of the glass fibre/epoxy composite could be over-estimated. In fact the fibre volume fractions (FVF) measured on the samples were slightly lower than those given for the mechanical properties that were used in the FE analysis.

Finally, it is clear that for the joints with load not parallel to the grain, the bending of the inclined timber member under load affects the results. However, there was also a slight eccentricity of the load during the experiments, but it was not that pronounced: The rig was made in order to always keep the sample in-line with the load. (i.e. by rotation of the pins that were holding the frame).

Nevertheless the interpretation of the results shows some relevant findings:

- The peak tensile stress in the timber interface appears to decrease with the angle of load to the grain. This is due to the tension strength of the timber that is high when parallel to the grain (low tensile stress) and low when perpendicular to the grain (high tensile stress).
- Alternatively the peak tensile stress in the composite interface appears to increase with the angle of load to the grain.
- The results of shear stresses are more difficult to analyse, as they are often inconsistent, mainly because of the bending of the inclined timber member.

As a conclusion, the FE analysis confirmed the non-uniform load transfer that occur on double lap joints, such as the wood/glass/epoxy joints that were tested in this research. However the distribution of shear stress at the interface between the composite and the timber is fairly different in terms of shape and range than those observed on CFRP joints presented in § 6.2.3. In fact the thickness of the composite layer (outer adherend) is so thin compared to the timber member (inner adherend) that the distribution of shear along the interface reach its maximum in the gap zone of the joint. At the end of the overlap, the shear always peaks but never exceeds the value in the gap zone. This is significantly different than for the joints presented in § 6.2.3, where the shear stress tend to peak at the end of the overlap. The reasons for that are:

- The two adherends on the wood/glass/epoxy joints are significantly different in terms of cross-sections: The inner adherend (the timber) cross-section is nearly 34 times larger than the outer adherend cross-section. The mechanical properties of the timber are lower than those of the composite, but with a lower multiplying factor. As a result the distribution of stresses can be more dispersed through the timber than through the composite.
- The inertia of the composite “plate” is very low because of its thin thickness. The plate is therefore very sensitive to the internal bending generated by the double-lap joint. For the joints presented in § 6.2.3, internal bending of the outer adherend were ignored in the analysis, as well as the stress variations through the thickness of the adherends. The FE models take those behaviours into account, which cause the peaks of stresses observed in the gap region.

The following chapter investigates another characteristic of the wood/glass/epoxy joint, which is essential to enable the use and design of this type of joint: The capacity of the wood/glass/epoxy joint to resist cyclic loading, in other words, its fatigue resistance.

CHAPTER 7

FATIGUE ASSESSMENT OF WOOD/GLASS/EPOXY JOINTS

7.1. Introduction

Wood/glass/epoxy joints were tested and analysed in static tension tests. The joints were loaded to failure at a specific rate in order to assess their strength and stiffness. However the strength of structural joints also depends on other factors.

For example, a structural joint can be efficient and suitable to connect members, but it may not have the capacity to withstand the load more than for a period of time. In other words, material strength can be affected by the load duration: This is known as creep, when the deformation increases with time under a constant load. Wood is subject to creep because of its viscoelastic response under load. The rate of creep in wood is influenced by the load duration, the moisture content, the temperature and the level of stress. Nevertheless creep contributes to affect the strength of wood. There are other parameters that can change the strength of a structural joint. One of them is considered as extremely important in order to validate the design potential of a structural joint: This parameter is known as the fatigue resistance. When a joint is subject to a number of varying stress cycles, its mechanical properties can be weakened and degraded. This phenomenon is identified as fatigue.

“It has been, estimated that at least 75% of all machine and structural failures have been caused by some form of fatigue” (Benham et al., 1996).

It is therefore essential to investigate the fatigue resistance of any material that will to be used for design purposes. As a result, it was decided to investigate the fatigue response of the wood/glass/epoxy joint before the research could be taken any further. In fact, a design method could not be developed for those adhesive joints without knowing whether their fatigue resistance is sufficient for their design life.

In this chapter, the experimental programme and the results are presented, including a detailed literature review used as background information for the results. In other words, a comprehensive assessment of the fatigue resistance of the wood/glass/epoxy joint is presented.

7.2. Fatigue test programme

7.2.1. Methodology

To investigate the fatigue response of wood/glass/epoxy joint, the cyclic pattern of stress has to be established. It is essential to highlight that fatigue failure of material occurs while the material is exposed to cyclic stress where the peak values are always lower than the material strength. Fatigue failure is a consequence of the progressive degradation of the material due to cyclic stresses that inevitably weakens its mechanical properties.

“Wooden structures are frequently subjected to dynamic loads, for example vehicle loads on factory floors and bridges and wind loads acting on timber roofs” (Ansell, Timber Engineering STEP 2, 1995).

Based on the potential use of wood/glass/epoxy joints for timber structures and particularly for timber trusses, it was decided that the joints would be loaded in order to simulate the fatigue behaviour of the connections under the effects of wind. In fact the wind is the appropriate dynamic load that could reasonably cause fatigue to the joints for building applications. To investigate the effects of dynamic loads on the joints under seismic conditions was not considered at this stage of the research.

To establish a realistic fatigue loading, the frequency of the loads has to be defined in order to simulate uplift or reversal load on the joints.

The wind is a dynamic load that acts on any structure with variable intensity in time. It has been monitored and studied for many years by the Meteorological Office in the U.K. and particularly by the Building Research Establishment, for the construction industry applications. Codes of practice such as CP3: Ch 5: Pt 2 “Code of basic data for design of buildings: Wind loads” and more recently BS6399: Pt 2 “Code of practice for wind loads” are the design standards for wind loading. The most relevant information was given in CP3: Ch 5: Pt 2, where the gust and wind speed averaging time are presented and developed in the codes appendix:

Maximum gust of the day and the mean hourly wind speed have been monitored for many years throughout the U.K using the network of anemograph stations. It was found that the maximum gust speed represents the mean wind speed averaged over about 3 seconds. Other research about the incidence and spread of gusts over a building suggested that the time interval over which maximum wind speeds should

be averaged will depend on the building size or part of the structure under consideration.

The standards adopted in CP3: Ch 5: Pt 2 are:

- The maximum 3-seconds gust speeds for all unit of glazing, cladding or roofing, whatever the size or portion of the building concerned,
- A wind speed with 5 seconds averaging time is used for the structural design of buildings or structures where neither the greatest horizontal nor vertical dimension exceed 50 m.
- For buildings or structures whose greatest horizontal or vertical dimension exceeds 50 m, a wind speed of 15 seconds averaging time is used.

The maximum 3-seconds gust duration is based on a 50 years design life, which corresponds to the average lifetime of most buildings according to the codes.

It was then decided to apply the 3-seconds loading period to the fatigue tests. In other words, the frequency proposed for the cyclic tests was:

$$N = \frac{1}{3} = 0.33Hz \quad (7.1)$$

With the frequency defined, it was then important to define the loading configuration in order to establish whether the load would be of varying amplitude, reversed, etc. Wood/glass/epoxy joints were analysed in tension only throughout this research, fatigue tests should then be carried out in tension only. To develop fatigue tests in compression could not be considered because static compression tests were not investigated. The results had to be interrelated with the research previously carried out.

The loading condition that simulates the effect of wind in a fatigue mode would be a loaded-unloaded cyclic pattern, where the minimum stress would correspond to 10% of the maximum stress. With this arrangement, the wood/glass/epoxy joint would remain in tension all the time. This cyclic pattern would have a “saw tooth” shape with constant amplitude, and the period would be of 3 seconds. It would be a similar loading pattern to the waveform shown in figure 7.1.

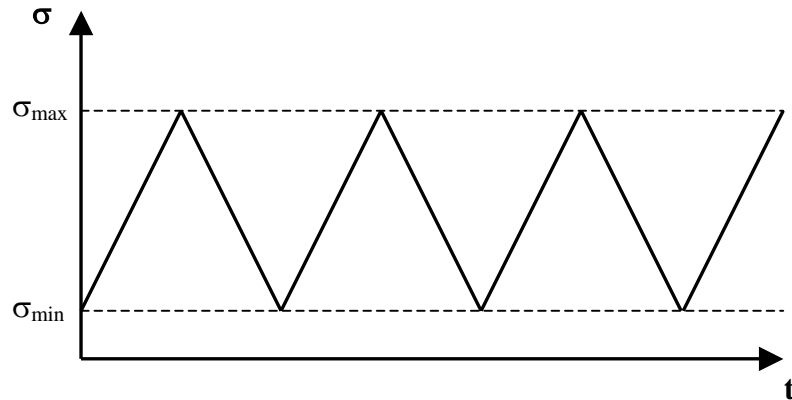


Figure 7.1 Typical saw tooth stress versus time waveform.

Sinusoidal or saw tooth stresses can be applied to fatigue test, but R ratios are the key to understand the loading mode, whether the test is in tension or compression only, or a combination of tension and compression. The R ratio is defined as:

$$R = \frac{\sigma_{\min}}{\sigma_{\max}} \quad (7.2)$$

Except for $R = 1$ that corresponds to static tension or static compression stress, the R ratios identify the fatigue loading mode:

$R = 1$ to 0	Tension-tension
$R = 0$ to -1	Tension-compression
$R = -1$ to $\pm\infty$	Compression-tension
$R = \pm\infty$ to -1	Compression-compression

As described previously, the minimum stress shall be equal to 10% of the maximum stress. As long as the tensile stress has a positive sign, the R ratio for that particular loading mode is equal to:

$$R = \frac{\sigma_{\min}}{\sigma_{\max}} = \frac{0.1 \times \sigma_{\max}}{\sigma_{\max}} = 0.1 \quad (7.3)$$

Stress-life (S-N) or strain-life (ϵ -N) curves are traditionally used to represent the fatigue life of any engineering materials. It is important to indicate for which R ratios the fatigue life is assessed. The S-N curves are usually plotted in a linear stress versus a logarithmic scale of the number of cycles. The S-N graph shown in figure 7.2 indicates wood fatigue curves for various R ratios.

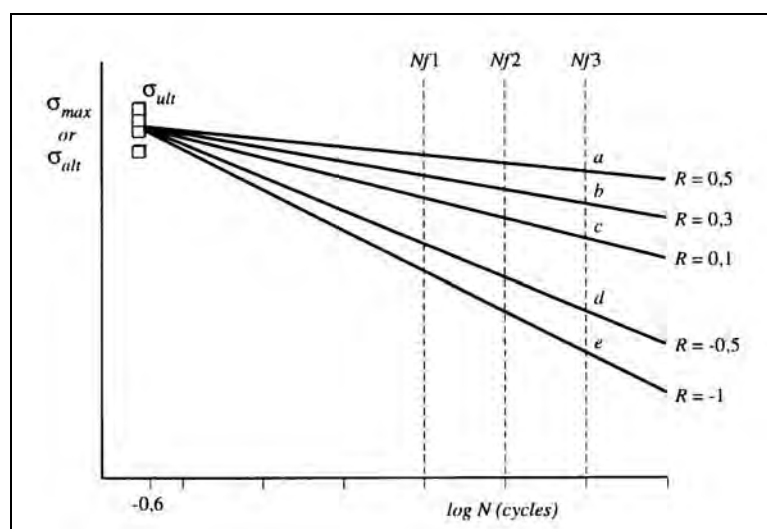


Figure 7.2 Set of σ -log N curves for tension-tension ($R = 0.1, 0.3$ and 0.5) and tension-compression ($R = -0.5$ and -1) cyclic stress configurations (Ansell, Timber Engineering STEP 2, 1995).

The ideal loading condition to simulate the effect of wind in a fatigue mode should have an R ratio equal to 0. But this is relatively difficult to achieve by adjusting the equipment to the exact minimum and maximum stresses, because of the frequency and the equipment used: The range of failure loads obtained for the wood/glass/epoxy joints tested in the static tension with load parallel to the grain was between 25 and 40 kN depending on glass fibres type and orientation.

A 3 seconds period corresponds to fairly fast loading and unloading rates, particularly if the maximum load is of, let us say 30 kN. The equipment can load and unload a joint to that range of loading rate, but the speed of the crosshead is such that it cannot stop at 0 kN precisely. The crosshead would tend to unload further and apply some compression to the sample. In order to make sure the sample will never be subjected to compressive stress, it was decided to limit the minimum stress to 10% of the maximum stress, to have a loading condition with an R ratio of 0.1.

The equipment used for the test is described in the following section.

7.2.2. Testing equipment

The wood/glass/epoxy joints configuration for the fatigue test was defined in accordance with the equipment that could carry out the fatigue test. Cyclic loading usually requires testing equipment that is run by a computer. Because a large number of cycles may be required to develop fatigue in the sample, each test can last for several days or even weeks without stopping. It also means that the equipment will be under severe working conditions. The J.J. Lloyds testing machine was selected to carry out the fatigue tests. This machine is equipped with a 100 kN load cell that works more efficiently in tension than in compression. The machine can clearly run cyclic loading and has a PC interface.

For the test, the J.J. Lloyds machine was connected to a PC, combined with a Translog E500 High Capacity Data Acquisition system. The Translog E500, which includes one module housing units and controller/interface module, translates the electric signals from both LVDTs and strain gauges into displacement and micro strains respectively. It means that wood/glass/epoxy samples were equipped with LVDTs and strain gauges to measure displacements and strains during the test. The position of LVDTs and strain gauges on the sample is described in the next section. Depending on the number of cycles the machine was programmed for, sets of readings known as “cycle-profiles”, were developed based on a period of approximately 3.2 seconds with readings taken at specific time intervals. These “cycle-profiles” are presented in table 7.1.

Profile	1 st reading after (cycles)	2 nd reading after (cycles)	3 rd reading after (cycles)	4 th reading after (cycles)	Total time
1	100	500	1000	1500	1h 20m 50s
2	100	1000	2500	5000	4h 27m 30s
3	1000	2000	3500	5000	4h 27m 30s
4	1000	5000	10000	20000	17h 47m 30s
5	5000	10000	15000	20000	17h 47m 30s
6	1000	10000	20000	30000	1day 2h 40m 50s
7	15000	30000	50000	75000	2days 18h 40m 50s
8	20000	40000	60000	80000	2days 23h 7m 30s

Table 7.1 Summary table of cycle-profiles used for the fatigue tests.

For each sample tested, profiles were selected depending on the estimated fatigue resistance of the sample. Once one profile was completed, another one was then programmed and so on up to the sample failure or test completion.

Strains and displacements were recorded at both maximum and minimum stresses.

The figure 7.3 shows the equipment that was used for the tests.



Figure 7.3 The J.J. Lloyds machine during the fatigue test of one of the sample.

Other equipment was used, particularly for the fabrication of the wood/glass/epoxy samples. The fabrication was identical to the one described in chapter 4.

A microscope was also used to inspect the glass fibre/epoxy composite layer after the fatigue test. Pictures of those observations are presented and analysed further on in this chapter.

7.2.3. Joint properties and configurations

The wood/glass/epoxy joints to be tested in fatigue had to be defined with a straight configuration for the following reasons:

- Because cyclic loading was applied to the sample, the configuration of the joint needed to be the same on both sides in order to have the same experimental conditions. With a weaker or stiffer bond on one side, due to the timber grain orientation, the sample would be unbalanced.
- Testing wood/glass/epoxy joints with the load not parallel to the grain would necessitate substantial equipment that would be fairly difficult to fabricate. Firstly, the sample should fit within the machine dimensions: Samples will have to be smaller than those tested in static mode. Secondly, the inclined timber member will have to be clamped differently because of the cyclic movement of the test. Therefore different connections and holding frame should be fabricated.
- To test a wood/glass/epoxy joint in fatigue would be of greater interest if it has exactly the same configuration as one of the joint tested previously. It would generate more substance for comparison.

It was decided to use wood/glass/epoxy joints having a straight configuration, with identical material and length of composite as previously used.

Testing a joint where the failure would occur by delamination of the composite was also required: tensile failure of the composite was not an option, as the strength of the bond between the composite and the wood was the interesting part to test in fatigue. As a result, the unidirectional glass fibre UT-E500 was selected for the joints.

The sample needed to be fixed to a testing machine at both ends with a strong fastening system that would resist the fatigue test. For both ends of the sample the same system was used as before: Two shear-plate connectors pressed between two steel plates and connected with a 20 mm diameter bolt. Details of this system were given in chapter 4 (in figures 4.7 and 4.8).

The wood/glass/epoxy samples were clearly made of two pieces of timber connected with butt ends with a 200 mm long glass fibre/epoxy overlap on each side, and were tested with the load applied axially to the timber direction.

As for the previous test, this type of samples was classified as **TPU00**, which means **Tension Parallel with Uniaxial glass fibre UT-E500**, where the load is applied in the glass fibre direction ($\alpha = 0^\circ$) and in the same direction than the timber grain ($\beta = 0^\circ$). The TPU00 sample is presented in figure 7.4.

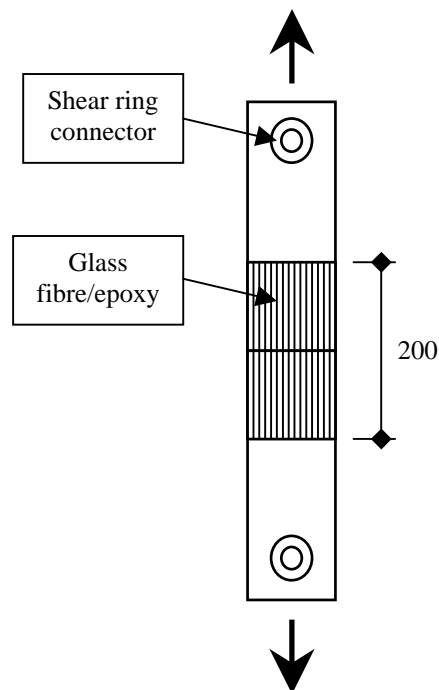


Figure 7.4 Sample configuration type TPU00 for fatigue test.

Measurements were carried out on these samples during test. With the load applied to the sample recorded, the displacements and strains at specific locations on the joint were measured. LVDTs and strain gauges were used to carry out those measurements:

- PVC and steel brackets fabricated for this purpose were glued onto the timber in order to hold the LVDTs in positions. The LVDTs measured displacements at the gap position between the brackets located on either piece of timber. They were fixed in a symmetrical arrangement to check any misalignment of the sample.
- Strain gauges were used only to measure strains in the glass fibre/epoxy layer. They were embedded directly at the surface of the composite matrix in the epoxy, with a thin coat added on top of it, while the samples were fabricated. Strain gauges were positioned in a same arrangement on each side of the sample.

LVDTs and strain gauges locations on the sample are shown in figure 7.5.

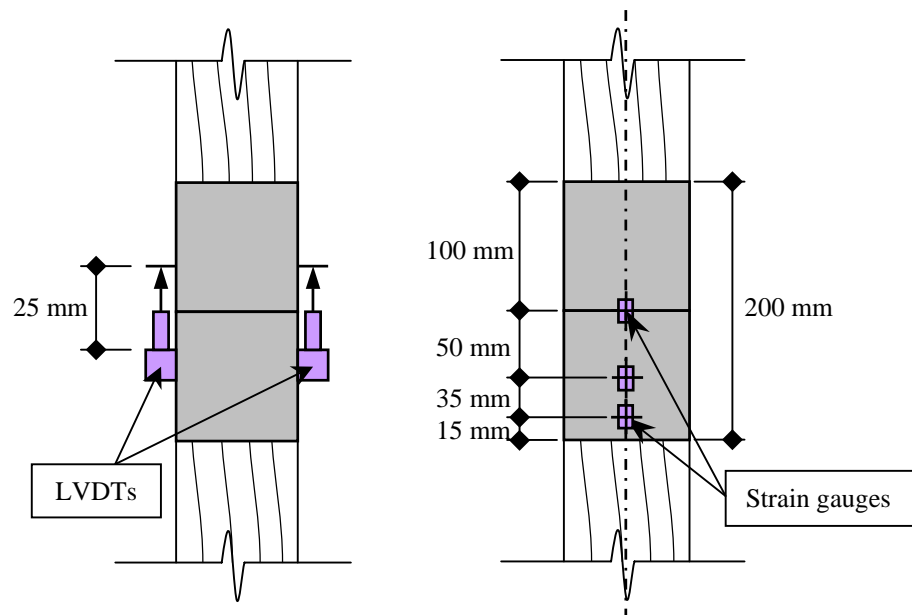


Figure 7.5 LVDTs and strain gauges positions on fatigue test samples.

Not all the samples had the same number of strain gauges. Half of them had 6 strain gauges (3 on each side, as shown in figure 7.5) and the other half had only two strain gauges, one on each side, located across the gap.

Some of the samples during the fabrication are shown in figure 7.6.



Figure 7.6 Strain gauges positions on fatigue test samples.

Samples with 6 and 2 gauges can clearly be identified in figure 7.6.

The figure 7.7 shows a sample set in position for the test in the J.J. Lloyds machine. The LVDTs are positioned with the holding brackets and the strain gauges with wires soldered to it, are connected to the Translog E500 acquisition system.



Figure 7.7 Sample in position ready for the fatigue test.

With the type of sample and the means of measurements defined, the numbers of sample as well as the loadings were established.

The straight configuration joints type TPU00 were tested statically previously and results from the tests were available at the time (table 5.8). It was initially decided to test two series of joints in fatigue having different R ratios, with 6 samples per test. However 6 samples sounded relatively low to draw the S-N curve. With six samples, there would have been only one sample tested for a given load. Using all 12 samples for only one series of test was more accurate because several samples could be tested in the same loading configuration. It was decided to use 12 samples for the fatigue test with an R ratio of 0.1.

Finally, 14 samples were fabricated with one sample used for preliminary tuning of the equipment. 13 samples were tested as part of the fatigue test. The results of those tests are presented in the next section.

7.3. Test results

The 13 samples were tested at different cyclic loading ranges in order to draw the S-N curve. Those ranges were based on the static estimated failure load of the joint. Using the results obtained in the previous tests, the static failure load was evaluated at 35 kN. The cyclic loading ranges presented in table 7.2 are based on a proportion of the estimated failure load and were used for the tests.

Sample	Wood	Percentage of estimated load (%)	Max cyclic load (kN)	Min cyclic load (kN)
1	D	83	29	2,45
2	E	65	22,5	1,9
3	C	65	22,5	1,9
4	B	53	18,5	1,6
5	D	53	18,5	1,6
6	E	53	18,5	1,6
7	A	50	17,5	1,5
8	D	50	17,5	1,5
9	A	46	16	1,4
10	C	46	16	1,4
11	A	46	16	1,4
12	B	39	13,5	1,25
13	C	33	11,5	1,05

Table 7.2 Cyclic loading ranges for the fatigue tests.

The sample 1D was the first sample to be tested. In fact, the fatigue tests started with high cyclic loads, reducing progressively with the successive samples. Eight samples with different cyclic loading ranges were initially tested. Additional tests were carried out in loading ranges where confirmations of the results were necessary.

Beside the fatigue resistance, other properties of the wood/glass/epoxy samples were measured. Those properties are presented in the next section.

7.3.1. Preliminary results

Other properties were measured on the wood/glass/epoxy samples. Some of those measurements were carried out before and some after the fatigue tests.

As for the static tests, the timber planks selected for the sample fabrication were tested in three points bending before being sawn in two timber pieces. The tests were carried out at very low load to avoid any structural damage of the timber. The mid-span deflection was recorded under load. This test enabled the calculation of the bending modulus of elasticity for each sample. This test was previously carried out for the timber grading. It was only used here to check whether the mechanical properties of the timber (that was of the same species) were similar. The test of a timber plank is shown in figure 7.8.

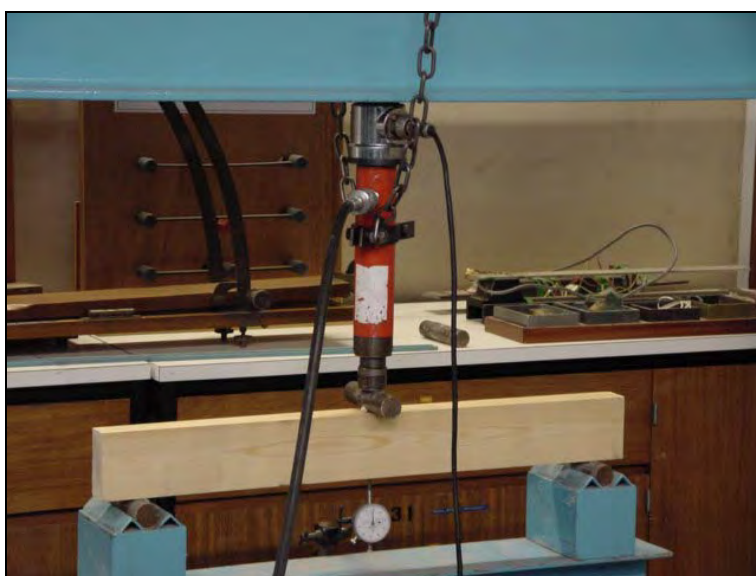


Figure 7.8 Three points bending test of one timber plank before joint fabrication.

Each wood/glass/epoxy samples was weighted before and after the gluing of the glass fibre/epoxy composite. This measurement enabled the calculation of the Fibre Volume Fraction (FVF), the ratio that defines the amount of glass fibre per unit weight of resin. The FVF was described in the previous chapter and this ratio is strongly linked to the strength of the composite.

After each tests, a sample of timber was sawn from the wood/glass/epoxy joint. This sample of timber was used to measure the moisture content, the specific gravity (i.e. wet density) and the nominal specific gravity (i.e. dry density) of the joint.

All those properties are presented and summarised in table 7.3.

Sample	Wood	Bending MOE (kN/mm ²)	Moisture Content (%)	Fibre Volume Fraction	Specific G. (kg/m ³)	Nominal S.G. (kg/m ³)
1	D	6,0	9,9	0,30	472	430
2	E	5,4	10,0	0,28	454	413
3	C	6,2	9,7	0,28	463	422
4	B	5,4	9,7	0,31	405	370
5	D	6,1	9,7	0,26	546	497
6	E	6,1	9,8	0,30	468	426
7	A	7,2	9,6	0,32	631	576
8	D	6,1	9,3	0,31	436	399
9	A	6,7	9,6	0,29	683	623
10	C	6,4	9,8	0,29	510	464
11	A	6,5	9,8	0,29	629	572
12	B	5,7	9,5	0,27	418	382
13	C	5,6	9,9	0,28	473	430
Average value		6,10	9,72	0,29	506,8	461,9
Standard Deviation		0,51	0,20	0,02	88,7	80,8

Table 7.3 Preliminary results from fatigue tests.

These properties are relevant for the two following reasons. Firstly each of them can interact on the strength and stiffness of the joint. It also has an effect on its fatigue resistance. Secondly those properties can be directly compared with those obtained from the TPU00 static tests because the samples were made with the same timber, the properties were measured with the same equipment and with the same methods and conditions.

The results are then discussed with reference to those of the static TPU00 tests, summarised in table 5.8.

- The average bending modulus of elasticity appears to be relatively lower than the value obtained from the TPU00 tests. It corresponds to a 22% reduction, which is significant, particularly with the standard deviation that is quite similar. However, this indicates that the quality of the timber is certainly lower than the timber used before, unless this is due to the moisture content.

- The measurement of moisture content indicates that the timber is drier than for the TPU00 tests. With almost 2% lower average moisture content and a very low standard deviation, the timber was left in dry conditions for a long time before the test and perhaps in slightly too dry conditions. With lower moisture content, the timber properties should be slightly better, but this is not the case. The quality of the timber is therefore lower than that used previously.
- The results of FVF are very close to those derived for the TPU00 tests. This confirms that the method used, the type of glass fibre and the resin are identical as before.
- The measurements of specific gravity and nominal specific gravity indicate fairly high average values for lower quality of timber than used for the static tests. The comparison of the standard deviation shows that the timber density is more variable in this test than in the previous static tests. More variations correspond to more discrepancy in the timber quality. However high values of specific gravity correspond to high values of bending modulus of elasticity. It confirms the accuracy of the experimental methods used to carry out those measurements.

Finally the results are all consistent considering the values obtained for the standard deviations.

The main test developed to evaluate the fatigue life of those joints is presented in the following section.

7.3.2. Fatigue properties and S-N curve

7.3.2.1. Experimental results

The fatigue life of any engineering materials or any structure is commonly represented with the stress-life (S-N) or strain-life (ε -N) curves. S and ε are respectively the stress and strain amplitude, N is the number of cycles to failure.

In the specific case of the wood/glass/epoxy joints, the fatigue life is represented as a load-life curve, for an R ratio of 0.1. For the 13 samples tested, the numbers of cycles to failure were recorded for each sample and those results are presented in table 7.4 with indication of maximum and minimum cyclic loads.

Sample	Wood	Max cyclic load (kN)	Min cyclic load (kN)	Cycles to failure
1	D	29	2,45	20
2	E	22,5	1,9	489
3	C	22,5	1,9	1391
4	B	18,5	1,6	2128
5	D	18,5	1,6	5454
6	E	18,5	1,6	30534
7	A	17,5	1,5	38400
8	D	17,5	1,5	54900
9	A	16	1,45	92330
10	C	15	1,4	98460
11	A	15	1,4	188500
12	B	13,5	1,25	+ 186500
13	C	11,5	1,05	+ 436250

Table 7.4 Tests results of loading ranges and cycles to failure.

For the samples 1 to 11, the joint failure occurred after the specified number of cycles. All samples displayed the same mode of failure: The delamination of the glass fibre/epoxy composite on both sides of the joint.

However samples 12 and 13 were tested up to the number of cycles indicated on table 7.4 without showing any visible sign of fatigue. Considering the large number of cycles those two samples endured, the fatigue tests were stopped. It was admitted that those two samples were tested below their endurance limit, on the assumption

that those joints have an endurance limit. The endurance limit is usually defined theoretically as the stress level below which the material can be cycled infinitely. The endurance or the fatigue limit is generally used for monolithic materials such as metals, and to some extent, to polymers. In the case of structural joint, this limit appears to be more complex to define as many parameters can affect it.

The results presented in table 7.4 are plotted in the S-N curve with linear maximum load versus logarithmic scale of the number of cycles, as shown in figure 7.9.

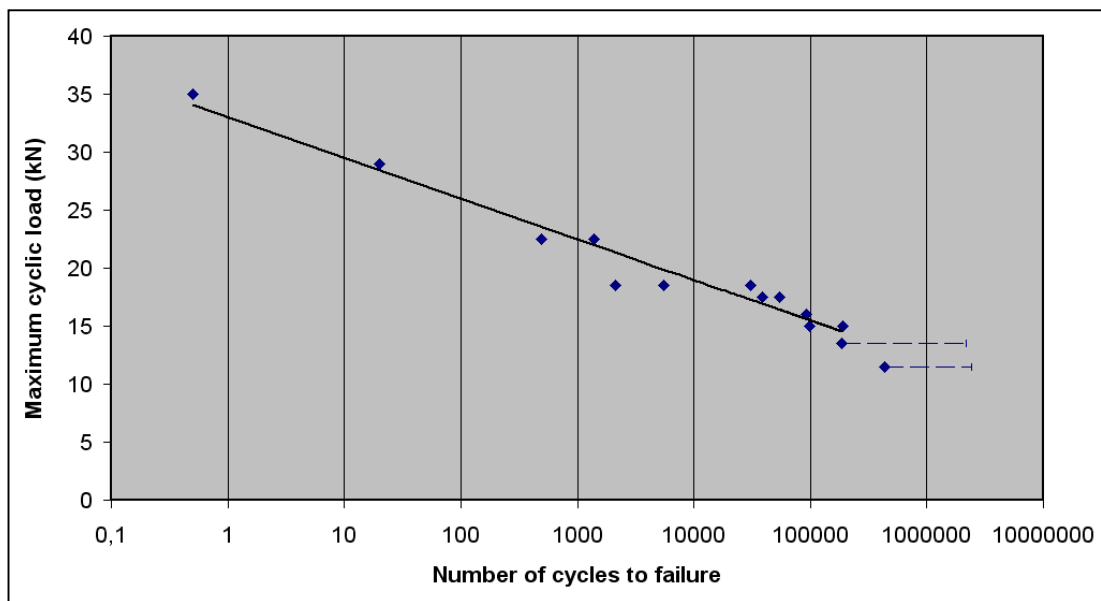


Figure 7.9 S-N logarithmic curves for wood/glass/epoxy joints tested in tension-tension at $R = 0.1$.

The graph clearly indicates the linear relationship between the results of maximum load versus logarithmic cycles form. Note that two results were left outside the graph for sample 12 and 13 because they were not tested to failure, as explained previously.

Samples 12 and 13 were careful removed from the testing rig following the fatigue tests. Visual inspection was carried out without revealing any visible sign of defects or cracks in the joint composite layers. Defects or cracks not visible to the naked eye could not be identified therefore it was inappropriate to state that those samples did not experience any damages from the fatigue tests. In order to estimate whether the samples were mechanically affected by the fatigue test, they were tested in static axial tension.

The tests were carried out using exactly the same procedures and equipment as used for the static tension tests described in the previous chapters, except for the two following items:

- No LVDTs or strain gauges were used for the tests,
- The test was carried out on the J.J. Lloyds machine instead of the strong floor rig that was used initially.

With a loading rate of 6kN/min, the samples were tested in tension to failure. The failure load and the modes of failure are presented in table 7.5.

Samples	Wood	Failure Load (kN)	Modes of failure
12	B	34.8	Composite delamination on both sides
13	C	33.7	Composite delamination on both sides

Table 7.5 Results of the static tension test for sample 12 and 13.

The failure loads are relatively high compared to the results obtained from the joints tested in tension statically (TPU00 tests), considering that the samples were previously tested in fatigue. Those results must be compared with the average failure load of the TPU00 tests of 34.9 kN. It clearly shows that sample 12 and 13 have not lost any of their tensile strength during the fatigue tests. Microscopic damage may have developed in the joints, but they were not significant enough to affect the strength of the two samples. Because they did not failed after a very large number of cycles and because after that their tensile strength was not affected at all, it can be assumed that sample 12 and 13 were tested in tension-tension fatigue towards their endurance limits (and maybe beyond), assuming they have a so-called “endurance limit”. This brings up the following question, which is to find out whether the concept of endurance limit is appropriate for the wood/glass/epoxy joints?

“In general, non-ferrous metals do not show a fatigue limit and fractures can still be obtained even after several hundred million cycles of stress” (Benham, 1996).

The fatigue properties for each material that compose the wood/glass/epoxy joints are presented in the literature review in the next section.

7.3.2.2. Fatigue properties of materials

It is necessary to identify the fatigue properties of each material (i.e. wood, wood/epoxy and glass fibre/epoxy) that compose the wood/glass/epoxy joints to understand the overall behaviour of the joints under fatigue.

Most fatigue theories usually admitted a so-called endurance limit for a monolithic material that was cycled 1 to 100 million times without failure, depending on the material considered.

But first it is essential to highlight that the use of S-N curves to assess the fatigue properties of a material is fully valid when the applied cyclic stress remains within the elastic range and the number of cycles to failure is large: This is known as the *high-endurance fatigue*. High-endurance fatigue relates to the endurance of a material from about 10^4 cycles to ‘infinity’. Alternatively *low-endurance fatigue* relates to the high cyclic stress to failure part of the curve (usually up to 10^4 cycles).

The approach regarding those two ranges of endurance is rather different:

- A material subjected to low-endurance fatigue is under high cyclic stresses and strains. In other words, significant plastic deformation is occurring in every cycle, resulting in strain-hardening or softening effects of the material. Plastic deformation is usually represented in the form of a stress/strain hysteresis loop. However stress/strain hysteresis loops were not produced during testing of wood/glass/epoxy joints because the measuring equipment could not monitor displacements and strains continuously or at very close intervals, considering it must record several readings for each cycle that last for 3 seconds.
- A material subjected to high-endurance fatigue is under low cyclic stresses and strains. Because the cyclic loading remains essentially elastic, the S-N curve approach is best suited for the high-endurance fatigue analysis. By reducing the cyclic stress level, the S-N curve of a material either becomes parallel to the N-axis or continues with a steadily decreasing slope. This is the case respectively for materials having an endurance limit such as steel, and for materials not having any endurance limit such as aluminium. This is confirmed on the S-N curves presented in figures 7.10 and 7.11 for both steel and aluminium materials.

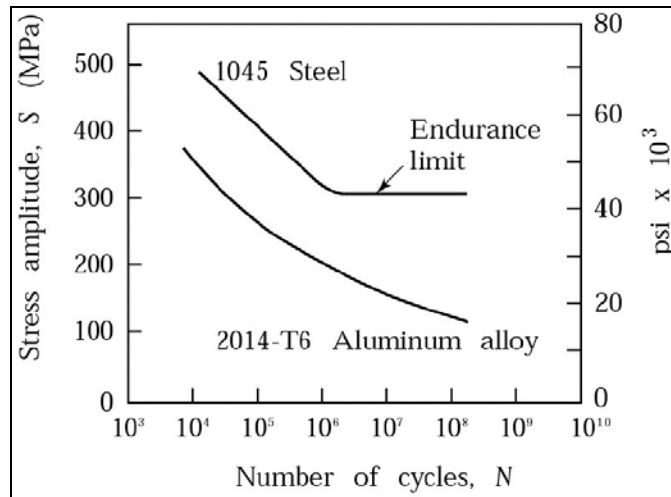


Figure 7.10 Typical S-N curves for 1045 Steel and 2014-T6 Aluminium alloy (Kalpakjian et al., 2001).

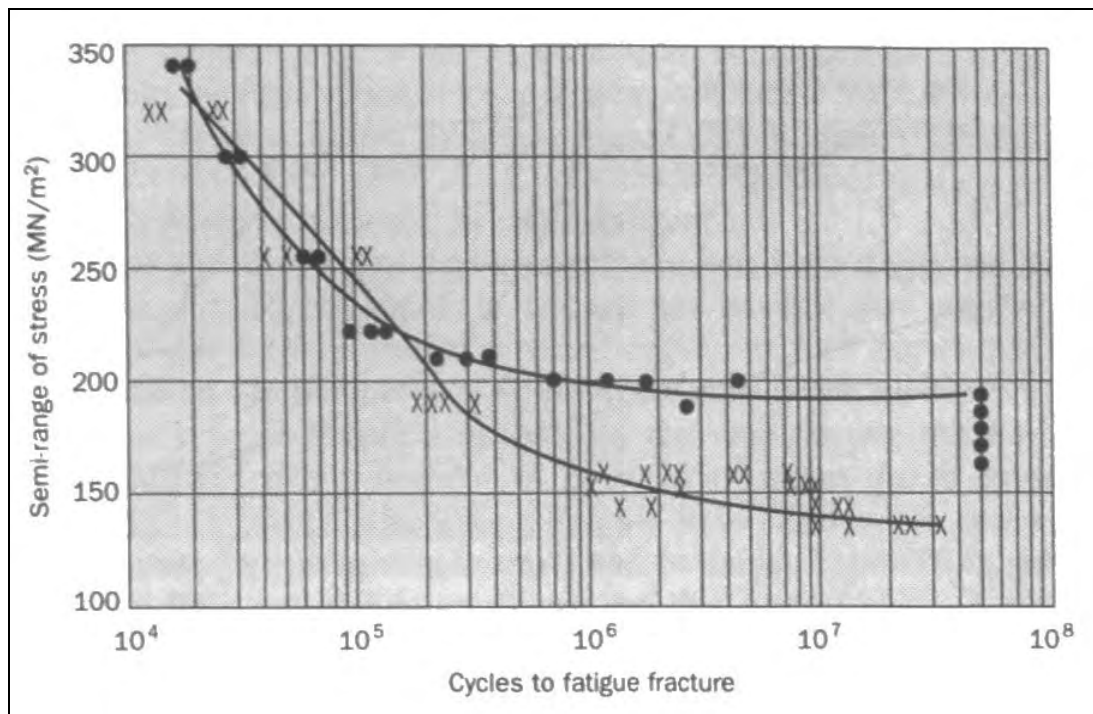


Figure 7.11 S-N curves of reversed axial stresses for mild steel (●) and 24S-T3 aluminium alloy (x) (Benham, 1996).

Aluminium is a non-ferrous metal and is a highly isotropic material. It is therefore likely that both glass fibre/epoxy composite and wood will not display any endurance limit because they are non-metallic materials (i.e. polymer and organic materials respectively) and are both anisotropic.

Fatigue properties of wood (or timber) have been studied for many years. It started with the use of timber for the Mosquito bomber and gliders in the early 1940s, to the more recent use of timber for the manufacture of blades for wind-powered generators. The S-N curves method is a convenient way to represent the fatigue life of wood, particularly as the results are linear in the form of S-Log N curves. Typical wood S-log N curves with various cyclic loading modes are presented in figure 7.2. Not all materials display that same linear S-Log N trend as timber, as illustrated by the S-Log N curves presented in figure 7.12.

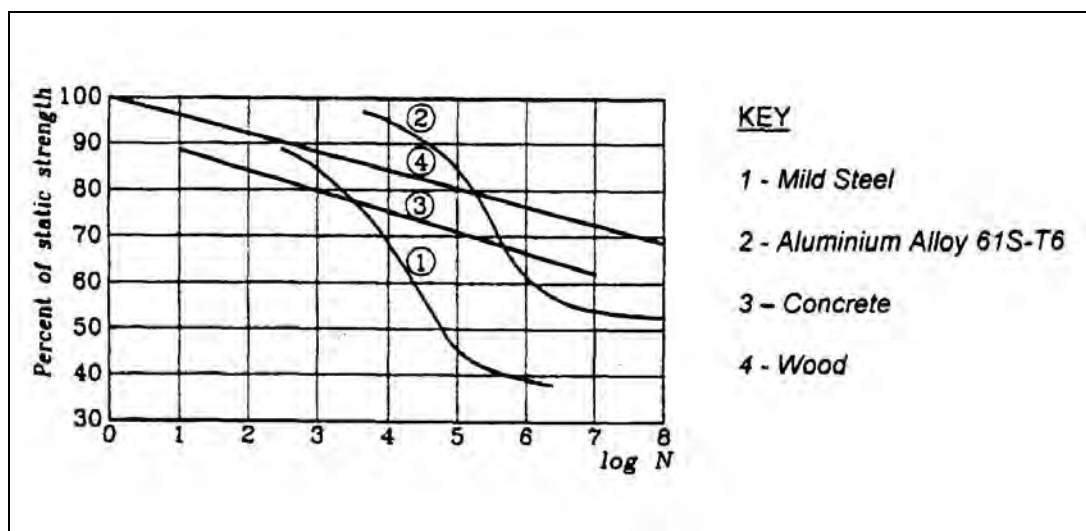


Figure 7.12 S-N curves for various construction materials at $R = 0.1$ (Hansen, 1991).

It is interesting to denote that the S-N curve for aluminium in figure 7.12 seems to show an endurance limit (i.e. horizontal end of the curve) towards 10^8 cycles as the mild steel does not. This S-N curve also indicates that timber can resist in cyclic stress in tension-tension ($R = 0.1$) up to 10^8 cycles with the maximum cyclic stress corresponding to 70% of its static (tension) strength. And this points out that timber has a better high-endurance fatigue resistance in tension than the other materials presented here, as long as this resistance is related to the static strength.

Much research work, such as that carried out by Tsai and Ansell (1990) was shown that the most severe mode of cyclic loading for wood material is fully reversed loading ($R = -1$). By testing different species of timber (Sitka spruce, laminated Khaya and beech) under load control in four-point bending and at five different R ratios and three different moisture contents, they found that fatigue lives were

independent of the species and were reducing with increasing moisture content. The effect of moisture content on sliced Khaya laminates fatigued at $R = 0$ in bending is shown on the S-N curves presented in figure 7.13.

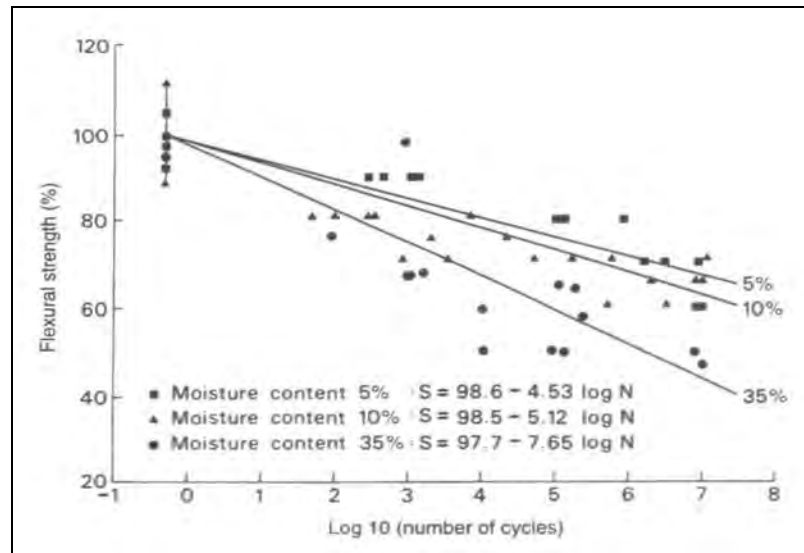


Figure 7.13 S-N curves for sliced Khaya laminates tested in bending at $R = 0$ (Tsai et al., 1990).

As for the mechanical properties, the moisture content seems to be an important parameter that affects the fatigue life of wood. They also found that the fatigue damage accumulation at cellular level was associated with the formation of kinks in the cell walls, compression creases and cracks in the wood.

Further research was carried out, such as that by Bonfield and Ansell (1991), which was part of a research program for the needs of the wind turbine blade industry in the UK. They explored fatigue in constant amplitude tests in axial tension, compression and shear for both Douglas fir and Khaya using various R ratios. The Douglas fir and the *Khaya ivorensis*, which is an inexpensive hardwood, were both laminated with 4 mm thick veneers and glued with epoxy resin. To reduce the defects in the glue line due to the air trapped between laminations, the samples were consolidated by vacuum bagging.

They found and confirmed that fatigue lives measured in all-tension loading are significantly longer than those in all-compression tests, mainly because the static tensile strength of wood is higher than the static compressive strength.

S-N curves for laminated Khaya tested in various tension-compression ($R = -1, -2$ and -10) and compression-compression ($R = 10$) modes are presented in figure 7.14.

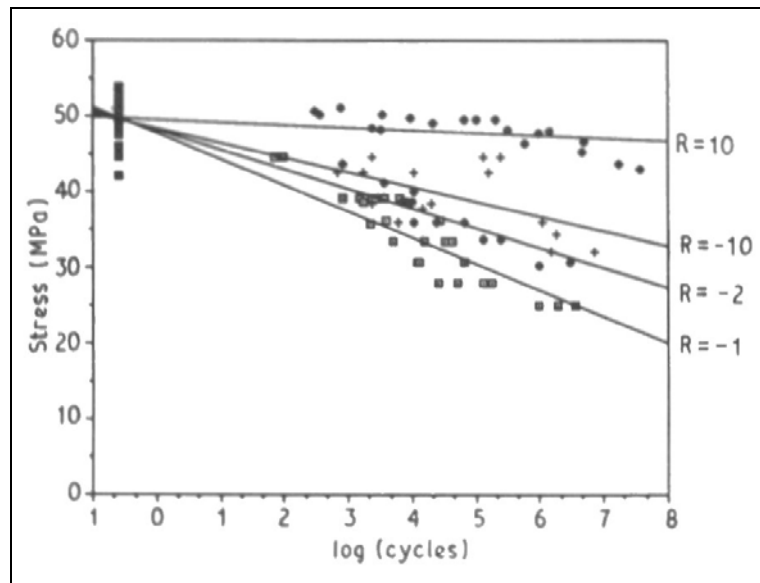


Figure 7.14 S-N curves for Khaya axially loaded at $R = -1, -2, -10$ and 10 (Bonfield et al., 1991).

The graph shown in figure 7.14 clearly indicates that the fatigue resistance of Khaya is significantly higher in all compression than in reverse modes. This is certainly the same for most wood materials. S-N curves for axial tension-compression ($R = -1$) for both Khaya and Douglas fir are presented in figure 7.15.

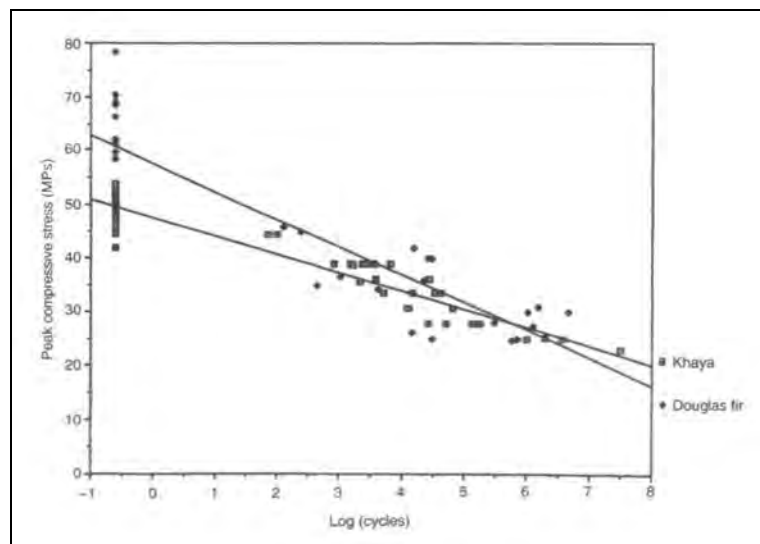


Figure 7.15 S-N curves for Khaya and Douglas fir tested in tension-compression at $R = -1$ (Bonfield et al., 1991).

The scattered results presented in figure 7.15 also point out the statistical nature of fatigue data that is emphasised by the highly variable properties of wood.

Finally the laminated Khaya was tested in shear in all-tension tests ($R = 0.1$). Compression and reverse tests could not be carried out with the sample configuration. The fatigue resistance in shear was measured along two shear plane orientations:

- Along the Radial/Longitudinal plane (RL), when the laminations were parallel to the sample face,
- Along the Tangential/Longitudinal plane (TL), when the laminations were parallel to the sample edge.

S-N curves for Khaya tested in shear at $R = 0.1$ for both the RL and TL orientations are presented in figure 7.16.

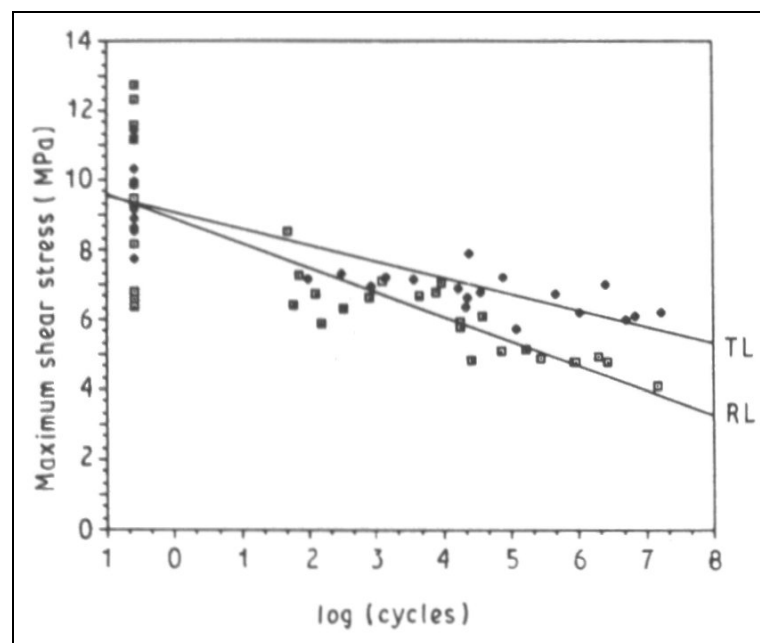


Figure 7.16 S-N curves for Khaya tested in shear at $R = 0.1$ (Bonfield et al., 1991).

The graph shown in figure 7.16 clearly indicates that the shear fatigue resistance of Khaya is significantly higher along the TL plane than the RL plane. This is due to the microscopic structure of wood material: The longitudinal cells must cleave before failure can occur on the TL plane, and this requires higher shear stress than cleavage of weaker ray cells on the RL plane.

Hacker and Ansell (2001) have investigated property changes and fatigue damage accumulation of wood-epoxy laminates under constant amplitude fatigue tests in tension-tension ($R = 0.1$), compression-compression ($R = 10$) and reverse loading ($R = -1$). They also found that the reverse loading is the most severe mode of cyclic loading. In this research as well, constant rate amplitude was used for the fatigue tests. The stress rate selected was $400 \text{ MPa}\cdot\text{s}^{-1}$, resulting in test frequencies varying between 4 and 7 Hz. As in the previous research, the wood-epoxy laminates samples were made of eight 4 mm thick laminated veneers of *Khaya ivorensis* glued with epoxy resin and consolidated by vacuum bagging.

S-N curves for laminated *Khaya* tested in tension-tension at $R = 0.1$ are presented in figure 7.17.

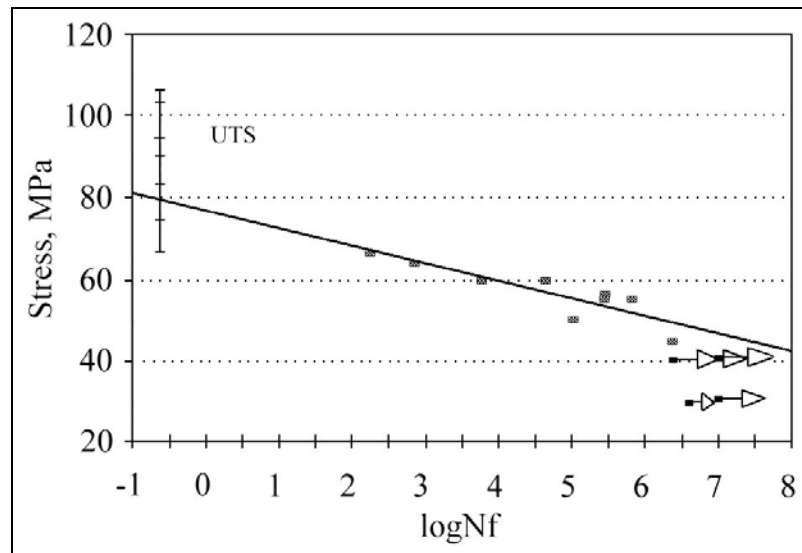


Figure 7.17 S-N curves for laminated Khaya tested in tension-tension at $R = 0.1$ (Hacker et al., 2001).

It appears on the graph shown in figure 7.17 that for fatigue lives up to 10^7 cycles, the fatigue failures always occur below the range of Ultimate Tensile Strength (UTS) data. The slope of the S-N curve in figure 7.15 is much higher than the S-N curve for the compression-compression $R = 10$ fatigue tests. As a result, the wood appeared to be more tolerant in compression-compression than in tension-tension.

Maximum and minimum fatigue strains were monitored during the fatigue tests. The results obtained at $R = 0.1$ for the samples tested with a peak tensile stress of 55 MPa are presented in figure 7.18.

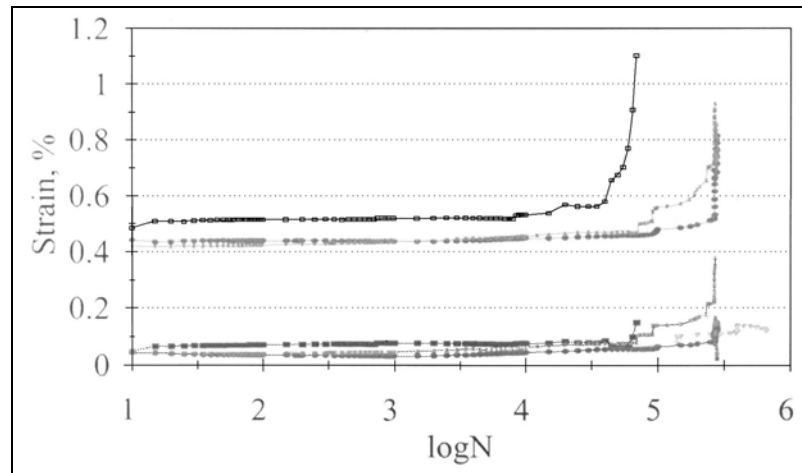


Figure 7.18 Maximum and minimum strain plotted versus log cycles for three *Khaya* samples tested in tension-tension fatigue at $R = 0.1$ and peak stress of 55 MPa (Hacker et al., 2001).

The strains are relatively constant, but close to failure they increase significantly. The same pattern is observed for maximum and minimum strains. The sudden increases of strains correspond to the initiation and growth of fatigue cracks along the wood grain, as each crack initiation causes a small step in strain.

The research carried out by Spera et al. (1990) investigated the laminated Douglas fir/epoxy as materials of choice for wind turbine blades. They characterised the fatigue properties of Douglas fir/epoxy joints. They tested scarf and butt joints in tension-tension at $R = 0.1$ with respect to grades and joint sizes. The S-N curves are presented in figure 7.19.

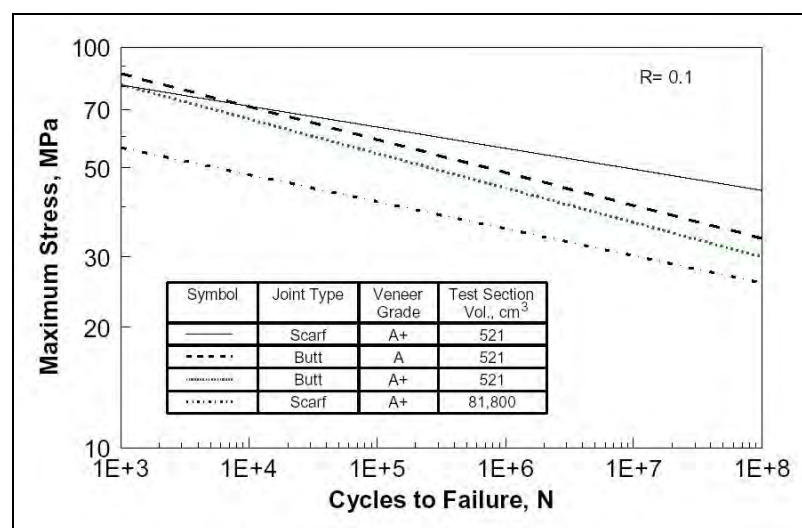


Figure 7.19 S-N curves for laminated Douglas fir tested at $R = 0.1$ (Spera et al., 1990).

It appears that the veneer grades do not govern the joint fatigue resistance: For the butt joints, the grade A veneer outperforms the grade A+ veneer, which is a higher quality grade. But the grade can be attributed visually or mechanically. The grading process mainly quantifies the straightness of the grain that is linked to the timber mechanical properties. But as wood is a natural material, this is not always true. Substantial variations in properties are still possible and can only be detected by destructive testing. A further effect illustrated in figure 7.19 is that the increased surface area of the scarf joints does not translate into an increase in strength and fatigue resistance. This could be due the fact that larger bonded areas contain more voids and therefore the bond is significantly degraded. Other reason could be that larger joints induce larger misalignment of the sample.

A further parameter that affects the fatigue life of timber is the load cycle frequency. The frequency seems to have a significant effect on fatigue behaviour, as shown on the graph presented in figure 7.20.

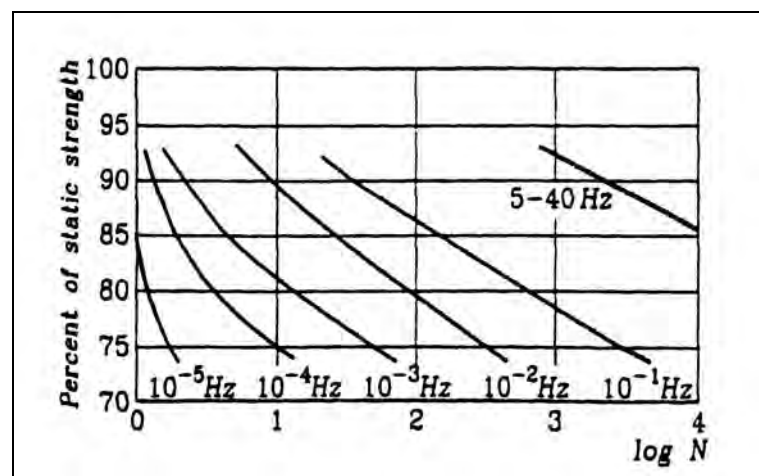


Figure 7.20 S-N curves for timber at various frequencies (Hansen, 1991).

On this graph, it emerges that higher the frequency, the lower is the fatigue life of timber for a given cyclic stress.

Fatigue properties of composite materials have been studied for a long time mainly because of the wide applications in almost all engineering field of composites. The fatigue approach to composite is rather complex.

“The major difficulty in this regard is that the application of conventional approaches to fatigue of composites, for examples, the stress versus cycles (S-N) curves or the application of Linear Elastic Fracture Mechanics (LEFM), is not straight forward” (Chawla, 1997).

It is known that the maximum efficiency in terms of stiffness and strength gains in fibre reinforced composites occurs when the fibres are continuous, uniaxially orientated and the properties are measured parallel to the fibre direction. At off-angle, the strength and stiffness drop sharply (as shown in chapter 3, figure 3.10). Also the role of the matrix becomes more important in the deformation and failure processes.

The fatigue of composite materials, as any other material, is characterised by mechanical property degradation that leads to fracture. But the fracture of a composite is rather different than for monolithic material: It is illustrated by a multiplicity of damage modes, such as matrix cracking, fibre fracture, delamination, debonding, void growth and multidirectional cracking. Some of those fatigue failure mechanisms are shown in figure 7.21.

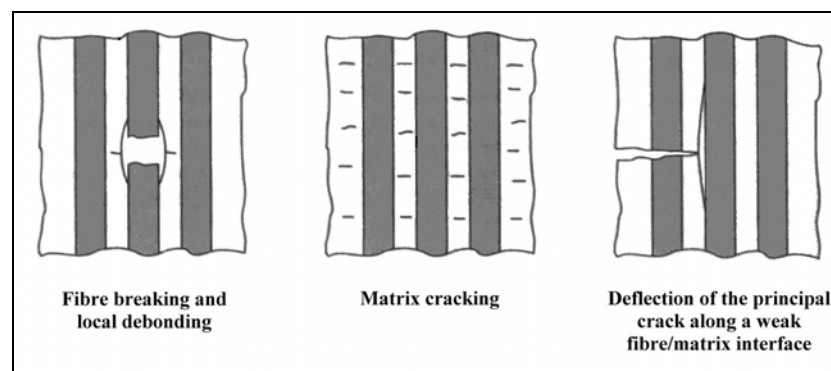


Figure 7.21 Fatigue failure mechanisms in composites (Benham et al., 1996).

It is also known that these modes of fracture appear rather early in the fatigue life of composites.

The damage mechanisms in unidirectional composites subjected to tension-tension fatigue parallel to the fibres also depends on the applied stress level. In the high stress region, the fracture mechanism would involve fibre breaking and matrix/fibre

local debonding. In the low stress region (high cycles), the fracture mechanism would involve matrix cracking with interfacial shear failure. These modes of fracture mechanisms are represented in the fatigue life diagram shown in figure 7.22.

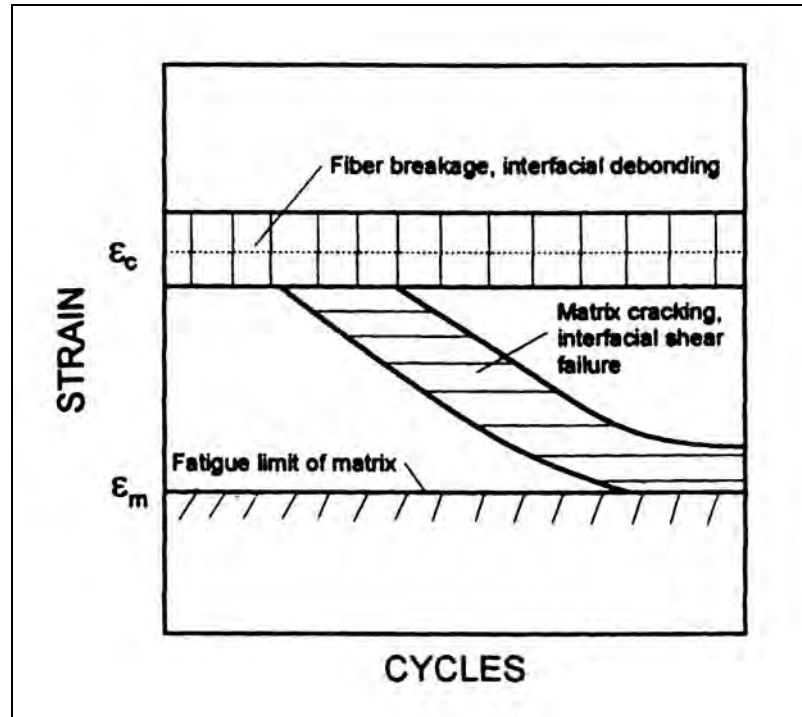


Figure 7.22 Fatigue life diagram with damage mechanisms for a unidirectional composite subjected to tension-tension stresses (Mallick, 1997).

This diagram is expressed in terms of strain instead of stress, where ϵ_c is the maximum composite fracture strain (in fact, the strain in the fibres and matrix is the same as long as no fracture occurs) and ϵ_m is the maximum matrix fracture strain.

The fibre-to-matrix strength ratio is also a significant factor in the fatigue resistance of axially stressed unidirectional composites. A composite with high fibre-to-matrix strength ratio would suffer early crack initiation. Then these cracks would grow for the major portion of its fatigue life along the fibre/matrix interface. It would be the same for a composite with low fibre-to-matrix strength ratio, but the cracks would be expected to grow also across the fibres and a poorer fatigue resistance will therefore result.

The fatigue resistance of composite materials varies depending on the type of fibres (as well as on the type of matrix material) used. It appears that because the fibres are carrying almost all the load when a unidirectional laminate is subjected to tension loading parallel to the fibres, the sensitivity of the fibres to fatigue is important to assess the composite fatigue life. The sensitivity of the matrix material is also relevant, as explained previously. However, normalised S-N curves for unidirectional composite materials having the typical epoxy material reinforced with graphite, glass and aramid fibres are presented in figure 7.23.

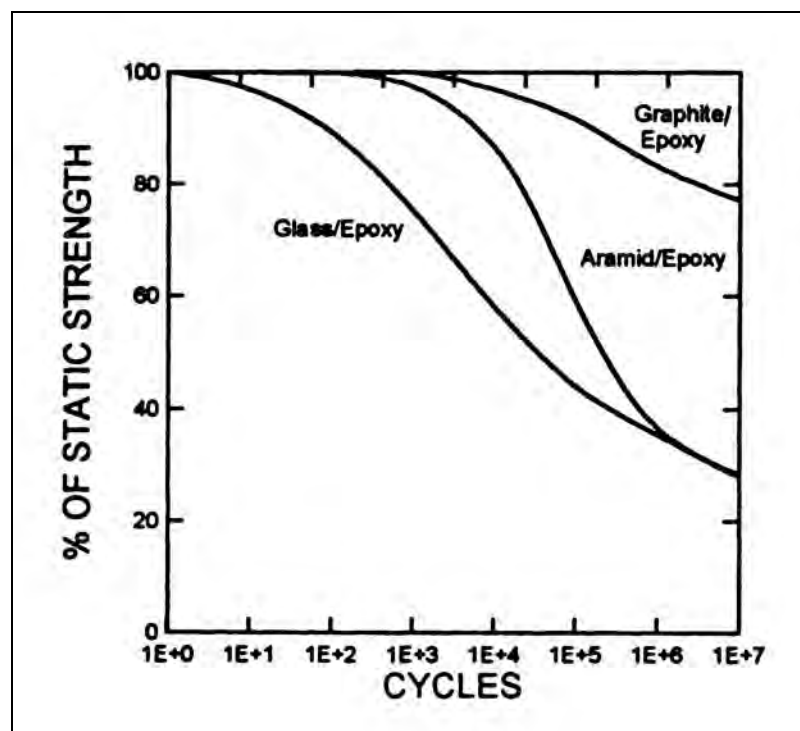


Figure 7.23 Normalised S-N curves for three unidirectional composite materials (Mallick, 1997).

The results obtained for the graphite fibres/epoxy give a very high fatigue strength ratio at 10^6 to 10^7 cycles, which corresponds to 75-80% of the ultimate static strength. Glass fibres/epoxy and aramid (Kevlar 49) fibres/epoxy converge toward the same lower fatigue strength ratio, which correspond to 30% of their ultimate static strength at 10^7 cycles. This clearly shows that the glass fibres suffer the maximum degradation in fatigue, graphite fibres exhibit much better fatigue resistance and are usually preferred in applications where fatigue is a primary concern.

Another property that characterised the fatigue resistance of composite is the high damping and low thermal conductivity of the polymeric matrix. This means that under cyclic stress, the heat generated is not dissipated quickly. This can cause a temperature difference between the interior and the surface of the composite that can lead to thermal softening failure if no precautions are taken to dissipate the heat. However, the internal heating phenomenon depends on the cyclic frequency the composite is subject to.

“For frequencies less than 20 Hz, the internal heating effects are negligible. For a given stress level, this temperature difference increases with increasing frequency” (Chawla, 1997).

As a result, thermal stress was not a concern through the fatigue tests of the wood/glass/epoxy joints because of the very low frequency of 0.33 Hz used for the cyclic loads.

Much research work has been carried out on the fatigue of composites, and particularly on glass fibre composites. Out of this research, one has to be mentioned because of its relevance to the subject: It is a large research programme about the applications of glass fibres to build wind turbine blades. This research programme that is presented in the report from Sutherland (1999) was undertaken in the early 1990s in the United States, sponsored by the Department Of Energy (DOE) and the Montana State University (MSU). This program aimed at the development of a glass fibre composite database for wind turbine applications. The DOE/MSU database for E-glass composites contains over 4500 data points for 130 material systems tested. A high frequency database provides a significant data set for unidirectional composites to 10^8 cycles. The database explores material parameters such as reinforcement fabric architecture, fibre content, matrix materials and loading parameters (R values).

The S-N behaviour of composite materials at a constant R value is typically characterised using either of the two following equations:

$$\log\left(\frac{\sigma}{\sigma_0}\right) = \log(C') - \frac{1}{m} \log(N) \quad (7.4)$$

$$\frac{\sigma}{\sigma_0} = C' - \frac{1}{m} \log(N) = C' - b \log(N) \quad (7.5)$$

Where σ is the stress level and σ_0 the static strength of the composite. C' is the material constant, N is the number of cycles and m , sometimes denoted b , is called the fatigue exponent.

In the forms of equations (7.4) and (7.5), C' has a value of 1 when the curve that fits to the S-N data set passes through the static strength at 10^0 cycles (i.e. at static failure in the first fatigue cycle).

Equation (7.5) was used to characterise the DOE/MSU database. This formulation has led to the “ten percent” rule that is typically used as a general rule-of-thumb for the tensile fatigue behaviour ($R \approx 0.1$) of unidirectional composites. The fatigue strength of the composite is reduced by ten percent by each decade of fatigue cycles, when

C is one and b is equal to 0.1 (i.e. the fatigue exponent m is equal to 10). This form is typically used for composites when comparing different material systems because it normalises out variations in the static strength. A large number of data points from the DOE/MSU database are plotted in figure 7.24.

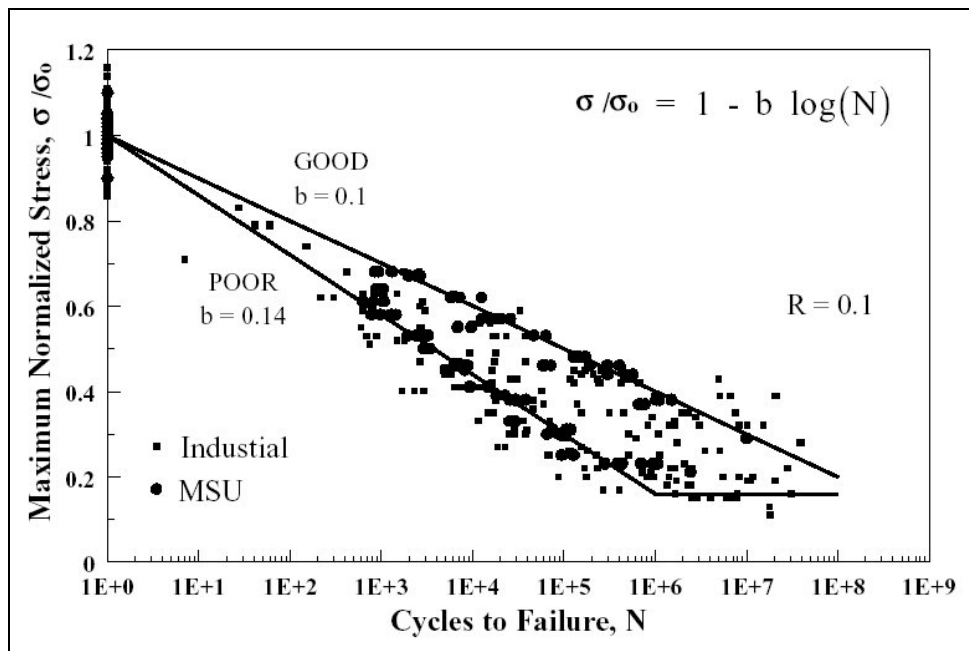


Figure 7.24 Extremes of normalised S-N tensile fatigue data from glass fibre laminate at $R = 0.1$ (Sutherland, 1999).

These data are for glass fibre composites with at least 25% fibre content in the loading direction tested at $R = 0.1$.

When applying equation (7.5), the good materials have a slope b of 0.10 and the poor have a slope b of 0.14. The good materials in this figure are approaching the best fatigue behaviour that can be obtained for glass fibre laminates in tensile fatigue. The small apparent variation in the fatigue slope b produces significant differences in high endurance fatigue performance. As shown in figure 7.24, at 20% of static strength, the good materials have almost 2.5 orders of magnitude longer life than the poor materials.

The fibre content has also an influence on the fatigue resistance of a composite. As part of the DOE/MSU database, it was found that many woven glass fibre fabric composites show poorer fatigue resistance than aligned and uniform systems. It also appeared that increasing the fibre content of a composite system generally reduces its fatigue performance. The fatigue sensitivity coefficient for glass fibre laminates as a function of fibre content is shown on the graph presented in figure 7.25.

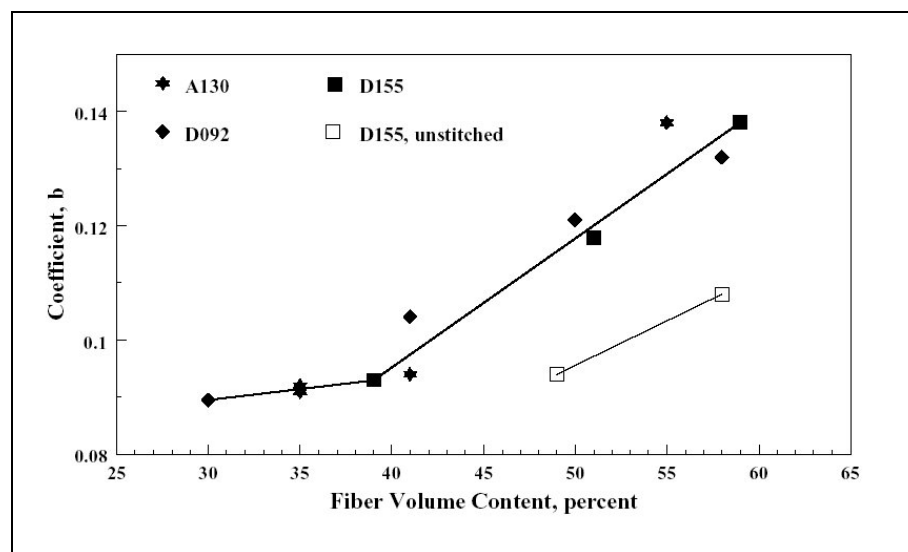


Figure 7.25 The fatigue sensitivity coefficient for unidirectional glass fibre laminates as a function of fibre content at $R = 0.1$ (Sutherland, 1999).

The fatigue sensitivity coefficient is expressed in terms of fatigue exponent b , which is also the slope of the normalised S-N curve. As shown on the graph in figure 7.25, the optimum fatigue performance is obtained with a fibre content of approximately 40% for unidirectional glass fibre laminates.

Finally, the influence of the matrix material is the last parameter revealed from the DOE/MSU database that is of interest in the review of glass fibre composite this chapter. Three matrix materials are commonly used in the construction of composite, particularly for wind turbine blades. They are vinyl ester, polyester and epoxy resins. The effect of matrix material on tensile fatigue in glass fibre laminates with 0° and $\pm 45^\circ$ plies (for $R = 0.1$) are presented in figure 7.26.

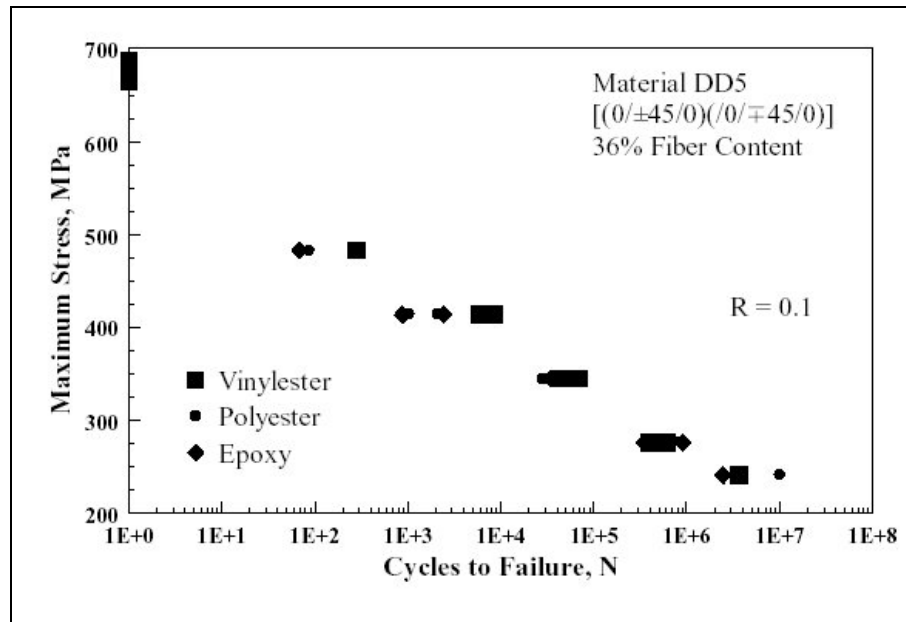


Figure 7.26 Effect of matrix material on tensile fatigue in glass fibre laminates with 0° and $\pm 45^\circ$ plies at $R = 0.1$ (Sutherland, 1999).

The matrix material has minimal effect on the static and fatigue properties, because the composite used are unidirectional and mainly stressed in the fibre direction. Note that the laminates used in figure 7.26 were unstitched $0^\circ/\pm 45^\circ/0^\circ$ composite plies. Similar results were obtained in both compressive and reverse loading.

The review of fatigue properties of wood, wood/epoxy laminates, glass fibre/epoxy composites presented in this section have shown many characteristics that can be found in wood/glass/epoxy joints. The next step before the fatigue characteristics of wood/glass/epoxy joints can be drawn, is to identify how fatigue is defined and applied in the current timber design codes.

7.3.2.3. Relationship with current design codes

It is necessary to identify how timber fatigue data is included in the current design codes to draw the fatigue characteristics of wood/glass/epoxy joints. The basis for fatigue verification is proposed in EC5: Part 2: 1997, which is the European timber code for bridges, through the use of a fatigue coefficient and a fatigue safety factor: For a structural element under a stress range $\Delta\sigma$ and for a periodic loading with N cycles, it should be verified that:

$$\Delta\sigma \leq f_{fat,d} \tag{7.6}$$

Where $f_{fat,d}$ is the design fatigue strength.

The design fatigue strength should be calculated as:

$$f_{fat,d} = \frac{k_{fat} f_k}{\gamma_{M,fat}} \tag{7.7}$$

Where f_k is the characteristic strength for static load,

$\gamma_{M,fat}$ is the material safety factor for fatigue (derived from EC1: Part 1: 1994) and

k_{fat} fatigue coefficient obtained graphically on table 7.6.

k_{fat} -Log N relationship	Structural element	$k_{fat,\infty}$
	Wooden members in	
	<ul style="list-style-type: none"> • Compression perpendicular and parallel to the grain [0,60] • Bending, tension and reversed tension/compression [0,30] • Shear [0,20] 	
	Joints with	
	<ul style="list-style-type: none"> • Dowels [0,25] • Nails [0,15] 	

Table 7.6 Relationship between k_{fat} and the number of cycles N and the corresponding values of $k_{fat,\infty}$ as presented in EC5: Part 2: 1997.

This form of fatigue verification relates directly the fatigue data to the timber static characteristic strength. It also confirms that 10^7 cycles is considered as an endurance threshold for timber bridge elements and connections under fatigue loading. For cyclic range below 10^4 cycles, the fatigue coefficient k_{fat} remains unchanged. In other words, the fatigue verification applies to high-endurance fatigue, mainly because high-endurance fatigue is a critical property for the design life of structures subject to dynamic loads such as bridges. Consequently low-endurance fatigue effects on timber members are included in the various design and materials safety factors for static design.

The fatigue performance of bonded-in rods in glulam, using three different adhesive types was investigated by Bainbridge et al. (2000). All the tests were carried out in tension-tension with $R = 0.1$ at constant test frequency of 1 Hz. Using commercial adhesives: epoxy (EP), polyurethane (PUR) and filled phenol resorcinol formaldehyde (PRF) resins, threaded steel rods (8 and 16 mm diameter) were glued in oversized holes in glulam host member and were axially loaded parallel to the timber grain in cyclic loading. A direct comparison was drawn between the results obtained from the tests and the fatigue factor k_{fat} -log N relationship as defined in EC 5: Part 2: 1997 (see also table 7.6). This comparison is presented in figure 7.27.

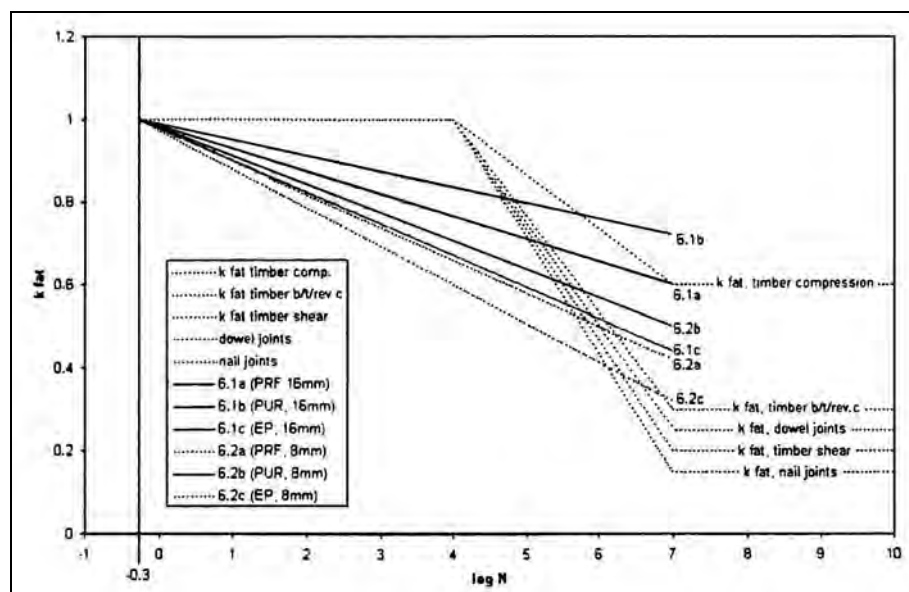


Figure 7.27 k_{fat} -log N relationship from EC5: Pt 2 combined with bonded-in rod connections test results (Bainbridge et al., 2000).

They identified various modes of failure that demonstrated the clear influence of the adhesive type upon both the fatigue life and likely failure mechanism. A direct comparison was also drawn between the observation of failure modes obtained from the tests and the fatigue factor k_{fat} -log N relationship as defined in EC 5: Part 2: 1997. This comparison is presented in figure 7.28.

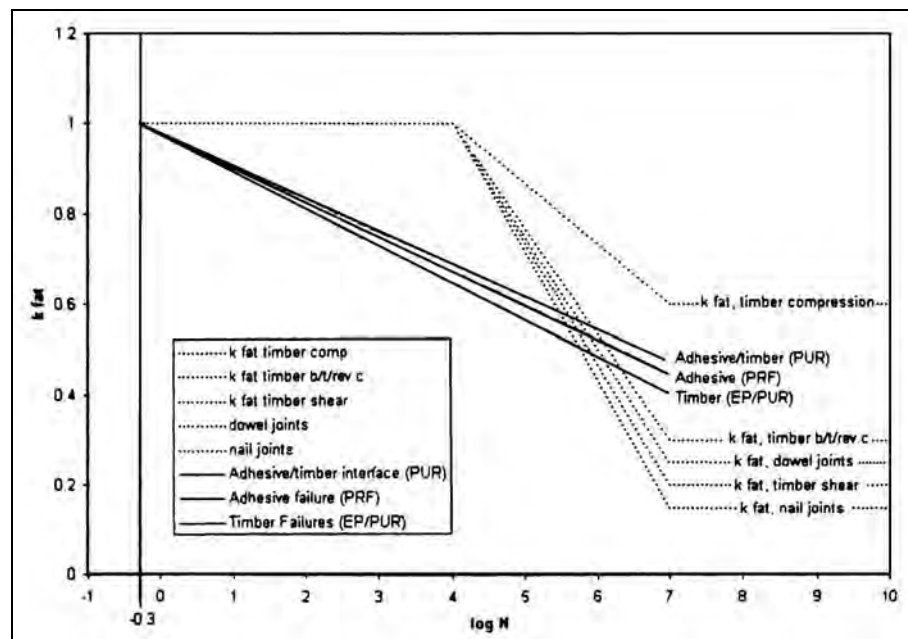


Figure 7.28 k_{fat} -log N relationship from EC5: Pt 2 combined with bonded-in rod connection test results by failure modes (Bainbridge et al., 2000).

The experimental results drawn on the graphs figure 7.27 and 7.28 must be carefully considered, as they do not take into account any probability factors. On the other hand, the derivation of the fatigue coefficient k_{fat} is probably based on characteristic values (i.e. the lower 5-percentile value of the population) derived from experimental results.

This research aimed towards the development of design rules for bonded-in rods timber connections in Eurocode 5. The authors also highlighted the limits of the results based on the extrapolations carried out because of the lack of data at high numbers of load cycles. They also mentioned that the general order of performance across the adhesive types was found to be consistent between specimen sets.

The same comparison was drawn between the fatigue experimental results of the wood/glass/epoxy joints and the fatigue factor k_{fat} -log N relationship as defined in EC 5: Part 2: 1997. This comparison is presented in figure 7.29.

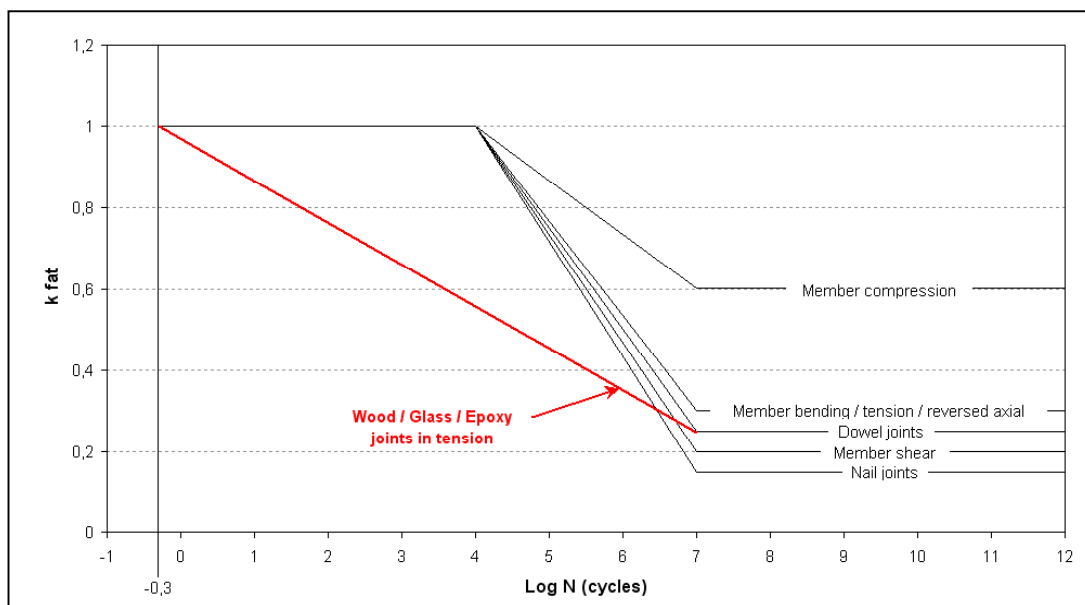


Figure 7.29 k_{fat} -log N relationship from EC5: Pt 2 and combined with the tension fatigue test results of wood/glass/epoxy joints at $R = 0.1$.

The curve for the wood/glass/epoxy joints in tension shown in figure 7.29 appears to end at a value of $k_{fat} = 0.25$ for 10^7 cycles. The value of 10^7 cycles is defined as the threshold of endurance limit in EC5: Part 2 as the k_{fat} factor remains unchanged beyond this value. The high endurance fatigue factor of the wood/glass/epoxy joints is the same as for dowel joints. It is also slightly lower than for a timber member in bending, tension and reverse tension/compression (i.e. $k_{fat} = 0.3$). As previously mentioned, those observations must be carefully considered because of the absence of statistical considerations in the fatigue results of wood/glass/epoxy joints. However, it can be said that the results reflect the good fatigue resistance of the wood/glass/epoxy joint compared to other timber joints. The joints efficiency, and therefore its fatigue resistance could be improved by increasing the bond length of glass fibre/epoxy composite for a given working load, as described in the Hart-Smith approach of adhesive joints (Adams et al., 1997). Other effects summarised are:

“As overlap lengths decrease [...]. This results in loss of damage tolerance because the joint strength is sensitive to bond length and creep in the adhesive under sustained or cyclic load” (Adams et al., 1997).

The results presented in figure 7.29 can be directly compared with those from Bainbridge et al. (2000), previously presented, for the following reasons:

- The fatigue tests were carried out in tension-tension with the same loading mode of $R = 0.1$.
- The fatigue tests were also carried out at similar frequency range (i.e. 0.33 Hz for the wood/glass/epoxy joints and 1 Hz for the bonded-in rods connections).

The fatigue results from bonded-in rod connections appear to display higher fatigue resistance than the wood/glass/epoxy joints, whether the comparison is made with the results obtained for various bonded-in rod configurations (see figure 7.27) or with the results obtained for various adhesive types (see figure 7.28). But here again, the anchorage length of the rods used (160 mm), their diameters (16 mm for 6.1 results and 8 mm for the 6.2 results) and the section of timber used (120×120 mm for 6.1 results and 70×70 mm for the 6.2 results) must be brought forward to enable a potential comparison of both systems.

Sections of timber are of the same size range as those used for the wood/glass/epoxy joints. However the anchorage length of the rods used is greater compared to the 100 mm length of composite bonded on both faces of either timber piece that compose the wood/glass/epoxy joints. As a result, the bonded-in rod connections and the wood/glass/epoxy joints cannot be compared because their geometrical configurations are radically different. However, in relation to their static failure loads, the fatigue resistance of bonded-in rods connections is generally higher than for the wood/glass/epoxy joints.

Other properties of the wood/glass/epoxy joints were also measured during the fatigue tests as described in the following section.

7.3.3. Other wood/glass/epoxy joints fatigue results

Other parameters, such as strains and displacements were recorded during the wood/glass/epoxy joint fatigue tests. The objective of those measurements was to identify how the joint properties were affected during the fatigue tests.

Using the Translog E500 High Capacity Data Acquisition system, minimum and maximum fatigue strains and displacements at minimum and maximum load were monitored during the tests. The readings were taken at various time intervals, depending on the expected joints fatigue life. The strains and displacements were recorded from strain gauges and LVDTs that were positioned as described previously in this chapter.

From those measurements, relatively good results were obtained from gap strain gauges (i.e. strain gauges positioned in the centre on the gap zone) and from LVDTs. Readings from the middle and end strain gauges were more scattered for most samples and therefore gave less precise results.

Fatigue strains and displacements generally increase with the number of cycles. The graph shown in figure 7.30 shows gap strains versus cycles recorded at maximum cyclic loads for several wood/glass/epoxy joints.

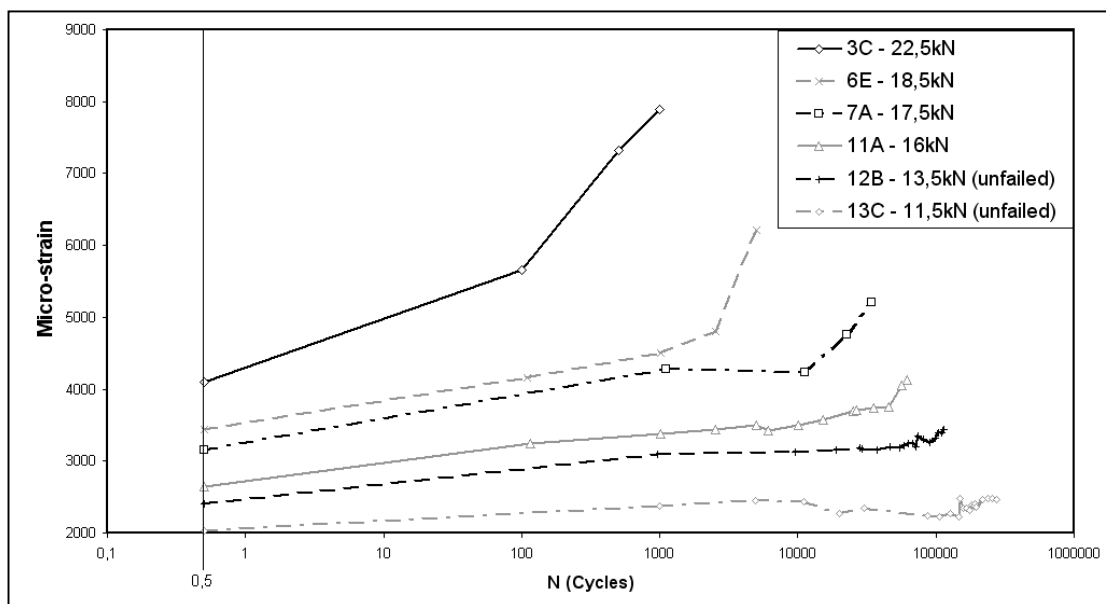


Figure 7.30 Maximum gap strain recorded for maximum cyclic loads for several wood/glass/epoxy joints tested in tension-tension at $R = 0.1$.

The curves shown in figure 7.30 clearly indicate that the strain in the gap area increases more steadily when the maximum cyclic load is reduced. For high maximum load (low endurance), the shape of the curve is almost parabolic (on the logarithmic scale). As the maximum cyclic load reduces, the shape of the curves becomes progressively linear. Nevertheless the slope of those curves significantly reduces with the maximum load. This is due to the plastic strain that is very significant at high cyclic loads. On the other hand, at low cyclic loads, the plastic strain is negligible or nil, therefore the slope is very close to the horizontal. However it should be noted that the results are plotted on a logarithmic scale. Finally the strains at failure reduce with the maximum cyclic loads. In fact the strain at failure has no direct incidence on the failure mechanisms because all samples failures occurred by delamination of the composite layer. The strain at the gap would be directly linked to failure if the joints had failed by tensile rupture of the composite, but this is not the case.

The displacements from LVDTs were also recorded in the gap zone. The graph shown in figure 7.31 shows gap displacements versus cycles recorded at maximum and minimum cyclic loads of two wood/glass/epoxy joints.

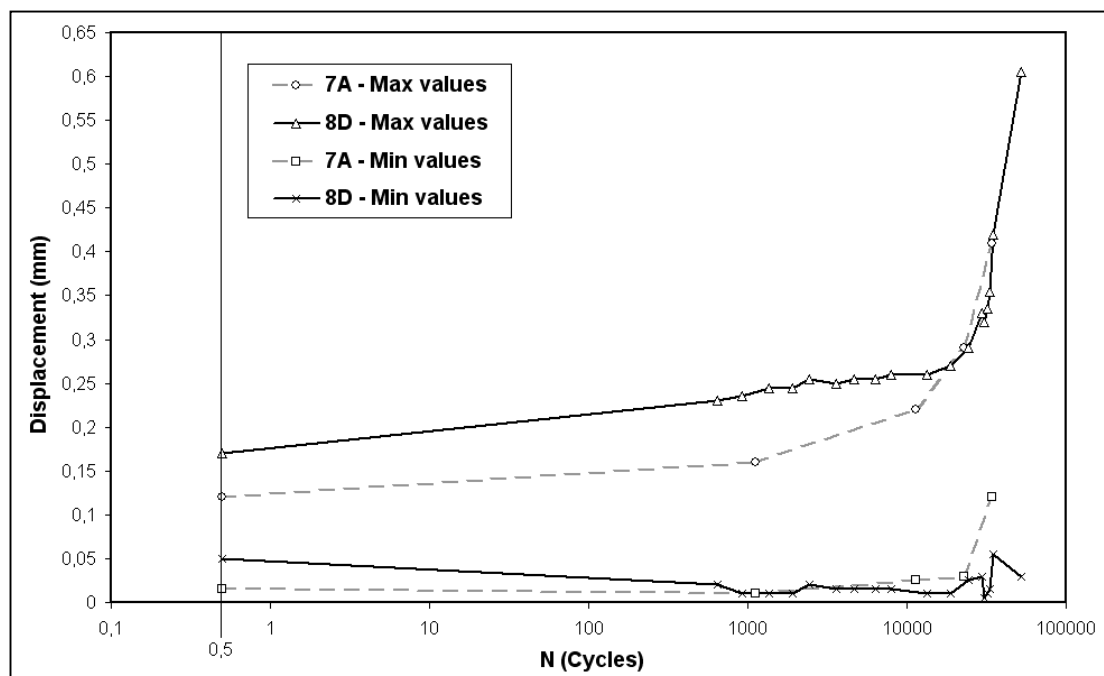


Figure 7.31 Maximum and minimum gap displacements recorded at maximum and minimum cyclic loads of 17.5 kN and 1.5 kN for two wood/glass/epoxy joints tested in tension-tension at $R = 0.1$.

On the graph shown in figure 7.31, it appears that the maximum gap displacements change much more significantly than the minimum gap displacements. The minimum gap displacements at low cycles even reduce up to 10000 cycles, and then rise up to the failure. The maximum gap displacements rise progressively up to approximately 10000 cycles and then rise more and more toward the failure.

As mentioned in the review of Hacker and Ansell (2001) and shown in figure 7.18, the same observation is also valid for figure 7.31: The first steps of strain increment correspond to the initiation and growth of fatigue cracks, as each crack initiation causes a small step in strain. Those cracks probably occur in the composite itself and at the interface between the timber and the glass fibre/epoxy. The observations and descriptions of cracks, as well as fracture mechanisms are described below.

The graph shown in figure 7.32 shows gap displacements versus cycles recorded at maximum and minimum cyclic loads of three other wood/glass/epoxy joints.

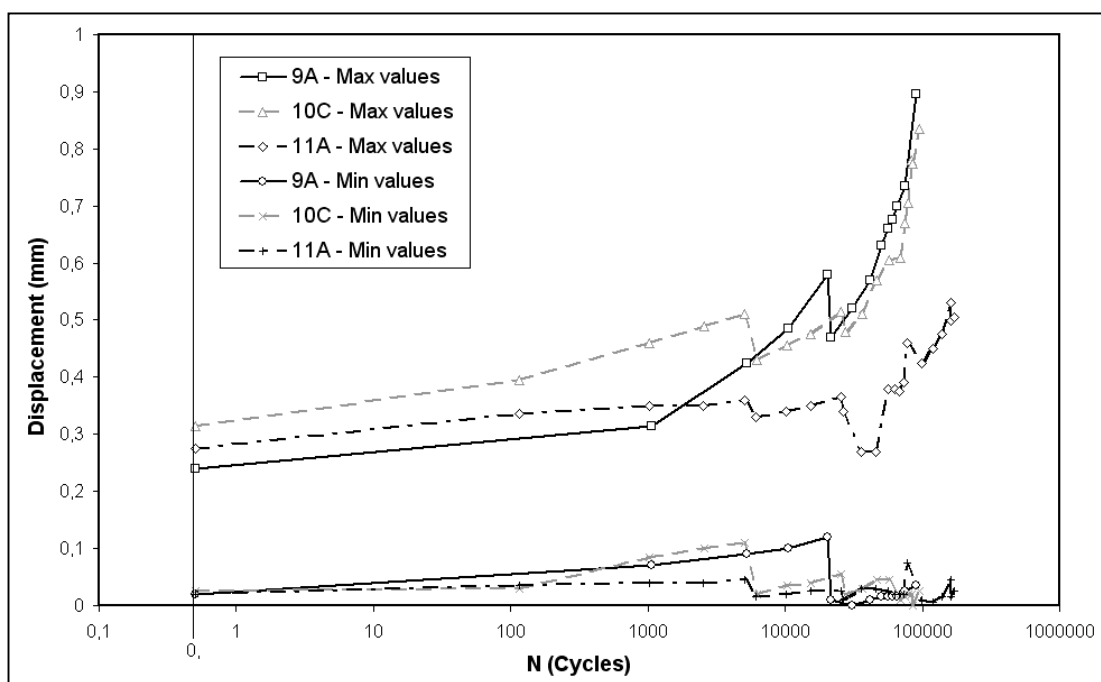


Figure 7.32 Maximum and minimum gap displacements recorded at maximum and minimum cyclic loads of 16 kN and 1.4 kN for three wood/glass/epoxy joints tested in tension-tension at $R = 0.1$.

The same observations can be made about figure 7.32 as figure 7.31: The maximum gap displacements change much more than the minimum gap displacements. However the maximum and minimum strains rise progressively up to around 10000 cycles and then the displacements become more chaotic: Minimum gap

displacements even reduce and remain relatively steady up to failure, while the maximum gap displacements increase significantly with some up and down steps that probably indicates some experimental errors or creep effects.

As previously described, some wood/glass/epoxy joints were equipped on both faces with strain gauges in the middle and end of the glass fibre/epoxy overlaps. Some of the results obtained are shown in figure 7.33. This graph illustrates the maximum and minimum middle and end strains versus cycles recorded at maximum and minimum cyclic loads of 18.5 kN and 1.6 kN for sample 4B.

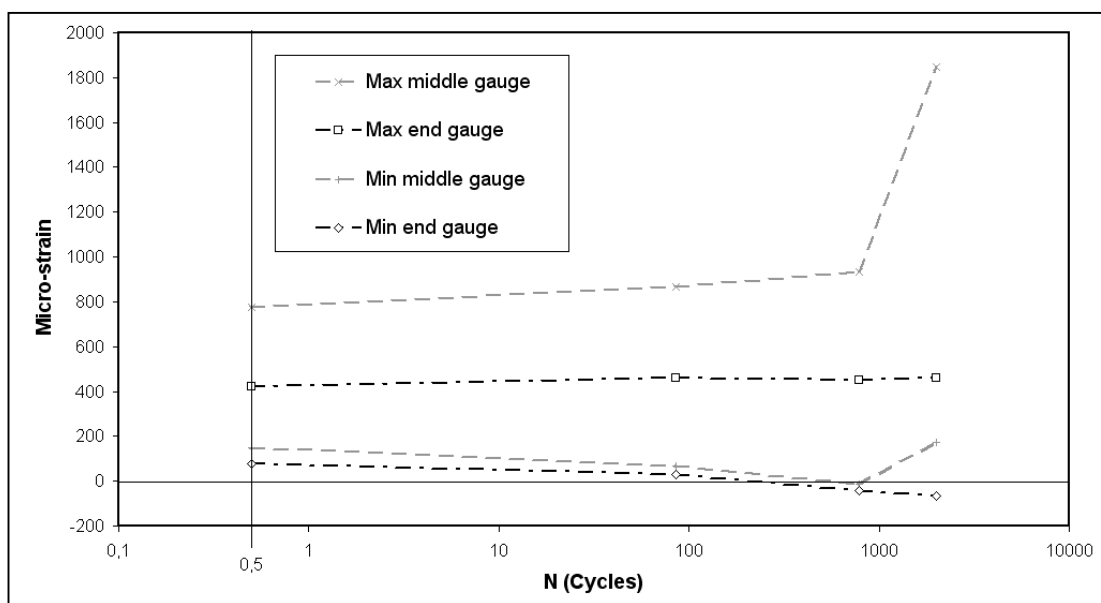


Figure 7.33 Maximum and minimum middle and end strains recorded at maximum and minimum cyclic loads of 18.5 kN and 1.6 kN for sample 4B tested in tension-tension at $R = 0.1$.

Because of the locations on the composite overlaps, the results of middle and end strains are always lower than those obtained from the gap strains. In figure 7.33 it appears logically that middle strains are always higher than end strains. Both maximum and minimum middle strains remain relatively constant up to 1000 cycles and increase significantly up to failure. Middle strains are still affected by the plastic strains that increase (towards sample failure) in the high strain gap region. On the other hand, maximum and minimum end strains remain relatively constant all the way up to failure. Unlike middle strains, it can be said that end strains are unaffected by plastic strains that built up within the sample as it reaches failure because the gauges are located relatively far away from the high strain region.

But those strain distributions are justified by the fact that sample 4B was tested at high cyclic loads and therefore a fair amount of plastic strain developed during the relatively short fatigue life of the sample.

For a sample that was tested at slightly lower cyclic loads, such as sample 11A the strain distributions are radically different. The graph shown in figure 7.34 illustrates maximum and minimum middle and end strains recorded at maximum and minimum cyclic loads of 16 kN and 1.4 kN for sample 11A.

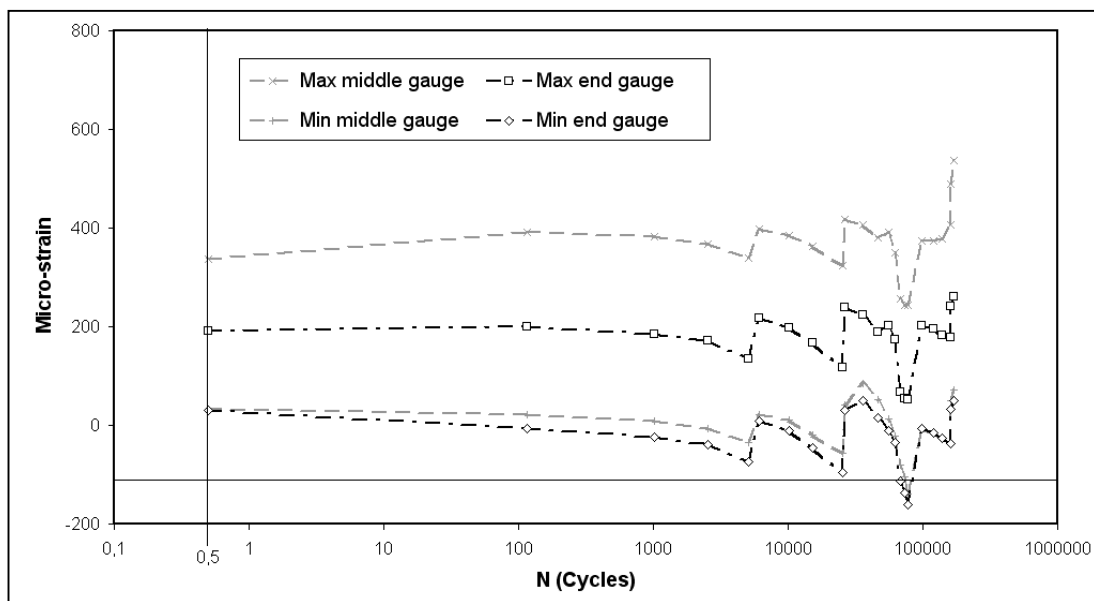


Figure 7.34 Maximum and minimum middle and end strains recorded at maximum and minimum cyclic loads of 16 kN and 1.4 kN for sample 11A tested in tension-tension at $R = 0.1$.

At lower cyclic loads, the middle and end strains behave in a different manner across the sample's fatigue life. Maximum and minimum values display the same curve shape. All values of strains remain very steady up to around 10000 cycles. Then the behaviour becomes more chaotic but still relatively constant up to the failure. It is interesting to notice that the strain distributions have the same shape and amplitude in the middle gauges as in the end gauges. Near failure, each strain has hardly increased. This clearly demonstrates that at lower cyclic loads there is less plastic strain developing. In fact middle and end strains are less affected by the cyclic loads. In theory, at some sufficiently low cyclic load, the strain distribution all over the composite surface will remain constant during the fatigue: This low load will correspond to the endurance limit of the joint.

The failure mechanism that was observed for all the wood/glass/epoxy joints that failed during the fatigue tests was the delamination of the glass fibre/epoxy composite layer on both faces of the samples. Some of those composite layers were collected after the tests and were examined using a microscope.

The microscope used could take black and white pictures (100 × 80 mm) with a maximum magnifying scale of × 250.

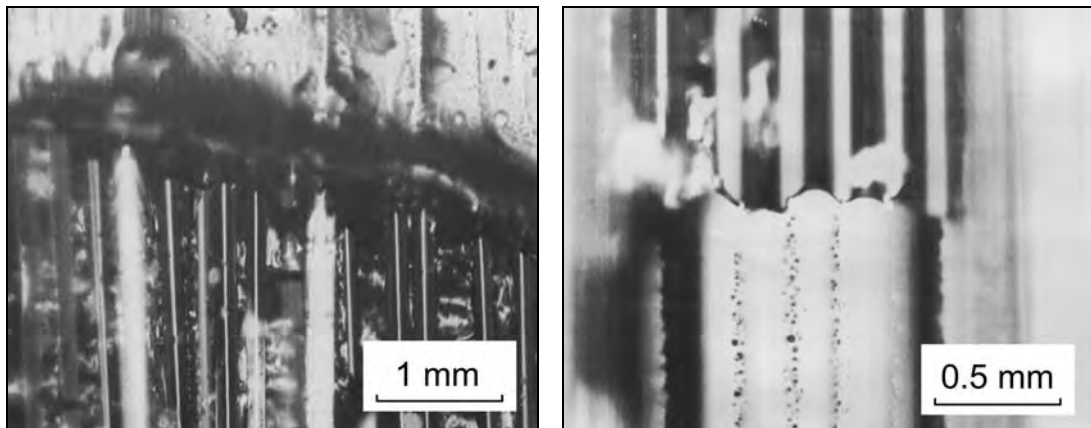
The pictures that are presented from figure 7.36 to 7.41 were taken from microscopic observations of the glass fibre/epoxy composite layers, in the gap zone. The gap of the glass fibre/epoxy composite layers is the zone where all the visible fatigue damage could be observed after the tests, as shown in figure 7.35.



Figure 7.35 Visible damage in the gap zone of the composite layer after the fatigue test.

Figure 7.35 was taken from a sample that did not fail as the composite layer is still bonded to the timber members. The delamination of composite from the timber surface is still visible in the gap zone (particularly on the right hand side) as well as surface matrix/fibre debonding.

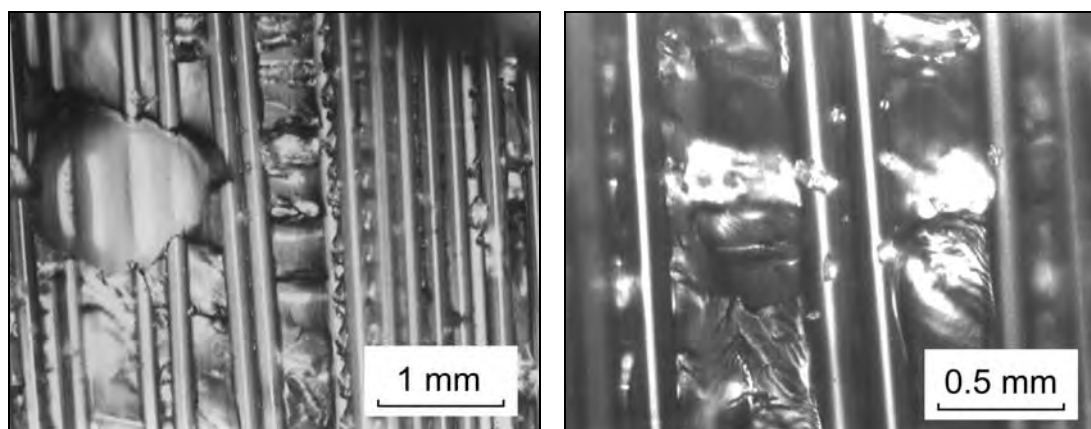
The microscopic observations of the gap zone of the composite layer, particularly the composite interface with the timber (i.e. its underside) revealed some interesting details of the mode of fracture, as presented in figures 7.36 to 7.41.



Figures 7.36 and 7.37 Matrix/fibre debonding details at the interface with the timber (underside of the composite layer) in the gap zone.

In these pictures, it appears that the matrix that once was bonded to the fibres is not there anymore. In figure 7.36, the matrix is visible at the top with some voids and below the fibres are not covered. The dark strip that separates the two zones is the fracture boundary, probably where the principal crack initiated in the matrix. In figure 7.37, the situation is rather different: the matrix is visible at the bottom (without showing any substantial voids) and the fibres are not covered at the top. The fracture boundary is clearly visible and is less regular than in figure 7.36: There are only six fibres that were debonded from the matrix. The presence of large voids in the matrix indicates substantial defect where cracks could initiate more easily.

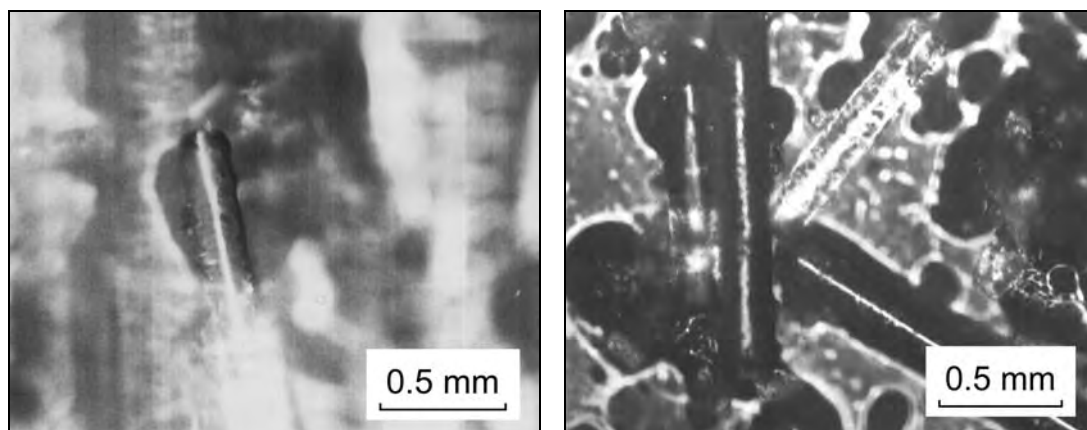
Other pictures were taken in zones where fibres were debonded, as shown in figures 7.38 and 7.39.



Figures 7.38 and 7.39 Other matrix/fibre debonding details at the interface with the timber (underside of the composite layer) in the gap zone.

In figure 7.38, the matrix that is in the background, behind the fibres has an irregular surface. This confirms that some matrix cracking occurred and that the surface matrix/fibre debonding was combined with the shear failure of the matrix. Figure 7.39 confirms the shear failure of the matrix and the matrix/fibre debonding, as some fragments of matrix still remain bonded to the fibres.

The pictures shown in figures 7.40 and 7.41 were taken in zones with broken fibres.



Figures 7.40 and 7.41 Fibre breaking and local debonding details at the interface with the timber in the gap zone.

Figure 7.40 shows a broken fibre in a local matrix debonding, which is a common fatigue failure mechanism in composites (see figure 7.21). This mode of failure was observed across the fatigue tests but was very minor because the main mode of failure of the joints was not fibre breaking but composite delamination. The figure 7.41 shows several broken fragments of fibres orientated in various directions in a debonded matrix with many voids.

Fibre breaking seems to be a local mode of failure that probably occurred in locations where the fibre/matrix bond was poor due to the presence of voids. However the microscopic observations confirm that the main failure mode observed for the wood/glass/epoxy joints was composite delamination from the timber all across the joint combined with fibre/matrix debonding in high stress regions such as the gap zone.

Finally all the fatigue characteristics and behaviour of the wood/glass/epoxy joints that were explored through this chapter are summarised in the conclusion.

7.4. Conclusion

Wood/glass/epoxy joints were subjected to cyclic testing in tension-tension at $R = 0.1$, which appears as a classic testing procedure used for most fatigue tests of structural materials.

The validity of the wood/glass/epoxy joints fatigue tests results has to be checked with existing data to find out how reliable the efficiency of those joints was in fatigue. By correlating the results obtained for E-Glass laminates in the DOE/MSU Database presented previously, with the S-N curves obtained for wood/glass/epoxy joints, it was found that the “ten percent” rule that typically applies to unidirectional composites also fitted perfectly to wood/glass/epoxy joints. The normalised S-N curve presented in figure 7.42 is the same as the one already shown on figure 7.9, except that this is expressed in percentage of maximum static load.

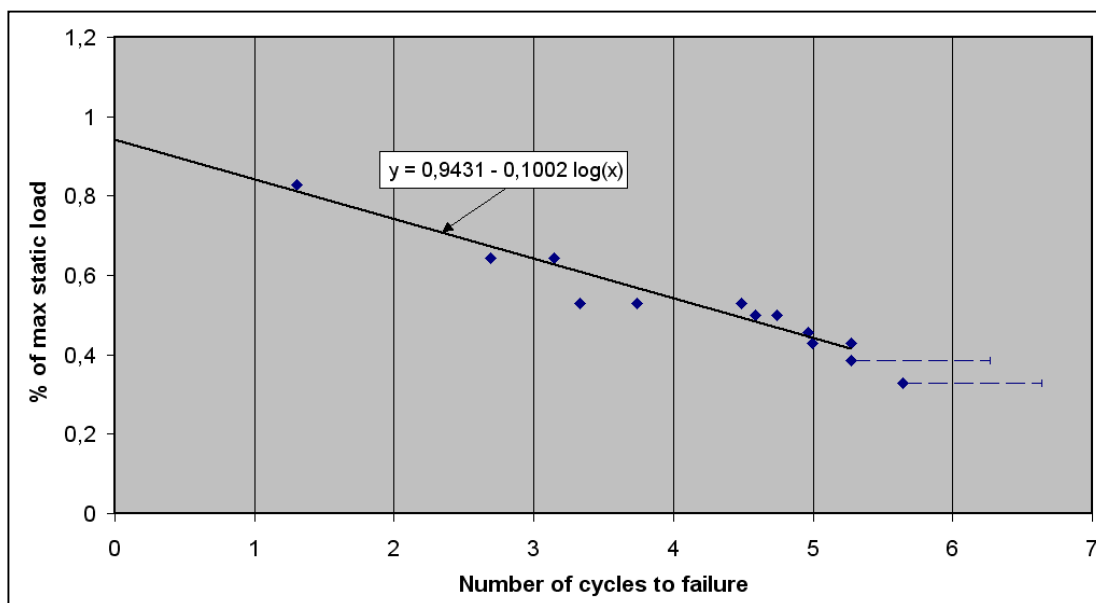


Figure 7.42 S-N normalised curves for wood/glass/epoxy joints tested in tension-tension at $R = 0.1$.

The trend line equation shown in figure 7.42 fits very well the previously presented equation (7.5) that characterised the S-N behaviour of composite materials. In fact, the material constant C' is equal to 0.9431, which is very close to one. The slope of the curve b is equal to 0.1002 that corresponds to the optimum slope, according to conclusions from the DOE/MSU Database: A slope b equal to 0.10 defines the good

materials as the curve is approaching the best fatigue behaviour that can be obtained for glass fibre laminates in tensile fatigue (see figure 7.24).

The similarities between the equations of the S-N curves indicate that the results obtained from the fatigue tests are reliable and reflect the fatigue response of well-fabricated wood/glass/epoxy joints. It also highlights that the fatigue response of wood/glass/epoxy joints is dominated by the composite behaviour rather than the main material that is timber.

Using the results obtained from the fatigue tests with the background information presented and described in the literature review of this chapter, the characteristics that define the fatigue response of the wood/glass/epoxy joints could then be drawn. The factors that affect the fatigue behaviour of the wood/glass/epoxy joints are related to the materials that compose the joints. The fatigue characteristics presented in the following bullet points were described in the papers review throughout this chapter

- Fatigue characteristics linked to the timber material:
 - Timber is a naturally grown material therefore its mechanical properties are very variable. It must always be graded according to the standards before being used for construction.
 - Tsai and Ansell (1990) found that fatigue life of timber is independent of the species and is affected by the moisture content. The fatigue life reduces with increasing moisture content (above 12%).
 - Tsai and Ansell (1990) identified that the fatigue damage accumulation at cellular level is associated with the formation of kinks in the cell walls, compression creases and cracks in the timber. As timber is an anisotropic material, the damage is of different nature depending on the stress direction.
 - Hansen (1991) highlighted that the fatigue resistance of timber is affected by the loading frequency. As a result, the higher the frequency, the lower is the fatigue life of timber for a given cyclic stress.
 - Tsai and Ansell (1990), as well as Hacker and Ansell (2001) observed that the most severe mode of cyclic loading for timber is the fully reversed loading at $R = -1$.

- Bonfield and Ansell (1991) identified that fatigue lives measured in all-tension are significantly longer than all-compression tests.
- Bonfield and Ansell (1991) found that the fatigue resistance of shear was higher along the TL plane than the RL plane for Khaya wood. Assuming the same behaviour could be obtained for European spruce, the fatigue resistance of wood/glass/epoxy joints could be improved as the delamination of the composite produced shear action of the timber members along the RL plane.
- Fatigue characteristics linked to the glass fibre/epoxy composite:
 - Maximum efficiency in terms of stiffness and strength is obtained with continuous, unidirectionally orientated fibres and properties measured parallel to the fibre direction. At off-angle, the strength and stiffness decrease (as shown in chapter 3, figure 3.10). Then the role of the matrix material becomes more important in the deformation and failure processes.
 - As a result, many woven glass fibre fabric composites show poorer fatigue resistance than unidirectional systems.
 - Matrix material has minimal effect on the static and fatigue properties in unidirectional composites loaded parallel to the fibres. However for the wood/glass/epoxy joints, the matrix has a prominent role because it bonds the materials together and carries the load from the timber to the composite.
 - There are many damage modes in composites, such as matrix cracking, fibre fracture, delamination, debonding, void growth and multidirectional cracking. Most of those damage modes were observed on the wood/glass/epoxy joints.
 - The fibre content is a significant parameter of composites fatigue resistance. Sutherland (1999) highlighted that increasing the fibre content of a composite system generally reduces its fatigue performance. The optimum fatigue performance is obtained with a fibre content of approximately 40% for unidirectional glass fibre laminates.
 - The fibre-to-matrix strength ratio is also a major factor in the fatigue resistance of axially stressed unidirectional composites. Composite with high fibre-to-matrix strength ratio will have higher fatigue resistance than the same composite with lower fibre-to-matrix strength ratio.

- Fatigue characteristics linked to the wood/glass/epoxy joints composite:
 - The quality of fabrication and particularly the bond of the glass fibre/epoxy composite to the timber are essential to the static and fatigue resistance of the wood/glass/epoxy joints.
 - The failure modes of the wood/glass/epoxy joints can be summarised as fatigue cracks initiation and growth that developed at the interface between the timber and the composite in the gap zone. Those cracks also occur in the composite itself in the gap zone, particularly where the composite has defects (air voids, unbonded matrix/fibre zones, etc). However the main damage mode that lead to failure of the joint is only the interface failure between the timber and the composite in the gap zone.
 - The distribution of stresses in the composite, further away from the gap zone is only significant a high cyclic loads. At low cyclic loads, most of the tensile stress is transferred from the composite to the timber in the gap zone. The length of composite has therefore a major role in the fatigue resistance of the joint. The Hart-Smith approach summarised by Adams et al. (1997) explains that increasing the composite length would always improve the fatigue resistance of structural adhesive joints, and therefore for wood/glass/epoxy joints.
 - Wood/glass/epoxy joints were found to have a good fatigue resistance compared to other timber joints, according to the EC5: Part 2: 1997 recommendations.

CHAPTER 8

CONCLUSIONS

8.1. General conclusions

The general conclusions summarise all the relevant results that were obtained throughout the research:

- Wood/glass/epoxy joints with uniaxial glass fibre tested in tension with load parallel to the grain were found the strongest in terms of failure loads and stiffness. Misalignment of glass fibres to the load and wood grain direction reduced significantly the strength and stiffness.
- Wood/glass/epoxy joints with biaxial glass fibre tested in tension with load parallel to the grain failed at lower loads because only half the amount of fibres was orientated in the load direction. However with the fibres orientated at 30 degrees to the load and the grain, the failure load was even lower but with higher stiffness.
- The joints were then tested in tension with load not parallel to the grain. For wood/glass/epoxy joints made of uniaxial glass fibre, the ones tested in tension at 90 degrees to the grain were the strongest in terms of failure loads and stiffness. Failure loads seemed to decrease as the grain/load angle reduced from 90 to 30 degrees.
- For wood/glass/epoxy joints made of biaxial glass fibre and tested in tension with load not parallel to the grain, Failure loads were fairly similar at 90 and 60 degrees, and slightly higher at 30 degrees to the grain.
- Performance of wood/glass/epoxy joints is mainly driven by the quality of the composite to timber bond. The load capacity is governed by the shear strength of the timber, which is not too affected by the grain orientation. This is confirmed in

the work by Gustafsson and Enquist (1993) and Avent (1986) presented in the literature review.

- The mechanical properties obtained from the small clear samples were in harmony with published figures of similar species. It confirms the validity of the tests and that the timber was correctly graded.
- More accurate finite element results were obtained with the 2D models than 3D models because convergence testing was carried out. FE results were very close to experimental results for joints made of uniaxial glass fibre and were generally lower for joints made of biaxial glass fibre.
- The FE analysis confirmed the non-uniform load transfer that occurs on double lap joints such as wood/glass/epoxy joints. The internal bending effect of the overlap was identified in the FE analysis and confirmed experimentally. This phenomenon strongly affected the stress and strain distribution in the joint.
- The S-N curve obtained from the fatigue tests of wood/glass/epoxy joints was compared with references and indicated that the results were reliable and were reflecting the fatigue response of well-fabricated joints. The fatigue of wood/glass/epoxy joints is dominated by the composite behaviour rather than the timber. The length of composite was found to have a major role in the fatigue resistance of the joint. Based on literature references (Adams et al., 1997), improving the fatigue resistance of the wood/glass/epoxy joints for a given cyclic loading could be achieved by increasing the composite length.
- Finally, the quality of fabrication and particularly the bond of the glass fibre/epoxy composite to the timber were found to be essential to the static and fatigue resistance of the joints and should be taken into consideration for design. The timber surface to be bonded with glass fibres should be preliminary planned or sanded down, free from defects and excessive humidity.

8.2. Suggestions for future work

There are several research subjects that should be investigated before a full design method for wood/glass/epoxy joints could be developed:

- Structural analysis of wood/glass/epoxy joints should be investigated in bending and compression. The glass fibre/epoxy composite will have a major role to overcome the premature buckling of the connected timber members (due to joint misalignment).
- Wood/glass/epoxy joints made of different species (particularly hardwoods) could be tested to investigate whether the differences between species or timber cell structures are affecting the strength and durability of the joints.
- Structural analysis of wood/glass/epoxy joints could be investigated with different bonded lengths and types of glass fibres and different resin types.
- Fatigue analysis of wood/glass/epoxy joints should be investigated in other loading modes, in compression and particularly in reverse mode ($R = -1$) as it appeared in all cited references that this mode is the most severe for fatigue resistance.
- The behaviour of wood/glass/epoxy joints under fire conditions should also be explored, in order to give a fire rating for that type of structural joint.
- In a broader research area, the effects of using glass fibres bonded on timber could also be investigated with the combination of mechanically fastened jointing systems. In other words, to investigate mechanical joints for wood/glass/epoxy structural material.

REFERENCES

1. Adams, R.D.; Comyn, J. and Wake, W.C. 1997. *Structural adhesive joints in engineering*. Second Edition, Chapman & Hall, London, U.K., 1997.
2. Allwork, M. 1997. *Research into the use of epoxy resin and glass fibre reinforcing joints*. BEng Civil Engineering Project Report, Coventry University, U.K.
3. Ashbee, K. 1993. *Fundamental principles of fiber reinforced composites*. Second Edition, Technomic, Pennsylvania, U.S.A., 1993.
4. Askeland, D.R. 1996. *The science and engineering of materials*. Third Edition, Chapman & Hall, London, U.K., 1996.
5. Avent R.R.; Emkin, L.Z. and Sanders, P.H. 1978. *Behaviour of epoxy repaired full-scale timber trusses*. ASCE Journal of Structural Engineering, Proceedings of the ASCE, 104(ST6): 933-951.
6. Avent R.R. and Issa, C.A. 1984. *Effect of fire on epoxy-repaired timber*. ASCE Journal of Structural Engineering, 110(12): 2858-2875.
7. Avent R.R. 1985. *Decay, weathering and epoxy repair of timber*. ASCE Journal of Structural Engineering, 111(2): 328-342.
8. Avent R.R. 1986. *Factors affecting strength of epoxy-repaired timber*. ASCE Journal of Structural Engineering, 112(2): 207-221.
9. Avent R.R. 1986. *Design criteria for epoxy repair of timber structures*. ASCE Journal of Structural Engineering, 112(2): 222-240.
10. Baker, A. 1997. *Joining and repair of aircraft composite structures*. Composites Engineering Handbook, Edited by Mallick, P.K., New York, U.S.A., 1997.

-
11. Barbero, E.J. 1999. *Introduction to composite materials design*. Taylor & Francis, Philadelphia, U.S.A., 1999.
 12. Benham P.P., Crawford R.J. and Armstrong C.G. 1996. *Mechanics of engineering materials*. Second Edition, Longman Group, Harlow, U.K., 1996.
 13. Biblis, E.J. 1965. *Analysis of wood-fiberglass composite beams within and beyond the elastic region*. Forest Products Journal 15(2): 81-88.
 14. Bonfield, P.W. and Ansell, M.P. 1991. *The fatigue properties of wood in tension, compression and shear*. J. Mat. Sci., 26, 4765-4773, 1991.
 15. Booth, L.G. and Reece, P.O. 1967. *The structural use of timber*. Spon, London, U.K., 1967.
 16. BS EN 408: 1995. *Timber structures – Structural timber and glued laminated timber – Determination of some physical and mechanical properties*. British Standards Institution, London, 1995.
 17. BS EN 1193: 1997. *Timber structures – Structural timber and glued laminated timber – Determination of shear strength and mechanical properties perpendicular to the grain*. British Standards Institution, London, 1995.
 18. BS EN 26891: 1991. *Timber structures – Joints made with mechanical fasteners – General principles for the determination of strength and deformation characteristics*. British Standards Institution, London, 1995.
 19. BS 373: 1957. *Methods of testing small clear specimens of timber*. British Standards Institution, London, 1957.
 20. BS 5268: Part 2: 1996. *Structural use of timber. Part 2. Code of practice for permissible stress design, materials and workmanship*. British Standards Institution, London, 1996.

21. BS 5268: Part 3: 1985. *Structural use of timber. Part 3. Code of practice for trussed rafter roofs*. British Standards Institution, London, 1985.
22. BS 6399: Part 2: 1995. *Code of practice for wind loads*. British Standards Institution, London, 1995.
23. BS 6948: 1989. *Mechanically fastened joints in timber and wood-based materials*. British Standards Institution, London, 1989.
24. Bull, J.W. 1994. *The practical design of structural elements in timber*. Second Edition, Gower, Aldershot, U.K., 1994.
25. Bulleit, W.M. 1984. *Reinforcement of wood materials: A review*. Wood and Fiber Science, 16(3): 391-397.
26. Chawla, K.K. 1998. *Composite materials, science and engineering*. Second Edition, Springer-Verlag, New York, U.S.A., 1997.
27. Chen, C.J. 1996. *An optimisation of timber joint by fiberglass reinforcements*. Proceedings pp. 811-818, Advanced Composite Materials in Bridges and Structures, 2nd Int. Conf., Montreal, Canada, 1996.
28. Claisse, P.A. and Davis T.J. 1998. *High performance jointing systems for timber*. Construction and Building Materials 12 (1998): 415-425.
29. CP3: Chapter V: Part 2: 1972. *Code of basic data for the design of buildings: Wind loads*. British Standards Institution, London, 1972.
30. Cramer, S.M., Shrestha, D. and Fohrell, W.B. 1990. *Theoretical consideration of metal-plate connected wood-splice joints*. ASCE Journal of Structural Engineering, 116(12): 3458-3474.
31. Davis, T.J. 1997. *An analysis of the performance of joints in wood composites*. EPSRC Report, Coventry University, 1997.

-
32. Dayer, P. 1994. *Renforcement par fibre de verre d'assemblages dans la construction en bois*. Mémoire de Diplôme, EPFL (Swiss Federal Institute of Technology), IBOIS, Lausanne, Switzerland.
 33. DD ENV 1991-1: 1994. *Eurocode 1 – Basis of design and actions on structures: Part 1: Basis of design*. European Committee for standardisation, Brussels, 1994.
 34. DD ENV 1995-1-1: 1994. *Eurocode 5 – Design of timber structures: Part 1.1: General rules and rules for buildings*. European Committee for standardisation, Brussels, 1994.
 35. DD ENV 1995-2: 1997. *Eurocode 5 – Design of timber structures: Part 2: Bridges*. European Committee for standardisation, Brussels, 1997.
 36. Dinwoodie, J.M. 2000. *Timber: Its nature and behaviour*. E & FN Spon, London, U.K., 2000.
 37. Dmitriev, P.A.; Strizhakov, Y.D. and Ushakov, V.I. 1991. *Wooden constructions with glass-reinforced plastic fastening units*. Proceedings vol. 3, pp. 157-163, Timber Engineering Conference, London, U.K., 1991.
 38. Dorey, A.B. and Cheng, J.J.R. 1996. *The behavior of GFRP glued laminated timber beams*. Proceedings pp. 787-794, Advanced Composite Materials in Bridges and Structures, 2nd Int. Conf., Montreal, Canada, 1996.
 39. Dorman, E.N. 1969. *Epoxy resins*. Handbook of Fiberglass and Advanced Plastic Composites, Edited by Lubin, G., New York, U.S.A., 1969.
 40. Dowling, N.E. 1999. *Mechanical behavior of materials - Engineering methods for deformation, fracture and fatigue*. Second Edition, Prentice Hall, New Jersey, U.S.A., 1999.

-
41. EN 28970: 1991. *Timber structures – Testing of joints made with mechanical fasteners – Requirements for wood density*. European Committee for standardisation, Brussels, 1991.
 42. GangaRao, H.V.S.; Sonti, S.S. and Superfesky, M.C. 1996. *Static response of wood crossties reinforced with composite fabrics*. Proceedings pp. 1291-1303, 41st International SAMPE Symposium, March 24-28, 1996.
 43. Gebremedhin, K.G. and Crovella, P.L. 1991. *Load distribution in metal plate connectors of tension joints in wood trusses*. ASAE (American Society of Agricultural Engineers), Structures and Environment Division 34(1): 281-287.
 44. Gilibert, Y.; Klein, M.L.L. and Rigolot, A. 1988. *Mechanical behavior assessment of epoxy adhesive in double-lap joint*. Adhesively Bonded Joints: Testing, Analysis and design, ASTM STP 981, Philadelphia, 1988, pp.39-53.
 45. Glos, P. and Horstmann, H. 1991. *Design of glued joints*. In proceedings vol. 3, pp. 77-84, Timber Engineering Conference, London, U.K., 1991.
 46. Grimes, G.C. and Bronstad, M.E.1969. *Test methods for composites*. Handbook of Fiberglass and Advanced Plastic Composites, Edited by Lubin, G., New York, U.S.A., 1969.
 47. Grinius, V.G. and Noyes, J.V.1969. *Design of composite materials*. Handbook of Fiberglass and Advanced Plastic Composites, Edited by Lubin, G., New York, U.S.A., 1969.
 48. Groom, L. and Polensek, A. 1992. *Nonlinear modelling of truss-plate joints*. ASCE Journal of Structural Engineering, 118(9): 2514-2530.
 49. Gupta, R. and Gebremedhin, K.G. 1990. *Destructive testing of metal-plate connected wood truss joints*. ASCE Journal of Structural Engineering, 116(7): 1971-1982.

-
50. Gustafsson, J. and Enquist, B. 1993. *Adherence of reinforcement to wood*. Advanced materials based on straw and wood – Fibre reinforcement of glulam. Report No 7, Lund University, Sweden, 1993.
 51. Hacker, C.L. and Ansell, M.P. 2001. *Fatigue damage and hysteresis in wood-epoxy laminates*. J. Mat. Sci., 36, 609-621, 2001.
 52. Haller, P.; Chen, C.J. and Natterer, J. 1996. *Experimental study on fiberglass reinforced and densified timber joints*. Proceedings pp. 308-314, Fourth Wood Engineering Conf., Oct. 28-31, New Orleans, U.S.A., 1996.
 53. Hamid, J.H.A. 1997. *Stress analysis on adhesive joints*. BEng Mechanical Engineering Project Report, Coventry University, U.K.
 54. Hansen, L.P. 1991. *Experimental investigation of fatigue properties of laminated wood beams*. Proceedings of the 1991 International Timber Engineering Conference 4, (Sub-Conference 15), 4.203 - 4.210, London, U.K.
 55. Harris, J.A. and Adams, R.D. 1984. *Strength prediction of bonded single lap joints by non-linear finite element methods*. Int. Journal of Adhesion and Adhesives, 4: 65-78.
 56. Hibbeler, R.C. 1997. *Mechanics of materials*. Third Edition, Prentice Hall, New Jersey, U.S.A., 1997.
 57. Hota, V.S. and GangaoRao, P.E. 1997. *Sawn and laminated wood beams wrapped with fiber reinforced plastic composites*. Wood design Focus, fall 1997, pp. 13-18.
 58. Jones, R.M. 1999. *Mechanics of composite materials*. Second Edition, Taylor & Francis, Philadelphia, U.S.A., 1999.

-
59. Juska, T.D. and Puckett, P.M. 1997. *Matrix resins and fiber/matrix adhesion*. Composites Engineering Handbook, Edited by Mallick, P.K., New York, U.S.A., 1997.
 60. Kalpakjian, S. and Schmid, S.R. 2001. *Manufacturing engineering and technology*. Prentice Hall, New Jersey, U.S.A., 2001.
 61. Kaw, A.K. 1997. *Mechanics of composite materials*. CRC Press, New York, U.S.A., 1997.
 62. Kirby, R. 1998. *An investigation into the strength of glass fibre and epoxy resin composites, and their use for the reinforcement of timber beams*. BEng Civil Engineering Project Report, Coventry University, U.K.
 63. Van de Kuilen, J-W.G. 1991. *Theoretical and experimental research on glass fibre reinforced laminated timber beams*. Proceedings vol. 3, pp. 226-233, Timber Engineering Conference, London, U.K., 1991.
 64. Laufenberg, T.L.; Rowlands, R.E. and Krueger, G.P. 1984. *Economic feasibility of synthetic fiber reinforced laminated veneer lumber (LVL)*. Forest Products Journal, 34(4): 15-22.
 65. MacLeod, I.A. 1990. *Analytical modelling of structural systems*. Ellis Horwood, Chichester, U.K., 1990.
 66. Mall, S. 1997. *Laminated polymer matrix composites*. Composites Engineering Handbook, Edited by Mallick, P.K., New York, U.S.A., 1997.
 67. Mallick, P.K. 1997. *Definitions, classifications and applications*. Composites Engineering Handbook, Edited by Mallick, P.K., New York, U.S.A., 1997.
 68. Matthews, F.L. 1987. *Joining fibre-reinforced plastics*. Elsevier Applied Science, London, U.K., 1987.

-
69. Matthews, F.L.; Kilty, P.F. and Godwin, E.W. 1982. *A review of the strength of joints in fibre-reinforced plastics. Part 2. Adhesively bonded joints*. Composites 31: 29-37.
 70. Mettem, C.J. 1986. *Structural timber design and technology*. Longman Scientific & Technical, TRADA, Harlow, U.K., 1986.
 71. Mettes, D.G. 1969. *Glass fibers*. Handbook of fiberglass and advanced plastic composites, Edited by Lubin, G., New York, U.S.A., 1969.
 72. Partridge, I.K. 1989. *Advanced composites*. Elsevier Applied Science, London, U.K., 1989.
 73. prEN 1075: March 1997. *Timber structures – Test methods – Joints made of punched metal plate fasteners*. Draft for Public Comment. European Committee for standardisation, Brussels, 1997.
 74. Richards, J.P. 1994. *A preliminary investigation into the use of glass fibre bonded to composite timber sections under simple loading conditions*. BEng Civil Engineering Project Report, Coventry University, U.K.
 75. Rowlands, R.E.; Van Deweghe, R.P.; Laufenberg, T.L. and Krueger, G.P. 1986. *Fiber-reinforced wood composites*. Wood and Fiber Science, 18(1): 39-57.
 76. Saucier, J.R. and Holman, J.A. 1975. *Structural particleboard reinforced with glass fiber – Progress in its development*. Forest Products Journal 25(9): 69-72.
 77. Sonti, S.S. and GangaRao, H.V.S. 1995. *Strength and stiffness evaluations of wood laminates with composite wraps*. Proceedings of the 50th Annual Conference, Composite Institute, The society of the plastics industry, Inc. Jan. 30-Feb. 1, 1995.

-
78. Sonti, S.S.; GangaRao, H.V.S. and Talakanti, D.R. 1996. *Accelerated aging of wood-composite members*. Proceedings pp. 1632-1641, 41st International SAMPE Symposium, March 24-28, 1996.
 79. Spera, D.A.; Esgar, J.B.; Gougeon, M. and Zuteck, M.D. 1990. *Structural properties of laminated Douglas fir/epoxy composite material*. DOE/NASA Reference Publication 1236, DOE/NASA/20320-76, Cleveland, 1990.
 80. Spaun, F.D. 1981. *Reinforcement of wood with fiberglass*. Forest Products Journal 31(4): 26-33.
 81. Staab, G.H. 1999. *Laminar Composites*. Butterworth-Heinemann, Woburn, U.S.A., 1999.
 82. Sutherland, H.J. 1999. *On the fatigue analysis of wind turbines*. SAND99-0089, Sandia National Laboratories, Albuquerque, New Mexico, 1999.
 83. Theakston, F.H. 1965. *A feasible Study for strengthening timber beams with fiberglass*. Canadian Agricultural Engineering, Jan. 1965, pp. 17-19.
 84. Timber Engineering STEP 1. *Basis of design, materials properties, structural components and joints*. First Edition, Centrum Hout, The Netherlands, 1995.
 85. Timber Engineering STEP 2. *Design – Details and structural systems*. First Edition, Centrum Hout, The Netherlands, 1995.
 86. Tsai, K.T. and Ansell, M.P. 1990. *The fatigue properties of wood in flexure*. J. Mat. Sci., 22, 865-878, 1990.
 87. Wangaard, F.F. 1964. *Elastic deflection of wood-fiberglass composite beams*. Forest Products Journal 14(6): 256-260.
 88. WIS (Wood information Sheets) 2/3 – 53. *Connectors and metal plate fasteners for structural timber*. TRADA, High Wycombe, U.K., 1996.

APPENDIX

A. Strains results from static tensile tests of wood/glass/epoxy joints

The results of strain gauges obtained through the static tests are summarised in table A.1 for all the samples made with uniaxial glass fibre and table A.2 for all the samples made with biaxial glass fibre.

Strains were recorded for loads of 6, 12, 18, 24 and 30 kN. To read the results of tables A.1 and A.2, refer to the strain gauge positions as shown in figure A.1 for a typical sample.

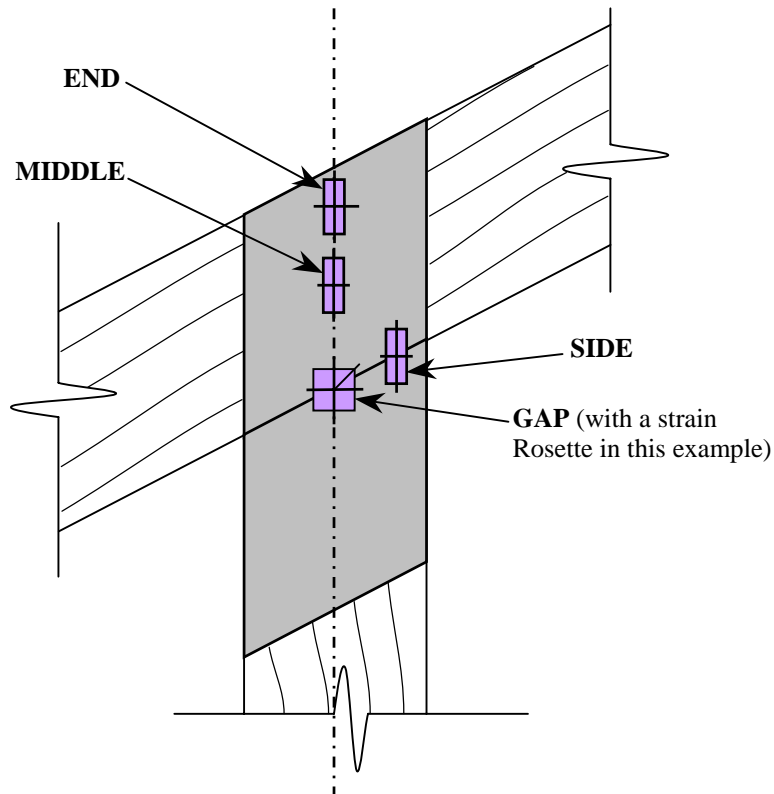


Figure A.1 Strain gauge positions on a typical composite layer.

The values of strain in table A.1 are expressed in micro strain (10^{-6} strain).

Sample	LOAD (kN)	END	MIDDLE	GAP (if Strain Rosette)			SIDE
				Longitudinal	Diagonal	Transversal	
7TPU00-Z	6	168	226	422	N/A	N/A	N/A
	12	342	508	2853	N/A	N/A	N/A
	18	503	758	4376	N/A	N/A	N/A
	24	662	1024	5917	N/A	N/A	N/A
	30	821	1308	7811	N/A	N/A	N/A
8TPU00-J	6	142	N/A	947	N/A	N/A	N/A
	12	287	N/A	2210	N/A	N/A	N/A
	18	428	N/A	3433	N/A	N/A	N/A
	24	581	N/A	4790	N/A	N/A	N/A
	30	772	N/A	7249	N/A	N/A	N/A
1TNU30-V	6	76	N/A	610	235	-219	837
	12	160	N/A	1628	679	-628	1954
	18	239	N/A	2893	1143	-1315	3274
	24	320	N/A	4560	1384	-1926	5155
	30	401	N/A	6573	2051	-2170	6856
5TNU60-η	6	134	N/A	974	670	-190	1059
	12	285	N/A	2147	1516	-419	2336
	18	438	N/A	3613	2721	-820	3767
	24	610	N/A	5348	4423	-1198	5377
	30	811	N/A	7617	6214	-1218	6784
5TNU90-Ω	6	95	N/A	991	N/A	N/A	N/A
	12	206	N/A	2259	N/A	N/A	N/A
	18	325	N/A	3738	N/A	N/A	N/A
	24	445	N/A	5228	N/A	N/A	N/A
	30	600	N/A	7519	N/A	N/A	N/A

Table A.1 Strain results obtained from samples made with uniaxial glass fibre.

The values of strain in table A.2 are expressed in micro strain (10^{-6} strain).

Sample	LOAD (kN)	END	GAP (if Strain Rosette)			SIDE
			Longitudinal	Diagonal	Transversal	
7TPB00- α	6	138	1401	N/A	N/A	N/A
	12	275	3817	N/A	N/A	N/A
	18	411	6093	N/A	N/A	N/A
	24	540	25394	N/A	N/A	N/A
	30	N/A	N/A	N/A	N/A	N/A
8TPB00- $\$$	6	152	1750	N/A	N/A	N/A
	12	296	3967	N/A	N/A	N/A
	18	463	6653	N/A	N/A	N/A
	24	621	9640	N/A	N/A	N/A
	30	N/A	N/A	N/A	N/A	N/A
6TNB30-U	6	55	862	866	-364	834
	12	123	2011	2048	-856	1991
	18	197	3956	3681	-1603	3666
	24	276	7405	6309	-2565	6495
	30	358	27160	15710	-3783	11554
5TNB60-W	6	231	1611	736	2	1653
	12	475	3660	1665	-90	3606
	18	731	6981	3293	-466	6364
	24	1151	11553	21708	-1506	24316
	30	N/A	N/A	N/A	N/A	N/A
6TNB90- ϕ	6	159	1769	N/A	N/A	N/A
	12	332	4180	N/A	N/A	N/A
	18	522	7007	N/A	N/A	N/A
	24	710	11022	N/A	N/A	N/A
	30	N/A	N/A	N/A	N/A	N/A

Table A.2 Strain results obtained from samples made with biaxial glass fibre.

B. Results of small clear samples tests

B.1. Static bending tests results

The results derived from the 20 sample beams tested in static bending test are summarised in table B.1.

Samples	Moisture Content (%)	Density (Kg/m³)	Bending MOE (MPa)	MOR (MPa)
A1	10,7	467	7568	73,8
B1	10,3	453	7596	73,8
C1	10,7	447	7515	73,0
D1	10,0	505	8965	86,5
E1	11,5	506	9070	82,4
F1	11,5	500	8375	79,6
G1	11,1	502	8298	79,7
H1	9,3	436	5064	74,6
I1	9,7	499	8895	84,9
J1	11,1	448	6944	69,2
A2	10,8	437	7232	70,5
B2	10,6	461	8023	79,0
C2	10,6	472	9163	84,0
D2	9,9	489	11568	104,4
E2	10,9	505	11091	96,4
F2	10,7	455	8441	77,1
G2	10,9	479	10190	89,8
H2	9,4	494	6818	79,0
I2	9,8	456	8563	82,3
J2	10,8	434	6282	87,7
Mean	10,52	472	8283	81
Standard deviation	N/A	N/A	1551	8,73

NOTE: MOE = Modulus Of Elasticity, MOR = Modulus Of Rupture or bending strength

Table B.1 Results obtained from the static bending tests.

B.2. Tension parallel to the grain tests results

The results derived from the 20 tension samples tested in tension parallel to the grain test are summarised in table B.2.

Samples	Moisture Content (%)	Density (Kg/m ³)	E _∥ (MPa)	σ _∥ (MPa)
A1	10,96	438	9949	57,3
B1	10,84	467	12012	95,1
C1	10,53	424	7432	57,1
D1	10,5	507	19060	136,4
E1	10	491	13531	77
F1	10,4	483	11944	90,7
G1	10,12	469	14144	106,4
H1	9,25	489	7175	42,6
I1	9,15	451	8906	77
J1	10,69	442	10319	65,4
A2	10,18	431	9532	62,7
B2	10,5	534	12231	92,2
C2	10,27	433	8323	68,3
D2	9,84	483	14745	104,3
E2	10,47	476	14988	106,1
F2	10,36	479	13845	109,3
G2	10,58	472	12287	84,2
H2	9,82	546	8035	70,8
I2	9,47	462	10294	90,5
J2	10,61	416	9563	59,3
Mean	10,23	470	11416	82,6
Standard deviation	N/A	N/A	3034	23,07

NOTE: E_∥ = Modulus of elasticity parallel to the grain, σ_∥ = Tension strength parallel to the grain.

Table B.2 Results obtained from the tension parallel to the grain tests.

B.3. Tension perpendicular to the grain tests results

The results derived from the 20 tension samples tested in tension perpendicular to the grain test are summarised in table B.3.

Samples	Moisture Content (%)	Density (Kg/m ³)	E _⊥ (MPa)	σ _⊥ (MPa)
A1	11,1	433	190	2,5
B1	10,8	505	218	1,1
C1	11,1	451	201	1,7
D1	10,2	461	220	1,3
E1	11,3	460	180	0,8
F1	10,9	434	174	1,4
G1	11,1	509	219	1,2
H1	9,3	420	189	1,9
I1	9,5	444	171	0,9
J1	11,2	431	224	1,7
A2	11	442	204	1,7
B2	10,7	505	263	2,3
C2	10,6	443	224	2,1
D2	9,1	455	447	2,6
E2	10,2	457	208	2,8
F2	9,8	439	185	2,2
G2	10,3	511	304	2,2
H2	8,7	407	202	2,1
I2	8,9	446	231	2,1
J2	10,3	427	295	2,9
Mean	10,31	454	227	1,86
Standard deviation	N/A	N/A	63	0,61

NOTE: E_⊥ = Modulus of elasticity perpendicular to the grain, σ_⊥ = Tension strength perpendicular to the grain.

The tension strengths σ_⊥ in grey background must be treated with caution, as they were derived from samples that failed by tensile failure of the resin bonded between the metal T-ends and the timber sample.

Table B.3 Results obtained from the tension perpendicular to the grain tests.

B.4. Shear parallel to the grain tests results

The results derived from the 40 shear samples tested in shear parallel to the grain test are summarised in table B.4.

Samples	Moisture Content (%)	Density (Kg/m ³)	τ (MPa)	Samples	Moisture Content (%)	Density (Kg/m ³)	τ (MPa)
A1	11,2	420	13,0	A3	10,9	490	4,6
A2	10,6	480	12,7	A4	9,3	424	N/A
B1	10,6	447	11,9	B3	9,7	438	4,2
B1	10,5	444	13,1	B4	9,1	432	4,1
C1	10,8	441	13,3	C3	9,9	434	N/A
C2	10,5	448	12,4	C4	9,7	449	N/A
D1	9,7	482	12,9	D3	9,4	491	12,5
D2	10,3	496	13,2	D4	9,5	490	15,0
E1	10,4	482	11,7	E3	9,3	474	9,8
E2	10,9	493	14,5	E4	9,6	484	12,5
F1	11,1	514	14,6	F3	10,3	499	12,9
F2	11,5	487	13,9	F4	11,5	505	14,7
G1	9,4	444	11,2	G3	10,1	448	9,5
G2	9,4	494	15,1	G4	10,2	500	15,1
H1	9,5	498	13,7	H3	9,3	477	13,1
H2	10,2	489	13,4	H4	8,9	461	13,2
I1	9,3	441	10,4	I3	9,4	452	11,2
I2	9,3	476	16,3	I4	9,8	490	12,5
J1	9,5	413	11,0	J3	11,7	412	10,8
J2	9,8	436	12,7	J4	10,4	436	10,2

	Moisture Content (%)	Density (Kg/m ³)	τ (MPa)
Mean	10,06	465	12,8
Standard deviation	N/A	N/A	1,63

NOTE: τ = Shear strength parallel to the grain.

Table B.4 Results obtained from the shear parallel to the grain tests.

C. Examples of in-plane and out-of-plane bending moment calculations

The examples are given for sample 6TPU00 – Z using the readings obtained from LVDTs at a tension load of 30 kN.

To calculate the in-plane bending moment that is applied to the sample at this load, the displacements measured with the small side LVDTs are 0.46 and 0.61 mm.

Using the moment area method, the eccentric fraction of tension load is calculated:

$$\text{Total surface area } A_T \text{ is: } A_T = \left(\frac{0.46 + 0.61}{2} \right) \times 94 = 50.29 \text{ mm}^2$$

$$\text{Portion of area applied to the eccentric load } A_e \text{ is: } A_e = \frac{(0.61 - 0.46) \times 94}{2} = 7.05 \text{ mm}^2$$

$$\text{The eccentric load } F_e \text{ is: } F_e = \frac{7.05 \times 30}{50.29} = 4.206 \text{ kN}$$

$$\text{Hence the in-plane bending moment } M_{in} \text{ is: } M_{in} = 4.206 \times 10^{-3} \times \left(\frac{94}{2} - \frac{94}{3} \right)$$

Then the in-plane moment is: $M_{in} = 0.0659 \text{ kN.m}$

To calculate the out-of-plane bending moment that is applied to the sample at this load, the displacements measured with the long face LVDTs are 0.38 and 0.46 mm.

Using the moment area method, the eccentric fraction of tension load is calculated:

$$\text{Total surface area } A_T \text{ is: } A_T = \left(\frac{0.38 + 0.46}{2} \right) \times 44 = 18.48 \text{ mm}^2$$

$$\text{Portion of area applied to the eccentric load } A_e \text{ is: } A_e = \frac{(0.46 - 0.38) \times 44}{2} = 1.76 \text{ mm}^2$$

$$\text{The eccentric load } F_e \text{ is: } F_e = \frac{1.76 \times 30}{18.48} = 2.857 \text{ kN}$$

$$\text{Hence the out-of-plane bending moment } M_{out} \text{ is: } M_{out} = 2.857 \times 10^{-3} \times \left(\frac{44}{2} - \frac{44}{3} \right)$$

Then the out-of-plane moment is: $M_{out} = 0.0209 \text{ kN.m}$

Those bending moments were found to be very low compared to the axial force applied to the sample and were therefore treated as negligible.

D. Technical details for the FE models

D.1. Models with load parallel to the grain TPU/B00 – 2D models

The two 2D models were built in a similar manner in terms of geometry but with different material properties.

File names:	Am12-Plane42 and Am14-Plane42
Materials number:	2 - Anisotropic
Element type:	PLANE42 - 2D Structural solid
Element description:	4 nodes planar element
Analysis type:	Static - Linear
Loading:	18 kN in tension
Number of Elements:	12393
Number of Nodes:	12685

Boundary conditions for the TPU/B00 – 2D models are presented in figure D.1.

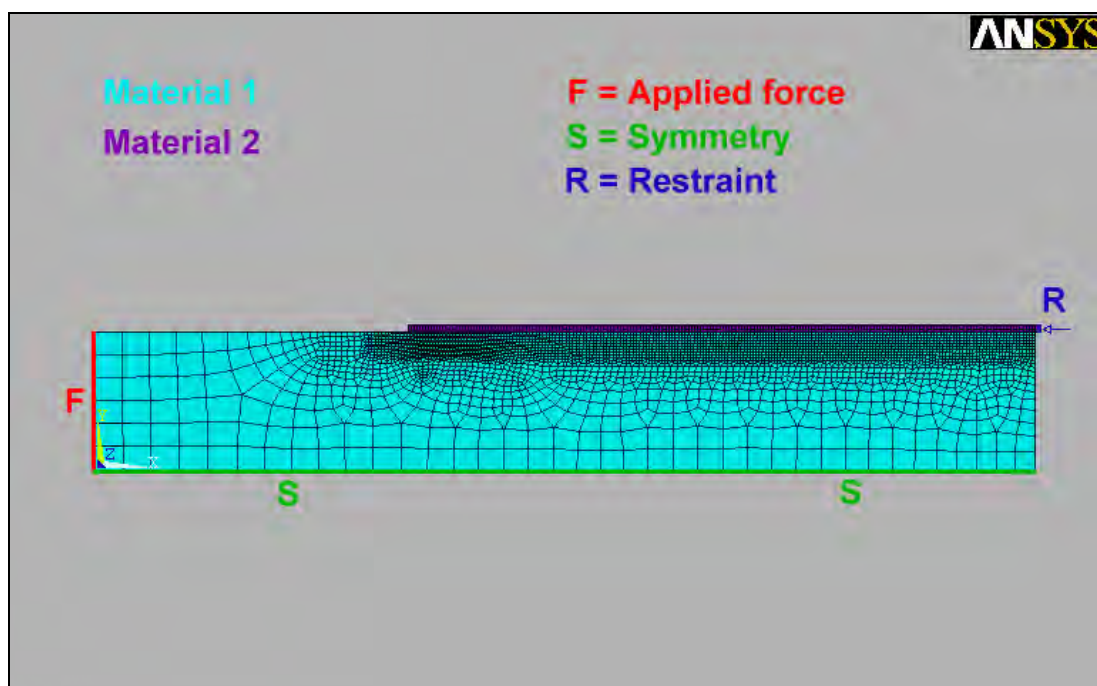


Figure D.1 Forces, restraints and symmetries for TPU/B00 – 2D models.

The 2D models were in fact 2 dimensional models with a thickness defined across the width of the sample, in the Z direction. The thickness was input as 94 mm.

The materials properties used for the FEM are given in table D.1 for the Am12-Plane42 model and in table D.2 for the Am12-Plane42 model. Materials

properties are defined with the three directions moduli of elasticity and three major Poisson's ratios.

Am12-Plane42 model						
	EX (N/mm²)	EY (N/mm²)	EZ (N/mm²)	NUXY	NUYZ	NUXZ
Material 1	11600	900	500	0.37	0.43	0.47
Material 2	28000	5000	5000	0.27	0.05	0.05

Table D.1 Materials properties forTPU00 – 2D models.

Am14-Plane42 model						
	EX (N/mm²)	EY (N/mm²)	EZ (N/mm²)	NUXY	NUYZ	NUXZ
Material 1	11600	900	500	0.37	0.43	0.47
Material 2	18600	5000	18600	0.091	0.091	0.05

Table D.2 Materials properties forTPB00 – 2D models.

The FE model geometry is defined in figure D.2 and the coordinates of the nodes are given in table D.3.

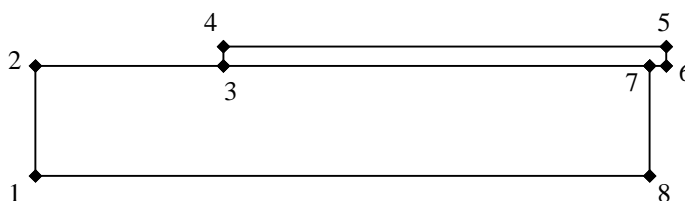


Figure D.2 Nodes locations forTPU/B00 – 2D models.

Am12-Plane42 and Am14-Plane42 Models		
Node	X (mm)	Y (mm)
1	0	0
2	0	22
3	50	22
4	50	22.65
5	150.5	22.65
6	150.5	22
7	150	22
8	150	0

Table D.3 Nodes coordinates forTPU/B00 – 2D models.

D.2. Models with load parallel to the grain TPU/B00 – 3D models

The two 3D models were built in a similar manner in terms of geometry but with different material properties.

File names:	Am01-Solid72 and Am02-Solid72
Materials number:	2 - Anisotropic
Element type:	SOLID72 - 3D Structural solid
Element description:	4 nodes tetrahedral solid element with rotations
Analysis type:	Static - Linear
Loading:	18 kN in tension
Number of Elements:	58886
Number of Nodes:	11788

Boundary conditions for the TPU/B00 – 3D models are presented in figure D.3.

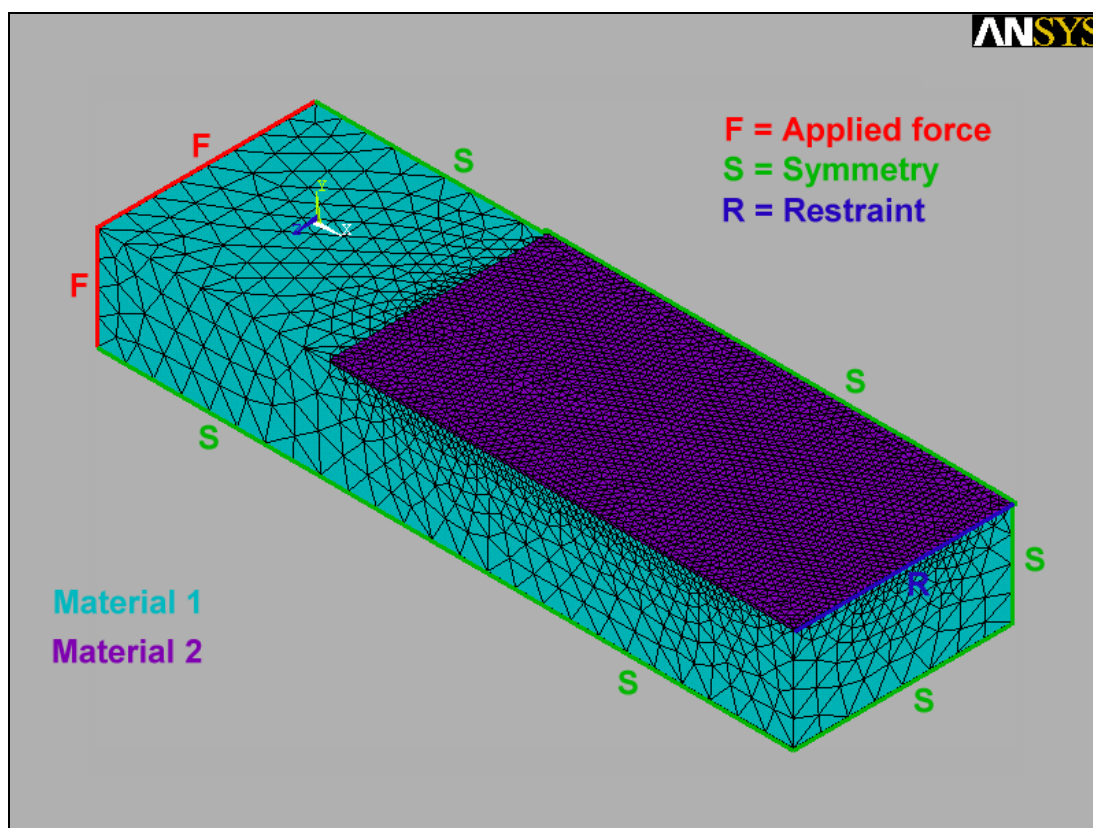


Figure D.3 Forces, restraints and symmetries for TPU/B00 – 3D models.

The materials properties used for the FEM are given in table D.4 for the Am01-Solid72 model and in table D.5 for the Am02-Solid72 model. Materials properties are defined with the three directions moduli of elasticity and three major Poisson's ratios.

Am01-Solid72 model						
	EX (N/mm ²)	EY (N/mm ²)	EZ (N/mm ²)	NUXY	NUYZ	NUXZ
Material 1	11600	900	500	0.37	0.43	0.47
Material 2	28000	5000	5000	0.27	0.05	0.05

Table D.4 Materials properties forTPU00 – 3D models.

Am02-Solid72 model						
	EX (N/mm ²)	EY (N/mm ²)	EZ (N/mm ²)	NUXY	NUYZ	NUXZ
Material 1	11600	900	500	0.37	0.43	0.47
Material 2	18600	5000	18600	0.091	0.091	0.05

Table D.5 Materials properties forTPB00 – 3D models.

The FE model geometry is defined in figure D.4 and the coordinates of the nodes are given in table D.6.

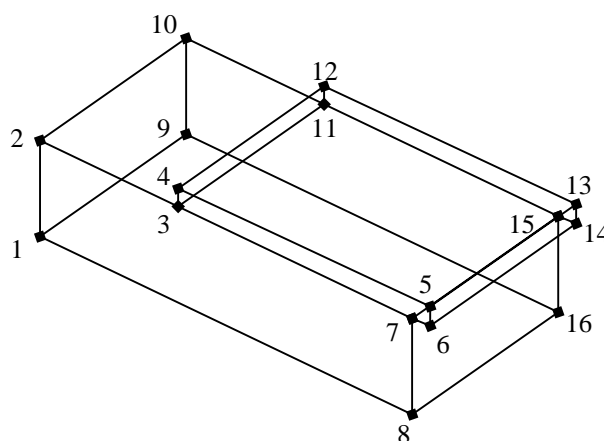


Figure D.4 Nodes locations forTPU/B00 – 3D models.

Am01-Solid72 and Am02-Solid72 Models							
Node	X (mm)	Y (mm)	Z (mm)	Node	X (mm)	Y (mm)	Z (mm)
1	0	0	94	9	0	0	0
2	0	22	94	10	0	22	0
3	50	22	94	11	50	22	0
4	50	22.65	94	12	50	22.65	0
5	150.5	22.65	94	13	150.5	22.65	0
6	150.5	22	94	14	150.5	22	0
7	150	22	94	15	150	22	0
8	150	0	94	16	150	0	0

Table D.6 Nodes coordinates forTPU/B00 – 3D models.

D.3. Models with load perpendicular to the grain TNU/B90 – 3D models

The two 3D models were built in a similar manner in terms of geometry but with different material properties.

File names:	Am03-Solid92 and Am04-Solid92
Materials number:	3 - Anisotropic
Element type:	SOLID92 - 3D Structural solid
Element description:	10 nodes tetrahedral solid quadratic element
Analysis type:	Static - Linear
Loading:	18 kN in tension
Number of Elements:	12650
Number of Nodes:	20557

Boundary conditions for the TNU/B90 – 3D models are presented in figure D.5.

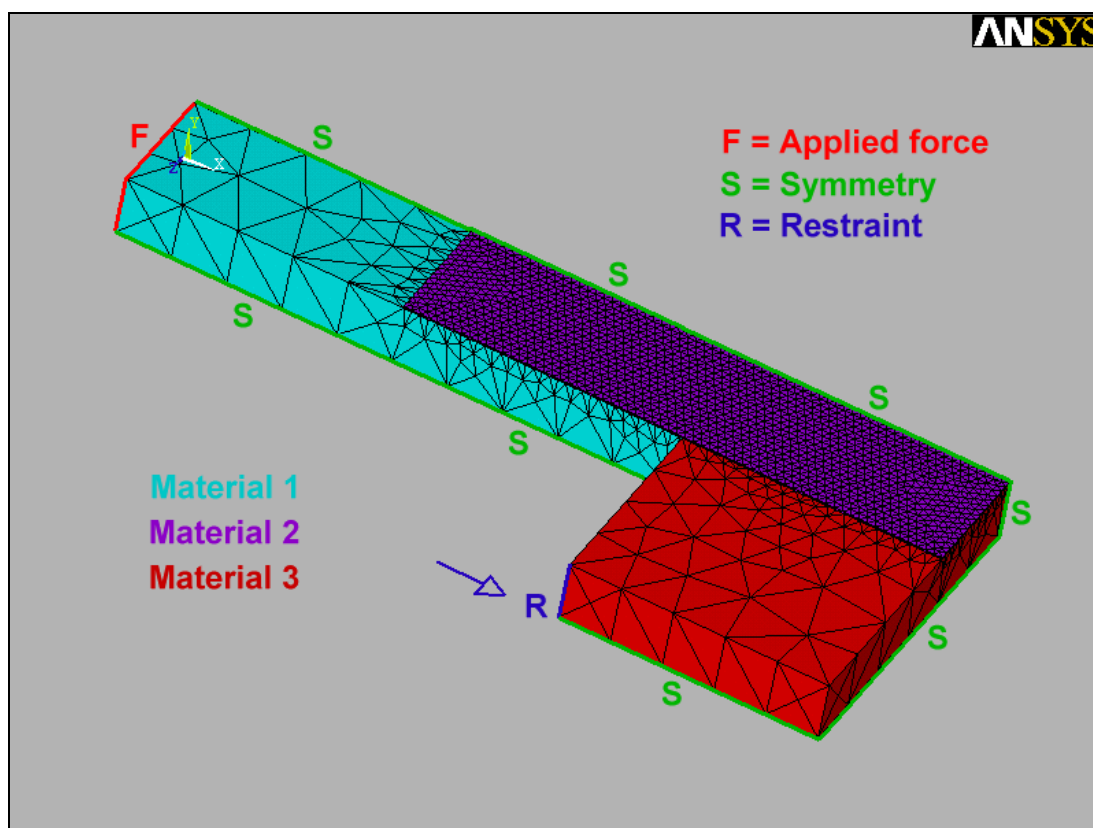


Figure D.5 Forces, restraints and symmetries for TNU/B90 – 3D models.

The materials properties used for the FEM are given in table D.7 for the Am03-Solid92 model and in table D.8 for the Am04-Solid92 model. Materials properties are defined with the three directions moduli of elasticity and three major Poisson's ratios.

Am03-Solid92 model						
	EX (N/mm ²)	EY (N/mm ²)	EZ (N/mm ²)	NUXY	NUYZ	NUXZ
Material 1	11600	900	500	0.37	0.43	0.47
Material 2	28000	5000	5000	0.27	0.05	0.05
Material 3	500	900	11600	0.25	0.029	0.02

Table D.7 Materials properties forTNU90 – 3D models.

Am04-Solid92 model						
	EX (N/mm ²)	EY (N/mm ²)	EZ (N/mm ²)	NUXY	NUYZ	NUXZ
Material 1	11600	900	500	0.37	0.43	0.47
Material 2	18600	5000	18600	0.091	0.091	0.05
Material 3	500	900	11600	0.25	0.029	0.02

Table D.8 Materials properties forTNB90 – 3D models.

With the geometry defined in figure D.6, nodes coordinates are given in table D.9.

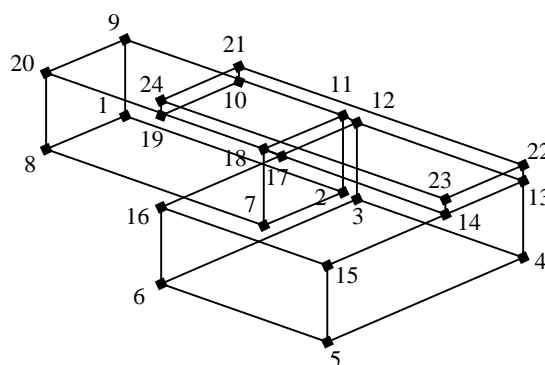


Figure D.6 Nodes locations forTNU/B90 – 3D models.

Am03-Solid92 and Am04-Solid92 Models							
Node	X (mm)	Y (mm)	Z (mm)	Node	X (mm)	Y (mm)	Z (mm)
1	0	0	0	13	295	22	0
2	200	0	0	14	295	22	47
3	201	0	0	15	295	22	122
4	295	0	0	16	201	22	122
5	295	0	122	17	201	22	47
6	201	0	122	18	200	22	47
7	200	0	47	19	100	22	47
8	0	0	47	20	0	22	47
9	0	22	0	21	100	22.65	0
10	100	22	0	22	295	22.65	0
11	200	22	0	23	295	22.65	47
12	201	22	0	24	100	22.65	47

Table D.9 Nodes coordinates forTNU/B90 – 3D models.

D.4. Models with load at 60° to the grain TNU/B60 – 3D models

The two 3D models were built in a similar manner in terms of geometry but with different material properties.

File name:	Am05-solid72 and Am06-solid72
Materials number:	3 - Anisotropic
Element type:	Solid72 - 3D Structural solid with rotations
Element description:	4 nodes tetrahedral solid element
Analysis type:	Static - Linear
Loading:	18 kN in tension
Number of Elements:	28932
Number of Nodes:	6753

Boundary conditions for the TNU/B60 – 3D models are presented in figure D.7.

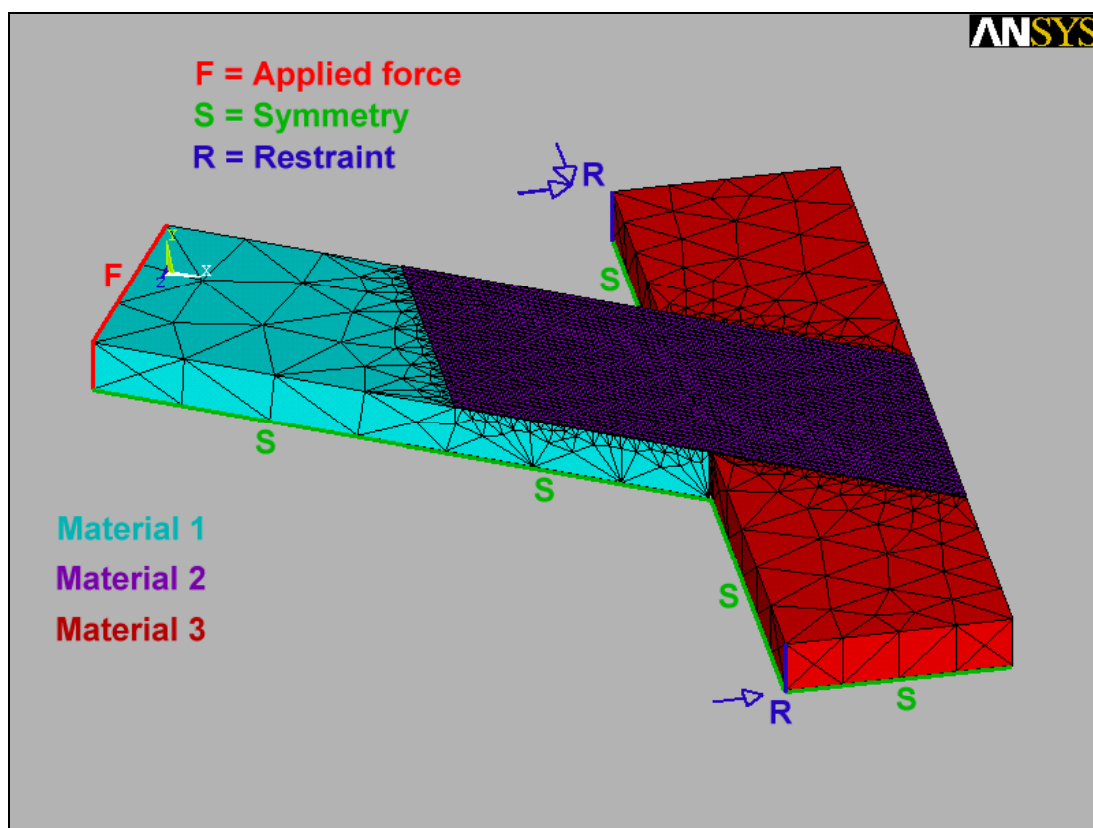


Figure D.7 Forces, restraints and symmetries for TNU/B60 – 3D models.

The materials properties used for the FEM are given in table D.10 for the Am05-Solid72 model and in table D.11 for the Am06-Solid72 model. Materials properties are defined with the three directions moduli of elasticity and three major Poisson's ratios.

Am05-Solid72 model						
	EX (N/mm ²)	EY (N/mm ²)	EZ (N/mm ²)	NUXY	NUYZ	NUXZ
Material 1	11600	900	500	0.37	0.43	0.47
Material 2	28000	5000	5000	0.27	0.05	0.05
Material 3	500	900	11600	0.25	0.029	0.02

Table D.10 Materials properties for TNU60 – 3D models.

Am06-Solid72 model						
	EX (N/mm ²)	EY (N/mm ²)	EZ (N/mm ²)	NUXY	NUYZ	NUXZ
Material 1	11600	900	500	0.37	0.43	0.47
Material 2	18600	5000	18600	0.091	0.091	0.05
Material 3	500	900	11600	0.25	0.029	0.02

Table D.11 Materials properties for TNB60 – 3D models.

Note that material 3 is defined in a different local coordinate system having node 11 as origin. This local coordinate system is translated in the X-axis by 237 mm and rotated by 30° anticlockwise around the Y-axis (i.e. in the X-Z plane).

With the geometry defined in figure D.8, nodes coordinates are given in table D.12.

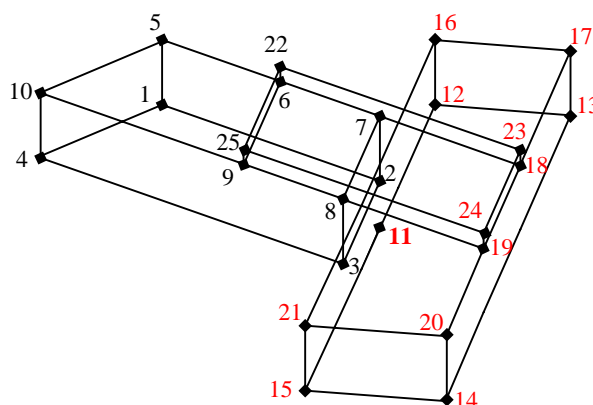


Figure D.8 Nodes locations for TNU/B60 – 3D models.

Am05-Solid72 and Am06-Solid72 Models							
Node	X (mm)	Y (mm)	Z (mm)	Nodes in local coordinated system 11			
				Node	X (mm)	Y (mm)	Z (mm)
1	0	0	0	12	0	0	-147.865
2	208.54	0	0	13	94	0	-147.865
3	262.81	0	94	14	94	0	202.135
4	0	0	94	15	0	0	202.135
5	0	22	0	16	0	22	-147.865
6	100	22	0	17	94	22	-147.865
7	208.54	22	0	18	94	22	0
8	262.81	22	94	19	94	22	108.54
9	154.27	22	94	20	94	22	202.135
10	0	22	94	21	0	22	202.135
11	237	0	47	23	94	22.65	0
22	100	22.65	0	24	94	22.65	108.54
25	154.27	22.65	94				

Table D.12 Nodes coordinates for TNU/B60 – 3D models.

D.5. Models with load at 30° to the grain TNU/B30 – 3D models

The two 3D models were built in a similar manner in terms of geometry but with different material properties.

File name:	Am07-solid72 and Am08-solid72
Materials number:	3 - Anisotropic
Element type:	Solid72 - 3D Structural solid with rotations
Element description:	4 nodes tetrahedral solid element
Analysis type:	Static - Linear
Loading:	18 kN in tension
Number of Elements:	67687
Number of Nodes:	15253

Boundary conditions for the TNU/B30 – 3D models are presented in figure D.9.

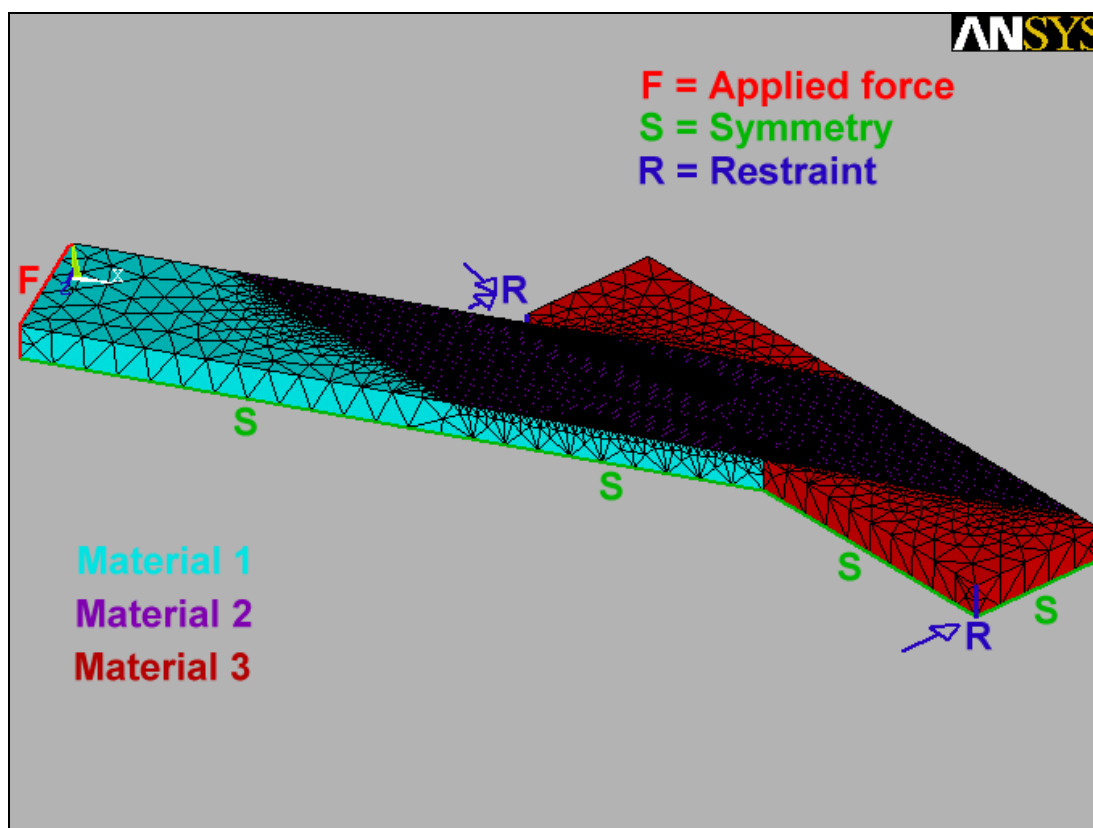


Figure D.9 Forces, restraints and symmetries for TNU/B30 – 3D models.

The materials properties used for the FEM are given in table D.13 for the Am07-Solid72 model and in table D.14 for the Am08-Solid72 model. Materials properties are defined with the three directions moduli of elasticity and three major Poisson's ratios.

Am07-Solid72 model						
	EX (N/mm ²)	EY (N/mm ²)	EZ (N/mm ²)	NUXY	NUYZ	NUXZ
Material 1	11600	900	500	0.37	0.43	0.47
Material 2	28000	5000	5000	0.27	0.05	0.05
Material 3	500	900	11600	0.25	0.029	0.02

Table D.13 Materials properties forTNU30 – 3D models.

Am08-Solid72 model						
	EX (N/mm ²)	EY (N/mm ²)	EZ (N/mm ²)	NUXY	NUYZ	NUXZ
Material 1	11600	900	500	0.37	0.43	0.47
Material 2	18600	5000	18600	0.091	0.091	0.05
Material 3	500	900	11600	0.25	0.029	0.02

Table D.14 Materials properties forTNB30 – 3D models.

Note that material 3 is defined in a different local coordinate system having node 11 as origin. This local coordinate system is translated in the X-axis by 371 mm and rotated by 60° anticlockwise around the Y-axis (i.e. in the X-Z plane).

With the geometry defined in figure D.10, nodes coordinates are given in table D.15.

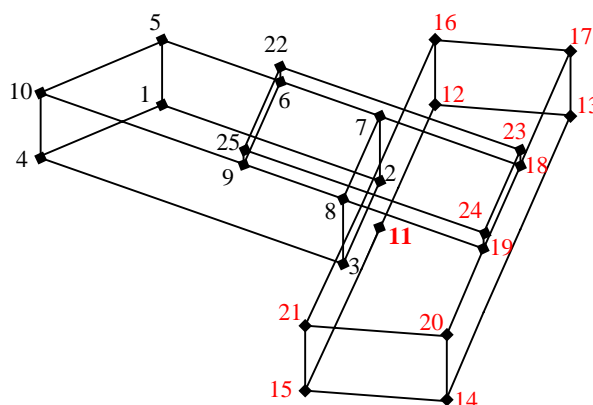


Figure D.10 Nodes locations forTNU/B30 – 3D models.

Am07-Solid72 and Am08-Solid72 Models							
Node	X (mm)	Y (mm)	Z (mm)	Nodes in local coordinated system 11			
				Node	X (mm)	Y (mm)	Z (mm)
1	0	0	0	12	0	0	-113.6
2	288	0	0	13	94	0	-113.6
3	450.8	0	94	14	94	0	276.4
4	0	0	94	15	0	0	276.4
5	0	22	0	16	0	22	-113.6
6	100	22	0	17	94	22	-113.6
7	288	22	0	18	94	22	68.8
8	450.8	22	94	19	94	22	256.8
9	262.8	22	94	20	94	22	276.4
10	0	22	94	21	0	22	276.4
11	371	0	47	23	94	22.65	68.8
22	100	22.65	0	24	94	22.65	256.8
25	262.8	22.65	94				

Table D.15 Nodes coordinates for TNU/B30 – 3D models.